COMSOL® HEAT TRANSFER MODELS

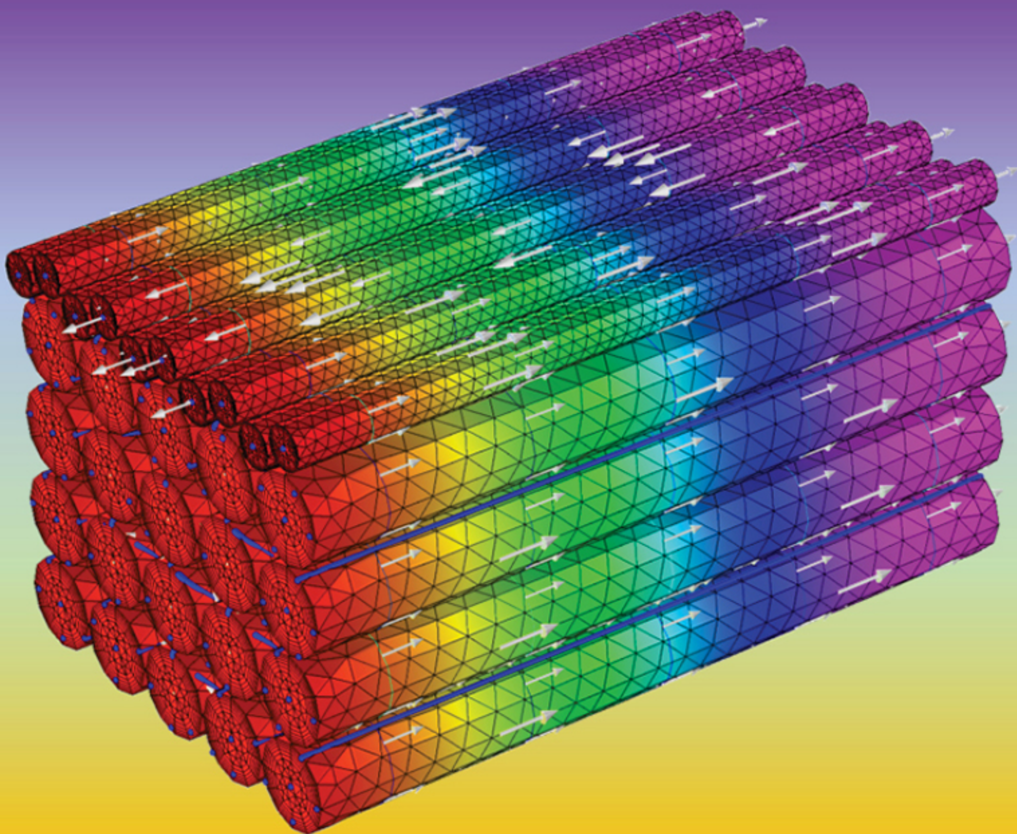

L. S. MAYBOUDI

COMSOL®
HEAT TRANSFER
MODELS

COMSOL®
HEAT TRANSFER
MODELS

Layla S. Mayboudi, PhD

MERCURY LEARNING AND INFORMATION
Dulles, Virginia
Boston, Massachusetts
New Delhi

Publisher: David Pallai
Mercury Learning and Information
22841 Quicksilver Drive
Dulles, VA 20166
info@merclearning.com
www.merclearning.com
800-232-0223

L. S. Mayboudi. *COMSOL® Heat Transfer Models.*
ISBN: 978-1-68392-211-7

Library of Congress Control Number: 2019940575

192021321 Printed on acid-free paper in the United States of America.

Our titles are available for adoption, license, or bulk purchase by institutions, corporations, etc. For additional information, please contact the Customer Service Dept. at 800-232-0223 (toll free).

All of our titles are available in digital format at *academiccourseware.com* and other digital vendors. *Companion files are also available for downloading by writing to info@merclearning.com*. The sole obligation of Mercury Learning and Information to the purchaser is to replace the book or disc, based on defective materials or faulty workmanship, but not based on the operation or functionality of the product.

To the Sunrise, Nights of Ten, Pair and Individual,

Time, and Green Rosary Beads…

CONTENTS

PREFACE

You are the one who created warm heat and cool shade.

—Great Mail, 62 [1]

This book can be considered a companion to the two previous publications by the author—*Heat Transfer Modelling Using COMSOL Slab to Radial Fin* [2] and *Geometry Creation and Import with COMSOL Multiphysics* [3]. For readers aiming to improve their heat transfer modeling skills, one possible sequence is to start with the present book, which will provide a broad perspective of the subject, and then continue to learn in greater depth about the geometry creation stage of model building. Those interested in the detailed exploration of heat transfer modeling of fins are directed to the related book. The same book will also provide an additional source of practice examples for the reader.

This section provides an outline of this work, a road map for the reader to this journey. The purpose is to become familiar with the field of heat transfer modeling through the examples from nature, the world surrounding us, such as animals and plants, but also the human body and the functions that help us live. Asking questions, learning, and trying to understand things are the most basic elements of humanity. If there is one single lesson that the author would like the reader to take from this publication, it is to never stop questioning and leaning; these are the privileges given to all, rich or poor, old or young. There exists nothing such as "*are we too curious*!"

The subject in the context of this publication is best understood if followed in the order the material is presented. The author encourages the reader to review the suggested approaches and to work through the presented problems, not only to visualize and understand them, but also to construct them manually as the first step and then use the finite element method tools to model the parts. There are multiple ways to approach each modeling problem, and this includes how one defines the relationships between the component physics. For example, you may decide to define multiple physics and solve each individually, feeding the results of one to the other, or to solve them simultaneously. You may decide to import the geometry or mesh into the modeling tool or to create the model geometry internally, using the built-in geometry-creation features. To gain a deeper understanding of the field, after completion of the related subject matter, the reader should attempt the Examples and Case Studies, exploring different possible ways to tackle the same problem using the building blocks of knowledge provided here.

While information learned from this book may be transferred to other FEM tools, the book's primary focus is on COMSOL Multiphysics modeling, with version 5.4 being used. This software consists of a core module and many specialized add-on modules. This book will present techniques which assume availability of the *Heat Transfer* module and the *CAD Import* module (or *LiveLink™* module connecting COMSOL Multiphysics with a specific CAD tool).

Chapter 1 shows the reader how the heat transfer phenomena can be found everywhere, from the smallest elements of the world to the universe in its entirety. Fire is perhaps the first thing one thinks of when heat is mentioned. Controlling fire may be considered as humanity's first step toward the creation of a civilized society. From the earliest days, humans learned how to manage this heat source for cooking, bringing light, protection, warmth, and even communicating with a divinity. From these ancient fires, as depicted in drawings on cave walls, humans have progressed to the most advanced heating technologies such as, for example, a laser, producing a collimated light that can be concentrated to deliver heat energy intensity surpassing that on the sun, but also able to treat the most sensitive organs, like our eyes.

While people could always tell whether something was hot or cold, to give a number to describe these "feelings" was something that required technological progress. This chapter thus reviews how temperature measurement technology has developed historically. The chapter continues by highlighting the interconnection between thermo-fluid sciences and the world around us, from the coldest possible state of matter to the hottest objects in the universe.

Thermal, flow and management are the essential elements of managing thermal sources—both hot and cold. These subjects are touched upon in this chapter, given that heat transfer modeling is done in order to achieve such competence in the long term and to understand the process in the short term. Defining physics for the modeling tool, including the methods of presenting them, addressing the variability and repeatability of some steps through variables and coding commands are also the items briefly discussed in this chapter.

Chapter 2 discusses modeling in general and how systems of different characteristics (thermo-fluids and other mathematical sciences) are modeled.

Before the advent of electronic computation tools, these models were tackled using analytical methods developed by physicists and mathematicians who introduced techniques such as the separation of variables and Fourier transforms. As our technological reach expanded, spurred on in particular by NASA's work on the *space program*, computational needs grew as well. Before electronic computers, human "calculators" were employed by NASA in the 1950s to perform the necessary computations, such as launch trajectories. These were done by a dedicated group of African American women, with Katherine Johnson being the most well-known among them, as depicted in the 2016 motion picture *Hidden Figures*. As the earliest electronic computers were introduced, these women also made significant contributions to their successful implementation in service of the space program. These first electronic computers themselves owed their existence in large part to the work of Alan Turing—recall the 2014 motion picture *The Imitation Game*. From the start of World War II, he developed electromechanical devices to help decode Nazi communications and, after the war, he worked on the theory and design of electronic computing devices [4,5]. Additional topics that this chapter covers include a discussion on validation and verification concepts, an overview of different thermal analysis types, and mathematical relations used to model such problems.

Chapter 3 introduces the thermo-fluid sciences and the knowledge areas that form their foundations. Fundamentals of heat transfer modeling, such as modes of heat transfer (conduction, convection, and radiation), energy balance equations, and material thermal properties are discussed.

Chapter 4 provides background on the finite element method of analysis. Material properties form the foundation on which these analyses are built. One needs to have a geometry to model, and that means choosing the appropriate number of dimensions to use and the method for geometry creation. Next, the choice of the analysis type is made, depending on whether one is interested in the variation of the model over time or in how the model behaves after reaching equilibrium. Boundary and initial conditions must be defined correctly, an appropriate mesh must be defined, the model is to be solved, and the results are to be presented.

Chapter 5 starts by providing an overview of the COMSOL Multiphysics model creation process. Next, options for geometry creation are examined in some detail, covering internal geometry creation, geometry import, and using the internal part library. Various approaches to carry out sensitivity analyses in COMSOL Multiphysics are described. These allow the user to quickly obtain a set of solutions which can be readily analyzed and compared, providing insight into the model's behavior. Finally, a more detailed review of the model setup, solution, and results processing is presented, covering such topics as the use of parameters and functions, as well as working with solution data sets, evaluation groups, plots, and reports.

Chapters 6 to 13 present a sequence of eight case studies. Model files used in these are available on the companion files. The companion files are located on the disc in the back of this book or for downloading by writing to the publisher (info@merclearning.com).

Chapter 6 is an introductory case study of hot water inside a cup. This is the heat transfer phenomenon that many of us experience several times every day. In this case study, thermal models are presented with an increasing level of complexity, starting from the analytical lumped-capacity method, followed by a 2D model, and concluding with the most complex conjugate heat transfer one, where the effects of conduction, convection, and surface radiation are modeled using Multiphysics nodes. To validate the model, a thermal imaging experiment is conducted that reproduces the modeled conditions. Test fundamentals and validation methods are discussed.

Chapter 7 models heat transfer in an insulated basement wall. Thus, the model consists of multiple layers, made of materials with different thermo-physical properties, and also layers that are arranged in different fashions with respect to one another. The variation in the thickness and height of the wall components affects the temperature distribution within the wall thickness. The multilayer wall is also simulated as an equivalent single-layer wall.

Chapter 8 models the heating of water inside a kettle. An electric kettle is represented by a transient model with a constant heat flux heat source. The model combines conduction with convection heat transfer and radiation. Water heating by a constant-temperature heat source, such as that provided by a tea candle, is recommended as a reader exercise.

Chapter 9 presents the model of a heated seat, such as those used in some cars. The model uses an electric source of heating that can be applied both by defining the resistance and the power. Although there are more specialized optional COMSOL Multiphysics modules, such as *AC/DC*, that are specifically made for modeling electric resistance heating, this case study demonstrates that the *Heat Transfer* module by itself is also capable of addressing problems of this nature.

Chapter 10 models non-isothermal gas flow inside a face mask. In addition to an overview of face mask applications, the study familiarizes the reader with the use of functions, both for geometry definition and analysis. Another aspect of modeling showcased here is use of virtual operations on the imported geometry. The influence of inlet and outlet conditions (temperature and flow) is also investigated.

Chapter 11 looks at the case of molten rock (lava) flowing inside a solidified rock channel. This example highlights handling of the phase change within a model. Results show the extent of the molten zone within the modeled domain.

Chapter 12 models a fin in the shape of rotini pasta. This shape, with triple helical surfaces, provides a large surface area for heat dissipation. A comparison is made to a simple cylindrical fin to demonstrate the effect of the large surface area of the rotini-shaped fin.

Chapter 13 presents the case study for flow inside a pipe. A pipe is a widely used engineering structure employed in the transport of a surprising range of materials. Another currently relevant application is in the harvesting of solar energy. Cases of pipe flow exposed to constant heat flux at the wall and constant wall temperature are presented as exercises for the reader. Non-isothermal flow within gas pipes and converging-diverging nozzles are also suggested as additional examples.

Chapter 14 talks about *good practices*—concepts of recommended methods versus *preferred* ones are clarified. It is emphasized that there is usually more than one way to create mathematical models. The purpose is therefore to select the method that is both efficient and compatible with the available FEM tool. Suggestions are provided for possible solutions to explore when difficulties are encountered.

Chapter 15 talks about the Lean Six Sigma application to the field. It is pointed out that all levels of the product lifecycle, including software-human interactions, should be considered when process improvement decisions are made. The concept of entitlement is presented as well as what it means to be *entitled* to something but not fully realizing it. The chapter talks about sources of waste and approaches to take in order to reduce waste.

Chapter 16 concludes this work. It reminds the reader that while there is a lot to be learned by studying, one must learn by doing as well. The chapter provides examples of responsible designs in the form of LEED projects.

ACKNOWLEDGMENTS

My family, teachers, and publisher—I am infinitely grateful to them all for their generous support and the positive influence on my life that they have had.

To my extraordinary classmate, the unknown warrior, wearing an oxygen mask, setting a firm example for divine sacrifice and honor, who defended and kept me and others safe from harm, and reciprocated the stare of death with firmness and generosity—the one whose memory summons awe-inspiring tears.

To the scientists and mathematicians who chose to be the outliers of their times; who worked ethically and diligently; who failed but persevered; and who lived happily forever and ever.

CHAPTER 1

INTRODUCTION

The term *heat* comes from Germanic roots, equivalent to contemporary Dutch *hitte* or German *heize*. In French, it is *chaleur*, which comes from the Latin *calor*, from which *calorie*, the term for a unit of energy or heat, was derived. The term *heat*, as used in English, refers to at least three different things: (1) temperature of something hot, (2) highly intense feelings, and (3) in a competition, a round of play before the finals [6].

Thus, in the first sense, we speak of the heat of the Sun and the heat of fire; the heat is conducted, convected, or radiated; additionally, it may be generated, stored, or released. It can be the quantity of energy required for a certain process to occur, or it is released as a result of a process: there is the heat of combustion or the latent heat of fusion. Sometimes you need to turn up the heat on a stove, perhaps as you are cooking that spicy recipe with chili pepper adding some heat to the food's taste. And while on the subject of cooking, as the saying goes, if you cannot take the heat in the chef's kitchen, you should leave. The amusement here comes from simultaneous reference to the first and second meanings of heat: the *literal* heat (high temperature) and the *figurative* heat (the highly intense psychological pressure).

In university studies, subjects such as *heat transfer* and *heat flow* are learned. Yet until the invention of the *thermoscope* by Galileo Galilei at the end of the sixteenth century, there was no numerical measure of the degree of heat. Greek philosophers, no matter how erudite they were, could not identify the temperature of water in a teacup. As far as heat itself, until the discoveries of the nineteenth century, scientists thought that it was a physical substance; therefore, they associated it with characteristics of a weightless liquid—also known as the *caloric fluid* or *frigorific particles* (particles of cold). This term (*frigorific*) is attributed to Robert Boyle, a seventeenth-century British natural philosopher, who hypothesized that *particles of cold* are transferred between objects [7].

Today, we know that heat is the measure of kinetic energy stored in the random motion of atomic particles in matter; temperature describes the intensity of this motion. Historically, extensive work has been conducted on the equivalency of heat, energy, and work. Heating processes such as quicker conduction heat transfer by aluminum compared to ceramic or plastic or convection heat transfer when boiling water are known facts. Nowadays, even young children know about *temperature*—they may be *running a temperature* when they are sick, where a thermometer is employed to measure their body temperature. This knowledge provides the ability to describe physical systems mathematically in order to model reality. This modeling is either done *analytically* or *numerically*. The analytical models include mathematical relations that express the physical relations between independent variables identifying the system behavior. Numerical models are the same as analytical models in terms of system behavioral representations, except that they define numerical algorithms that are applied to the analytical models. For example, they are discretized for a domain filled with elements.

Thermodynamics, fluid mechanics, and heat transfer are known collectively as *thermo-fluid sciences*. They find applications just about all of nature's phenomena as well as in most of humanity's technological fields. In nature, from the Sun's heating of the Earth's surface, to the atmospheric phenomena, to the movement of oceanic currents—all are connected to these sciences. In human technological endeavors, from the internal combustion engine of a car to the turbofan engine of an airliner, from the floating of a ship on an ocean to the buoyancy forces that keep the airplane in the air, from the frying of your morning eggs to the heating of your house—all are connected to thermo-fluid sciences. The rest of this chapter explores the connections between these fields and the phenomena we are all familiar with.

1.1 Fire

Controlled use of fire is one of the most fundamental and deeply rooted of human abilities. In fact, it predates the Homo sapiens (the modern humans), and in a sense it defines us. Earliest evidence found for controlled use of fire goes back 1.4 million years, to what is known as the *Early Stone Age* (or *Lower Paleolithic*), and was in the form of burned clay clasts found at sites located in Kenya. This evidence attributes the first controlled use of fire to the earlier human species (Homo erectus). More definite evidence shows the ability to create fire around 750,000 years ago, with sites on Jordan River and Pacific Islands [8,9,10]. Before learning to control it, in their daily lives, early humans encountered wildfires caused by lightning and by volcano eruptions. These natural fires taught them that some materials burn better than others. They learned to make fire themselves using friction, for example, by rubbing hard and soft woods against one another or by a spark from flint stones. They learned to transport this fire by keeping it burning for an extended period of time in a controlled fashion.

The ability to control fire made a major contribution to the improvement of human life and technological development. As it still does today when we visit the wilderness, the fire kept us warm, warded off wild animals, and cooked our food. Humans quickly learned that to process food, they needed to expose the food ingredients to a certain heat intensity for a specific period; otherwise, their food would have been either burned or undercooked. The capability to cook food led to the discovery of food ingredients that could be processed in a way that they could be more easily received and digested by the body. Our bodies gradually adopted to these new food types, with varieties that expanded with time, thanks to the capabilities that cooking with fire introduced.

This enhanced human capability led to further development of human faculties that included searching for new ingredients, making tools to acquire them (e.g., hunt), and new ways of processing the food. The hunted animals and gathered plants that were food sources started to be used for other applications as well, such as their fur for covering the body, bones to create shelters, and internal organs (e.g., stomach and bladder skin) for storing items. When humans learned to hunt the mightiest of creatures (such as whales), they discovered that they could employ the fat layer under the creatures' skin to start and feed their fire more reliably. They learned not only to decorate themselves and their environments with the bones and teeth of mighty creatures but also to draw using them, leading to the growth of art and culture. However, just like with all other human powers, fire has also found less harmonious applications, as a tool of war and destruction. Today, the study of burning processes is known as the *science of combustion* and is one of the thermo-fluid sciences.

1.2 Concept of Heat through the Ages

To ancient people, the concept of heat was connected with that of fire. They believed that all matter was made up of the four elements—air, fire, water, and earth. This concept of four elements existed in the ancient cultures of Greece, Babylonia, Persia, India, and Japan [11]. A modern, scientific understanding of heat only started to be developed from the seventeenth century. Francis Bacon, a British scientist, philosopher, and statesman, first distinguished between heat and temperature in 1620. Due to the close connection between heat and the process of combustion, they were mistaken for each other. This was also known as the *caloric theory of heat*, first presented in the middle of the seventeenth century; it proposed that heat was an invisible, weightless fluid, a substance that could flow from areas of higher values to lower ones within liquids or solids, by replacing the molecules or penetrating through the pores in the case of solids. Since the conservation of matter was an accepted hypothesis at the time, conservation of heat was also inferred.

Johann Joachim Becher and Georg Ernst Stahl introduced the *phlogiston theory of combustion* at this time, where temperature was thought to be the substance of heat. This theory suggested that a fire-like element (named *terra pinguis* by Becher, being the combustible one of the three forms of the *Earth* elements) is an ingredient of combustible bodies that is released when any substance burns. Georg Ernst Stahl, a German physician and chemist, renamed Becher's *terra pinguis* to *phlogiston* and further developed this theory, which was still accepted until the late eighteenth century. To find evidence for his theory, he worked with metals in order to separate this element from the rest of the ingredients. He suggested that metal composition (calx, ash, and phlogiston) reduces to the former two (calx, ash), since phlogiston leaves the composition. Antoine-Laurent Lavoisier, a French chemist in 1772, later proposed the *theory of oxidation*. Due to the large influence Stahl's *theory of phlogiston* had at the time, it is recognized as serving as the transitional function between alchemy and chemistry [12,13,14,15,16].

In 1761, Joseph Black, a Scottish physician and chemist, quantitatively distinguished between heat and temperature. He applied conservation of mass—earlier suggested by Newton and adopted by Antoine-Laurent Lavoisier, for all chemical reactions—and developed calorimetry and the *theory of latent heat*. His theory for *specific heat* (heat capacity for unit mass) is also well-known. He applied heat to ice when it was ready to melt (melting point) and noticed that the temperature during the melting process remained the same while water content increased. He repeated the same experiment for boiling water and noticed that the temperature also did not increase; however, steam content increased. He concluded that the applied heat was added to the solid and liquid particles and became latent—it existed but did not manifest itself. Some scientists consider these experiments as the beginning of thermodynamics as an independent science. Based on the similar experiments, Black concluded that materials had different specific heats, since they responded differently to the added heat.

Around 1775, James Watt, a Scottish inventor and mechanical engineer and a student of Black, employed the latent heat concept in his work on *power generation from steam engines* [17,18,19]. Since the water was widely available and its latent heat was considerably higher than other common liquids, it became the generally used working fluid in steam engines. Watt was not the first to build a steam engine. In 1712, British inventor Thomas Newcomen built the *atmospheric engine*, which can also be considered a steam engine, to lift water in a tin mine using the *thermic siphon* principle. A thermic siphon, also known as the *thermosiphon*, passively exchanges heat using natural convection, resulting in circulating fluids without the use of a mechanical pump.

The theory that heat was connected with motion and not some substance contained in matter was presented in 1798 by Sir Benjamin Thompson, an American-born British physicist and innovator. While working in Germany on the manufacturing of cannons, he noticed that as a cannon's bores were drilled in cold metal, the temperature of the metal in contact with the drill increased, to the point that the metal started to glow red. However, Thompson made no attempt to further quantify the heat generated or to measure the mechanical equivalent of heat. In 1824, Thompson's theory was further developed by French physicist Sadi Carnot, who proposed the idea of the equivalency of heat and mechanical work [20,21,22]. Carnot measured the equivalent work done by a gas expanded under isothermal conditions. In 1851, William Thompson, a Scottish mathematician more commonly known as *Lord Kelvin*, reemphasized this equivalency, stating that heat was not a substance; he presented the *dynamical theory of heat*, which grew into the *science of thermodynamics*, the study of the connection between heat and work. Terms such as *specific heat*, *calorimetry*, and *combustion*, introduced in the nineteenth century, are rooted in this theory.

Robert Brown, a Scottish botanist, distinguished himself through his innovative use of the microscope to observe biological phenomena. In 1827, during his microscopic observations of water-suspended pollen from the plant Clarkia pulchella, he noticed that particles expelled from the pollen grains, now known as the *amyloplasts* (starch organelles) and *spherosomes* (lipid organelles), were undergoing continuous "jittery" motion. He repeated the same tests on inorganic matter and observed similar motion, concluding that this motion was not life related. Notably, Brown was not the first one to report this phenomenon, as in 1785, Jan Ingenhousz, a Dutch biologist, reported on the similar irregular motion of coal dust floating over the surface of alcohol. Nonetheless, the phenomenon became known as the *Brownian motion* [23,24].

In 1905, nearly eighty years after Brown's observations, Albert Einstein published a paper which used statistical physics principles to present the hypothesis that the random motions of these particles were caused by the movement of the liquid's molecules. This paper was one of the four ground-breaking papers published by Einstein that year, though perhaps it was not as famous as the ones on special relativity or mass-energy equivalence. The significance of this paper was that it showed experimental evidence for the existence of atoms, which was still a subject of scientific debate at that point. Einstein's paper presented the *molecular kinetic theory of heat*, showing how the movement of molecules was directly related to the temperature, thus illustrating that the three states of matter all relate to molecular freedom to move.

Leonhard Euler, a Swiss mathematician, physicist, astronomer, and engineer, is well-known for his work in fluid dynamics and mechanics, as well as for his development of modern mathematical vocabulary and symbolization. He concluded that bodies do not possess the same capability to contain heat, receive it, or transmit it across their surfaces or through the interior of their masses. He published his continuity and momentum equations in 1757 in their general form. The energy balance equation was developed a century later. His work applied to incompressible fluids and represented the first steps toward the introduction of the Partial Differential Equations (PDE). PDEs are differential equations that represent functions of multiple variables and their partial derivatives [25].

In 1804, Jean Baptiste Biot, a French physicist, astronomer, and mathematician, employed Newton's law of cooling to introduce a distinction between the conduction of heat within the body and into the surrounding atmosphere. In 1807, Joseph Fourier, a French mathematician and physician, published his initial work on *propagation of heat in solids*. Among his influential contributions are Fourier series, transcendental functions, Fourier integral, and operator calculus methods. His masterpiece on *Analytical Theory of Heat* was published in 1822 and translated into English in 1878. His derivation of the transient heat transfer equation took a macroscopic approach to that of the Euler's derivation of continuity of mass and motion for a frictionless fluid in 1761. Fourier set up his convective boundary condition using *Biot number*, which is a dimensionless number representing the ratio of the convective to conductive heat transfer forces. Fourier's law of heat conduction is similar to Newton's law of viscosity, with temperature difference substituted for velocity difference. Later on, Fourier also studied radiation heat transfer as well as dimensional analysis relevant to parametric studies [26,27].

Fourier's energy equation in convective heat transfer differs from that of the Navier-Stokes'. In Fourier's work, heat flux is proportional to the temperature gradient in solids, while Navier-Stokes relationships represented a more general form of heating by advection due to the transportation of the bulk of liquid. These equations were introduced in 1822 by Claude-Louis Navier—a French engineer and physicist who specialized in mechanics—and further developed in the 1840s by Sir George Gabriel Stokes, the first Baronet—a British-Irish physicist and mathematician. Stokes also developed equations for drag force over spherical objects, where *Reynolds number* (*Re*) is very small.

Ohm's law, presented in 1827 by Georg Simon Ohm, a German physicist and mathematician, and Fick's law of diffusion in 1855, presented by Adolf Fick, a German physician and physiologist, later used Fourier's law of heat conduction for their analogies [28,29,30,31]. Fick presented a mathematical model for a general diffusion equation that was then adopted as a special case in the form of a heat equation. A Laplace operator (a differential operator obtained from the gradient divergence of a given function in Euclidean space) was used to simplify the heat equation and make a generalization over time and space. The adiabatic conditions were defined where no heat exchange happened between the system and its surroundings. The *Laplace operator* is named after the French mathematician Pierre-Simon, marquis de Laplace, who used this operator in 1825 to study celestial mechanics [32].

1.3 Temperature Measurements through the Ages

Temperature is the most fundamental property in thermo-fluid sciences; therefore, a brief overview of how and where this concept originated is beneficial to understanding the many related physical phenomena. The first attempts to visualize *temperature* have been attributed to Heron of Alexandria from the Roman province of Egypt (about 10 AD to 70 AD), who observed air expansion with heating and contraction with cooling within a tube partially filled with air, one end of which was submerged inside a tub of water and the other sealed.

The term *temperature*—the atomistic conception of heat transfer—was still unknown in the 1600s at the time of Galileo Galilei, the famous Italian polymath. In 1593, he used an idea similar to Heron's to develop a thermoscope, which worked based on the changes in sensible heat. Sensible heat is the heat that can be *sensed* and which causes temperature changes without changes of some thermo-physical properties such as pressure or volume. The thermoscope was made from a large glass bulb-shaped container from the bottom of which a thin tube extended and was submerged in a container of water. Increasing the air temperature inside the bulb increased its pressure, caused expansion, and so lowered the water level in the tube. Cooling the air led to the opposite result. This functionality made it an ancestor to today's thermometers based on the expansion of a liquid. Note that thermoscopes had no scales and only provided a relative indication of one environment being warmer or colder than the other [33].

Jean Leurechon, a French mathematician in 1624, first used the term *thermometer* for a device that was actually a barometer. Galilei's student, Joseph Solomon Delmedigo, an Italian physician, mathematician, and music theorist, allegedly was the originator of the idea of a sealed liquid-in-glass thermometer. However, it was Ferdinando II de' Medici in 1654 in Italy who first produced the instrument which was independent of air pressure and only depended upon the expansion of the liquid. A number of thermometers were then tested using different liquids and tubes. The first reliable one that was suggested based on the melting and boiling points of water was produced in 1694 by Carlo Renaldini, a French philosopher and experimenter. The one proposed by Sir Isaac Newton in 1642 was based on the twelve-degree scale between the melting point of ice and body temperature.

It was only in 1714 that Daniel Gabriel Fahrenheit, a Dutch-German-Polish scientist, introduced the concept of the contemporary thermometer with the correct scale, which was based on the mercury's high thermal expansion coefficient. Fahrenheit noticed that the temperature of three points always remains the same—water-ice mixture (0.01 °C), body temperature (37 °C), and brine mixture (i.e., ammonium chloride, liquid water, and ice mixture, 0 °C). In 1742, Anders Celsius, a Swedish scientist, suggested a 100-degree scale between the freezing and boiling points of water. In 1848, Lord Kelvin proposed the idea of absolute zero, a negative reciprocal of the gas expansion coefficient (0.00366) at the water-freezing temperature per degree Celsius. Therefore, one Kelvin was defined as the fraction (1/273.16) of the triple point of water (0.01 °C), which equals one degree Celsius [34,35,36, 37,38,39,40,41].

One of the most important characteristics of a thermometer is its response time. Reportedly, early devices needed twenty minutes to identify accurate temperature. Sir Thomas Clifford Allbutt, a British physician in 1866, was able to reduce this response time to five minutes, and therefore the first generation of clinical thermometers was developed. In 1999, after over a century of technological progress, Francesco Pompei, an American innovator and entrepreneur, developed a high precision two-second-temporal artery thermometer [42,43].

1.4 Temperature and Matter

Temperature change can affect the structure of matter and it can change matter into another form or cause it to disintegrate, forming new phases, shapes, and applications that would not be possible at room temperature. Extreme conditions, either cold or hot, can also affect the performance of any system. On the other hand, in living beings, temperature stability is paramount. The following sections provide examples of the effects of extreme thermal conditions and of the importance of temperature. The story of temperature and matter is told, ranging from the human body to the materials used in space and onward to the stars.

1.4.1 Is It Cold Enough for You?

The temperature story starts from the logical point—the lowest temperature possible. The process of lowering temperature (just like raising temperature) requires energy. If matter is gradually cooled and the diagram of absolute temperature versus molecular motion (average velocity) is plotted, temperature being plotted on the vertical axis, a linear function with positive slope (showing an increase of temperature with velocity) is obtained. This crosses the zero-velocity axis at absolute zero. The lower the temperature is, the lower the velocity is; however, reaching the value of zero is reportedly unachievable. This theoretically unachievable temperature is known as the *absolute zero*, equal to −273.15 °C (0 K) [44].

A recently published article reported that reaching absolute zero has been proven as impossible. Physicists, including Albert Einstein, have been working on this for at least a century. The reason is associated with the entropy of the matter that cannot be zero. In other words, nothing exists that is completely stationary; this is also supported by the third law of thermodynamics, which states that heat moves from the place of higher temperature to that of the lower one [45].

In 2014, scientists at an Italian institute, participating in an international collaboration named *Cryogenic Underground Observatory for Rare Events* (CUORE), have been able to record a temperature as low as −273.144 °C (0.006 K) [46]. One method to achieve ultracold temperatures is to use liquid helium and attempt to slow the atoms by directing laser light onto the molecules in motion. The energy of the laser beam deters motion through the collision of the laser photons with the molecules. Slowing down the molecules means that they are getting colder. If an array of laser lights in the correct composition is applied to the molecules, they can reach very low temperatures, coming close to absolute zero in their quantum state.

Cooling certain materials (e.g., Yttrium Barium Copper Oxide—YBCO) too far below the freezing point, in this case to the temperature of liquid nitrogen, −196 °C (77 K), can change their atomic structure, spontaneously producing a magnetic field and therefore manifesting superconducting properties. When such cold matter is placed close to a magnet, it can start levitating, suspended over the magnet. It conducts electricity by pairing the electrons, which can easily navigate through an open field. This open field is due to the nearly immobile atoms causing the attracted electron pairs to move with almost no resistance through the crystal passages, therefore creating electric and magnetic fields. Maglev trains, contactless melting, and magnetic bearings are among the magnetic levitation applications. Magnetic Resonance Imaging (MRI), which is a medical imaging method to create radiological images of body parts as well as bodily physiological processes, needs strong and uniform magnetic fields. One way to create these is by use of superconducting magnets that require temperatures as low as liquid helium, −270 °C (3 K) [47,48].

The University of Basel, Switzerland, presented a version of the electron-hole-based quantum computer, which uses low-temperature (a few milli-Kelvin) semiconductor electron holes for computing purposes. The low temperatures help address the decoherence issue (instead of using the alternative approach of manipulating electron spins). Decoherence is due to the interaction of the system with its environment, and therefore isolating it prevents such intrusion and resultant errors. This computer is also known as the *positronic quantum computer* [49,50].

When water molecules freeze, though they still experience vibrational motion, their average positions become fixed in space, forming a regular hexagonal lattice. Molecules occupy more space in this case, and ice becomes less dense than water. This causes the ice to float on water, which is a critical condition for the survival of many species living in cold regions. In these areas, water is in a frozen state for most of the year, and the majority of creatures, such as bears and seals, do not travel long distances to survive. These creatures as well as those in the ocean are then capable to live in the liquid water under the ice that also acts as a blanket, moderating the water temperature.

For humans, however, the ice sometimes gets in the way, and so we use icebreaker ships to navigate through the Arctic. Steel used to make icebreaker hulls undergoes specialized heating and cooling treatments to make it withstand extreme cold. The hull steel can break ice when conditions are right, which is due to the modified steel's behavior under cold temperatures, improving its strength and decreasing brittleness in low surrounding temperatures and under high loads. Some claim that the RMS *Titanic*, a passenger liner that sank in the North Atlantic in 1912 on its maiden voyage from Southampton to New York City, was made of hull steel that was incapable of tolerating extreme North Atlantic cold. The steel became too brittle and, therefore, hitting the iceberg caused sufficiently high stress concentrations at rivet holes to result in crack formation and catastrophic hull rupture [51].

1.4.2 At the Movies

Scientists, when taking a well-deserved break from their research, enjoy munching on popcorn as they watch a movie, just like most people do. But what makes popcorn pop? Corn kernels, from which popcorn is made, contain water, which makes up 14 to 20 percent of their weight. As the kernels are heated, the water molecules move faster and faster inside, forming water vapor, thus making each kernel into a tiny pressure cooker. At the same time, the heating gelatinizes the hard starch within the kernel. Eventually, the kernel's hull ruptures and, as the steam escapes from the tiny container, the pressure drops rapidly and the internal contents, such as starch and proteins, expand, making the kernel up to fifty times larger than its original size. This puffy popped kernel then cools down, convecting the heat away to its surroundings via its newly expanded surface area.

Note that the outer skin of corn is impenetrable to water; therefore, water vapor cannot escape easily as the corn is heated, which is what causes the popping. However, the kernel tip, where it is attached to the cob, is partially permeable. Thus, the steam molecules may escape if the rate of heating, which causes the water and oil heat to build up pressure, is the same as the rate at which the solid starch gelatinizes. Therefore, the heating process should be fast; otherwise, the kernel will not pop. The steam partial pressure is about 135 psi (930 kPa), which happens at about 180 °C (453 K).

Popcorn degree of expansion affects the profitability of its sales and so the corn growers try to develop products that expand more. When you buy popcorn at the movie theater, it is sold to you by volume, but the theater buys the corn by weight. Therefore, the puffier it is, the faster the bag fills up, and the more profits are made. Corn moisture content also needs to be carefully controlled. The high moisture content of the freshly harvested corn causes kernels to expand poorly and the popped result, if any, to be chewy. Drying the kernels too much, on the other hand, leads to a large fraction of them not popping at all. So, neither extremes are desirable [52].

1.4.3 Temperature in Nature

Just like fire (in the form of the Sun's energy), water is also essential to life on the Earth. The covalent bonds between the atom of oxygen and the pair of hydrogen atoms are so strong that the Sun's energy cannot decompose it, which is a good thing for all of the Earth's living beings. Water is an excellent energy (heat) storage medium. In its liquid form, its heat capacity is 4,180 J/kgK at 20 °C at constant pressure. For comparison, the heat capacity of mercury is about 139 J/kgK, while for sunflower oil it is 1,910 J/kgK at 20 °C. Thus, the enormous mass of water in our planet's oceans retains enough energy to act as a giant heat sink for the planet [53].

Converting liquid water to vapor can store an additional substantial quantity in the form of latent heat, which would be released upon condensation. The vapor in the atmosphere also absorbs light energy from the Sun, leading to the greenhouse effect. Deep down under the ocean, geysers (thermal vents) on the ocean floor eject steam to the surface and therefore moderate the ocean's temperature. These two mechanisms, high above and at the bottom of the ocean, cause temperature moderation and stabilize the climate.

In the absence of the ocean's heat sink and the greenhouse effect, the Earth would be as uninhabitable as Mars, which has almost no atmosphere. Of course, too much atmosphere can be as bad as not enough. The atmosphere of Venus weighs ninety-three times that of the Earth and is composed mostly of carbon dioxide, with thick clouds of sulfuric acid vapor. The resulting greenhouse effect causes its surface temperatures to be around 400 °C, making the environment highly hostile to life. So, having just the right temperature is what makes life on the Earth possible. And even the slightest increase of the global average temperature can lead to dramatic consequences, as the changes due to global warming, much in the news recently, illustrate [54].

Having evolved over billions of years in the Earth's cradle, life on our planet has adapted to seasonal temperature variations (away from the tropical zone), daily (diurnal) temperature variations, and both cold and hot climate extremes. Regulating body temperature, known as the *thermoregulation*, helps animals to find food, mate, avoid predators, and resist disease. Based on this characteristic, they are divided into two main groups—endotherms and ectotherms. *Endotherms* are warm-blooded animals; they generate most of the required body heat from food by metabolic processes. *Ectotherms* are cold-blooded animals; they use external heat sources to control their body temperature. Thinking of animals' body temperature in terms of a heat transfer model, endotherms are equivalent to a stationary system, while ectotherms are equivalent to a transient system. Regardless of type, their bodies include a temperature-regulating control feedback mechanism in order to reach homeostasis (i.e., an equilibrium state maintained by the body). This control feedback loop consists of stimulus, receptor, modulator, and effector [55,56].

When in extreme cold climates, birds and mammals adapt to conditions by various means: growing larger; distorting skin surface by means of small muscles (called the *arrector pili* in mammals) under their skin, making them get *goose bumps* (standing hair) and therefore reducing air movement across the skin; gaining fat in order to be able to store energy (polar bears); developing short bodies (e.g., Yakutian horse); and having countercurrent blood flow, where the warm arterial blood warms the cool venous blood in a countercurrent heat exchange process (e.g., penguin and arctic wolf). In conditions of extreme heat, they show physiological changes that are essentially behavioral adaptations, such as living in burrows (e.g., lizards), evaporating liquids (e.g., sweat) from their skin or sweat glands, storing fat in a strategic location (e.g., camel hump), and developing extremely vascularized parts (e.g., legs in Arabian horses and ears in African elephants). Think of horse legs as extended surfaces with embedded cooling flow channels and elephant ears as extended surfaces of another shape—radial fins, effectively removing excess heat from their large surface areas.

Endotherms, the warm-blooded animals, respond to cold conditions by increasing their metabolic rate, consuming fats and sugars. In a hot environment, they use evaporation of water from their skin surfaces if they have sweat glands. Animals with fur covering their body use panting (fast breathing through their open mouths) in order to reduce their body temperature, since their fur acts as an insulator. The rapid airflow increases evaporation from wet surfaces such as lungs and tongues. Some animals, such as cats, dogs, and pigs, have sweat glands only in foot pads and snouts. This offers little additional cooling—the thin layer of moisture on their foot pads is mainly useful for enhancing grip during locomotion.

The use of fur as an insulator is seen in animals that have adapted to extreme cold. For example, a Yakutian, unlike other horses, has evolved a long-hair coat to survive in the extreme cold climate of Siberia. Thick, insulating fur also works in the high heat of the deserts. Camels have such fur to protect them from high temperatures. A fur coat, however, is only one of many incredible adaptations that these animals have evolved to live in their extreme environment. While most endotherms can only tolerate a few degrees of body temperature variation (remember how you feel when you are running a 39 °C fever – that is only about 2.5 °C above normal), camels regularly tolerate temperature rise from 34 °C in the morning to 40 °C by the late afternoon.

The network of vessels through which blood passes to and from their brain is arranged as a counterflowing heat exchanger to cool the incoming blood. Camels sweat very little and the moisture evaporates from their skin, not their coat, taking advantage of the cooling effect. Other water conservation measures include trapping the exhaled water vapor in the thick hair of their nostrils and then reabsorbing it, having highly efficient kidneys produce urine as thick as syrup, and having feces so dry that the local tribes can use them for fires without the need of extra drying. Camels even have red blood cells that are elongated (not spherical as in other animals), which improves blood flow during dehydration and allows them to tolerate drinking large volumes of water very quickly—a 600 kg camel can consume 200 L of water in just three minutes. All of these adaptations allow camels to survive up to ten days without water [57].

To keep themselves cool, birds take advantage of gular fluttering, the quick vibration of their throat skin, which is one of the few areas on their body not covered by feathers. The layer of down feathers underneath the main feathers acts as an insulator. That explains why you should choose a down jacket for your own temperature regulation if you decide to visit the Arctic. Mammals have thicker skin than birds, with a fat layer under their skin acting as an insulator. This is also seen in marine mammals, such as whales, and the ones living in extremely cold climates, such as polar bears. Their fat layer is also known as the *blubber*. *Torpor* is a special thermal regulation mode that endotherm animals can deploy to lower their body temperature and metabolism in order to survive periods of food scarcity or harsh weather. Some animals (hummingbirds, mice, bats) enter this state nightly; others (ground squirrels, and bears) do it on a seasonal basis. Among mammals, elephants have one of the lowest body temperatures (36.5 °C) while goats are the warmest of all (39.7 °C).

A giraffe's coat pattern not only camouflages them but also helps with thermoregulation. There is a complex pattern of small blood vessels under the dark patches. These vessels connect to large ones at the patch boundaries. Think of the dark patches as thermal shields, managing heat on this large body surface. Also, the surface emissivity of the darker fur is higher, facilitating radiative heat transfer to the surrounding environment. Giraffes' brains also generate a large amount of heat, and therefore they are equipped with very sophisticated breathing systems to be able to thermally manage this generated high temperature; breathing in the air causes evaporative cooling as oxygen reaches the blood vessels. This cools down the local blood flow, which exchanges heat with the warm blood, traveling to the brain via a structure called the *karate route*, acting like a heat exchanger. Giraffes' elongated necks and legs also act as extended convective surfaces, creating large surface-to-volume ratios [58].

Ectotherms are cold-blooded animals; they use external heat sources to control their body temperature. They bask in the Sun or take shelter in the shade to respond to their body temperature changes. Ectotherms exhibit a body temperature range similar to endotherms. These animals use effective thermal management strategies to regulate their body temperature by taking advantage of three modes of heat transfer. They employ vaporization (using sweat and other fluids), convection (sending blood flow to surfaces or climbing to higher elevations such as trees), conduction (coming in contact with cold or hot surfaces such as swimming or lying on the ground or in the mud), and radiation (radiating heat away or basking in the Sun, folding skin, and exposing or concealing wing surfaces). In insects this depends on their body mass and morphology. For their smallness, some have very small internal body heat generation; however, this generated heat along with a high flight metabolism can make them overheat [59,60].

The Komodo dragon is the largest known living lizard species; they are around 3 m long and can weigh 70 kg. This cold-blooded animal absorbs heat from its environment during the day and maintains the warmth during the night by nesting inside burrows. Pogona, a genus of reptiles also known as the *bearded dragons*, change body color as temperature changes and turn black when they need to absorb heat. During extreme heat times, they go dormant. When there are extreme cold conditions, they hibernate; this is also known as the *brumation*, going on a fast for months with occasional water drinking. The lowest body temperature they can tolerate is about 16 °C during the night and 24 °C during the day. These reptiles rely on basking under a light-emitting heat source, requiring heat and UV for their bodily functions. The egg's incubation temperature even changes the gender of the baby inside the egg. Higher temperatures (above 34 °C) result in female pogonas, while the lower ones result in males [61,62].

Humans also have their ways of dealing with external temperature variations and have multiple means to control their body temperature in all conditions. For example, while exercising, the body warms up, inducing increased sweating as a measure to remove excess heat. Underarms usually show the highest exterior surface temperature within the body. This is also complemented by the blood vessels dilating. When humans encounter a cold environment, their blood vessels contract, constricting the blood flow and minimizing heat loss through their extremities. Human skin forms its own microclimate and possesses a complex thermal management plant. Humans can survive their body temperature decreasing to 21 °C (294 K) for an unknown amount of time, depending on pressure and humidity levels (hypothermia).

The maximum body temperature that humans can tolerate is about 41 to 45 °C (hyperpyrexia) [63,64]. Extreme heat (hyperthermia) can be used in medical treatments, such as destroying overgrown tissues at temperatures of about 45 °C to make tumors shrink. To increase tissue temperature, energy can be transported to it by microwaves, radio frequencies, or ultrasound. This is also occasionally referred to as the *tissue ablation*. Extreme cold conditions cause the blood flow to slow down considerably and even to form clots. This characteristic is employed in a variety of medical treatments such as surgery and treating cancer. In the former case, known as the *cryosurgery*, extreme cold (below -100 °C for two to four minutes) is used to destroy the diseased or abnormal tissues (e.g., a wart). In the latter case, known as the *cryoablation*, a thin needle is inserted through the skin into the tumor. Gas is pumped through the needle, which freezes the tissue; the tissue is then thawed, and the process is repeated several times [65,66,67].

1.4.4 A Lot of Hot Air

The idea of using heated air trapped in an enclosure to create a buoyant flying object dates back to the Three Kingdom era in China (the third century AD), were airborne lanterns where used for military communication purposes. Centuries later, in France, brothers Joseph-Michel and Jacques-Étienne Montgolfier, who ran a paper manufacturing business, had a similar idea. Their first successful public flight took place in 1783 and used an unmanned hot-air balloon that floated in the air for about ten minutes, covering 2 km at an altitude of about 5,000 feet. The balloon was made of sack cloth lined with layers of paper and covered with a fishnet for reinforcement.

People had grave concerns at the time about the possible ill effects of raising living creatures to high altitudes. French King Louis XVI even suggested using convicted criminals as test subjects. To allay these fears, later the same year the Montgolfier brothers conducted an experiment with animals placed in the balloon's basket. They even designed this experiment using a scientific approach: the animals included a sheep (a normally earth-bound animal), a duck (an animal that should do fine in the air but was included as a control for any ill effects due to the airship itself), and a rooster (also a bird but one that cannot fly on its own). Despite concerns, all the experiment participants survived, but perhaps not for too long—they may have ended up on the menu for the dinner to celebrate the experiment's success! Louis XVI, who witnessed this demonstration, then gave permission to attempt human flight.

The balloon built for this purpose was 75 ft tall and 50 ft in diameter. It was richly decorated with fleur-de-lis and suns with the king's face in them, all on a deep blue background. Étienne Montgolfier was the first to try a tethered ascent successfully to a few tens of meters. Shortly after these trials, on November 21, 1783, the first free human flight took place when Pilatre de Rozier, a physicist, and marquis d'Arlandes, an army officer, flew 3,000 ft above Paris over a 9 km distance. Reports of these flights became widely known through the Western world and led to similar endeavors by others.

Today's typical hot-air balloon uses an on-board heat source in the form of a propane burner, which was developed in 1960 by American inventor Ed Yost. The highest altitude reached by a hot-air balloon is reported to be 21,027 m (68,986 ft), achieved in 2005 by Vijaypat Singhania, an Indian textile businessman and aviator, at the age of 67 [68,69,70,71].

About a decade later, in 1972, Dominic Michaelis, an Anglo-French inventor and architect, invented a solar balloon. It took advantage of the available solar radiation to increase the balloon's lifting capacity. The air inside this balloon is heated by the solar thermal radiation, in addition to the regular propane burner. The balloon fabric is either covered by a coating that is highly absorptive to the Sun's spectral-directional radiation (given the wavelength and direction) or is made from a material that has similar high absorptivity. The color may be black or any other color (e.g., diffusive gray) with high absorption properties. It is also possible to make the balloon out of a material that reflects the thermal radiation. In this case, the thermal radiation is not absorbed by the surface and, although the emissivity of the surface may be close to 100 percent (given the wavelength and direction of the irradiance, also known as the *radiant flux*), the thermal radiation absorption is minimal. Radiation intensity is the total energy reaching the surface per unit time per unit area.

It is possible to either make the entire balloon surface of the absorptive material or have a balloon in which part of the fabric is absorbing and the rest is reflecting. With this arrangement, by rotating the balloon to the direction of the source of irradiance (the Sun), the exposed exterior heated surface warms the air inside the balloon adjacent to the interior of the heated surface and the convective flow on the interior facilitates the heat transfer. As a result, the density of the air inside the balloon decreases, and lift force is generated due to the buoyancy. On the other hand, when the balloon is rotated to expose the reflective surface to the Sun's radiation, the thermal radiation is reflected back to the environment, the gas molecules adjoining the interior surface cool down, the temperature of the interior air decreases, and the lift force is reduced.

The envelope of a hot-air solar balloon is made of a special grade of Nylon, known as the *Nomex*, which is a polymer with a special molecular structure of aromatic backbones. The balloon envelope consists of two laser-joined hemispheres. One half is made of Nomex pigmented with absorbing agents, which results in an absorptivity of about 0.8. The other half is made of a special grade of Nomex with an absorptivity of about 0.2. Due to the pigmentation, the color of the absorbing half is darker than the reflective half. Note that absorptivity is the percentage of the energy that is absorbed by the surface. It is assumed that the pilot is capable of controlling the orientation of the balloon so that either the absorptive or the reflective part of the balloon is exposed to the Sun. The minimum value for solar radiation is about 1,000 W/m^2 and the maximum value is 1,361 W/m^2, reaching the Earth's surface depending on the atmospheric conditions, day of the year, time of the day, and geographical location. The balloon operates in the temperature range of 20 to 120 °C.

1.4.5 The Heat Is On

Glass is one of the most useful materials known to humans. Typical glass, such as that used for bottles or windows, is made up of 75 percent silicon dioxide, with the remainder being oxides of sodium and calcium. Glass has an amorphous atomic structure, meaning that there are no distinct crystals making it up and its atoms are not arranged in an organized crystalline structure. This is what gives it its transparency, as the light can pass straight through without multiple refractions, and thus scattering, at the crystalline boundaries. Its amorphous structure also means that with heating it softens gradually, becoming progressively less viscous with increasing temperature. This property allows glass to be shaped by introducing air pockets into it, using the craft known as the *glassblowing*, which was first practiced around the first century BC.

Glass is formed from the raw materials by heating them to about 1,300 °C, at which point the glow is nearly white. The furnace is cooled down to about 1,100 °C, with the glass now glowing orange; it is then collected to be shaped by glassblowing. After the hot molten glass leaves the furnace, it gradually cools down, starting from the exterior surface. The air pocket blown by a pipe inserted into the glass blob also creates a thin cooler skin on the interior. The cooler glass is more viscous and allows the glass to be worked into the desired shape by the glass maker. The glass is shaped by controlling the rate of heating and cooling. That is why the glass maker blows at different stages when making glass, rotating and moving it skillfully, making its surfaces cool in a controlled manner. In addition to the furnace where the glass is made, the process uses two more furnaces—one for reheating the glass while it is being worked and another for annealing, at around 400 °C, where the completed piece is left to gradually cool down over a number of hours in order to prevent cracking from thermal stresses [72].

Metal work, also known as the *blacksmithing*, has some similarity to glassblowing, in the sense that the heated material behaves as a highly viscous fluid and can be shaped as needed; however, the shaping techniques differ between these two crafts. Iron becomes workable for blacksmithing around 820 °C (1,093 K), where it has a taffy-like consistency. The term *black* refers to the black layer of fire stain (fire scale) that is formed on the surface of the heated metal. Pieces that are usually made of wrought iron or steel are heated to the softening point; therefore, they become workable using an anvil, a hammer, and a chisel. Heating of metal is done in a forge using fuels such as natural gas, charcoal, or coke. As the metal is heated, its color changes from red to orange, to yellow, and to white.

The best workability temperature is where the metal becomes yellowish-orange; for this reason, the artisans work in an environment where they can easily detect the color, keeping the workshop lighting subdued. The process involves different activities: (1) forging—including drawing, bending, upsetting, and punching, where the softened metal is shaped to the correct form by elongation, winding, thickening, and creating decorative patterns, respectively; (2) welding—where similar or dissimilar metals are joined; in this case, the blacksmith and a sticker work together to ensure the parts are joined at the right temperature; and (3) finishing—in which the excess parts such as bursts and sharp edges are removed by filing and brushing [73].

1.4.6 Up in the Air

Aerodynamic heating happens when a solid object passes through the air (or another fluid) at very high speed. The total energy of the solid consists of kinetic and potential energies. The kinetic energy is transformed into heat due to the fluid friction with the skin of the solid. This friction energy is a function of the velocity of the object squared and fluid density and viscosity. As the object passes through the fluid, a layer of the flow over the surface, called the *boundary layer*, is created due to the viscosity of the fluid. This can be visualized by imagining a stack of papers sitting on a table surface. If you push on the stack so that the side of the paper stack forms an inclined surface, this will represent layers of fluid shifting with respect to one another. The magnitude of shift from *page* to *page* represents shear. The fluid's resistance to this shearing motion (a frictional force) is the shear stress. The shear becomes progressively smaller as one gets further away from the solid surface.

The shear stress is proportional to the gradient of the velocity in the direction normal to the surface (wall) and to flow viscosity. The energy consumed by this viscous friction (drag) is viscous dissipation, which can become significant for high flow velocities. This is the heat that conducts to the object's surface due to the reduced flow velocity inside the boundary layer. Potential flow is an area outside the boundary later, where the flow conditions are close to those of the environment and the flow velocity is 99 percent of the free-stream flow velocity. The higher the flow velocity, the larger the velocity gradient normal to the wall surface, and the higher the boundary flow slope and the shear stress; as a consequence, the viscous energy dissipation is higher too [74,75].

Aerodynamic heating becomes a significant factor for supersonic aircraft and meteoroids or space vehicles passing through the Earth's atmosphere. It is this heating that causes the meteoroids to burn up and produce streaks of light in the night sky. It is for this reason that the skin of the Lockheed SR-71 Blackbird reconnaissance aircraft, capable of flight at over Mach 3, had to be made from titanium, so it would not soften due to aerodynamic heating. Space vehicles reentering the atmosphere experience speeds much greater than that of the SR-71, reaching up to Mach 20. Unless special measures are taken to thermally manage the heat generated, they would meet the same fate as the meteoroids. One of these techniques is to design the vehicle so that the generated thermal shock waves are kept away from the main body, producing a standoff bow. The excess heat is then released into the surrounding environment. The vehicle reentering the atmosphere typically has a blunt bottom and semispherical or spherical top, or an optional conical bottom. Spherical models have been historically employed due to their relative ease of mathematical modeling. With the advancement of numerical tools and enhanced computer capabilities, more complex design geometries became possible. The angle of attack is also an important factor, causing more or less flow to pass by the object and hence affecting the temperature at the boundary layer.

Vehicles traveling through the air at supersonic speeds of Mach greater than two require Thermal Protection System (TPS) as part of their design. If such a vehicle is not designed to meet the thermal requirements, the parts exposed to extreme heat melt (or are ionized), the heat is conducted to the interior parts such as capsules, and structural integrity is jeopardized. Material choice is critical in these designs. To keep the heat away from the sensitive parts (in direct contact with the high-velocity flow stream), they are made of or coated with special thermally resistive materials. For very high Mach velocities, such as reentry vehicles, they can also employ ablative materials, meaning that they are vaporized in a direct sublimation process. During this process, a large amount of energy (latent heat of sublimation) is consumed, therefore reducing the heat transferred to the vehicle.

The protective materials should have a relatively low thermal expansion coefficient and high strength. Glass-reinforced aluminum is one common choice—it was employed in the construction of the Mercury space capsule. This material can tolerate temperatures as high as 1,100 °C (1,373 K), above which temperature it evaporates. It is believed that Columbia space shuttle thermal shield got damaged and that lead to its destruction as it entered the Earth's atmosphere. Due to the damage of some of the tiles covering the capsule surface, the heat was conducted to different parts at different rates, causing the materials to expand unevenly, hence leading to the fracture of the structure [76].

The intermediate components, in between the exterior and interior surfaces, are made of insulating materials. This is to ensure that minimum heat is conducted into the interior, delaying the heating process until the speed is reduced enough so that cooling by convection becomes more effective. There are materials with negative thermal expansion coefficients that contract versus expand with heating. Zirconium tungstate is one such material; it has a negative thermal expansion coefficient from near absolute zero up to 777 °C (1,050 K). It is possible to use composite materials made of a combination of negative and positive thermally expansive materials. In this case, it is possible to achieve zero overall expansion at selected temperatures (e.g., special grades of silica-ceramics) [77].

1.4.7 To Infinity and Beyond

An optical telescope sees darkness in the background of stars and galaxies. A radio telescope, however, shows a background noise or isotropic glow that is independent of the stars or galaxies, which is stronger in the microwave region of the recorded noise spectrum. Cosmic Microwave Background (CMB) radiation has a black body temperature of about −270.4 °C (2.73 K). This color temperature reduces gradually as the universe expands. This cosmic microwave radiation is everywhere, encompassing all the information ever generated and to be generated, while being invisible to the naked eyes. It is possible to record temperature at various locations and translate that to the color temperature of an ideal black body radiator, therefore bringing color to the universe, making color temperatures above 5,000 K appear bluish (cool) while those between 2,427 °C (2,700 K) and 2,727 °C(3,000 K) appear yellowish (warm). The lower the temperature, the longer the wavelength becomes, according to the Wien's displacement law ($\lambda_{in}T = b$) applicable to black bodies. In this relation, λ_{max} is the maximum wavelength (m), T is absolute temperature (K), and b is Wien's displacement constant (2.8978×10^{-3} mK). Longer wavelengths make light appear redder and dimmer.

The Sun is powered by a nuclear fusion reaction in its core where temperatures reach 15.7 million K. The Sun's radiation emitted from its surface has an effective temperature of 5,505 °C (5,778 K), resulting in a peak at a wavelength of about 635 nm, the red part of the spectrum. However, only a small fraction of the Sun's radiation is within the visible spectrum (380 to 740 nm).

As another example, consider the Orion constellation, one of the most prominent in the sky, the one with the three-star belt, visible at night during the winter in the Northern Hemisphere (being summer in the Southern Hemisphere). Its three brightest stars are Betelgeuse (T = 3,300 K, yellowish), Rigel (T = 12,100 K, warmer blue, greenish), and Bellatrix (T = 22,000 K, cooler bluish). Mars's average temperature is about −60 °C (213 K), while near its poles, the temperature can be as low as −125 °C (148 K). The Moon's surface temperature is about 127 °C (400 K) where its surface is exposed to the Sun and −173 °C (100 K) when it is in the shade. Other factors such as the existence of elements (e.g., vapor) in the planet's atmosphere may also affect the color temperature. One may conjecture that if other planets are found with the similar atmospheric temperature as that of the Earth, they may be similar to the Earth in other ways, and therefore possibly inhabitable.

X-ray telescope images obtained by the Suzaku satellite have detected a cosmic hotspot that is as hot as 15 million K. This cluster of galaxies is known as the *RXJ1347* and is five million light-years away from the Earth. It is believed that in order to achieve the highest temperature in the universe, it has to arrive at thermal equilibrium (1.416×10^{32} K, 0.1416 decillion), also known as the *absolute hot* or *Planck temperature*. At the other temperature extreme, it is believed that the Boomerang Nebula, belonging to the constellation Centaurus, which is 5,000 light-years from the Earth, is the coldest known place in the universe, at about −272 °C (1.15 K) [78,79].

In 1964, Robert Wilson and Arno Penzias, American radio astronomers, discovered CMB radiation. This is hypothesized as the ancient light that saturated the universe 380,000 years after the big bang explosion, creating the universe from a small seed about 13.8 billion years ago. This discovery was made at Bell Labs' Holmdale Complex in New Jersey in the United States. The antenna's receiver recorded a hum from sources unknown to the scientists. The hum came from all parts of the sky in a continuous fashion. They eliminated all possible sources for the humming sound and eventually concluded that they had discovered the thermal echo of the universe's birth. For this discovery they, together with Soviet scientist Pyotr Kapitsa, won the 1978 Nobel Prize in physics [80,81]. It is believed that cosmic rays are the oldest electromagnetic radiation in the universe.

1.5 Thermal, Flow, and Test Management

Thermal management, either in the form of heating or cooling, dates back centuries. In fact, the industrial revolution was not responsible for the invention of heating, ventilation, and cooling in buildings, nor for the invention of refrigerators. Persian (Iranian) engineers used *Yakhchal*, meaning *ice container* in Farsi, as early as 400 BCE to store over the summer months the ice created in winter. Aqueducts, called *Qanat* in Farsi, transported water to *Yakhchal's* tall conical structures, where it was cooled to the freezing point by its surroundings. To make the heat transfer more efficient, the flow was directed through the northern wall to use its shadow and keep the water cooler, and an additional eastern-western wall was made to protect the northern wall from the Sun's radiation. The word *Yakhchal* is still used for refrigerator and freezer in modern-day Iran.

Abanbar, a Persian (Iranian) cistern, is another thermal engineering example where a water reservoir with an insulating structure built below ground level was able to manage water temperature and the ventilating effect due to installation of windcatchers, helped to avoid the creation of mold and mildew due to stagnation. The windcatchers, also known as the *Badgir* in Farsi, were a traditional ventilating system used in ancient Iran and which are still in use; they can be unidirectional, bidirectional, and multidirectional. Many examples of these can be seen in the city of Yazd. The structure is even resistant to earthquakes, which are common in this area. If you wonder what material was used to make such an insulating structure, think of baking a low-fat sand cubed cake with two-meter sides: egg white, sand, clay, lime, goat hair, and ash—a recipe rooted in vernacular architecture. One wonders if Marco Polo truly appreciated this innovation while he rested in the caravanserai of Yazd as he followed the Silk Road.

Many engineering systems generate heat during their operation. The heat generation mechanism may be of a mechanical nature, such as friction between subcomponents, or it can be electrical or electromagnetic. In most cases, the heat generated needs to be dissipated as effectively and efficiently as possible. The study of methods for dissipating heat from the environment is thermal management. Thermal management may be carried out by methods categorized into three groups: (1) varying geometry configuration by designing extended surfaces, also known as the *fins*, and introducing cooling channels; (2) implementing additional mechanical systems such as fans and heat pipes; and (3) interfacing the parts so that the contact areas are increased for efficient heat transfer by using thermal patty, oil, or thermal tape at the adjacent surfaces.

To implement an effective thermal management strategy, one needs to understand how heat is generated, accumulated, and removed within the system. One way to accomplish this is to build a prototype, which can be full scale or scaled up or down, and then operate this prototype under conditions similar to those in the field. Building such prototypes (also known as the *mock-ups*) effectively and efficiently, however, requires extensive resources and following the 5M principles (Materials, Manpower, Machinery, Methodology, and Measurement methods).

Depending on the test type, mock-ups may be either reusable or not. For example, in cases where destructive tests are conducted or if for whatever reason the experiments do not result in the desired outcomes, a new mock-up will need to be built. Building a mock-up from scratch is a time-consuming activity requiring equipment and financial, and human resources. Therefore, it may not be practical for large-scale projects or ones with tight timelines. One example of a test requiring significant resources is evaluation of a passenger train car's underframe for tolerance to fire exposure. A typical requirement is that the temperature within the train's interior should remain below a safe limit up to 15 min after a fire starts to allow for safe passenger egress, according to the NPF-130 standard. Another example where one may choose to build a physical mock-up is in diffuser flow balancing for the train car's Heating, Ventilation, and Air Conditioning (HVAC) system. It is clear how time-consuming and expensive this task would be.

An alternative approach to employ in order to predict the behavior of a system, mechanically, thermally, and electrically, is to create a computational model. By exposing the model to different conditions—boundary and initial conditions—it is possible to predict physical system responses without the need to build multiple mock-up iterations. One may still want to build a physical mock-up, but it would be based on the predictions of mathematical computations and not a gut feeling, resulting in a much greater likelihood of success, with a minimal number of iterations.

Let us look at the example of a train car's HVAC design in more detail. Imagine a situation where a train car is being used by a customer in a warm and humid climate such as Las Vegas. After initial delivery of the product, dissatisfaction among train passengers rises since the airflow is not being distributed appropriately within the train interior to meet their comfort. For example, the airflow is too high in some areas, while others receive insufficient airflow. This negative feedback creates a strong incentive for a redesign.

Given that the existing HVAC duct design is a result of much effort and many hours spent building and flow balancing of physical mock-ups, the lead engineer decides to explore an alternative approach by incorporating computational modeling as the first step in the duct design (based on the timely proposal from a thermo-fluid specialist). The specialist proposes to create a model for the airflow inside the duct and then to adjust its geometry to achieve better performance. Flow models are created for the existing design, confirming the flow nonuniformities as the air exits the outlet diffusers. The specialist improves the design, considering manufacturing and space limitations. For each design iteration, a new flow model is developed and tested for flow distribution and formation of eddies resulting in turbulent flows. The iterative changes of the duct geometry based on the flow pattern output result in a major performance improvement after analysis completion.

In the next step, the physical prototype of the duct is made based on the computational flow model and tests are conducted. The tests show that the new diffusers' designs deliver the airflow uniformly to different sections of the duct. The conclusion is that the resources spent on iterating the computational models are much less than those that would have been required for physical prototypes. In addition, as the cost and time for each iteration is lower, more design iterations can be carried out, leading to a better product and fewer complaints from the future passengers.

CHAPTER 2

Modeling Systems

The use of mathematical models to solve physical phenomena followed the establishment of theories in physics and other sciences (e.g., social, economic, and biological). Brilliant mathematicians such as Khwarizmi, Newton, Lagrange, Gauss, and Euler have each contributed to the establishment of fundamental mathematical techniques such as algebra (to solve linear and quadratic equations by reduction and balancing); Newton-Raphson (to obtain successively better approximations to roots of a real function); Lagrange (to interpolate polynomials); Gaussian elimination (to solve systems of linear equations); and Euler's forward difference (to solve ordinary differential equations). These methods are still employed, and numerical calculations are still derived from the original analytical models.

2.1 Analog Computing through the Ages

Before the digital computing devices of today, there were analog computers. They did not look anything like what we would associate today with the word *computer*. These devices were dedicated to a specific function. The earliest devices would have been mechanical in nature, using the rotation of gears and other mechanical elements to provide the required information based on the user's input. After the invention of electricity, voltages or currents could be used to provide the answers sought by the user. In all of these cases, some analog quantity, be it mechanical or electrical, was varied and could assume a continuous range of values, unlike in digital computers, where discrete values of quantities are used. Also, unlike digital computers, analog ones by their nature could be affected by random errors—for example, due to electrical noise.

Through the centuries, the primary use of mechanical calculators and aids was for astronomical and navigational purposes. Perhaps the earliest analog computer was the south-pointing chariot, invented in China in the first millennium BC. It had a human figure standing on top of it that was pointing to a direction; this figure was connected by gears to the chariot's wheels and used the mechanical differential system to keep pointing in the same direction, no matter which way the chariot turned. This functioned like a compass, helping travelers to keep going in the desired direction.

Another ancient, and more complex, analog computer dates circa 100 BC; it was found off the Greek island of Antikythera in 1901. It had a system of thirty-seven geared wheels able to represent astronomical movements with high precision and predict events like eclipses years into the future. Skills for the creation of such devices were lost in subsequent centuries and not regained until similar astronomical clocks were built in the thirteenth to fourteenth centuries in the Middle East and Europe [82].

An astrolabe was a device widely used in the ancient and medieval times. Some books listed hundreds of applications for it. One could think of it as a smart tablet of its day! It was so common that a well-educated twelve-year-old person was supposed to know how to use it. The astrolabe's invention is attributed to the Greek geometer Apollonius of Perga around 200 BC. The device was much refined by astronomers of the medieval Islamic world such as Persians (Iranians) al-Bīrūnī (1000 AD) and Abi Bakr al-Farīsī (1235 AD) [83,84,85].

An astrolabe is made up of a circular base plate (mater, for *mother* in Latin) with a pin passing through its center. A circular flat plate (called the *tympan*) was fitted onto this base. Tympans were marked with lines corresponding to azimuth and elevation circles using stereographic projection of the celestial sphere onto the flat plate. Different plates would be used depending on the latitude of the location where the measurement was taken. Then, an overlay *web* (called the *rete*, for *net* in Latin) was placed on top, with locations of significant celestial bodies marked on it with arrows. A ruler that spun about a central pin was attached to the back. This ruler was used for sighting the celestial bodies and reading the elevation from the marks on the rim. When used, the astrolabe was suspended by a ring attached to its circumference.

One important application was to tell the time. The steps were: (1) select a known celestial body marked on the astrolabe's rete, such as the Sun or one of the bright stars; (2) sight it using the ruler to obtain its elevation angle above the horizon; (3) rotate the rete until the point corresponding to the chosen sky object lines up with the elevation angles marked on the tympan plate; and (4) rotate the ruler around the astrolabe to align with the current month and date and then read the time of the day on its perimeter ring. This sounds like a lot of work, but remember that reliable mechanical portable clocks were not available and that the device also provided a lot of other information, such as the location of all the significant objects in the sky, the time of sunrise and sunset, and the Sun's trajectory [86,87,88].

A more modern analog computing tool, a slide rule, is in some sense a descendant of the astrolabe—it also uses a set of sliding scales to obtain the desired information. Slide rules were invented around 1630, after the concept of the logarithm was developed. Until the introduction of digital hand calculators in the second half of the twentieth century, slide rules were widely used for division and multiplication. Slide rules (and similar manual calculating tools) are still used in aviation to solve time-distance problems and obtain values such as true airspeed and heading. Pilots are expected to have these skills in case modern electronic aids fail or are not available [89].

Through the first half of the twentieth century, a number of electromechanical analog computer devices were developed for military applications. For example, Dumaresq (invented in 1902 by Lieutenant John Dumaresq of the Royal Navy) was an analog computer that calculated the parameters for a ship's gun firing, taking into account the movement of one's own ship and the target. During WWII, mechanical analog computers were used extensively for directing gunfire and for bomb sights.

From the 1950s to 1970s, many electronic analog computers were developed and employed. For example, Project Typhoon, an analog computer used to analyze and design dynamic systems, was developed by RCA in 1952, comprising more than 4,000 electron tubes, 100 dials, and 6,000 plug-in connectors used to program it. Analog computers, with mechanical integrators and analog controllers, were extensively used for industrial process control (e.g., temperature, flow, and pressure) [90, 91,92,93].

Manhattan Project was among the first to extensively employ numerical tools for its calculations. This project started in 1939 in the United States, in collaboration with Canada and the UK, with the objective of harnessing nuclear fission and fusion processes, and it led to the development of nuclear weapons in addition to nuclear energy generation technologies. Although analog computers were extensively used, digital computers were subsequently developed at a rapid pace to meet the project's needs [94,95].

Digital computers that we use today can trace their origin to the ideas of Charles Babbage (c. 1834). He proposed to build *Analytical Engine*, a general-purpose mechanical computer, but the project did not proceed far due to funding and technology limitations. However, it was the ideas of Babbage that were of much greater historical importance. He essentially described the architecture of a modern computer, with an arithmetic logic unit, program flow control (conditional branching and looping), and memory. The machine could receive digital input via the media of punched cards and could produce output by punching holes in cards or plotting curves. Ada Lovelace worked with Babbage and realized the tremendous future potential of his ideas. Her published article (c. 1842) explained how such a machine could be used for general-purpose computing and published the first algorithm, thus making her the first computer programmer.

In 1936, Alan Turing, a British mathematician and scientist, invented what came to be known as the *Turing machine*. It was not a physical machine but a mathematical theory formally describing the concept of a computing machine; it built upon the legacy of Babbage's *Analytical Engine*. Conceptually, Turing machine operated symbols on a strip of tape according to a table of rules. Turing machine's importance is that it laid a theoretical foundation for the development of digital computers that started in the 1940s and led to the world-changing effects that we all witness today.

2.2 Model Categorization

Physical phenomena may be represented by models based on the mathematical relations. For example, in natural sciences, calorie intake may be modeled based on the gender, age, and activity level; heat of combustion may be described as a function of the reactant heat values and other characteristics. In an engineering application, for example, stresses imposed on a suspended bridge are predicted for the given environmental conditions such as wind and heat. In social sciences (e.g., economics), the behaviors of supply and demand on macro and micro levels may be described. No matter the discipline within which the model is employed, it is used to explain the system it is associated with by describing the effect of input parameters (predictors) on the response.

Mathematical models may be developed and solved using different approaches, which may fall within one of two main categories: *statistical* or *dynamical* models. Statistical models investigate the behavior of a system within a population, while dynamical models consider transient behavior of the individual system. There are variations of each model; for example, if the effect of time can be ignored in a dynamical system, a stationary model is used. If derivatives of the predictors and responses are included in the model, differential equations can be created. To make a model, the governing equations that represent the behavior of the modeled system are introduced, followed by the boundary and initial conditions and constraints. The first two (boundary and initial conditions) are usually sufficient for the results to be obtained; however, for the results to be meaningful, the initial and boundary conditions define the acceptable limits within which the system can operate. Constraints can also identify the optimized conditions for the response based on an optimum combination of the predictors. In other words, the input parameters are selected to achieve a certain goal defined by an objective function calculated from the predictors.

The approach of using an objective function with predictors is similar to game theory, in which the rational interaction between the state variables of different groups is modeled and which is based on the zero-sum principle. If you were to add the action and reaction forces in a system that is mechanically balanced, the sum of zero is obtained—that is because based on Newton's third law of motion, all interactions between bodies produce forces that are the same in magnitude and opposite in direction. The acceleration in this case is zero, unless it is included as part of the equation ($F - ma = 0$). Although game theory is a concept that is widely used in computer and social sciences, you see that Newton's third law of motion in physics can take advantage of the zero-sum principle. The same law may even be applied to modeling human-life interaction. The natural zero-sum rule—that for every action there is a reaction, equal in magnitude but opposite in direction—applies to the universe.

The frame in which the physical system is represented may be fixed or moving. This is also applicable to the model that represents the system. For example, for the case of a dynamic system, the frame of the model may remain stationary, and therefore a transient model may be employed, or it may move with the system, in which case a quasi-stationary model is appropriate. Consider as an example a model of a laser beam scanning process, where a laser light source is moved relative to an object's surface. To model this process, the scientist may choose to "ride" the laser beam, watching the object move underneath, or they may choose to remain attached to a fixed spot on the object and watch the laser beam move by. The benefit of "riding" the laser beam is that in many cases, from the beam's perspective, the effect on the object remains constant in this coordinate frame. If the beam is heating the surface, the temperature peaks at the trailing edge of the beam spot and then decays as the distance from the beam increases. In the beam's coordinates, this temperature distribution will remain constant if there is no variation of the object's properties over space or time. In such a case, a quasi-stationary model can be employed, much simplifying the modeling task.

The chosen modeling approach will also dictate the appropriate experimental approach to validate the model. Thus, if the model's frame is attached to the object, a thermal camera fixed relative to the object could be used to observe the movement of the hot spot produced by the beam; if the model's frame is attached to the beam, the camera would be fixed relative to the moving beam and the distribution of temperature in the beam's vicinity should appear constant.

In some cases, the physical phenomena may not be easily modeled, for example, due to a system's physical or operational complexity. In these cases, the model would need to be simplified. As a consequence, the modeling results may deviate to some extent from those of the experiments. This discrepancy is sometimes used to understand the physical system and seek solutions for the unknown physics that were ignored when setting up the model. Correlations may be developed as a result that show the relations between the predictors and response variables, and then a proportionality coefficient is defined to make the relationship meaningful. This coefficient may be constant or vary as a function of the input variables. The relation between the predictor and response variables may be linear or nonlinear. An example is the power law for the velocity over the boundary layer for a turbulent flow when setting up a flow model over a flat surface. Another example is *Nusselt number* that represents the ratio of the convective forces to the conductive forces and is used to obtain the convective heat transfer coefficient for the modeling of the heat transfer between a solid and its adjoining fluid.

Models can be developed for cases where the physical phenomena are not directly modeled; in other words, these models do not involve the governing equations. Instead, this approach employs the state variables in order to obtain a relation between them and a response variable. The response variable is directly influenced by the state variables. An example of this modeling is *Buckingham Pi Theorem*, in which the effect of physical and flow characteristics on a variable such as velocity is investigated. In other words, the behavior of a system (e.g., a flow problem) is modeled, assuming that certain characteristics (state variables) are the determining factors in how the flow behaves.

Let us assume that you are interested in modeling the behavior of a sphere in a viscous fluid flow. The critical variables are sphere diameter (D), flow velocity (V), fluid density (ρ), and kinematic viscosity (ν). The objective is to predict the drag force (F) on the sphere. Assuming that the drag is a function of the identified critical variables—$F = f_1(V, \rho, \nu, D)$—there exists a number of linear combinations of parameters raised to power that can result in a relation for drag $F = f_2(V^a, \rho^b, \nu^c, D^d)_i$, where the subscript i may vary from 1 to n, representing the number of possible scenarios. Presenting the variables' dimensions (F [kg m/s^2], V [m/s], ρ[kg/m^3], ν[m^2/s], D[m]) and equating them on the right and left side of the equation f_2, it is possible to find the superscripts (a, b, c, and d). A dimensionless combination can even be found—$F/\rho V^2D^2 = f_3(VD/\nu)$. Functions (e.g., f_3) are unknown, meaning that the scientist finds a relationship between the drag (response) and the rest of the critical variables (predictors) that follow the general equation presented previously, related by means of mathematical equations, as well as a calibrating coefficient to make the equations exact (versus an approximation). This calibrating coefficient therefore depends on the experimental *conditions* (e.g., ambient temperature and pressure) and *methods* (e.g., thermal imaging versus the use of thermocouples).

The aforementioned example was related to a *quantitative* test. It is also possible to associate values to *qualitative* observations and present a relationship for multiple qualitative variables, assuming a sufficient number of samples are available and the input (qualitative) variables are defined properly. An example for this scenario is employing a Likert scale, where 5-, 7-, or 10-point scales are used that represent qualitative variables in a range varying from the "best" (e.g., strongly agree and extremely likely) to the "worst" (e.g., strongly disagree and extremely unlikely) scenarios.

The use of statistical tools is reported in many fields; one of these is the atmospheric sciences used for weather forecasting. In aviation, Terminal Aerodrome Forecast (TAF) is used by pilots to predict the weather (i.e., provide weather-related data such as pressure and temperature). The data are provided by weather stations located at selected sites (e.g., airports) and so are not available at all locations. Using the weather reports from neighboring sites is possible but may not result in accurate decisions when making flight plans, especially when weather conditions are close to minima (i.e., the minimum acceptable conditions in order for specific flight rules to be valid). Model Output Statistics (MOS) are one approach for predicting the weather at unknown locations versus the predicted and variable data. These models present trends for historical data that include uncertainties for the given conditions. The predicted data can be obtained by interpolating the known data between the two known locations or conditions (e.g., altitude or distance).

It is also possible for the data to be extrapolated. For example, some weather data may not be available for a 3,000-ft altitude while they may be available for 6,000-ft and 9,000-ft altitudes. The data for a 3,000-ft altitude can be obtained by extrapolating the available data. Model results are presented in the form of diagrams, charts, and plots. These visual presentations are based on the calculated raw data that are post-processed to represent the desired effect. For example, contour plots represent the precipitation type, temperature, and pressure as a function of the altitude.

Models can be further categorized as either *discrete* or *continuous*. The qualitative model discussed previously, where a discrete number of samples are required to perform a statistical analysis, is an example of a discrete case, whereas the stress model predicting the structural stress for a bridge is an example of a continuous model. Furthermore, there are *explicit* models in which the response is generated from the known predictors, meaning that all the outputs are found based on knowing the inputs. On the other hand, *implicit* problems are the ones with the outputs known fully or partially; however, some of the input variables are unknown and need to be determined when solving such a model.

These concepts may be applicable to a variety of numerical models both in terms of the approach to solve the problem and also the type of analysis to be performed. For example, assume you model a physical problem of operating a Linear Induction Motor (LIM). A LIM may be used for propulsion of a train, one application example being a SkyTrain in Vancouver, BC. A LIM consists of coil windings energized by an alternating current. When modeling a LIM, one uses the known thermo-physical properties and amount of heat generated by the systems as a function of the current in order to find the temperature distribution, for example, within the coils. This forms an *explicit* model, since all the input variables—which are required to feed the governing equations and represent the heating within the system—are known. These variables belong to the thermal, electromagnetic, and mechanical aspects of the involved systems.

Now consider a different situation: the desired operating temperature for certain components of the LIM system is given. For example, you know that for the system to operate at its optimum, the ferrite within the coil assembly is to be maintained at 70 °C. Some input variables, such as thermo-physical properties of the assembly parts, are also known. However, you are to select the material in the vicinity of the ferrite with appropriate heat transmission properties to maintain its temperature at 70 °C. It is also possible that the properties of the adjoining materials or components are known but the thermal layer in between the parts is to be selected to achieve the optimum temperature. Such a problem formulation is an example of an implicit model. It is similar to a reverse engineering problem, where the known output values are employed in order to obtain the corresponding input variables.

Another example for the implicit model is the scenario where a westerly hurricane approaches the East Coast and you are to predict the severity of the storm and the velocity of the hurricane, given the extent of damage that will occur at certain locations along its path. A damage prediction model can be made to evaluate the output (weather and storm severity) versus the inputs (e.g., quantitative estimate of damage, infrastructure, and geographic variables) for three to five years of historical data (transient model). Some models can use up to fifty-five variables for more than eighty weather events. Using an explicit model for the same scenario, the extent of damage is predicted for the via-point residences (i.e., the damage experienced by the houses located at the storm-stricken regions) using weather and storm severity data [96]. In this case, extrapolation techniques may be employed in order to predict the exact severity at the via points.

A different type of categorization occurs when setting up models in the *deterministic* versus *stochastic* fashion. This consists of known predictors (inputs) that fully determine the response (output) in the case of deterministic models and models whose inherent randomness, employing the same input variables (predictors), results in multiple outputs (responses). These stochastic models are more complex than the deterministic ones, as they need to take into account the uncertainty. An example is the LIM scenario discussed previously (the reverse engineering example) for a deterministic model. In the latter scenario (stochastic nature), probability is present. This modeling is the foundation for the statistical analysis. An example for the latter case is the qualitative model presented previously (service). Let us re-examine the said examples. Using the applicable governing equation for the LIM model, it is possible to predict the temperature distributions. Let us assume that the findings support the scientific observations when the system is in operation. It can be concluded that the model is valid based on the input process parameters and physics; however, you are not certain how accurate the model is. Process parameters are the conditions at which the system operates or the model is run, which may slightly vary since obtaining the exact parameters (e.g., current or resistance defined for the model) may not be achievable when conducting tests. There may be errors introduced into the tests that are associated with operational limitations such as stability. For example, you may wish to make a model for when the system is exposed to a 10 A current, while it may only be able to have stable performance at a 15 A current or higher. Varying the process parameters and finding the sensitivity of the test results to input conditions, you are able to predict the validity of the model or the conditions under which it is applicable. In other words, with stochastic models one accounts for the degree of certainty with which one knows the input parameters by predicting the certainty with which one knows the model output.

Induction works from specific observations to wider theories or generalizations (bottom-top approach) while deduction works from general to specific observations (top-bottom approach). When employing induction, you measure specific events, quantify them, and try to find regularities and patterns, present tentative theories, and develop conclusions. When employing deduction, knowing one of the variables results in deducing other variables in which models are tried and tested and outputs are very accurate. You deduce from more general to more specific theories, narrowing down the possibilities, resulting in observations to determine critical variables.

A system that is easier to deal with is when you know the exact outcome of exposing the system to certain process parameters with high accuracy based on the measurements. For example, you are certain that sending a known current into the copper coils results in the generation of a known electrical field around the copper coil. The associated magnetic field may also be predicted as a result. In this scenario, the output is predicted with high accuracy, since there are exact formulae predicting the relationship between these variables. In other words, in knowing one of the variables, the other two may be deduced. These models are deterministic—the fully developed, tried, and tested theory can identify the output with high accuracy.

Now consider a different case. You decide to run wind tunnel tests to identify the airflow pressure over an aircraft fuselage in order to obtain the temperature distribution over its wings. The purpose of this study is to know the conditions at which ice crystals may form on the wing's leading edges; as they grow, they may eventually cause flow separation from the airfoil (wing) surfaces. As a result, the generated lift forces reduce and eventually may fail to be sufficient to keep the aircraft aloft. Although there are theories that may explain the reasons for the reduction of the lift forces on the airfoil surfaces when separation of flow occurs, the exact temperature at which this may occur given the environmental conditions in which the wind tunnel tests are performed is unknown. Conducting experiments at the given conditions should determine the physical relationships that exist for this specific scenario. This scenario presents an example for an *induction* model versus the LIM thermal model that can be interpreted as a *deduction* case. In other words, you are correlating the test results (responses) with the process parameters (predictors).

Another point to keep in mind is that the processes may be *reversible* or *irreversible*. For example, consider the process of heating a frying pan on a stovetop (before oil and other food ingredients are added). After the heat source is removed, the frying pan will cool down to room temperature, given enough time. This is a reversible process. In irreversible physical phenomena, however, the changes cause the system to not return to its original state, and it either remains in the same condition it experiences after eliminating the source of the disturbance (neutral stability) or continues experiencing the change even after removing the source of the disturbance (negative stability). This is in contrast to the behavior of a system that returns to its original state (positive stability) after removing the source of the disturbance, as in the previous frying pan example. Cooking food ingredients inside the said frying pan is an example of an irreversible cooking process.

2.3 Analytical Models

Analytical models are indispensable tools in science and mathematics. The term *analytical* model means mathematical models whose sensitivity to their input parameters are analyzed by means of solutions using mathematical relations to make logical conclusions. An example of an analytical model for physics problems are the wave equations in which the second derivatives of inputs or state variables (predictors) are defined versus the second derivatives of the output variable (response).

Different types of analytical models have been created where the first derivatives or the interactions (e.g., their multiplications) of these derivatives are introduced into the relations. These models generally fall into two categories: *logic* and *linguistics*—use of words in defining the concepts and their order in the former and latter cases applies. Linguistic variables involve a linguistic term that is derived using quantitative or qualitative reasoning (e.g., probability, statistics, fuzzy sets, and systems). Logical variables can be either *true* or *false*. In mathematics, a connection between a model's elements is achieved by means of equations, variables, parameters, constants, and operators. The equations and analytical functions do not only equate terms but also represent the scenarios in which the inequalities—differences in magnitude, expressed by *greater or less than* relationships—exist. Newton's second law of motion falls into this category, expressed by an equality relation, while *Mie scattering theory* employs an inequality relation. A statistical analysis can be a form of analytical function when a regression analysis is performed, resulting in fitting a curve to the critical input variables and predicting the response variable as a result.

There are *surjective* functions, where for each set of input variables, a specific output variable is obtained; in other words, for at least one value for each input variable, a specific output variable is calculated. For example, $z = f(x, y) = 2x + 10y - 12$ is an analytical relation that equates z, which is a function of x and y, to a linear combination of two variables (x and y). Assuming that $x = 2$, one can obtain the value for y ($y = 0.8$), which makes $z = 0$. These variables are a combination of numbers used to calculate z. The *objective* function may consist of any combination (linear or nonlinear) of the variables or their derivatives.

It is also possible that the derivative combinations of variables are related by mathematical operators, presenting both surjective (at least one-to-one) and *injective* (one-to-one) functions. For example, Newton's second law of motion states that the net force applied to a body is proportional to the body's mass (m) and the derivative of the distance (x) derivative (i.e., the derivative of the speed—the acceleration—a). The third variable (time—t) is hidden in this formula, introduced by the *derivative* operator—$F = ma = md^2x/dt^2$.

Optimization is another method for modeling in which an objective function is defined, showing the relationship between a set of variables. These variables may each have their own limitations (e.g., maximum and minimum values). The purpose of such analysis is usually to optimize (maximize or minimize the function) given the input limitations. For example, if the objective is to reduce the carbon footprint, you need to define a carbon footprint magnitude function as the output variable, which should be minimized based on the critical input variables affecting the carbon footprint. For example, fossil fuel compounds, generated by burning gas in the furnace or driving a gasoline-powered vehicle, can be assumed as input variables to the said functions.

In other words, objective functions are affected by the imposed constraints. Any functions defined for a process to be optimized belong to this group. Consider a case such as $f(x, y) = \min(2x + 10y)$ where $x < 2$ and $y > 1$, and both x and y are positive integers ($x >= 0$ and $y >= 0$). This relation results in a minimum value of 20 for the function $f(x, y)$. This objective function does not accept any values for the input variables, and its conditionality is beyond the single-variable relations presented by the said subjective case. Nevertheless, it is possible to introduce variables that have been operated upon (e.g., derivatives and gradients) to form equations similar to a *surjective* function. The advantage of analytical formulae over numeric ones is that they allow one to make a quick and precise evaluation of the influence of the input variables on the output variable. For example, looking at function $f(x, y)$ in the previous equation, one concludes that this function (response) is linearly dependent on the input variables (predictors).

2.4 Numerical Models

Numerical analyses use algorithms that employ numerical approximation versus the symbolic manipulations performed in analytical or parametric studies. A numerical method is a mathematical method (tool) that is created to solve numerical problems by means of a programming language. It is also known as the *numerical algorithm*. Numerical models still employ the mathematical relations of analytical approaches (or models); however, for these models, in order for the solution to be obtained, the equations are solved using numerical techniques and by assuming initial values for the input variables (predictors) that are iteratively improved upon or by using omission techniques.

Iteration techniques are repetitions of steps taken to obtain new variable values. The process continues until the variation of the calculated predictors or response at the iteration m is within a predefined tolerance from the previous step, the iteration $m - 1$. In omission techniques, one or more variables are omitted by assuming they are zero and the rest are predicted. The predicted values are then substituted in the equations, reducing the number of variables from m to $m - 1$, assuming one variable is calculated at a time. This process continues to the point that all variables are predicted. The process may need to be repeated if the last variable does not meet the operator requirement (e.g., 2 = 1). In most cases, it is not possible to identify the exact relation between the input (predictor) and output (response) variables. This method is particularly useful if there are multiple mathematical relations to be solved, meaning that there are systems of equations which should be satisfied. If these systems are connected at their boundaries (in case of spatial variables), a continuity relation should also be observed, meaning that, depending on the order of the equation, the associated variables at the boundary should be the same for the two equations sharing the same boundary as well as their derivative(s).

Numerical models have some disadvantages compared to analytical ones. Numerical models would normally take longer to solve and the relationship between the inputs and output may not be as clear. For example, in an analytical model of drag force on a spherical object, we can immediately predict that the force will be proportional to the square of air stream velocity. However, numerical models are indispensable when dealing with problems that are too complex to be solved using analytical techniques (e.g., PDE). For this reason, different numerical methods such as the Finite Difference (FDM), Finite Element (FEM), Finite Volume (FVM), or Discrete Element (DEM) methods have been developed.

Due to their capability to handle complex systems, they are used to model thermal systems in the field of weather forecasting, such as predicting pressure and temperature over a certain period of time, geological observations, such as thermal history of rocks, and movement of the Earth's layers. The process of discretization, which is describing a system by equations for a set of elements (FEM), nodes (FDM), or volumes (FVM), is common among numerical methods. Computational Fluid Dynamics (CFD) falls into the DEM category, where the motion and influence of many small particles are considered. This method is generally used to tackle engineering problems in continuous and discontinuous manners and with respect to moving elements (flow), such as in the field of thermodynamics.

To start a complex modeling task, the scientist designs an analysis flow chart, which is the diagram for the methods of interaction and the locations at which any model components (e.g., thermo-physical properties and process parameters) are introduced to the systems of equations. An algorithm, a written computer program, is then composed for the problem with elements that include the inputs, which are then applied to the physics, incorporating the constraints. Solving the problems based on a specific numerical method is the last step. The numerical data from the analysis are then extracted and shown in the form of diagrams and plots using the same tool that was used to perform the analysis or a new post-processing-dedicated tool. Occasionally, data are exported to other programs and are processed and used for the desired purpose—such as further data analysis or as inputs for different sets of physics that cannot be coded or modeled using the original tool. The environment (tool) in which the numerical processing (equations assembly combined with process parameters) takes place is either a coding compiler such as C++ or a commercial software package in which the physics are already defined along with the method of interaction. The scientist sets up the problem to the extent of accuracy possible, interacts with the setup, produces the solution, and then post-processes the results.

2.5 Verification and Validation

Let us assume that a numerical model explaining a physical phenomenon is created using a commercial FEM software to output information for given inputs. The inputs to such a model may be material properties or manufacturing process parameters. They are included in the form of boundary conditions or any other terms defined in the energy balance equations. How does a scientist know if the calculated numerical results are valid? Generally speaking, outputs are only as good as inputs; however, there are additional factors to consider. The following aspects enhance the validity of a solution: (1) setting up physics as accurately as possible—meaning introducing a comprehensive set of equations which represent the physical phenomena, (2) making simplifying assumptions that do not jeopardize the problem integrity, (3) creating geometry that accurately represents the real system—including the correct interfaces and boundaries, (4) defining model inputs accurately, (5) solving the model using proper techniques, and (6) selecting outputs that closely follow the questions sought when setting up the physical system.

Comparing the results of the solution available in the literature (or obtainable by means of available formulae) and the ones obtained by employing custom numerical analysis—either by means of commercial software packages or programming languages (coding)—is called the *validation*. One approach to validating a model is to change some of the setup conditions to a simpler case to allow comparison with either available analytical formulations or with reputable literature sources. For example, it is possible to zero the inhomogeneous heat gradient at the boundary of a physical system and obtain a homogeneous problem with insulated boundaries whose numerical analysis, analytical model, or methodologies to obtain any of the said results are available in the literature. One can then claim that since the model produced correct results for one set of inputs, the model is a valid one and should produce correct results for different inputs.

Validation can be carried out either numerically or analytically. One very useful approach is to use known analytical solutions. A variety of these models can be found in heat transfer textbooks. Although analytical solutions can be developed for a number of physical phenomena, they usually can only represent a simplified form of a more complex physical system. Attempting to fully model a very complex problem by analytical solutions is either very inefficient or impossible. Unless the scientist is interested in investing hours to develop complex mathematical models for the pure joy of challenging themselves (which they often like to do), they can employ numerical coding or commercial software packages as a more efficient approach to analyzing physical phenomena.

Another approach to validate the results of numerical analyses is to employ experimental results for a system that closely matches the boundary and initial conditions of the mathematical model. One may argue it is more practicable to simulate the experiments numerically, as the reverse process is more challenging in the majority of cases. This is not necessarily the case and depends on the complexities associated with the numerical model and experiments. There are examples in which experiments face limitations and interpolating or extrapolating the results is the only way of moving forward. The limitations may be due to process parameters or geometry. Conducting physical experiments is generally expensive and time-consuming; one may only be able to carry them out for a limited set of conditions. With a numerical model, the scientist may run it for any conditions, even those that may not be possible to achieve with the available equipment. However, the model may be validated by comparing its results with those of the experiments for a few selected settings.

As an example, one can look at a challenging task of heat transfer modeling in Laser Transmission Welding (LTW) of thermoplastics. In this process, a laser-transmitting part is joined with a laser-absorbing part by passing the laser beam through the former until the laser radiation is absorbed by the latter part, and the resulting heating causes both parts to melt at the interface, thus forming a joint. Selecting the optimal combination of process parameters to join parts is time-consuming. The possible range of variation of the laser power may be limited by the available equipment, both at the low end where only a certain minimum operating power may be feasible, and at the high end. Therefore, selecting process parameters for numerical models requires careful design of experiments—in addition to identifying upper and lower process limits. Thermal imaging is a method that can be used to verify the results of numerical analysis. The model should be set up to be as similar as the experiments as possible. Correct thermal imaging techniques must be used to ensure that the experimental temperature observations are recorded properly. For example, the scientist needs to ensure that the camera lens is parallel to the surface. The test part facing the camera should have a known emissivity or be coated with a known material (e.g., soot or black electric tape). This is in addition to calibrating the thermal camera by means of a black body heat source to ensure the thermal camera converts the object signal to the temperature correctly.

Complex analytical and coded numerical models should be carefully *verified* to ensure the applicable physics are functioning as they should in representing the system(s). Commercial software packages, before being released to the consumer, would normally have already been verified. If a scientist is interested in confirming the correctness of commercial software packages, they can review the verification documents released with each new product revision. Some commercial codes (e.g., Code-Aster, a commercial FEM code designed for solving structural mechanics) are also accompanied by an ISO-9001 qualification certificate. Note that the end-user agreement for some commercial software may not allow direct comparison of the numerical results obtained from their platforms with those of the competitors' tools.

In applications where analysis results are highly sensitive and safety is of great concern—such as the operation of nuclear reactors for power generation—it is common to employ multiple commercial software platforms to ensure the results are consistent, reproducible, reliable, and accurate. You may wonder why the model built using software from a *certified* commercial developer still needs to be validated to ensure the model is correct (since they were already verified). To clarify this, it is not the commercial package which is validated, but the *model*. For example, it is possible that the physics are not accurately assigned to the regions or boundaries, variables are not defined properly among the list of parameters, variables are locally defined while they are needed globally, or that parameters and conditions (boundary or initial) are not implemented correctly.

If numerical coding is employed to represent a mathematical model, meaning that you are using a suitable programming language such as

Fortran or C++ to set up and solve a physical phenomenon, there are extra challenges of verifying the solution in addition to validating the solution. Validating the model requires the steps described earlier. Verifying, on the other hand, requires that the physical equations be investigated for both precision and accuracy—correctness.

2.6 Physics Governing Equations

Computational models are based on the mathematical relations and governing equations, known as the *physics*, that describe the behavior of a system. They can be based on the analytical formulae developed from fundamental physics principles, such as the conservation of mass, energy, and momentum. For example, when modeling a system for thermal responses, Newton's law of cooling, Fourier's law, and Boltzmann's relations are applicable for the convection, conduction, and radiation modes of heat transfer, respectively.

They can also be based on the empirical relations obtained from experiments or experiments calibrating the physical models by means of mathematical laws. The latter can be achieved by analyzing test data using statistical analysis. This technique uses mathematical relations (e.g., regression formulae) to identify key variables (predictors) and then generates linear, quadratic, or higher order equations to calculate the dependent (response) variable. Empirical relations are in fact a variation of these models, as they also describe the effect of one or more variables (predictors) on a single or multiple variables (responses).

One benefit of statistical models is that they estimate the weight of each variable (degree of *significance*). It is also possible to calculate the degree of *confidence* associated with the model. When setting up a heat transfer model, for example, for a case where radiation is the dominant mode of heat transfer, the convection coefficient may have little significance. In fluid flow modeling, when calculating drag force over a surface, one may decide that the flow velocity is the more important input variable compared to surface roughness.

The mathematical models based on the dominant physics can be either solved *analytically* or *numerically*. For simple physical systems, it may be possible to use analytical tools to solve the problems; however, with increasing complexity, both in associated physics and geometries, this turns into a challenging task. Therefore, numerical analysis methods become necessary. The choice of the numerical technique is the next step, as the problem is to be solved as efficiently as possible, with errors that are within acceptable ranges, solutions that are stable, and with a minimum of ill conditioning (i.e., conditions resulting in singularities).

Generally speaking, a simpler modeling solution that achieves accuracy comparable to a more complex one is the best approach. Even if its faithfulness to the physical system is slightly less than that of a more complex model, faster solution times will mean that more design iterations and computational tests can be conducted, which can lead to a better design than would be achievable with a more faithful but complex model.

For example, in a past research project the author was faced with a problem of modeling heat transfer in the cornea of a human eye exposed to an intense source of the thermal radiation. A choice needed to be made between an FDM or FEM. A model was developed using a forward iterative FDM with Gauss elimination method and compared with the FEM approach. It was found that the FDM approach was nearly as accurate but was much faster to solve.

The number of conditions applied to a model (boundary or initial) depends on the number of predictors (state variables) and their derivatives that are introduced into the model (physics). The total number of conditions (constraints) is the summation of the number of conditions (constraints) required for each single state variable. For example, the second-order equation with respect to the predictor x requires two boundary conditions that show the relationship between the response and predictor x—one of them is most probably a linear relation of variable x and the second one is that of its derivative. In the third-order equation involving variable y, three sets of conditions are required, and the third constraint may be the second derivative of variable y. If the problem consists of a combination of the two scenarios—where the second-order derivative of predictor x and the third-order derivative of predictor y are present—five boundary conditions should be employed.

Assuming that the problem is time-dependent (the first-order time derivative), the initial condition is also to be included, resulting in six conditions. If the number of conditions is smaller or larger than the required conditions, there are either an infinite number of solutions in the former case or the problem is over-constrained in the latter case, each leading to a failed solution. Furthermore, the conditions should be linearly independent for the constraints to be independent entities, so that a finite number of responses are achieved. For example, having a boundary condition that is a linear function of the two other linearly independent boundary conditions, with the three of them presenting the same state predictors, results in having two constraints (even though there are *apparently* three constraints defined). This results in an infinite number of solutions, similar to the case where the number of conditions is insufficient.

2.7 Modeling with Custom Programs versus Commercial Software

Programming languages or commercial software packages may be adopted as methods to carry out the numerical analyses based on the governing equations in combination with the initial and boundary conditions. Programming languages such as Fortran and C-derivatives (e.g., C++) are among the popular ones used by scientific communities for decades, with new subroutines built upon the previous versions or as add-on features. Depending on the physics in which the problem is set up and modeled and the available resources, either a commercial package or a custom-written program may be selected. There are also situations where a combination of both may be used to solve a problem. One example is the use of ANSYS® Parametric Design Language (APDL), which involves writing subroutines, also known as the *scripts*, in the format of an input file for its classic platform. In Abaqus FEA, the subroutines may be written in Python. In COMSOL Multiphysics, parameters for mathematical functions may be set up using *Mathematical* module—an add-on feature to COMSOL Multiphysics.

One factor which may discourage the use of a commercial software package (versus custom programming) is the higher cost of the former. For educational institutions, discounts are usually provided with the stipulation that the programs are to be used only for training purposes, which would also serve in fact to promote the use of the company's software. Students who are exposed to these tools graduate and become decision makers or influencers regarding the choice of the tool to be used in their organization. Therefore, the educational pricing is well-justified. Also, most software packages allow for a free trial period. Software costs can be in the form of an annual license or as an outright purchase. However, the latter may still require ongoing purchases of annual maintenance, without which access to future software updates or support will not be granted.

Examples of general-purpose software packages which require the purchase of an annual license include ANSYS (for linear analysis) and Abaqus FEA (for nonlinear analyses). Following a similar pricing model are also more specialized tools such as ESATAN-TMS (*Thermal Module Suite*) that are focused on thermal modeling of satellites. COMSOL Multiphysics follows the second (ownership with annual maintenance) approach. Since 1998, when COMSOL Multiphysics was developed from its predecessor, FEMLAB, its core application and add-on modules have undergone numerous changes, with regular updates. With every update, the core and existing modules are improved with new capabilities. Also, the number of add-on modules keeps multiplying, each one addressing an ever-narrower application field.

COMSOL Multiphysics marketing approach is to start with a core package with its base capabilities, addressing the basic physics in different fields, and then expand on it with discipline-specific modules. To use any of these modules, the user must have the core COMSOL Multiphysics package. Additional capabilities such as advanced geometry operations—to either create geometry internally or via the CAD tools—may require additional modules and associated initial and ongoing costs.

For the purpose of this publication, thermo-fluid physics with heat transfer effects and temperature distribution are an essential requirement. Therefore, although COMSOL Multiphysics core application is equipped with some basic features that may be used to pre-process, analyze, and post-process a thermo-fluid model, *Heat Transfer* module is selected as an add-on. It is also possible that the combination of COMSOL Multiphysics and *Mathematical* module is employed to form customized differential equations with the applications in a variety of fields. Note that having decided to take this path, the model would need to be as thoroughly validated as when writing a custom computer code.

On occasion, advanced features of a specialized module may have equivalent counterparts in the base module. For example, when setting up a flow problem, the velocity may be set for a base module while mass flow—which is derived from velocity knowing the flow properties and geometry configurations—may be set as the flow inlet or outlet conditions in the specialized module. The emissivity for the radiation heat transfer model may be set in the base module while for the more specialized one, a particular radiation model (e.g., opacity approach) may be selected. Therefore, you may be able to find the features in the base module that can partially or fully perform the tasks of the specialized modules. The current version of COMSOL Multiphysics is 5.4, and it is employed for all modeling in this publication.

2.8 Modeling Using Commercial Software Packages

When setting up models, required physics are selected, such as heat transfer, structural mechanics, or fluid flow. For some models, more than one physics are needed. When solving such numerical problems, there are two possible approaches: either to solve the physics sequentially, feeding the output of one physics solution as the initial or boundary condition to the next one, or all the physics are solved simultaneously. Sequential solutions are usually less demanding in terms of computer resources than simultaneous solutions, but they may also produce less accurate results. The physics may be set up and solved within the same commercial software package using either the same or two different environments. Alternatively, a different software package may be used for each physics solution, with the results being exported from one and imported into the other.

For example, in COMSOL Multiphysics, you may choose to solve a thermal-stress problem in an iterative fashion, defining a multiphysics scenario for the heat transfer and structural mechanics physics, and then solve each physics either simultaneously or in steps. In this case, the heat transfer solution will provide the initial conditions as input to the structural problem. When solving problems involving heating due to electric current, COMSOL Multiphysics *AC-DC* module may be employed to solve the electrical problem in combination with *Heat Transfer* module.

Another approach would be to use a specialized electromagnetic field simulation tool, such as ANSYS Maxwell, to set up and solve the physics related to the electric current by calculating the B-fields, H-fields, and hysteresis magnetic data, and then export the solution results (e.g., temperature distribution). This export is usually in the form of nodal raw data as a function of the nodal coordinates. These exported spatial data may be then processed in a third-party software (e.g., MATLAB® or SciLab) to make the data compatible with the software in which the next analysis step is to be performed (e.g., COMSOL Multiphysics). This in-between processing may include reorganizing of the data so that the order of the coordinates may vary or reprocessing the raw data to calculate the input variable values to be used in the next-stage solution.

In addition to transferring data between different physics solutions, another point to consider when choosing the software packages for analysis is the import of model geometry. For highly complex geometries, the analysis software should be able to carry out the import with relative ease and should be able to perform geometry processing steps such as repairing the parts within the specified tolerance, treating the parts as individual components or as an assembly, or simplifying the geometry by removing unnecessary features. These are the capabilities that a typical modern commercial software package is expected to have. The latter capability (known as the *part defeaturing*) is very important in dealing with geometrical structures such as slits and sharp corners. If left unrepaired, they can lead to non-converging solutions.

If geometrical features are not created using built-in capabilities such as *Design* module or other add-ons, they may be repaired either before or after importing them into the analysis tool, considering appropriate tolerances. In some cases, it is possible to import the geometry as an assembly or as a unified object. Importing as an assembly makes it possible to treat the subcomponents individually, allowing the definition of layers with space gaps between components or the introduction of contact areas. When employing this scenario, it becomes possible to have common nodes and elements, which should be then merged, satisfying the continuity conditions. When the geometry is imported as a union, tolerances should be set. In this case, there is perfect contact between the subcomponents. The contact variation between the surfaces can be defined by introducing contact elements and nodal and elemental conditions (e.g., constraints, surfaces with contact resistance, and thin conductive and resistive layers)—given material thermo-physical properties. Examples of commercial software packages capable of such functionalities are ANSYS, Abaqus FEA, and COMSOL Multiphysics.

It must be remembered, however, that since the main function of the analysis packages is to solve the physics, their internal geometry creation and manipulation capabilities are limited, and so complex geometries are built most often with dedicated CAD tools (e.g., CATIA, SolidWorks®) from where they may then be exported for use in the analysis tool. On occasion, though, the geometric information may travel in the opposite direction as well. It is possible that the geometry is originally created in an analysis tool and then, after being analyzed and optimized within it, exported to a CAD tool for further processing, and later being reimported to the analysis tool or being embellished to include the design details such as grills, cables, onboard electronics, and control surfaces. Afterward, the design can be sent to manufacturing for production. For example, for the HVAC duct case discussed earlier, the problem of the flow distribution inside the duct is first addressed by the analysis tool and, after finding a solution that meets passenger comfort requirements, the duct geometry can be exported to a CAD tool to refine the design, accounting for space clearances, manufacturing limitations, and other necessary details.

In some cases, there are specific CAD tools that interface particularly well with the chosen FEM tool, and so their selection may provide strong additional benefits. For example, COMSOL Multiphysics has an optional built-in feature, called *LiveLink*, that makes it possible for the analysis software to communicate directly with a specialized CAD tool such as Solid Edge® or SolidWorks. This is done by making accessible in COMSOL Multiphysics the geometry-defining parameters in the CAD tool. Thus, if a brick-shaped block were to be created in Solid Edge CAD, its three dimensions could be defined as multiples of a user-defined *brick_Scale* internal variable. If the CAD software is running with the brick part open simultaneously with COMSOL Multiphysics FEM tool that includes the optional Solid Edge LiveLink add-on feature, this CAD geometry could be imported as LiveLink, making the *brick_Scale* variable now accessible from COMSOL Multiphysics as part of a list of its own local variables. Thus, the user would be able to change the geometrical parameters in either the CAD or FEM tool and have the geometry update simultaneously in both environments.

CHAPTER 3

HEAT TRANSFER AND FLOW THERMAL SCIENCES

Heat transfer modeling is founded on the principles of thermodynamics. This science focuses on the motion of particles making up the matter stimulated by the heat that causes a change of internal energy and its manifestation as heat or work. For example, if a hot-air balloon is filled with hot gases, its envelope keeps pushing its boundaries to the point that it cannot expand anymore. The process of energizing the molecules has first caused the process of expansion (work) and then exciting the molecules to go beyond expanding the envelope, to lift the balloon and keep it floating. In thermodynamics, the four laws are as follows: (1) the zeroth law—two bodies, each in equilibrium with the third body, are in equilibrium with one another; (2) the first law—internal energy of bodies remains constant; (3) the second law—entropy of the universe increases over time and its changes cannot be negative for any given system; and (4) the third law—entropy of a body approaches zero when its temperature approaches absolute zero. The term *body* used in this context is interchangeable with *system*, since both define a cluster of molecules with the equation of states ruling over them [97].

Interacting forces within fluids (e.g., gases, liquids, and plasmas) are governed by fluid mechanics. This is also known as the *third law of Newtonian mechanics*, sometimes called the *action-reaction law*—for every action, there is a reaction equal in magnitude which is in the opposite direction. Fluid mechanics is further categorized into fluid *statics* and *dynamics*, based on the temporal status of the fluid molecules—the former relating to stationary (equilibrium state) and the latter to transient systems. An example where statics is applicable is the variation of the atmospheric pressure with altitude. Hydrostatics is the reason for self-leveling concrete liquid pouring over your bathroom floor—making it flat—similar to fluids inside a container that not only take the shape of their vessel but also stay level. Fluid dynamics apply, for example, in shock absorber systems, such as those used in car and aircraft wheel suspensions. Depending on the type of fluids, either liquids or gases, more specialized disciplines such as hydrodynamics and aerodynamics have evolved. Aerodynamics investigates the flow patterns and forces over an aircraft, or any flying object in general, and predicts the evolution of weather.

Heat transfer is a thermo-fluid science that focuses on the transportation of heat in a continuous medium. The continuum consists of its molecules and is identified by its boundaries. Depending on the spacing between the molecules and atoms, the particles that agglomerate to form the matter, and the ratio of the mean free path to the characteristic length—also known as the *Knudsen number* (*Kn*)—the medium forms a fluid or a solid. A larger space introduces the possibility for the molecules to freely move in their environment without interacting with the molecules in their vicinity. It is similar to a large field with areas of farmland that are sparsely distributed versus an urban setting with houses sitting side by side. If *Knudsen number* is larger than one, free molecular flow is observed, where molecules can freely move to occupy the available space with only their container shape limiting their motion (gas). Molecules with a smaller Kn (about 1) have their movement constrained to greater extent (as in fluids). Therefore, fluids, which are further divided into gases and liquids subcategories, are identified by the spacing between their molecules. Fluids adopt the shape of their container. In solids, *Knudsen number* is considerably smaller than 1 and the molecules are tightly packed.

Energy (as heat) can be transferred either by mechanical interaction between the matter's elemental particles or by transmission and absorption of electromagnetic waves. Thus, a medium (gas, liquid, or solid) is required for the former mode, while no medium is needed for the latter mode. Heating a skillet on the stove results in raising the skillet temperature that starts locally in the heated area first and then affects the rest of the skillet as time passes. For example, you may feel the heat touching the handle some time after the burner is turned on. This is an example of heat transfer by mechanical interaction of the skillet's atoms. Alternatively, if you direct your open palm toward that same hot skillet and feel the warmth, then you are detecting the electromagnetic waves transferring energy by radiation.

During a phase change, when the matter changes from solid to liquid (melting) to gas (vaporization) and going in the opposite direction, when the matter freezes or condenses, the temperature remains constant and this phase change is described according to the process in progress (e.g., melting and boiling points versus freezing and condensation points).

In heat transfer, the movement of heat in single or multiple objects is investigated. Since heat is directly related to the temperature, the variation of this property is the determining factor in the creation and transportation of this energy. Spatial and temporal changes of internal and external energies result in heat generation, either in a closed system or in a control volume. In a closed system, energy in the form of heat crosses the boundaries while in a control volume both energy and mass can do the border crossing. This energy is either in the form of heat or work.

Heat transfer problems can be categorized in the following terms: (1) isothermal—a process in which temperature remains constant; (2) isobaric—a process in which pressure remains constant; (3) isovolumetric (or isochoric)—a process in which volume remains constant; (4) adiabatic—a process with no energy transfer; (5) isentropic—a process in which entropy remains constant; and (6) isenthalpic—a process in which enthalpy remains constant.

All thermal sciences are governed by natural physics and employ analytical laws (derived from mathematical relations), empirical laws (obtained from experimental observations), and hybrid relations (predicted from correlating the two physical modeling approaches). These studies focus on calculating spatial fluid properties such as temperature, pressure, density, and velocity in a time domain. When processing thermal science data, either interpreting or presenting them, it is possible to take advantage of certain special cases. If the system properties do not vary over time, a steady-state or stationary condition is reached. If these properties do change with time, then the system can be described as in a transient or time-dependent state.

When post-processing the results of any system study, if multiple variables are plotted against each other, by keeping one property constant, the *iso* contour lines or surfaces can be produced. You may be familiar with the isotherms (lines of equal temperature) and isobars (lines of equal pressure) plotted on weather charts. There are also less familiar plot types employing the same concept. For example, when interpreting weather data, you may create contour plots using isogeotherms (lines of constant mean annual temperature) and isodrosotherms (lines of constant dew point).

This chapter looks next at material thermal properties, which are the critical inputs required when solving heat transfer models. A section on thermal analysis discusses the advanced methods used to obtain accurate material properties. The three dominant modes of heat transfer are considered next, followed by a review of the energy conservation principles on which heat transfer modeling is founded.

3.1 Thermal Properties of Materials

Thermal properties of materials usually involve a combination of energy (J), temperature (K), mass (kg), length (m), or time (s). Adding (or taking away) energy from a material increases (or decreases) the degree of *excitement* in the form of translational, rotational, and vibratory motion of the material's elementary particles; the level of this *excitement* is expressed by the material's temperature.

Specific heat capacity is the amount of energy that is needed to increase the temperature of material by one degree Celsius (J/kgK). For example, for water, it is 4,200 J/kgK, while for cast iron it is 460 J/kgK. *Thermal conductivity* describes how much energy (J) can travel per unit time (s) per unit length (m) for a temperature gradient of one degree Celsius. For example, for alumina, a high-strength ceramic material, it is 27 W/mK, while for copper, known for its high thermal conductivity, it is 401 W/mK, which is almost fifteen times greater than that of the ceramic material.

The three thermo-physical properties of density, thermal conductivity, and specific heat capacity form the foundation of all heat transfer problems. A fourth property, *thermal diffusivity*, may also be used to characterize the material, though it is only a combination of the previous three properties, given by the ratio of thermal conductivity to the product of density and specific heat capacity. It is proportional to the rate of heat transfer in the material. As it is derived from the other properties, it is not one of the inputs required to define thermal properties of a material in a model.

Any type of conservation, either in the form of mass, energy, or momentum, employs one or more of the three previously listed properties. Temperature is the driving force in many heat transfer problems, either directly or indirectly, by relating other types of energy to heat. Although material properties are vital ingredients of any modeling, some properties are more dominant than others, depending on the thermo-fluid regimes, modes of heat transfer, or the analysis types. These properties may vary in space (*spatial*), time (*temporal*), or under environmental conditions (environmental). Nonconstant properties introduce nonlinearities and inhomogeneities to the physics that make the problem more challenging to tackle.

If a material is a mixture of two or more distinct elements or compounds, it can be classified as *homogeneous*, *inhomogeneous*, or *heterogeneous*. In a homogeneous material, the components are mixed at such a fine level that any small macroscopic sample of the material has an equal proportion of the constituents. In an inhomogeneous material, taking similar samples results in sample-to-sample variation of the constituent proportions. In other words, homogeneous materials are consistent in composition and character (e.g., some metals), while inhomogeneous materials are inconsistent in composition or character due to the substantial material variations (e.g., rice pudding). Heterogeneous materials are inconsistent in composition or character for similar materials (e.g., chocolate chip cookie).

For example, after stirring sugar or milk in your morning tea, you can no longer identify the components individually, making a homogeneous mixture. An example for an inhomogeneous case is making your favorite marinating sauce recipe and including pepper grains; you can distinguish the mixture ingredients (pepper from the rest) with unaided eyes. If you decide to make a marinating sauce that uses vinegar and olive oil, however, you notice that they do not mix, maintaining an independent coexistence with the pepper grains. This is an example of a heterogeneous mixture. Here, you are using two completely different non-mixing ingredients. If the mixture's thermal properties are not available, one way to approximate them is to use a rule of mixtures. It provides an estimate of the property from the sum of products of individual component property values and the corresponding mass fractions.

Spatial properties can change within a geometry or specific domains within a geometry. This introduces inhomogeneities in properties (e.g., physical and thermal). The change can be spatial (non-isotropic, e.g., varying thermal conductivity as a function of the location or direction), thermal (e.g., change of specific heat capacity with temperature), or temporal (as can happen in a living organism).

Properties that are expressed per unit length (e.g., thermal conductivity—W/mK) or length squared (e.g., elastic modulus—Pa = N/m^2) can also vary depending on the direction within the material. If such variation exists, the material is said to be *anisotropic*. Furthermore, anisotropic materials may be transversely *isotropic* or *orthotropic*. The former has invariant properties within a plane but different properties in the direction orthogonal to this plane. Think of a thin membrane—properties within its plane are the same in all directions, but they are different in the transverse direction. Orthotropic materials have properties which differ along three orthogonal directions. For example, a sheet of rolled steel has different properties in the direction of rolling, in the sheet plane but perpendicular to the rolling direction, and transverse to the sheet plane.

3.2 Thermal Analysis of Materials

In the context of this section, *thermal analysis* refers to the evaluation of material properties as a function of the temperature. This meaning should not be confused with another common usage of *thermal analysis* to describe heat transfer modeling. Thermal analysis describes the thermal response of a system as a function of the predictors affecting this response. These predictors may be material characteristics—such as thermo-physical and optical properties—or process parameters that describe the system's operational conditions.

A material's thermo-physical properties are typically obtained using experimental thermal analysis techniques—occasionally in combination with the simulated analytical or numerical models of the same experiments. For example, Differential Scanning Calorimetry (DSC) is employed in order to characterize the heat capacity of the material as a function of the temperature during a heating cycle. In this method, the heat required to increase the temperature of the sample is recorded for both the part, whose property is of interest, and also a reference part with known properties that is exposed to the same heating cycle. A similar approach is taken in a Differential Temperature Analysis (DTA), where a reference material and the material whose properties are to be investigated are exposed to identical thermal cycles, and temperature differences between the two are recorded against temperature and time to identify the exothermic or endothermic reactions.

The Thermogravimetric Method (TGM) is used to record changes of the sample's mass as a function of the temperature. This method is used to determine the degradation temperature, which is the temperature at which the sample's mass starts decreasing, and it is used to determine the upper limit of the material's processing temperature. In methods such as evolved gas analysis, the material is exposed to heat and, as a result, the time at which it starts to evaporate (i.e., generate gas) along with the composition of the released vapor can be recorded. This method combines the DSC and TGM technology with a Quadruple Gas Spectrometer (QGS).

In Thermomechanical Analysis (TMA), changes of the sample dimensions with temperature are examined (thermal expansion). The sample is exposed to a small load, and the variation of a linear dimension when exposed to a heating cycle is recorded to measure strain. From this data, a material's elastic (e.g., tensile modulus) or viscoelastic properties as a function of the temperature are obtained.

The thermal expansion coefficient—defined as a derivative of a specimen's relative volume change with respect to the temperature—is another thermal material property that is useful in applications such as the making of thermometers using mercury, for example. The equipment used to measure this property, known as the *dilatometer*, identifies the expansion of the mercury as a function of the temperature to create a thermometer with a graduated scale.

There are applications in which the thermal response to environmental conditions needs to be examined to determine properties such as *thermal setting*—setting of material properties by exposing the matter to specific temperature patterns, for example, pottery clay—and viscoelastic behavior of materials. In these scenarios, the response of the sample to sinusoidal electric and mechanical fields (for the former and latter cases, respectively) causes the temperature of the part to vary during the test, which results in measuring the process derivatives such as permittivity and strain. These properties are then used to deduce the desired information such as the setting behaviors of adhesives and paints.

Occasionally, a combination of several thermal properties is investigated. For example, thermal diffusivity can be determined versus the temperature using the Laser Flashing Analysis (LFA) technique. In this method, the part is exposed to a heat pulse on one side, and the temperature increase on the other side is measured versus the time.

Note that in an endothermic process, heat (energy) is absorbed from the surroundings and the surroundings are cooled as a result. The term *endothermic* is from the Greek for *endon* (within) and *therm* (hot). Thus, the process needs heat to take place. In an exothermic process, heat is released into the surroundings and causes the temperature of the surroundings to increase. The term *exothermic* comes from the Greek words *exo* (outward) and *therm* (hot).

An example of an exothermic process is the food that is heated inside a special self-heating packaging that hikers use or the care bag you pack with you for the next Mars expedition. The package consists of multiple layers. The food or drink can be located anywhere inside the interior or exterior of the package. The heat is generated after the membrane between the heating substance (e.g., calcium oxide) and water is removed and the two are mixed. Examples of endothermic processes include water phase changes from solid to liquid (melting) and gas (evaporation) and photosynthesis. Examples of exothermic processes comprise water phase change from gas to liquid (condensation) to solid (freezing) and any combustion process (e.g., burning of coal).

Combustion is fast oxidation of a combustible material. Therefore, slow oxidation (e.g., rusting of your car's muffler) does not comprise an exothermic process. Combustion involves the mixing of a combustible material (such as gasoline or wood) with an oxidant (typically oxygen found in air) in an appropriate ratio, with the combustion process then initiated by the introduction of sufficient heat to start the reaction, which then becomes self-propagating, until either the fuel or the oxidant are no longer available.

Typically, combustion produces water (H_2O), which is a product of oxygen in the air and hydrogen found in combustible organic compounds. For a stoichiometric (i.e., complete) combustion process, just the right ratio of oxygen is available for the given quantity of combustible material so no excess oxygen is generated nor carbon monoxide produced due to an incomplete combustion. Since the process releases a large quantity of heat, the temperature of the reactants (the inputs to the chemical process) may increase by over a thousand degrees Celsius. This is called the *adiabatic flame temperature*, and the released heat is the heat of combustion. This heat is the difference of the enthalpy of the products and reactants (given the temperatures at which they interact), and no other form of energy in the form of work or heat is generated or consumed from the system (adiabatic process). The adiabatic flame temperature is the maximum achievable temperature during a combustion process.

Thermo-Optical Analysis (TOA) is another method in which optical properties of the material (e.g., emissivity) are measured versus the temperature. Note that the emissivity is defined as the percentage of the received energy that is emitted from the body. Employing a black heat source whose emissivity is known and increasing its temperature while looking at the black body source through the camera, one can calibrate the infrared (thermal) camera. This calibrated camera then may be used to measure the emissivity of any material (e.g., plastic parts) as a function of the temperature.

Thermal cameras are a very useful tool for directly observing the temperature distribution of any experimental sample over time. These cameras can either generate the raw data in the form of object signals, which can then be translated into the temperature (using a black body source), or the temperature data are directly output by internal translation of the raw data using built-in formulae. To ensure the built-in formulae translate the raw data correctly, the infrared cameras should be sent out to the manufacturer for calibration as specified by manufacturer. The user can also calibrate the camera, but this is different from the calibration offered by the manufacturer, which involves making changes to the camera's internal parameter values. To calibrate the camera by the user, a black body heat source is used, as described previously for the TOA application.

3.3 Modes of Heat Transfer

Dependent variables are the driving forces for defined physics. When modeling *Heat Transfer* physics in solids and fluids, temperature is the dependent variable. This is analogous to pressure being the dependent variable when modeling fluid flow. Heat is transferred from the point with the higher temperature to that with the lower one. Fluid moves from the point with higher pressure to that with the lower one. Heat or fluid movement continues until all points reach an equilibrium state, meaning that their temperature or pressure equalizes.

The dependent variable is to be measurable so that the derivative may be calculated. In order for heat flow to be determined, temperature is the state variable. The variation of temperature throughout the matter—either in the form of solid or fluid—is either time-dependent (temporal) or space-dependent (spatial). The gradient of temperature (i.e., spatial variation) results in heat conduction—from a region with a higher temperature to that with a lower temperature. The rate at which this equalization takes place is proportional to thermal diffusivity and the second spatial derivative of temperature. As you recall, thermal diffusivity is the ratio of heat conductivity to the product of density and specific heat capacity. This property is the characteristic of the material that explains the variation of temperature within matter over time (i.e., transient temperature).

The mechanism of heat transfer depends on the medium in which the heat is being transferred. On the microscopic level, matter is made of molecules and atoms. The main difference between the gas and solid states of matter is the proximity of the molecules. The relative distance between the matter's molecules can be characterized by a statistical thermodynamics concept known as the *mean free path*. *Knudsen number (Kn)*, defined as the ratio of the mean free path to the characteristic length, is a dimensionless number that defines the scale of a physical system, effectively describing the molecular level of freedom. This freedom is greatest for molecules in a gaseous state. *Knudsen number* less than one characterizes a fluid in a state of continuum flow, values equal to one are associated with *slip flow*, and values greater than one define a *free molecular flow*.

When a continuum nonslip flow passes over a wall (i.e., any solid boundary), the magnitude of the flow velocity adjacent to the wall will be zero, while for a slip flow this value is not zero, since the fluid can slide relative to the wall. The parabolic velocity profile associated with the continuum flow passing over the wall changes to a linear profile in a free molecular flow, meaning that the flow velocity, starting at a nonzero magnitude at the wall, changes (increases) linearly with increasing distance from the wall.

The mechanism by which the heat is transferred depends on the material state. The heat transfer is achieved primarily by the mechanisms of conduction and radiation. For conduction to happen, either in its pure or subsidiary forms (such as convection), molecules need to be present. While in the radiation form, electromagnetic waves are the energy-transmitting agents and no intervening molecules are needed. This is how the Sun's radiant energy reaches the Earth's atmosphere and passes through the atmospheric layers to be absorbed by the planet's surface. This is also the reason spacecraft, such as Soyuz (Сою́з), for example, need to be covered with thermal blankets—they protect the spacecraft from overheating. When spacecraft designers need to estimate the intensity of solar radiation at any location in space, they use *isohels*—lines of constant solar radiation (just like *isotherms* are lines of constant temperature on weather maps). They use such data in thermal modeling of satellites in planetary orbits. Excessive heat in any of the planetary explorative equipment caused by the Sun's radiated energy may damage the electronics and main structure—in addition to the indirect adverse effects on the human body—but it can also be harvested to generate electrical power for the onboard equipment.

For solids, in which molecules are in close proximity to each other, the conduction mode of heat transfer is dominant. For molecules flowing in the form of a fluid (i.e., liquid or gas), heat transfer takes place by means of advection, which is the combination of convection and conduction due to the fluid flow and also the solid surface they may come in contact with. When a gas comes in contact with a solid, a hybrid heat transfer mechanism results—a combination of the conduction and convection heat transfer modes, both in the solid and liquid as well as their interface. Additionally, the momentum of the fluid bulk transfers some of the energy in the form of heat.

In the three main modes of heat transfer (conduction, convection, and radiation), temperature difference is the driving force. Heat transfer occurs from the point of higher temperature to that of the lower one, until the temperature equalizes among all regions and the rate of heat transfer approaches zero, reaching the state of thermal equilibrium. If there are also no internal forces due to thermal effects in any part of the system (*mechanical* equilibrium), no chemical reactions or movement of reactants (*chemical* equilibrium), and no temperature difference between the surroundings and system (*thermal* equilibrium), *thermodynamic* equilibrium is reached. In this condition, no spontaneous change occurs.

3.3.1 Conduction Heat Transfer

Temperature difference is the driving force for the movement of heat energy; heat is transferred from the location with a higher temperature to that with a lower one. This heat flow rate (q in W = J/s) depends on the heat conduction coefficient (k in W/mK), which is the proportionality factor, area of the body normal to the heat flow (A in m^2), and temperature change (dT in K) with respect to the distance (dx in m). This is described by Fourier's equation—$q = -kA(dT/dx)$. Thermal conductivity depends on the material and demonstrates how fast the molecules get excited and show signs of increased activity as temperature increases. Metals have higher thermal conductivity compared to nonmetals. The closer the molecules are to one another, the easier it is for them to transfer their motion, which corresponds to thermal energy.

The heat conduction transfer direction is along the direction of the temperature gradient. Temperature gradient is a vector. For three-dimensional space, each of the vector's three components is obtained by calculating the derivative of temperature with respect to the distance along that component. Thus, a vector (dT/dx, dT/dy, dT/dz) is obtained in Cartesian coordinates. The area that is normal to the heat transfer gradient vector is considered when calculating the total power passing through a plane. For example, if the heat transfer along the x-coordinate is to be determined, the *y-z* plane is perpendicular to the heat transfer direction and therefore the surface to which the heat flux density is applied.

3.3.2 Convection Heat Transfer

Newton's law of cooling, which describes the convection heat transfer mode, states that heat transfer is a function of the difference between the surface temperature of a solid in contact with the fluid (T in K) and the bulk temperature of the fluid surrounding it (T_∞ in K) —$q = Ah(T - T_\infty)$. In this equation, A is the area of the convective surface (m^2) and h is the convection heat transfer coefficient (W/m^2K) that depends on bulk flow characteristics, such as its velocity; it determines the magnitude of the heat flux between the fluid and the solid. Surface characteristics such as roughness or position also affect this heat constant. It is expected to be greater for a vertical surface (due to the gravity effect, more pronounced at higher temperatures) versus a horizontal surface under the same conditions.

Occasionally, the bulk temperature is assumed to equal the average temperature between the wall surface temperature and the flow temperature at a distant location, if this temperature difference is considerable. The factors that make this proportionality an equality are the area of the surface and a proportionality coefficient that is called the *convection heat transfer coefficient*. For a motionless fluid, this coefficient may be obtained from experimental observations. For example, for a horizontal wall adjacent to an air volume, this coefficient is about 5 W/m^2K, while for a vertical wall, this value is about 10 W/m^2K. The larger the coefficient of the convective heat transfer, the larger the heat transfer is from the surface to the environment. The reason is that the heat transfer is facilitated by the flow in the proximity of the vertical surface, where the fluid can move freely due to its buoyancy. A wall which is colder than air will cool it; a hotter wall will heat the air. Since the cold air is denser, it will move downward, while the warm air will move upward, creating an airflow in the vicinity of the wall which would promote the heat transfer and would be represented by the higher h value. The horizontal surface, however, generally exhibits a lower heat transfer rate.

The mechanism of convection heat transfer that occurs only due to the natural buoyancy of the fluid is called the *free convection*. In this case, when the solid surface comes in contact with the fluid, no additional mechanism exists to facilitate the heat transfer. An example is warming a room by hot-water radiators. In *forced convection*, on the other hand, the fluid flow in the vicinity of the surface is facilitated by mechanical means, such as fans. An example is heating a room by means of an electric heater with a built-in fan. Forced convection may increase the convection heat transfer coefficient by a factor of 10, to about 100 W/m^2K or more.

3.3.3 Radiation Heat Transfer

Radiation is the mode of heat transfer which does not require a physical medium for heat to propagate. In this mode, the energy is transferred by electromagnetic waves radiated by one body and absorbed by another. One example of this phenomenon that human beings are all very familiar with, and one we all depend upon for our very existence, is the radiation emitted from the Sun and received by the Earth. This radiation is emitted in a broad range of wavelengths but, because of the atmosphere, only part of that broad spectrum reaches the Earth's surface and the intensity is reduced (to about 1,000 W/m^2 on average).

Being an electromagnetic wave, solar energy travels through space at the speed of light (3×10^8 m/s). To understand the concept of electromagnetic energy waves, imagine throwing a stone into a still lake—the wave ripples will radiate in all directions along the water surface from the point where the stone hits. If you imagine being stationary over any point by which the wave passes, you can measure how many waves pass that point per second—this gives you the frequency. If you freeze the motion for an instant and measure the distance between the wave crests, you will get the wavelength. Measuring the speed at which the wave crests move by you gives the propagation speed. These three quantities can be related by an equation—$c = \lambda\nu$, where c is the speed of light (m/s), λ is the wavelength (m), and ν is the frequency (1/s or Hz).

Any body at a temperature higher than absolute zero emits the thermal radiation. The Stefan-Boltzmann law describes the emitted energy (q in W) as proportional to the difference between temperatures, each raised to the fourth power. One temperature is that of the emitting body (T in K) and the other of the surroundings (T_∞). This energy is also proportional to the emissivity of the emitting body (e, dimensionless), the Stefan-Boltzmann constant ($\sigma = 5.670374419 \times 10^{-8}$ W/m^2K^4), and the area of the emitting body surface (A in m^2)—$q = A\sigma\varepsilon(T^4 - T_\infty^4)$. The emissivity property is a proportionality constant that describes how good a body is at emitting the thermal radiation, as determined by its optical and surface properties, and it can vary from 0 to 1.

Radiation heat transfer can be also modeled similar to a convection heat transfer approach. An equivalent convective heat transfer coefficient can be associated with the summation of the temperature squares of the two bodies multiplied by the Stefan-Boltzmann constant—$h_r = \sigma\varepsilon(T^2 + T_\infty^2)(T + T_\infty)$, where ε is the emissivity of the receiving body.

Emissivity is the percent of the incoming radiative energy that leaves a surface. Depending on the size of this surface and how it is situated with respect to other surfaces, this energy is distributed to the external entities (surfaces). An object that emits whatever energy it receives is known as the *black body* and has an emissivity of one. For this body, the emission and absorption of light are equivalent through Kirchhoff's law, which describes how the radiative energy is emitted as a function of the wavelength. The total spectrum (all wavelengths) of emitted energy is expressed by the equation shown in the previous paragraph, integrated over the entire spectrum forming the black body radiation.

A *cavity* is an example of a black body. A pinhole cavity functions as a light trap; as the light passes through its opening, it hits the opposite surface, and then it continues bouncing within this cavity until its energy is fully absorbed. The walls of the cavity are assumed to be opaque to the incoming radiation beam, meaning that it will not allow any light to escape. A black body radiates energy in all directions in equal fashion, so the radiation intensity is both independent of the direction (diffuse) and wavelength (gray). There are cases in which the emissivity of the surface is large while the absorptivity is small. An example is white paint, with large emissivity of about 0.93 and a low absorptivity of about 0.16. This is why the roofs of some houses in arid regions are painted white—this provides effective thermal management. In the same way, a white car should be cooler than a black one if both are left parked outdoors on a sunny summer day.

When modeling the radiation mode of heat transfer, one can think in terms of the surfaces and the media. Radiative energy can be emitted by a surface or medium. It can also be absorbed by these. In a model, any component can be designated as opaque (and thus not able to transmit radiation).

Surfaces can absorb or emit. The absorption is a function of the wavelength of the radiation and the incident angle. Emission can be *diffuse* (multidirectional) or *specular* (when the radiation is reflected without scattering). The medium between the surfaces can completely *transmit* the radiation (like air or a vacuum), it can partially *absorb* and *reflect* the radiation, it can absorb and *scatter* the radiation, or it can be *opaque*. To model the radiation, one needs to calculate the radiative energy reaching the surface as well as leaving the surface. The simplest case is that of a surface facing the ambient (surroundings). If the ambient is cooler than the surface, the surface will lose heat, and vice versa.

Things get more complicated when there are surfaces that can *see* one another. Consider for example a brick-shaped block. Figure 1 illustrates such a block by a 2D rectangle. A block will have six surfaces. Each surface can either face the interior or exterior. Four surfaces, marked by letters from "*a*" to "*d*," are identified in the figure. An external point heat source (like the Sun) is also shown.

Some surfaces will be visible to this radiation source ("*b*" and "*c*" exterior) and some will not (both sides of "*a*" and "*d*," the interior of "*b*" and "*c*"). Also, each point on a surface can see some surfaces but not others. The exterior "*a*," "*b*," "*c*," and "*d*" surfaces in the example cannot see each other. They are on a convex surface where this is always the case, like an exterior of a sphere. The interiors of these four surfaces can all see each other, which is the case for concave surfaces (like the interior of an ellipse). For more complex shapes and a greater number of objects, there will also be shadowing to account for.

If a surface is visible from any point on another surface (such as Point "1" on the interior of "*a*" in the figure), the radiation it receives from the surfaces that it *sees* will also depend on the angle between the line from this point to the point on that surface. This is accounted for in a *view factor* calculation. The view factor is the percent of the energy sent out, which is received by the other object.

Thus, Point "1" will see *less* of the infinitesimal surface patch at Point "3" then at Point "2", since the incident angle is smaller for Point "3". It is

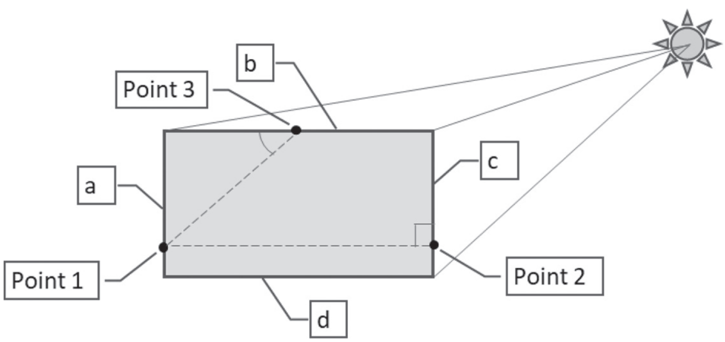

Figure 1. An illustration showing the concept of view factor in radiation heat transfer.

for the same reason that there are seasons on the Earth—the tilted Earth axis means each hemisphere will see larger or smaller angles of incidence between the Earth's surface and the Sun during the year.

To calculate how much heat is lost or gained by the surface, one needs to integrate over all the other visible surfaces. This means the larger the surface area of a receiving body is, the higher percentage it receives of the total energy sent from the emitting body.

3.4 Energy Conservation

When solving numerical models, either FDM or FEM, the conservation of energy principle must be applied to all elements or nodes. For nodes, the total energy of zero confirms that the balance of energy at each node has been met, meaning that the total nodal incoming energy equals the total outgoing energy. Since an element occupies a line, area, or volume, as determined by its spatial dimension, the balance of energy should still be satisfied; however, in this case, the total elemental incoming energy should equal the total outgoing energy. The outgoing energy is the incoming energy plus the variations of the energy along the length where the energy is transported, expressed in the form of the derivative of the energy along the direction of transportation. This energy balance applies along each of the three coordinates (x, y, and z).

For transient analysis, where the temporal variation is desired, the time predictor is considered either as an additional coordinate to the three spatial ones or as a separate variable where it influences the thermo-physical properties—expressed in terms of the temporal variation of the boundary conditions. An example is the definition of the *volumetric heat generation* term for the case of a laser contour welding process, where the profile of the heat source changes along the x, y, and z-coordinates and also varies with time (since the beam is scanning the part). The heat source can be applied cyclically—turning on and off—to study the effect of the heating and cooling (after the heat source is no longer active). The time-varying volumetric definition of the heat source, either in the form of heat generation inside the geometry or boundary conditions applied to the internal or external borders, follows similar rules. They are formed by a hierarchical buildup and can be likened to "lines," "paragraphs," "pages," and "chapters" of a "book" [98].

The following analogy may be useful when you create a script for the input file that may be used as the input to some FEM commercial software such as ANSYS. Assume that your simplest form of heat generation term is a constant value. This constant value can be applied per volume of solid at any desired coordinate; therefore, it is expressed in W/m^3. Now, let us assume the heating term varies along a certain coordinate (e.g., x-coordinate); the heat per unit volume is applicable to all the locations that vary along the desired coordinate. Therefore, it remains constant along the rest of the coordinates (i.e., y- and z-coordinates).

This is similar to defining an array for the heat generation term within the problem (the "line" of the "book"). If you have multiple arrays, meaning that this time you are presenting variations along a new coordinate (e.g., y-coordinate), you are forming a matrix (n_y rows and n_x columns). Each such matrix is a "page" of the "book". Putting multiple "pages" together, you make a "chapter"; this adds the dependency on the third coordinate (i.e., z-coordinate). This "chapter" represents the heat generation in your model at a certain point in time. If the heat generation changes over time, you define a new "chapter" at each chosen time interval. A "book" is created as a result. In most cases, the latter is done by defining new files, each presenting a time-related event. Each "chapter" can be stored as a separate file, as it is more convenient to keep the three spatial coordinates together in one file.

The events may include any time-related process, changing the status of the system or control volume. For example, it can be turning on and off a heat source (e.g., inserting LED lights in an oven in order to cure the adhesive by which they are attached to a substrate). It is possible for the time-related effects to be observed during any transient analysis. For example, the process of curing the adhesive involves gradual heating. After the maximum curing temperature is reached, the part remains in the oven for the setting period and the heat is then turned off, while keeping the lamps inside the oven for an additional cooling period. This gradual cooling after an extended period of heating may cause the formation of residual thermal stresses. These stresses vary with time and employ the temperature distribution at given times as input variables to the stress model. If steady-state stress distribution is sought, the steady-state temperature is fed into the steady-state stress (structural) model.

3.4.1 Energy Balance

Conservation of energy requires that the total energy inputted into and generated within the system is the same as the total outputted from and stored by the system (including the stored energy). Figure 2 shows the schematic of the general form of the energy balance for a continuum—equation (1).

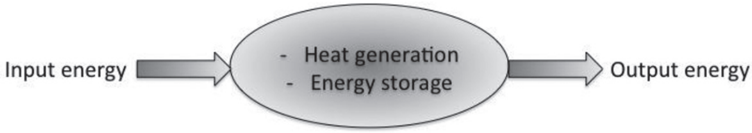

Figure 2. Energy balance diagram for a continuum (e.g., a parcel of air).

$$\dot{E}_{\text{in}} + \dot{E}_{\text{generated}} = \dot{E}_{\text{out}} + \dot{E}_{\text{storage}} \tag{1}$$

The conservation of energy requirement means that the energy balance is to be complied with for any small and identifiable portion (element) of the material that satisfies the continuity of mass, energy, and momentum. Energy can enter and exit the continuum; however, the boundaries remain constant, and so it forms a closed system. The continuum is identified by its size, mass, and thermo-physical properties. Thermo-physical properties may be temporal (transient—change with time), spatial (nonhomogeneous—change with direction and location within the geometry), temperature-dependent, or constant.

Energy is defined in different forms inside this environment. It is either in the form of heat entering the continuum by conduction, heat generation (HG) inside the continuum, changes of internal energy (or energy storage), or heat leaving the continuum by conduction. The heat leaving the continuum by conduction is the same as the heat entering the continuum by conduction plus the spatial variations over the length of travel $(E_{x+dx} = E_x + (dE_x/dx)dx)$, and it is time-independent (steady-state). The internal energy on the other hand is time-dependent (transient); it represents the variation of internal energy (or energy storage) expressed in the following form, using the thermal capacity of the continuum—$mc_p(dT(x,y,z)/dt)$, where m is mass (kg), c_p is specific heat capacity (J/kgK), T is temperature (K), t is time (s), and E is energy (J).

3.4.2 Energy Balance Diagram

Energy balance for the case studies presented in this work is set for a system where mass does not enter or leave the system boundary—only energy in the form of heat and work does. There are some cases in which mass crosses the boundary as well—this is a control volume (versus the system) problem. The boundary of a system may expand or contract. For a control volume, however, both energy and mass may enter and leave the boundaries that do not expand or contract. Your body as a source of heat, the sensible heat you experience transported by sweat, a rush of blood, and tears, is a control volume, with the possibility for organic fluids entering and leaving the body parts. Each body part has a set boundary that essentially does not change, though it may expand or contract.

Geometry in which heat transfer takes place can be defined by Cartesian coordinates in 1, 2, or 3 dimensions. For some 3D shapes, cylindrical or spherical coordinates can facilitate the modeling task. There are a number of scenarios where the model can be simplified by reducing the number of dimensions. One scenario is the case where the length of the plane transverse to the heat transfer direction is large compared to the other dimensions (including the dimension along which heat is transferred); the heat transfer along that direction (transverse to the heat transfer direction) can be ignored. This is where a 3D model can be simplified to a 2D model.

Experimental correlations have been the basis of many thermo-fluid formulae. In this approach, tests are carried out to investigate the influence of the change of a single parameter or number of them on a control volume or system. The parameters can be either thermo-physical properties of the material such as heat capacity and thermal conductivity or temperature-induced ones such as stress, creep and oxidation lives, magnetic fields, and phase change. In a complex system such as a heat exchanger, water temperature, pressure, and velocity are the determining factors for heat transfer mechanisms and its efficiency as well as flow regimes.

Experiments need to be conducted in order for the mathematical correlations representing the physical phenomena to be derived. The following are the steps involved: (1) conception of ideas, (2) setting objectives, (3) identifying design approaches, (4) establishing pros and cons of each technique, (5) selecting the approach that is best suited to the objective of the tests given the resources, (6) designing the experiments, (7) conducting the tests, (8) collecting relevant data, (9) analyzing the data objectively, (10) reporting analysis results, (11) presenting analysis results, (12) publishing analysis to share with peers, (13) presenting a technical version of research findings, and (14) presenting a scholarly consumable (but not necessarily specialist) version of research findings.

When analyzing data, the relationship between the parameters is identified to the best knowledge of the experimenter. One must be careful to avoid prejudices during the analysis so that they will not affect your judgment. With an open mind, an experimenter can extract new unexpected findings from the data that may contradict established theories. Examples include the discovery of the element Polonium by Marie (and Pierre) Curie and the *theory of black hole radiation* by Stephen Hawking; they either challenged previous findings or set the platform for future challenges.

Theoretical relations derived from experiments show a parametric relationship between two or more variables affecting the experimental outputs; for example, they identify that selected critical variables are directly or inversely related through different mathematical functions (e.g., linear, quadratic, and polynomial). The parameters that make this connection between the test results and mathematical models are correlation factors, which can be material-dependent (e.g., conductivity in Fourier's law) or not material-dependent (e.g., the convective heat transfer coefficient in Newton's law of cooling). The correlated value obtained from this analysis identifies the thermo-physical property of the material.

An example is *Nusselt number* used to obtain the convective heat transfer coefficient employed in Newton's law of cooling. In some cases, the correlation value is a constant parameter, which may be of general significance in physics; an example of such a parameter is Stefan-Boltzmann's constant that correlates radiated electromagnetic energy to an object's temperature in Stefan-Boltzmann's law. There are cases in which no exact mathematical relations can be achieved by fitting an experimental relationship into a theory; this is the definition for an *empirical* relationship. Examples include the release of magnetic energy during a solar flare, heat transfer in external flows, and shear stress in non-Newtonian fluids.

Figure 3 shows the general form of conservation of energy, including all modes of heat transfer. The radiation and convection terms shown are applied at the exposed boundaries. As in other disciplines, such as forces in solid mechanics, the energy conservation law can be expressed separately

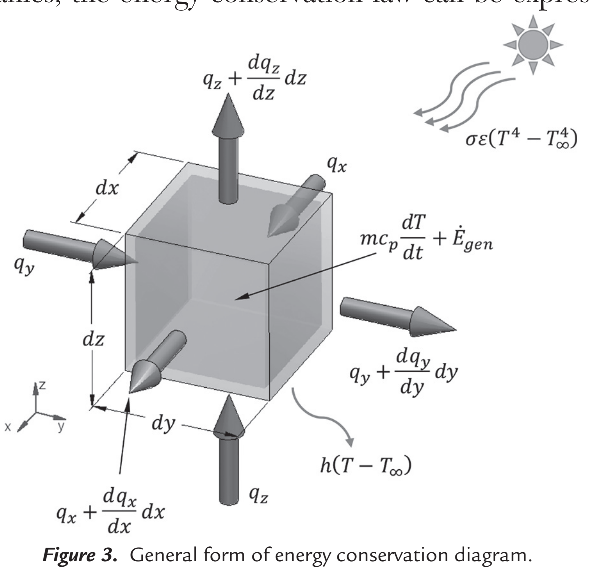

Figure 3. General form of energy conservation diagram.

for each x, y, and z direction (m)—equations (2) to (8). A matrix can then be created that is a linear combination of the conservation in three dimensions in addition to the time component. T, q, k, dx, dy, dz, and t are temperature (K), heat flux (W/m^2), thermal conductivity (W/mK), distances in the x, y, and z directions, and time (s), respectively. The heat flux defined by equations (2) to (7) is proportional to the temperature gradient (dT), where the conductivity (k) is the proportionality constant. Equation (8) shows the rate of energy change as a function of the variation of internal energy ($\dot{E}_{\text{internal}}$ in W) over time and energy generated inside the material due to any heat source or sink ($\dot{E}_{\text{gen}}$ in W)—m is mass (kg), and c_p is specific heat capacity (J/kgK).

$$q_x = -k_x\left(\frac{dT}{dx}\right) \tag{2}$$

$$q_y = -k_y\left(\frac{dT}{dy}\right) \tag{3}$$

$$q_z = -k_z\left(\frac{dT}{dz}\right) \tag{4}$$

$$q_{x+dx} = q_x + \left(\frac{dq_x}{dx}\right)dx \tag{5}$$

$$q_{y+dy} = q_y + \left(\frac{dq_y}{dy}\right)dy \tag{6}$$

$$q_{z+dz} = q_z + \left(\frac{dq_z}{dz}\right)dz \tag{7}$$

$$\dot{E}_{\text{internal}} = m\,c_p\,\frac{dT(x,y,z)}{dt} + \dot{E}_{\text{gen}} \tag{8}$$

Substituting the previous relations into the energy balance in equation (1) results in equations (9) and (10), where spatial and temporal temperature profiles are related to the change of internal energy and heat generation within the material. $\dot{q}_{\text{gen}}$ is volumetric heat generation (W/m^3).

$$\left(\frac{dq_x}{dx} + \frac{dq_y}{dy} + \frac{dq_z}{dz}\right)dx\,dy\,dz + m\,c_p\,\frac{dT(x,y,z)}{dt} + \dot{E}_{\text{gen}} = 0 \tag{9}$$

$$\frac{d}{dx}\left(k_x\frac{dT}{dx}\right) + \frac{d}{dy}\left(k_y\frac{dT}{dy}\right) + \frac{d}{dz}\left(k_z\frac{dT}{dz}\right) = \rho\,c_p\,\frac{dT}{dt} + \dot{q}_{\text{gen}} \tag{10}$$

3.5 Example—Heat Transfer in a Sandwich

Let us provide an example in which these thermo-physical characteristics may be put to use. Imagine making a FLT sandwich (Fish burger, Lettuce, and Tomatoes). The sandwich is to be made from the bun, tomatoes, lettuce, pickles, and a semi-frozen cooked fish burger. You assemble the sandwich, put it on the baking sheet, and decorate the sheet with vegetables and yams. The ingredients may be sprinkled with some olive oil and maybe a touch of paprika. For this example, let us ignore any chemical reactions among the ingredients. The next step is to set the oven to the desired temperature, preheat the oven, and place the baking sheet inside to cook for the intended period. At the end of this period, you remove the baking sheet from the oven and review the results. You may notice that the vegetables are soft enough with the yams in their saffron-gold condition, almost ready to be consumed, and the bun is charred on the edges. Perhaps you are too hungry to investigate if the fish is cooked enough, but the first bite quickly informs you that the center of the fish burger is not properly cooked.

Even though it is hard to make oneself stop in the middle of eating a sandwich, there is nothing else to do but return it to the oven to ensure that it is properly cooked. You decide to heat the sandwich for another 25 percent of the original heating time. The timer beeps and you approach the oven with trepidation. As you take out the meal, your starving face is frozen by the sight of mushy vegetables, burned bun, and merely OK fish burger. The pickles are not crunchy anymore, the lettuce is all soggy, and the tomatoes have changed to patches of red skin on the fish-burger. The disappointment is written all over your face. You ruined a perfect meal.

Given that a FLT sandwich is one of the best "fast" foods you may choose to have; the ingredients were the best in the market; the assembly was done properly; the oven is an efficient one with a convection baking capability; you are hungry enough to enjoy the food; and your stomach is generally in good working order; the experience is not the best one you have ever had. You launch an investigation and figure out that the input variables (predictors) defined for the process of heating (i.e., heating time and temperature) are to be adjusted so that better results will be obtained in the future.

Your investigation is a methodical one. You are to test three possible levels (increase, decrease, and constant) for the two predictors (cooking time and temperature). This gives nine possible combinations. However, despite your most thorough methodology, you do not end up with an edible sandwich. Reviewing your methodology, you decided to deal with this complex system by looking at each component separately. This time, you choose to adjust the cooking time for each ingredient, and thus place them in the oven in stages and in a certain order—introducing the frozen fish burgers first, adding the potatoes next, vegetables third, and the buns last. The heated ingredients are then combined with the cold pickles, tomatoes, and lettuce to make a sandwich worthy of being written about in a heat transfer report.

The methodology employed to create the perfect FLT sandwich is the method often used when thermally managing the systems that generate heat. This delicious example examines the heat transfer phenomena on multiple levels and may be explained from both microscopic and macroscopic points of view. The method explained previously in order to reach a desired final product consists of multiple steps: (1) variation of the process parameters (temperature and time), (2) physical arrangements of the ingredients, and (3) introducing the ingredients into the process in a particular order. The layers of the sandwich consist of ingredients that have different thermo-physical properties (e.g., thermal conductivities and heat capacities). Depending on the thermal conductivity, the heat is transferred more slowly or quickly through the layers, and depending on the heat diffusivity, it takes more or less time for the heat to be absorbed or dissipated, causing the temperature of the ingredients to rise.

Table 1 shows thermo-physical properties of some food ingredients used in the FLT sandwich. Meat burgers are also presented as a possible substitute for fish burgers. Thermal diffusivity (α in m^2/s), which is the ratio of the thermal conductivity (k in W/mK) to density (ρ in kg/m^3) multiplied

Table 1. Thermo-physical properties of foods in the FLT sandwich [99,100,101,102,103,104,105]

Food	K (W/mK)	ρ (kg/m^3)	c_p (J/kgK)	α (m^2/s) × 1E+07
Bread	0.410	341.75	1420	8.45
Meat burger	0.380	1019.5	3520	1.06
Cucumber	0.620	957	4100	1.58
Fish burger	1.054	1080	2970	3.29
Lettuce	0.625	1095	3700	1.54
Onion	0.420	1110	3770	1.00
Tomato (red)	0.505	565	3980	2.25

by specific heat capacity (c_p in J/kgK), shows the ratio of heat conduction to convection for a transient heating process—$\alpha = k/\rho c_p$. The convection mechanism happens between the solid parts and the surrounding ambient. It is seen that the baked bun has the highest heat diffusivity followed by the fish-burger, while the onion has the lowest value of all. The higher the diffusivity is, the faster the heating process is throughout the material. This is why you would expect that the bread would take a shorter time to heat than the onions or fish burger.

CHAPTER 4

FINITE ELEMENT ANALYSIS

The Finite Element Method (FEM) is a numerical technique in which geometry is divided into a finite number of small pieces called the *elements*. One advantage of defining such elements is that it enables the division of regions into smaller portions that can more accurately represent the associated physics. Element size and shape may vary for regions, depending on the physics they represent. Each element can have its own distinct properties. Elements are in contact with the adjacent elements.

Solving an FEM problem consists of solving m conservation equations, where m equals the number of nodes when there is only one field variable. For each node, an equation is written for each field variable (such as temperature in heat transfer models) in order to find the value for the associated variable at the given location. The field can be defined in 1D, 2D, or 3D spaces. For example, if there are eight nodes with a single field variable (e.g., temperature), eight equations will be required; if there are two field variables (e.g., x and y displacements), sixteen equations will be required (Figure 4).

Each node requires its own boundary and initial conditions. From algebra you may recall that if, for example, you have an equation with two independent variables and would like to solve it to get a unique solution, you will need to solve it in combination with the second linearly independent equation which includes at least one of these two independent variables. Expanding the equation from 2 to m state variables requires m independent equations. The same concept applies to FEMs.

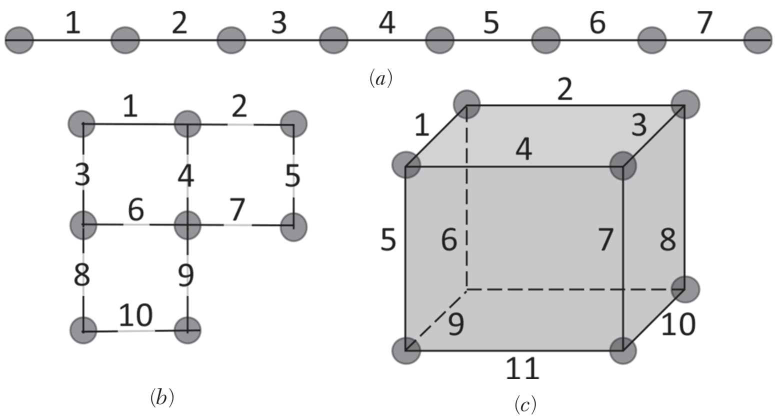

Figure 4. Elements and nodes: (a) 1D, (b) 2D, (c) 3D.

4.1 Material Properties

Material properties are essential constituents of any modeling. One should endeavor to obtain the most accurate material properties possible to assure accurate model predictions. However, obtaining accurate property values is sometimes challenging. Thus, an analyst should be aware of which properties have greater impact on the solution and which have little effect. The relative importance of different material properties may be determined by the thermo-fluid regime, mode of heat transfer, or analysis type. One can use sensitivity analysis methods (see Section 5.4) to determine the effect of uncertainty in any property on the desired model output.

Material properties may vary in space (spatial), time (temporal), or as a function of environmental conditions (environmental). Nonconstant properties introduce nonlinearities and inhomogeneities to the physics that make the problem more challenging to tackle. To describe temperature-dependent material properties, an FEM tool may use a table or a function if the relationship can be described by a function. A table will contain a list of combinations of known temperature-property value pairs. For temperature values between those listed, interpolation is used; this can be a linear interpolation or one of a higher order. If the temperatures in the solution exceed the limits of the range of temperatures for which the property values are given, one can choose to either extrapolate linearly or to keep the value constant, equal to the property value at the nearest extreme point.

For example, the specific heat capacity of a thermoplastic polymer is temperature dependent. The values of this property versus the temperature may be obtained from DSC measurements of the material sample (as discussed in Section 3.2). The relationship thus obtained could then be approximated by listing several key points in a table. The specific heat capacity of water is also temperature dependent. It can be described by a function plotted in Figure 5.

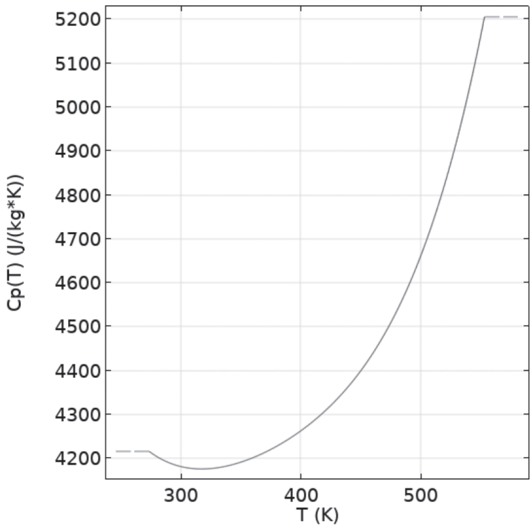

Figure 5. Specific heat capacity of water versus the temperature (diagram created in COMSOL Multiphysics).

Material properties may also vary with the direction in space. For example, if you have a sandwich-like plate structure made up of several layers, it may be modeled as having poor thermal conductivity transverse to the plane of the plate but good conductivity within the plane. If this plate is oriented so that it is parallel to the x-y plane, the following matrix would be used as input to describe its directional thermal conductivity—$[k_x, k_y, k_z]$. For this example, k_x, k_y would be equal and both greater than the k_z value. Position-dependent properties change as a function of the location in space. The property can be defined as a function of the location in 3D—$k(x, y, z)$.

Let us review next the material property settings which may be required as inputs for a physics model set up in a typical FEM software tool. Usually such tools have a built-in library of materials, which may be expandable with optional add-ons. Thus, if the material you need for your model is available within one of these sources, simply selecting it defines common inputs such as density, specific heat capacity, and thermal conductivity. If needed, any predefined properties may be changed, missing properties can be added, or a completely new material may be defined from scratch. For example, thermal conductivity may be defined as an *isotropic*, *diagonal*, *symmetric*, and *anisotropic* property. Note that when performing stationary analysis of a heat transfer model, only thermal conductivity is needed. Density and heat capacity, which combined with thermal conductivity give thermal diffusivity, are not part of the steady-state heat transfer equation.

Fluids have settings similar to solids; one additional property is the *ratio of heat capacities*, which is the ratio of the heat capacity at constant pressure to that at constant volume. This ratio is widely used in thermodynamically reversible processes, especially for ideal gases; for example, the speed of sound within a fluid medium depends on this property. The fluid type may be set to be ideal gas, gas/liquid, or moist air. For moist air, the *vapor mass fraction* (mass of vapor to the total mass), *concentration* (volume of the constituent to the total volume of the mixture), *moisture content* also known as the *absolute humidity* (water content in air regardless of its temperature), and *relative humidity* (water content in air given its temperature) need to be defined. If an ideal gas fluid type is selected, *mean molar mass* and *specific gas constant* are to be defined. In this case, it is possible to choose a specific heat capacity at a constant pressure or the ratio of the heat capacities as an alternative to the ratio of specific heat (per mass) variables. For example, if specific heat at a constant pressure or volume or their ratio are available, one can use thermodynamic relations in order to determine the missing property.

When setting up a radiation problem, wavelength-dependent surface properties can be selected, which are either constant, depending on the solar and ambient conditions, or have multiple spectral bands and hence have wavelength dependence. In most cases for transmitting media, the refractive index needs to be defined. The *refractive index* of a medium is the ratio of the speed of light in a vacuum to that of the medium and is therefore always more than one. For water this value is 1.33, meaning that light travels 33 percent faster in a vacuum than in water. For air, the refractive index is close to 1. A transmitting medium needs to be defined for a domain enclosed by diffuse surfaces that face each other.

The surface-to-surface radiation method is used to model cases where heat transfer by conduction, convection, and radiation are present in combination with radiation from internal or external surfaces. To model this phenomenon, one needs to define several settings. First, the method is selected as *direct area integration*, *hemicube*, or *ray shooting*. In the direct area integration method, the radiation between surfaces is calculated directly, not taking into account the obstructing (shadowing) surfaces, eliminating the surfaces that do not face each other. In the hemicube method, shadowing effects are included. The ray shooting method calculates the view factors given the wavelength and direction. To complete these settings, the radiation integration order, radiation resolution, tolerance, and maximum number of adaptations are set. Solution techniques include setting up the *surface radiosity* that can be linear, quadratic, cubic, quartic, or quantic. Surface radiosity is the amount of radiation flux emitted from the surface given versus the radiation wavelength; it is also known as the *radiant intensity*. There are a variety of techniques in order to estimate this energy intensity, which result in formulae that can be linear, quadratic, cubic, quartic, or quantic functions.

4.2 Geometry

The choice of the dimensions in which physics are set up depends on the shape of the model, boundary conditions, and available time and computational resources. The first question to ask is what kind of information a three-dimensional (3D) model can produce that a two-dimensional (2D) model cannot, or if the physics captured by a 2D model can produce meaningful results. A 3D model may seem a sophisticated choice, but it may be possible to start with a simpler approach to work out the physics and validate the results more efficiently before moving on to a more complex representation of the problem. Remember that for a given element size, the higher-dimensional model will have significantly more elements, leading to longer solution times, a greater amount of Random-Access Memory (RAM) needed during the solution, more disk storage space used to keep the solution, and longer post-processing time for the solution results.

For very large 3D models consisting of millions of elements, the benefit of model dimension reduction can be very significant. Such models may take many days to solve, even if using a High-Performance Computing (HPC) facility. Reducing the model to 2D in such a case will likely bring significant time savings and potentially may no longer require the use of the HPC facility. But even for smaller models, when considering time resources, you may think that there is not much difference between two minutes and thirty seconds. However, one should realize that to fully develop an accurately working numerical model, multiple repeated solutions will likely be needed, numbering in tens if not hundreds of times, so the time savings can add up to a significant number, even for such a relatively small difference.

The simplest model can be of zero dimension; more complex models can be of one (1D), two (2D), and three (3D) dimensions. The zero-dimension approach, also known as the *lumped capacity technique*, assumes that the temperature is spatially uniform throughout the model. In a 1D numerical analysis, one coordinate is required to identify the position of a point and heat is transferred in only one direction (e.g., x-coordinate), meaning that heat transfer along the remaining coordinates, which form a plane, is ignored or heat is integrated over the remaining plane. One advantage of 1D numerical analyses is that they allow comparison with simplified analytical solutions, thus enabling validation of the numerical analysis. In a 2D numerical analysis, two coordinates are needed to identify the position of a point and heat is transferred in two directions (e.g., x- and y-coordinates). In other words, the heat transfer transverse to the active *Work Plane* is ignored or the heat is integrated over the third dimension of the geometry. In a 3D numerical analysis, the most comprehensive approach, three coordinates are needed to represent the position of a point within the geometry (x-, y- and z-coordinates) and heat is transferred in all three directions.

In cases where the geometry, material properties, and boundary conditions have *axial symmetry*, one can reduce the model by one dimension. Thus, for example, a cylinder has axial symmetry, and so this 3D shape can be represented by a 2D axisymmetric model without any loss of fidelity. A 2D shape, like a flat ring, can be replaced by an equivalent 1D axisymmetric model.

Symmetry about a plane can be also used to reduce the model size. For a geometrical shape, such *reflectional symmetry* can exist in 3D space about one, two, or three planes. Again, if boundary conditions are also symmetrical, the model can be reduced to one-half, one-quarter, or one-eighth of the original size, respectively. A similar concept applies to 2D space, where reflectional symmetry can exist about one or two lines.

Another type of symmetry that can be taken advantage of is *rotational symmetry*. Here, the model can be represented by rotating a particular shape m times about an axis, giving an m-fold symmetry. Thus, a shamrock flower can be considered to have a threefold symmetry, while a four-leaf clover has a fourfold symmetry. Such models can then be reduced by modeling only the repeating element.

Some shapes will have multiple symmetries. You can decide which one will be most advantageous to use. For example, a hexagonal nut (ignoring threads) has reflectional symmetry about the three principal planes in addition to a six-fold rotational symmetry (Figure 6). Here you can reduce the model to one-twelfth the size by utilizing the six-fold symmetry together with the reflectional symmetry about the horizontal plane, as shown in the figure. The extra up-front time spent to identify these geometry characteristics is effort well spent, since it forms the foundation of all subsequent steps.

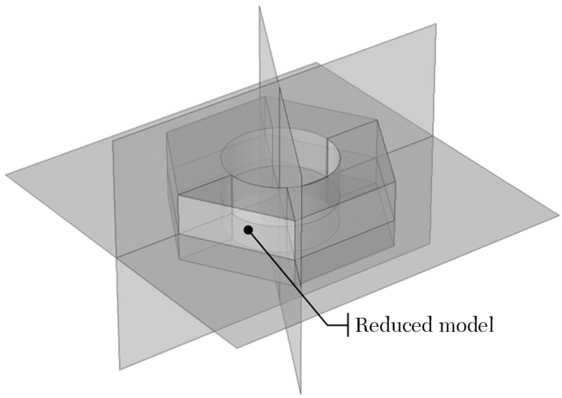

Figure 6. Hexagonal nut shape with symmetry planes.

4.3 Analysis Types

Any set of solution settings for a model may be referred to as the *study*. Analysis type selection specifies whether the study will be time-independent (i.e., stationary) or time-dependent (i.e., transient). A stationary study does not mean that the actual modeled physical system never changes over time but that the analyst is interested in finding out what happens after the system has reached a steady-state condition. This is the state of the system at some theoretically infinite time. In a time-dependent study, the analyst is interested in the state of a system as time passes. If the study is run over a sufficiently long time, for some cases, a steady state may be reached as well. For example, temperature may not rise any further for a given fixed rate of heat input in a thermal problem. A steady state may be reached only if the model boundary conditions are constant. Thus, if the model is exposed to a heat input that increases linearly over time, a steady-state temperature distribution will never be reached.

Selecting the analysis type may also depend on the objective of the analysis. If the analyst is interested in studying the thermal response of a train underframe to fire to make sure it complies with the ASTM 2061 standard for the fire test code for rail transportation vehicles, they will want to study the time response for the first 15 min of exposure time. Knowing that the structure is made of a grade of steel with a softening temperature of 400 °C and a melting temperature of 1,300 °C, and that the fire temperature-time curve has a steep rise for the first 15 min, they would need to perform a transient analysis by which they can obtain the temperature-time history of the structure exposed to fire. The temperature profile as a function of time provides valuable information in this case. It not only provides data on the transient structural integrity of the part when exposed to fire, but also provides an insight as to the areas that need to be structurally strengthened. Such thermal reinforcements can be achieved by introducing additional materials in areas with a minimum of limitation for space and weight to thermally insulate the part or applying intumescent coatings as a fire retardant in areas that are less accessible or have limited space available.

Knowing the transient spatial temperature profile inside the train when exposed to fire will ensure passenger safety by estimating the maximum safe evacuation time at different locations. On the other hand, if the analyst is interested in evaluating the thermal performance of a heat exchanger, they may not be interested in plotting the transient temperature but instead want to identify the spatial temperature profile along a specific path, such as the liquid cooling channel, after the heat exchanger has been operating for a prolonged time and temperatures have stabilized.

4.4 Boundary and Initial Conditions

Just as material properties are important to accurately represent the modeled system, the boundary and initial conditions are important to correctly describe the conditions to which the modeled system is exposed. For heat transfer problems, setting the initial conditions means defining the temperature from which the solution will start. For example, a room temperature of 20 °C (293.15 K) is a typical default starting point. Boundary conditions at the specified boundaries may be defined as insulated (a default always applied automatically), a fixed temperature, a constant heat flux, or as subject to convection or radiation modes of heat transfer. For 2D models, these boundary conditions apply at edges or points; for 3D models, they apply at the domain surfaces, edges, or points.

The boundary conditions are usually known relationships for the elements located at the boundaries. The interior elements do not have conditions of their own unless where specific contact conditions such as contact resistance, internal heat generation, temperature, and heat sink (or source) should be introduced to the interior boundaries of assembled parts. Boundary condition settings can be part of a sensitivity analysis. For example, one can assess the effect of different temperature values for the surroundings when implementing the convection boundary condition.

4.5 Mesh Size and Time Step

FEM involves dividing the geometry into small elements and solving the energy and mass governing equations for each element and for the number of time steps required in order to reach the total analysis time (for transient problems) or steady state (for stationary problems). The number of iterations required for a solution to converge depends on the initial conditions that the solver employs to start the solution, and it may increase or decrease depending on the residuals. Residuals are the estimates of the difference between the calculated and desired values. The temporal and spatial steps can be controlled when setting up the analysis. Spatial step is related to mesh size, which may vary within the geometry. The temporal (time) step is varied by the solver as the solution progresses.

The choice of the element size for meshing in FEM is a little like the choice for image resolution. If the image pixels are large relative to the detail in the picture that you would like to see, you are not going to get a clear image of these details. Thus, a smaller pixel size is needed. However, if you just want to get an overall impression of an image, you may increase the pixel size, reducing the total number of pixels (or elements in FEM). When meshing, unlike in images, you can effectively vary your *pixel* (element) size throughout the model. For example, intense heating processes such as laser welding require fine detail resolution around the exposed regions, where temperature is changing rapidly in space and time, and so require local reduction of the element size and time step.

There are engineering tools such as the Engineering Equation Solver (EES) that may be employed to estimate the optimized time step for a certain element size and vice versa. The user may even create a parametric table to help determine which element size to use with which time step to generate the most accurate results (i.e., by minimizing an error function). A similar approach may be taken by using Microsoft Excel® or MATLAB.

Assume that one decides on the optimized mesh size using one of the said techniques. The next step is to make sure the element size produces converging results that are reasonable. One way to achieve this is to change the element size from larger to smaller values and review the variation of the numerical results (i.e., sensitivity analysis). The sensitivity analysis is usually conducted for the independent variable whose numerical analysis is being performed. If heat transfer analysis is the main focus of the investigation, temperature is the most common independent variable.

It is assumed that the mesh size is sufficiently small if successive size reductions result, for instance, in temperature changes which are judged to be insignificant. For example, if the total temperature change in a heat transfer problem is 10 °C and one is off by 1 °C, it is already a 10 percent error. However, if the former is 100 °C and the latter remains the same, it becomes a 1 percent error. So, if you are modeling the average temperature of the Earth's oceans, an error of 1°C is very significant; however, if you are modeling laser welding of steel, an error of 1°C is acceptable. On the other hand, there is no need to select a very fine mesh over a coarse one if the objective is purely to provide methodology examples for educational purposes. Also, there is no point in refining the solution to 1 percent accuracy if there is much higher uncertainty in other model data, such as material properties or boundary conditions.

Some FEM specialized tools are equipped with adaptive meshing capability. If this feature is activated as the solution is performed, the element size gets reduced at the locations where most attention is required. In a time-dependent study, this element size refinement happens at selected solution time points; in a steady-state study, the solution is performed, the results are assessed, and the solution is repeated after the mesh refinement. The refinement is usually applied at sharp corners, high-stress areas, curvatures, and wall boundaries where fluids interface with solids. In other words, the mesh adapts to the conditions. Activating *Adaptive Mesh* may lead to significant solution time increase, however. Some tools are capable of multicore and parallel features where the solution is divided into sections and solved simultaneously, speeding up the solution and allowing larger models to be solved.

When a meshed model is solved, there are two types of errors: (1) round-off, and (2) truncation errors. The former occurs when one decides to round the number to the closest value, using only the desired number of decimals. The latter case is when one decides to keep only a specific number of decimals. A simple example is to represent 14.647123 as 14.65, 14.64, or 14.647. The first two examples show the same number when it is either rounded off or truncated with two figures after the decimal; the third example could be either rounded off or truncated to the same number when three figures after the decimal are employed. There is a balance between the two errors, especially where they are accumulated due to the increased number of numerical equations, which is the case if the number of elements is increased. They usually show an opposite trend—decreasing versus increasing for the roundoff and truncation errors, respectively. Time step and mesh sensitivity analyses provide good compromises. It is due to accumulation of the previous computational errors that with decreasing element size, after converging to the most accurate solution, the solution may start diverging (i.e., getting less accurate).

4.6 Solution Control and Convergence

Conservation laws are satisfied when solving physics for the heat transfer of any type. Dependent variables are to be calculated using independent variables as well as initial values. Dependent variables are inputted into the model. The equations are solved, and the residuals are obtained. The residuals are the actual sum difference from the zero-sum case. For example, for the energy conservation law to be valid, the total energy entering an element should equal the total energy leaving an element, including energy storage and energy generated within the element.

Ideally, zero residuals should be obtained, meaning that this difference should approach zero. Zero residuals are not normally possible, and so a small nonzero tolerance value needs to be used. If the residuals are below the defined tolerance, it means a solution considered as “good enough” has been achieved. This is where the iterations stop and the solution step has converged to an acceptable value that can then be used as input for the next step for a transient analysis or as a complete solution, as in a steady-state analysis. For instance, if a user sets a 10^{-5} tolerance value for a solid heat transfer analysis problem, most probably they will be happy with the results: the solution should converge to reasonable values and in a reasonable time. However, if the user were to employ the same tolerance for a flow problem, there is a good chance that the analysis may require an excessive number of iterations, leading to very long solution (convergence) times or in some cases to not converging at all; ill-conditioned solutions may be another consequence of incorrectly setting the tolerance. They may then decide to relax the tolerance to, say, 10^{-3}. Thus, the tolerance value setting should be chosen with care.

Figure 7 is an example of a convergence plot for a single-parameter time-dependent analysis. It shows the reciprocal of step size versus time for a transient analysis using a logarithmic vertical scale. Step size identifies the time in between the analysis steps required for accurate computation of the solution. A new data point is added to the plot at every iteration while the analysis progresses. The user is also able to view the message console under the convergence plot providing information related to the previous steps taken before running the analysis, such as number of degrees of freedom, number of domains and boundaries, number of domain elements, the name under which the file was saved, and solution time in seconds. The figure shows a window of the convergence plot, together with the *Messages* tab below it.

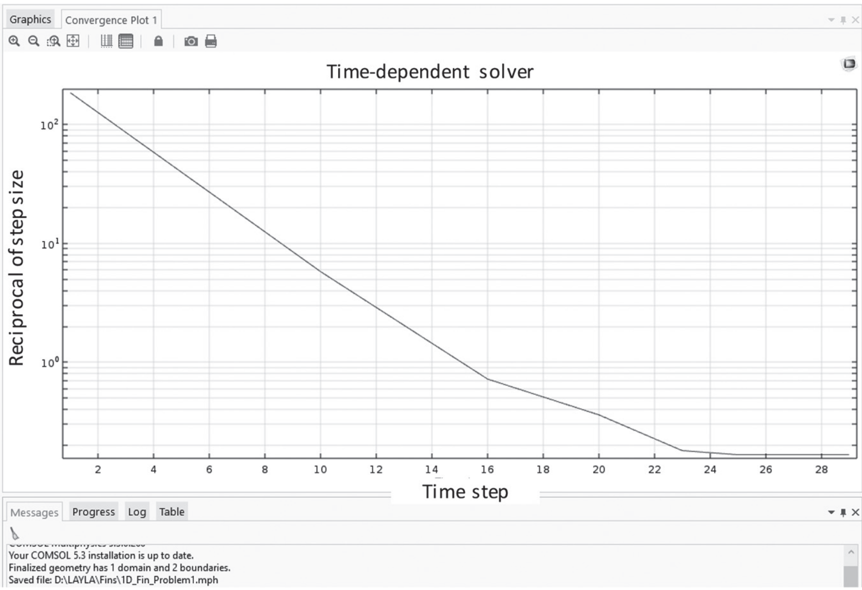

Figure 7. Example of a convergence plot (Reciprocal of step size) for a 3D analysis for a heat transfer model.

Figure 8 is an example of a convergence plot for a parametric analysis, showing the reciprocal of step size versus the iteration number. This type of analysis, which investigates the sensitivity of the model to different parameters, will be discussed in Section 5.4. Each plot represents data (the reciprocal of the step size versus the time for a transient analysis) associated with a new set of parameters that are added to the diagram with every iteration as the analysis progresses. If the analysis were stationary, there still would have been the same number of plots as the number of cases selected to explore variable variations.

Figure 9 is an example of a convergence plot for a parametric analysis, showing error. Data (error versus the iteration number for a steady analysis)

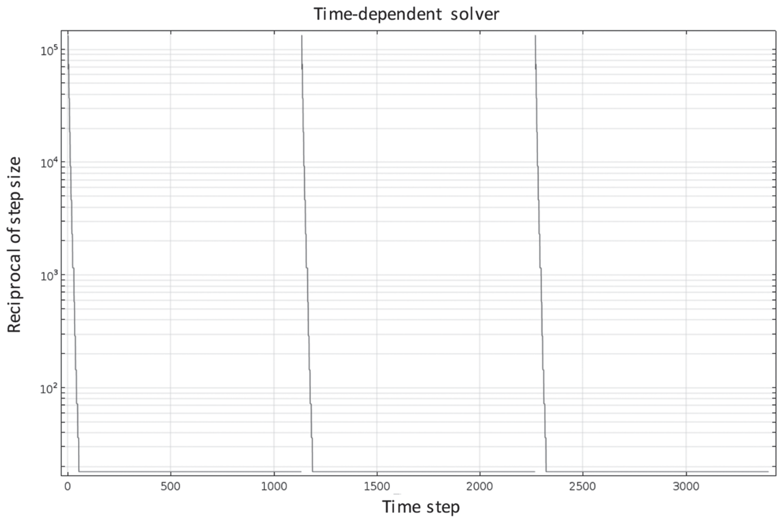

Figure 8. Example of a convergence plot (*Reciprocal of step size*) for a parametric study for a 3D analysis for a solid heat transfer model.

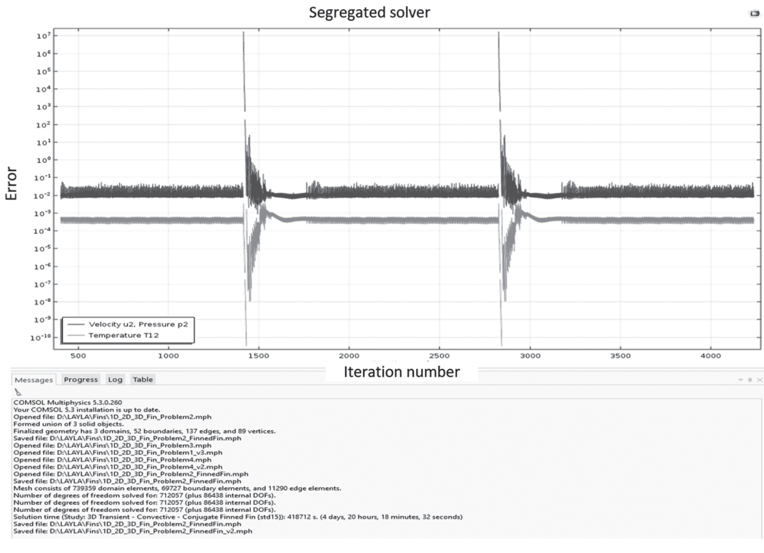

Figure 9. Example of a convergence plot (*Error*) for a 3D analysis for a conjugate heat transfer model.

has been presented using a linear scale. This is a multiphysics analysis including solid heat transfer and non-isothermal physics, with plots showing velocity-pressure (upper curve) and temperature (lower curve). Depending on the type of flow analysis, the user may display additional plots such as one associated with a segregated solver to represent dissipated turbulent energy that is supposed to converge to the equivalent temperature-related one for the acceptability of the results. The plot is populated with new data with each iteration. The message console is similar to the previous example and includes information such as the number of degrees of freedom, number of domains and boundaries, number of domain elements, file name, and solution time in seconds. The latter is particularly informative in flow applications where computational resource allocation is paramount. Figure 9 is not *Parametric Sweep*, but an iteration of the solution until convergence is reached.

CHAPTER 5

COMSOL MULTIPHYSICS MODELS

The process of heat transfer analysis using FEM is carried out in three stages: (1) model set up or pre-processing, (2) solution, and (3) post-processing. Model setup steps are:

1. number of spatial dimensions (zero to three) in which the physical phenomena are to be modeled are selected;
2. model geometry is created or imported;
3. dominant physics are identified (e.g., thermal and/or mechanical);
4. conditions at which the boundaries interact with their environment(s) are identified (e.g., zero gradient and constant value);
5. time-dependency is selected (i.e., steady state or transient);
6. initial conditions are identified;
7. model geometry is meshed;
8. numerical technique is selected for the solution; and
9. solution parameters are set up (e.g., duration of interval simulated and time intervals at which the solution is saved.

After running the solution, the post-processing steps are:

1. extracting the solution (e.g., output commands);
2. evaluating the solution (e.g., taking an integral or average over a region);
3. reporting the results (i.e., web applications and defined templates); and
4. processing the solution output (by means of diagrams, contour plots, and probes).

This chapter discusses how to work with models in COMSOL Multiphysics (using the current version, which is 5.4). The first section reviews considerations pertinent to setting up a heat transfer model. The second section outlines the initial steps of setting up a model in COMSOL Multiphysics. The next section focuses on the geometry creation process, covering importing the geometry as an independent part or assembly from a dedicated CAD tool such as Solid Edge and creating it using the built-in geometry creation tools. Sensitivity analysis and how to carry it out in COMSOL Multiphysics is explained next, followed by a brief summary of all the steps involved in carrying out an analysis, from the model setup, to solution, and to visualization of the results.

5.1 Heat Transfer Modeling Considerations

To model a heat transfer problem using any tool, including COMSOL Multiphysics, the modes of heat transfer applicable to the problem are to be identified. The dominant modes of heat transfer are conduction, convection, and radiation. The term *dominant* is used to signify that in most heat transfer problems all three modes are present; however, in some problems, certain modes may only have negligible contributions and so may not need to be included.

Methods of setting up the models do vary for solids and fluids. Conjugate heat transfer is defined as the combination of solid and fluid interaction (or modes of heat transfer); these modes may be combined with other modes of heat transfer such as radiation as the model becomes more complex. Gravity may also play a more important role where the flow in the vicinity of a vertical surface is examined—for example, the scenario of free convection where the ratio of the buoyancy to viscosity forces is dominant. In radiative problems, the sources of radiation may vary; for example, it may include solar radiation heat rate—hitting the surface of an object and thus defined in the units of W/m^2—or radiative heat due to an intense heat source such as fire with temperature variation over time. An example is performing a thermal analysis for the train underframe with different radiative properties to ensure it complies with fire test codes. In each of these methods, the details such as the models chosen to represent the physics, methods by which the heat convection coefficient is calculated, ways of physics interfacing with each other, and proper capture of the temporal and spatial variations of the thermo-physical properties are all important.

The choice of transient versus stationary solutions should also be carefully considered. For some models, a stationary study may result in a solution while a transient one will not converge. However, the choice of the stationary study does not provide the information on the system state development over time.

When setting up the physics between two materials of different thermo-physical properties, sharp variations of the temperature gradient between the two bodies at the interface may result, causing potential solution instability or inaccurate model predictions. In such cases, care is to be taken when setting up the physics and solving it at the interface. The large local temperature variations may result in thermal stress at the onset of the heat exposure and also residual stresses as the heat source is removed. This is what occurs when a part is exposed to an intense localized heat source, such as when welding thermoplastic components by scanning with a laser beam.

Consider, for example, a thermoplastic laser welding process known as the *Laser Transmission Welding (LTW)*. In an LTW process, the laser spot size may be on the order of 0.5 to 3 mm and laser power may range from 5 to 50 W. For the laser beam to join two thermoplastic parts, the light passes through the laser-transmitting part (in a lap-joint configuration) and hits the surface of the laser-absorbing part. The absorbed laser radiation heats the material, melting both parts to form a joint under pressure. The laser-absorbing part typically contains an additive which causes the laser energy to be quickly converted to heat once the light reaches this part's surface. This results in a sharp increase in local heat generation. The optical and absorptive properties of the plastic materials need to be accurately specified.

The time exposure to the heating source combined with other process parameters, such as laser power and beam scanning speed, are key factors determining the heat generated at the interface; modeling this generated heat accurately is important. An accurate model can only be achieved by selecting appropriate elements (size and capabilities). For example, when using a commercial software package such as ANSYS, one must use plane or volume elements capable of addressing heat transfer problems; one also needs to choose whether higher or lower order element versions are used. In COMSOL Multiphysics, the specialist may not be able to pick a specific element (e.g., *link32*, *plane55*, or *solid70* for 1D, 2D, and 3D elements in ANSYS) as such; however, they are able to manipulate the size of the elements or their shapes (e.g., *quads* versus the *tetrahedral* elements and *free* mesh versus the *mapped* mesh methods). It is also possible to divide a complex geometry into smaller regions in which individual meshing parameters are applied, such as mesh size, type, and method.

In general, to obtain a good model solution, one will need to iteratively adjust various settings. For example, one may need to do this to determine appropriate model solution step size or mesh size. This type of study, also known as the *sensitivity analysis*, starts by assuming a reasonable initial parameter value (e.g., mesh element size) and changing it—increasing or decreasing—to the point that the response remains unaffected, within some small tolerance.

This process is started and iterated based on the educated guesses. However, there are techniques to conduct such iterations based on the mathematical principles as opposed to guesses. For example, to select element size, conservation of energy methods may be used. Also, to obtain appropriate initial guesses, one can use an FDM method or a commercial package such as EES. Using EES, one can vary time and space steps when solving transient FEM models in order to develop educated guesses for initial values. This technique can save resources required for computation and reduce the volume of data to be analyzed. Steps of carrying out various types of sensitivity analyses are described later in this chapter in Section 5.4.

5.2 Creating a Model in COMSOL Multiphysics

To set up a new model, open COMSOL Multiphysics software. Before continuing, you may wish to check for the latest software updates by going to *File > Help*. After selecting *File > New*, a window opens that offers the choice of *Blank Model* or *Model Wizard* (Figure 10). If you select *Blank Model*, a new model is created; if you had a previously opened model in the same window, it will be closed (after a warning message). *Blank Model* is usually used to set up specialized models by inputting the mathematical functions. However, for most applications, it is much simpler to set up the model based on the applicable physics. For this purpose, *Model Wizard* should be activated (Figure 10a). A new window opens where you can select the appropriate space dimensions (e.g., *1D* or *2D Axisymmetric*)—(Figure 10b). Now you need to decide which physics to include in the model (e.g., heat transfer, solid mechanics, fluid flow, or a combination of several physics). For example, if you wish to study the *Structural Mechanics* of your model, you can select *Solid Mechanics* physics option and click on *Add* button (Figure 11).

Note that in the image shown you only see one option available to be picked (*Solid Mechanics*); the reason is that the optional add-on *Structural Mechanics* module was not included in this installation. This shows that even without optional specialized modules, the user still has some basic capabilities available. In most cases, it is possible to revise some input equations and create the desired specialized physics. Figure 12 shows the physics selection when a specialized add-on module is available (*Heat Transfer*). In this case, there are twelve different physics available—*Heat Transfer in Solids* is highlighted in the image.

After the physics is added, the dependent variable for it (e.g., temperature—T) is set. It is possible to change the dependent variable name; however, no matter what you name it (whatever name and subscript number you prefer), it represents the temperature in the model, such as T_1 or T_2 (T_i). After completing this step, click on *Study* button at the bottom of the window to display *Study Selection*, where *Study* type is to be defined. These can be either the most commonly chosen *General Studies* or more specialized types (e.g., *Thermal Perturbation*)—Figure 13. In this example, a *Time Dependent* (transient) study is selected. Selecting *Stationary* study allows the performance of the steady-state analysis.

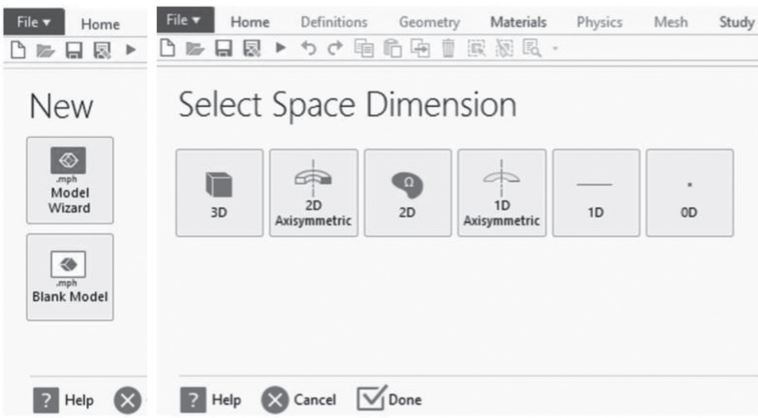

(*a*) (*b*)

Figure 10. (a) Setting up a new model, (b) Selecting space dimension.

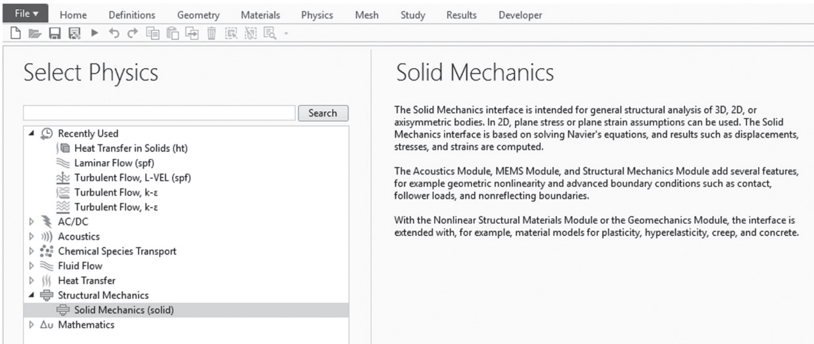

Figure 11. Selecting physics, *Structural Mechanics* (*Solid Mechanics*).

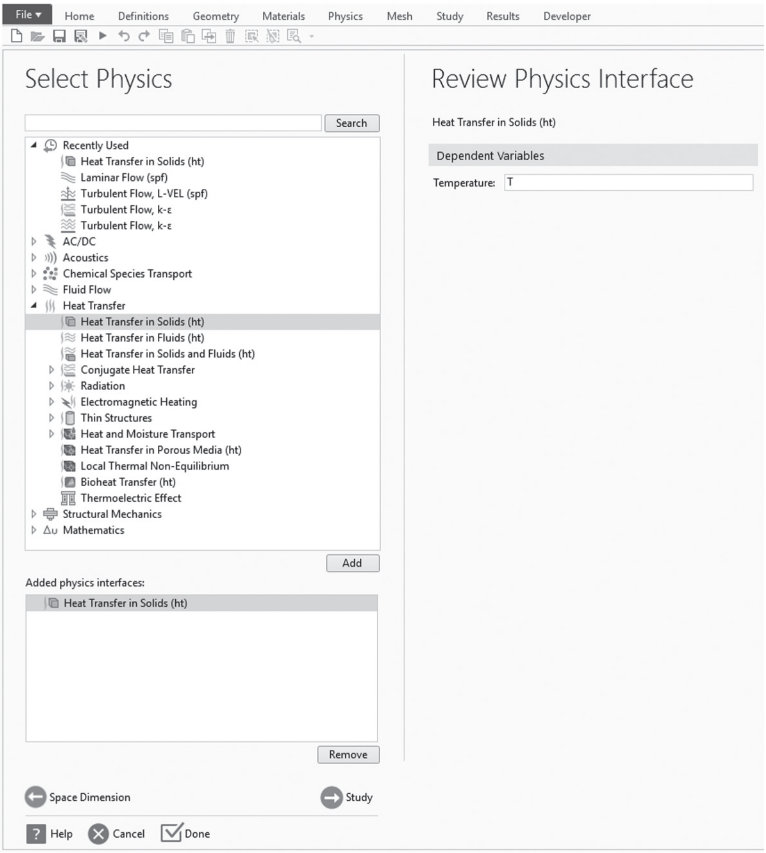

Figure 12. Selecting physics, *Heat Transfer* (*Heat Transfer in Solids*).

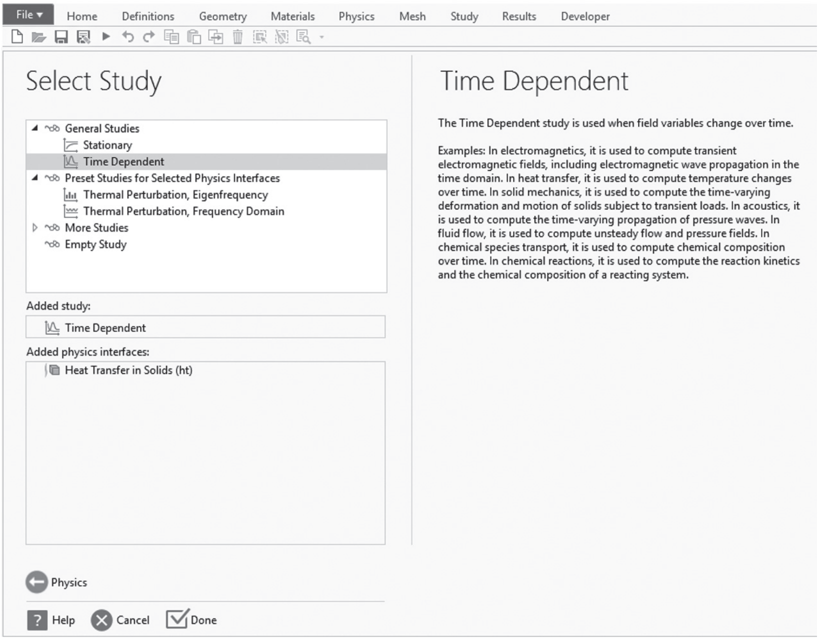

Figure 13. Selecting study, *General Studies* (*Time Dependent*).

Clicking on *Done* button after the previous steps are completed takes you to the modeling window, a home for your brand-new model (Figure 14). Here, you have multiple regions or windows (four in the provided example). You may choose to pin down more regions to the ribbon or reduce the number of regions as desired. Most of the "construction work" on your

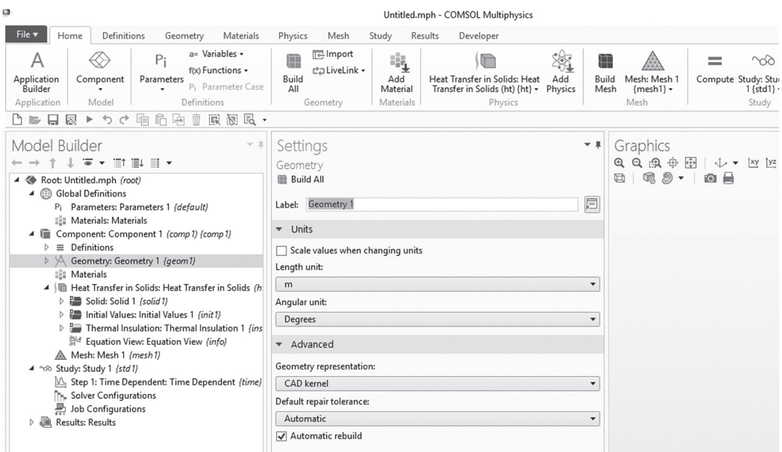

Figure 14. COMSOL Multiphysics model window.

model will be done in *Model Builder* window. It has a tree structure starting with *Root* named after your model, with the main branches of *Global Definitions*, *Component*(s), *Study*, and *Results*.

Model Builder's neighbor to the right shows *Settings* pertaining to the selection made in *Model Builder* window. In the example shown in the figure, *Geometry* is highlighted. In this case, *Settings* window presents the related geometrical characteristics such as *Length unit* (e.g., m, nm, and GM)—Figure 15, *Angular unit* (Figure 16), *Geometry representation* kernel (Figure 17), and *Default repair tolerance* method (Figure 18). A kernel is the fundamental geometrical language used to describe the model geometry. In this example, two geometrical kernels are available—*CAD* and *COMSOL Multiphysics*; the former is only available with the optional *CAD Import* module while the latter is part of the base package.

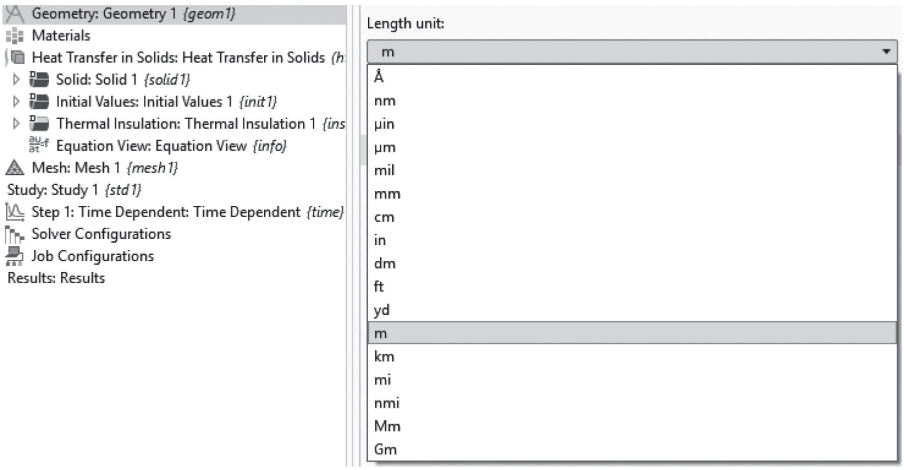

Figure 15. *Geometry, Length unit.*

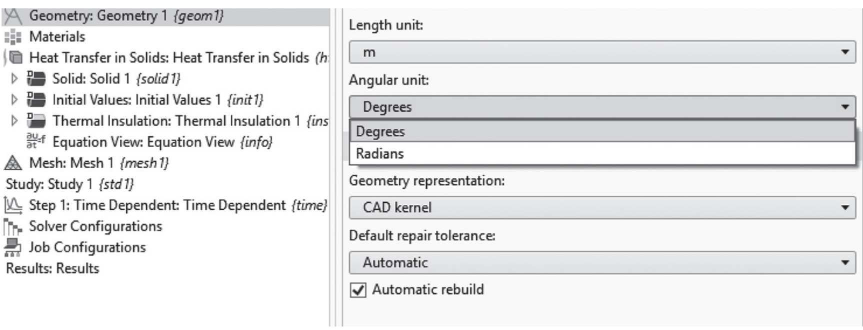

Figure 16. *Geometry, Angular unit.*

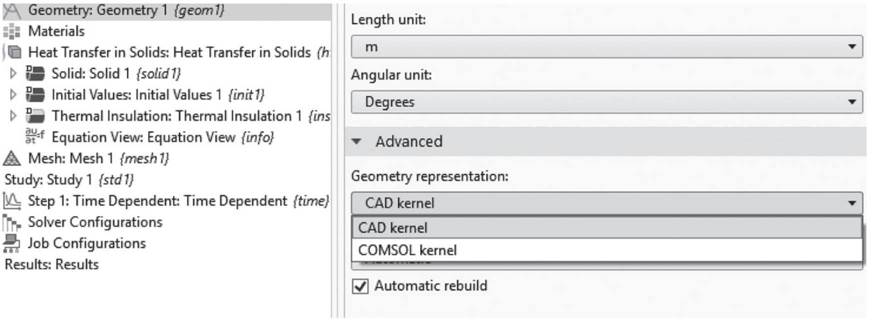

Figure 17. *Geometry, Geometry representation* kernels.

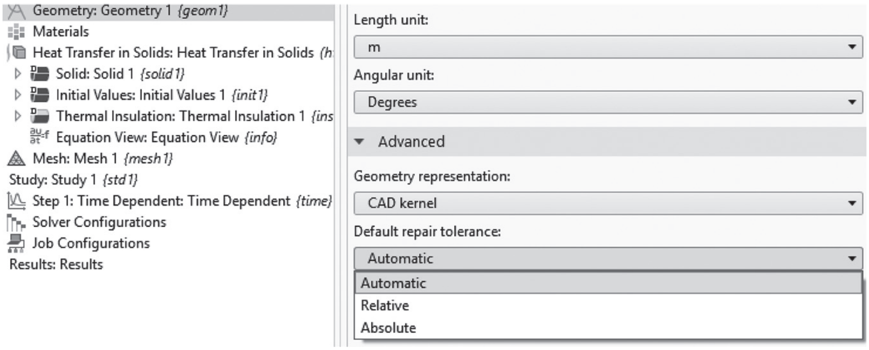

Figure 18. *Geometry, Default repair tolerance* options.

Default repair tolerance is applied when geometry is imported or when Boolean operations are performed. It defines a threshold below which the geometry entities may be considered coincident and appropriate repairs are made to avoid, for example, cases of vertices which are very close to one another. Selection of *Relative* setting expresses the tolerance as a ratio between the error dimension and the maximum model coordinate. *Absolute* tolerance is expressed in the length units of the model. *Automatic tolerance* (the default choice) sets it at a relative value of 10^{-5} and takes adjustment steps if needed.

After the model geometry is created (by import or internally), the next step is to add one or more materials—a material needs to be assigned to each domain of the model. Materials can be added from the list of built-in basic ones that are included with the core COMSOL Multiphysics package, from an optional *Material Library* add-on module, or by introducing a blank material and filling in the associated fields (e.g., mechanical and thermo-physical properties).

Once a working model is set up, an additional functionality that is available in COMSOL Multiphysics is creation of an application based on the model. Such an application gives users a simplified interface where they can adjust a limited set of input variables (chosen by the application designer) and observe their effect on outputs such as geometry, mesh, and solution results expressed by diagrams and contour plots. Thus, those users who do not wish to or have no need to learn the details of FEM tool operation (e.g., manufacturing or design engineers) can still have the ability to use it to explore the "what-if" scenarios; students can use applications as an educational tool to study the modeled system behavior. With these applications, the user does not need to have a local COMSOL Multiphysics installation; they can run the application over the local or external network via a web browser interface by connecting to a COMSOL Multiphysics Server installed on a remote computer. With an optional COMSOL Multiphysics Compiler, one can even create completely stand-alone applications, able to run the model via the application interface without the need for a local or a remote server-based COMSOL Multiphysics installation.

Items such as variables, parameters, and materials may be added either at the local (directly under the subcomponent—tree leaf: local) or global (under the upper level component—tree trunk: global) levels. In the latter case, a link needs to be created that connects the local property or entity (child) to the global property or entity (parent). Any of the preset parameters (or variables), including the material properties and solution control options, may be revised at any time.

Note also that even after the physics and study selections have been made during the model setup, it is possible to add a new physics under the current *Component* or a new study under *Root* (top-level tree). It is also possible to add a new *Component* (of any dimension) under *Root*. The user may add *Study Steps* as well as a variety of sweeps (e.g., *Parametric*, *Function*, and *Material Sweep*). *Study Extensions* may also be activated under each of *Study Steps*. The latter two features make it possible to perform sensitivity analysis for the selected parameter (or variable).

The sub-physics and conditions (e.g., boundary conditions such as inflow, symmetry, heat flux, and loads) are added under the main physics. The user should ensure that these sets of input data are provided so that the problem solution can be attempted. In case a boundary condition is missing, the program may employ the default conditions for the missing regions (e.g., lines, areas, and volumes) if the user has not excluded them from the physics. For example, when defining the material for the first time, its properties are propagated to the entire geometry (whose analysis is to be performed upon). However, this is not the case if the user decides to exclude parts of the geometry from the physics or material definition. Leaving the properties of the materials the same as the default values is advantageous in the sense that errors due to the lack of attributes (types) and properties (attribute values) are avoided; however, the disadvantage of this method is when the user inadvertently neglects setting up the attributes that are not shared among all the features such as radiation properties. Therefore, care should be taken when setting up the features' attributes and properties.

If a model consists of multiple components and physics, they are solved in the order in which they were defined. The user can choose which components-physics to solve by placing a checkmark in the corresponding box (under *Study Step*, *Physics*, *and Variable Selections*). Additionally, component mesh for the selected physics is shown so that the user can ensure that the correct physics and component mesh are selected. This means the user can exclude analyses if they are not interested in solving them by not placing checkmarks in their related box. This may be done either to perform the analysis in steps where the output of one analysis is to be used as the input to the next analysis (in whatever order desired), or when there is no interest in performing all analysis steps simultaneously when, for example, the effect of including or excluding certain features (e.g., heat flux versus the convection boundary condition) is to be studied using *Parameter Sweep*.

5.3 Creating Geometry

This section presents a brief overview of geometry creation in COMSOL Multiphysics. Much more detail is available in the author's publication *COMSOL Multiphysics Geometry Creation and Import* [4]. In COMSOL Multiphysics model file, geometry is created in *Geometry* found under each *Component*. The parameters used for the geometry may be defined either on the local or global level. There are three different ways to create a geometry: by creating and manipulating elementary geometric entities, by importing, or by bringing the geometry in from a part library.

To import from external CAD tools such as SolidWorks, Solid Edge, Autodesk®, or Inventor™, the analyst needs to have either *CAD Import* module or *LiveLink* module, the latter being associated with a specific CAD tool. On the other hand, any of the software-specific *LiveLink* modules include *CAD Import* module functionality. Using *LiveLink* module allows one to update *Geometry* in COMSOL Multiphysics as soon as the changes are made in the CAD software. In addition, if variables are employed to define the CAD model (such as lengths or angles), these can be accessed in COMSOL Multiphysics and used as part of the parametric solutions or in any internal calculations. As these variables are updated in CAD, they will be synchronized with COMSOL Multiphysics.

Using external CAD tools may become necessary as the model complexity increases. Another way to deal with more complex modeling tasks is to use COMSOL Multiphysics *Design* module, which adds expanded modeling functionality. One benefit of using COMSOL Multiphysics internal geometry generation tools is that all creation steps are accessible and can be modified by adjusting internal variables. Sensitivity to dimensions using solution sweep features can also be easily investigated. Another benefit is that the model file does not require any external software, which means fewer demands on the expertise of the analyst or the need for assistance from others; this also means that if the model file is shared with users at other locations, they are not required to also have access to a CAD tool or to have one of the optional modules in order to work with the model.

5.3.1 Using Elementary Geometric Entities

In this method, the geometry is created by defining basic geometrical entities, such as: (1) intervals and points (1D); (2) lines, curves, rectangles, and circles (2D); and (3) blocks, cylinders, and spheres (3D). Various transformations can then be applied to these entities, such as Boolean operations of union and difference; copy, mirror, rotate, and scale transforms; extrude, revolve, or sweep of a profile; and modifications such as fillets or chamfers. All of these steps are then processed sequentially to build the desired geometry. Any step can be disabled temporarily and thus excluded from the build processing. This is a convenient way to test different geometry-creation methods or even to modify the geometry quickly by selectively enabling/disabling creation steps. In addition, each step can be duplicated and the copy modified as needed. This is an efficient way to add new steps.

For example, to create the 3D ring shown in Figure 19, the following sequence may be used: (1) cylinder of radius 0.03 m and height of 0.015 m (*cyl1*); (2) cylinder of radius 0.024 m and height of 0.015 m (*cyl2*); and (3) *Difference*, *cyl2 – cyl1* (*dif1*).

For 3D parts, *Work Planes* are a powerful tool that can aid in geometry creation. They can be used to sketch 2D shapes which can then be extruded or revolved to create 3D objects. They can also be used as partitioning tools to split any 3D geometry. The split volumes can then be used for subsequent

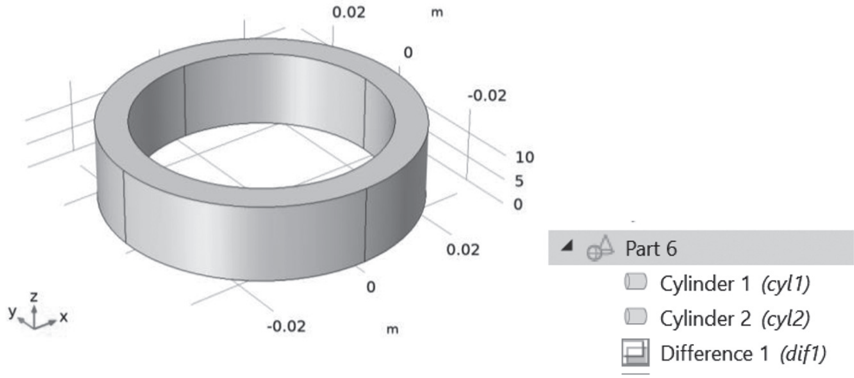

(*a*) (*b*)

Figure 19. (a) An example of a 3D ring geometry, (b) The geometry sequence shown.

modeling steps, allowing for example, different material properties or meshing for each volume, or deletion of the unneeded volume.

As an example of *Work Plane* use, you can create a more complex cylindrical shape, a 3D ring with a groove, by first drawing the profile of this ring on *Work Plane* (*wp1*) and then revolving (*rev1*) this profile about the ring's central axis (Figure 20). Figure 21 shows how the revolved profile is created by using circle (*c1*) and rectangle (*r1*) 2D shapes (Figure 21a) and performing a Boolean difference (*dif1*), where the circle is subtracted from the rectangle (Figure 21b). *Revolve* operation is then performed, which uses this profile and defines a revolution axis to create the 3D shape shown.

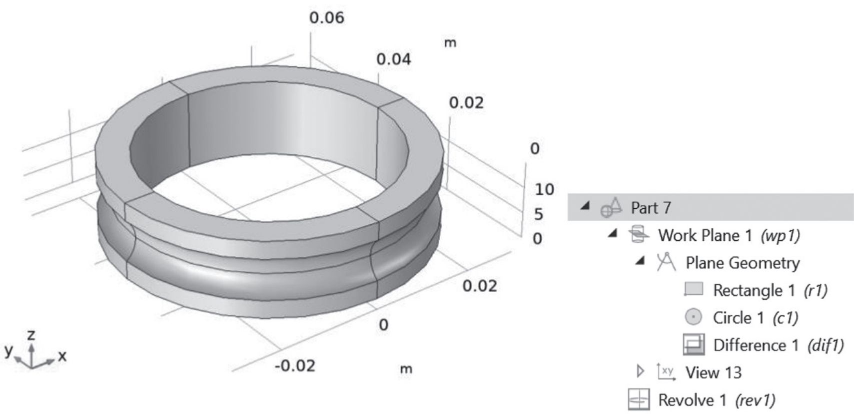

(*a*) (*b*)

Figure 20. (a) A 3D ring with a groove created by revolving 2D shapes, (b) The geometry sequence shown.

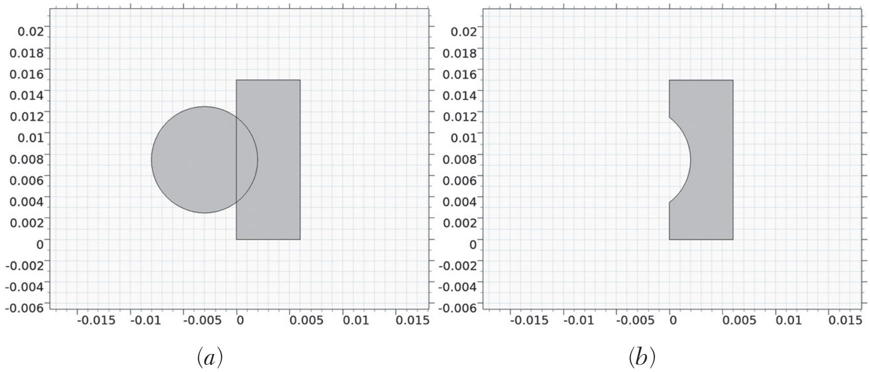

Figure 21. (a) Work Plane used to define input 2D shapes, (b) Finished profile for a 3D ring with a groove.

5.3.2 Importing Geometry

Geometry import is performed by right-clicking on *Geometry* and selecting *Import*. Sources available for bringing in the geometric entities into the file are: (1) geometry sequence; (2) mesh; (3) *STL* (3D geometries only); (4) COMSOL Multiphysics file; and (5) 3D CAD File (3D geometries only).

Geometry sequence option allows you to bring a set of geometry creation steps from another component of compatible dimensions (1D, 2D, or 3D) within the same model file into the current component. This option allows you to reuse the geometry you created in one component within another component.

Mesh import takes a mesh from another component within the same model file and brings it as a geometry (shape) into the current component. The two components must have the same number of spatial dimensions (e.g., if you have a 2D component, only a mesh from another 2D component can be used).

STL import only applies to 3D components. It allows you to bring into your model file a geometry defined using an *STL* file format, which is a common way to store information used for 3D printing of objects. *STL* format describes surfaces of 3D objects by flat triangular surface patches, with coordinates of all triangle vertices stored in *STL* file. Thus, curved surfaces will be approximated by these flat patches. For curved surfaces with small radii, small triangles are needed in order to have an accurate surface representation, possibly leading to very large file sizes for highly complex objects.

COMSOL *Multiphysics file* option allows you to import into the definition of the current component a geometry extracted from another

COMSOL Multiphysics file. Such a source geometry file can be created in the first place by right-clicking on *Geometry* and selecting *Export*. A file in a **.mphbin* format is then created, which can be selected for import via this option.

The *3D CAD File* option is only available for 3D components and will only be visible if you have one of several optional add-ons which include this functionality, such as *CAD Import* module or one of *LiveLink* modules allowing real-time communication with a specific CAD software. CAD files of several different formats can be imported. These include non-proprietary geometry exchange formats, such as *STEP*, *SAT*, and *IGES*, and proprietary ones, such as SolidWorks part (**.sldprt*) and assembly (**.sldasm*).

5.3.3 Using Part Library

This approach provides a way to take advantage of what can be described as geometry generation templates to quickly create new geometry customized by adjustment of the template parameters. Such geometry templates can be either made by the user or selected from *Part Library* parts provided with COMSOL Multiphysics core program and its optional modules.

User-made templates are created by adding *Geometry Parts* node under *Global Definitions* by right-clicking on the latter and then adding 1D, 2D, or 3D parts under this node by right-clicking on the newly created *Geometry Parts* node. For each part node thus made, the corresponding *Settings* window allows the definition of *Input Parameters* which will be used to control its shape. A geometry sequence is then built using these parameters.

To add one of these templates to your component's geometry, right-click on *Geometry* and select *Parts*. You can then choose a part from *Part Library* or one of the parts that you defined in *Geometry Parts* node as described previously. After this part is brought in, you can adjust its definition parameters as desired. Thus, the same template can be used to quickly generate an infinite variety of shapes, which may save you a lot of time in some applications.

For example, you can create a template for a 2D ring shape as shown in Figure 22a. Do so by first adding a 2D Part under *Geometry Parts* as described previously. Name it *Ring_2D* and define the parameters listed in Figure 22b. Use these parameters to define the dimensions of an outer circle (*c1*), inner circle (*c2*), and then perform a Boolean difference operation (*dif1*) of (*c1-c2*) to get the ring shape, resulting in the geometry sequence in Figure 22c. Having created this template, you can use it to quickly define a ring of any shape and place it as desired (Figure 23).

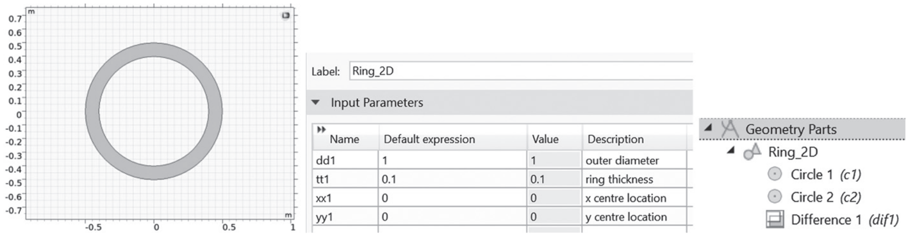

(*a*) (*b*) (*c*)

Figure 22. **2**D ring part template: (a) Shape, (b) *Input Parameters,* (c) *Geometry Parts*.

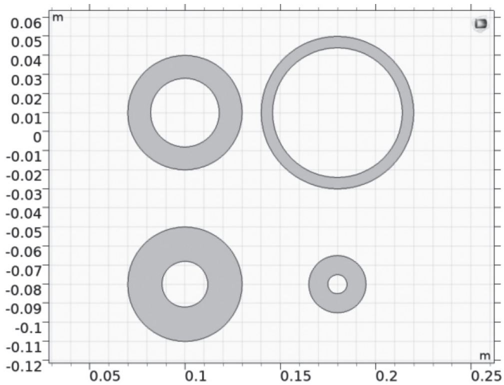

Figure 23. Four 2D rings created from the example 2D ring template.

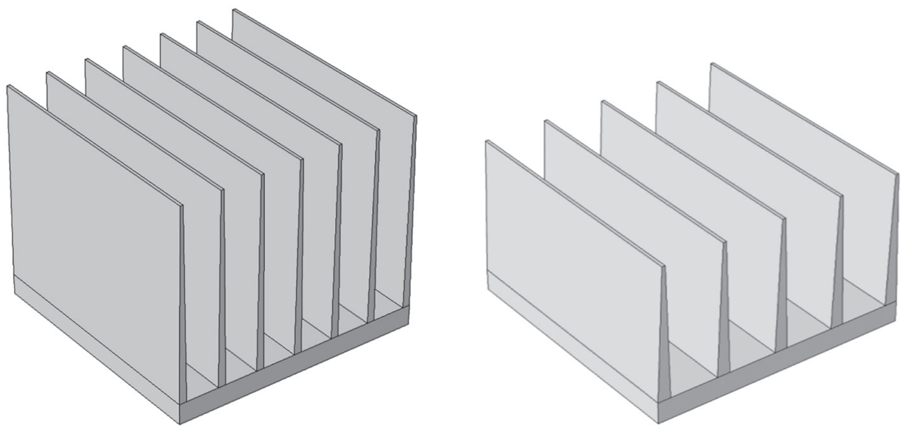

(*a*) (*b*)

Figure 24. Importing a *Heat Sink, Straight Fins* library part (*Heat Transfer* module) (a) Default, (b) Customized.

As an example of how *Part Library* can be used, you can import *Heat Sink—Straight Fins* template (Figure 24). It is included with optional *Heat Transfer* module. *Part Library* parts can be brought in either under *Global Definitions* or directly into your component's geometry sequence. For the former method, right-click on *Geometry Parts* and select *Part Libraries*; for the latter method, right-click on *Geometry* of your component and select *Parts* > *Part Libraries*. The advantage of using the former (*Global Definitions*) method is that this part can then be directly accessed from *Geometry* > *Parts* of all components, without the need to browse repeatedly through the libraries.

After you bring in the example part template into your *Geometry* sequence using one of the previous methods, you will see in *Settings* window a list of many parameters which can be used to customize the shape. The base dimensions, fin height, fin top and bottom dimensions, and number of fins are just a sample of parameters which can be adjusted. Figure 24b shows the same heat sink part but with the default settings modified by changing the number of fins, their height, and their base thickness. If you can create the geometry you need for your model from such a template, it can save you a lot of time. It also allows you to easily modify the geometry's shape if you are trying to investigate how the shape affects the solution results.

5.4 Sensitivity Analysis

5.4.1 Parametric Sweep

An analyst can use *Parametric Sweep* to investigate the sensitivity of the results with respect to material properties, initial conditions, geometry features, mesh characteristics, and boundary conditions such as coefficients, fluxes, and temperatures. The following example shows the steps for setting up such an analysis. Assume that the convective heat transfer coefficient is the focus of this investigation; its value determines the effectiveness of the environmental cooling. A good approach to perform such studies is to set up parameters (or variables if they are interconnected to the import geometry), varying as required with distinct identifiers (names). Under *Study* branch, pick *Parametric Sweep* (Figure 25). *Parametric Sweep* is added as a new item under *Analysis* node.

In the corresponding *Settings*, one needs to select one or more parameters to be varied in this sweep. In the example shown herein, the user-defined parameter n is selected as the parameter whose sensitivity analysis should be performed. This parameter is a dimensionless multiplier for the heat transfer coefficient (h_c in Figure 25). The parameter units must be defined carefully. If h_c were to be selected as a parameter to vary instead of n, the analyst would need to ensure that the parameter dimension is repeated in this window for each value of h_c listed. The author recommends that a dimensionless parameter such as n be used instead; it makes it possible to scale any given value without changing the parameter value itself. Another advantage for setting up such a variable is that there is no need to define the units for each individual set of parameters.

Therefore, for example, instead of defining h_c variables that should be inputted into the model as (5 W/m^{2}K, 10 W/m^{2}K, and 20 W/m^{2}K), the model input can be set to equal $5n$ W/m^{2}K (where $n = 1$ for the base condition) and then an array of (1, 2, 3) can be used as a set of n values. Other items that can be defined in *Settings* window allow the user to activate plotting of the results for the analyses as they run or selecting a probe (e.g., temperature) to collect data for a desired location. This is to display the value at the probe during the solution iterations and is especially useful to monitor the value of a property, such as temperature, at a specific point while the solution is progressing.

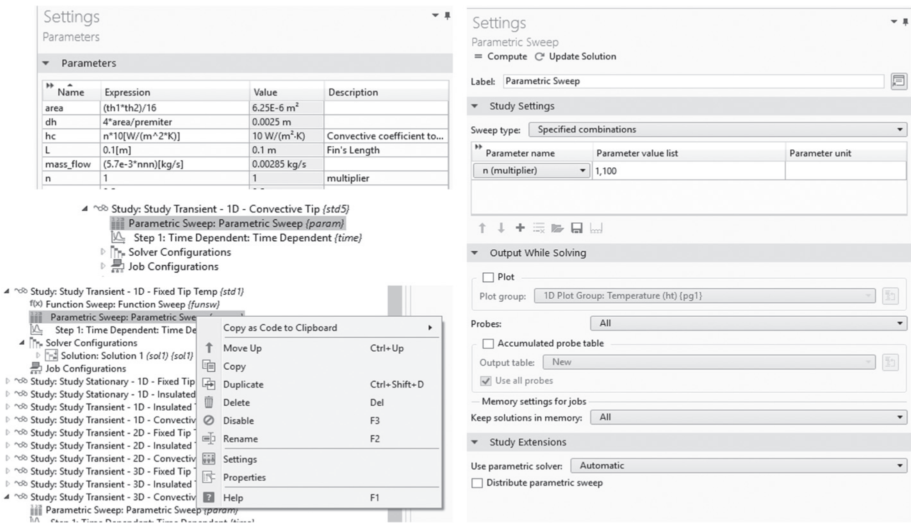

(*a*) (*b*)

Figure 25. (a) Adding *Parametric Sweep* under *Study* node, (b) *Parametric Sweep* settings.

5.4.2 Function Sweep

The analyst may employ functions (e.g., analytical, interpolation, random, step, and waveform) when defining material properties, initial conditions, geometry features, mesh characteristics, and boundary conditions such as coefficients, fluxes, and temperatures. Note that the function definition can be made either under *Global Definitions* or *Definitions* node for each component (e.g., analytical, piecewise, and step) or for individual components. To perform such a sweep, the user needs to have selected *Function Sweep* under the component which they wish to analyze (Figure 26). These functions are listed under the predefined *Switch* in *Study Settings*. The next step is to communicate the intention to the analysis node (e.g., stationary and transient) in which you are interested in performing *Function Sweep* by adding the capability under *Function Sweep* settings, *Study Settings*. *Switch* can be chosen by selecting its name in *Study Settings* window (Figure 26).

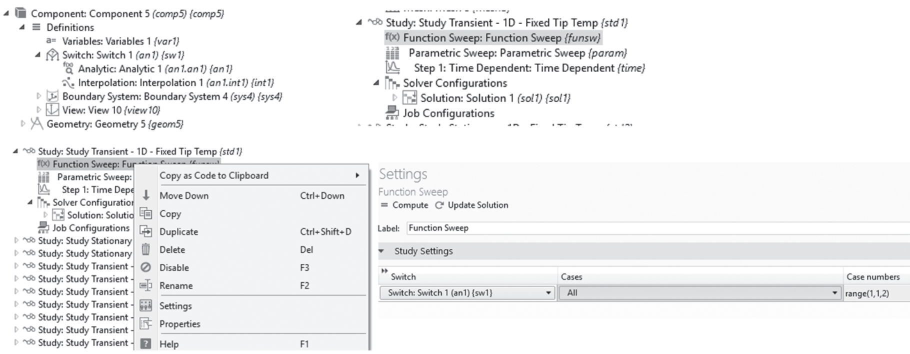

(*a*) (*b*)

Figure 26. (a) Adding *Function Sweep* under *Study* node, (b) *Function Sweep* settings.

5.4.3 Material Sweep

If there is an interest in learning how varying a component material affects the results, the analyst can employ *Material Sweep* feature. Consider the case where one wants to investigate, for example, the influence of a cooling agent (e.g., liquid) with the choice of six substances—ethylene glycol, water, mercury, air, transformer oil, and engine oil. Recall that materials may be set either on the global or local level. When setting up materials locally, it is possible to add materials as separate nodes or to define them in groups under *Material Switch*, where blank or predefined materials can be added. To add this *Switch* node, right-click on *Materials* node within your component, then select *More* > *Switch*. Let the newly created family group name be *Switch 1*.

To add materials to this *Switch 1*, go to *Add Material* tab, select the material you would like to add, and click on the small downward-pointing triangle on the right of *Add to Component* button. You will see a complete list of all places where you can add this material, including *Switch 1*, which you should now select. Select other materials you would like to add—they will then be ordered within *Switch* group in the sequence in which they were added. *Switch 1* will consist of ethylene glycol (member 1), water (member 2), and so forth.

To add *Material Sweep*, right-click on *Study* node and select this feature. Under *Study Settings*, you can select *Switch 1* and specify the sweep settings (Figure 27). You can select any number of sensitivity studies. For example, for the group family of six, the user can select any family members in any order using their sequence numbers such as 1, 3, 6, and 4, equivalent in this case to ethylene glycol, mercury, engine oil, and air, respectively (Figure 27). One reason to choose different sequence orders is to facilitate solution convergence in applications such as turbulent flow analysis. The example in Figure 27 shows range (1,1,3) when defining *Material Sweep*. This specifies that the material index is to be incremented by 1, from 1 to 3, equivalent to listing them as 1, 2, and 3.

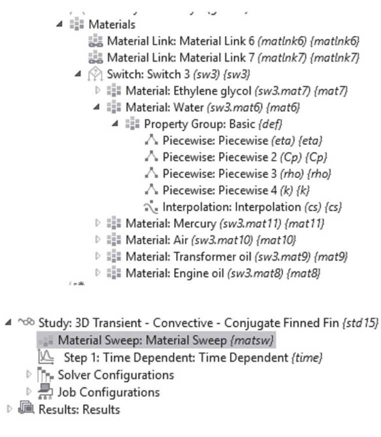

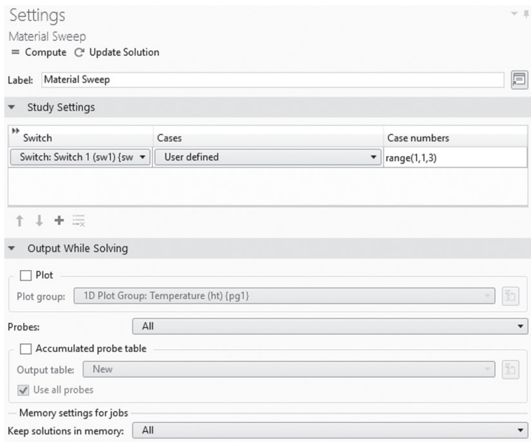

Figure 27. (a) Adding *Material Sweep* under *Study* node, (b) *Material Sweep* settings.

5.4.4 Auxiliary Sweep

Auxiliary Sweep feature can be used to investigate the sensitivity of the results to material properties, initial conditions, geometry features, mesh characteristics, and boundary conditions including coefficients, fluxes, and temperatures. It can be found under *Study* node, within one of *Study* steps, under *Study Extensions* listed in the corresponding *Settings* window. It is available for stationary, transient, and frequency domain studies. Let us consider the example discussed earlier where the effect of the convective heat transfer coefficient was studied. Under *Study* node, one can define as many steps as needed, for stationary or transient cases—independently, or as input to the next analysis step. Under the specific step in which the sensitivity analysis should be performed, *Auxiliary Sweep* feature may be activated and the related parameters selected. In this example, the dimensionless multiplier n for the convective heat transfer coefficient is selected as the parameter whose sensitivity analysis should be performed, and values 1 and 10 are chosen (Figure 28).

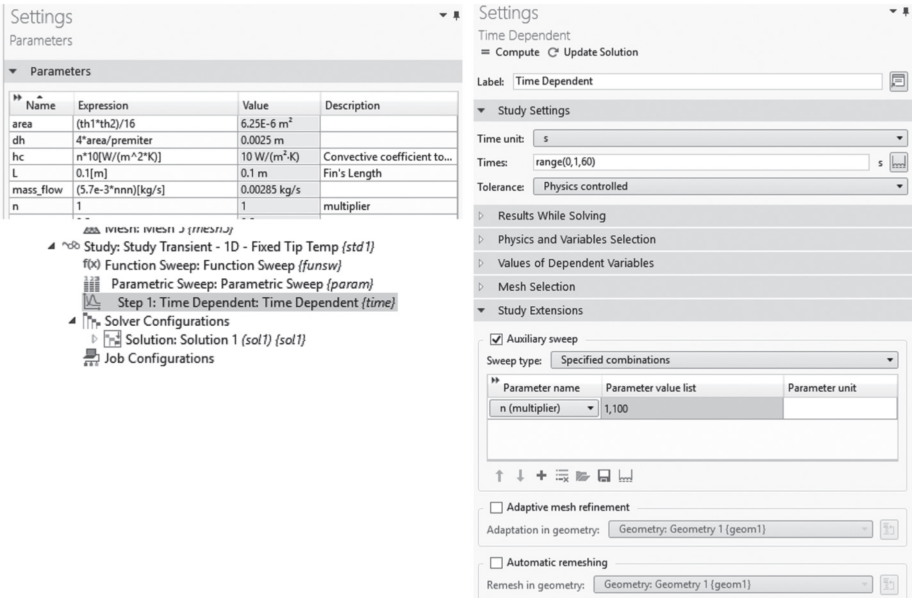

(*a*) (*b*)

Figure 28. (a) Adding *Auxiliary Sweep* under *Study* node, (b) *Auxiliary Sweep* settings.

5.5 Modeling Process Overview for COMSOL Multiphysics

This section reviews the steps to be taken in order to set up models, run the solutions, and visualize the results. Note that *Settings* and *Properties* are available for all subcomponents of the model tree. Although the following description focuses on thermal flow analysis, a similar methodology applies to other physics as well.

5.5.1 Components and Studies

Under the model *Root*, new components and new studies can be added to the model (Figure 29). Using *Add Component*, a new geometry component of any desired dimension can be added. It is also possible to insert a component from an existing COMSOL Multiphysics model. *Add Study* is another available feature under *Root*. A study is where the computation of the analysis takes place. *Settings* is where the model characteristics such as title, description, author's information, systems of unit, graphics information such as color and font type and size, thumbnail, and computation time are defined. This type of information may appear, for example, in automatically generated reports. *Properties* are a separate tab with the node *Properties* under *Root*, identifying the file name, version, date of model creation and last modification, the license number, and application version.

Copy as code to Clipboard is also available under *Root*. This allows the code for the associated block of the model to be copied from the program and made available to paste to wherever the user chooses (e.g., another code or a text editor). For example, under *Root*, the expression *model* can be copied. Note that you may also save your model as a Java program. This program then can be modified by adding loops or conditions using the Java programming language. Code editing can be done with a basic text editor or, for example, Eclipse, which is a popular Integrated Development Environment (IDE) for Java. It has a base workspace as well as a plug-in

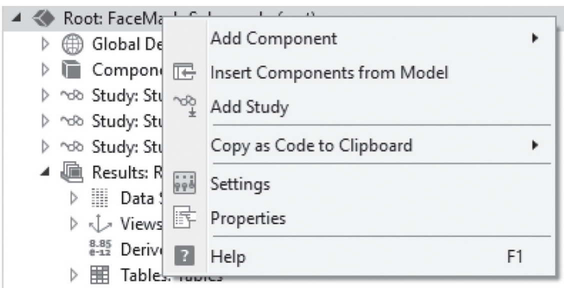

Figure 29. *Root* node and related components.

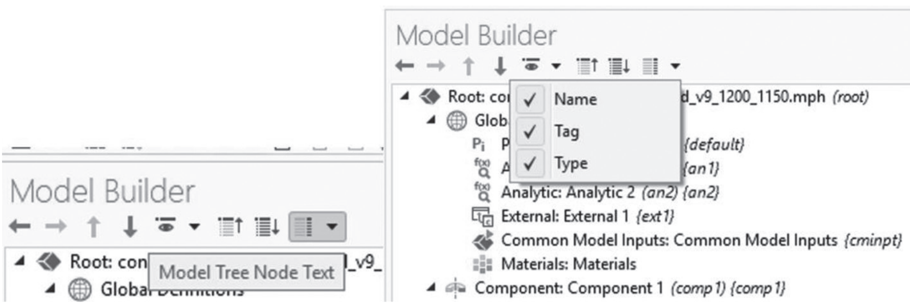

Figure 30. *Model Tree Node Text* options available to activate Java-related tags.

system to customize the environment. Eclipse is written mainly in Java and can be employed to develop Java and other applications such as Ada, C++, Fortran, PHP, and Python via special plug-ins. Note that you can activate *Name*, *Tag*, and *Type* under *Model Tree Node Text* in order to view these variables, which may be useful when writing scripts (Figure 30).

5.5.2 Parameters and Variables

Parameters and *Variables* are defined under *Global Definitions*, the first item under *Root* (Figure 31). *Variables* can be created under *Global Definitions* or under *Component*. *Parameters* can be created only under *Global Definitions*. There is always one *Parameters* node available. Extra *Parameters* nodes can be added, if desired, to group parameters for better organization. Parameters are mainly useful in defining the geometry and in mesh size control. They can reference other parameters and use built-in mathematical functions and constants (such as *pi*). Variables can be used, for example, in the definition of material properties.

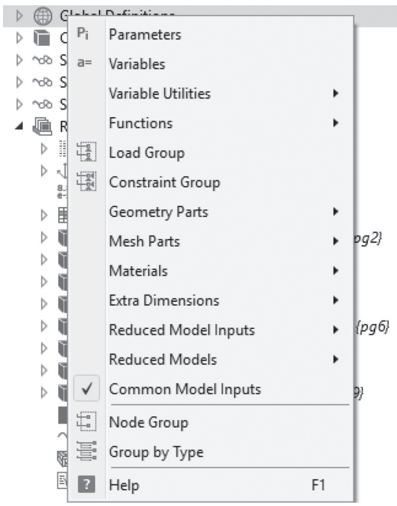

Figure 31. *Parameters* and *Variables* menu selections along with their features available under *Global Definitions*.

Proper use of parameters and variables is a mark of an expert user. Using parameters and variables in setting up a COMSOL Multiphysics model is strongly recommended. It brings benefits similar to those of using meaningful names and comments when writing program code. As your model complexity increases, parameters will allow you to easily modify the model while minimizing the chance of error. They will allow you to return to your model in the future and more easily remember what you were doing. Avoid using numerical values when defining any quantity that may be changed in the future. If you give it a name, you will be able to easily modify the value. If it is just a number, you may forget why you chose that value or make an error when editing it. By using parameters, you can define one value and then reference it in multiple places, thus minimizing the possibility of making an error and speeding up the model changes. In addition, *Description* field for each parameter (or variable) should be used to provide a useful explanation for the purpose of this item (Figure 32).

When using parameters, one can define *Case* node under each *Parameter* node. Each new case is given a sequential number. Under each one, you can define a complete set of parameters, using the same names but varying their values. Then, when setting up *Parametric Sweep* under *Study* node, *Parameter Switch* option can be selected, allowing you to select cases by their number in order to carry out solutions for different sets of parameter values, as opposed to just varying individual parameters.

Copy to Clipboard command results in the expression *model.param()*. Under this expression, one can define the code for this section of the model block.

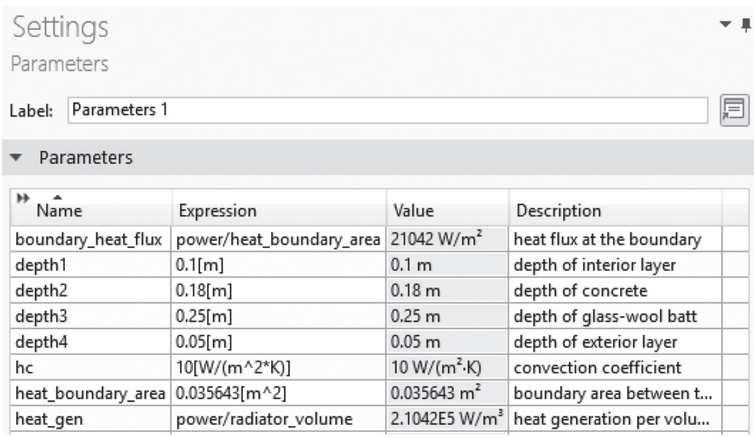
Settings
Parameters
Label: Parameters 1
Parameters

Name	Expression	Value	Description
boundary_heat_flux	power/heat_boundary_area	21042 W/m²	heat flux at the boundary
depth1	0.1[m]	0.1 m	depth of interior layer
depth2	0.18[m]	0.18 m	depth of concrete
depth3	0.25[m]	0.25 m	depth of glass-wool batt
depth4	0.05[m]	0.05 m	depth of exterior layer
hc	10[W/(m^2*K)]	10 W/(m²·K)	convection coefficient
heat_boundary_area	0.035643[m^2]	0.035643 m²	boundary area between t...
heat_gen	power/radiator_volume	2.1042E5 W/m³	heat generation per volu...

Figure 32. An example of *Parameters Settings*.

5.5.3 Functions

Functions are defined under *Global Definitions* or under *Component*, *Definitions* (Figure 31). Examples of functions include analytic, interpolation, piecewise, Gaussian, and step (Figure 33). Required settings differ, depending on the function. The analytical function requires a list of arguments (e.g., x_1, x_2) and a mathematical expression that uses these

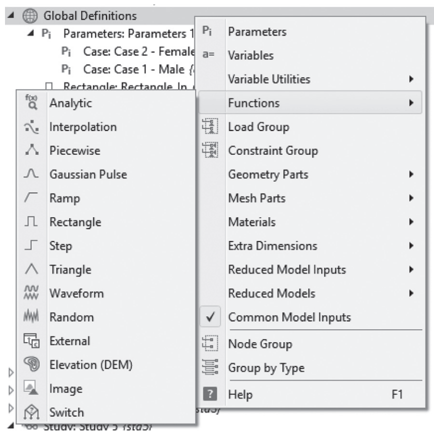

Figure 33. *Functions* menu selections along with their features available under *Global Definitions*.

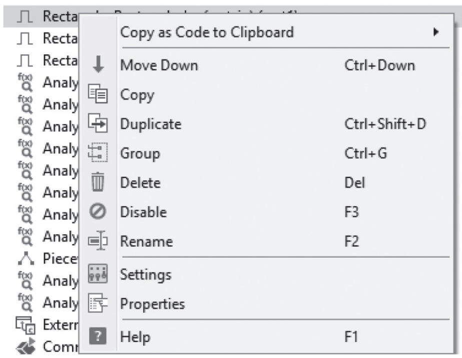

Figure 34. *Functions* options available to process related data.

arguments (e.g., $x_1^2 + x_2^2$). The argument names are local to the function and can be replaced with any other variable when the function is used, such as temperature (T). Functions such as Gaussian, step, or triangle only require function-specific parameters to be defined. Generally, they use a single input argument (e.g., x or t, representing location and time) which is defined when the function is called. For example, a step function represents a rise of the value listed in *From* field up to the value in *To* field, and this rise occurs when the function argument exceeds the value in *Location*. *Step* and other similar functions can also be smoothed to achieve derivative continuity at the transitions. It is also possible to duplicate, import, and copy functions from other programs in the form of a table that consists of *Function name* and *Arguments* (Figure 34); this is done under *Global Definitions*, *Functions*, *External* node.

Copy to Clipboard command results in the expression *model.func().create(an6, Analytic)*.

5.5.4 Geometry and Mesh Parts

Geometry and *Mesh Parts* (under *Global Definitions*) can be created locally or imported from another model or built-in COMSOL Multiphysics library to be used later on in *Geometry* of each *Component*. More information on geometry creation has been given previously in Section 5.3. *Mesh Parts* node will allow you to import part geometry descriptions from either mesh data (from an export of COMSOL model mesh or a NASTRAN file) or *STL* files.

5.5.5 Physics and Mesh

Physics and *Mesh* are added under *Component* (Figure 35). *Multiphysics* is available as a separate item. It allows coupling between physics to be defined. Physics may also be added from a previously generated model.

Copy to Clipboard command results in the expression *model.component().create (comp1)*.

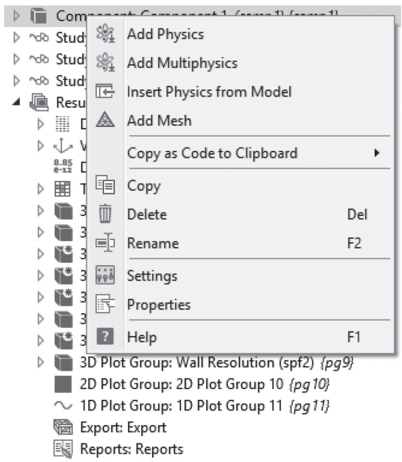

Figure 35. Menu selections under *Component*.

5.5.6 Study

Study node is where solution options such as *Parametric*, *Function*, and *Material Sweep* are set (Figure 36). Study steps are created in this section. This means a number of study steps can be made with their specific requirements and settings, consisting of stationary, transient, eigenfrequency, and frequency domains. These may be independent, meaning that the number of cases can be set and solved for the model with the possibility to feed the results of one step to the next step. A useful feature is to employ *Batch* option under *Study* node for the solution steps and methods under a single umbrella in order to run a number of cases in the order selected. This makes it possible to employ high performance computing capabilities and also run multiple cases without the need for the analyst to manually control the solutions one at the time. *Statistics* is also available for selection; this generates statistical data for the corresponding study that includes the number of degrees of freedom, as well as the name of the dependent variables such as temperature or pressure. It is possible to move the studies up or down within *Study* block by either choosing *Move Up*, *Move Down* commands or dragging the node to the desired location.

Copy to Clipboard command results in the expression *model.study (std5)*.

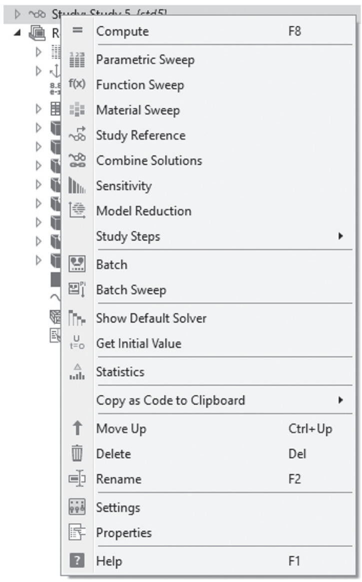

Figure 36. Menu selections under *Study* node.

5.5.7 Results

Results node contains the results of all the solutions in *Data Sets* node as well as all the post-processing steps (Figure 37). Additional sub-nodes are *Evaluation Group*, *Export*, and *Reports*.

Copy to Clipboard command results in the expression *model.result()*.

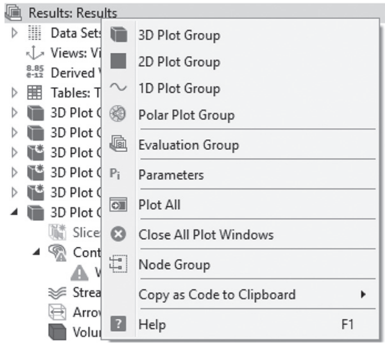

Figure 37. Menu selections under *Results*.

5.5.7.1 Data Sets

Data Sets (under *Results*) is the node where all the solution data can be found (Figure 38). It is a node that an analyst should get to know well. In addition to the solutions, it provides numerous other ways to manipulate the results to extract useful information from them. This information can then serve as input for the plots. For example, for heat transfer modeling results, one can extract temperature data for any point, line, or surface (for 3D models). For time-dependent solutions, the extracted values are a function of the time; for *Parametric Sweep*, results from each solution in the sweep are available.

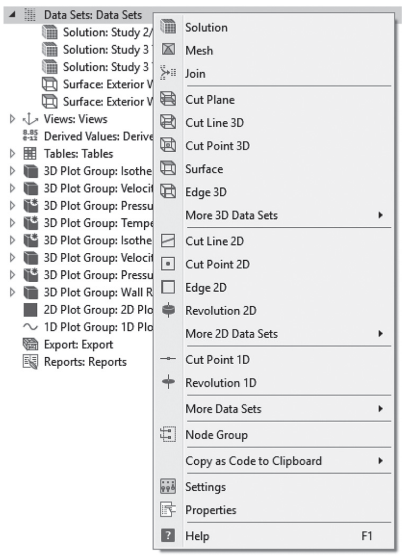

Figure 38. Menu selections under *Data Sets*.

Another useful feature is that the results for 2D or 1D axisymmetric geometry solutions can be revolved about their axis of symmetry to produce data sets simulating the original axisymmetric geometry. Using these revolved data sets, it is possible to produce an impressive-looking visual 3D effect using only a fraction of the computation time required for a true 3D model.

Other operations under *More 2D* (Figure 39) and *More 3D* (Figure 40) *Data Sets* are available that allow for the selection of array, mirror, sector, and parametric surfaces to extract the associated data. Mathematical functions can be applied to *Data Sets* under *More Data Sets*, and selections such as data integration, maximum and minimum, time average, extrusion, and array are available (Figure 41).

Copy to Clipboard results in the expression *model.result().dataset()*.

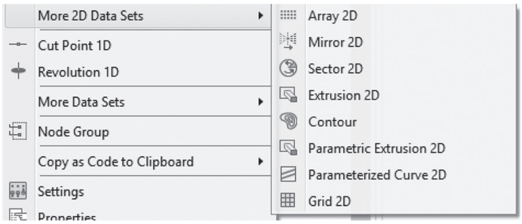

Figure 39. Menu selections under *More 2D Data Sets*.

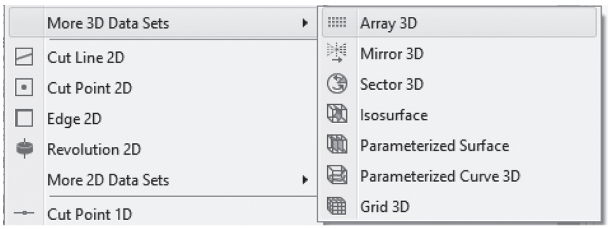

Figure 40. Menu selections under *More 3D Data Sets*.

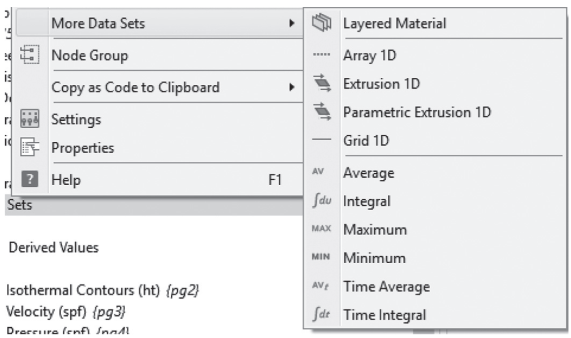

Figure 41. Menu selections under *More Data Sets*.

5.5.7.2 Evaluation Group

One interesting feature in COMSOL Multiphysics available for post-processing of the results is *Evaluation Group* option under *Results* (Figure 42). The output of the chosen evaluation appears under *Evaluation Group* under *Results* block. Using this capability, it is possible to interactively select vertices from the geometry and select any calculated or associated variables. When the evaluation command is executed, the points along with the calculated variable are listed in columns versus the time (for transient analysis). The data in the table can be plotted for visualization purposes. It is also possible to export the data to a text file or copy to the clipboard. This file can then be opened in other data processing programs, such as Microsoft Excel, for further processing. If exported, it appears under *Table*, which is part of *Results* block.

Copy to Clipboard results in the expressions *model.result().evaluationGroup (eg1)* for the definition of the evaluation group and *model.result().table()* for the contents of the table.

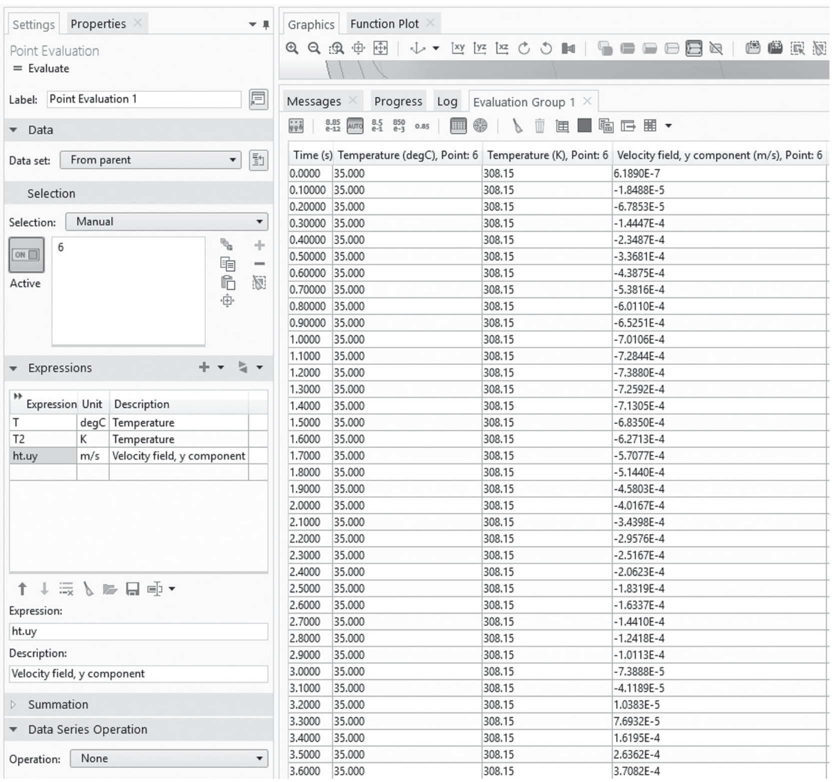

Figure 42. An example of generating data using *Point Evaluation*.

5.5.7.3 Derived Values

Derived Values node allows you to define point, global point, global matrix, system matrix, and mathematical evaluations (Figure 43). The latter include integration, maximum, and minimum operations. The defined parameters can then be evaluated as single or cluster, with the results exportable to the clipboard or text files. Data extracted either in the form of *Evaluation Group* or *Derived Values* can be exported to tables (Figure 44).

Copy to Clipboard results in the expression *model.result().numerical().*

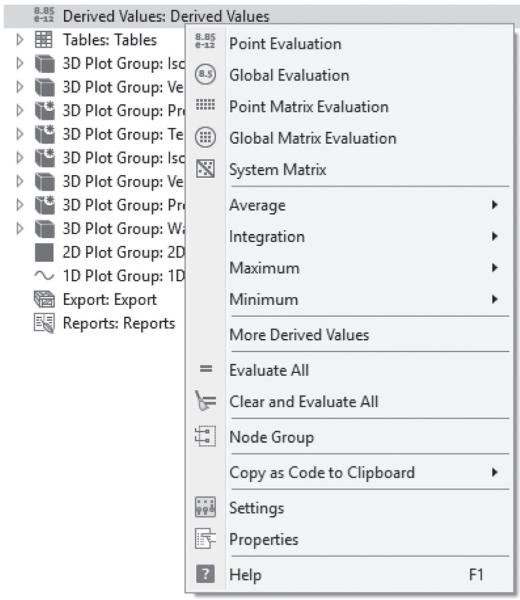

Figure 43. Menu selections under *Derived Values*.

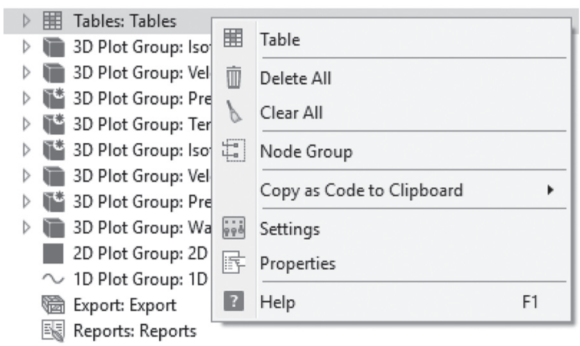

Figure 44. Menu selections under *Tables*.

5.5.7.4 Plots

Plots are used to visualize the data in *Data Sets* or *Tables* (Figure 45, Figure 46, and Figure 47). There are many ways to visualize this data. All plots are created by first defining 3D, 2D, or 1D plot groups to which can be subsequently added any number of volumes, surfaces, lines, edges, and point plots. For a 3D model, all three types of plots and contours are available, while for a 2D model, typically 2D and 1D diagrams are available. For example, one may wish to plot how the temperature varies at a particular point within a 3D time-dependent heat transfer model. To do this, one first needs to define *Cut Point 3D* under *Data Sets*, specifying the location of this point of interest. Then, one creates *1D Plot Group* under *Results*, where one references the previous *Cut Point 3D*. Under this *1D Plot Group*, one creates *Point Graph*, which can be set to use the data from its *Parent* (*1D Plot Group*). Here, the *y*-coordinate data is set as an expression equal to the temperature variable of interest, the units are set (°C or K), and the *x*-coordinate data is set to be *Time*. Adding other graphs to the same plot group will combine them on the same displayed plot.

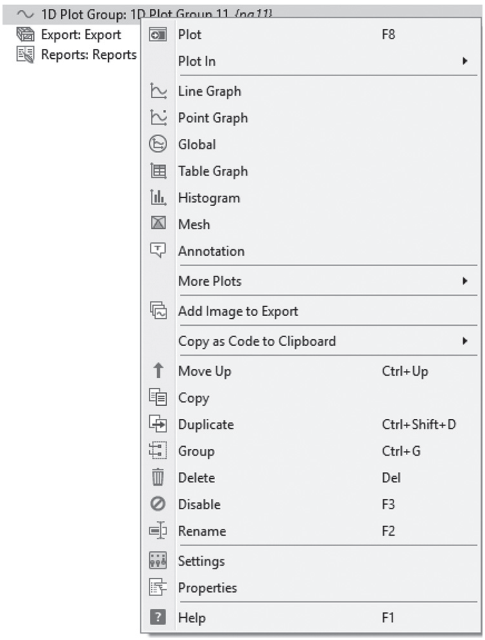

Figure 45. Menu selections under *1D Plot Group*.

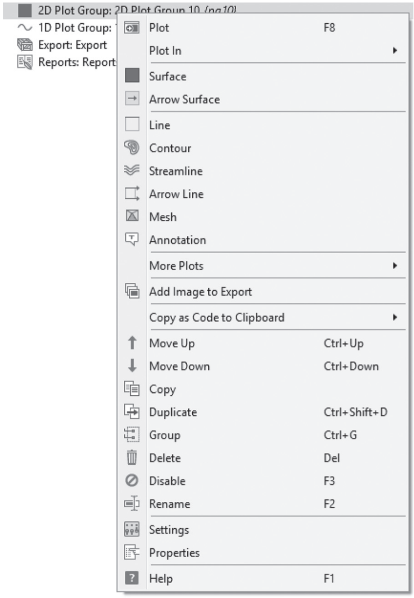

Figure 46. Menu selections under *2D Plot Group*.

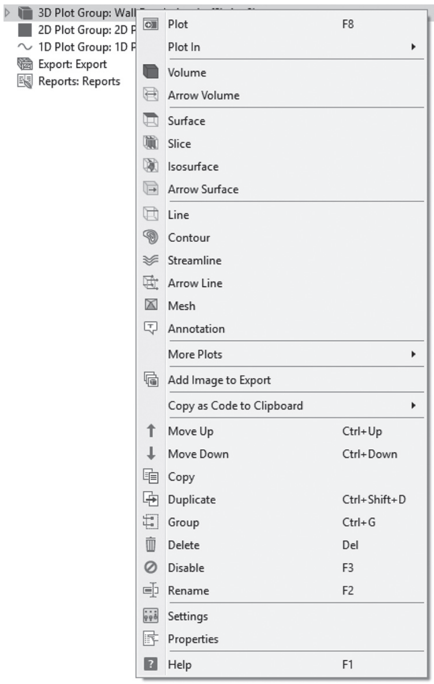

Figure 47. Menu selections under *3D Plot Group*.

5.5.7.5 Views

Views under *Results* allow control of the 3D and 2D visualization of the results (Figure 48 and Figure 49). Figure 50 is the result of the expanded *View 3D* case, which shows the direction of the light defined in three directions using *Direction* and adjusting the settings for coordinate, light intensity, specular intensity, and color.

Copy to Clipboard results in the expression *model.view()*.

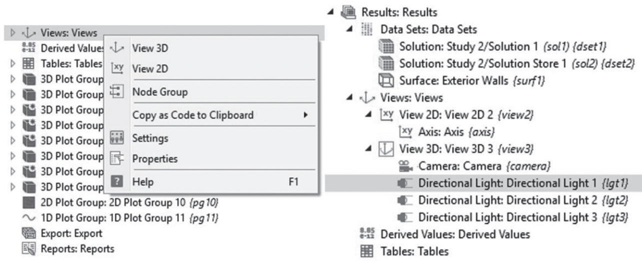

(*a*) (*b*)

Figure 48. (a) Menu selections under *Views*, (b) Options available for *View 3D*.

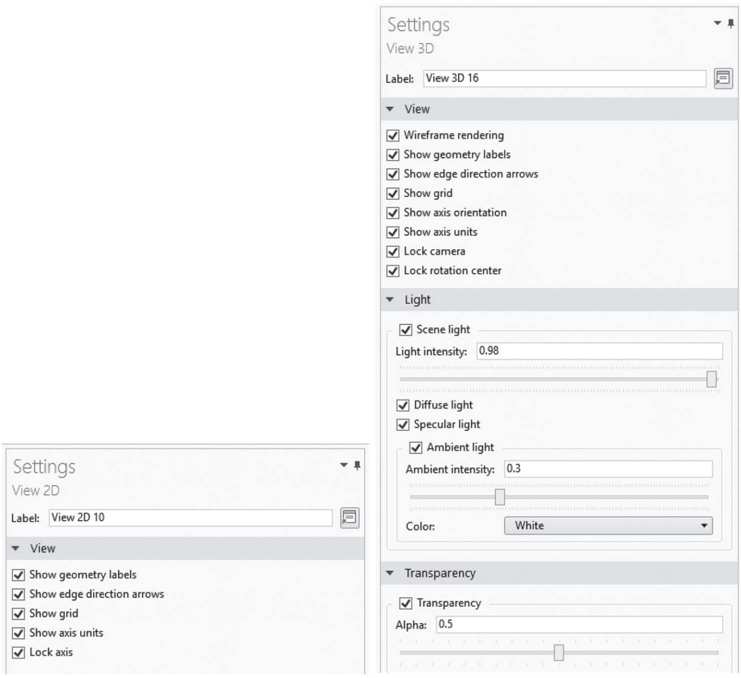

(*a*) (*b*)

Figure 49. *Settings***:** (a) *View 2D* options, (b) *View 3D* options.

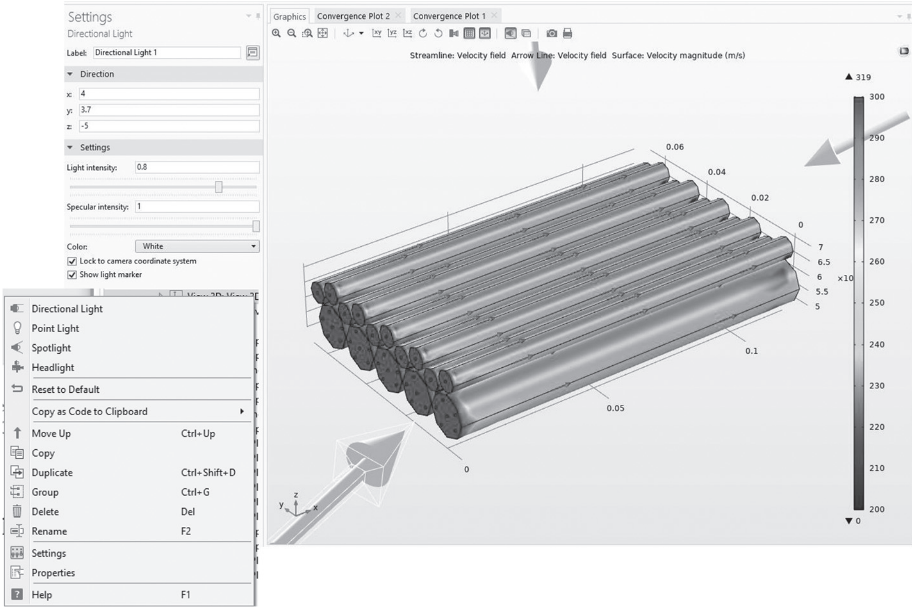

Figure 50. *Settings*, *Directional Light* under *View 3D*, an example of thermal flow model for Beesat Bridge on the southern section of the river Arvand, discussed in Chapter 13.

5.5.7.6 Export

Export node allows you to select the data plots which will be exported, typically in a text file format, for import into a spreadsheet (Figure 51).

Copy to Clipboard results in the expression *model.result().export()*.

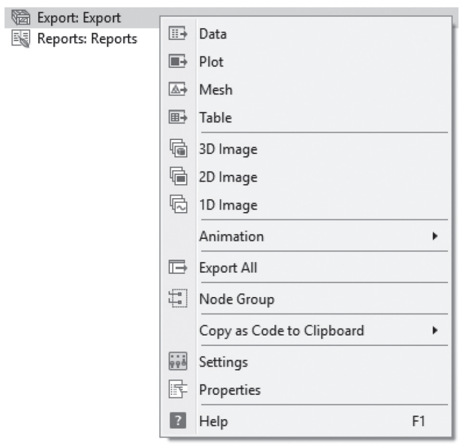

Figure 51. Menu selections under *Export*.

5.5.7.7 Reports

Reports node allows the analyst to define and then automatically generate reports of the model runs (Figure 52a). These reports allow organized presentation of the plots, diagrams, and parameter settings with minimal effort. Predefined report templates are available, identified as brief, intermediate, or complete. Custom reports can also be created, with the option to import your own template or set up a new one. The report normally starts with a table of contents and global definitions; it continues to components, study, and results, with the related subcomponents such as definitions, geometry, material, physics, study steps, data sets, and plot groups. Physics equations are presented for each scenario, together with the boundary and initial conditions formulae. After the report is generated, it is possible to modify any of its individual components (Figure 52b).

Copy to Clipboard results in the expression *model.result().report()*.

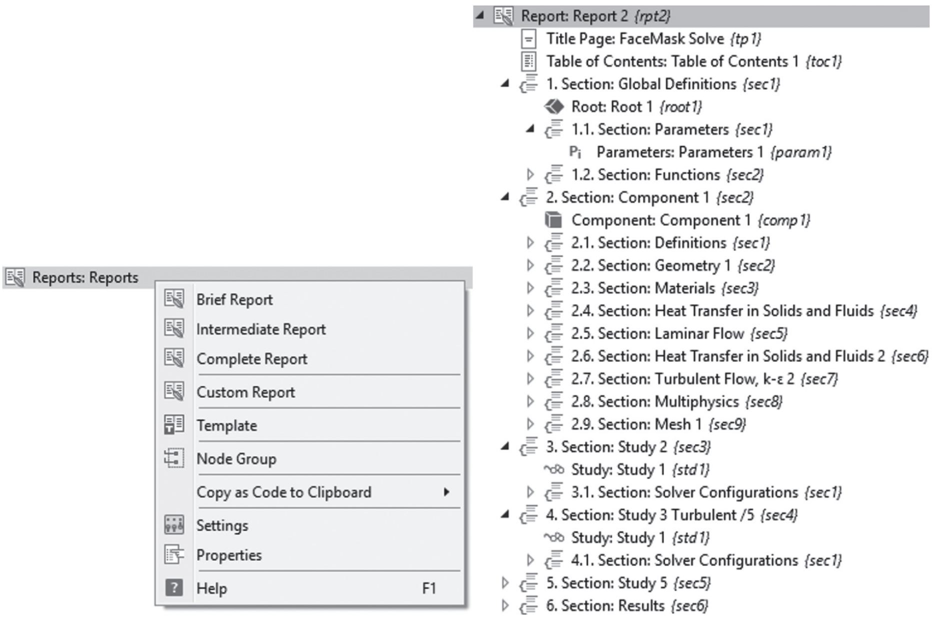

(*a*) (*b*)

Figure 52. (a) Menu selections under *Reports*, (b) Table of contents of the generated report.

5.6 Case Studies

The eight chapters following this one present case studies on the topic of heat transfer. They employ thermal-fluid models created using COMSOL

Multiphysics. When choosing their subjects, examples were selected based on what readers may experience in their daily lives (or on a few special occasions). You probably boil water in a kettle every day; some times you may keep your teapot warm using a tea candle, so that you can relax with that cup of hot tea. You probably sat in a car with a heated seat or used a hose to water plants. If you live in a cold climate, you need insulated walls to keep warm in winter. Have you worn a face mask and wondered how the air flows inside it? On the other hand, as far as molten rock coming out of a volcano, most likely you only saw that on television. But it does make for an interesting heat transfer problem!

In most case studies, the conduction heat transfer mode is present, with fluids, as liquid or gas, being involved as well. Interaction of solids and fluids brings with it conjugate heat transfer modeling, which describes the interaction between a non-isothermal flow and a solid. For cases where sufficiently high temperatures are reached, radiation heat transfer mode is included. A variety of materials are used for the models. For fluids, air and water are involved in many cases. For some of these, more viscous fluids are substituted for water to demonstrate the effect of higher viscosity.

COMSOL Multiphysics model files are made available for the majority of the cases presented. The reader is encouraged to think about the concepts illustrated by the case studies, review the model files, and make their own models, which they can solve and post-process using the guidelines provided in this book. True learning happens only by doing! The author would be happy to hear from the readers about their own FEM modeling experiences.

CHAPTER 6

CASE STUDY 1—A CUP OF HOT TEA

This chapter examines a system where heat transfer plays a key role. It is a system that we all have likely observed on a daily basis. As the title of the chapter suggests, we are talking about a cup of hot beverage, be it tea, coffee, or just plain hot water. From the perspective of heat transfer modeling, they are all going to be treated as plain water here. So, throughout this chapter, when a reference is made to hot tea, physical properties of water are to be assumed.

First, let us characterize the system from the heat transfer perspective. The components are a cup and a liquid beverage that has been heated to its boiling point and poured into the cup. The cup is made of glass. It is a non-metallic solid with relatively low conductivity. The problem can be characterized as transient in nature since the temperatures of the liquid and the cup are quickly changing after the cup is filled. Thus, a time-dependent model would be appropriate here. A steady-state model would be of no benefit. You already know what the solution of that model will predict—the cup and water will eventually end up at room temperature.

Looking at the modes of heat transfer, there is conduction happening as the heat is transferred from the hot liquid to the cool cup. There are two cases of solid-fluid interaction here: first, between the cup and the hot liquid inside it and, second, between the cup's exterior surfaces and the surrounding air. In both cases, there will be convective heat transfer taking place. There is also a gas-liquid boundary between the hot liquid and the air above it. Here, in addition to convective heat transfer, there will be some heat loss due to phase change as the hot liquid evaporates. Finally, there will be radiative heat loss from the hot water and the cup exterior.

The information to be obtained from the model is a variation of water and cup temperatures over time, for a time period of up to eighty minutes. When considering a suitable modeling approach for any system, the first question to ask is what the simplest approach will be that can be used to provide the desired information with satisfactory accuracy. Thus, next an analytical model will be presented and then FEM models will be introduced that can be compared to the analytical approach.

6.1 Analytical Model of Water and Spoon

This analytical model introduces another object that frequently joins the water and cup pair—a metal teaspoon. When you insert a teaspoon inside a hot cup of tea, the temperature of the metal increases from the initial room temperature to that of the liquid. A calculation using basic physics can estimate the amount of energy required by the spoon to be heated after being immersed in the liquid. Physics predicts the heat absorbed by the spoon is a function of its mass, specific heat capacity, and temperature difference between the initial spoon temperature and its surroundings.

Assume that the spoon (domain 1) is submerged completely within the hot water (domain 2), which is itself surrounded by the ambient air (domain 3). To allow for analytical model development, it is assumed that each of the domains has uniform spatial temperature distribution at any point in time. The analysis adopts an outside-in approach, starting from the ambient (the most exterior domain) to hot water (the middle domain) to spoon (the innermost domain). The initial temperature of domain 1 (the spoon) and 3 (the ambient) is assumed as 26 °C, and for domain 2 (the hot water), it is 97 °C. The water's temperature is reduced by 3 °C to account for cooling while the water is transferred to the cup.

An available example stainless steel teaspoon was weighed on an electronic scale and found to weigh 34 g. The example spoon was made of 18/10 stainless steel. This material's specific heat capacity is about 500 J/kgK. The difference between the initial spoon temperature of 26 °C and the hot water temperature of 97 °C is 71 °C. Thus, the total energy required to raise the spoon temperature from 26 to 97 °C can be found as: $(mcp)_{\text{spoon}}(T - T_{\text{amb}})_{\text{spoon}} = 0.034 \times 500 \times 71 = 1{,}207$ J.

Assuming no heat loss to the surroundings, if the spoon is immersed in water and the temperature in the two bodies is let to equalize, one can obtain this temperature by equating the energy balance for the two domains—energy given by one is assumed to be received by the other. This temperature is 93.93 °C, which is obtained from the following relation (ignoring the time effects): $(mc_p)_{\text{water}}(T_{\text{water}} - T_{\text{equlibrium}})_{\text{water}} = (mc_p)_{\text{spoon}}(T_{\text{equlibrium}} - T_{\text{spoon}})$.

The thermo-physical properties of water and the spherical "spoon" are presented in Table 2. In order to predict the equilibrium temperature from the said relation, there are number of approaches; one is to use the iteration technique and substitute temperatures, obtaining the difference between the left and right terms and continuing this substitution until it approaches to zero.

Table 2. Thermo-physical properties of water and stainless steel spherical "spoon" used for the lumped capacity technique.

Water			Teaspoon		
Heat Capacity (c_p)	4,180	J/kgK	Heat Capacity (c_p)	475	J/kgK
Density (ρ)	1,000	kg/m^3	Density (ρ)	7,850	kg/m^3
Radius (R)	2.38	cm	Radius (R)	1.01	cm
Height (h)	5.0	cm	Height (h)	11.4	cm
Area (A)	0.0123	m^2	Area (A)	0.001279	m^2
Volume (V)	8.44E-05	m^3	Volume (V)	4.30E-06	m^3
Mass (m)	0.0844	kg	Mass (m)	0.0338	kg
Convection Coefficient (h_c)	10	W/m^{2}K	Convection Coefficient (h_c)	10	W/m^{2}K
$Ah_c/\rho c_p$	3.49E-04	1/s	$Ah_c/\rho c_p$	7.98E-04	1/s
5 $Ah_c/\rho c_p$	3.74E-03	1/s	5 $Ah_c/\rho c_p$	3.99E-03	1/s
10 $Ah_c/\rho c_p$	3.49E-03	1/s	10 $Ah_c/\rho c_p$	7.98E-03	1/s
Temperature Difference ($T_{\text{hot}} - T_{\text{amb}}$)	71	°C (K)	Temperature Difference ($T_{\text{amb}} - T_{\text{hot}}$)	–71	°C (K)
Ambient Temperature (T_{amb})	26	°C	Spoon Temperature (T_{spoon})	26	°C
Hot Water Temperature (T_{hot})	97	°C	Hot Water Temperature (T_{hot})	97	°C

For the conditions where transient thermal analysis for a system is of interest, spatial temperature variations as well as heat generation terms can be ignored, and the only heat loss from the system is due to convection. Equation (10) can be simplified to include only the time-dependent temperature and convection terms $\rho V\, c_p(dT/dt) = -A\, h_c(T - T_{\text{amb}})$. Temperature ($T$) is the temperature of each domain (either the spoon or the water), which is assumed to be uniformly distributed in space and only varies with time (t). The solution to this analytical equation depends on the initial condition (T_0), thermo-physical properties of the domain (ρ and c_p), domain volume (V), and convection coefficient between the domain's exterior boundaries and the ambient (h_c)—between the hot water exterior and the air in one case and the hot water interior and teaspoon in the other.

The spoon is modeled as a single-domain object submerged in a single-domain hot water with their temperature being uniform throughout their volume. The heat transfer between the spoon and the liquid is assumed to be due to convection and is described by a convection coefficient.

The solution expressing temperature of the teaspoon or hot water versus the time can be written in terms of dimensionless temperature, defined as the ratio of the temperature difference at a given time to that of the initial state $\theta/\theta_0 = (T - T_{\text{amb}})/(T_0 - T_{\text{amb}}) = \exp(-Ah_c/\,\rho V c_p)t$.

The transient temperature for the liquid (starting from 97 °C) is presented in Figure 53, which assumes the hot water is surrounded by the air.

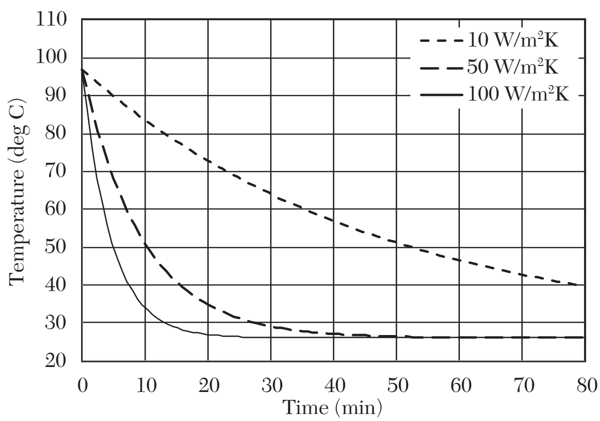

Figure 53. Transient temperature for hot water.

Figure 54 presents the transient temperature for the same spoon submerged in hot water for three different assumed convection heat transfer coefficient values between the ambient and water. It is seen that the higher the convection coefficient, the lower the maximum temperature reached by the spoon. Transient temperature for the equilibrium state, the temperature at which the cold spoon and hot water equalize to after the spoon has been submerged in the water, is presented in Figure 55. Note that the transient equilibrium temperature is in fact the temperature obtained from equating energy balance relations at each selected time step. The transient temperatures calculated in Figure 53 and Figure 54 are used as the inputs to Figure 55.

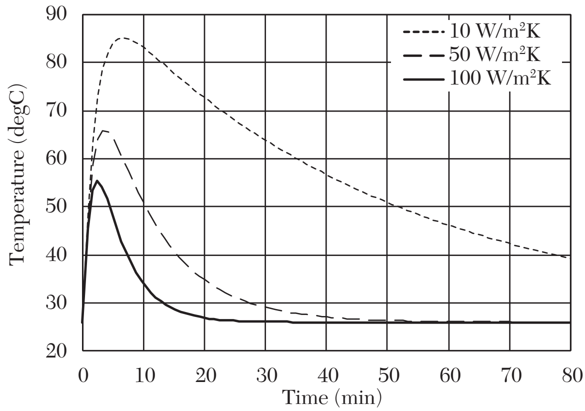

Figure 54. Transient temperature for spherical "spoon."

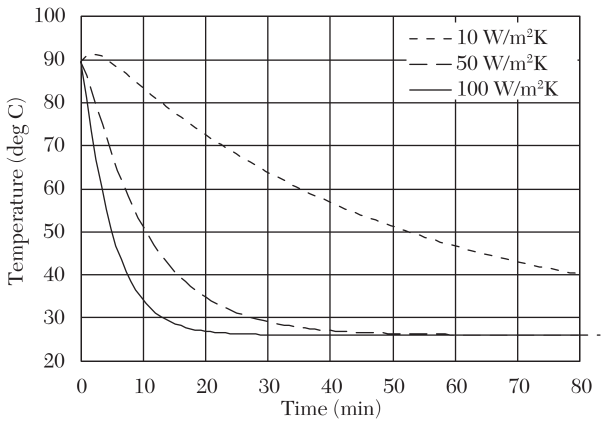

Figure 55. Transient temperature for spherical "spoon" submerged in hot water.

After about 10 min (see Figure 55), the temperatures of the spoon submerged in hot water for the three coefficients between the water and spoon, which is constant at 100 W/m^{2}K, and that of the ambient which varies (10, 50, and 100 W/m^{2}K), are about 83.6, 50.9, and 34.8 °C, respectively. Note that one would generally expect convection coefficients of about 5 to 10 W/m^{2}K for a horizontal and vertical wall, respectively, which has been the base of selection for convection heat transfer coefficients in this case study.

6.2 2D Axisymmetric FEM Model of Water and Spoon—Conduction Mode

In this section a numerical model will be developed that will then be compared to the analytical model presented in the previous section. The modeled system consists of hot water, metal spoon, and ambient. The hot water in a cup shape will be approximated by a cylinder. The teaspoon will be represented by a sphere of equivalent mass, with its dimensions obtained from the observed mass and density from literature. The spherical "spoon" will be located in the center of the water cylinder. Figure 56 shows that the volume of the sphere is equal to the spoon volume of 4.3 mL and the water volume is 84.7 mL. The intent of using these simple shapes is to approximate the behavior of a lumped-capacity model. As both shapes have axial symmetry, a 2D axisymmetric model will be employed (Figure 59a). The semicircle highlighted with purple in Figure 59b represents the spherical domain approximating the metal teaspoon.

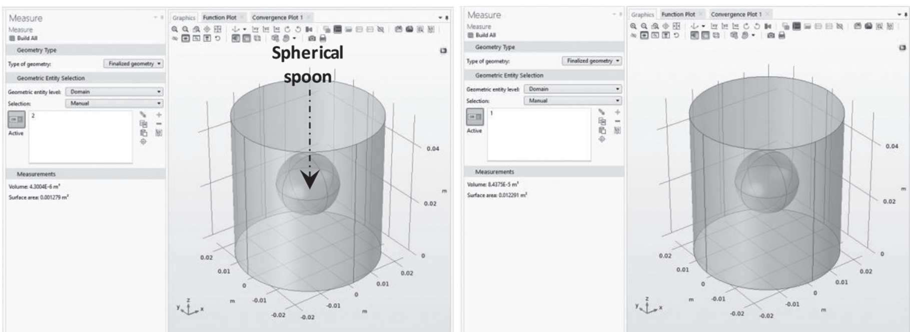

(*a*) (*b*)

Figure 56. Domain volume measurements: (a) Spherical "spoon" submerged in hot water, (b) Water.

The study in this section models the interaction of the hot water and the teaspoon using conduction heat transfer only. The next section combines conduction with a fluid flow using a conjugate heat transfer model, where the non-isothermal hot water flow is modeled in combination with a solid conduction heat transfer.

The solid spherical "spoon" domain has properties of stainless steel and the surrounding water domain has properties of water. Material properties for both were obtained from COMSOL Multiphysics material library and are listed in Figure 57 and Figure 58. The water's exterior boundaries exchange heat with the ambient by means of convection (Figure 60a). Sensitivity to the convection coefficient on the water's exterior surface will be investigated by running the model with it set to low and high values of 10 and 100 W/m²K. These will be controlled in the model settings by parameter *nnnn* with values of 1 and 10, which will be multiplying the base

Material Contents

	Property	Variable	Value	Unit	Property group
☑	Dynamic viscosity	mu	eta(T)	Pa·s	Basic
☑	Ratio of specific heats	gamma	gamma_w(T)	1	Basic
☑	Heat capacity at constant pressure	Cp	Cp(T)	J/(kg·K)	Basic
☑	Density	rho	rho(T)	kg/m³	Basic
☑	Thermal conductivity	k_iso ; kii = k_iso, kij = 0	k(T)	W/(m·K)	Basic
	Coefficient of thermal expansion	alpha_iso ; alphaii = alpha_iso, alphaij = 0	alpha_p(T)	1/K	Basic
	Bulk viscosity	muB	muB(T)	Pa·s	Basic
	Electrical conductivity	sigma_iso ; sigmaii = sigma_iso, sigmaij = 0	5.5e-6[S/m]	S/m	Basic
	Speed of sound	c	cs(T)	m/s	Basic

Figure 57. Water thermo-physical properties.

Material Contents

	Property	Variable	Value	Unit	Property group
☑	Heat capacity at constant pressure	Cp	475[J/(kg*K)]	J/(kg·K)	Basic
☑	Thermal conductivity	k_iso ; kii = k_iso, kij = 0	44.5[W/(m*K)]	W/(m·K)	Basic
☑	Density	rho	7850[kg/m^3]	kg/m³	Basic
	Relative permeability	mur_iso ; murii = mur_iso, murij = 0	1	1	Basic
	Electrical conductivity	sigma_iso ; sigmaii = sigma_iso, sigmaij = 0	4.032e6[S/m]	S/m	Basic
	Relative permittivity	epsilonr_iso ; epsilonrii = epsilonr_iso, epsilonrij = 0	1	1	Basic
	Coefficient of thermal expansion	alpha_iso ; alphaii = alpha_iso, alphaij = 0	12.3e-6[1/K]	1/K	Basic
	Dynamic viscosity	mu	1	Pa·s	Basic
	Young's modulus	E	200e9[Pa]	Pa	Young's modulus and Poisson's ratio
	Poisson's ratio	nu	0.30	1	Young's modulus and Poisson's ratio
	Murnaghan third-order elastic moduli	l	-3.0e11[Pa]	N/m²	Murnaghan
	Murnaghan third-order elastic moduli	m	-6.2e11[Pa]	N/m²	Murnaghan
	Murnaghan third-order elastic moduli	n	-7.2e11[Pa]	N/m²	Murnaghan
	Lamé parameter λ	lambLame	1.15e11[Pa]	N/m²	Lamé parameters
	Lamé parameter μ	muLame	7.69e10[Pa]	N/m²	Lamé parameters

Figure 58. Stainless steel thermo-physical properties.

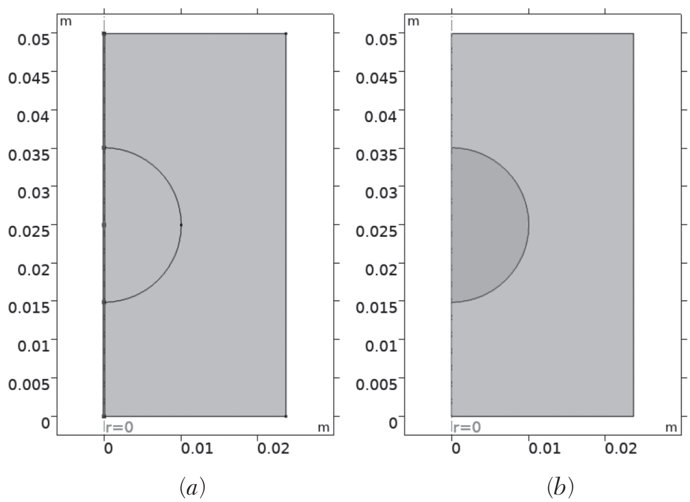

Figure 59. Spherical "spoon" submerged in hot water, modeled in COMSOL Multiphysics: (a) Axis of symmetry, (b) Solid spherical domain of the "spoon."

value of 10. Initial temperature values are set as 97 °C for water and 26 °C for the spoon. Meshed geometry is displayed in Figure 60b. Parameters used for this study are presented in Figure 61.

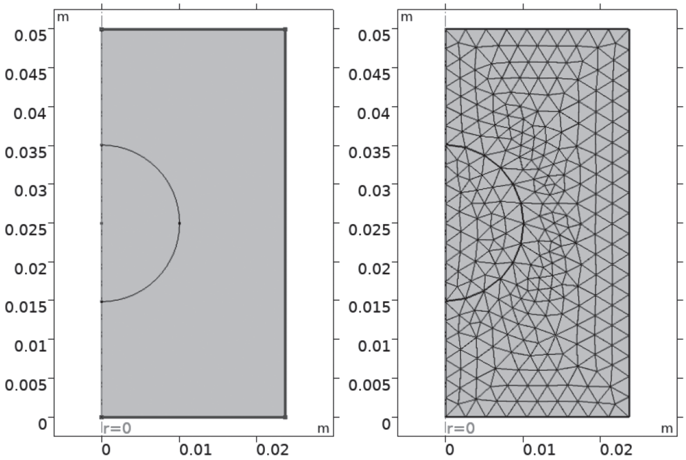

(*a*) (*b*)

Figure 60. Spherical "spoon" submerged in hot water, modeled in COMSOL Multiphysics: (a) Convective boundaries, (b) Solid-fluid model meshed geometry.

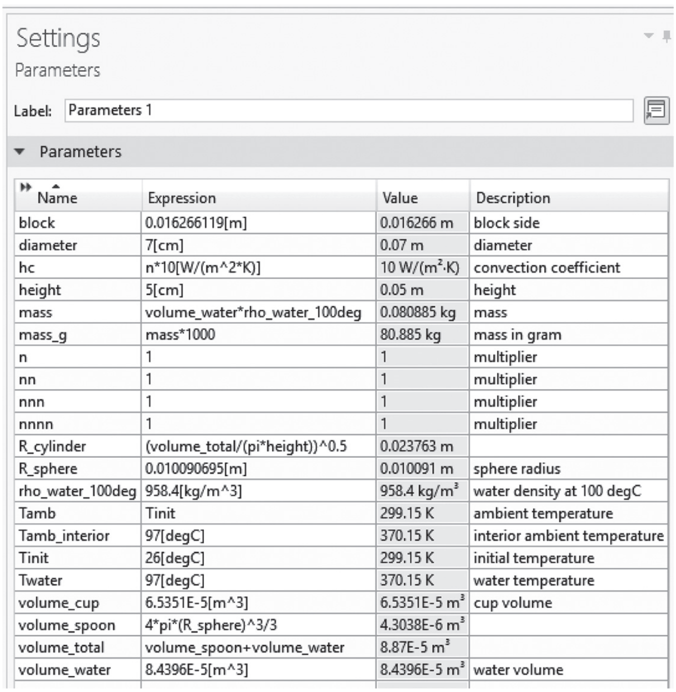

Settings
Parameters

Label: Parameters 1

Parameters

Name	Expression	Value	Description
block	0.016266119[m]	0.016266 m	block side
diameter	7[cm]	0.07 m	diameter
hc	n*10[W/(m^2*K)]	10 W/(m²·K)	convection coefficient
height	5[cm]	0.05 m	height
mass	volume_water*rho_water_100deg	0.080885 kg	mass
mass_g	mass*1000	80.885 kg	mass in gram
n	1	1	multiplier
nn	1	1	multiplier
nnn	1	1	multiplier
nnnn	1	1	multiplier
R_cylinder	(volume_total/(pi*height))^0.5	0.023763 m	
R_sphere	0.010090695[m]	0.010091 m	sphere radius
rho_water_100deg	958.4[kg/m^3]	958.4 kg/m³	water density at 100 degC
Tamb	Tinit	299.15 K	ambient temperature
Tamb_interior	97[degC]	370.15 K	interior ambient temperature
Tinit	26[degC]	299.15 K	initial temperature
Twater	97[degC]	370.15 K	water temperature
volume_cup	6.5351E-5[m^3]	6.5351E-5 m³	cup volume
volume_spoon	4*pi*(R_sphere)^3/3	4.3038E-6 m³	
volume_total	volume_spoon+volume_water	8.87E-5 m³	
volume_water	8.4396E-5[m^3]	8.4396E-5 m³	water volume

Figure 61. Parameters used for spherical "spoon" submerged in hot water study (global level).

Temperature contours for the low and high values of the convection coefficient are presented in Figure 62. Maximum temperature is at the sphere's center; it reduces from 82.6 to 37.7 °C if the convection coefficient is increased by 10. Note also the very narrow range of temperature variation of only a fraction of a degree for both plots (as seen on the temperature scale). This is due to the large thermal conductivity used in this case (1,000 W/mK) to simulate the behavior of a lumped-capacity model. Large thermal conductivity results in large thermal diffusivity (that is the ratio of heat conduction to convection), resulting in a uniform spatial temperature. A lumped-capacity model does not account for temperature variation within each body, and a high conductivity value will minimize these variations.

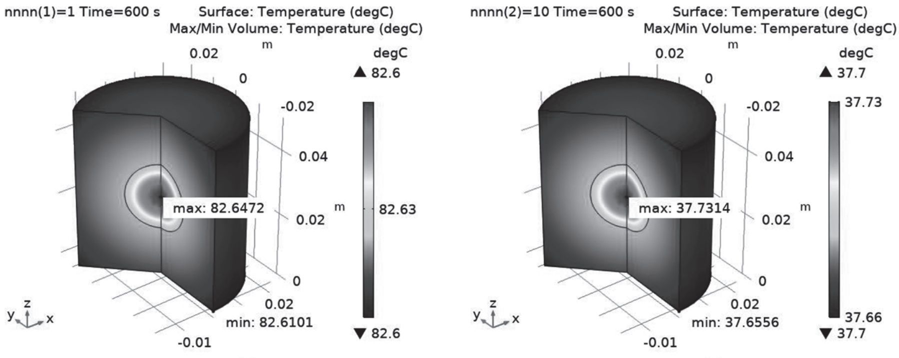

(a) (b)

Figure 62. Temperature contours for spherical "spoon" submerged in hot water, modeled in COMSOL Multiphysics, t = 10 min: (a) *nnnn* = 1 (h_c = 10 W/m²K), (b) *nnnn* = 10 (h_c = 100 W/m²K).

Temperature distributions for *Cut Points 3D* presented in Figure 63 are shown in Figure 64 for the two convection coefficient values. Point "*a*" is located at the spherical "spoon's" center and Point "*b*" is within the water domain. There is little difference between the temperature at points "*a*" and "*b*." However, the convection coefficient setting has a very strong effect on the model results. With the lower coefficient value, the temperature drops by about 14.4 to 82.6 °C (from 97 °C) after 10 min (600 s); when the coefficient is increased tenfold, during the same interval the temperature drops by 59.3 °C (from 37.7 °C), nearly approaching the ambient temperature setting. Thus, choosing the correct convection coefficient value for this system will be critical to obtaining an accurate result.

Figure 65 compares the FEM model results with those from the lumped-capacity method. For the FE results, the temperature at Point "*b*" (from the previous plot) is shown. These results show how close the

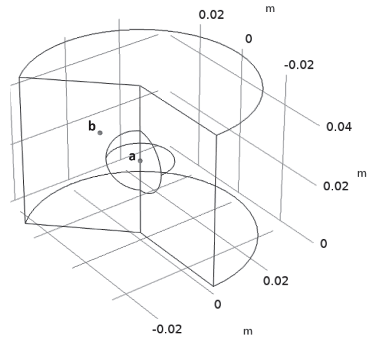

Figure 63. *Cut Points 3D* for spherical "spoon" submerged in hot water, modeled in COMSOL Multiphysics.

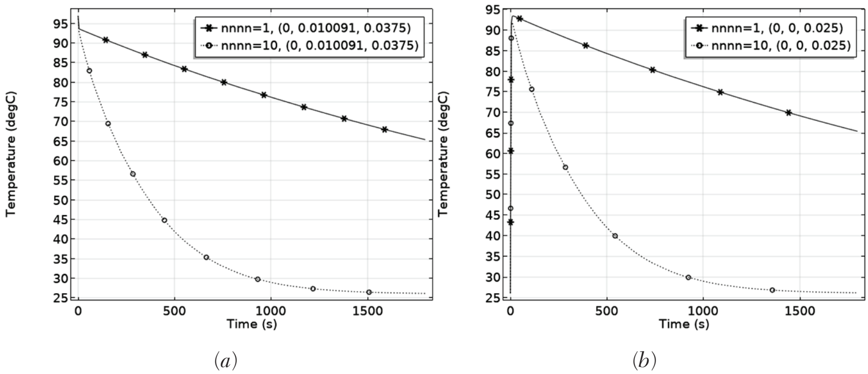

Figure 64. Transient temperature profiles at selected points for spherical "spoon" submerged in hot water modeled in COMSOL Multiphysics for the base condition *nnnn* = 1 (h_c = 10 W/m²K): (a) Hot water, Point "*b*" (b) Spherical "spoon" submerged in hot water, Point "*a*".

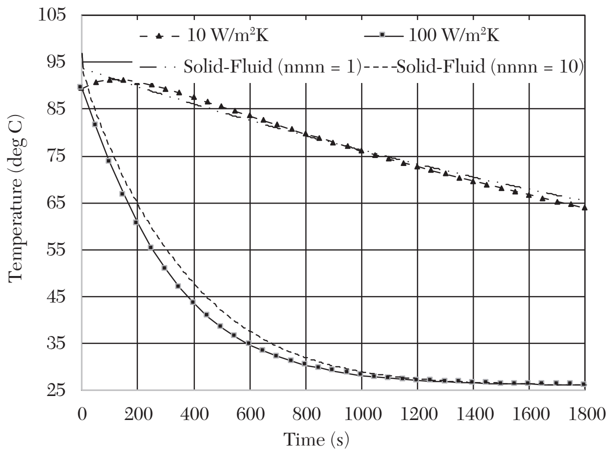

Figure 65. Comparison between transient temperature profiles at selected points for spherical "spoon" submerged in hot water for the conduction heat transfer model (modeled in COMSOL Multiphysics) versus the analytical model for spherical "spoon" submerged in hot water at Point "*b*" for the base condition *nnnn* = 1 (h_c = 10 W/m²K).

analytical and FEM model results are. The trends in both cases are very similar. The analytical model predictions are at most about 3 °C lower than the FEM model. If such accuracy were acceptable for the intended application, one would be able to use the analytical model.

6.3 2D Axisymmetric FEM Model of Water and Spoon—Conjugate Heat Transfer

The conduction-only heat transfer model presented previously does not account for the heat transfer by convection flow due to the buoyancy forces produced by the temperature variations within the hot fluid. This section presents a more complex model that adds the flow model to the thermal model. This is accomplished by defining a conjugate heat transfer model. In this model, a combination of the solid-fluid physics (as discussed in the previous section) and the flow model (a laminar compressible flow with Mach under 0.3) are employed. These two physics interact through *Multiphysics* node added to the model.

The geometry is the same as in the previous case, with a fluid domain having an external shape of a cylinder and a solid spherical "spoon" at the center. The fluid domain within a 2D axisymmetric model is highlighted in Figure 66a. The fluid symmetry axis is shown in Figure 66b.

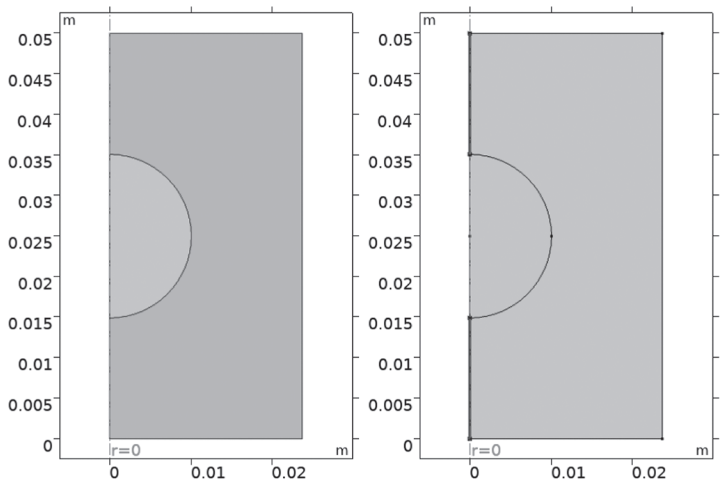

(a) (b)

Figure 66. Spherical "spoon" submerged in hot water, modeled in COMSOL Multiphysics: (a) Fluid domain, (b) Axial symmetry.

Similar to the previous case, material properties (water and spoon) are adopted from COMSOL Multiphysics material library (Figure 57 and

Figure 58). As in the previous section, the water domain's exterior boundary exchanges heat with the ambient by means of convection, with two values being tested—a low value of 10 W/m^{2}K (*nnnn* = 1) and a high value of 100 W/m^{2}K (*nnnn* = 10). The initial temperature for water was set at 97 °C and for the spoon at 26 °C; the ambient temperature was set to 26 °C.

Meshed geometry is seen in Figure 67b. Comparing this mesh to the one for the previous case, one may observe the presence of the boundary wall elements—two layers of quad elements adjacent to the walls surrounding the fluid domain. These are added for the purpose of fluid flow modeling. Parameters used for this study are presented in Figure 61.

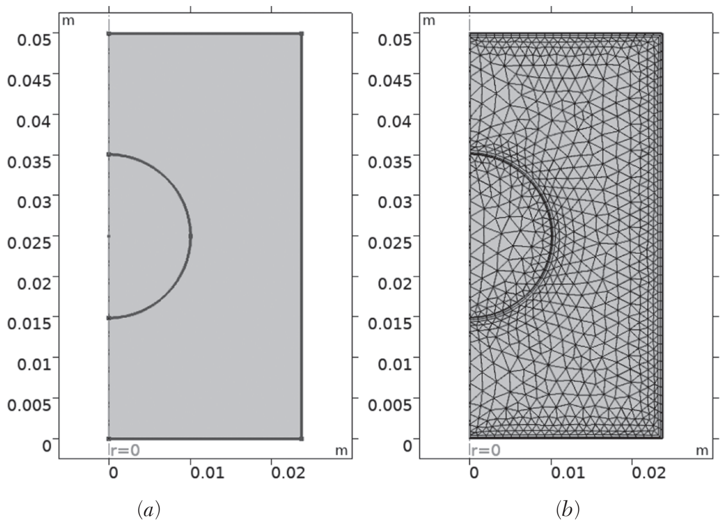

Figure 67. Spherical "spoon" submerged in hot water, modeled in COMSOL Multiphysics: (a) Convective boundaries, (b) Conjugate model meshed geometry.

Figure 68 and Figure 69 present the 3D velocity contours for the conjugate heat transfer model at time points 10 s and 10 min for the two convection coefficients of 10 W/m^{2}K (*nnnn* = 1) and 100 W/m^{2}K (*nnnn* = 10). The maximum velocity magnitude is 39.92 mm/s at 10 s; it decreases to 4.24 mm/s after 10 min for *nnnn* = 1. For the higher convection coefficient (*nnnn* = 10), the initial velocity magnitude is slightly lower, at 37.25 mm/s at 10 s, and it decreases to 4.13 mm/s at 10 min. The general trend for velocity decrease with time is due to the cooling of the fluid and thus reduction of the temperature difference that drives the flow.

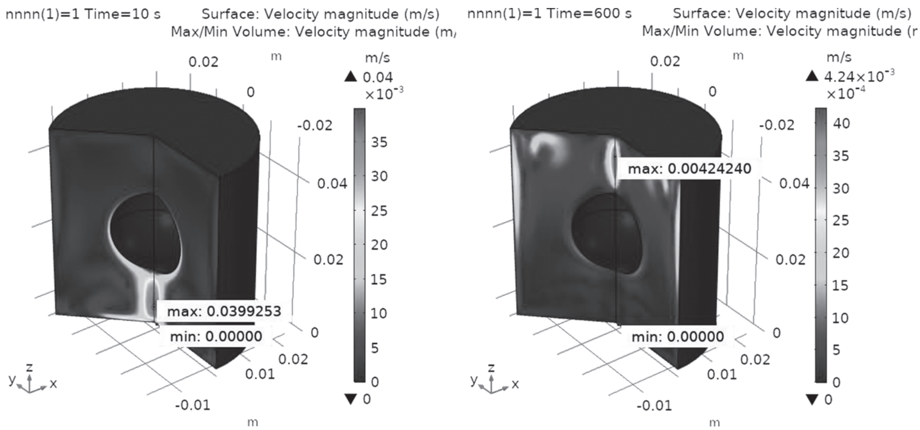

(a) (b)

Figure 68. Flow velocity contours for spherical "spoon" submerged in hot water, modeled in COMSOL Multiphysics, *nnnn* = 1 (h_c = 10 W/m^{2}K): (a) t = 10 *s*, (b) t = 10 min.

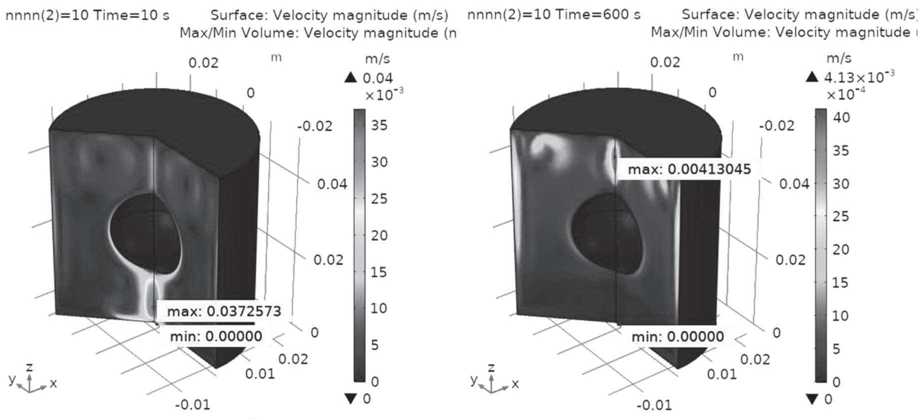

(a) (b)

Figure 69. Flow velocity contours for spherical "spoon" submerged in hot water, modeled in COMSOL Multiphysics, *nnnn* = 10 (h_c = 100 W/m^{2}K): (a) t = 10 *s*, (b) t = 10 min.

2D contour plots on the axisymmetric plane shown in Figure 70 and Figure 71 add arrows that show flow velocity direction (*Arrow length* set to *Normalized*). Here one can see that a circulating flow is formed. The flow is downward at the exterior walls, where the denser cooler fluid descends, warms up by mixing with the interior warmer fluid, and rises again to the top through the central region. An interesting difference can be seen between the initial flow at 10 s and the stabilized one after 10 min. For

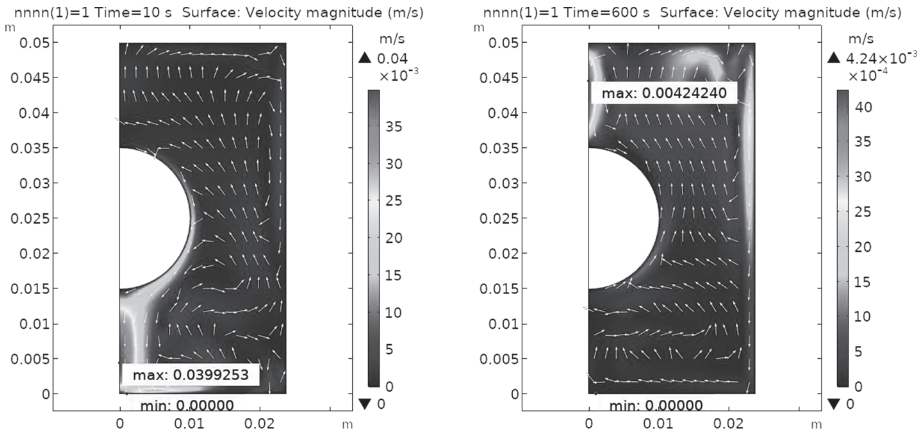

(*a*) (*b*)

Figure 70. Flow velocity contours for spherical “spoon” submerged in hot water, modeled in COMSOL Multiphysics, *nnnn* = 1 (h_c = 10 W/m^{2}K): (a) t = 10 s, (b) t = 10 min.

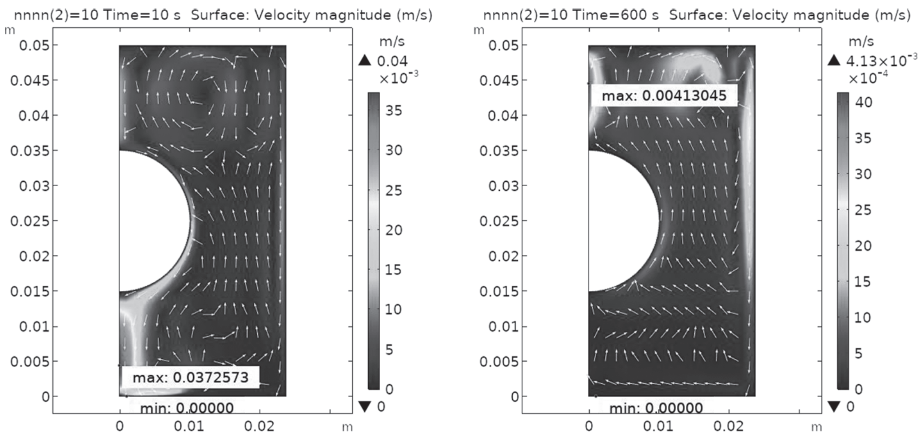

(*a*) (*b*)

Figure 71. Flow velocity contours for spherical “spoon” submerged in hot water, modeled in COMSOL Multiphysics, *nnnn* = 10 (h_c = 100 W/m^{2}K): (a) t = 10 s, (b) t = 10 min.

the former, the peak velocity is on the central axis below the sphere. It is a strong downward current due to the cool fluid produced by heat transfer with the cool sphere at the start of the modeled interval. For the flow at 10 min, the same region below the sphere now shows an upward flow.

Temperature contours are presented in Figure 72 and Figure 73 for the same previous conditions. The plots for the initial conditions at 10 s confirm the presence of the cooled fluid flow at the central axis below the sphere. The higher convective coefficient of the latter plot results in cooler fluid collecting at the bottom even at the 10 s point. After 10 min, a stratification trend develops, with cooler water layers collecting near the cylinder's bottom.

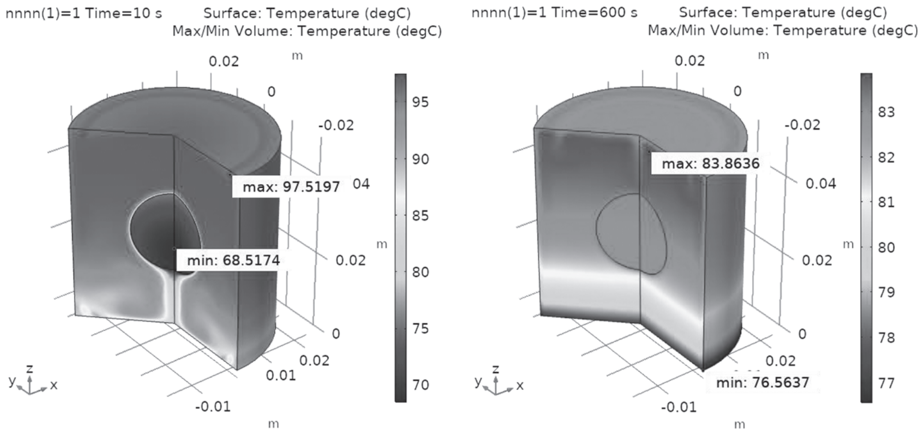

(*a*) (*b*)

Figure 72. Temperature contours for spherical "spoon" submerged in hot water, modeled in COMSOL Multiphysics, *nnnn* = 1 (h_c = 10 W/m²K): (a) t = 10 s: (b) t = 10 min.

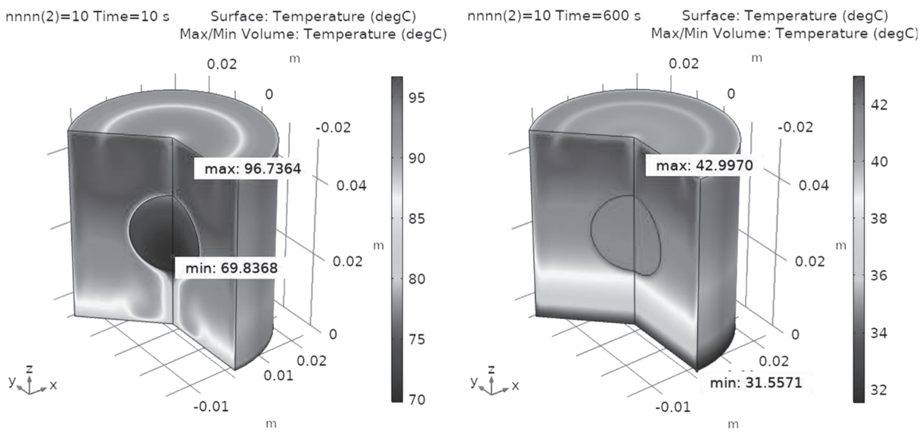

(*a*) (*b*)

Figure 73. Temperature contours for spherical "spoon" submerged in hot water, modeled in COMSOL Multiphysics, *nnnn* = 10 (h_c = 100 W/m²K): (a) t = 10 s: (b) t = 10 min.

Figure 74a shows the spatial temperature profile for the horizontal radial line passing through the center of the solid domain. Figure 74b shows the same for the vertical line along the axisymmetric axis. For the vertical profile, the plot clearly shows the presence of the cooler layers for z values up to about 1.5 cm. Figure 75 presents a comparison of the transient temperatures for the cases of the analytical, conduction, and conjugate heat transfer models for the two convection coefficient settings of 10 W/m²K (*nnnn* = 1) and 100 W/m²K (*nnnn* = 10). The transient temperature distributions for the corresponding convection coefficients show very similar behaviors among the three cases, with the analytical model slightly underpredicting the temperature distribution at most about 2 to 3 °C for the conduction model case and about 5 to 10 °C for the case of the conjugate model.

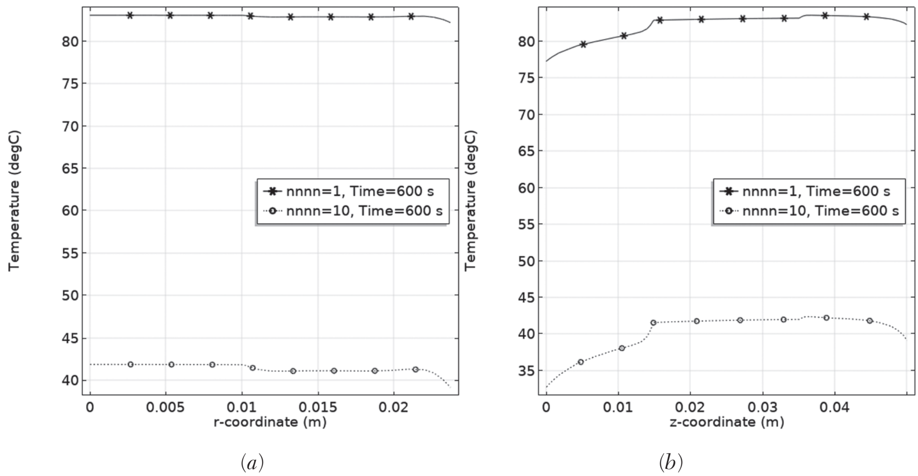

Figure 74. Spatial temperature profiles at selected lines for spherical "spoon" submerged in hot water modeled in COMSOL Multiphysics for the base condition *nnnn* = 1 (h_c = 10 W/m²K), *t* = 10 min: (a) Radial distance from the axisymmetric axis, *r*-coordinate, (b) *Cut Line 2D* at axisymmetric axis height, *z*-coordinate.

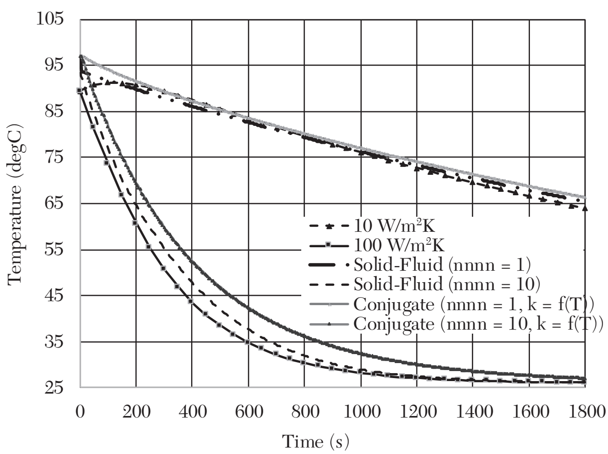

Figure 75. Comparison between transient temperature profiles at selected points for spherical "spoon" submerged in hot water for the conduction and conjugate heat transfer models (modeled in COMSOL Multiphysics) versus the analytical model for spherical "spoon" submerged in hot water at Point "*b*" for the base condition *nnnn* = 1 (h_c = 10 W/m²K).

It is seen that thermal behavior is well predicted for the three scenarios and the temperature predictions are close. It can be concluded that the FEM model validation is achieved. Additionally, adjusting thermal conductivity and using an only the conduction model will result in temperatures identical to those of the analytical ones predicted through the lumped capacity method. It may be concluded that using a simplified version of the model (i.e., conduction) should result in sufficiently accurate predictions; using such a model would save computational resources.

6.4 3D FEM Model of a Cup of Hot Tea

In this section, a full 3D model of a cup with hot tea (water) is developed. As this model is more complex than the previous ones, the geometry was simplified by removing the spoon and just having the water and cup in the model. Parameters used for this study are presented in Figure 61. For this case study, a cup including a water solid model was created in Solid Edge CAD tool from an available physical cup after carrying out careful measurements. Dimensioned drawing and a rendered image of the model are presented in Figure 76.

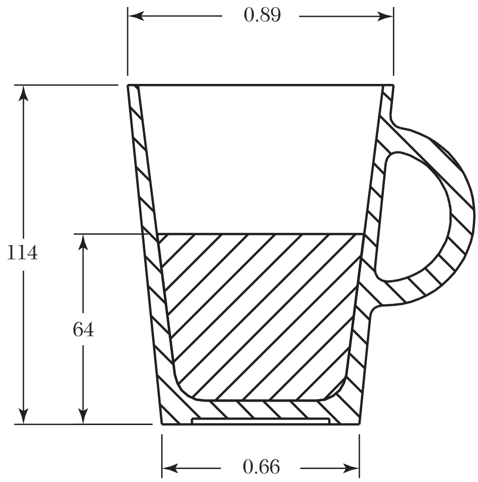

(*a*) (*b*)

Figure 76. The glass cup with water, models created in Solid Edge: (a) Dimensioned section view, (b) Rendered image.

When setting up this study, one key point to address is how to carry out the thermal modeling of the water. The most accurate approach would be to use the water's temperature-dependent thermal properties in addition to incorporating conjugate heat transfer that includes the flow model within the water domain, similar to the model presented previously in Section 6.3. However, the conjugate heat transfer model developed in Section 6.3 was for a 2D model; for 3D geometry, such a model is significantly more challenging to solve. The solution of a 3D conjugate heat transfer model is described for an oxygen facemask in Chapter 10, and it did prove to be very demanding of computer resources and time.

In view of these considerations, the teacup model will be solved by following two approaches. In the first approach, actual temperature-dependent water thermal conductivity will be used, as defined in COMSOL Multiphysics material library. However, the water will be treated as a *solid* domain. This is not a realistic model, as an actual fluid water convection mechanism is to a large extent the mode of heat transfer. This model will serve as a baseline for comparison with the other models.

In the second approach, the water's thermal conductivity will be set to various higher values in order to emulate the increased heat conduction due to the convection flow, which is not modeled. These values will range from 10 to 500 W/mK. However, without experimental observations, it would be difficult to deduce which thermal conductivity value provides the closest approximation of reality. Thus, the next section reports on thermal imaging experiments intended to provide a reference for calibrating this model by the adjustment of the heat transfer coefficient.

6.4.1 FEM Model of a Cup of Hot Tea—Model Setup

The 3D geometry of the cup with water is shown in Figure 77a. The geometry was created in Solid Edge CAD software, with water and cup forming two separate bodies, and with the water geometry being driven by the cup's internal shape. An assembly of these two bodies was formed and then exported using an **.igs* format. This exported file was then imported into COMSOL Multiphysics. As the geometry is symmetrical about a vertical plane, it was partitioned into two halves using *Work Plane*, and one half was discarded. The model was meshed using a tetrahedral mesh, resulting in 10,793 elements, as shown in Figure 77b. Fluid domain is presented in Figure 78.

Model initial temperature settings are 26 °C for the glass cup, 97 °C for the water in the cup, and 26 °C for the ambient temperature. The water initial temperature is set to be 3°C below the boiling point to account for the cooling while the water is transferred from the kettle and poured into the glass.

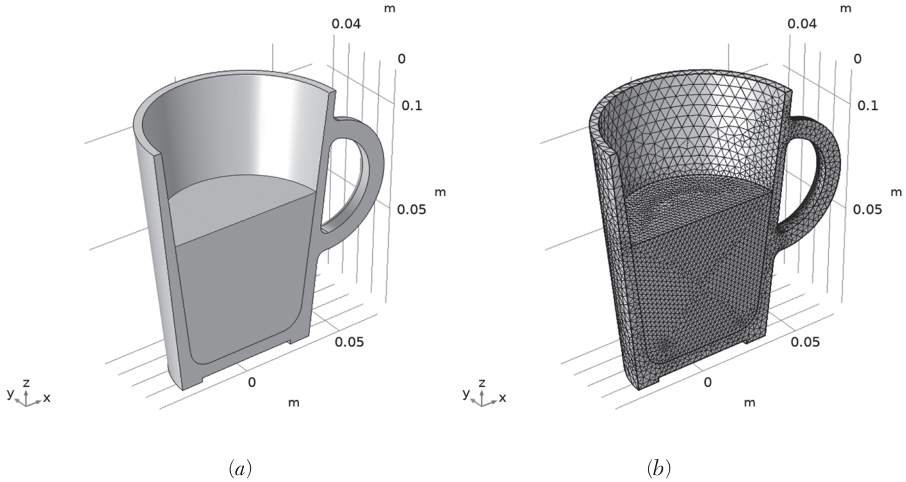

Figure 77. Cup of hot tea model: (a) Convective liquid top surface losing heat by evaporation, (b) Meshed geometry.

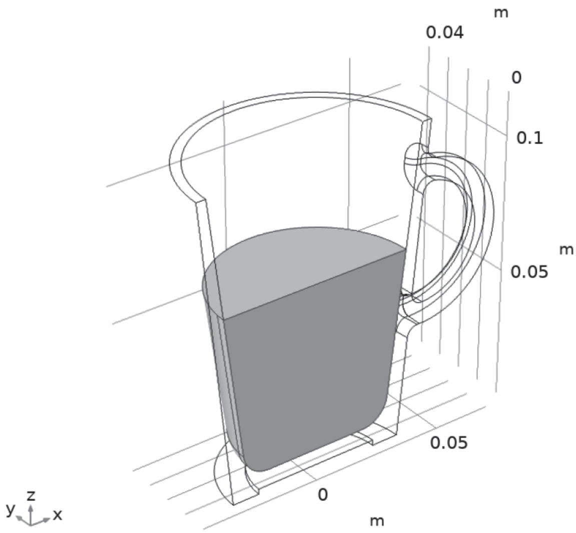

Figure 78. Cup of hot tea model, fluid domain.

It is possible to define ambient properties and include the environmental conditions such as humidity, pressure, and wind velocity. This information then can be employed in whatever ambient-related physics are to be used in the model. This approach is used in this model. Under *Component*, *Definition* one defines *Ambient Thermal Properties*, which represent *Ambient Conditions* (e.g., *Ambient temperature*, *absolute pressure*, *relative humidity*, *Wind velocity*, *Clear sky noon beam normal irradiance*, and *diffuse horizontal irradiance*)—Figure 79. Not all of these settings will necessarily be used in all models.

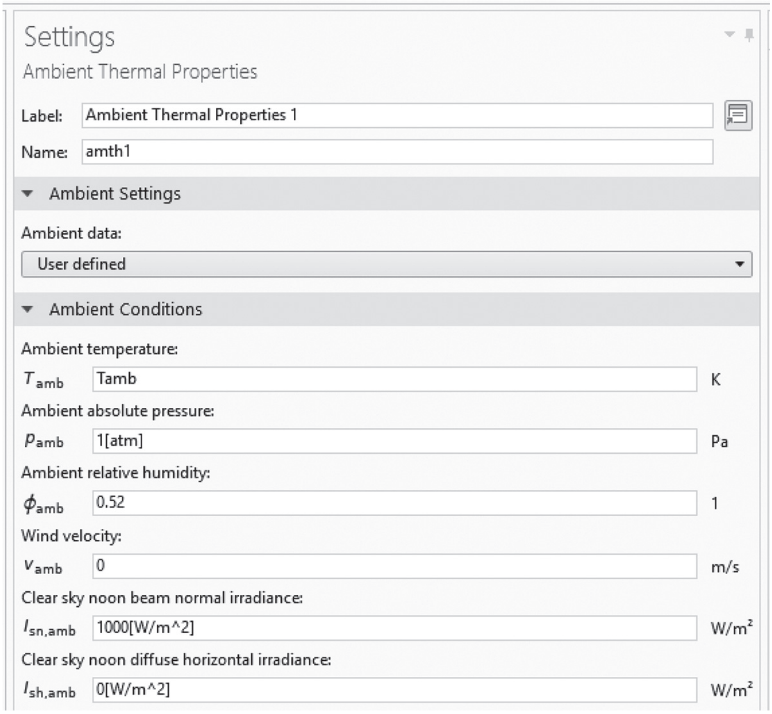

Figure 79. Ambient thermal properties.

The material properties of glass are shown in Figure 80. Most of the values were taken from the built-in material library of the core COMSOL Multiphysics. However, the actual density of the glass from which the cup was made was not precisely known. Glasses have varying densities, depending on the type of glass [106]. For example, borosilicate glass, similar to Pyrex, has density of 2.235 g/cm^3, while soda-lime glass has density of 2.52 g/cm^3. As the mass of the glass is important for accuracy of the model, the glass density was adjusted so that the model's cup volume had a mass that matched the mass obtained by weighing the glass using an electronic scale. The glass weight measurement was confirmed using two different scales, with the results matching within 1 g. The adjusted glass density is 2.482 g/cm^3, which falls within the range of the reported densities.

An important parameter, as demonstrated by the previous models of the cooling hot water, is the heat loss modeling at the exterior boundaries. This is what determines the rate of the system's cooling. Three heat

Material Contents

Property	Variable	Value	Unit	Property group
Heat capacity at constant pressure	Cp	703[J/(kg*K)]	J/(kg·K)	Basic
Density	rho	2481.6[kg/m^3]	kg/m³	Basic
Thermal conductivity	k_iso ; kii = k_iso, kij = 0	1.38[W/(m*K)]	W/(m·K)	Basic
Relative permeability	mur_iso ; murii = mur_iso, murij = 0	1	1	Basic
Electrical conductivity	sigma_iso ; sigmaii = sigma_iso, sigmaij = 0	1e-14[S/m]	S/m	Basic
Coefficient of thermal expansion	alpha_iso ; alphaii = alpha_iso, alphaij = 0	0.55e-6[1/K]	1/K	Basic
Relative permittivity	epsilonr_iso ; epsilonrii = epsilonr_iso, epsilonrij = 0	3.75	1	Basic
Young's modulus	E	73.1e9[Pa]	Pa	Young's modulus and Poisson's ratio
Poisson's ratio	nu	0.17	1	Young's modulus and Poisson's ratio
Refractive index, real part	n_iso ; nii = n_iso, nij = 0	1.45	1	Refractive index
Refractive index, imaginary part	ki_iso ; kiii = ki_iso, kiij = 0	0	1	Refractive index

Figure 80. Glass thermo-physical properties.

transfer mechanisms can be identified: (1) convective losses from all the cup surfaces, (2) heat loss from the exposed water surface, and (3) radiative heat loss.

Convective heat loss was defined separately for (1) the exterior walls and handle of the cup (Figure 81a); and (2) for the interior walls of the cup, above the water surface (Figure 81b). There are two approaches to define *Convective heat flux* under the settings for *Heat Flux* node in COMSOL Multiphysics, by: (1) employing *User defined* option, where the heat transfer coefficient value is entered directly; and (2) selecting from the four built-in options (e.g., *Internal and External natural convection*). The latter approach is shown in Figure 82. This approach was attempted but did not produce satisfactory results. An additional disadvantage of this approach is that the actual value of the heat transfer coefficient is not readily available. Therefore, the first approach was used by specifying the two convection coefficient settings of 10 W/m²K (*nnnn* = 1) and 100 W/m²K (*nnnn* = 10) for the interior and exterior surfaces.

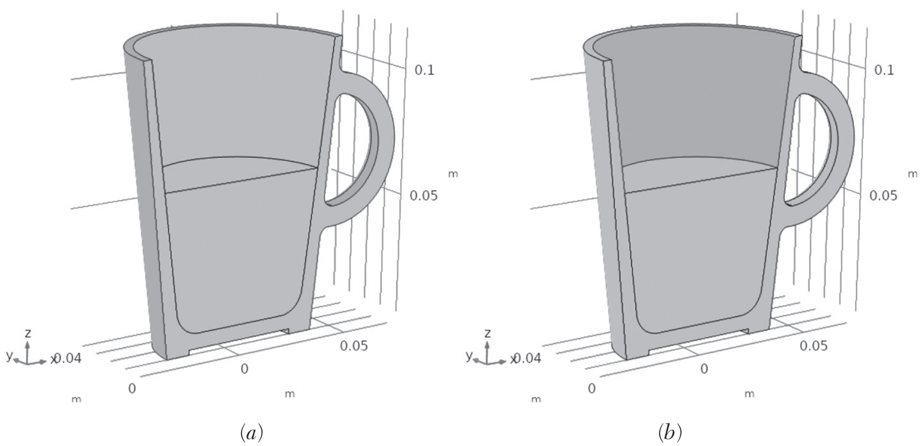

Figure 81. Convective surfaces: (a) Exterior walls, (b) Interior walls.

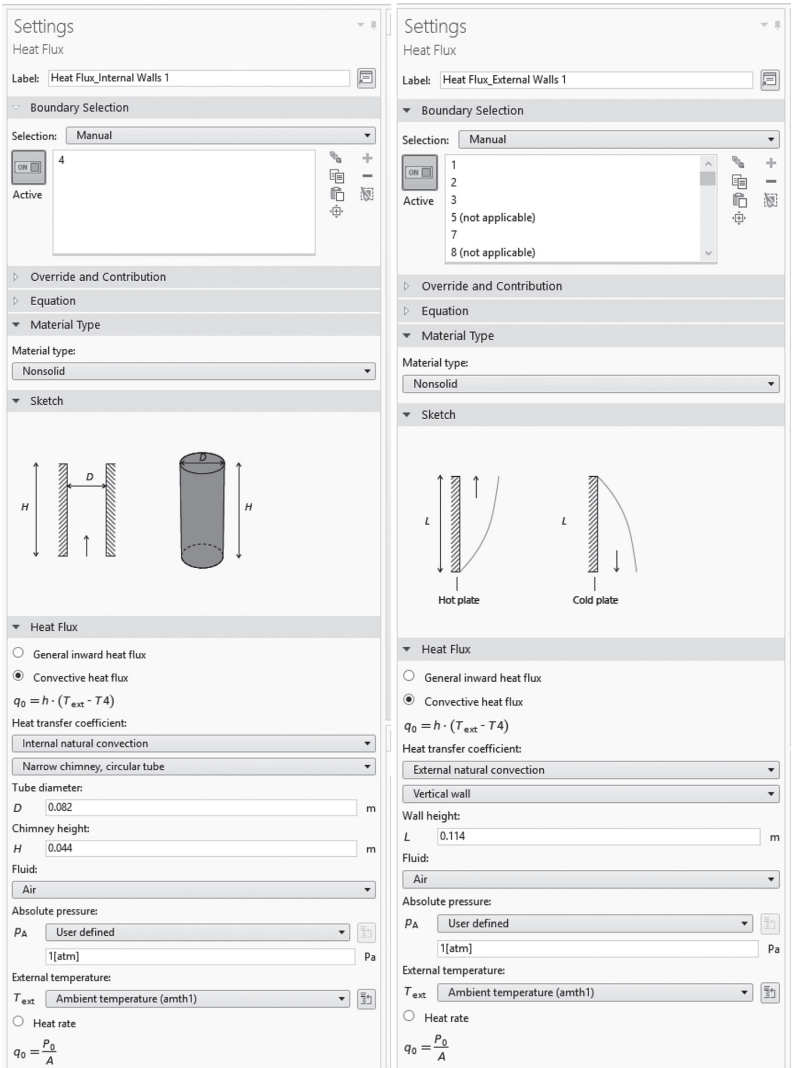

(*a*) (*b*)

Figure 82. Cup of hot water model convection loss boundary conditions: (a) Interior walls, (b) Exterior walls.

Significant heat loss is expected to occur from the open water surface due to evaporation, convection, and radiation. The rate of this heat loss as a function of the water temperature was obtained from online source, defined as a table (plotted as a function shown in Figure 83) and used as input for a temperature-dependent boundary heat source (Figure 84a). Radiative heat transfer was not modeled in this case study, since the water-exposed surface radiative loss was already included in the heat loss from the water surface (Figure 83). Radiation heat transfer from the external or internal cup surfaces were not included in this study (Figure 81).

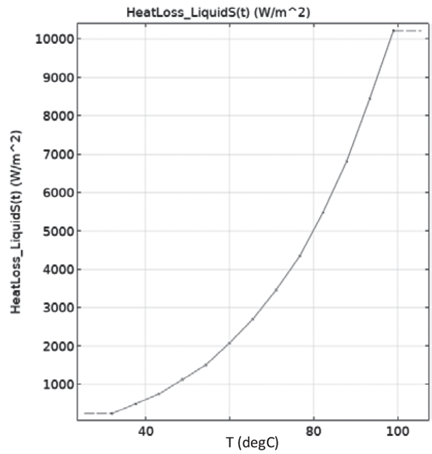

Figure 83. Temperature-dependent heat loss for water top surface versus the water temperature (plot data taken from [107]).

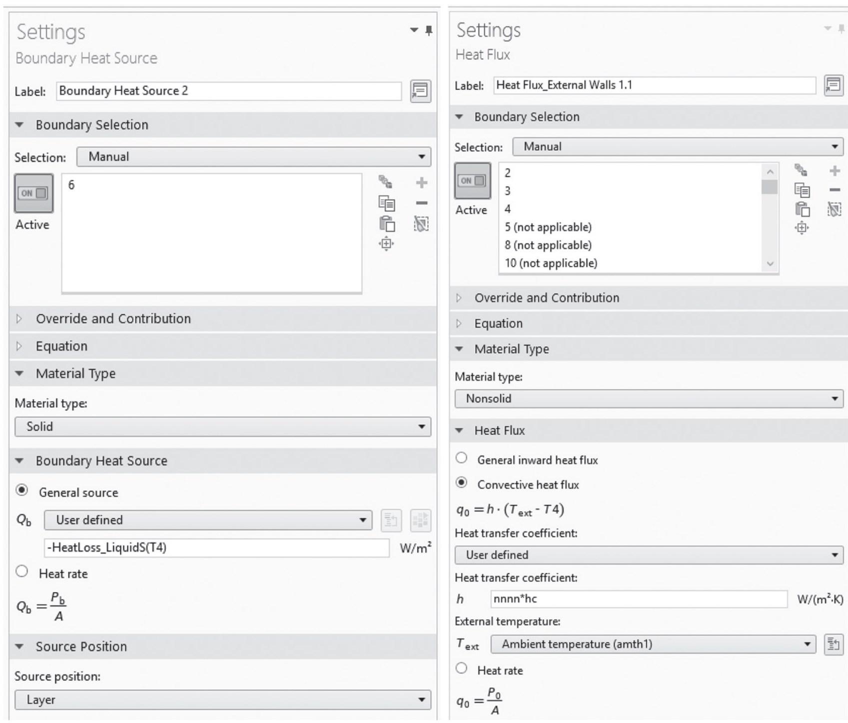

(a) (b)

Figure 84. Cup of hot water model boundary conditions: (a) Convection loss from the liquid surface, (b) Convection heat transfer from exterior surfaces.

The thermal analysis model tree for the 3D cup of hot liquid is shown in Figure 85; it includes all the nodes discussed previously. The model was meshed using *Finer* element size setting, generating 100,793 tetrahedral elements. A time-dependent study was defined, with the solved-for time equal to 30 min and the solution data saving at 5 s intervals.

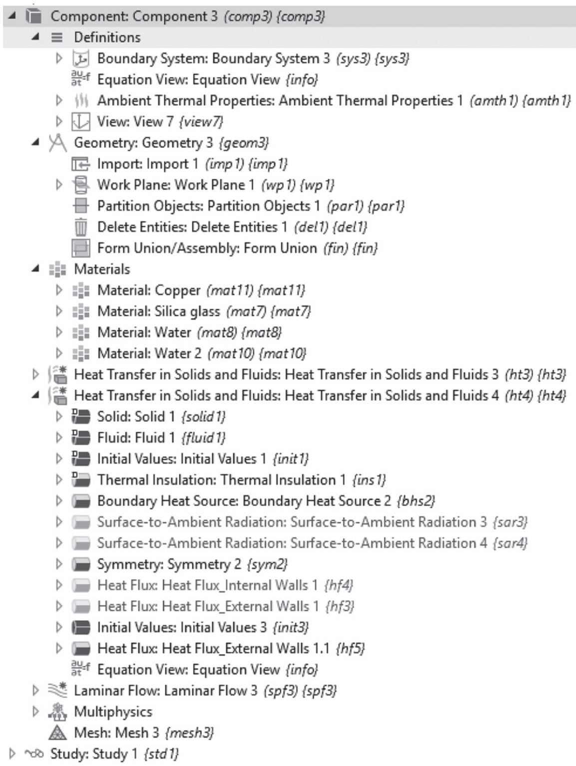

Figure 85. Thermal analysis model tree for cup of hot water.

6.4.2 FEM Model of a Cup of Hot Tea—Solution Results

As mentioned previously, two different approaches were taken to model the conductivity of water. In the first approach, the actual water conductivity was used. Solution results for this approach are shown in Figure 86 through Figure 90. Temperature contours displayed in Figure 86 and Figure 87 show the variation of the temperature, from the cool upper part of the cup and the handle to the hot center of the water. Note the significant variation of the water temperature, from the center to the cup boundary, that develops over time. This development can be more clearly observed by displaying temperature profiles (Figure 88b and Figure 89b) along *Cut Lines* passing through the water center, horizontally (Figure 88a) and vertically (Figure 89a). The Figure 88b horizontal profile shows how over time the flat-top temperature distribution changes into a curved shape with a peak.

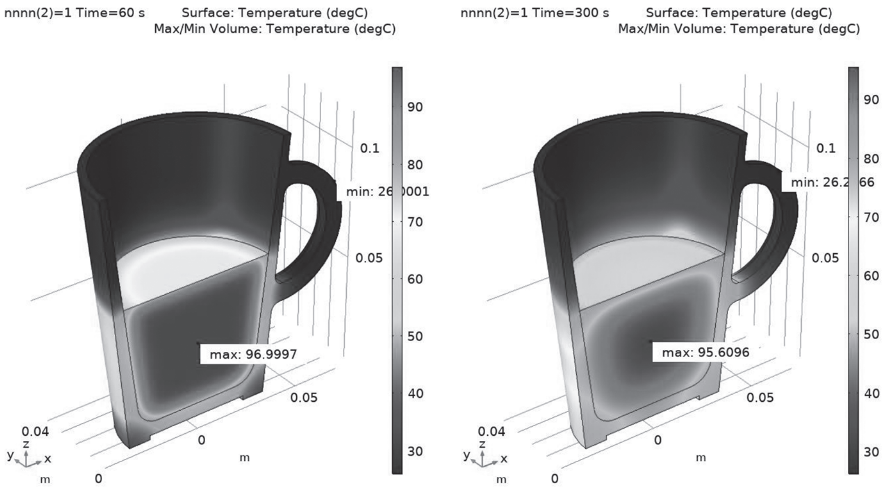

(*a*) (*b*)

Figure 86. Temperature contours for cup of hot water modeled in COMSOL Multiphysics, *nnnn* = 1 (h_c = 10 W/m^{2}K): (a) t = 1 min: (b) t = 5 min.

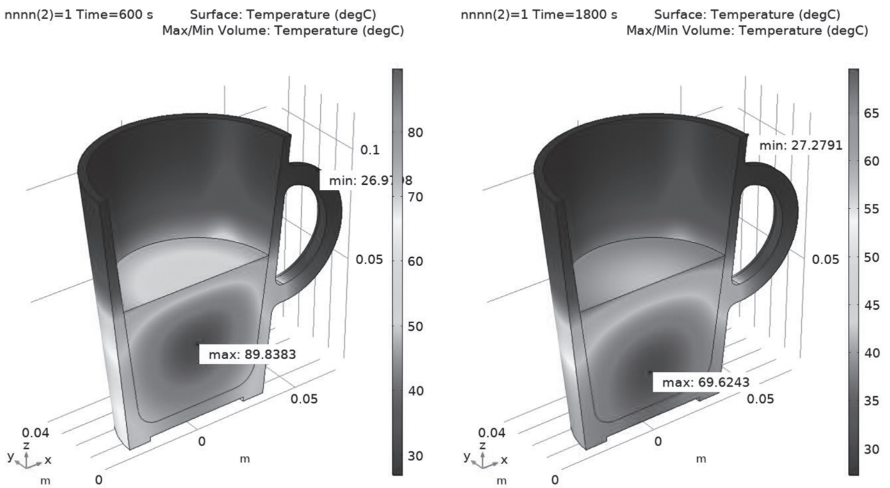

(*a*) (*b*)

Figure 87. Temperature contours for a cup of hot water modeled in COMSOL Multiphysics, *nnnn* = 1 (h_c = 10 W/m^{2}K): (a) t = 10 min: (b) t = 30 min.

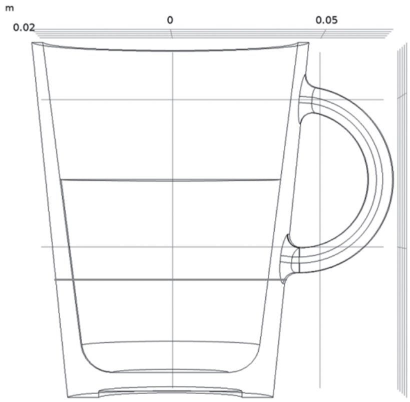

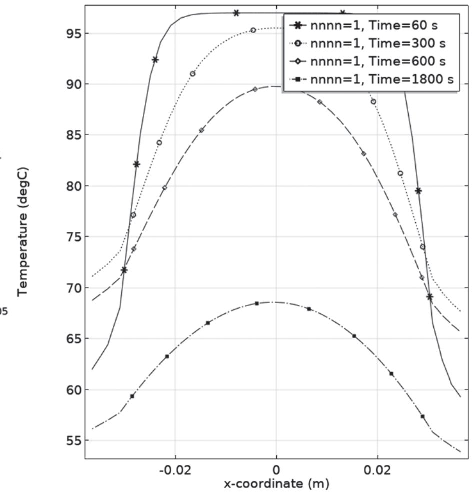

(*a*) (*b*)

Figure 88. Spatial temperature profiles at selected line for cup of hot water modeled in COMSOL Multiphysics, *nnnn* = 1 (h_c = 10 W/m^{2}K): (a) *Cut Lines 3D* (*x*-coordinate), (b) Spatial temperature profiles.

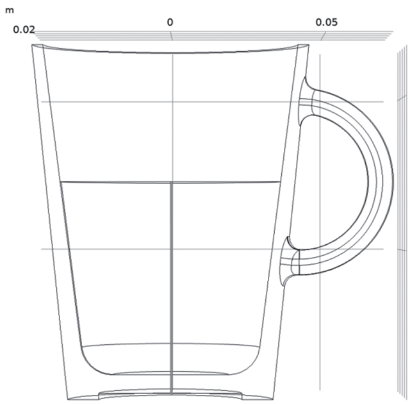

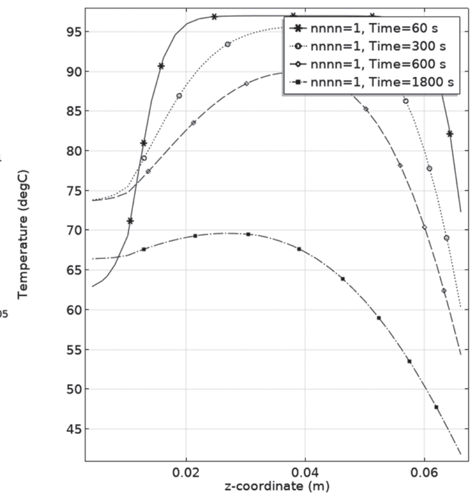

(*a*) (*b*)

Figure 89. Spatial temperature profiles at selected line for cup of hot water modeled in COMSOL Multiphysics, *nnnn* = 1 (h_c = 10 W/m^{2}K): (a) *Cut Lines 3D* (*z*-coordinate), (b) Spatial temperature profiles.

Figure 90b shows the transient temperature for *Cut Points* defined in Figure 90a. Over the 30 min of simulated time, the temperature at the center of the cup (Point "*b*") is seen to drop to about 68 °C from the 97 °C initial value. The bottom of the cup (Point "*a*") heats up after the hot water

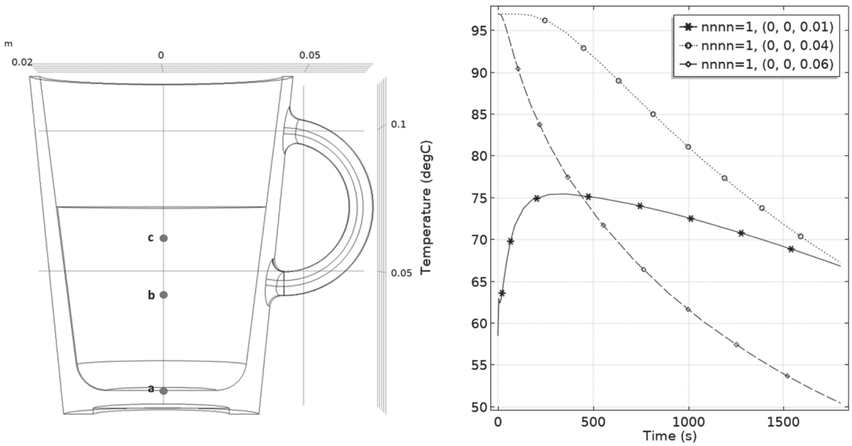

(*a*) (*b*)

Figure 90. Transient temperature profiles at selected points for cup of hot water modeled in COMSOL Multiphysics, *nnnn* = 1 (h_c = 10 W/m²K): (a) *Cut Points 3D*, (b) Transient temperature profiles.

is added, reaching a peak of 76 °C and then declining to about the same temperature at the water's center. Point "*c*" close to the water's top surface is seen to decline in temperature quickly, dropping to 51 °C at the end of the simulated interval.

For the second approach, the water's thermal conductivity was set to a high value to approximate the effect of conductive heat transfer. Values from 50 to 500 W/mK were tested, with similar results. Solution results for the case of a water thermal conductivity setting of 50 W/mK are shown in Figure 91 through Figure 95. Note that this conductivity value is over fifty times higher than the actual value for water (about 0.6 W/mK). For comparison, aluminum's thermal conductivity is about 240 W/mK.

Temperature contours are shown in Figure 91 and Figure 92. The effect of the increased thermal conductivity setting is immediately apparent in these plots when comparing them to those in Figure 86 and Figure 87. For the high conductivity setting, the water temperature is much more uniformly distributed throughout the simulated time interval. As the water cools by heat being removed from its boundaries, the temperature within the liquid quickly equalizes due to the high thermal conductivity.

This trend can be verified numerically by plotting the temperature distribution along the horizontal (Figure 93a) and vertical (Figure 94a) cut lines through the water's center. Temperature distributions plotted in Figure 93b and Figure 94b are nearly uniform through the water domain

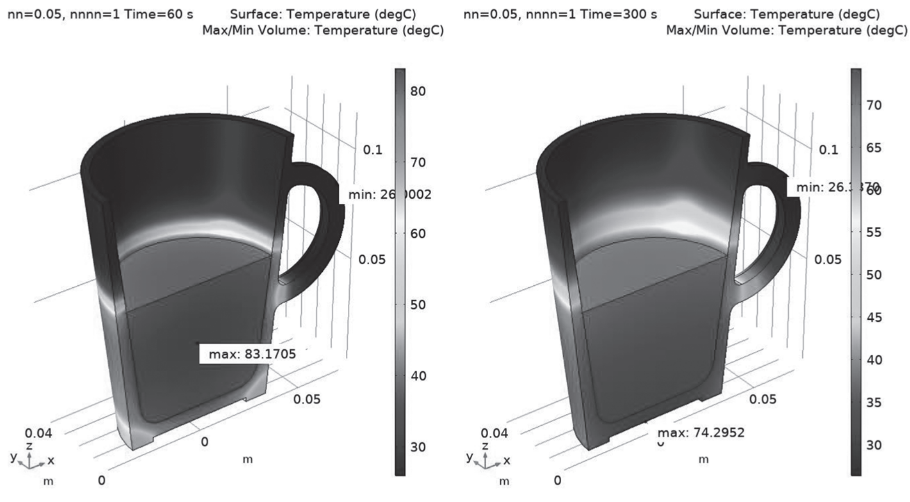

(*a*) (*b*)

Figure 91. Temperature contours for cup of hot water modeled in COMSOL Multiphysics, *nn* = 0.05 (*k* = 50 W/mK), *nnnn* = 1 (h_c = 10 W/m^{2}K): (a) *t* = 1 min: (b) *t* = 5 min.

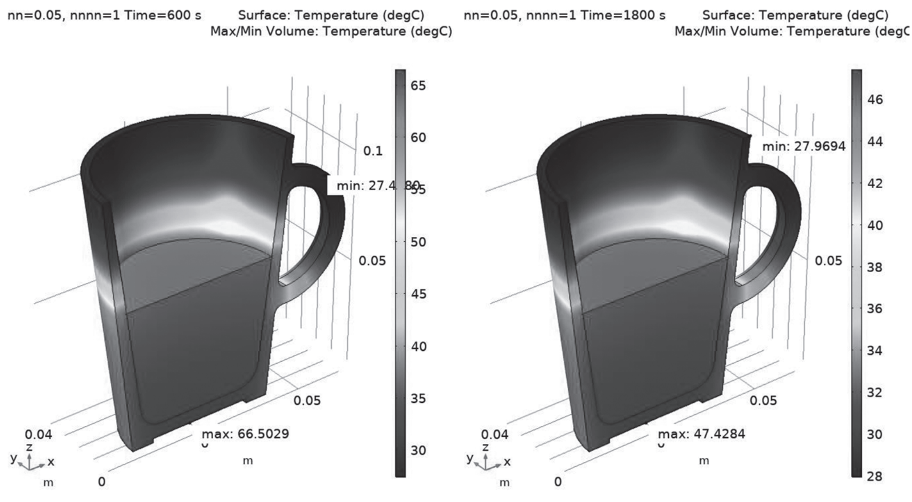

(*a*) (*b*)

Figure 92. Temperature contours for cup of hot water modeled in COMSOL Multiphysics, *nn* = 0.05 (*k* = 50 W/mK), *nnnn* = 1 (h_c = 10 W/m^{2}K): (a) *t* = 10 min: (b) *t* = 30 min.

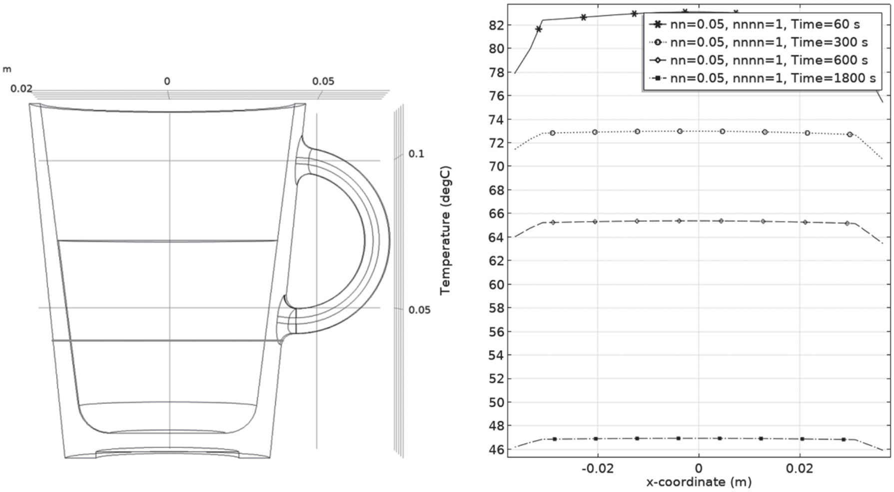

(*a*) (*b*)

Figure 93. Spatial temperature profiles at selected line for cup of hot water modeled in COMSOL Multiphysics, *nn* = 0.05 (*k* = 50 W/mK), *nnnn* = 1 (h_c = 10 W/m^{2}K): (a) *Cut Lines 3D* (*x*-coordinate), (b) Spatial temperature profiles.

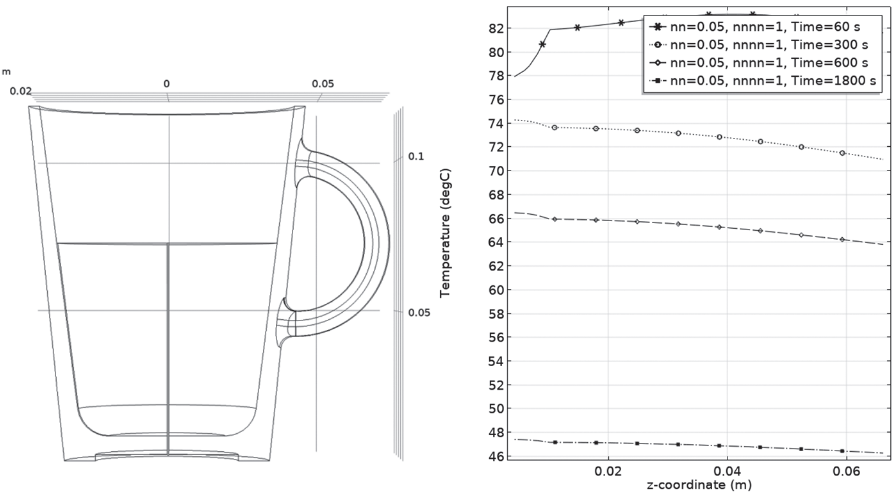

(*a*) (*b*)

Figure 94. Spatial temperature profiles at selected line for cup of hot water modeled in COMSOL Multiphysics, *nn* = 0.05 (*k* = 50 W/mK), *nnnn* = 1 (h_c = 10 W/m^{2}K): (a) *Cut Lines 3D* (*z*-coordinate), (b) Spatial temperature profiles.

width, remaining within 1 or 2 °C, from maximum to minimum, through the simulated time interval. Vertical distribution shows slightly more variation; it reaches about 3 °C at most. The left and right ends of the horizontal distribution also show temperature variation through the cup's walls, which is nearly linear, with the difference between the interior and exterior walls ranging from about 5 °C initially to about 1°C at the end of the simulated time.

Figure 95b shows the transient temperature for the locations presented in Figure 95a. These plots show a very different behavior compared to the equivalent plots with the lower thermal conductivity setting. The temperature shows a nearly identical trend for all three points, with temperature differences within about 2 °C through most of the simulated time. At 30 min, the temperature is seen to have decreased to about 47 °C.

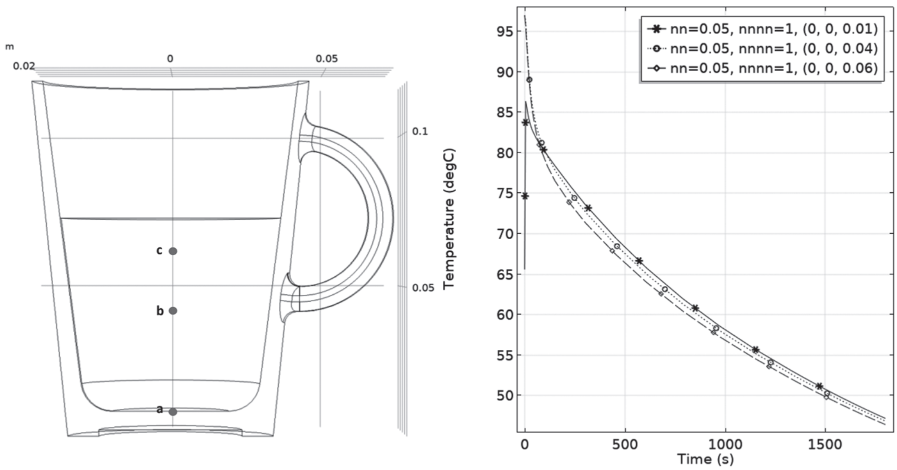

(a) (b)

Figure 95. Transient temperature profiles at selected points for cup of hot water modeled in COMSOL Multiphysics, *nn* = 0.05 (*k* = 50 W/mK), *nnnn* = 1 (h_c = 10 W/m^{2}K): (a) *Cut Points 3D*, (b) Transient temperature profiles.

6.5 Thermal Imaging Observations of a Cup of Hot Tea

Thermal imaging experiments were conducted to validate the analysis results. In these experiments, a glass cup was filled with boiling water and a FLIR One Pro infrared (IR) thermal camera was used to observe the temperature on the cup's surface [108]. FLIR One Pro is a small camera designed to connect directly to a mobile phone (e.g., iPhone). The camera is controlled via a FLIR One application written for the IOS operating system.

This camera is not well-suited to carrying out advanced research, since its output cannot be used with IR thermal analysis software such as FLIR IR Researcher software. With such software, one would be able to import individual images or video files containing raw thermal data. This data could then be sampled by a spot or a line and the temperature at this spot or along this line could be automatically plotted versus the time.

The FLIR One Pro camera can still be useful to carry out on-site inspection and obtain quick observations with relatively modest investment. It is priced at about US$400, while research-grade thermal imaging cameras can cost from ten times this number to up to tens of thousands of dollars. The camera can capture still images, movies at up to 8 fps, or time-lapse recordings. Its battery life is about one hour, thermal image resolution is 160×120 pixels, measurement accuracy is ±3 °C, and resolution is 0.1 °C. One can define up to three sample spots, sample rectangles, or circles of fixed size.

The temperature observed at the spot or the average of the area is displayed on the image. It is also possible to adjust the thermal scale bar to fixed minimum and maximum temperature values or let the two limits adjust automatically as temperatures in the image vary. After capturing the recording, it can be played back, and the observed temperature values can be read from the image and recorded manually versus the time. The time value must be tracked manually by adding up the time intervals of the time-lapse recording.

6.5.1 Experimental Setup

The phone with the attached thermal camera was secured to a tripod stand (Figure 96). Camera height was adjusted so that it was level and viewing the middle of the glass cup; it was located about 17 cm from the cup's exterior surface. A black electrical tape strip was placed vertically on the glass cup exterior wall to ensure that the camera measured the surface temperature accurately, as it can be assumed that the tape's surface emissivity is 1.0. Three temperature sample spots were defined as seen in Figure 97b—one above the water line, one around the air-water interface level, and one near the center of the water.

Water was first boiled to 100 °C and then poured inside the glass cup with minimal delay. The camera was set to capture images using time-lapse recording at an interval of 20 s, with the video recording thus created displaying one frame per second. The first image capture was synchronized

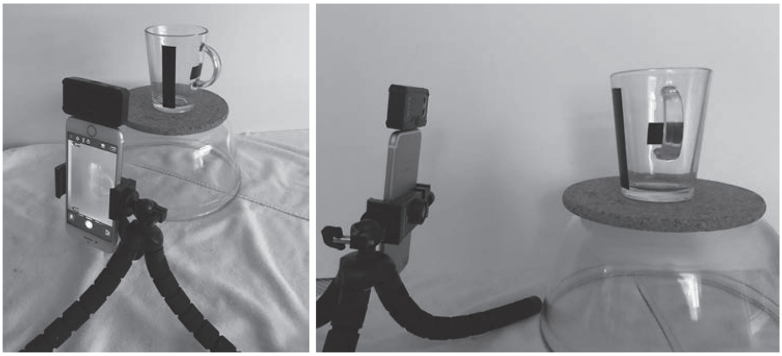

(*a*) (*b*)

Figure 96. Thermal imaging setup for cup of hot water experiment, setup: (a) View of the screen, (b) Side view.

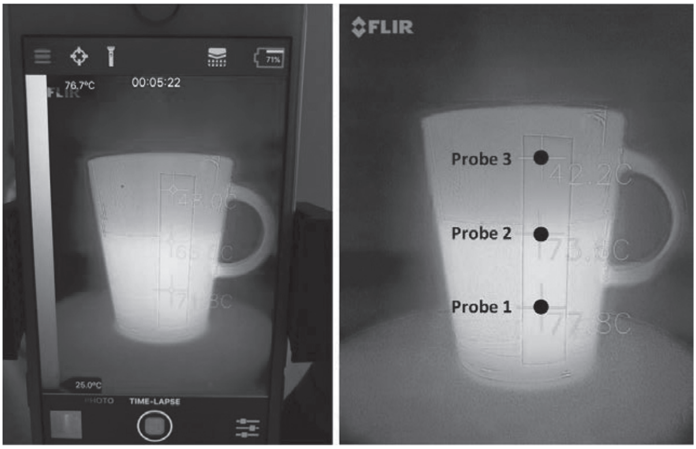

(*a*) (*b*)

Figure 97. Thermal imaging window for cup of hot water experiment: (a) FLIR One application display, (b) Recorded IR image of cup of hot water.

with the time the water was added. The temperature values were extracted afterward by viewing the video, one frame at a time, and manually entering in a spreadsheet the three displayed spot probe temperatures versus the time.

Although the tape was well attached to the wall, since its thermal conductivity is lower (likely about 0.2 to 0.3 W/mK) than that of the glass wall (1.38 W/mK) and there is an adhesive layer in between, a resistive layer is introduced, which would be expected to delay the temperature rise on the tape's surface compared to the temperature of the glass. The glass cup initial temperature equaled that of the ambient (26 °C) [109].

6.5.2 Comparison with FEM Model of a Cup of Hot Tea

Experimental temperature data for Probes 1, 2, and 3 identified in Figure 97 are plotted in Figure 98. Corresponding locations on the model are shown in Figure 99. Experimental data shows a fast temperature increase followed by gradual decrease as the glass surface cools. The temperature peak is highest for Probe 1 located about midway between the glass bottom and the water surface. A value of 77.8 °C is reached at 120 s (2 min). Probe 2 peaks at a slightly lower 74.4 °C, as it is located near the water surface level. Probe 3 temperature shows a more gradual rise and reaches only about 48 °C. This probe is located on the cooler upper wall of the glass, which was not in direct contact with the hot water.

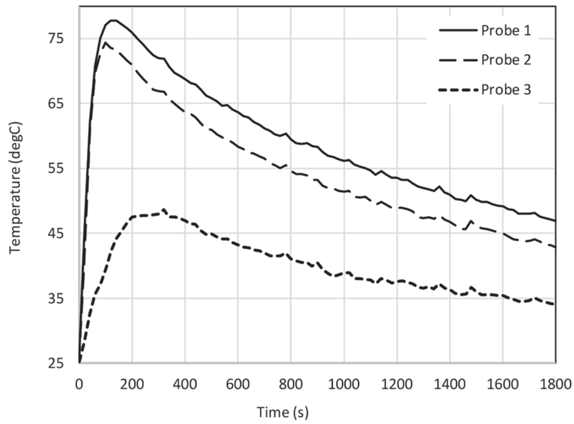

Figure 98. Thermal imaging data for cup of hot water at the probe locations presented in Figure 97.

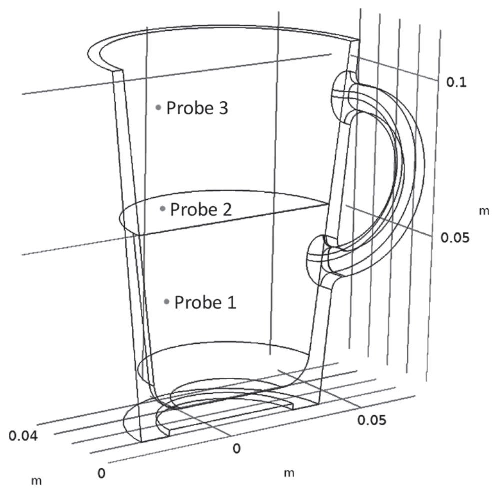

Figure 99. Probe locations to compare thermal imaging data with those of the model.

When attempting to calibrate the model with the experiment observations, one should focus on the model parameters which are known with the least certainty and which are the most influential on the model predictions. For this model, two such parameters have been identified: (1) water thermal conductivity value, and (2) cup-surface-to-ambient convection coefficient.

The water thermal conductivity is the "artificial" value that has been assigned to emulate the convective heat transfer within the liquid. Thus, it is essentially a guess aimed to improve the accuracy of the model in representing the physical phenomenon which is not modeled, and so its value is highly uncertain. The ambient convection coefficient to a large extent determines the rate at which the heat is removed from the system. Its strong influence on the model prediction was shown for the 2D axisymmetric FEM model of water and spoon. A general range for this value given the physical arrangement of the setup is known, but there is still some uncertainty. Typical free convection coefficients for a vertical wall would be about 10 W/m^2K.

In the results presented, the water thermal conductivity is varied by changing multiplier *nn* between 0.01 and 0.5, with the base condition of $nn = 1$ ($k_{\text{water}} = 1{,}000$ W/mK), giving a range from 10 to 500. The ambient convection coefficient is varied by changing multiplier *nnnn*, with values equal to 1 and 1.5 reported for the base condition of $nnnn = 1$ ($h_c = 10\ W/m^2K$), thus giving values of 10 and 15 W/m^2k.

Thermal model data and those of the experiments are compared (Figure 100 through Figure 103). Figure 100 compares observations to model predictions for Probe 1 and 2 locations, with varying values of *nn* and $nnnn = 1$. Figure 101 plots the same data, except the ambient heat transfer coefficient is increased by setting $nnnn = 1.5$ ($h_c = 15\ W/m^2K$). Both Probe 1 and Probe 2 results show that the model predictions follow the observed temperatures and general trends fairly closely. The peak temperature is predicted within 3 °C and the maximum deviation is about 6 °C.

For Probe 1, increasing the water conductivity (*nn* parameter) results in an overall temperature decrease during the cooling stage by about 3 °C. The effect is likely due to the higher conductivity allowing the water to transfer heat to the glass surface faster, leading the water temperature to decrease faster, which leads to the cooler glass walls, as they are in immediate contact with the water. The peak temperature prediction is not affected and closely matches the experiment.

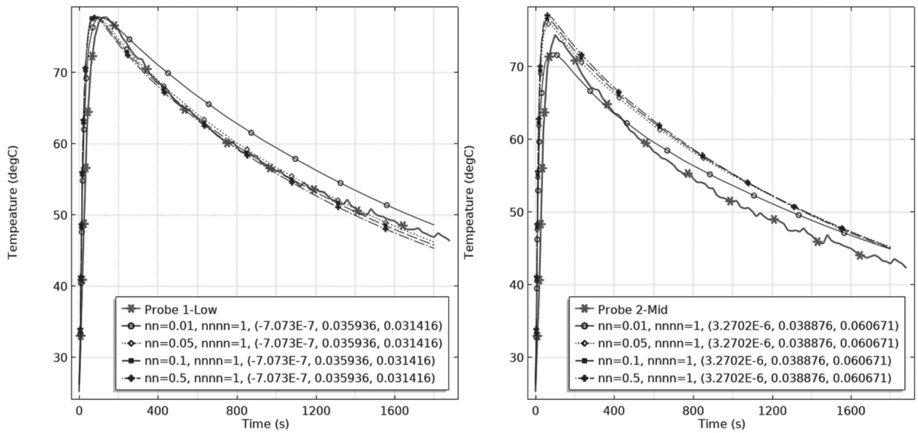

(*a*) (*b*)

Figure 100. Comparison between transient thermal imaging data for cup of hot water and FEM temperature profiles for the base condition *nn* = 1 (k = 1,000 W/mK), *nnnn* = 1 (h_c = 10 W/m^{2}K): (a) Probe 1, low point, (b) Probe 2, middle point.

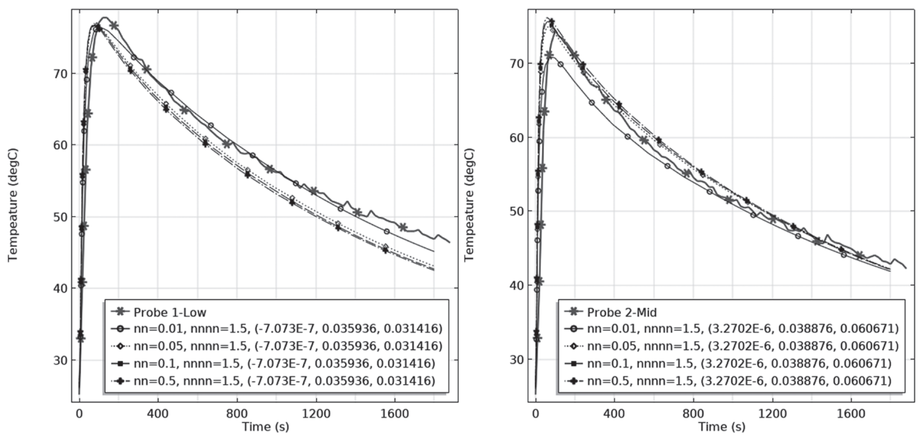

(*a*) (*b*)

Figure 101. Comparison between transient thermal imaging data for cup of hot water and FEM temperature profiles for the base condition *nn* = 1 (k = 1,000 W/mK), *nnnn* = 1.5 (h_c = 15 W/m^{2}K): (a) Probe 1, low point, (b) Probe 2, middle point.

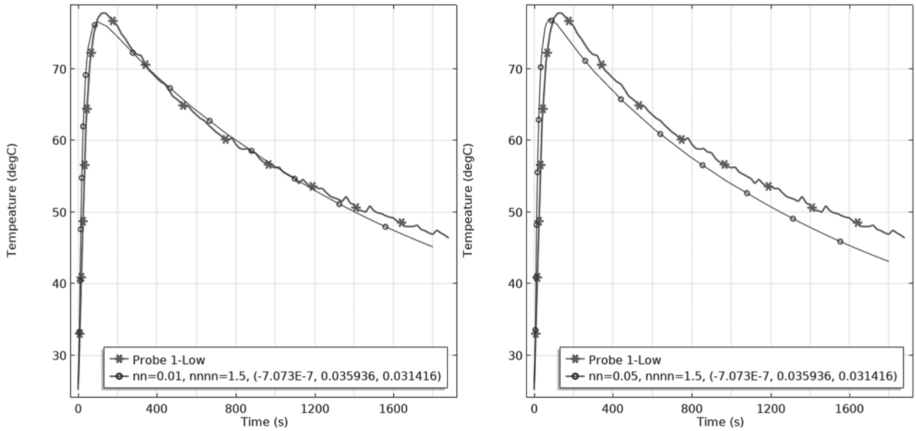

(*a*) (*b*)

Figure 102. Comparison between transient thermal imaging data for cup of hot water and FEM temperature profiles at Probe 1, low point, *nnnn* = 1.5 (h_c = 15 W/m^{2}K): (a) *nn* = 0.01 (k = 10 W/mK), (b) *nn* = 0.05 (k = 50 W/mK).

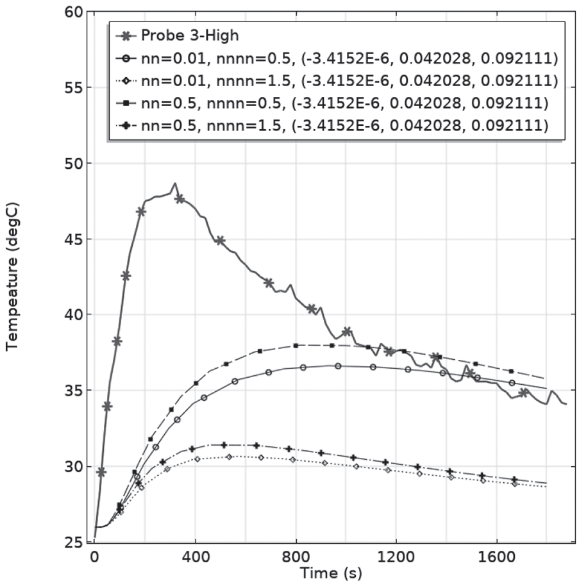

Figure 103. Comparison between transient thermal imaging data for cup of hot water and FEM temperature profiles at Probe 3, high point for the base conditions of *nnnn* = 0.01 (h_c = 10 W/m^{2}K) and *nn* = 0.01 (k = 10 W/mK).

For Probe 2, increasing the water conductivity causes the opposite effect, with overall temperature increasing during the cooling stage. This can be explained by the higher water conductivity being able to distribute the heat faster through the glass body. This also leads to the peak temperature at Probe 2 to increase at higher *nn* values by about 6 °C. One can also observe that for *nn* values of 0.05 and higher, there is little difference in the model predictions for both probe locations.

Figure 101 shows that increasing the convective coefficient from 10 to 15 W/m^2K leads to faster heat loss from the glass surface, leading to a decrease of predicted temperature by about 3 to 4 °C during the cooling stage and for the peak value for both Probes 1 and 2. Figure 102 highlights the two plots for Probe 1 from the previous figure with the highest and lowest *nn* values.

Figure 103 compares the model predictions with the experimental results for Probe 3, which was located on the upper part of the glass surface, the interior of which was not in direct contact with water. The model results for the lowest (0.01) and highest (0.5) values of water conductivity (*nn*) are shown, combined with the ambient heat transfer coefficient multiplier (*nnnn*) values of 0.5 and 1.5. The lower multiplier of 0.5, which gives the heat transfer coefficient of 5 W/m^2K, produces the two upper plots in the figure; the higher value of 1 produces the two lower plots. The effect is due to reduced heat loss to the ambient, in the former case producing a higher temperature.

The comparison shows a significant difference in behavior between the model and the experiment. The experiment shows a much faster temperature increase and a higher peak value reached (48 °C) than any of the model predictions. The reason for this variance is conjectured to be due to the steam escaping from the hot water surface, particularly during the first few minutes of the test, condensing on the interior glass surface, transferring its latent heat to it, and thus warming it up. Another factor that would result in higher temperature is that the model assumes the interior surfaces to be facing the same ambient conditions as the exterior. However, this is not the case, as the interior of the cup is much warmer. This would lead to the model overpredicting the heat loss.

This variation between the model and the experiment shows that the real systems often have certain aspects of their behavior which are not captured by the model. This also shows how invaluable the experiment is, even in a relatively simple system such as the one examined here. Another lesson is that the modeling process is iterative in nature. If a more accurate representation of this system was needed, these additional effects could be captured with further model refinement. This also shows that an analyst should make every effort to find experimental validation for their model from the existing literature, by carrying out their own tests, or by collaborating with others.

In summary, the temperature variations seen between the analysis and test results may be due to the following uncertainties: (1) heat loss from the fluid (hot water) surface, (2) convection heat transfer coefficient for the interior and exterior glass wall, and (3) radiative heat transfer modeling for the glass cup interior and exterior surfaces.

CHAPTER 7

CASE STUDY 2—BASEMENT INSULATION

For those living in colder climates, basements are needed to insulate the rest of the house from the coldness of the ground in winter. If you were to build a house in Canada on a simple concrete slab, as is done for some homes in the southern United States, for example, your floors would feel uncomfortably cold. The only way to build without a basement in cold climate is to have an in-floor heating system, which can be water- or electricity-based. This study looks at the case of a typical basement in winter for a northern country, such as Canada. Of course, as long as you have that basement, it does not have to serve only its thermal function—it can also be transformed into a useful living space such as an office.

When designing the heating and cooling systems for any type of building (e.g., a three-story office building), the designer learns that the walls that include windows transfer heat at different rates. There are data tables available providing the heat transfer rate for these walls. The heating profile for the entire building and each room is calculated, and based on that, radiators or HVAC ducts and systems are designed. The designer cannot expect to obtain a comfortable rate of cooling and heating if a proper system is not selected. The system's selection on its own requires considering factors such as the efficiency of the system in addition to the cost considerations. For the economical considerations but also the environmental impacts that any of the said design decisions introduce, in addition to the social responsibility that has become an integral part of life today, it is important that the design choices are fully integrated with the purpose of the structure.

In most cases, designers will need to develop environmental robustness plans that consider the effect of the elements, such as the wind, rain, sun, sand, and heat. A windy or hurricane-prone area will need extra structural reinforcements. Occasionally, environmental conditions provide such strong motives that old-fashioned approaches to living become an attractive option. Modern cave living is an example of such an approach that considers this primitive method of living entwined with modern amenities such as water circulation systems and green heating and cooling options that take advantage of geothermal energy.

The scenarios presented herein are very real and provide a powerful tool for scientists or researchers to get inspiration and insight as to how to proceed when such social, economical, and environmental understandings are required when building the structures to harness peace and comfort in living spaces.

7.1 Problem Definition

Imagine that you bought an older home with a poorly insulated basement. The walls are covered with wood paneling, in direct contact with the concrete blocks behind them. The cinder block exteriors are partly above ground, in contact with the outside air, and partly below ground. As part of your renovation plans, you know that you should insulate the basement before putting the finishing touches on it. The building codes require that you draw the plans and get approval by acquiring a city permit. In order to do so, you need to know what thickness of insulation is required based on the insulation type you choose. For example, using the common pink batt insulation requires a thicker layer given its lower density and *R*-value, versus the denser Styrofoam that has lower compressibility. One can also use spray-foam insulation. There are environmentally friendly versions of these (brown ones made of soy), blue ones made from artificial materials, and purple ones made from recycled artificial materials.

The *R*-value characterizes the capability of an insulating material; the higher it is, the more insulating the material is. The *R*-value is proportional to the temperature difference across the insulation thickness and inversely proportional to the heat flux (W/m^2) flowing through the insultation. Thus, for example, for the same temperature difference between the interior and exterior of the insulation layer, doubling the *R*-value will reduce the heat flux by half.

Depending on the available products, characteristics of the location to be insulated, restrictions such as the need for covering the insulation to meet fire codes, and space limitations, an insulation type may be selected. For example, if the walls and corners are to be foam sprayed, all the little crevices can be fully filled; however, the foam must be covered by drywall so that, in case of fire, the toxic fumes released by the insulation do not spread quickly to the rest of the building. As you see, there are options available, and these options—from the choice of the material, its characteristics, the thickness, and the method of applying it—are all to be made based on the effectiveness and efficiency of the finished product to meet your requirements. Your personal preferences also may come into play. For example, if you are dedicated to improving life on the Earth and are environmentally conscious, you may choose the option of using the soya-based insulation—if available. You may choose the pink batt if the environment is a nursery, just to be on the safe side (Figure 104).

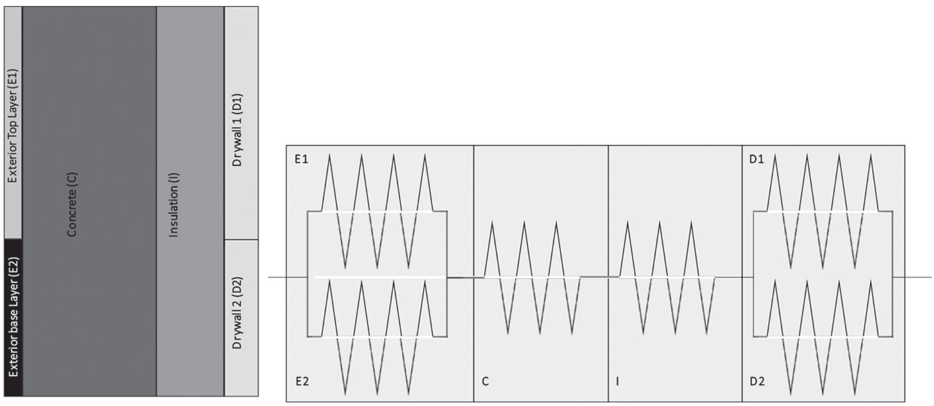

(*a*) (*b*)

Figure 104. (a) Wall layers, (b) Equivalent electric circuit to determine the equivalent thermal conductivity.

Let us identify the components of this problem. The simplified form of this problem consists of the wall and the parallel layers adjacent to it. The layers may be selected to be either of the insulating materials, with or without the vapor barrier. It is assumed that the exterior of the house is also to be covered with a thin layer of asphalt. All the layers are placed vertically and are parallel. In layers of hard materials, the dominant mechanism of heat transfer is conduction mode; the aboveground exterior surface and the entire interior surface experience a natural convection heat transfer mode.

If details of temperature variation within the wall assembly are not of interest and only the temperature difference between the interior and exterior as well as the heat loss to the exterior are important, it is possible to simplify the sandwich layer by replacing it with a single composite material equivalent to all the wall layers. To achieve this, the resistance of the composite material as a whole (lumped thermo-physical properties) should simulate the total effect of the individual layers of the sandwich.

In this case study, the exterior surface of the wall is partially covered by bricks (upper part) and concrete (bottom part). The vertical wall and horizontal floor intersect at the ground level, forming a T-joint. The layer adjoining the exterior layer is made of concrete. Adjoining this layer, toward the interior, is a layer of glass-wool batt insulation. The interior basement wall is covered by two materials: (a) pine wood (top part) and (b) gypsum board (bottom part and trim). The baseboard heater is made of aluminum and consists of five adjacent elliptical shapes; it is located on the selected *Work Plane*, which is spaced out from the interior surface using a 2D sketch created using polygons (Figure 105). Figure 106 shows the 3D model as well as the layers that make up the wall.

There are four layers, with two of them composed of two parts. The equivalent electric resistance model is presented in Figure 104b. The letters indicate the resistive layers having the same values. The equivalent resistive element consists of the parallel and series resistors. The parallel resistors receive and transmit the same electric voltage (equivalent to the temperature difference), while the ones in series receive and transmit the same electric current (equivalent to the heat flux).

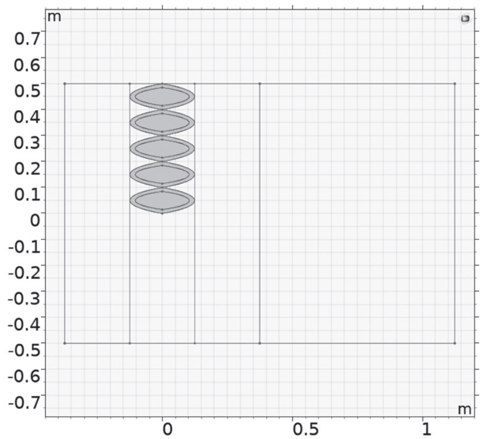

Figure 105. 2D sketch of the heating elements using 2D polygons.

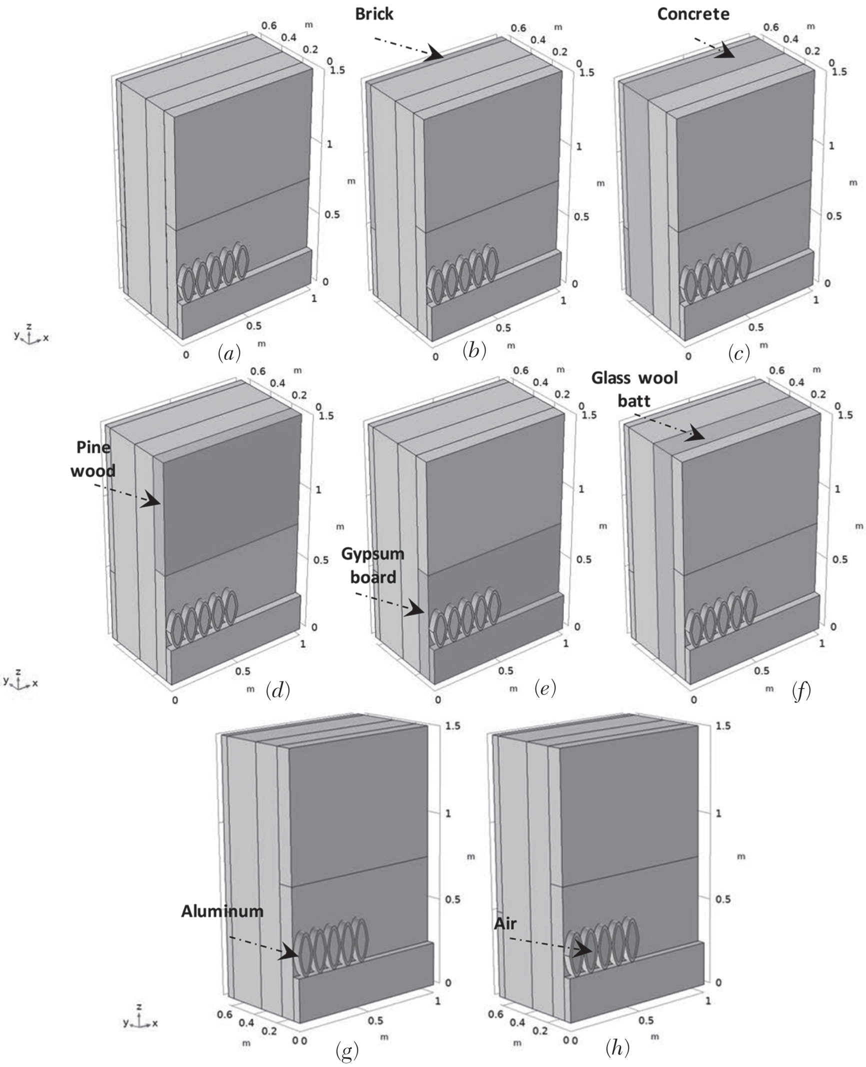

Figure 106. Wall model and its components: (a) Wall, (b) Brick, (c) Concrete, (d) Pine wood, (e) Gypsum board, (f) Glass wool batt, (g) Aluminum, (h) Air.

Figure 107 shows the boundary conditions for the 3D model presented. The two main heat transfer modes are conduction and convection. Note that the surfaces with unidentified boundary conditions are assigned to be insulated. The interior and (partially) exterior surfaces are transferring heat by a convection mechanism to the surroundings. The top and bottom surfaces are assumed to be insulated, as they are in contact with the

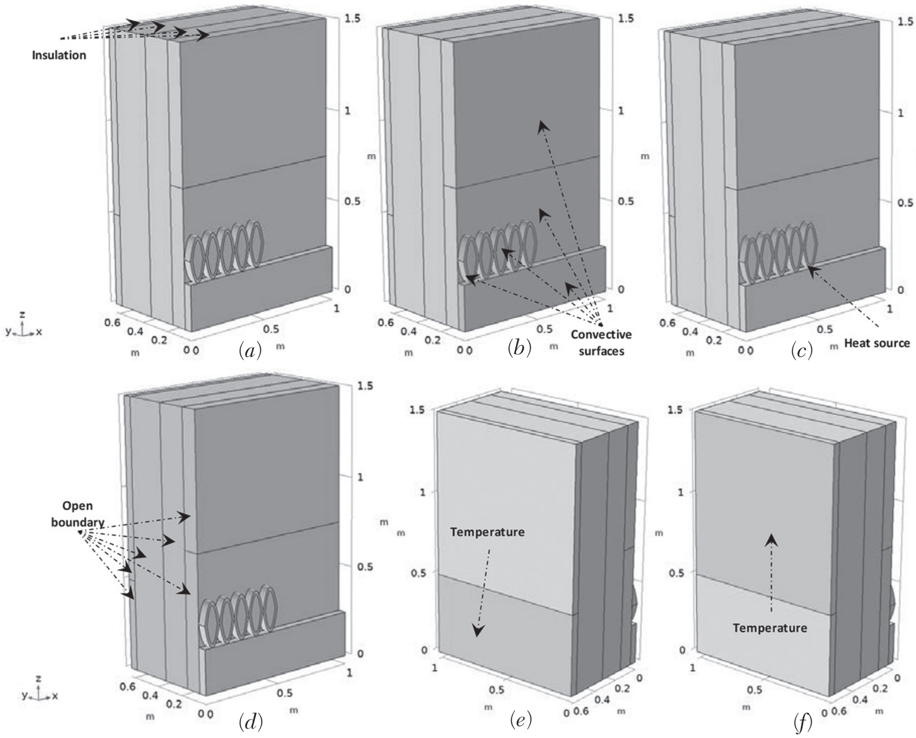

Figure 107. Wall model boundary conditions: (a) Insulation, (b) Convective surfaces, (c) Heat source, (d) Open boundary, (e) Temperature, (f) Temperature.

other insulating objects such as the ground and the upper-level insulation materials. Only a segment of the wall needs to be modeled, because the heat flow gradient is mostly directed transverse to the wall. You expect little heat flowing parallel to the wall. The sides are assumed to have periodic boundary conditions with the zero-temperature offset. The radiator heats up the room and is made of a coil-like material.

Three are three main scenarios when incorporating heating: (a) the radiator is treated as a heat source with a constant heat rate—as part of the original physics; (b) the radiator is incorporated as a boundary heat source, transferring heat to the environment in a constant fashion—not as part of the original physics but as a separate condition applied to the boundaries; and (c) the equivalent thermal conductivity is applied for stationary problems, representing multi- and single-layer cases. A transient analysis considers the effect of a specific heat capacity and density in addition to thermal conductivity (presented in the form of thermal diffusivity).

In order to isolate the effect of thermal conductivity on the model, a stationary thermal model is also solved. The results of this 3D single-layer model are then compared to those of the multilayer ones. The last scenario assumes constant temperatures at the exterior surfaces, and the analyses are performed for both multi- and single-layer cases for the stationary study.

Note that the wall also could have been treated as a 2D model, with the model plane showing the wall's cross section (*y*-*z* plane). A 2D model implies that the wall extends as an infinite solid along the *x*-coordinate.

Figure 108 shows how the model is meshed, using free tetrahedral elements. The transient solution simulates one hour of operation. Of course, in an actual implementation, the heating system would be controlled by a thermostat, turning it off once the set temperature is reached. Figure 109 shows the parameters used in these scenarios. Initial values are considered as the ambient and reference temperatures (T_{amb} = 22 °C) for the entire wall. For the fluid pockets surrounded by the radiator coils, the atmospheric conditions are assumed. Vertical surfaces convect heat, with the heat transfer defined by the heat transfer coefficient (h_c) and the ambient temperature (T_{amb}); the vertical wall inside the ground is assumed to be constant at the base temperature (T_{base1} = 10 °C), while the temperature at the top exterior surface is at a lower constant temperature (T_{base2} = −10 °C). Figure 110 through Figure 116 present the thermo-physical properties of the materials used for the analyses. Figure 117 presents the thermo-physical properties of the single equivalent layer used for this analysis.

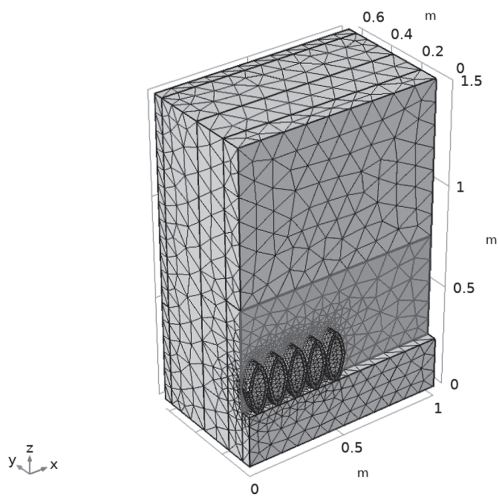

Figure 108. Meshed wall.

Settings

Parameters

Label: Parameters 1

Parameters

Name	Expression	Value	Description
boundary_heat_flux	power/heat_boundary_area	21042 W/m^2	heat flux at the boundary
depth1	0.1[m]	0.1 m	depth of interior layer
depth2	0.18[m]	0.18 m	depth of concrete
depth3	0.25[m]	0.25 m	depth of glass-wool batt
depth4	0.05[m]	0.05 m	depth of exterior layer
hc	10[W/(m^2*K)]	10 $W/(m^2{\cdot}K)$	convection coefficient
heat_boundary_area	0.035643[m^2]	0.035643 m^2	boundary area between t...
heat_gen	power/radiator_volume	2.1042E5 W/m^3	heat generation per volu...
height1	1[m]	1 m	height of exterior concrete
height2	height1/2	0.5 m	height of exterior brick
power	750[W]	750 W	radiator heat rate
radiator_surface	0.57525[m^2]	0.57525 m^2	radiator surface
radiator_volume	0.0035643[m^3]	0.0035643 m^3	radiator volume
Tamb	22[degC]	295.15 K	ambient temperature
Tbase1	10[degC]	283.15 K	external surface temperat...
Tbase2	-10[degC]	263.15 K	external surface temperat...
time	3600[s]	3600 s	exposure time
Tref	20[degC]	293.15 K	reference temperature
width	1[m]	1 m	wall width

Figure 109. Parameters used for basement insulation study (global level).

Link Settings

Material: Material: Brick (mat10) {mat10}

Material Contents

	Property	Variable	Value	Unit	Property group
☑	Density	rho	2000[kg/m^3]	kg/m^3	Basic
☑	Heat capacity at constant pressure	Cp	900[J/(kg*K)]	J/(kg·K)	Basic
☑	Thermal conductivity	k_iso ; kii = k_iso, kij = 0	0.5[W/(m*K)]	W/(m·K)	Basic
	Coefficient of thermal expansion	alpha_iso ; alphaii = alpha_iso, alphaij = 0	6e-6[1/K]	1/K	Basic
	Young's modulus	E	17e9[Pa]	Pa	Young's modulus and Poisson's ratio
	Poisson's ratio	nu	0.2	1	Young's modulus and Poisson's ratio

Figure 110. Thermo-physical properties of brick.

Link Settings

Material: Material: Concrete (mat1) {mat1}

Material Contents

	Property	Variable	Value	Unit	Property group
☑	Density	rho	2300[kg/m^3]	kg/m^3	Basic
☑	Thermal conductivity	k_iso ; kii =...	1.8[W/(m*K)]	W/(m·K)	Basic
☑	Heat capacity at constant pressure	Cp	880[J/(kg*K)]	J/(kg·K)	Basic
	Coefficient of thermal expansion	alpha_iso ;...	10e-6[1/K]	1/K	Basic
	Young's modulus	E	25e9[Pa]	Pa	Young's modulus and Poisson's ratio
	Poisson's ratio	nu	0.20	1	Young's modulus and Poisson's ratio

Figure 111. Thermo-physical properties of concrete.

Link Settings

Material: Material: Glass wool batt (mat5) {mat5}

Material Contents

	Property	Variable	Value	Unit	Property group
☑	Density	rho	22	kg/m³	Basic
☑	Heat capacity at constant pressure	Cp	850	J/(kg·K)	Basic
☑	Thermal conductivity	k_iso ; kii = k_iso, kij = 0	k(T)	W/(m·K)	Basic
	Water content	w_c	wc(phi)	kg/m³	Basic
	Vapor resistance factor	mu_vrf	1.2	1	Basic
	Vapor permeability	delta_p_iso ; delta_pii = delta_p_iso, delta_pij = 0	delta_p(phi)	s	Basic
	Diffusion coefficient	D_iso ; Dii = D_iso, Dij = 0	1e-14	m²/s	Basic

Figure 112. Thermo-physical properties of glass wool batt.

Link Settings

Material: Material: Wood (pine) (mat3) {mat3}

Material Contents

	Property	Variable	Value	Unit	Property group
☑	Density	rho	532	kg/m³	Basic
☑	Heat capacity at constant pressure	Cp	2700	J/(kg·K)	Basic
☑	Thermal conductivity	k_iso ; kii...	k(phi)	W/(m·K)	Basic
	Diffusion coefficient	D_iso ; Dii...	Dw(phi)	m²/s	Basic
	Water content	w_c	wc(phi)	kg/m³	Basic
	Vapor permeability	delta_p_is...	delta_p(phi)	s	Basic
	Vapor resistance factor	mu_vrf	mu_vrf(T,pA...	1	Basic

Figure 113. Thermo-physical properties of pine wood.

Link Settings

Material: Material: Aluminum (mat11) {mat11}

Material Contents

	Property	Variable	Value	Unit	Property group
☑	Heat capacity at constant pressure	Cp	900[J/(kg*K)]	J/(kg·K)	Basic
☑	Thermal conductivity	k_iso ; kii =...	238[W/(m*K)]	W/(m·K)	Basic
☑	Density	rho	2700[kg/m^3]	kg/m³	Basic
	Relative permeability	mur_iso ;...	1	1	Basic
	Electrical conductivity	sigma_iso ;...	3.774e7[S/m]	S/m	Basic
	Relative permittivity	epsilonr_is...	1	1	Basic
	Coefficient of thermal expansion	alpha_iso ;...	23e-6[1/K]	1/K	Basic
	Young's modulus	E	70e9[Pa]	Pa	Young's modulus and Poisson's ratio
	Poisson's ratio	nu	0.33	1	Young's modulus and Poisson's ratio
	Murnaghan third-order elastic moduli	l	-2.5e11[Pa]	N/m²	Murnaghan
	Murnaghan third-order elastic moduli	m	-3.3e11[Pa]	N/m²	Murnaghan
	Murnaghan third-order elastic moduli	n	-3.5e11[Pa]	N/m²	Murnaghan

Figure 114. Thermo-physical properties of aluminum.

Link Settings

Material: Material: Air (mat9) {mat9}

Material Contents

	Property	Variable	Value	Unit	Property group
☑	Ratio of specific heats	gamma	1.4	1	Basic
☑	Heat capacity at constant pressure	Cp	Cp(T)	J/(kg·K)	Basic
☑	Density	rho	rho(pA,T)	kg/m³	Basic
☑	Thermal conductivity	k_iso ; kii =...	k(T)	W/(m·K)	Basic
	Coefficient of thermal expansion	alpha_iso ;...	alpha_p(pA,T)	1/K	Basic
	Mean molar mass	Mn	0.02897	kg/mol	Basic
	Bulk viscosity	muB	muB(T)	Pa·s	Basic
	Dynamic viscosity	mu	eta(T)	Pa·s	Basic
	Electrical conductivity	sigma_iso ;...	0[S/m]	S/m	Basic
	Speed of sound	c	cs(T)	m/s	Basic
	Parameter of nonlinearity	BA	(def.gamma+1...	1	Nonlinear model

Figure 115. Thermo-physical properties of air.

Link Settings

Material: Material: Gypsum board (mat7) {mat7}

Material Contents

	Property	Variable	Value	Unit	Property group
☑	Density	rho	574	kg/m³	Basic
☑	Heat capacity at constant pressure	Cp	1100	J/(kg·K)	Basic
☑	Thermal conductivity	k_iso ; kii =...	k(phi)	W/(m·K)	Basic
	Diffusion coefficient	D_iso ; Dii =...	Dw(phi)	m²/s	Basic
	Water content	w_c	wc(phi)	kg/m³	Basic
	Vapor resistance factor	mu_vrf	6.9	1	Basic
	Vapor permeability	delta_p_iso...	2.9e-11	s	Basic

Figure 116. Thermo-physical properties of gypsum board.

Material Contents

	Property	Variable	Value	Unit	Property group
☑	Density	rho	2300[kg/m^3]	kg/m³	Basic
☑	Thermal conductivity	k_iso ; kii =...	k(T,phi)	W/(m·K)	Basic
☑	Heat capacity at constant pressure	Cp	880[J/(kg*K)]	J/(kg·K)	Basic
	Coefficient of thermal expansion	alpha_iso ;...	10e-6[1/K]	1/K	Basic
	Ratio of specific heats	gamma	1	1	Basic
	Young's modulus	E	25e9[Pa]	Pa	Young's modulus and Poisson's ratio
	Poisson's ratio	nu	0.20	1	Young's modulus and Poisson's ratio

Figure 117. Thermo-physical properties of single equivalent layer.

7.2 Scenario 1—No Heat Source

This case study considers the most basic form of steady-state heat transfer for the given problem between an external surface, kept at the two constant temperatures (upper and lower portions) defined previously, and an internal wall at a fixed temperature with no heat source. Temperature contours are presented in Figure 118. The temperature along the wall depth is presented in Figure 119. The temperature profile within the wall consists of nearly linear line segments with varying gradients that depend on the thermal conductivity of each layer's material. Steeper slope corresponds to lower conductivity.

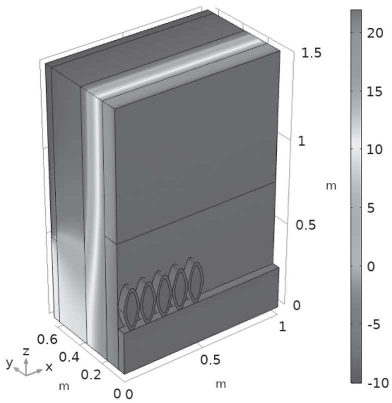

Figure 118. Temperature contours.

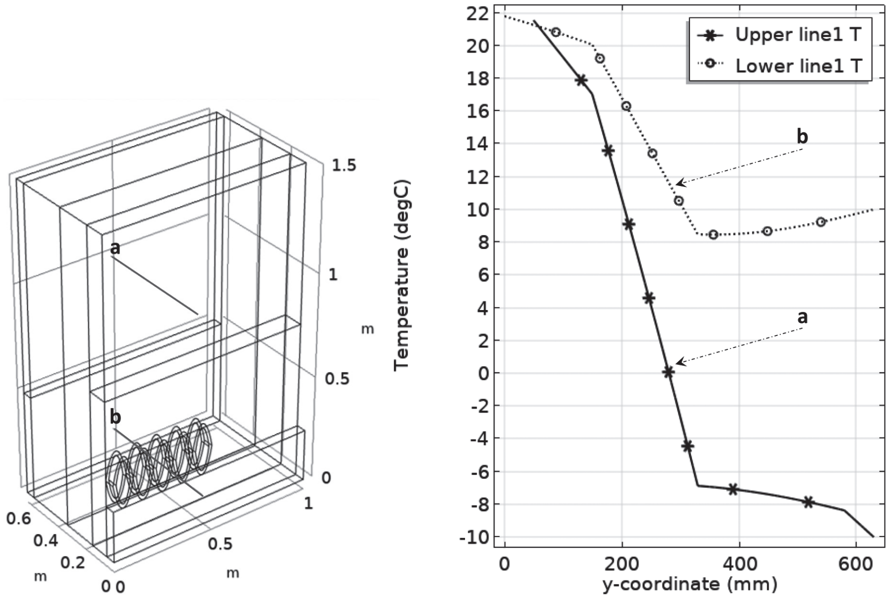

(*a*) (*b*)

Figure 119. (a) *Cut Lines 3D* versus the wall depth (*y*-coordinate), (b) Spatial temperature profiles versus the wall depth.

7.3 Scenario 2—Heat Source: Constant Heat Source Rate, Transient, Multilayer

Figure 120 shows the heat source incorporated into the thermal model and defined by a constant heat rate (750 W). It is also possible to include the term in the form of a general source (volumetric power) or a linear source (volumetric power per temperature). In order to calculate the volumetric heat generation, one method is to obtain the volume of the heating elements and combine this with the element power in order to obtain the heat generation rate (W/m^3)—Figure 120. This volumetric measurement can be done through the measurement built-in tool available in COMSOL Multiphysics (Figure 120). Note that an actual heater would not normally be on for the time duration that was modeled, since a thermostat would be used to control the temperature in the room. For this analysis, a prolonged time has been selected to show the effect of continuous heating over time.

Figure 121 shows the transient analysis results after an exposure time of one hour. Boundary conditions are as described previously. In order to gain a better understanding of the temperature distribution inside the volume, one can set a color range with an identified maximum temperature

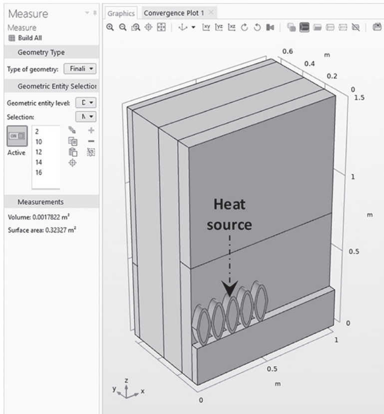

Figure 120. Constant heat rate heat source boundary condition.

range. This is to better visualize how the maximum temperature within the chosen domains changes. Figure 121 shows a two-scale temperature, full scale and 30 °C scale. It is seen that a majority of the temperatures falls in the temperature ranges above the initial state (22 °C), with the temperature of the wall gradually increasing around the radiator area.

It is possible to show the maximum and minimum temperatures (volume or surface) for the temperature contour diagrams. This added functionality is available under *3D Plot Group, More Plots, Max/Min Volume*. Activating this feature on the *Messages* tab window under the appropriate table (Figure 122) displays the exact location of the peak temperatures in the domain (3D space). If these temperatures are sought for the surfaces, the surfaces

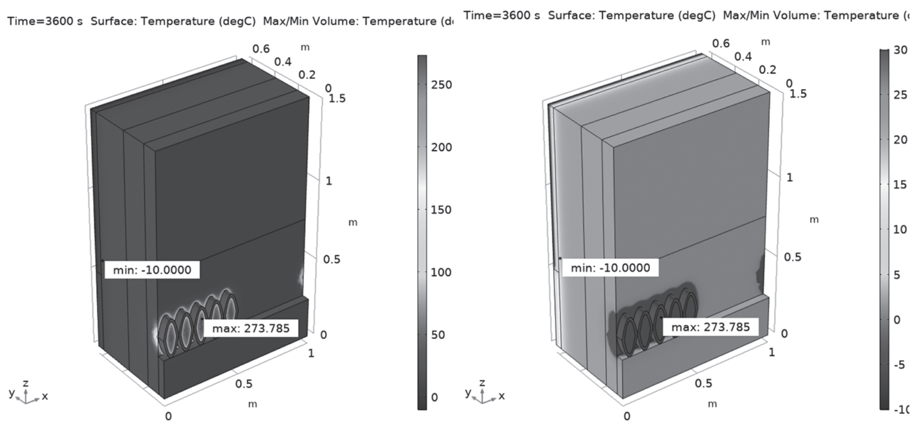

(*a*) (*b*)

Figure 121. Temperature contours (60-min heat exposure): (a) Full scale, (b) 30 °C scale.

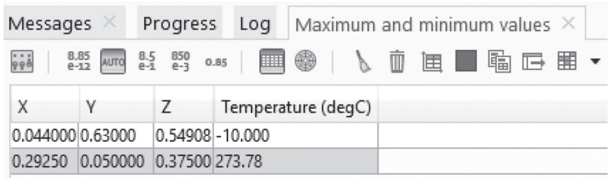

X	Y	Z	Temperature (degC)
0.044000	0.63000	0.54908	-10.000
0.29250	0.050000	0.37500	273.78

Figure 122. Maximum and minimum volume temperatures, one-hour exposure time.

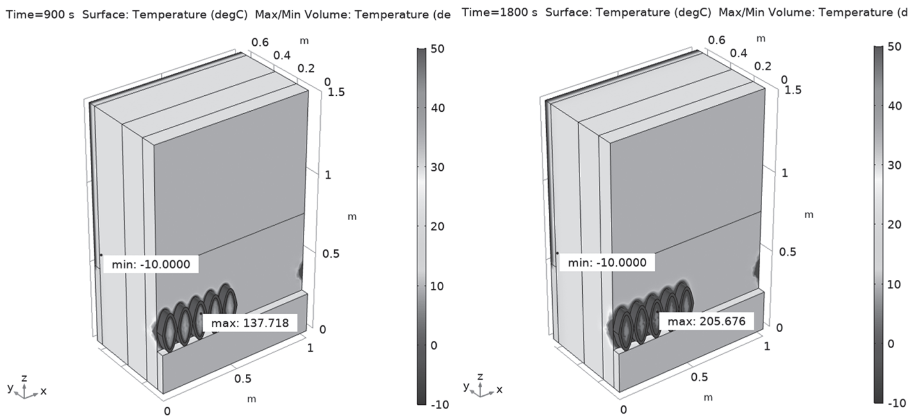

(*a*) (*b*)

Figure 123. Temperature contours, 50 °C scale: (a) 15-min heat exposure, (b) 30-min heat exposure.

are first selected and peak temperatures for those surfaces are extracted. Figure 123 presents temperature contours for the 3D model after a 15 and 30 min exposure time for a set scale with a maximum of 50 °C. It is noted that due to the periodic boundary condition with zero-degree temperature offset, identical temperatures to those of the left region are seen in the right region of the presented domain (wall cross section). This is seen in the identical colors presented. It is assumed that the same wall continues to the right part of the geometry (repeated pattern).

Figure 124b presents the temperature profiles versus the depth of the 3D model. It is seen that the temperature has its peak value in the vicinity of the heating elements, at about 206 °C, at the coil surface on the opposite side from the wall interior surface. The locations of the lines where the temperatures have been sampled are seen in Figure 124a. Figure 125 shows the location of the lines along the length of the 3D model with the temperature profiles shown in Figure 126. This figure presents the three temperature profiles in one diagram (Figure 126a) and also zooms in on the two plots in which the temperatures are lower (Figure 126b). Figure 127 shows the location of the points for which temperature distributions versus the time are presented. The profiles show temperatures that are still increasing, meaning that the system had not yet reached a steady state when the simulation ended.

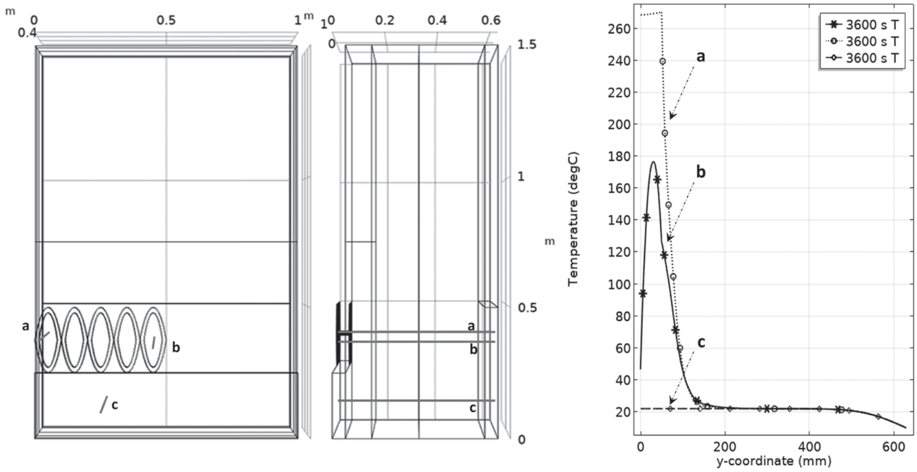

(a) (b)

Figure 124. (a) *Cut Lines 3D* versus the wall depth (*y*-coordinate), (b) Spatial temperature profiles versus the wall depth.

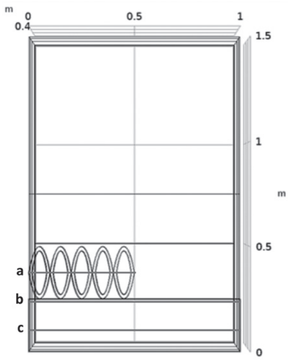

Figure 125. *Cut Lines 3D* versus the wall length (*x*-coordinate).

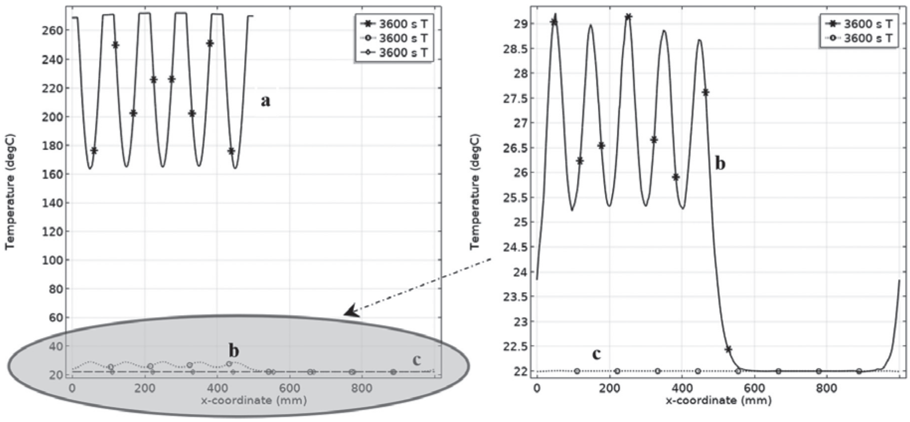

(*a*) (*b*)

Figure 126. Spatial temperature profiles versus the wall length (*x*-coordinate): (a) Lines "*a*," "*b*," and "*c*", (b) Lines "*b*" and "*c*".

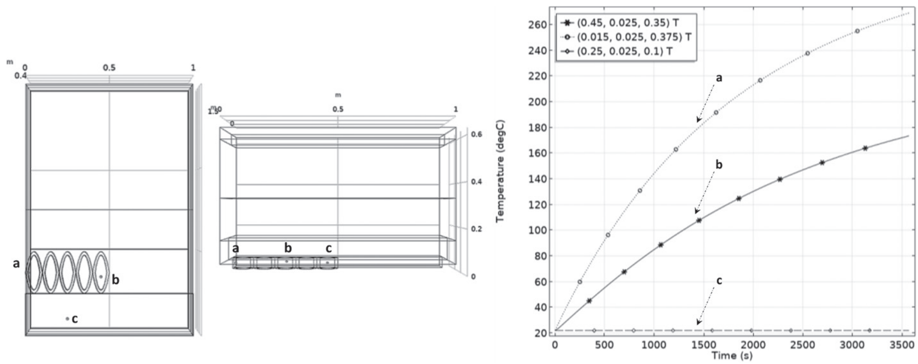

(*a*) (*b*)

Figure 127. (a) *Cut Points 3D*, (b) Transient temperature profiles at selected points.

7.4 Scenario 3—Heat Source: Constant Boundary Heat Rate, Transient, Multilayer

Figure 128 shows the boundary heat source introduced to the thermal model as a source with a constant heat rate (750 W). In other words, the boundary of the radiators in contact with the wall is assumed to hold a constant heat rate, transferring this energy to their surroundings. The difference between this and the previous scenario (Scenario 1) is that in Scenario 1, the heat source is part of the heat conduction equation, while in Scenario 2, the heat source is defined as the boundary source, complementing the defined thermal conduction equation. It is also possible to include the term in the form of a general source (power density in w/m^3). In order to calculate the value of the volume heat source, one method is to identify the volume of the heating elements, then divide the element power by the volume obtained by measuring in COMSOL Multiphysics. If the total power is already known, the total value may be used. To obtain the area or volume of the heating element boundary, one can use the measurement built-in tool available in COMSOL Multiphysics (Figure 128).

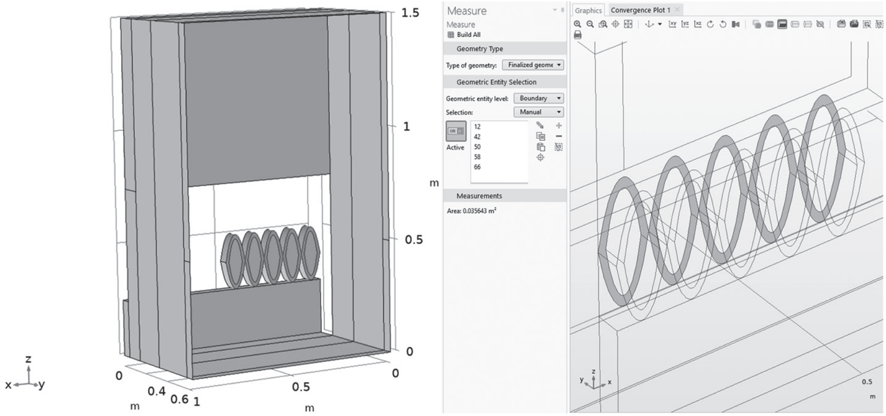

(*a*) (*b*)

Figure 128. Constant heat rate boundary condition: (a) 3D interior view, (b) Wired-frame view.

Figure 129 shows the transient analysis results after one hour of exposure time. In order to gain a better understanding of the temperature distribution inside the volume, one can set a color range with an identified maximum temperature range. Noting the temperature variation along with the peak temperatures, it can be concluded that the temperature variations are almost identical as expected for the conduction problem presented herein. This scenario presents the case that the heat source is in direct contact with the wall. The exterior surfaces convect heat to the surroundings as in the previous scenario; however, there is no heat exchange with the environment at the identified boundary.

The convection heat transfer mechanism is similar to the previous case; therefore, the temperature contours are similar to those of Scenario 1. Figure 129 shows a two-scale temperature, full scale and 30 °C scale. The majority of the interior wall domains are within the temperature range between the initial (22 °C) and ambient (22 °C) ones. The temperature around the radiator areas shows the highest values. Peak temperatures are seen in the message console window (Figure 130) along with the exact values and their locations within the 3D domain. Figure 131 presents temperature contours for the 3D model after 15 and 30 min of exposure time for a set scale of maximum 50 °C. The periodic boundary condition

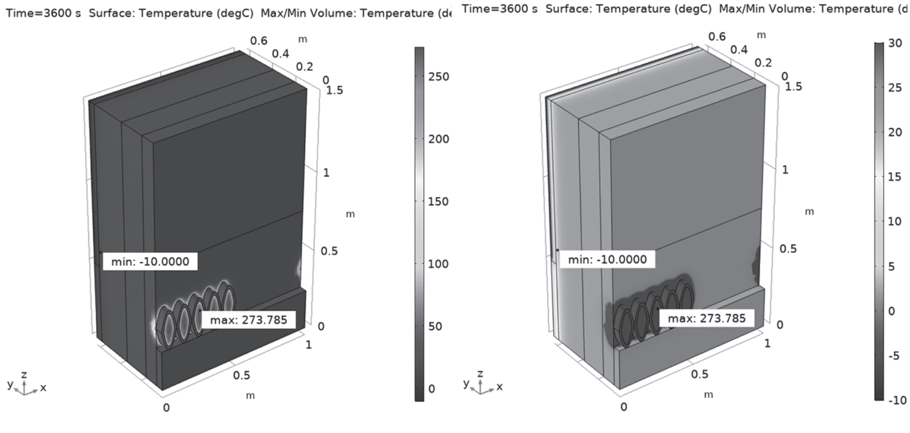

(a) (b)

Figure 129. Temperature contours, 60-min heat exposure: (a) Full scale, (b) 30 °C scale.

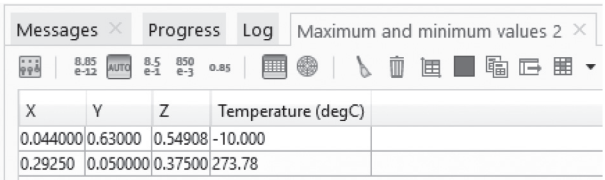

X	Y	Z	Temperature (degC)
0.044000	0.63000	0.54908	-10.000
0.29250	0.050000	0.37500	273.78

Figure 130. Maximum and minimum volume temperatures, one-hour exposure time.

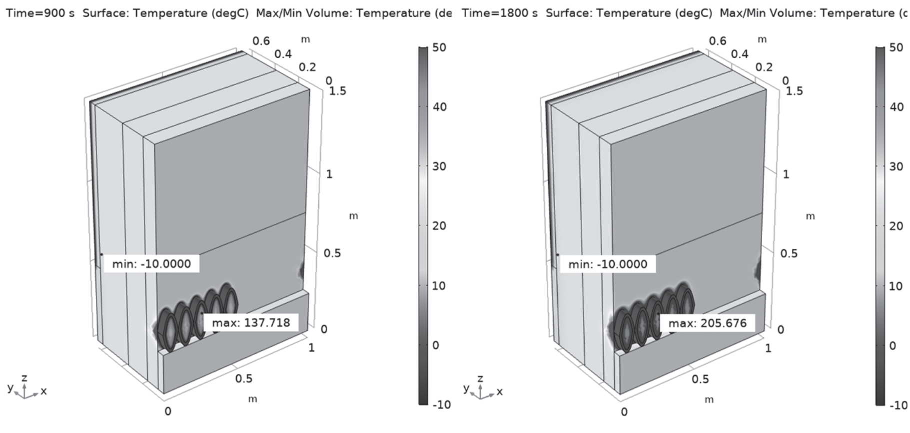

(a) (b)

Figure 131. Temperature contours, 50 °C scale: (a) 15-min heat exposure, (b) 30-min heat exposure.

with zero-degree temperature offset behaves similar to Scenario 1, where for the expected repetition results in the same temperature variation on the right boundary as the left boundary.

Figure 132b presents the temperature profile versus the depth of the 3D model for this example. It is seen that these temperature distributions are almost identical with those of Figure 124b, with the maximum temperature seen at the vicinity of the heating elements reaching a peak value of 267 °C at the coil surface, away from the wall interior surface. The lines along which temperatures are sampled are shown in Figure 132a. Figure 133 presents the locations of the lines along the length of the 3D model with the temperature profiles shown in Figure 125. This figure presents the three temperature profiles in one diagram (Figure 133a) and the domains in which heat is not generated (*Cut Lines 3D* "*b*" and "*c*") as shown in Figure 133b.

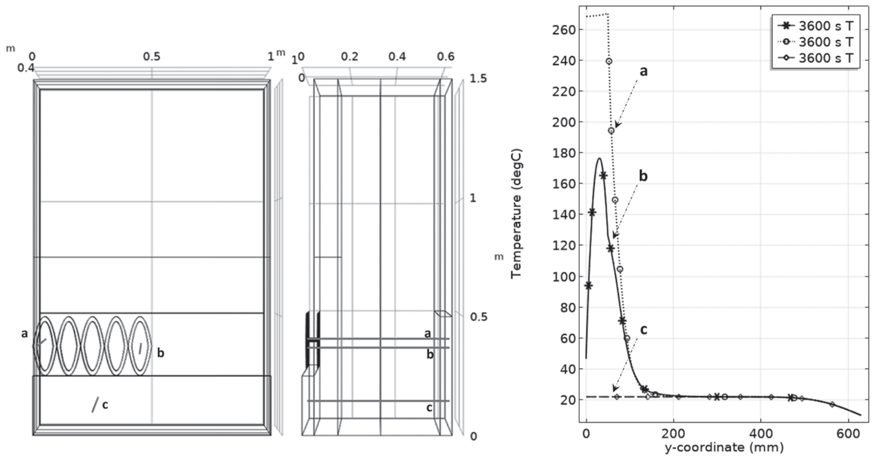

(*a*) (*b*)

Figure 132. (a) *Cut Lines 3D* versus the wall depth (y-coordinate), (b) Spatial temperature profiles versus the wall depth.

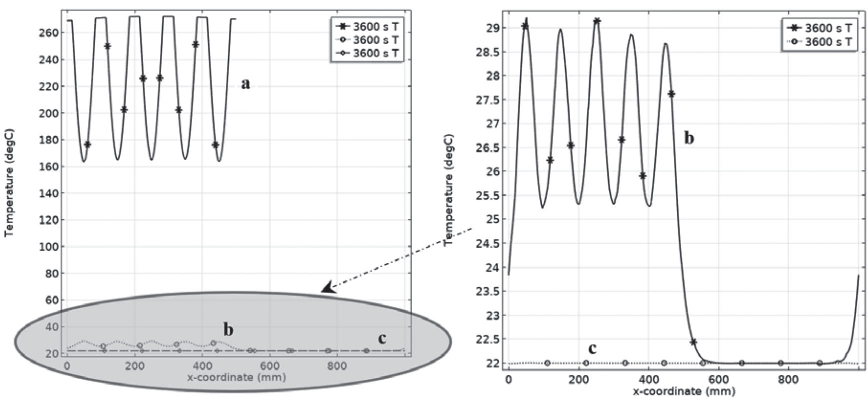

(*a*) (*b*)

Figure 133. Spatial temperature profiles versus the wall length (*x*-coordinate): (a) Lines "*a*," "*b*," and "*c*", (b) Lines "*b*" and "*c*".

Figure 134 shows the locations of the points for which transient temperature distributions are presented—with a continuous rise reaching after one hour about 260 °C at *Cut Lines 3D "a"* at the interior surface opposite the radiator element and 180 °C at *Cut Lines 3D "b"* at the interior surface in the gap between radiator elements.

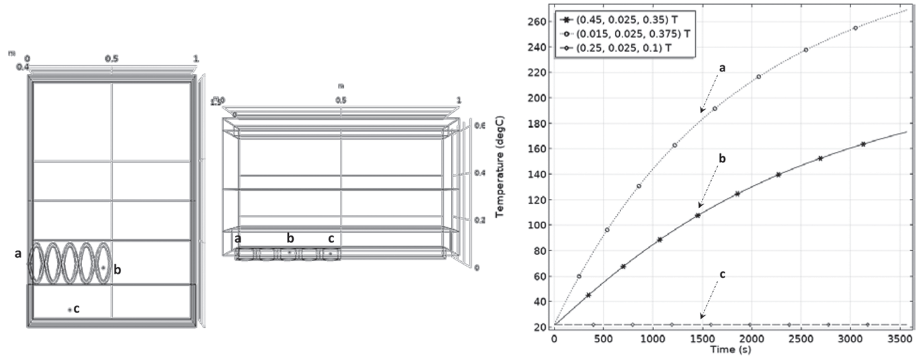

(*a*) (*b*)

Figure 134. (a) *Cut Points 3D*, (b) Transient temperature profiles at selected points.

7.5 Scenario 4—Heat Source: Constant Boundary Heat Rate, Stationary, Multilayer

Figure 135 presents the stationary solution to the transient problem presented in Scenario 2. It is seen that temperature is fully developed in this case with the maximum temperature of about 350 °C. The interior zone surface temperatures remain above the ambient temperature (22 °C) originally set for the problem. As a reminder, a boundary heat source with a constant heat rate (750 W) is assumed in this case. Figure 135 is a two-scale temperature, full scale and 30 °C scale. Peak temperatures along with exact locations are presented in Figure 136. In this scenario, the heat source and interior wall are directly in contact with one another. Temperature variation is more pronounced in Scenario 4 compared to that of Scenario 3. This is due to the extended heating time and higher maximum resulting temperature. Figure 137 presents temperature contours for the 3D model for a set scale of maximum 50 °C. The periodic boundary condition with zero-degree temperature offset presented in this case produce similar results with those of Scenario 2, showing the same temperature distribution on the left side as that of the right side.

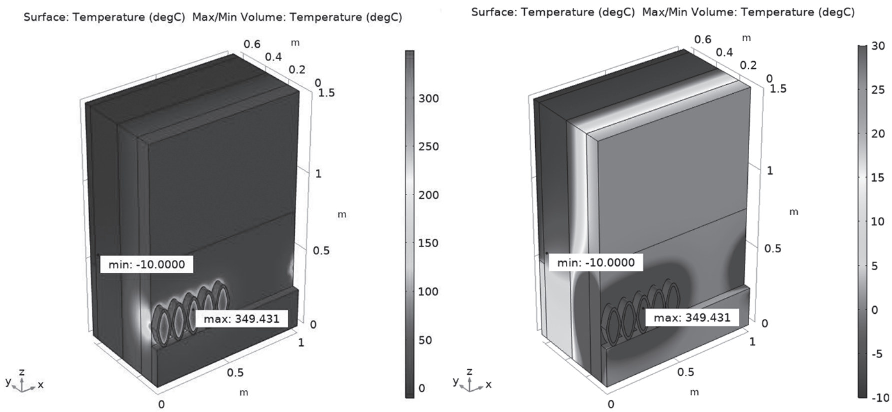

(*a*) (*b*)

Figure 135. Temperature contours (steady-state analysis): (a) Full scale, (b) 30 °C scale.

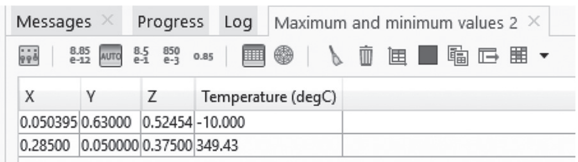

Messages Progress Log Maximum and minimum values 2

X	Y	Z	Temperature (degC)
0.050395	0.63000	0.52454	-10.000
0.28500	0.050000	0.37500	349.43

Figure 136. Maximum and minimum volume temperatures, steady-state analysis.

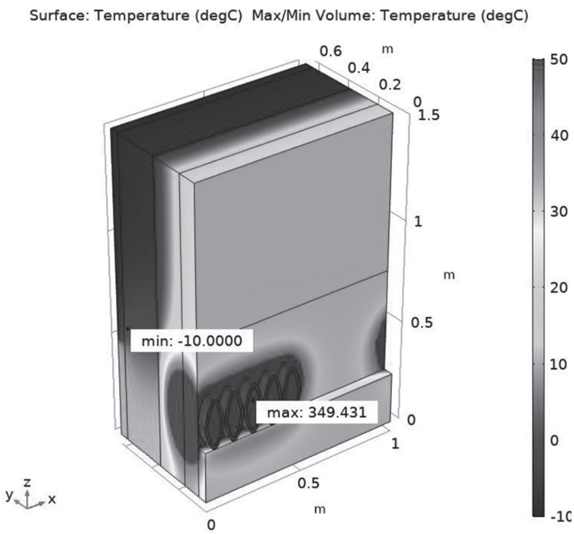

Figure 137. Temperature contours (steady-state analysis), 50 °C scale.

Figure 138b presents the temperature profile versus the depth of the 3D model for the steady-state condition. The peak temperature is higher than that of the transient case as expected. Temperature profiles show a parabolic shape. The locations of the lines are seen in Figure 138a. Figure 125 presents the locations of the lines along the length of the 3D model with the temperature profiles shown in Figure 139. This figure presents the three temperature profiles in one diagram (Figure 139a) and zooms in on the domains with lower temperatures in Figure 139b.

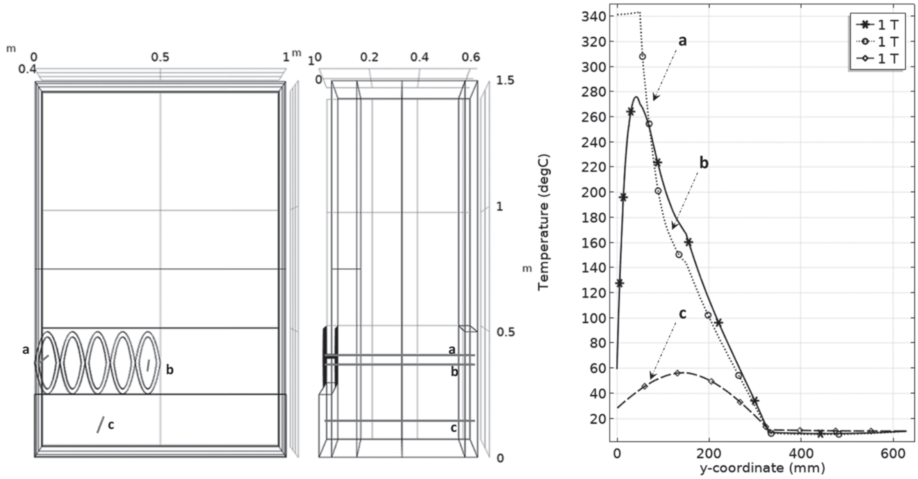

(*a*) (*b*)

Figure 138. (a) *Cut Lines 3D* versus the wall depth (*y*-coordinate), (b) Spatial temperature profiles versus the wall depth.

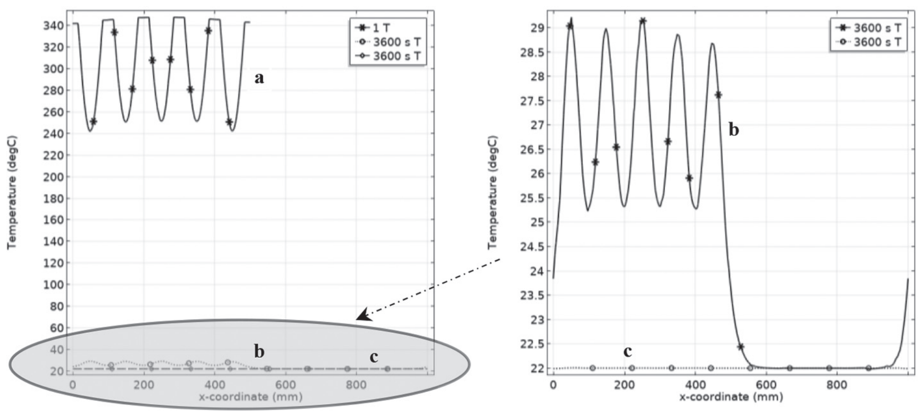

(*a*) (*b*)

Figure 139. Spatial temperature profiles versus the wall length (*x*-coordinate): (a) Lines "*a*," "*b*," and "*c*", (b) Lines "*b*" and "*c*".

7.6 Scenario 5—Heat Source: Constant Boundary Heat Rate, Stationary, Single Layer

This scenario examines the case where an equivalent thermal conductivity using a thermal resistance model is employed in order to replace multiple layers with a single one (equation 11). In heat transfer, temperature difference is the driving force, causing heat flow from the location of the higher value to the lower one. Temperature is equivalent to the voltage that drives the current in an electrical system. The resistance is then the reverse of the thermal conductivity, since thermal conductivity describes how easily the heat flow moves within a domain, while resistance shows how resistive the circuit is to the electric current. The equivalent thermal resistance is presented by equation sets (11). The k_i coefficient is the thermal conductivity related to layer, $depth_i$ is the thickness of the associated layer, and R_i is the thermal resistance value for the layer. The total k defined is the total thermal conductivity of the layer. T shown in brackets indicates the temperature dependence of the parameters, while ϕ in brackets means dependence on the moisture content. Some properties are dependent on temperature (e.g., glass wool), pressure (e.g., air), location, and humidity level (e.g., pine and gypsum); other layers have constant thermal conductivities (e.g., concrete, aluminum, and brick).

Note that the parts associated with gypsum and pinewood walls consist of parallel thermal resistors that are added, while these parts combined (as a single thermal resistor) as well as the thermal resistors associated with the glass-wool and concrete walls form series of resistors. For parallel resistors, the inverse of the total resistance (R_t) equals the sum of the inverses of individual resistances. For the series scenario, the total resistance equals the summation of the individual resistances as shown in equation 11. Figure 140 shows the equivalent thermal conductivity (as a function of the temperature and humidity) versus the humidity level and temperature, calculated from equation sets (11).

$$\begin{cases} R_1 = \dfrac{\text{depth}_1}{k_{gyp}(\varphi) + k_{pw}(\varphi)} \\ R_2 = \dfrac{\text{depth}_2}{k_{gw}(T)} \\ R_3 = \dfrac{\text{depth}_3}{k_{\text{con}}(T)} \\ R_t = R_1 + R_2 + R_3 \\ k = \dfrac{1}{R_t} \end{cases} \tag{11}$$

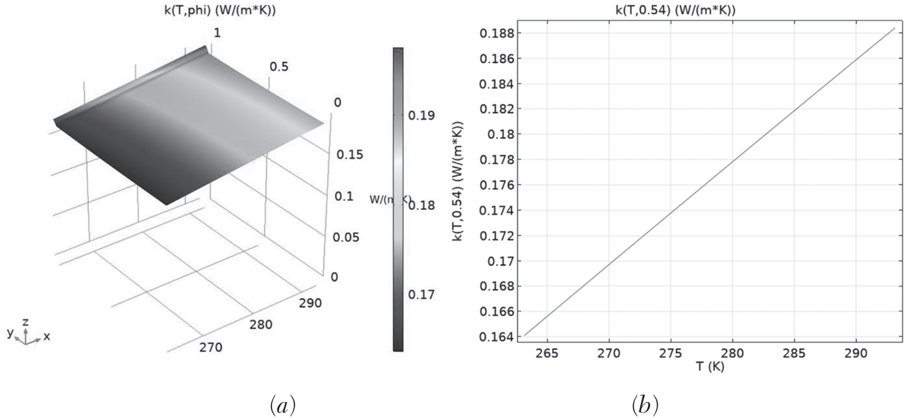

Figure 140. Thermal conductivity with single middle layer as a function of: (a) Temperature and humidity, (b) Temperature at 54 percent humidity level.

Figure 141 presents the wall system with a single (equivalent) mid layer; the model is meshed using the free tetrahedral elements. Figure 142 presents the stationary solution to the transient problem presented in Scenario 3 (assuming that the middle layers are joined). It is seen that the maximum temperature in this case is about 326 °C. The interior zone surface temperatures are at about the original ambient temperature (22 °C). A boundary heat source with a constant heat rate (750 W) is assumed in this case. Figure 142 is a two-scale temperature, full scale and 30 °C scale. Peak temperatures along with exact locations are presented in Figure 143.

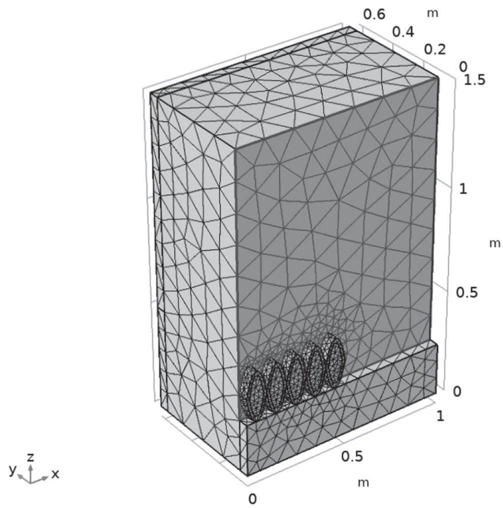

Figure 141. Meshed wall.

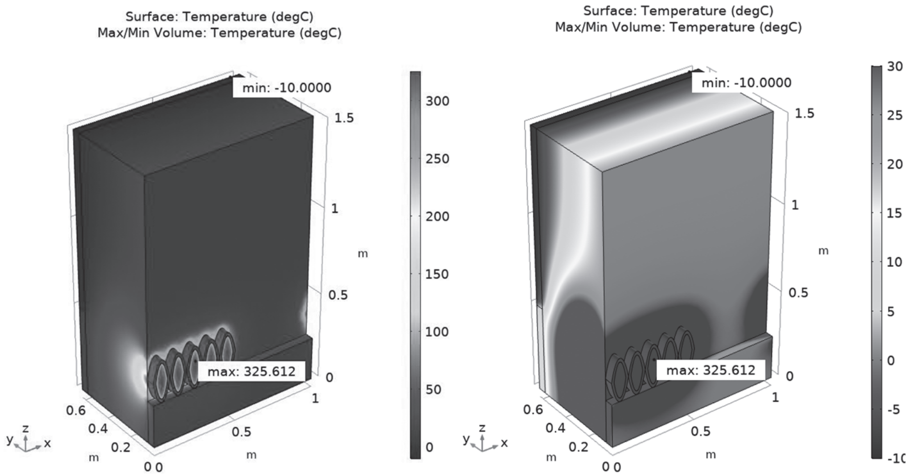

(*a*) (*b*)

Figure 142. Temperature contours (steady-state analysis): (a) Full scale, (b) 30 °C scale.

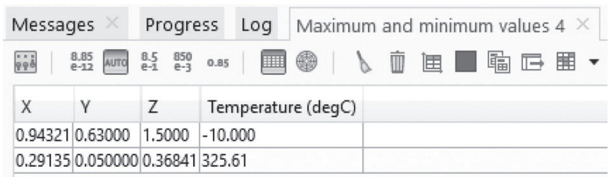

X	Y	Z	Temperature (degC)
0.94321	0.63000	1.5000	-10.000
0.29135	0.050000	0.36841	325.61

Figure 143. Maximum and minimum volume temperatures, steady-state analysis.

In this scenario, the heat source and interior wall are touching one another. Maximum temperature shows a higher value in Scenario 5 compared to that of Scenario 4. It is expected that these two values show similar behaviors; however, they do not. Figure 144 shows temperature contours for the 3D model for a set scale of a maximum of 50 °C. The periodic boundary condition with zero-degree temperature offset generates similar trends to those of Scenario 4—similar temperature distribution to the left side is seen on the right side. A comparison between the temperature profiles along the depth of the domains at the vicinity of the radiators is presented at the identified locations (Figure 145). It is seen that these profiles are not identical. They show a similar trend inside the unified layers until halfway inside this layer, where temperature variations become significant.

Figure 145b presents the temperature profile versus the depth of the 3D model for the steady-state condition. The peak temperature is higher than that of the transient case as expected. Temperature profiles show a parabolic shape. The locations of the lines are seen in Figure 145a.

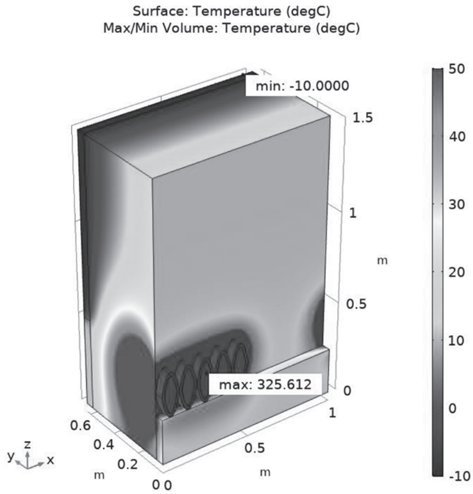

Figure 144. Temperature contours (steady-state analysis), 50 °C scale.

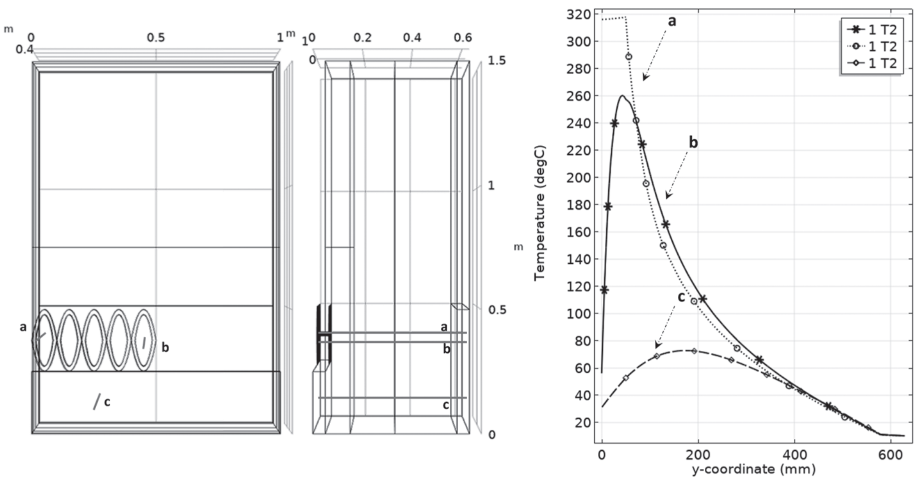

(*a*) (*b*)

Figure 145. (a) *Cut Lines 3D* versus the wall depth (*y*-coordinate), (b) Spatial temperature profiles versus the wall depth.

Figure 125 presents the locations of the lines along the length of the 3D model with the temperature profiles shown in Figure 146. This figure presents the three temperature profiles in one diagram (Figure 146a) and zooms in on the domains with lower temperatures in Figure 146. Figure 147 shows the temperature profiles along the depth of the 3D model for the three said locations compared to the previous scenario.

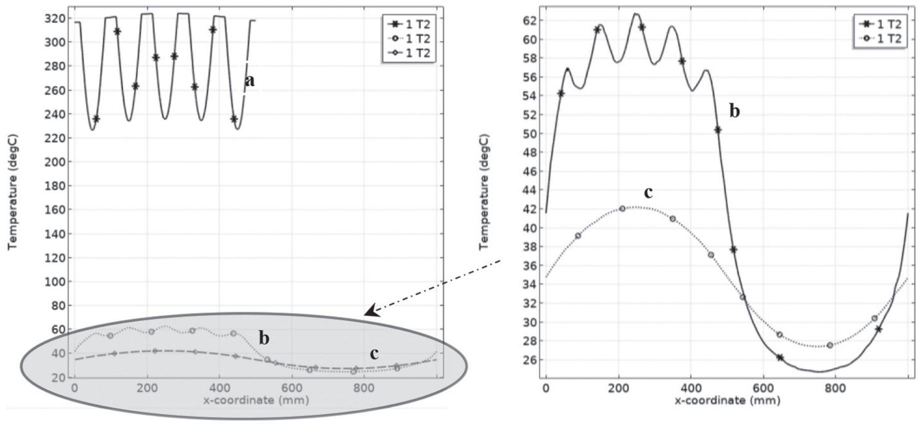

(*a*) (*b*)

Figure 146. Spatial temperature profiles versus the wall length (*x*-coordinate): (a) Lines "*a*," "*b*," and "*c*", (b) Lines "*b*" and "*c*".

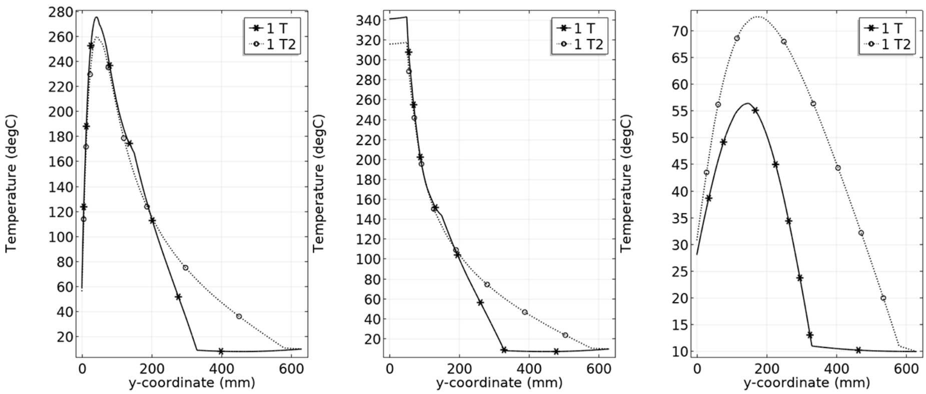

(*a*) (*b*) (*c*)

Figure 147. A comparison between spatial temperature profiles versus the wall depth (*y*-coordinate): (a) Line "*a*", (b) Line "*b*", (c) Line "*c*".

7.7 Scenario 6—Heat Source: Constant Interior Temperature, Stationary, Single Layer

This example is similar to the one presented in Scenario 5; however, temperatures of all interior surfaces (walls) are now constant at 22 °C (Figure 148). This scenario examines the case where a single thermal resistance as the equivalent one is assumed for the middle layers. This means that the middle layers can be substituted with a single layer, which is expected to produce results similar to those of the multilayer representation.

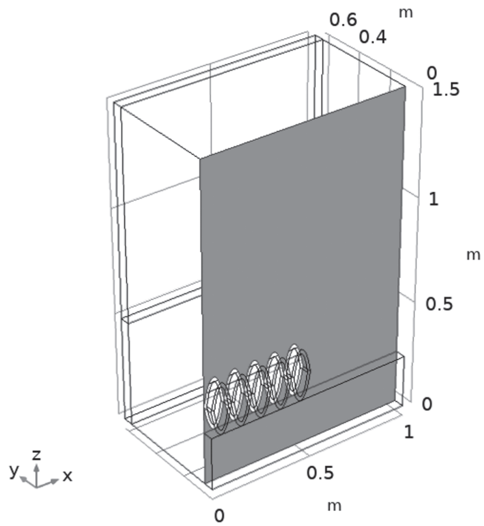

Figure 148. Constant temperature boundary condition.

To compare the solutions for the multilayer and single-layer representations, the temperature profiles along the depth of the domains in the vicinity of the radiators (that are turned off in this case) are presented (Figure 149). It is seen that these profiles are close but not identical. They show a similar trend for the reference plane (y = 0), and this is due to the fact that the imposed wall temperature isolates the domains on either side of the walls with a constant temperature. The rest of the temperature variation is then similar to modeling two different physics. Figure 149b presents the temperature profile versus the depth of the 3D model for the steady-state condition for when temperature at the interfacing walls is constant (22 °C). Temperature profiles are parabolic. The locations of the lines are seen in Figure 149a. Figure 125 presents the locations of the lines along the length of the 3D model with the temperature profiles shown in Figure 150. This figure presents the three temperature profiles in one diagram (Figure 150a), with the right plot showing a zoomed-in view of lower temperatures in Figure 150. Figure 151 shows the temperature profiles along the depth of the 3D model for the three said locations compared to the previous scenario.

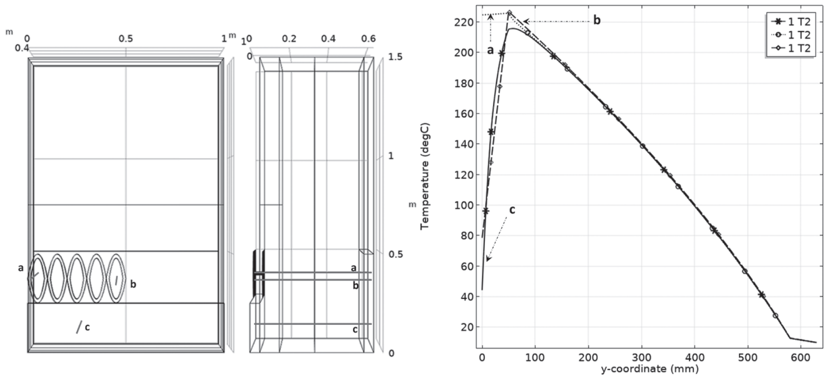

(*a*) (*b*)

Figure 149. (a) *Cut Lines 3D* versus the wall depth (*y*-coordinate), (b) Spatial temperature profiles versus the wall depth.

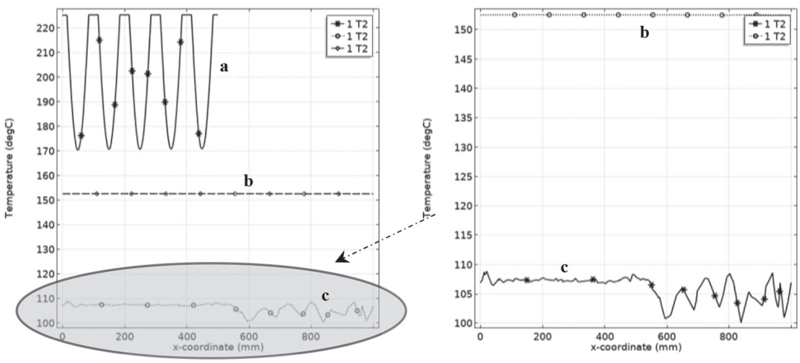

(*a*) (*b*)

Figure 150. Spatial temperature profiles versus the wall length (*x*-coordinate): (a) Lines "*a*," "*b*," and "*c*", (b) Lines "*b*" and "*c*".

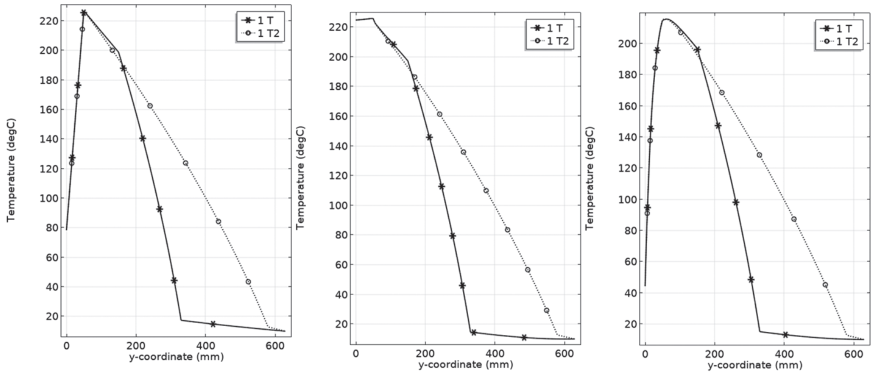

(*a*) (*b*) (*c*)

Figure 151. A comparison between spatial temperature profiles versus the wall depth (*y*-coordinate): (a) Line "*a*", (b) Line "*b*", (c) Line "*c*".

7.8 Scenario 7—Constant Exterior-Interior Temperatures, Stationary, Single Layer

This case study considers the heat transfer for the given problem between an external surface, kept at the two constant temperatures specified previously (upper and lower portions), and no heat source. It is assumed that the middle wall layers (i.e., concrete, glass wool batt, pine wood, and gypsum board) are joined so that they form a single layer with the thermo-physical properties presented in Figure 117. Temperature contours are presented in Figure 152. Temperature along the wall depth is presented in Figure 153. The temperature profile within the wall is almost linear with the varying gradients as material varies, the temperature gradient slope depending on the thermal conductivity of the layer. Note that the middle layer, which is the combination of the three layers presented by equation (11), has a constant temperature slope with a negative gradient. The beginning and end of these profiles are similar to that of the multilayer. The comparison between the two sets of temperature profiles is shown in Figure 153. In the plot, *Dependent variable T2* corresponds to the single-layer physics while *Dependent variable T* is related to the multilayer physics.

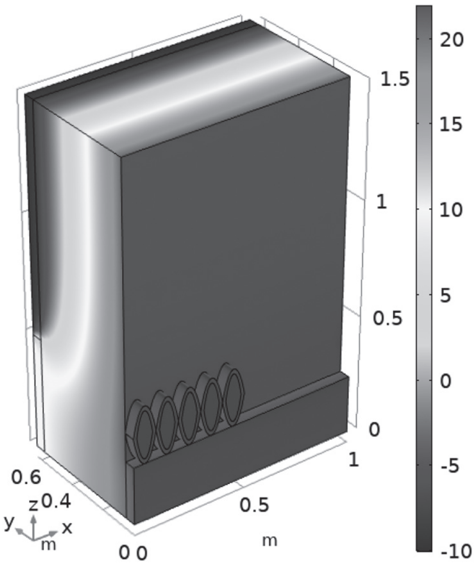

Figure 152. Temperature contours (steady-state analysis).

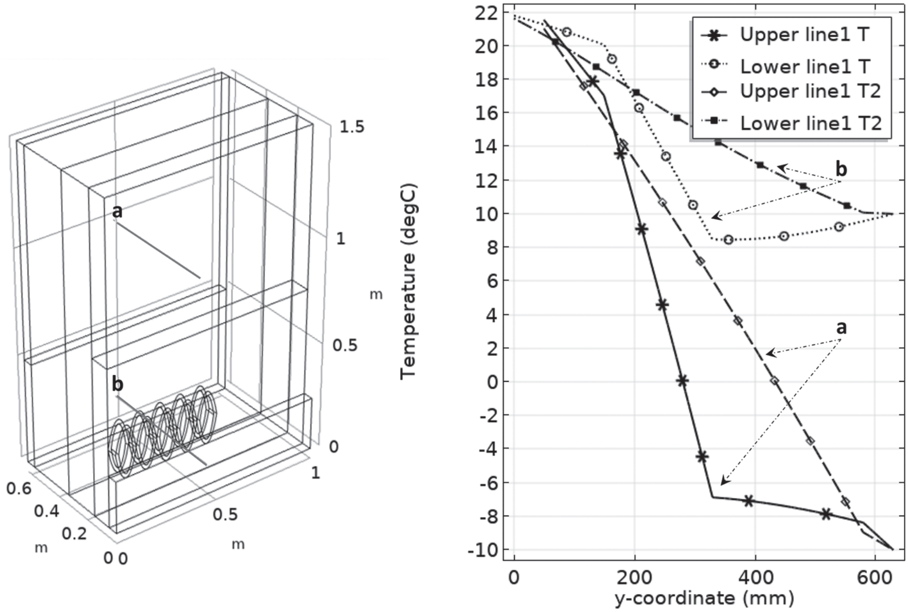

(*a*) (*b*)

Figure 153. (a) A comparison between *Cut Lines 3D* versus the wall depth (*y*-coordinate), (b) Temperature profiles versus the wall depth.

CHAPTER 8

Case Study 3—Heating Water Inside a Kettle

Learning to harvest mechanical power from heated water led to a great leap in humanity's progress, known as the *First Industrial Revolution* (1760–1840). Reliable mechanical power from steam could be deployed wherever it was needed and did not need to be tied to the source of moving water or be dependent on unpredictable winds. Steam power is obtained by the conversion of energy from one type (thermal) to another (mechanical). Today, the power of steam is still used in fossil fuel power plants to generate electricity. The combustion heat of a fossil fuel (coal, oil, or natural gas) is used to heat the water, converting it to high-pressure steam that drives the turbine connected to an electrical generator.

The high amount of thermal energy that can be stored in water (both in liquid and steam forms) also makes it an efficient medium for distribution of heat in hot-water heated homes (with radiators or in-floor heating) and, on a larger scale, in district heating systems. And, of course, we have all used hot water for cooking as well as washing dishes, clothing, and ourselves.

Another common way of heating water is by electrical current used to heat a resistive element, as is done in electric domestic water heaters. The third way, gaining in importance as humanity is trying to reduce its reliance on fossil fuels, is heating by solar radiation. We have all experienced the radiant energy of the Sun on a personal level—on a sunny day, you can feel its warmth on your face. The same energy can be concentrated to generate massive amounts of electricity. Currently, the world's largest concentrated solar power plant is the Ouarzazate Solar Power Station located in Morocco, generating 510 MW since 2016. It uses large molten salt tanks to store the Sun's heat; the molten salt is then used to convert water to steam, driving the electricity-generating steam turbines. In the Mohave Desert of California, Ivanpah Solar Power Facility, operating from 2014, is capable of producing 392 MW of electricity. It uses mirrors to concentrate the solar radiation, producing steam that drives the turbines.

8.1 Problem Definition

This study examines the case of a kettle filled with water (Figure 154). A *kettle*, as used in this case study, could also stand for a pot or container with any liquid. It is also possible to consider a combination of fluids (gases and liquids), as is presented as a special example for this case study. Such a container can be made of a range of materials and have a variety of sizes and shapes, with its subcomponents (e.g., lid, spout, and handle) situated at different locations with respect to one another. There are both stovetop and electric kettles. Other forms of kettles are Kelly kettles that are used outdoors to boil water, made of water jackets that surround a fire chamber warmed with twigs and other similar materials. Boiling vessels are another example of water-heating containers. These are used in military applications, where the crew can heat water and cook food by using the vehicle electric supply.

A samovar is another appliance used to heat water to make tea; it originated in Russia and has been adopted by many neighboring countries such as Iran as well as Eastern and Central European countries. A samovar uses a heating technique known as the *double-pot method*—water boiled

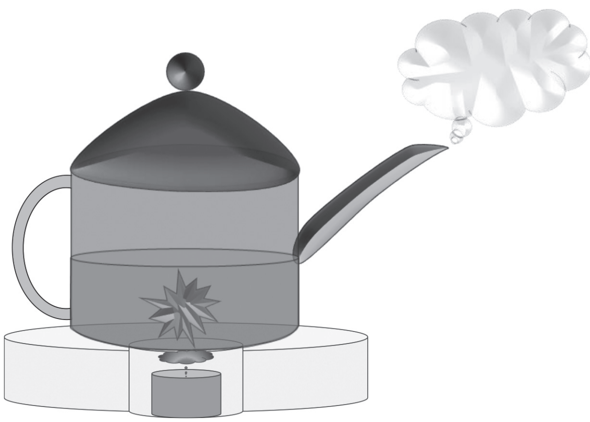

Figure 154. A kettle with a heating source.

inside the large vessel is transferred to a smaller pot. This smaller pot is then placed on top of the samovar, where it continues to be warmed using the latent heat of the water still being heated inside the main vessel. The tea is brewed and also kept warm for the duration of the exposure to this heat. A metal pipe located in the middle of the samovar is filled with combustible solid material that heats the water [110].

A Windermere kettle, with its name adopted from the English lake, is a steam-operated samovar that was used on steamboats. A heating copper coil is located inside the water vessel. The steam from the boat propulsion boiler is passed through the coil, after opening a valve to the vessel, and the water is heated in a matter of seconds. These steam vessels are essentially rapid boilers [111]. A teasmade is an automatic tea-maker machine that was used extensively in the United Kingdom and some of the Commonwealth countries, meant to serve as an alarm clock, with lamps with ornamental shades and a tea maker to be placed at the bedside. That should have started your day on the right foot, with the whistle of steam as it escapes the spout [112].

The previous examples show the relevance of this case study to a variety of industrial and domestic applications. Two scenarios are considered here. The heating is either done by: (1) an electric current, or (2) a tea candle. The first scenario is presented as follows as a complete case study. The second scenario is then introduced as an exercise for the reader.

8.2 Kettle Geometry

The kettle geometry consists of both solid and fluid domains. The geometry is created as a drawing in Solid Edge, exported in the*.dxf* format, and then imported into a 2D axisymmetric model. Since after the import, the geometry was at a distance r and z from the axisymmetric axis, it was moved to (0,0). The exterior surfaces consisting of the kettle walls, lid, and base are solid; the kettle interior is partially filled with water. The top boundary of water is in contact with the empty space inside the kettle (surrounding). The modeled kettle's overall shape can be considered to be axially symmetric, if one ignores the spout and the handle. Since there are significant computational resource savings by going from a 3D model to a 2D one, and since this problem involves complex physics modeling, it was decided to use a 2D axisymmetric model as an approximation, while neglecting the effect of the handle and the spout. The 2D model can be seen in Figure 155a, while Figure 155b shows its 3D visualization, obtained by rotating the 2D model about its symmetry axis. This visualization can be obtained by creating a *3D Plot Group* and selecting *Revolution 2D*, which is found under *Data Sets* (*Results*), about the axisymmetric axis (z-coordinate) at a distance r (zero) from this axis in COMSOL Multiphysics. Note that

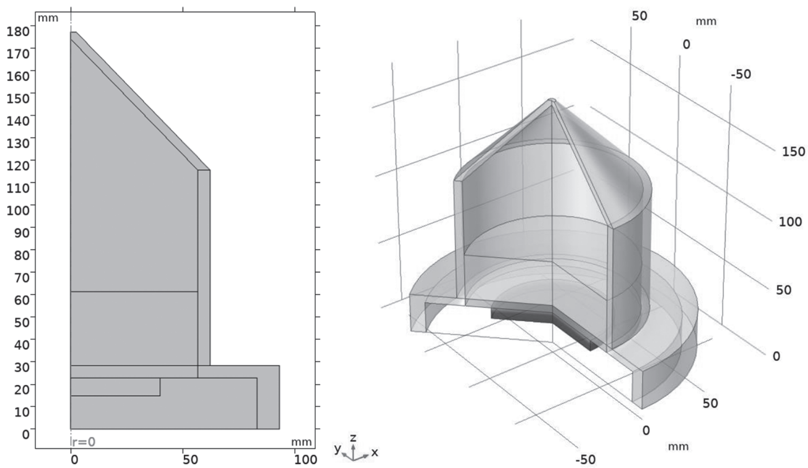

(*a*) (*b*)

Figure 155. A kettle with a heating element: (a) 2D axisymmetric model geometry, (b) 3D representation of a 2D axisymmetric model.

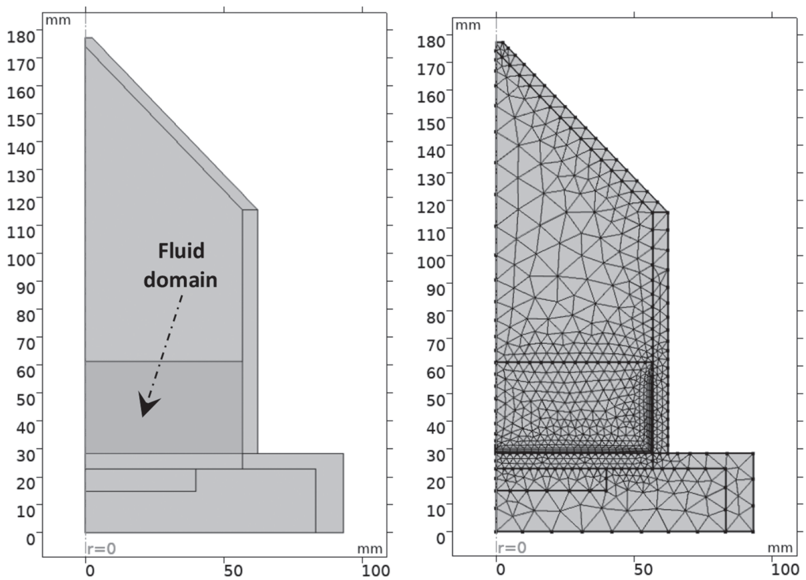

(*a*) (*b*)

Figure 156. 2D axisymmetric model for a kettle with heat source, *r-z* plane: (a) Highlighted fluid domain, (b) Meshed geometry.

by default, the *Revolution 2D*, data set is created under *Data Sets*, *Results*. Since the heat source is also located centrally and is uniformly distributed, it can be represented within this 2D axisymmetric model. The fluid domain (the liquid being heated) is highlighted in Figure 156a, and the mesh is shown in Figure 156b.

When meshing the parts, note that the domains involved in the flow model are to be meshed so that the boundary layers—which are the boundaries between the solids and fluids—are properly defined (Figure 156b). To mesh the model, *Fine* setting was used to generate an automatic mesh consisting of under 5,000 triangular elements.

8.3 Kettle Physics Selection

In this case study, where the kettle is partially filled with water and the space above it is empty, the entire system is modeled as a multiphysics solid-fluid domain interacting with a fluid domain through a conjugate heat transfer node. The effects of the thermal radiation emitted from the exposed hot surfaces are also included. Note that the kettle walls have two surfaces, internal and external (due to the wall thickness). The interior surfaces are directly in contact with the fluid inside the kettle, while the exterior surfaces are in direct contact with the ambient. The latter exchanges radiative heat that is received from the interior surfaces with the surroundings. The interior surfaces receive the heat generated by the electric source. This heat is then transferred by conduction and radiation to the external surfaces. This is done through *Surface-to-Surface Radiation* feature. The surfaces in contact with the ambient (external diffuse surfaces) use ambient conditions (i.e., temperature) as the input temperature, while the internal diffuse surfaces use the calculated dependent variable (T) as the input temperature. The effect of gravity is also accounted for as part of the flow model.

As stated previously, the air above the water is not modeled here. It is possible to also include the air fluid domain above the water to fully model the physics with multiple flows. However, such a model would require considerable additional computational resources and may in fact exceed the capabilities of a typical PC workstation. If such a setup is of interest, the free boundary at the upper water surface will not be applicable, and the walls in contact with the fluids (water and air) would be expanded to the entire interior kettle surface in contact with the fluids.

When setting up the physics in COMSOL Multiphysics, two individual physics are selected from the physics tree (Figure 157): (1) *Conjugate*

Heat Transfer physics that presents a multiphysics interface, coupling the three modes of heat transfer for the solid with flow convection physics—in this example, the fluid is assumed to follow a laminar flow regime; and (2) *Surface-to-Surface Radiation* physics that combines the three modes of heat transfer for the solid along with surface-to-surface radiation. The three modes of heat transfer referenced previously are conduction, convection, and radiation, defined in the form of boundary or domain conditions. In conjugate heat transfer, the fluid flow can be assumed to be laminar or turbulent. In the case study presented herein, the flow model is assumed as laminar and compressible with Mach under 0.3.

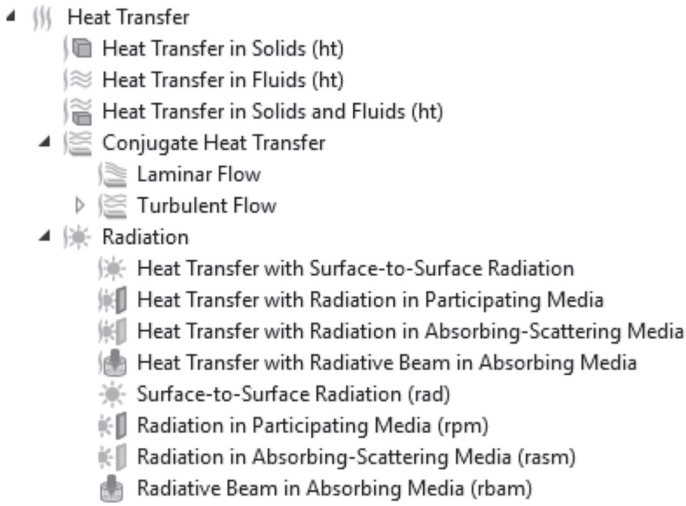

Figure 157. *Heat Transfer* physics tree to set up heating water inside a kettle study.

When setting up the physics for radiation heat transfer, one must select all the boundaries and spaces in between the surfaces that can transfer heat by radiation. The radiosity equation is then defined on these boundaries. For the surface-to-surface radiation to be modeled, the radiosity method is identified. The latter is a boundary condition that is added to the radiation parent.

When modeling radiation heat transfer, external surfaces are usually defined as diffuse surfaces, transferring heat in all directions to the internal surfaces and also to the ambient. It is important to know the emissivity of these two surfaces (internal and external). This can be done by defining a boundary material (e.g., surfaces or boundaries of the radiative domains in 3D or planes in 2D scenarios) as part of the defining materials on the global or component levels. Note that temperature conditions are applied to the boundary and not the domain. Doing so, the optical properties of the material are also added or a placeholder is considered where such properties including the emissivity of the matter can be included or revised to desired values. Alternatively, it is possible to identify the emissivity of the material when setting up the physics at the component physics level and boundary condition level (diffuse to diffuse surface)—i.e., user-defined versus the material-defined optical properties.

Note that when setting up the conjugate and surface-to-surface radiation physics, two sets of physics are created for each set of multiphysics problems. The flow and radiation modes are in addition to the solid-fluid modes of heat transfer for each set of groups, which are connected through the temperature (T) dependent variable under *Multiphysics* node. This dependent temperature in the solid-fluid physics is shared among the two sets of physics. In other words, when defining variables for the physics (e.g., ambient temperature), they should be the same dependent variable as that of the related solid-fluid physics. In *Multiphysics* nodes that use physics couplings in order to solve the physics simultaneously, the defined inter-dependent physics, fluid flow, heat transfer models, and surface-to-surface radiation physics are applied to the applicable domains and solved in pairs (solid-fluid and radiation heat transfer).

8.4 Kettle Materials, Boundary Conditions, and Meshing

The flow model follows Naiver-Stokes equations with the gravity forces acting downward, in the negative z direction. The fluid density is calculated based on the gas/liquid relations. In the non-isothermal node found under *Multiphysics* node, *Non Isothermal Flow*, when setting up a multiphysics model, the selection of fluid density is either from *Heat Transfer* or *Fluid Flow Interface*—$\rho = \rho(p_{\mathrm{ref}}, T)$, where temperature ($T$) and reference pressure (p_{ref}) are employed. Density can also be user defined, predicting the density varying linearly with temperature. In this case, reference density (ρ_{ref}) along with the thermal expansion coefficient (α_p) and reference temperature (T_{ref}) are given in order to provide the density for the given condition, $\rho = \rho_{\mathrm{ref}}(1 - \alpha_p(T - T_{\mathrm{ref}}))$. Another scenario to define density for *Multiphysics* node is to associate a constant value to it at reference temperature. Note that reference temperature is 20 °C by default. However, it can be changed as desired and can be selected from *Heat Transfer* or *Fluid Flow Interface* or chosen to be constant.

In this example, both density and reference temperature are adopted from the heat transfer interface. The analyst should ensure there is consistency when selecting the sources of reference temperature and density from which the non-isothermal flow properties are adopted; otherwise, there will be convergence issues when solving the problem.

Extensive research has been conducted into finding the best choice for the kettle material from the perspective of long-term negative health effects. Borosilicate glass was determined to be the safest choice; there are reports that aluminum or stainless-steel kettles can release nickel and chromium into the water. If a glazed ceramic pot is used for heating water, it is possible for lead to be released into the water. Borosilicate glass is used to make laboratory glassware; thus, it resists heat well above the water boiling temperature in addition to not releasing harmful chemicals into the liquid. In this example, water is warmed in such a glass container [113]. The base of the teapot stand is assumed to be made of copper to maximize heat transfer to the pot. The lid is also made of copper—for decorative reasons.

This scenario models the kettle where water is heated by electricity at a constant power setting. This heat is provided through Joule's heating, which can be calculated from the resistance and current or entered directly in terms of electrical power. There are different ways to represent such a heat source: (1) *General Source* (volumetric energy source in W/m^3); (2) *Line source* (q_sT) in W/m^{3}K, knowing *Production/absorption coefficient* (energy per unit temperature (q_s); or (3) *Heat rate* ($Q_0 = P_0/V$) in W. For this model, the entire area of the heating element shown with purple in Figure 158 generates heat at a constant rate of 1,500 W for the entire simulated time interval (5 min). It is assumed that the heat source area's lower and right boundaries are insulated.

The surfaces not exposed to the fluid (air) are insulated in this scenario. The initial conditions are assumed as those of the ambient with reference pressure and temperature of 1 atm and 20 °C, and ambient temperature of 25 °C. Reference pressure and temperature are used as the default conditions when setting up the models for any thermo-fluid analysis. For the fluid flow, it is possible to assume initial values for the velocity field in case of existence of currents; however, in this example the initial velocity is set to equal zero.

To take into account radiative heat transfer, diffuse surface boundary conditions are selected where heat is expected to be transferred by the surface-to-surface radiation. These conditions are applied to edges highlighted in Figure 160. The internal and external diffuse surfaces transmit the radiative energy with the surface emissivity assumed equal

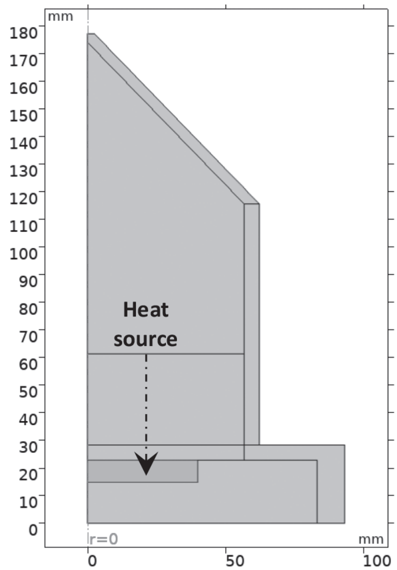

Figure 158. 2D axisymmetric model for a kettle highlighting the heat source (*r-z* plane).

to 0.9. In the radiation coupled *Multiphysics* node, domain opacities are either selected as *Transparent* or *From the heat transfer interface*. The latter is selected in this scenario.

This means that the view factor is nonzero on the diffuse surfaces. The view factor is the portion of the energy that leaves one surface and reaches the other one and is inversely proportional to the areas of the surfaces facing each other by the reciprocity law. For this scenario, the radiation direction may be selected as negative (inward) or positive (outward), both sides, opacity controlled, or none of them. Radiation direction is *Opacity Controlled* in this case. Opacity is the percentage of the absorption and scattering of radiation within a medium. A transparent or translucent object lets all or some light pass through. An opaque object lets no light pass, therefore letting other modes (scattering, absorption, and reflection) happen. Glass may be transparent (transmitting) when exposed to visible light but opaque to an infrared wavelength. Radiation physics settings are set so that the refractive index equals one to represent the optical properties of the air.

Figure 159 highlights the surfaces defined as the open boundary and the walls (for the fluid-filled domain). The open boundary is a free surface in contact with the empty space above it. A *Normal stress* of zero at the open boundary is assumed for the flow model. Another option would be to select

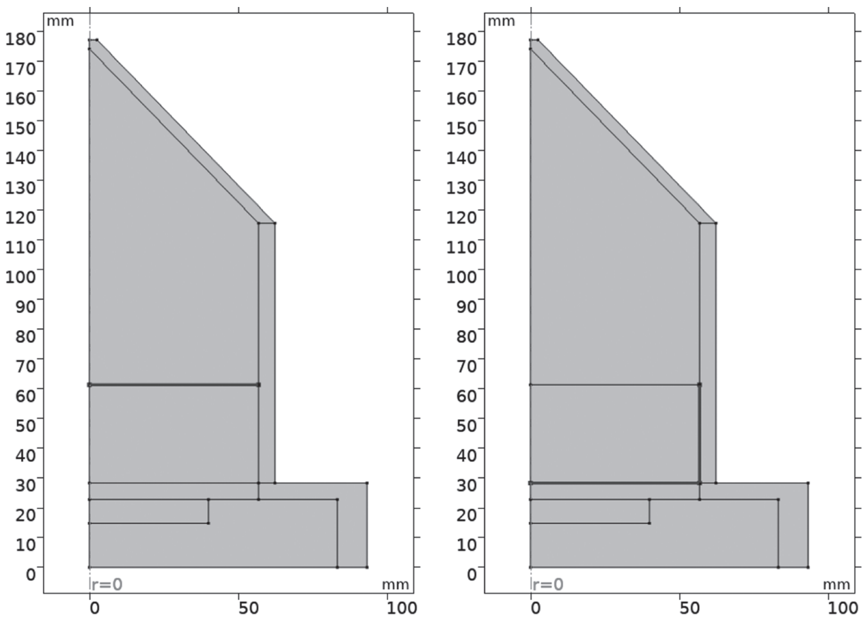

(*a*) (*b*)

Figure 159. 2D axisymmetric model for a kettle with heat source (*r-z* plane): (a) Open boundary, (b) Walls.

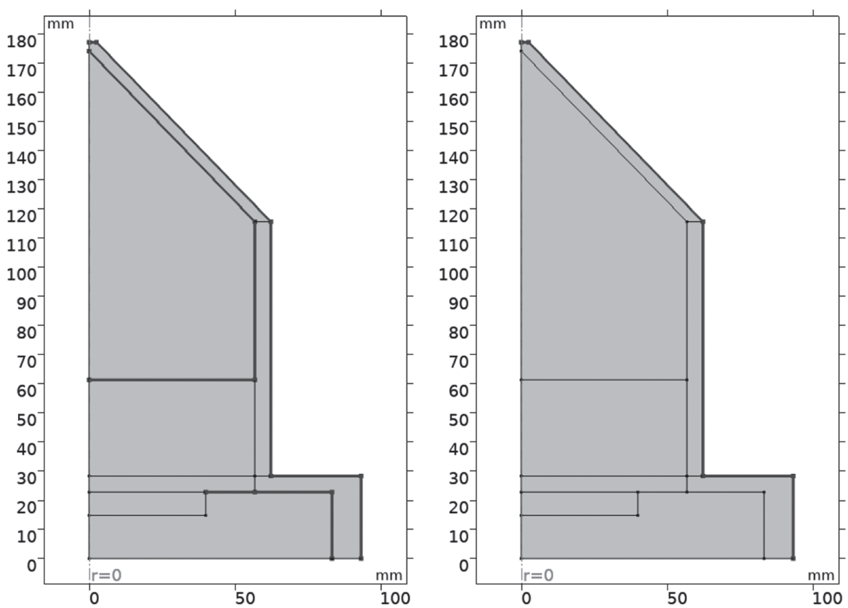

(*a*) (*b*)

Figure 160. 2D axisymmetric model for a kettle with heat source (*r-z* plane): (a) Diffuse surfaces, (b) External diffuse surfaces.

No viscous stress. Since the fluid (water) is exposed to the empty space, it can be treated as a free boundary (Figure 159a). The kettle's interior surfaces in contact with the fluid are treated as walls (Figure 159b). The environment is at the atmospheric conditions.

It is assumed that the system is exchanging heat with its environment by the convection mode of heat transfer. Convective heat transfer is set for the external surfaces. Note that the teapot wall temperature increases the convection of the fluid flow (gas or liquid) inside the pot as well as the energy convected to the ambient.

Since the radiation model is coupled with the solid model, the ambient temperature is assumed to be user defined. The same independent variable defined in the solid-fluid model (e.g., T) is adopted for the ambient temperature of the radiation model for the internal surfaces. The exterior surfaces mode of radiation transmission is by surface-to-ambient radiation. This means that there is no radiation by reflection from the surroundings. Therefore, the surface is assumed as a black body in this scenario, meaning that it is emitting energy over the entire spectrum in all directions. Diffuse irradiance can be a user-defined variable that is assumed to be zero in this case. In this scenario the solid parts are considered opaque, while the liquid parts are assumed transparent (transmitting).

Surface emissivity is an important optical property when setting up radiation models. It is possible to define the surface emissivity from the predefined material property or, when at the physics level, as a user-defined property. The interior and exterior surfaces of the kettle are assumed to have an emissivity of 0.9. Ambient is the environment that surrounds the exterior portion of the surface. Therefore, the ambient for the interior wall surfaces is the wall exterior surfaces and for the exterior wall surfaces is the ambient air surrounding them. The surface-to-surface radiation method is *Hemicube*, and a *Radiation resolution* of 256 along with *Linear* method under *Surface radiosity*, *Discretization*, are selected for *Real* selection under *Value type* when using *Splitting of complex variables*.

8.5 Kettle Solution Results

For the problems presented herein, transient studies were carried out. It is also possible to carry out a stationary study to see if the system ever reaches a steady state. However, if the heating is continuously turned on and heat cannot escape as fast as it is generated, the temperature predicted by the model is expected to rise indefinitely, making a stationary study inappropriate in this case.

A heating period of 5 min is assumed for this problem, and this is the period for which the results are shown. *Values of Dependent Variables* for the solution variables are selected as *User controlled* with *Initial values of variables solved for, Initial expression, Zero solution*—this is to clear the problem from the residue that might have been left from the previous solutions, starting from a clean slate. In case the problems do not converge as easily as one hopes, it is possible to solve the problem for the solid physics and use the data as inputs to the coupled physics to generate initial conditions, which are in the approximate range of the solutions—a big difference between the initial values and the solution steps may result in convergence issues. Figure 161 presents the parameters used for the scenarios presented in this case study.

Settings

Parameters

Label: Parameters 1

Parameters

Name	Expression	Value	Description
area	(2*pi*40*8)[m^2]	2010.6 m^2	area
dH	2260[kJ/kg]	2.26E6 J/kg	
dT	15[K]	15 K	
h0	5[W/(m^2*K)]	5 W/(m^2·K)	vertical convection coefficient
height	33[mm]	0.033 m	
HG_applied_area	Power2/area	0.74604 W/m^2	
HG_applied_vol	Power2/volume	0.037302 W/m^3	heat generation
HGen	2334254.144[W/m^3]	2.3343E6 W/m^3	heat generation
HLine	2106.442398[W/((m^3)*K)]	2106.4 W/(m^3·K)	line heat source
Power	33.8[W]	33.8 W	heat flux as heat rate
Power2	1500[W]	1500 W	heat source as heat rate
Pref	1[atm]	1.0133E5 Pa	reference pressure
q_source	2334254.144[W/m^3]	2.3343E6 W/m^3	heat generation
radius	56.81795363 [mm]	0.056818 m	
Tamb	22[degC]	295.15 K	ambient temperature
Tcandle	830[degC]	1103.2 K	candle temperature
time	10[s]	10 s	exposure time
time2	300[s]	300 s	
Tinit	25[degC]	298.15 K	initial temperature
Tm	100[degC]	373.15 K	
Tref	20[degC]	293.15 K	reference temperature
Twater	100[degC]	373.15 K	water temperature
vol_water	pi*(radius^2)*height	3.3468E-4 m^3	
volume	(pi*(40^2)*8)[m^3]	40212 m^3	

Figure 161. Parameters used for a kettle with heat source partially filled with hot water study (global level).

Solution tolerance was set to 0.001 for this analysis. This is a relatively tight tolerance and results in a longer solution time. The solution time was about six hours on a Windows 10 PC, with Intel Core i7-3770K CPU and 32 GB RAM. The finer the mesh is, the longer the solution will take to run. Having a multiphase flow also introduces challenges to the model in order to find consistent initial values and for the results to converge.

Solution results for this transient study are presented in Figure 162 and Figure 163 for two time points (2.5 and 5 min). The diagrams on the left (Figure 162a and Figure 163a) show the temperature contours using a reduced scale range, where the maximum temperature is set to 40 °C. Diagrams on the right (Figure 162b and Figure 163b) use the full-scale temperature contours, where the maximum temperature is set automatically. The reduced-scale plots allow one to observe the details of the temperature variation within the water.

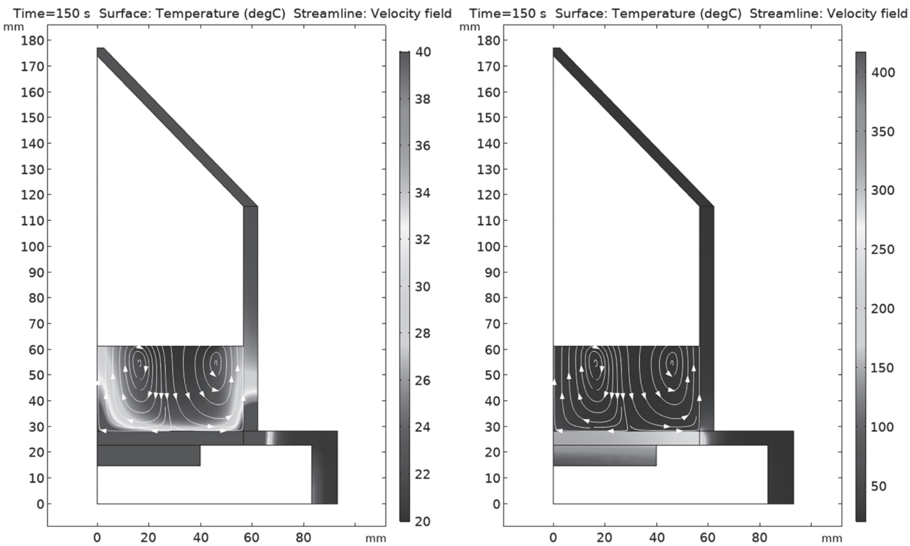

(*a*) (*b*)

Figure 162. Surface temperature contours for a kettle with heat source, partially filled with water after 2.5 min (*r-z* plane): (a) Partial 40 °C scale, (b) Full scale.

Since the problem is set up with 2D axisymmetric geometry, the results may be displayed in a 3D form by revolving the 2D axisymmetric results about the *z*-coordinate. Figure 164 shows such a plot and also uses the reduced scale with a maximum temperature of 40 °C. All of these plots include temperature contours and the arrow lines and streamlines presenting the flow velocity field (u,v,w).

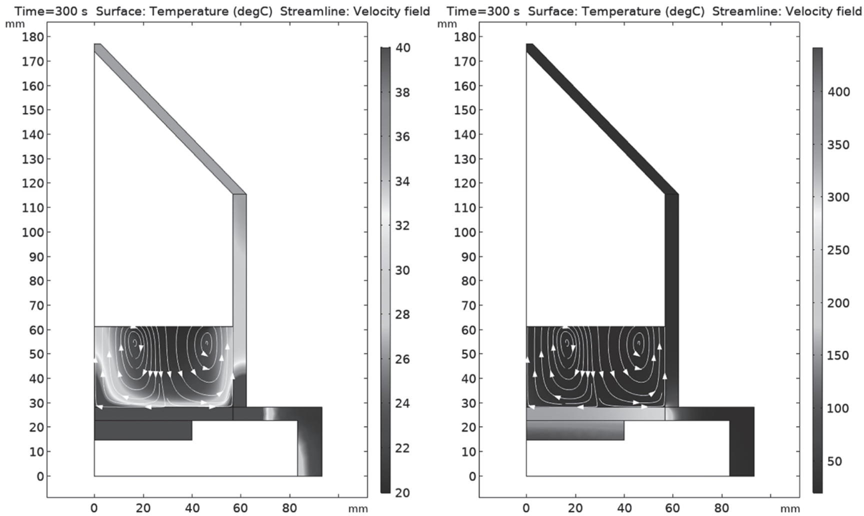

(*a*) (*b*)

Figure 163. Surface temperature contours for a kettle with heat source, partially filled with water after 5 min (*r-z* plane): (a) Partial 40 °C scale, (b) Full scale.

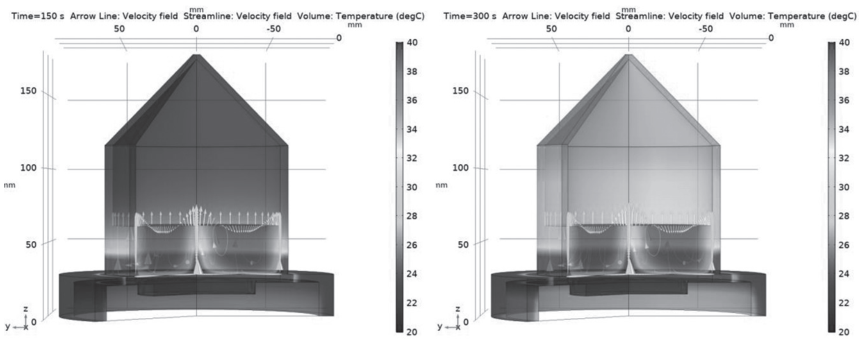

(*a*) (*b*)

Figure 164. Volume temperature and surface velocity contours for a kettle with heat source, partially filled with water, shown in 3D view, partial 40 °C scale: (a) t = 2.5 min, (b) t = 5 min.

The following plots show temperature distributions along vertical and horizontal directions at time exposures of 0.6, 1.23, 2.5, and 5 min. Figure 166 shows temperature distributions along the center axis (vertical direction) for the locations identified in Figure 165. Figure 166a shows temperature profiles starting from the top surface of the liquid to the bottom of the kettle, while (Figure 166b) only includes the liquid. It is seen that the temperature is at its peak value at the heating source and decreases as one gets farther away from it. The profiles have a sharp downward step at the interface between liquid and solid. Note that the temperature of the

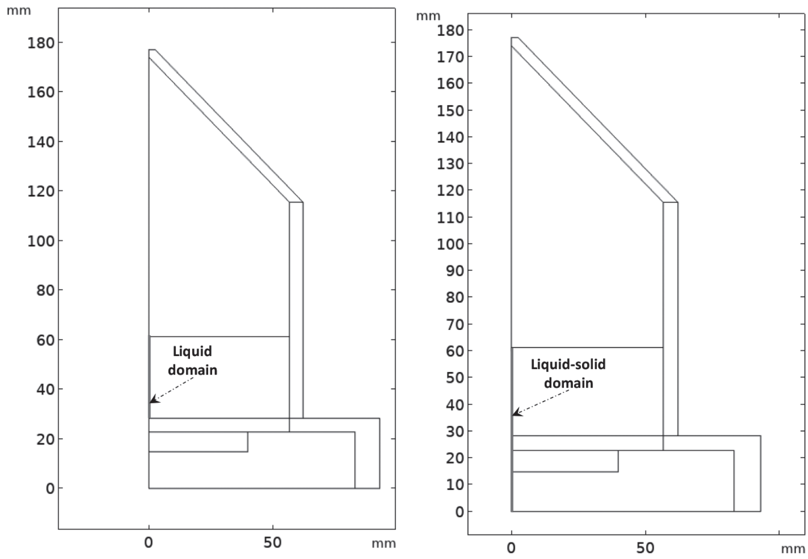

(*a*) (*b*)

Figure 165. 2D axisymmetric model for a kettle with heat source, partially filled with water *Cut Lines 2D* (*r-z* plane), vertical line along the axisymmetric axis (*z*-coordinate): (a) Liquid-solid domain, (b) Liquid domain.

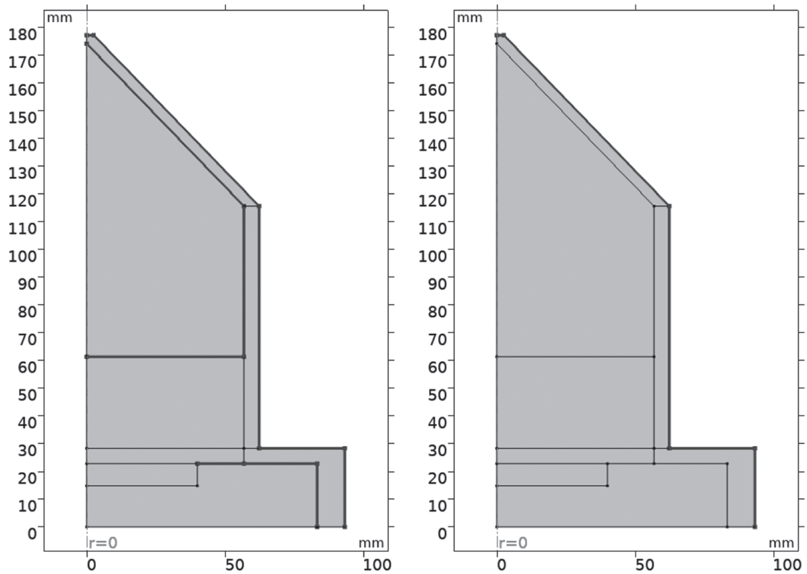

(*a*) (*b*)

Figure 166. Spatial temperature profiles for a kettle with heat source at selected lines, partially filled with water for *Cut Lines 2D* (*r-z* plane) within the depth of the kettle: (a) Liquid-solid domain, (b) Liquid domain.

heating element (Figure 166a), embedded in the copper base, increases and eventually becomes almost uniform in a short amount of time. Also note the parabolic temperature contours surrounding the heating element, which are expected to have a constant heat rate.

Figure 167b presents temperature profiles along the diameter (r-coordinate) of the kettle for the locations presented in Figure 167a. It is seen that for the selected locations, this profile is relatively uniform inside the liquid domain and increases quickly at the walls.

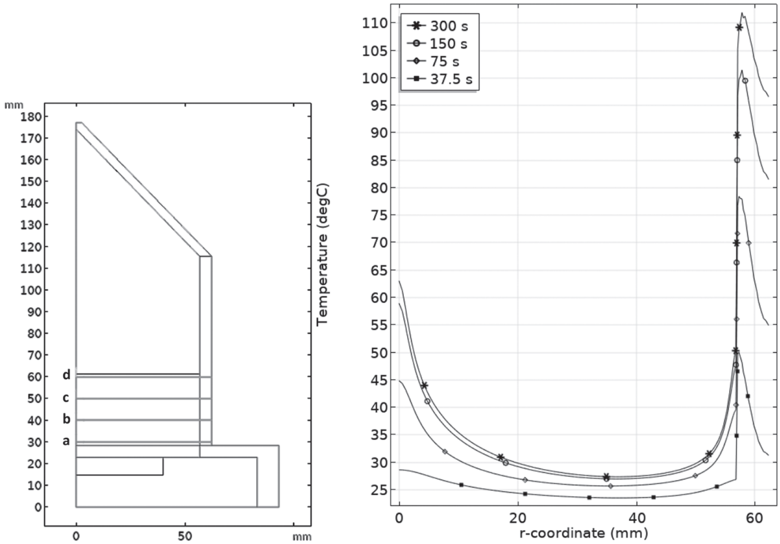

(a) (b)

Figure 167. A kettle with heat source, partially filled with water (r-z plane): (a) *Cut Lines 2D* (r-coordinate), (b) Spatial temperature profiles.

Figure 168b presents temperatures versus the time at several locations shown in Figure 168a. They are located at 5 mm from the middle of the base (red reference line), progressively increasing by 10 mm increments up to a 35 mm height above the reference line (indicated by points "*a*" to "*d*"). Maximum temperature is observed at Point "*a*" that is 5 mm above the copper base, being closest to the heat source. Note that the plot legend displays the (r, z) coordinates of the selected locations. As time increases and heat exposure increases, the temperature of the bottom of the kettle made of copper increases. This heat is transferred through conduction to the liquid above this surface. Some heat is also transferred by conduction to the kettle walls and lid, and this heat is partially transferred to the fluid in contact with the walls.

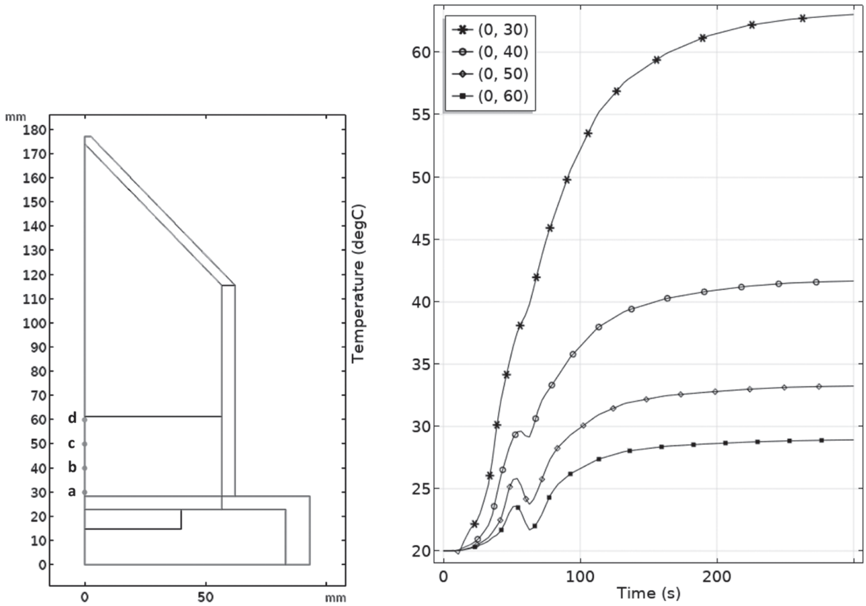

(a) (b)

Figure 168. A kettle with heat source, partially filled with water (*r-z* plane): (a) *Cut Points 2D*, (b) Transient temperature profiles.

8.6 Exercise—Kettle Model, Heat Source: Constant Temperature

This scenario is a variation on the electric kettle model presented previously, with the heating source being replaced by a candle. It is added as an exercise to be completed by the reader. A tea candle would be normally used with water that had already been boiled. Thus, the initial value in the model would be set to a higher value (closer to the boiling temperature). If phase change physics is desired, this feature is activated under *Fluid* node in which *Phase change temperature*, *Transition interval* between the two phases, and *Latent heat* are set. The candle's function would be to brew the tea in the container gradually while keeping it warm. Additionally, it may be used to gently warm water containing other ingredients (e.g., fruits and herbs) to generate a pleasant aroma.

The reader needs to know how to introduce the tea candle into the thermal model. Knowing that the candle temperature varies from the central part (minimum value) to the outer part (maximum value)—where the flame color is blue, indicating that the combustion process is complete—it is possible to select the flame temperature value (e.g., average or maximum flame temperature). Thus, the candle is treated as a heat source with a constant temperature of 830 °C (Figure 169).

A teapot stand gets heated with this temperature at exposed locations that could be a spot or an extended surface. It is possible for the temperature to vary by location or over time as well [114]. Since there is a large temperature difference between the fire and the ambient, a radiation mode of heat transfer is also added to the conjugate heat-flow model. This applies to the surfaces that are exposed to the radiative heat due to the fire. Recall the energy balance diagram presented in Figure 3, showing modes of heat transfer [115,116].

In this scenario, fire temperature is assumed to have a constant value of 830 °C, the maximum tea candle flame temperature value as reported in the literature. It is also possible to use the energy flux (per area), energy density (per volume), and heat rate (per time) in order to incorporate the heat source into the problem. The said heat sources can either be included as a heat generation term inside the heat conduction equation or as a boundary or volumetric heat source. Another method of modeling this problem is to use a constant heat rate for the heat source (boundary flux) to represent the

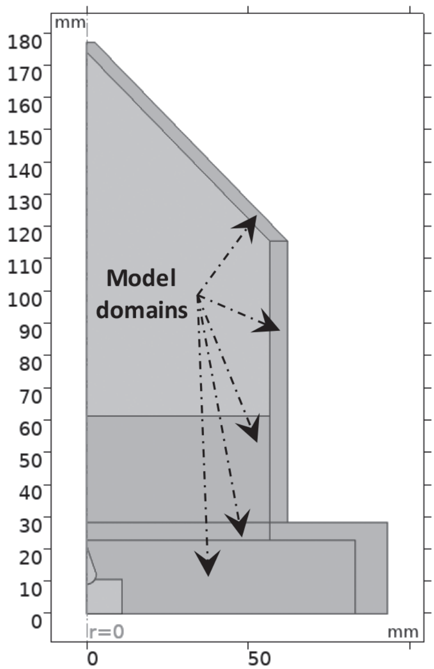

Figure 169. 2D axisymmetric model for a kettle with candle temperature boundary source partially filled with water (*r-z* plane).

candle flame power. To calculate a suitable heat generation rate, tea candle size (radius and length), wax density, and energy rating for the candle—which depend on the wax heat value—would need to be used. Note that not all the candle energy reaches the teapot stand. It is estimated that 75 percent of the candle energy appears as light and the rest is converted to heat [117].

A 2D axisymmetric thermal model of the kettle, similar to the previous study, is to be used. The heat source temperature remains constant for the entire duration of the heating. The environment surrounding the tea candle is filled with air. Air convection is modeled in the space under the teapot base. All areas exposed to the ambient transfer heat by convection. The liquid (water) that partially fills the teapot is also transferring heat by a convection mechanism and is designed as part of the flow model. The space above this water is filled with air. This air transfers heat by a convection mode of heat transfer as part of the flow model but also as conduction as part of the solid model. The latter is valid for liquid (water) as well.

The location of the fixed-temperature boundary condition is shown with purple lines in Figure 170a; these lines correspond to the tea candle flame boundary. The exterior surfaces consisting of the kettle walls, lid, and the base are solid. The upper highlighted domain in Figure 170b is water; the lower is the air surrounding the candle.

This exercise can also be attempted when the space above the water is assumed empty and the boundary between the water and this space is treated as an open boundary (Figure 171a). In this case, Figure 171b presents the walls that are in contact with the fluids. Figure 172 presents the internal and external diffuse surfaces that transfer radiative energy in all directions to the internal (fluids) and external (ambient) environments.

A transient study should be set up, modeling heating over a period of 10 min. Meshed geometry is presented in Figure 173. The zoomed-in image on the right shows the quadrilateral boundary layer elements defined at the walls of the fluid domains. Figure 174 presents the lines at which spatial temperature profiles are to be predicted. Figure 174a shows the line along the axisymmetric axis, while Figure 174b shows the radial temperature location at z = 30 mm. Figure 175 shows the points for which the transient temperature should be predicted. They are located at 5 mm from the middle of the base (red reference line), progressively increasing by 10 mm increments up to a 35 mm height above the reference line (indicated by points "*a*" to "*d*"). Point "*e*" is located in the middle of the glass kettle wall at 60 mm from the axisymmetric axis and at the same height as Point "*a*".

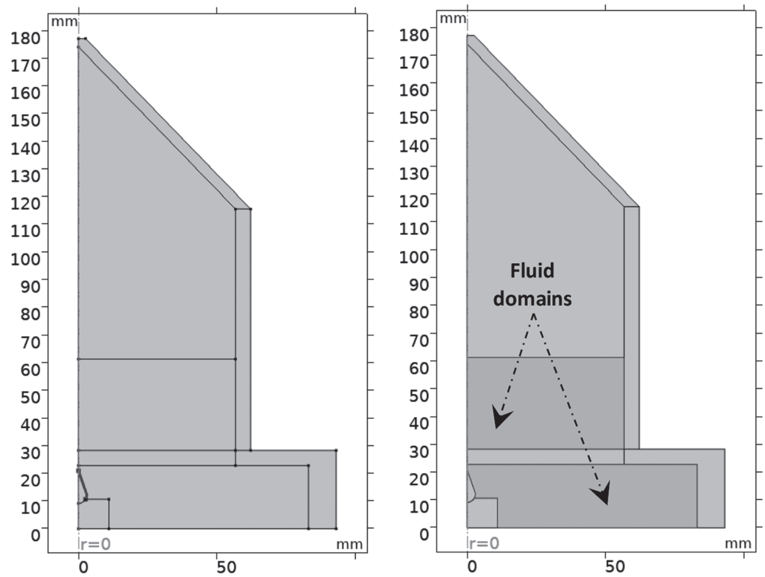

(*a*) (*b*)

Figure 170. 2D axisymmetric model for a kettle with candle temperature boundary source partially filled with water (*r-z* plane): (a) Constant temperature heat source, (b) Fluid domains.

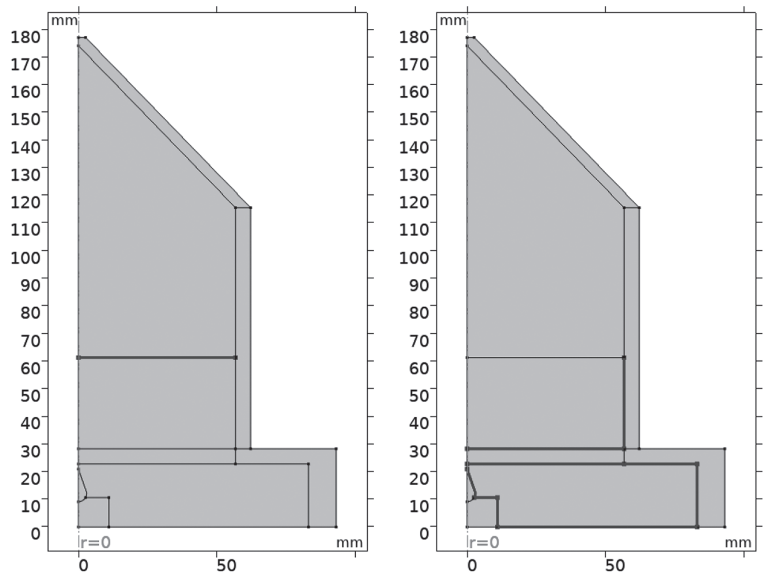

(*a*) (*b*)

Figure 171. 2D axisymmetric model for a kettle with candle temperature boundary source partially filled with water (*r-z* plane): (a) Open surface boundary condition, (b) Walls.

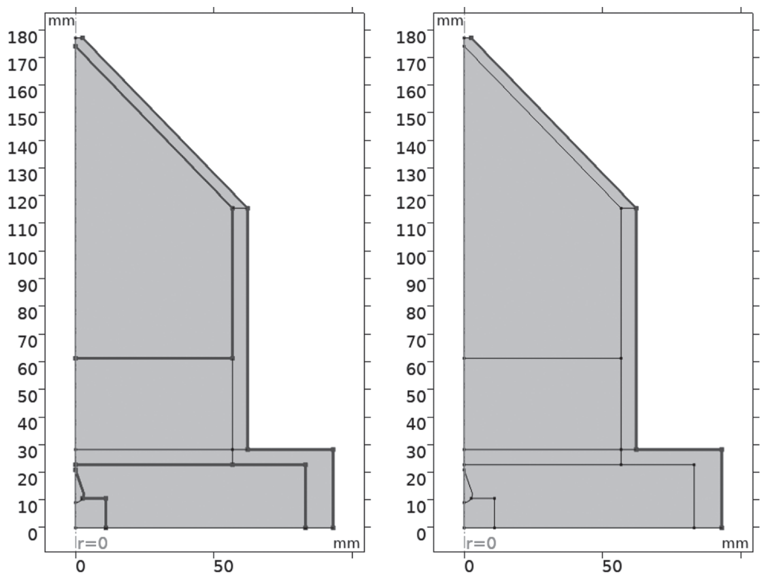

(*a*) (*b*)

Figure 172. 2D axisymmetric model for a kettle with candle temperature boundary source partially filled with water (*r-z* plane): (a) Diffuse surfaces, (b) External diffuse surfaces.

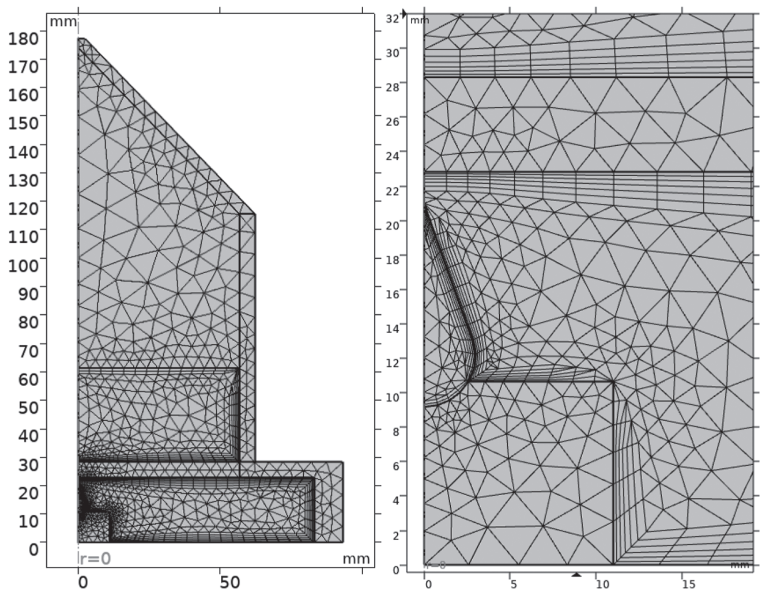

(*a*) (*b*)

Figure 173. 2D axisymmetric model for a kettle with candle temperature boundary source partially filled with water, meshed geometry (*r-z* plane): (a) Complete meshed geometry, (b) Zoomed-in meshed domains.

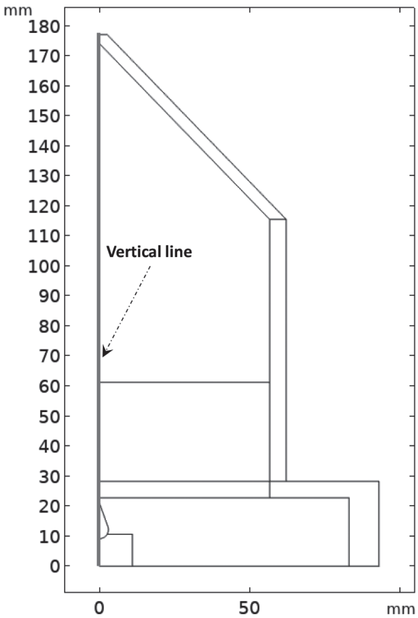

(*a*)

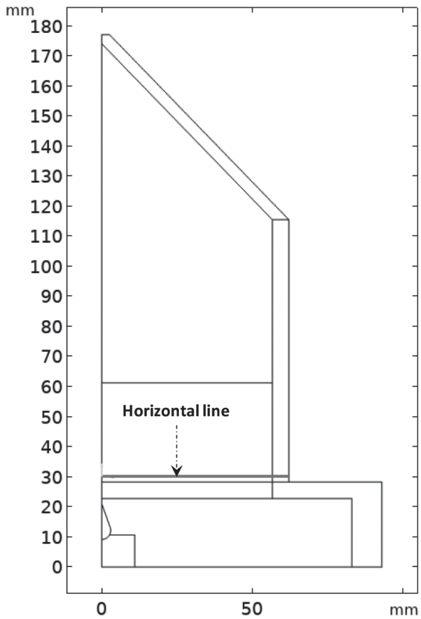

(*b*)

Figure 174. 2D axisymmetric model for a kettle with candle temperature boundary source partially filled with water, *Cut Lines 2D* (*r-z* plane): (a) Vertical line along the axisymmetric axis (*z*-coordinate), (b) Horizontal line along the radial axis (*r*-coordinate).

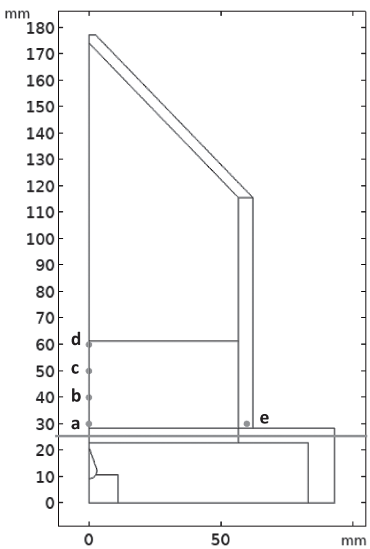

Figure 175. 2D axisymmetric model for a kettle with candle temperature boundary source partially filled with water (*r-z* plane), *Cut Points 2D*.

CHAPTER 9

Case Study 4—Heated Seat

Humans have sought comfort by adjusting their environment from the earliest times, when they learned to control fire and seek shelter in caves. Environments that are either too cold or too hot affect our ability to effectively perform everyday activities, including both physical and mental ones. Our bodies have complex internal systems which provide thermoregulation to keep our body core temperature at an optimum value, ensuring that all vital organs are able to function as intended. Activities such as exercise increase the internally generated heat, partly due to the increase of body metabolism and partly due to release of the sensible heat to the skin as blood rushes to this organ in order to reject the excess heat. Our effectiveness is also reduced when the body temperature is decreased due to tiredness, lack of sleep, or a cold environment.

Driving and flying are activities that require a high degree of concentration and fine control of actions with your hands and feet. It is hard to precisely move the controls and push pedals with cold toes and fingers. Any deterioration in these abilities may jeopardize the safety of oneself and others. Some pilots, if their cockpit is cold and drafty, resort to putting gloves under their hips or under their arms to warm them up. The use of heated seats in these applications not only improves comfort but also general safety.

9.1 Problem Definition

Heated seats, like heated clothing, blankets, toilet seats, and mattresses, use internal electrical elements to generate the required heat. This case study models the temperature distribution in an electrically heated seat. Such seats first appeared in luxury car models but have now spread to even modestly priced vehicles; more recently, heated seats have started to appear in airplane cockpits. A car seat consists of three sections: (1) a cushion, which supports most of the body's weight; (2) a backrest; and (3) a head rest. Typically, the heated parts are the cushion and the backrest. These two will be considered for this case study. Depending on specific implementation, the seat heating controls may be just on/off, have low, moderate, and high settings (e.g., some Honda vehicles), or allow for setting of the desired temperature using a thermostat-based regulation (e.g., Tesla).

A heated seat normally includes electric wires (coils), soft material to provide cushioning, and exterior leather or fabric that contains the cushions and provides durable surface protection (Figure 176). Arrangements of electric wire may be in the form of two mirrored coils dedicated to the left and right sides of the body or a u-shaped coil. The thermo-physical properties of a seat, required for heat transfer modeling, are affected by the method of seat construction, layers, thickness, and materials. When modeling this structure, it is possible to consider the seat as a single unit and define effective thermo-physical properties. Recall the example of the FLT sandwich discussed earlier. The effective thermal conductivity (or any other thermo-physical property) is the property that can allow a replacement of a complex multi-material structure with a single region possessing equivalent property values.

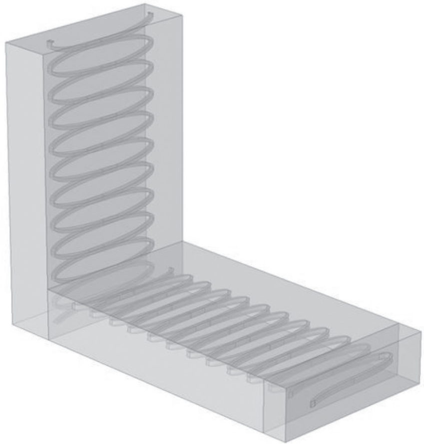

Figure 176. Heated seat model geometry.

These equivalent values would be obtained by combining the individual elements of the structure in a series or parallel fashion, as appropriate. The series arrangement case occurs if the seat layers are set one on top of another, similar to lap-joint weld geometry, starting from the interior core (e.g., wires) to its external surface (soft material and skin). This scenario may consist of a single-coil layer. The parallel arrangement is the case where the components are arranged side by side. Imagine using multiple parallel coil wires as sources of heating. After the effective properties are modeled, given their position with respect to one another, and their individual thermo-physical properties (e.g., thickness, thermal conductivity, density, and specific heat capacity), the resistive model (including parallel and series components) is made. Using the series and parallel laws, the total resistance or thermo-physical properties are obtained as a result. The reader may review Chapter 7 ("Basement Insulation") to review the multilayer (parallel and series) implementation of the resistive layers.

There have been few research studies into thermal modeling of heated seats for a variety of applications. Their assumptions ranged from using a lumped capacity model to a detailed representation of all the heating sources and seat structures, enough for a doctoral engineering degree. This study does not include a model of the human body. The purpose of this study is not to implement a full model, including all the elements of the heated seat and the human body, but to acquaint the reader with the methodology used to model such a system and to provide an overview of the process of experimental designing (or *test design*, as it is called in the industrial environment). At the end of this chapter, a section is included providing background information on the addition of the human body to the heated seat model. The reader may attempt to incorporate it as an exercise.

9.2 Heated Seat Thermal Model

The data employed in this study, such as the heat generated by the elements, exposure time, and thermo-physical properties of the seat, have been adopted from well-known international sources that reported on the investigation into human comfort and body response to thermal sensations. Figure 177, Figure 178, and Figure 179 present thermo-physical properties of the materials used for the analyses [118].

This study examines three different cases. The first case considers the situation in which there is a seat with built-in heating elements of a chosen

Label: Nylon

▷ Material Properties

▼ Material Contents

Property	Variable	Value	Unit	Property group
Heat capacity at constant pressure	Cp	1700[J/(kg*K)]	J/(kg·K)	Basic
Relative permittivity	epsilonr_iso ; epsilonrii = epsilonr_iso, epsilonrij = 0	4	1	Basic
Coefficient of thermal expansion	alpha_iso ; alphaii = alpha_iso, alphaij = 0	280e-6[1/K]	1/K	Basic
Density	rho	1150[kg/m^3]	kg/m³	Basic
Thermal conductivity	k_iso ; kii = k_iso, kij = 0	0.26[W/(m*K)]	W/(m·K)	Basic
Young's modulus	E	2e9[Pa]	Pa	Young's modulus and Poisson's ratio
Poisson's ratio	nu	0.4	1	Young's modulus and Poisson's ratio

Figure 177. Thermo-physical properties of nylon.

Label: Copper 1

▷ Material Properties

▼ Material Contents

Property	Variable	Value	Unit	Property group
Heat capacity at constant pressure	Cp	385[J/(kg*K)]	J/(kg·K)	Basic
Density	rho	8960[kg/m^3]	kg/m³	Basic
Thermal conductivity	k_iso ; kii = k_iso, kij = 0	400[W/(m*K)]	W/(m·K)	Basic
Relative permeability	mur_iso ; murii = mur_iso, murij = 0	1	1	Basic
Electrical conductivity	sigma_iso ; sigmaii = sigma_iso, sigmaij = 0	5.998e7[S/m]	S/m	Basic
Coefficient of thermal expansion	alpha_iso ; alphaii = alpha_iso, alphaij = 0	17e-6[1/K]	1/K	Basic
Relative permittivity	epsilonr_iso ; epsilonrii = epsilonr_iso, epsilonrij = 0	1	1	Basic
Young's modulus	E	110e9[Pa]	Pa	Young's modulus and Poisson's ratio
Poisson's ratio	nu	0.35	1	Young's modulus and Poisson's ratio
Reference resistivity	rho0	1.72e-8[ohm*m]	Ω·m	Linearized resistivity
Resistivity temperature coefficient	alpha	0.0039[1/K]	1/K	Linearized resistivity

Figure 178. Thermo-physical properties of copper.

Label: Cushion

▷ Material Properties

▼ Material Contents

Property	Variable	Value	Unit	Property group
Heat capacity at constant pressure	Cp	1100[J/(kg*K)]	J/(kg·K)	Basic
Density	rho	175[kg/m^3]	kg/m³	Basic
Thermal conductivity	k_iso ; kii = k_iso, kij = 0	0.033[W/(m*K)]	W/(m·K)	Basic
Relative permittivity	epsilonr_iso ; epsilonrii = epsilonr_iso, epsilonrij = 0	4	1	Basic
Coefficient of thermal expansion	alpha_iso ; alphaii = alpha_iso, alphaij = 0	280e-6[1/K]	1/K	Basic
Young's modulus	E	2e9[Pa]	Pa	Young's modulus and Poisson's ratio
Poisson's ratio	nu	0.4	1	Young's modulus and Poisson's ratio

Figure 179. Thermo-physical properties of cushion material.

design with the heating elements using a constant power level, time-dependent power density, and time-dependent temperature boundary conditions for the modeled period. This means the heating remains on for the duration modeled, without considering whether the resulting temperature is within the passenger's comfort level.

The second case models a time-varying power density in the electrical elements. Hence, sensitivity of the results to both power density and exposure time are investigated. This model provides the opportunity for using functions (e.g., step and analytical) when defining the input process parameters.

The third case assumes a temperature variation within a certain period for the wires. This is a reverse engineering of the second scenario and is a new method of presenting the input process parameters, where thermostats are used to control the heating of the seat pad and based on the desired temperature.

The model of the seat along with the embedded wires has been created using the combination of COMSOL Multiphysics *CAD Import* module and Solid Edge CAD tool (Figure 180). The seat model with dimensions presented in Figure 180a is about a 1/3 scale of a regular car's seat; the reduced scale allows for elements with smaller dimensions while keeping the solution time reasonable. Solid Edge was employed to create the geometry presented in Figure 180a. This geometry was then imported into COMSOL Multiphysics where additional processing steps were carried out.

First, to create the wire model, a cap operation was carried out. The *wires* visible in the CAD model are actually hollow spaces produced by using a cutout operation. This hollow space is capped on both ends to create a domain in COMSOL Multiphysics to which material properties and meshing can be applied. In order to make the wire design more complex, a mirrored copy of the wires seen in Figure 180 was added to the geometry. This was done by copying and linearly offsetting the wiring to the desired location (Figure 181). The newly created geometry (the offset block and wire) is then partitioned, using the original block. The unneeded additional domain (the purple highlighted part on the left side of Figure 181) was deleted. Next the resultant cushion model is used to create the backrest by copying, rotating, and moving it to align with the end of the original cushion (Figure 182).

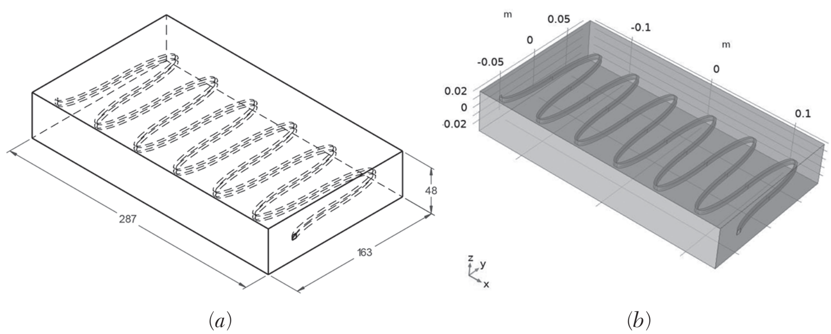

Figure 180. Seat cushion created in Solid Edge: (a) Dimensioned CAD model (dimensions in mm); (b) CAD geometry imported into COMSOL Multiphysics.

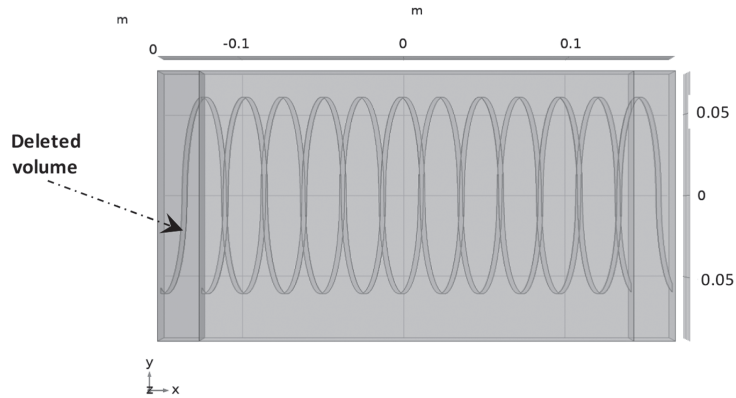

Figure 181. CAD seat geometry modified in COMSOL Multiphysics by copying and offsetting to create the second set of wires.

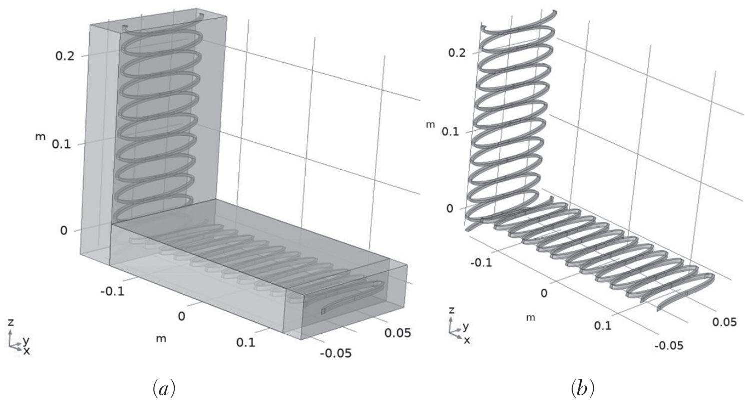

Figure 182. Seat backrest created in COMSOL Multiphysics by using the original seat pad: (a) Coils embedded in the seat and back rest, (b) Coils.

The material definitions are introduced within *Global Definitions* of COMSOL Multiphysics. This is done by adding the materials at the global level, defining links under each component, and assigning the defined materials to the 3D domains to which they apply (Figure 183).

The model is meshed using physics-controlled tetrahedral elements with *Fine* size setting (Figure 184a). While it may be possible to make the elements coarser, one must ensure that the element size does not exceed the size of the smallest features when meshing this part. Mesh statistics (element type, size, and quality) are shown in Figure 184b. When setting up *Study*, *Parametric Sweep* feature is used during the solution step. It runs the solution for three different power levels (half, full, and double the power).

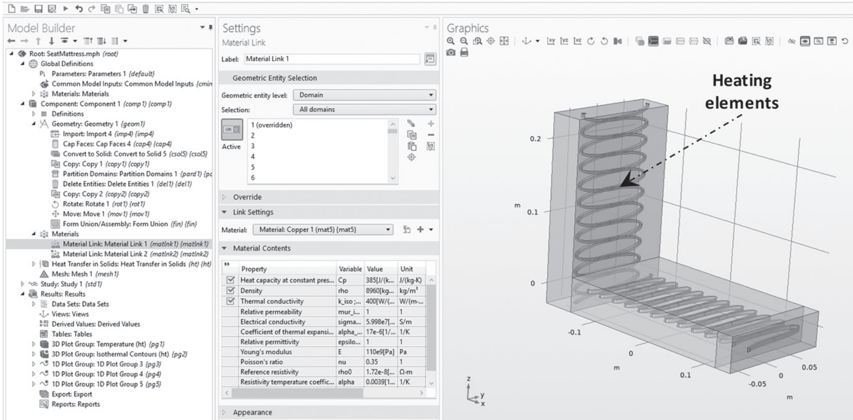

Figure 183. Adding material links under *Component* of the seat model.

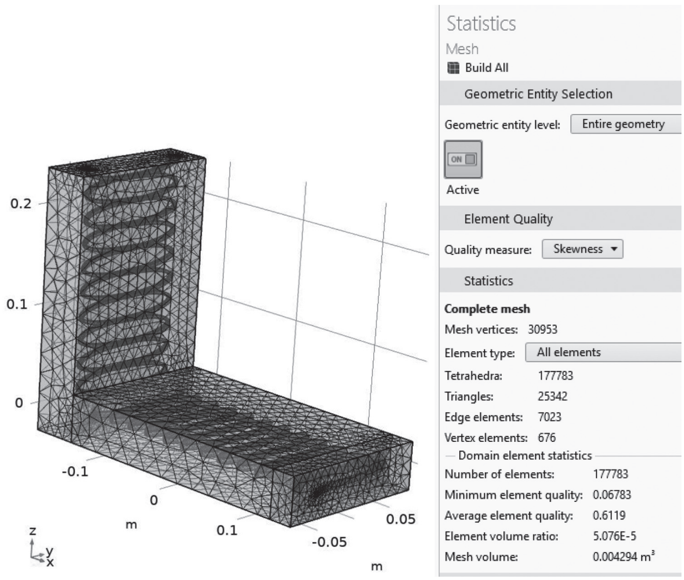

(*a*) (*b*)

Figure 184. (a) Meshed seat model, (b) Mesh statistical data.

The physics in this scenario is heat transfer by means of conduction in solids; the heat source is modeled by Joule heating (i.e., heating due to electrical resistance) defined by the energy rate (*Power* parameter in W). Additional settings are initial conditions (*Tinit*), ambient temperature (*Tamb*), no insulating surfaces, thermal contact (*contact_p*), and heat flux in the form of convection from the horizontal and vertical surfaces with associated heat transfer coefficient (*h_horizontal* and *h_vertical*, respectively)—Figure 185. Parameter settings are presented in Figure 186.

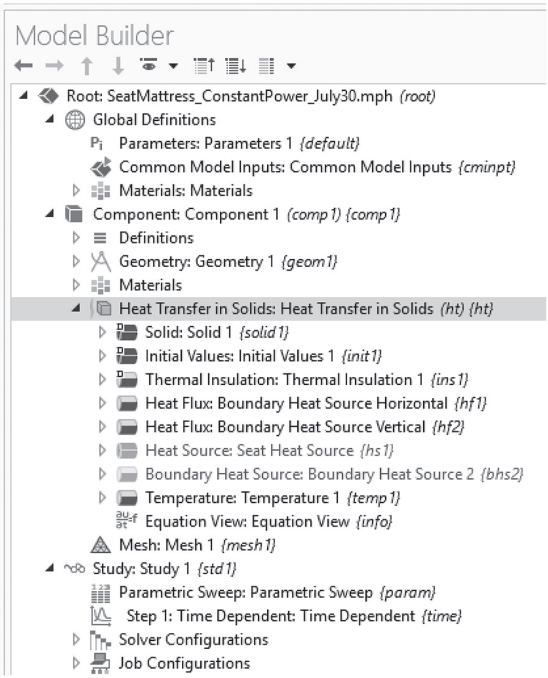

Figure 185. *Heat Transfer* physics tree for heated seat study.

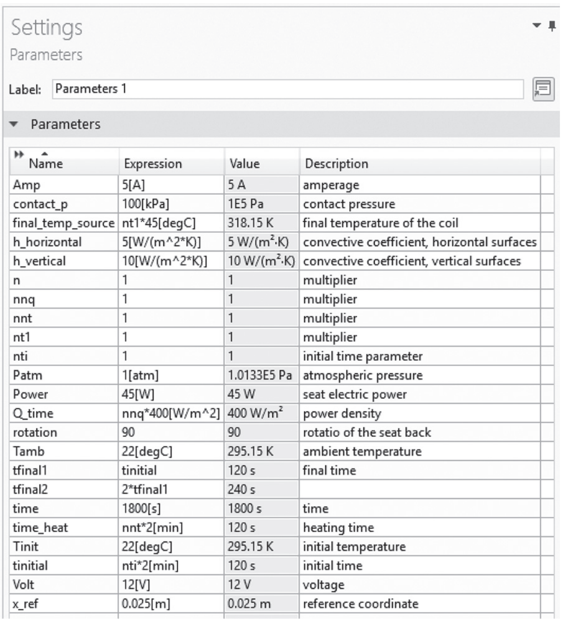

Name	Expression	Value	Description
Amp	5[A]	5 A	amperage
contact_p	100[kPa]	1E5 Pa	contact pressure
final_temp_source	nt1*45[degC]	318.15 K	final temperature of the coil
h_horizontal	5[W/(m^2*K)]	5 W/(m²·K)	convective coefficient, horizontal surfaces
h_vertical	10[W/(m^2*K)]	10 W/(m²·K)	convective coefficient, vertical surfaces
n	1	1	multiplier
nnq	1	1	multiplier
nnt	1	1	multiplier
nt1	1	1	multiplier
nti	1	1	initial time parameter
Patm	1[atm]	1.0133E5 Pa	atmospheric pressure
Power	45[W]	45 W	seat electric power
Q_time	nnq*400[W/m^2]	400 W/m²	power density
rotation	90	90	rotatio of the seat back
Tamb	22[degC]	295.15 K	ambient temperature
tfinal1	tinitial	120 s	final time
tfinal2	2*tfinal1	240 s	
time	1800[s]	1800 s	time
time_heat	nnt*2[min]	120 s	heating time
Tinit	22[degC]	295.15 K	initial temperature
tinitial	nti*2[min]	120 s	initial time
Volt	12[V]	12 V	voltage
x_ref	0.025[m]	0.025 m	reference coordinate

Figure 186. Parameters used for heated seat study (global level).

Figure 187 presents the lines for which spatial temperature profiles are reported in this study. These lines are along the seat length, depth, and width. For each line, two views are presented to clarify the location. Figure 188 presents the locations of the points at which temperature

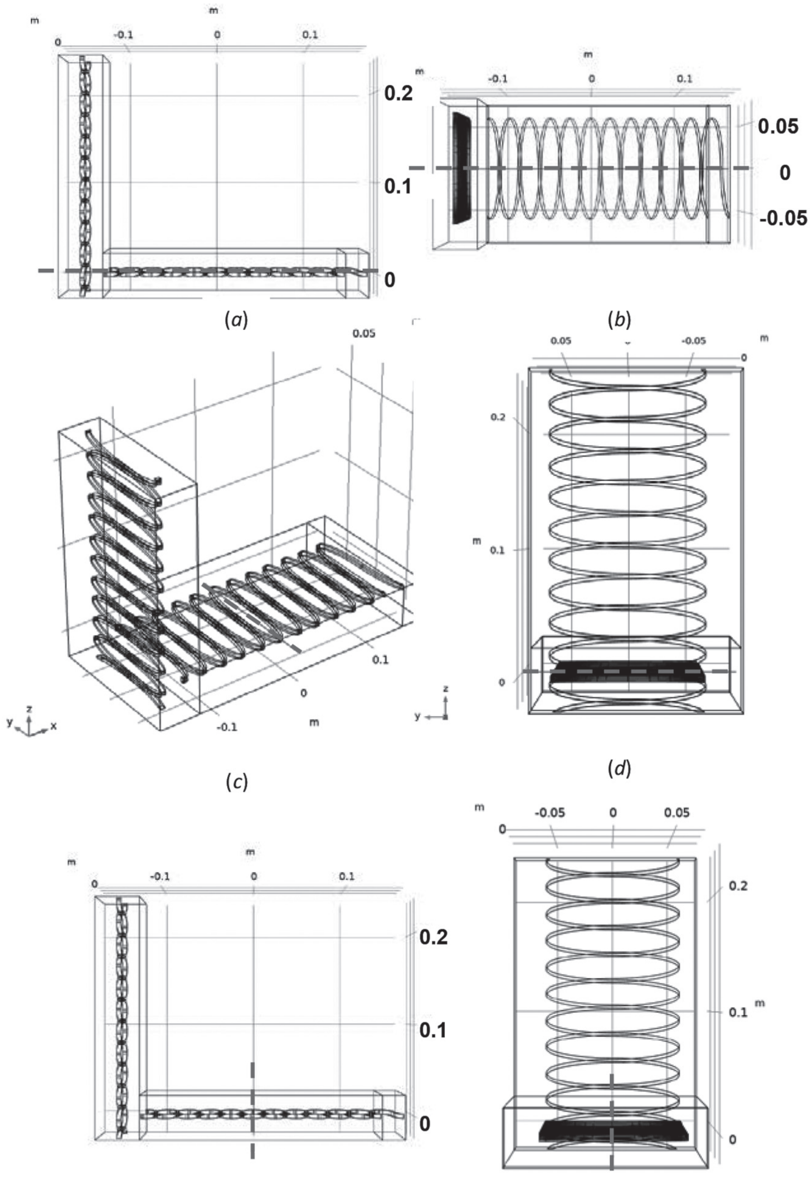

Figure 187. *Cut Lines 3D* for heated seat along: (a) Length side view (*x*-coordinate), (b) Length top view (*x*-coordinate), (c) Width isometric view (*y*-coordinate), (d) Width top view (*y*-coordinate), (e) Depth side view (*z*-coordinate), (f) Depth top view (*z*-coordinate).

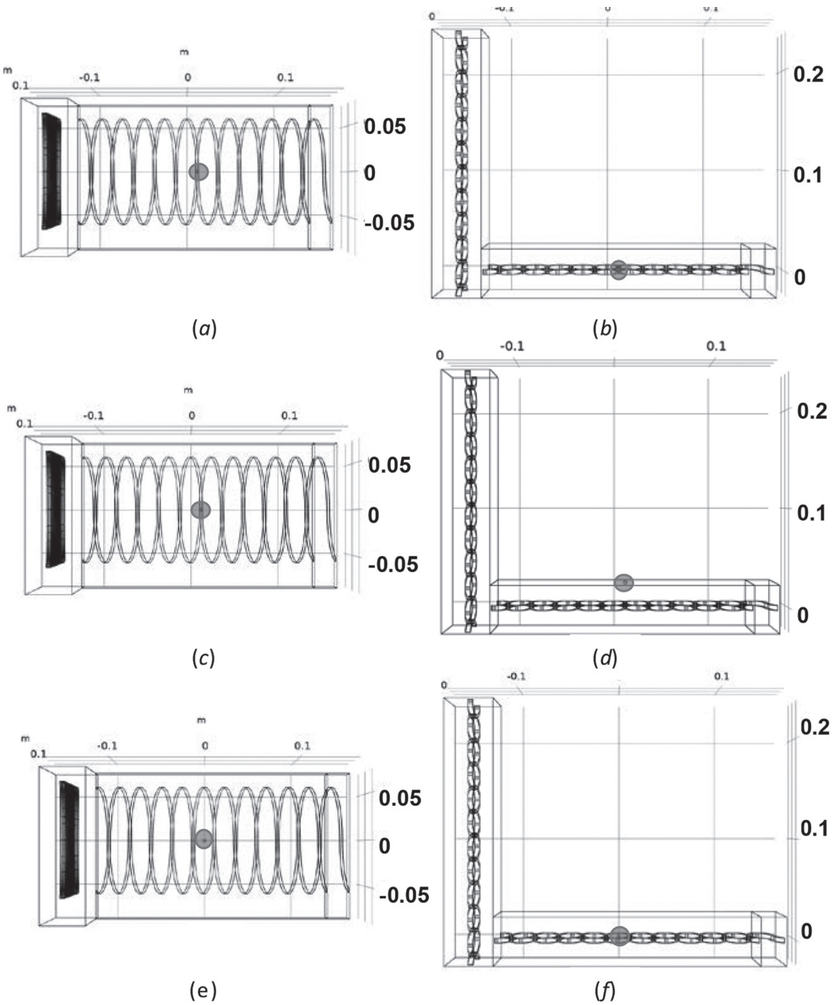

Figure 188. *Cut Points 3D* for heated seat: (a) Central wire top view, (b) Central wire side view, (c) Seat surface top view, (d) Seat surface side view, (e) Middle seat top view, (f) Middle seat side view.

variation is reported. These points are located on the wire, in the middle of the wires, and on the external surface of the seating area. The temperature distributions at these locations are important, since they affect passenger comfort and wire thermal performance criteria.

9.2.1 Scenario 1—Constant Heat Flux

In this case study, constant heat (*pw(t)* in W) is applied to the wires in the bottom cushion and back rest (Figure 189). The purpose is to identify what level of heat produces a comfortable temperature for the person occupying the seat. A base heating power value of 45 W is used, which is then varied to produce three levels of heating—low (half of base setting), medium (base setting), and high (double the base setting). A time interval of 30 min (1,800 s) is modeled, where heat is applied at a constant level for the duration of this period.

The solution is obtained with the surface and volume contour plots shown in Figure 190. The surface plot identifies the contours for the vertical and horizontal as well as the coil surface at the specified times, while the volume plots present the temperature for the volume. Maximum and minimum temperatures in the latter scenario are presented after 20 min (1,200 s), boxed inside the related figures. The values are 75.2 and 21.4 °C for the low-power cases (22.5 W) (Figure 190a) and 234.8 and 19.5 °C for the high-power cases (90 W) (Figure 190b). The results show that increasing the power by 4 times results in a significant rise (3.1 times) of the maximum temperature, as expected.

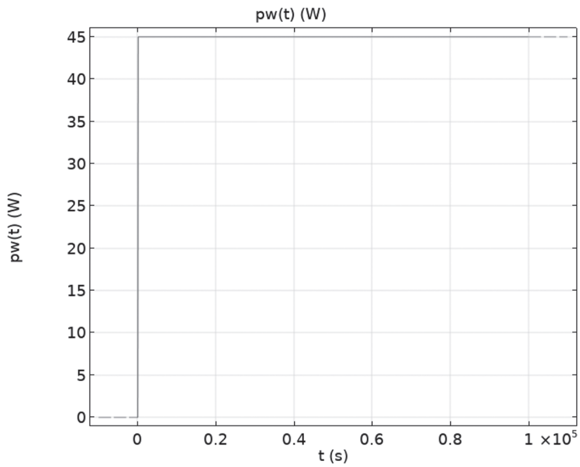

Figure 189. Time-dependent heat source, power is multiplied by *n* ($n \times pw(t)$).

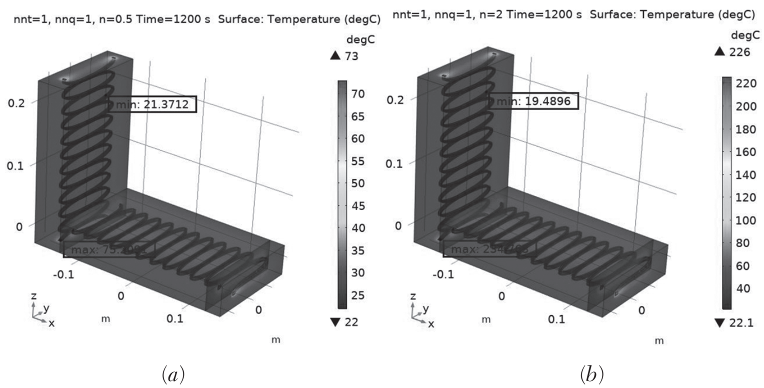

Figure 190. Surface temperature contours for heated seat after 20 min, *nnt* = 1 (2 min), *nnq* = 1 (400 W/m²): (a) *n* = 0.5 (22.5 W), (b) *n* = 2 (90 W).

Maximum temperatures predicted are seen on the wires, while the minimum temperatures are observed on the seat cushion. Figure 191 shows the temperature isotherms. This generally shows the temperature distribution range on the seat, with the corner areas cooler than the rest. For higher seat heating power (90 W), the maximum and minimum surface temperatures are 225.9 and 22.1 °C, seen on the back rest and front edge of the seat, respectively. For the lower seat heating power (22.5 W), the maximum and minimum surface temperatures are 73.0 and 22.0 °C, seen on the back rest and front edge of the seat, respectively. This produces an increase of temperature of about 3.1 times for the surface temperature increase, which is identical with that of the said scenario. For the regular power (45 W), the maximum and minimum predicted temperatures are in the order of 124.0 and 22.0 °C, respectively.

Maximum seat surface temperature versus the power level is presented in Figure 190; it is seen that temperature distribution follows a linear behavior. This diagram can be employed in order to predict the effect of heat input on the maximum seat surface (i.e., back rest).

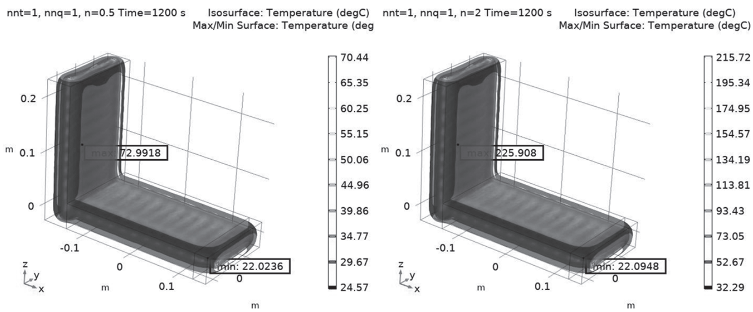

(a) (b)

Figure 191. Isosurface temperature contours for heated seat after 20 min, *nnt* = 1 (2 min), *nnq* = 1 (400 W/m^2): (a) *n* = 0.5 (22.5 W), (b) *n* = 2 (90 W).

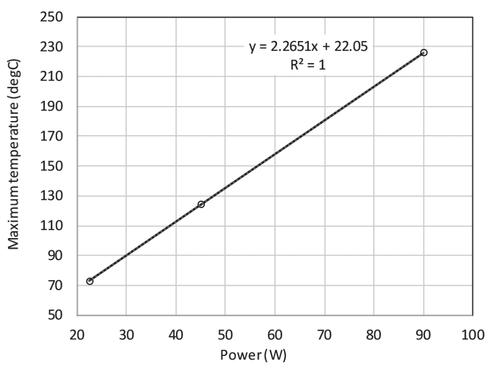

Figure 192. Maximum seat surface temperature versus the power level.

Figure 193 shows temperature profiles along the seat length for the line shown in Figure 187a. It is seen that for the selected locations (Figure 187a), the temperature shows a periodic variation that corresponds to the locations of the heating wires. Peak temperatures at the wires are about 73 °C for the low heat setting and 223 °C for the high setting. Note that in a typical installation, a built-in thermostat is responsible for regulating the heating element so that it does not overheat while producing appropriate temperature for the user. In this case, you can note that the predicted temperature is much lower than the copper melting point of about 1,085 °C. Additionally, the seat occupant may decide to turn the heating off if they are uncomfortable at a certain temperature level. Some of the studies focusing on passenger comfort level regarding the heated seats are presented in the bibliography, and the reader is encouraged to review them if interested in the subject.

Figure 194 presents the temperature distributions along the seat width (Figure 187c). It is seen that for the selected locations, temperature shows a parabolic trend, with lower values reported at the central part of the seat where the hips and central back are in contact with the seat. This temperature is about 50 °C at the vicinity of the wires.

To examine the temperature experienced at the seat's external surface, the temperature distribution along the vertical line passing through the middle of the bottom cushion (as seen in Figure 187e) is shown in Figure 195. Note that the line where the temperature is sampled is passing through the empty space between the coils, and not through the wire directly. The distribution peaks at the center where the heating elements are located. On the seat external surface (0.01125, 0, 0.024), for the low heat setting, the maximum temperature of about 25 °C after 20 min is seen, which becomes about 27 °C at the 30-min point. For the high heat setting, the maximum temperature of about 32 °C after 20 min is seen, which becomes about 40 °C at the 30-min point.

Figure 196 shows the temperatures at three points (Figure 188) over time, where the maximum heating element temperature reached is about 85 °C (on the wire) and 30 °C (where legs come in contact with the seat) for the low-power setting (22.5 W). For the high-power setting (90 W), the maximum temperatures of about 280 and 60 °C are predicted for the said locations.

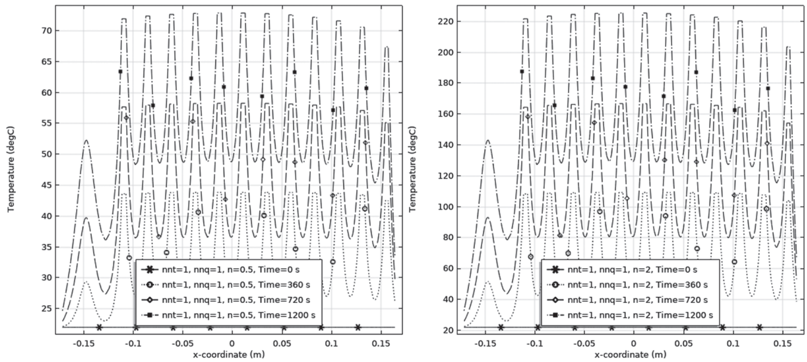

(*a*) (*b*)

Figure 193. Spatial temperature profiles at selected line along the seat length (*x*-coordinate), *nnt* = 1 (*2* min), *nnq* = 1 (400 W/m^2): (a) *n* = 0.5 (22.5 W), (b) *n* = 2 (90 W).

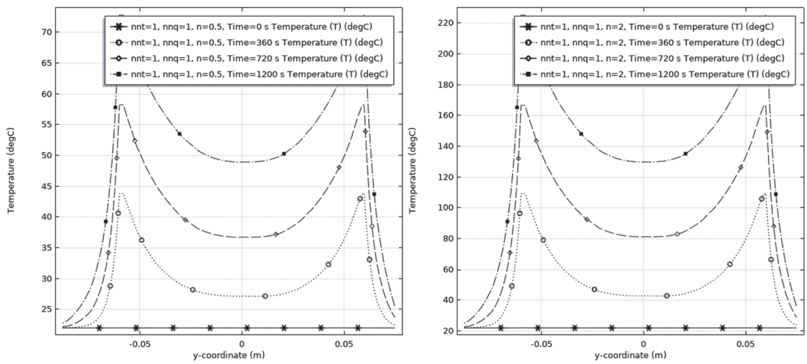

(*a*) (*b*)

Figure 194. Spatial temperature profiles at selected line along the seat width (*y*-coordinate), *nnt* = 1 (2 min), *nnq* = 1 (400 W/m^2): (a) *n* = 0.5 (22.5 W), (b) *n* = 2 (90 W).

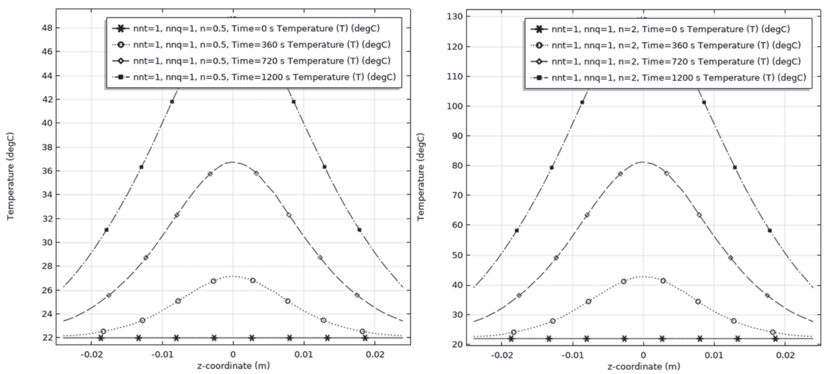

(*a*) (*b*)

Figure 195. Spatial temperature profiles at selected line along the seat height (*z*-coordinate), *nnt* = 1 (2 min), *nnq* = 1 (400 W/m^2): (a) *n* = 0.5 (22.5 W), (b) *n* = 2 (90 W).

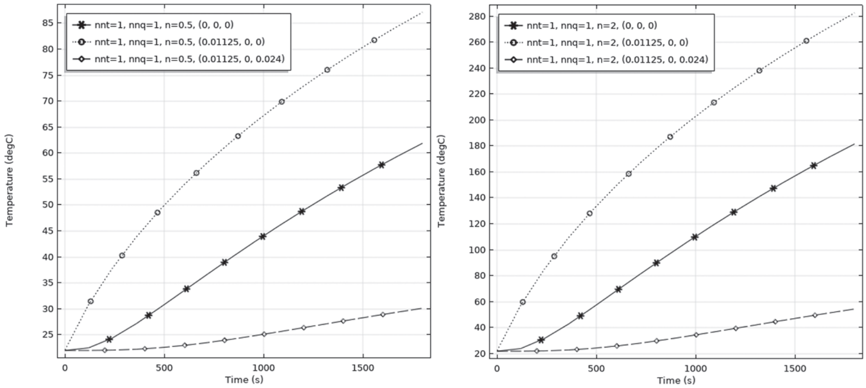

(*a*) (*b*)

Figure 196. Transient temperature profiles at selected points for heated seat, *nnt* = 1 (2 min), *nnq* = 1 (400 W/m^2): (a) *n* = 0.5 (22.5 W), (b) *n* = 2 (90 W).

9.2.2 Scenario 2—Transient Heat Flux

In this case study, transient constant heat flux ($pw2(t)$ in W/m^2) is applied to the wires (Figure 197). The heating is turned on at a constant setting for a certain period and then turned off. Three heating intensity levels are tested—low, medium, and high. The heating intensity is controlled by parameter *nnq*, while the initial heating interval duration is controlled by parameter *nnt*. *Heat flux* is set to equal *nnq* × 400 (W/m^2); the heating time is set equal to *nnt* × 2 (min). Results for *nnq* values of 0.5 and 2 and *nnt* values of 0.5 and 3.5 are reported. There is a solution covered time duration of 30 min, with results at the 20-min point being presented.

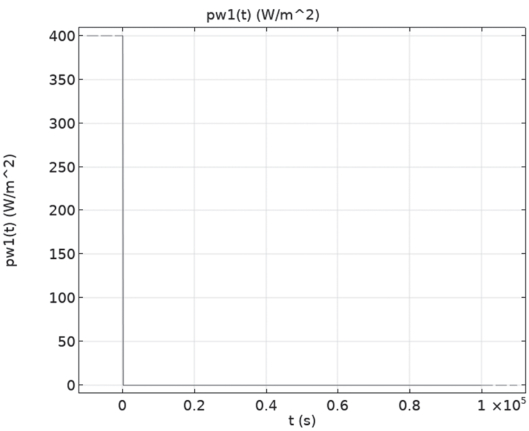

Figure 197. Time-dependent heat source, power density is multiplied by *nnq* (*nnq* × *pw*1(*t*)).

The surface plots (Figure 198 and Figure 199) display the contours for the vertical and horizontal cushions as well as the coil surface at 20 min. The maximum and minimum volume temperatures after 20 min, shown in the surface plots, indicate the maximum and minimum values of 23.2 and 22.0 °C for the low power and a 20-min heating time (Figure 199a), and 55.2 and 22.0 °C for the high power and a 20-min heating time (Figure 199b).

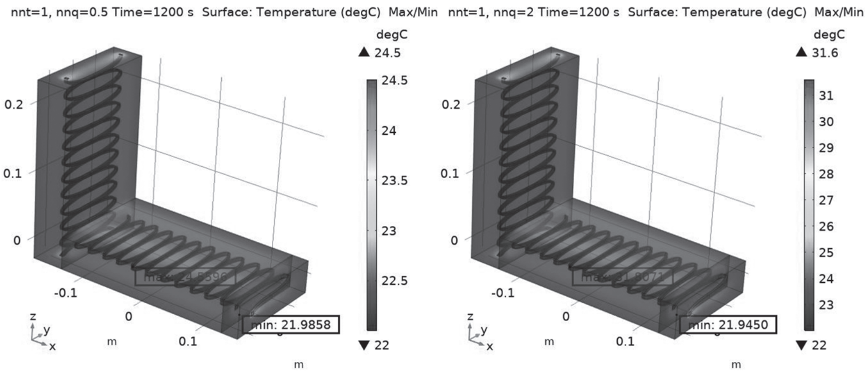

(*a*) (*b*)

Figure 198. Surface temperature contours for heated seat after 20 min, *nnt* = 1 (2 min): (a) *nnq* = 0.5 (200 W/m^2), (b) *nnq* = 2 (800 W/m^2).

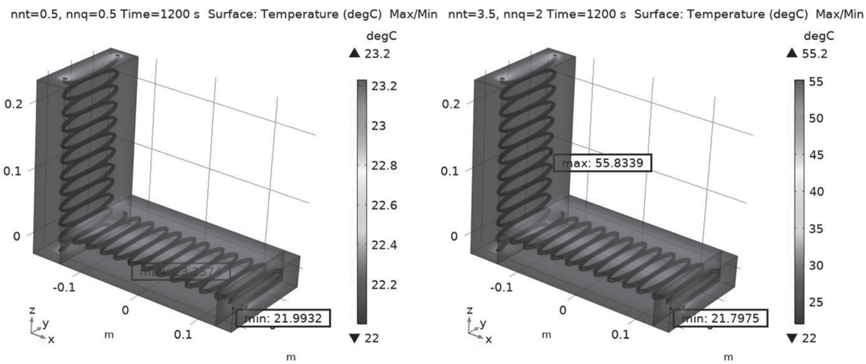

(*a*) (*b*)

Figure 199. Surface temperature contours for heated seat after 20 min: (a) *nnt* = 0.5 (1 min), *nnq* = 0.5 (200 W/m^2), (b) *nnt* = 3.5 (7 min), *nnq* = 2 (800 W/m^2).

Figure 200 predicts temperature along the seat height (Figure 187e) for several times, showing a peak in the middle. In this case, the heating is minimal, showing a maximum temperature in the center inside the wire of only about 23 °C, and the seat surface temperature remaining within a fraction of a degree of the initial setting. The temperature along the vertical line is important as it shows the cushion surface temperature, which is the most important thing for the heated seat.

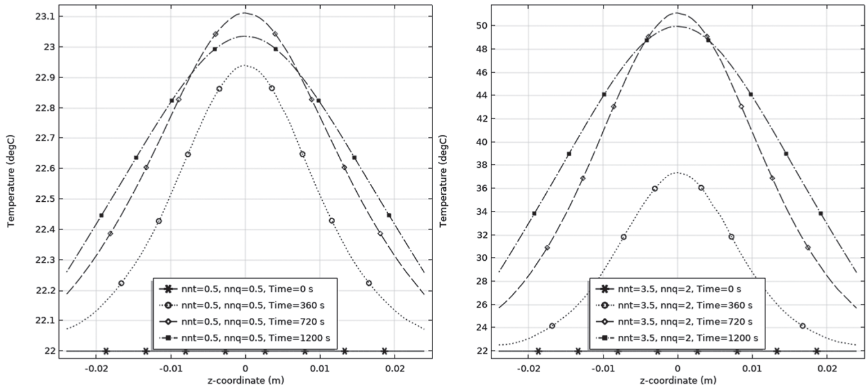

(*a*) (*b*)

Figure 200. Spatial temperature profiles at selected line along the seat height (*z*-coordinate): (a) *nnt* = 0.5 (1 min), *nnq* = 0.5 (200 W/m^2), (b) *nnt* = 3.5 (7 min), *nnq* = 2 (800 W/m^2).

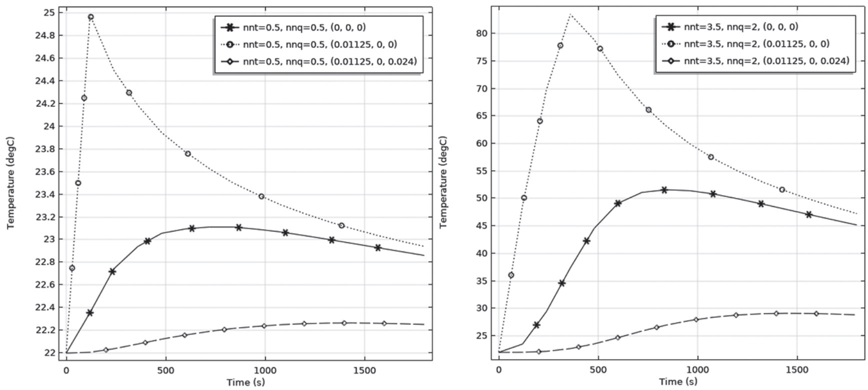

(*a*) (*b*)

Figure 201. Transient temperature profiles at selected points for heated seat: (a) *nnt* = 0.5 (1 min), *nnq* = 0.5 (200 W/m^2), (b) *nnt* = 3.5 (7 min), *nnq* = 2 (800 W/m^2).

Figure 201 shows the temperature versus the time for the three locations identified in Figure 188. This is the most interesting plot for this scenario. The highest temperatures are shown for the point located on the wire itself, at (0.01125, 0, 0)—(x,y,z). The plot shows the temperature reaching a peak point at the end of the heating period and then sharply changing to a downward slope when the heating stops. This is a characteristic behavior for the point where the heat is being generated. For longer heating and higher power, this peak is at about 83 °C.

The next lower temperature is shown for the point within the central horizontal plane but between the heating wires, at (0, 0, 0). As this point is some distance from the heat source, there is a delayed peak temperature reached after the heating stops and the peak is rounded. For the longer heating at a higher power, the peak is at about 51 °C.

The most important temperature, as far as the seat occupant is concerned, is the one at the seat surface, at (0.01125, 0, 0.024). This point is at a greater distance from the heat source than the previous one and is separated by material of low thermal conductivity. This leads to the peak temperature being reached here at an even later time (about 10 min after the heating stops) and the peak being lowest, at about 29 °C, for the longer time (or higher power) case. Information obtained here on the time delay and the temperature reached at the seat surface would be of importance to the design of the control system for this heated seat.

9.2.3 Scenario 3—Time-Dependent Temperature

In this case study, time-varying temperature is applied to the wires. From Scenario 2 the reader can observe that the heating element reached the temperature of about 45 °C (44.8 °C) after approximately 2 min. In an attempt to reverse-engineer this problem, one can assign this temperature (or its multiples) to the heating element. It is possible, for example, that a control system for the seat heating is designed with a temperature sensor at the heating wire, thus allowing a controlled variation of the wire temperature over time.

Function *pw2(t)* in K is defined to specify the required temperature versus the time. The function's definition is given in Figure 202 and it is plotted in Figure 203. The function is trapezoidal in shape, with linear rise and fall segments, and a constant temperature in the middle. This function is applied as a temperature boundary condition to the wire surfaces. The total simulated time interval is 30 min (1,800 s).

The sensitivity of results to the heating level is explored by varying *nti* (heating time) and *nt1* (temperature level) parameters. Heating time parameter (*nti*) is an integer multiplier defining the heating time in minutes (*nti* × *2* in min). Temperature level parameter (*nt1*) is an integer multiplier defining the peak temperature (*nt*1 × 45 in °C). The temperature is set to start and return to the initial state of 22 °C.

Three levels of heating are assumed for the scenario—low, medium, and high. This means *pw2(t)* in K is defined as (*nt*1 × 45 in °C). A time of 2 min (*tinitial*) is assumed for the total heating period. The scenario was applicable to where *nnt* = 1, resulting in the total heating time of 2 min along with the associated heat flux, *nnq* = 2, resulting in the boundary

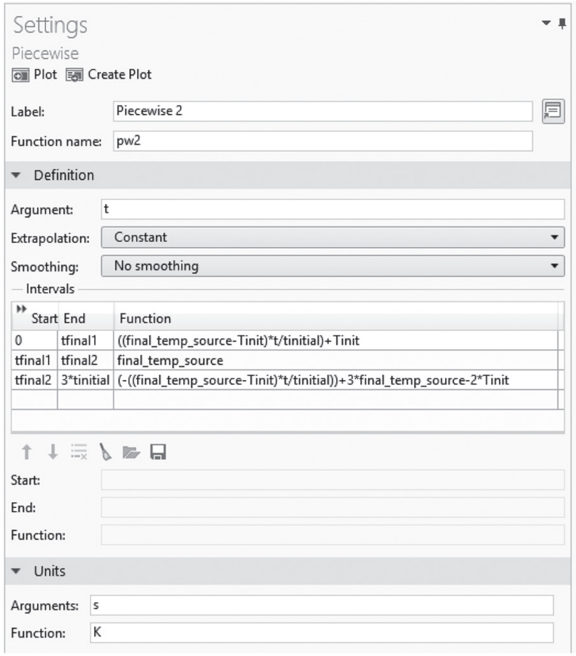

Figure 202. Piecewise temperature function for Scenario 3 of the heated seat ($pw2(t)$).

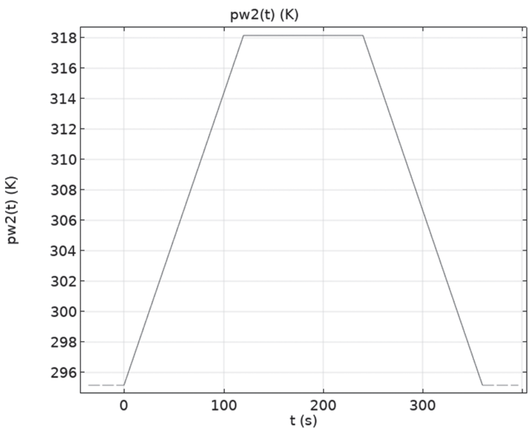

Figure 203. Time-dependent temperature, temperature is multiplied by *nt1* ($nt1 \times pw2(t)$).

temperature of 45 °C. In Scenario 2, it was assumed that the heating was turned on for 2 min at the beginning of the heating process and then turned off. For the current scenario, it is assumed that temperature reaches 45 °C in 2 min, remains at 45 °C for 2 min, and then returns to the initial state (22 °C) in 2 min.

Figure 204 presents the temperature contours for the domains. These contours are associated with the base conditions (45 °C for 2 min exposure time)—Figure 204a. Figure 204b presents the temperature sensitivity of the results for the total duration of 6 min, where a maximum temperature of 82.7 °C is reached. Figure 205 shows the spatial temperature distribution along the height (*z*-coordinate) (Figure 187e).

Figure 206 shows the temperature variation versus the time for the three points defined in Figure 188. The highest temperature is reached at the point on the wire, at (0, 0, 0). As expected, it follows the profile of the trapezoidal boundary condition function $pw2(t)$, reaching a peak of 43 °C for the lower power and 360 °C for the higher power.

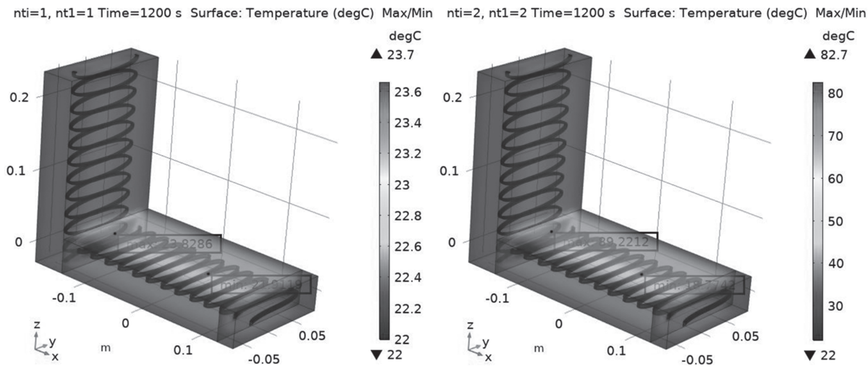

(*a*) (*b*)

Figure 204. Surface temperature contours for heated seat after 20 min: (a) *nti* = 1 (2 min), *nt*1 = 1 (45 °C), (b) *nti* = 2 (4 min), *nt*1 = 2 (90 °C).

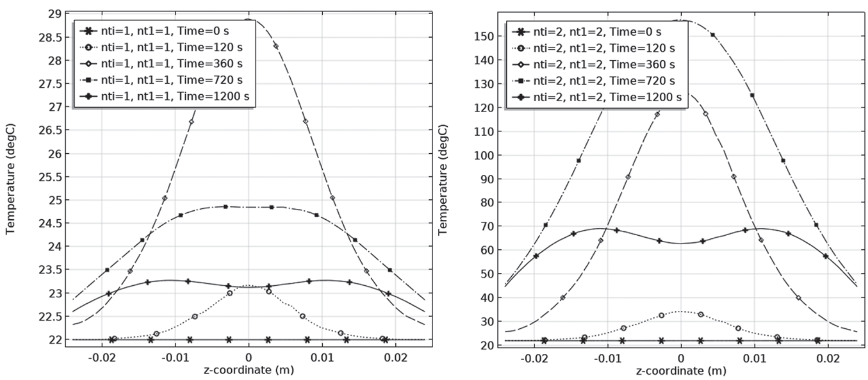

(*a*) (*b*)

Figure 205. Spatial temperature profiles at selected line along seat height (*z*-coordinate): (a) *nti* = 1 (2 min), *nt*1 = 1 (45 °C), (b) *nti* = 2, *nt*1 = 2 (90 °C) (4 min).

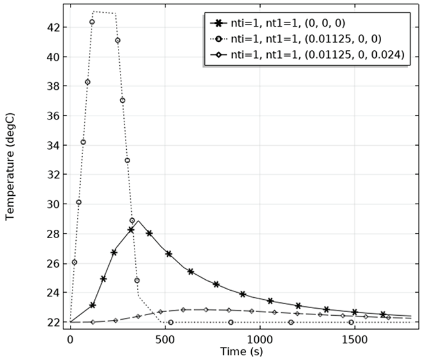

(*a*)

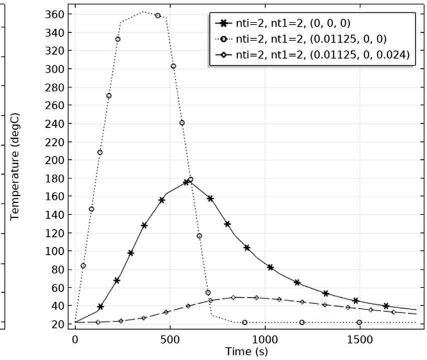

(*b*)

Figure 206. Spatial transient temperature profiles at selected points for heated seat: (a) *nti* = 1 (2 min), *nt*1 = 1 (45 °C), (b) *nti* = 2 (4 min), *nt*1 = 2 (90 °C).

The next lower temperature curve is for the point in the middle of the seat, but between the wires, at (0.01125, 0, 0). A smoothed peak shape is seen, which is delayed from the time of the peak temperature at the wires. A maximum of 180 °C is reached for the high-power case, while for the low-power case, the peak is about 29 °C.

For the point at the cushion exterior, at (0.01125, 0, 0.024), there is an even longer delay to reach the peak temperature, and this peak is very broad. For the low-power case, the temperature peaks only about one degree Celsius above the initial value (23 °C), showing that this power setting is insufficient. For the high-power case, the peak at the cushion surface reaches about 50 °C after approximately 5 min from the time the wire temperature begins to decrease.

9.3 Exercise—Adding the Human Body to the Heated Seat Model

As an additional challenge, the reader may attempt to augment the heated seat model with a representation of the passenger's body. The most accurate method would be to model the body as a separate domain, which is connected to the seat via contact resistances. This is to account for the clothing roughness and lack of perfect contact in areas where the body-seat contact is poor.

The human body in these cases can be approximated by a multilayer cylinder, consisting of three components—body core, skin and its adjoining cells, and the body cover or clothing. In a human, the heat is generated within the body core in order to regulate the core temperature to 37 °C and thus can be represented as a fixed-temperature volume. However, the skin temperature is slightly less than that of the core (about 36 °C).

Due to the contact resistance between the skin and its cover (mainly filled with air), the temperature of the clothing is less than that of the skin. The thicker the clothing material is (e.g., denims or winter jacket), the greater the temperature gradient is observed from the skin to the exterior shell (clothing). Additionally, in the proximity of the skin, the heat is transferred by means of convection but also advection due to the blood flow. If the person feels too hot (due to external heat or internal muscle activity), the arterial blood vessels dilate to remove more heat. Additionally, sweat glands get activated. This is why you sweat when you exercise and you feel thirst, since a lot of extra heat and moisture evacuates the body by exhalation. On the other hand, when you feel cooler than your comfort level, the arterial vessels constrict, reducing the blood flow and, therefore, keeping the heat inside the body. Also, heat generation is increased via body shivering.

The mechanism of heat transfer from surfaces exposed to the environment, both dress and skin, is by heat convection and radiation. The convection coefficient may vary for the two cases, depending on the method by which the body is modeled. Similar to the heated seat scenario, effective thermo-physical properties may be calculated for the passenger body. The body also generates heat by blood flow and may lose it through perspiration and sweat. These additional factors distinguish a human from a mannequin and would need to be accounted for to create an accurate heat transfer model.

The interface between the passenger body and the seat determines the rate at which the heat is conducted to the body. The more pressure the body applies to the seat, the better the contact and, therefore, the less thermal resistance between the two surfaces. A variety of studies have been conducted in which the pressure distribution of the passenger body over the seat area was mapped. It was found that most contact occurs at the head rest, upper portion of the back, and upper to lower parts of the hips.

For this exercise, include the body contact area as a surface boundary and apply the conditions that simulate best what describes the passenger body, in the form of a heat flux, for example, consisting of the body-generated energy due to blood flow, sensible heat, and convection due to sweat. The presented studies are mainly applicable to the cases in which the purpose is to understand how long it takes for a heated seat to be warmed so that it reaches a safe temperature, capable of providing passenger comfort. Generally speaking, after reaching such a temperature level, human physiology responds almost uniformly to the heated boundary (seat), and the defined (or felt) comfort level can be further accessed through the literature with extensive qualitative and quantitative data, presented using numeric or Likert scales [119,120,121,122].

CHAPTER 10

Case Study 5—Face Mask

While masks can be used to beautify, protect one's face from external natural (e.g., sand storms) and artificial (e.g., ball hits received by a hockey goalie) hazards, or conceal one's identity (e.g., circuses), they can also be used to provide breathable air to humans in environments where such air is not naturally available. Such breathing masks can be classified into those that filter the incoming air and those that supply it from an external source. For example, a respirator can be used to prevent the wearer from inhaling harmful chemicals. A filter in the form of fine meshes at the inlet of the mask traps the incoming contaminants.

There is a long history of people trying to protect themselves from inhaling noxious substances. In the sixteenth century, Leonardo da Vinci proposed the use of wet woven masks by sailors to protect them from the fumes produced by the exploding gunpowder of the cannons. In the nineteenth century, animal bladder skins were used to protect the Romanian miners working in toxic environments. As mining technology developed, so did the face masks. As materials and manufacturing methods improved, it became possible for the dust particles to be separated from the air with multiple filters made of porous materials of different sizes so that variety of particles could be absorbed before entering the human respiratory system. Additional materials, such as charcoal, lime, and glycerine, have been employed to absorb the unwanted gases.

Filtering masks can also work in reverse, shielding the environment from the wearer. For example, surgical masks protect patients from the liquid precipitations and aerosols generated by health professionals. Masks that provide such reverse protection are commonly used in East Asian countries by ill persons trying to prevent spreading of germs and airborne diseases—practicing social responsibility and showing respect for others. During the flu pandemic of 1918, these protective masks were also a common sight, with people not being allowed to use public transit without them in some areas (e.g., Seattle in the United States).

Looking at the masks that provide breathable air from an external supply source, one common application is in scuba diving. The word *scuba* itself was originally an acronym SCUBA, standing for Self-Contained Underwater Breathing Apparatus, coined by Christian James Lambertsen, an American environmental and diving medicine specialist in 1952. The apparatus invented by Lambertsen was actually a rebreather type, where exhaled air is recycled and its carbon-dioxide content reduced, and it is enriched by oxygen. Today, the term *scuba* is usually applied to what is known as the *open-circuit breathing apparatus*. In it, the exhaled air is released into water and new air is supplied from the pressurized cylinder storage. The currently used safe design for the open-circuit breathing device was invented in 1943 by Jacques-Yves Cousteau, the famous French underwater explorer. Cousteau wanted to sell his device in English-speaking countries under the name *Aqua-Lung*. This term is still used for this device, but *scuba* is much more common [123,124].

In today's scuba sets, compressed air cylinders store air at pressures of up to 240 bar; the pressure is reduced by a regulator when supplied to the diver. Note that as one descends further below the water surface, pressure increases; therefore, the difference with the atmospheric pressure at the surface is to be minimized so that the breathing conditions remain the same as on the surface. In this scenario, the exhale of the diver does this pressure equalization. Note that when the chest cavity enlarges by moving the diaphragm downward (during inhalation), pressure inside the lungs decreases. This is when the inhale process takes place, where air enters the lungs. After this, exhalation occurs, where the diaphragm relaxes by moving upward and air leaves the lungs. This causes pressure equalization; flow moves from the location of higher pressure to that of lower pressure. The demand valve built into the scuba diving system supplies the required air needed for the inhalation process; in other words, it regulates diving.

As the diver ascends, the air automatically leaves the mask to relieve the excess pressure. In addition to breathing capability, scuba masks also provide improved vision under water. To focus the image on the retina correctly, the eye's lens needs to be in contact with the surrounding air, which has a refractive index of 1. However, the refractive index of water is higher (1.3), meaning that the light rays bend differently when passing from water to the eye's lens, causing poor vision. The mask provides a clear space filled with air in front of the face to produce correct focusing by the eye's lens.

Masks can also be used to provide oxygen-enriched air in applications other than underwater diving. They may be used for medical reasons (e.g., oxygen therapy) or to aid firefighters, high-altitude climbers, aviators, airplane passengers, and astronauts. These masks may be covering the nose and mouth only or the entire face; alternatively, the mask structure may not be used at all—a tube supplying the oxygen may be inserted directly in the nasal channel (nasal cannula). Masks are made of a variety of soft materials (e.g., plastic, rubber, and silicon) that are not only comfortable for the wearer but also have the flexibility to conform to the wearer's face shape, providing a good seal.

As in the scuba sets, the gas is delivered to the mask by tubing from a high-pressure storage tank (reservoir), with a regulator valve adjusting the supply pressure and flow rate (Figure 207). Some masks are also equipped with breathing bags made of plastic or rubber to support deep breathing. In some applications (such as air supply to military jet pilots), larger-diameter hoses instead of tubes are used, allowing a greater amount of air to be delivered with less resistance. Such hoses will also use ribs or corrugations in their design to minimize the possibility of kink formation that can constrict the flow. Recall the hose you use to water the outdoor plants; if bent excessively, water constriction may be experienced. This does not present any danger to the plants but may be life-threatening for a military pilot at high altitudes.

Medical use of oxygen for treatment of chronic or acute conditions is a common practice that started around 1917. It is listed among the most essential medicines by the Wold Health Organization (WHO). It provides the oxygen needed for cell metabolism. Depending on the condition and type of treatment, different saturation rates are prescribed (mostly 94 to 96 percent), though excessive oxygen may cause toxicity, lung damage, or dry nose. Such oxygen treatment, for example, has been used for those affected by chemical weapon attacks (such as mustard gas) [125,126].

Supplementary oxygen is also used to allow humans to function effectively or even survive at elevated altitudes. Hemoglobin in our blood, which distributes oxygen to all tissues, saturates when exposed to oxygen at partial pressure found at sea level. This partial pressure is proportional to the oxygen fraction in the air (about 20 percent) and the atmospheric pressure. The oxygen fraction in the air remains constant at altitudes below 100 km and thus is not a factor. But the atmospheric pressure declines substantially with altitude. Symptoms of altitude sickness may appear at altitudes as low as 2,000 m (6,600 ft), where pressure is about 80 percent of that at sea level, and include headaches, nausea, tiredness, and dizziness. The atmospheric pressure falls to 50 percent of sea level pressure at 5,500 m (18,000 ft). Altitudes above 8,000 m (26,000 ft) are called the *Death Zone* in mountaineering. Here, supplementary oxygen is a requirement for survival for most people, which is why it is commonly used to ascend Everest's 8,840 m height. Until 1978, when Reinhold Messner (Italy) and Peter Habeler (Austria) succeeded, it was thought to be impossible to reach the summit without the use of oxygen. Now, about 5 percent of Everest ascents are made without supplementary oxygen.

The earliest reported use of oxygen in an aircraft was in 1919, for two passengers who were taken to a 15,000 ft altitude. For flights at altitudes above 12,500 ft that last longer than 30 minutes, all aircraft need to be equipped with oxygen masks for all passengers. At altitudes above 14,000 ft, pilots are required to wear oxygen masks in unpressurized cabins. For pilots and in small business jets, the oxygen supply is generally provided by a compressed gas tank storage unit. For large aircraft, passenger emergency oxygen is normally supplied via a chemical reaction. This exothermic reaction is initiated when masks are deployed in case of depressurization and is expected to last at least 15 min, providing sufficient time for the aircraft to descend to a safe altitude.

Three kinds of masks are used for flying at high altitudes: (1) providing continuous flow during the inhalation and exhalation—the exhalation breath is accumulated inside a rebreather bag that allows deeper breathing during inhalation; (2) diluting the flow—increasing the oxygen flow rate with increasing altitude so that oxygen pressure remains constant at high altitudes, activated during inhalation; and (3) changing the flow pressure—providing oxygen above the ambient pressure, making it easier to inhale while more difficult to exhale; therefore, it is activated mainly during inhalation. All of theses masks require a good seal between the wearer's face footprint and the mask; a good seal is of particular importance in the latter two cases [127].

Jet fighter pilots may experience symptoms similar to those of the scuba divers due to the fast ascents and descents; therefore, they wear G-Suits that are pressurized and wear oxygen masks at all times. A G-Suit is worn when pilots experience high G-loads (acceleration) due to the fast maneuvers that may cause a sudden rush of blood to or away from the brain—a redout or a blackout [128]. Face masks for these pilots cover face sides, providing protection against flash burns, particles, and high velocity air streams when an emergency arises (e.g., seat ejection). The G-Suit helps with adjusting the blood pressure to prevent blood's excessive accumulation or lack of it by pressing against the body parts, to provide resistance to the blood flow and therefore delaying these adverse effects. The astronauts who are sent to outer space fall within the same category.

In his autobiography, Chris Austin Hadfield, a Canadian engineer, pilot, and astronaut, talks about his experience when doing one-on-one combat training in a CF-18 fighter plane. He found that his G-Suit's hose was accidentally disconnected during maneuvers by his elbow [129]. As a result of this malfunction, C. A. Hadfield became unconscious for 16 s while his training mate was trying to communicate with him. He employed his operational awareness and got back on the ground first before trying to find what happened in the air. His experience resulted in modifications to the G-Suit connection in the CF-18 to improve safety. It is also required for the space shuttle crew members to wear oxygen masks after Soyuz 11 (Союз 11) incident in 1971, resulting in the death of Soviet cosmonauts after the cabin air leaked, when the cabin vent valve opened accidentally before entering the atmosphere while the crew members were not wearing oxygen masks.

10.1 Problem Definition

In this case study, an oxygen mask is modeled. The mask includes an inlet and outlet. The flow is treated as a non-isothermal one, assuming density varies with temperature, even though not significantly. The flow is assumed incompressible with Mach under 0.3. There are two main parts to the mask that fit onto the patients' face: (1) the inlet, where the gas enters the mask through the inhale mechanism; and (2) the outlet, where the exhaled gases exit the mask. It is assumed in this scenario that the gas is pure oxygen, entering the mask at the ambient temperature and leaving it at the atmospheric pressure. Heat transfer to the surroundings is done by convection and conduction.

For this study, human inhale and exhale patterns are modeled. The oxygen mask (respirator) is impermeable. To define the inhale-exhale flow patterns, parameters such as gender, age, weight, height, and activity level are used. Modeling of breathing can be approached in different ways. For example, different thermal-flow models for the inhale and exhale may be developed in which laminar or turbulent flows with inlet and outlet flows that are constant or follow a function are introduced. It is also possible to define a multi-flow pattern, where the combination of the inhale and exhale functions is introduced into the model. This is achieved by offsetting the related periods, so that the mask lets the air in or out in a transient fashion. Figure 207 shows an example of an oxygen breathing system; a modified version of the face mask was modeled in this case study.

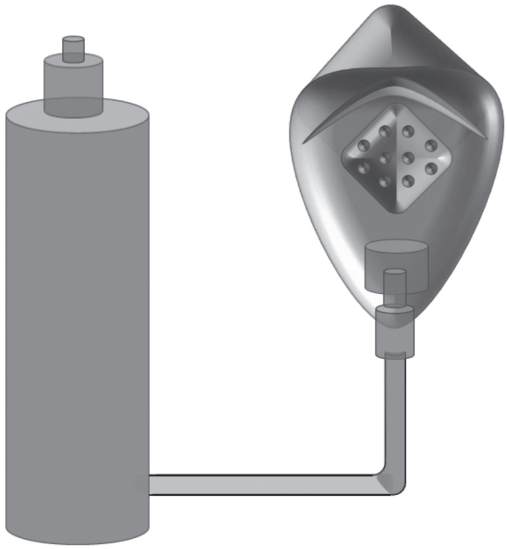

Figure 207. A respirator mask connected to an oxygen tank.

To define the mask shape, it is possible to make a mold of the patient's face, similar to those made when making sculptures, or use scanning methods in order to estimate dimensions for different regions of the face. The regions considered may be as few as three (forehead, nose, and chin areas) or as many as seven (forehead, cheeks, nose, chin, neck, and back of the head). The shape of each of these parts is identified through the multilayer bones under the skin projected to the visible skin. This head (including the facial structure) is also known as the *head form*.

Given the complexity of the mask's shape, the easiest way to define its geometry in an FEM tool is via import of a solid model from an external

CAD tool. For this model, it is assumed that the mask has a thickness of 5 mm and is made from vinyl. The inlet and outlet operate using a one-way valve that only allows flow in one direction, as appropriate. Although in this case study the inflow and outflow are normal to the inlet and outlet openings, in general, they can be guided to follow a specific spatial direction. For this model, flows inside the tank and tubing are not modeled [130,131,132].

The model employs inhale-exhale flow patterns that have cycle times similar to actual breathing. The flow temperature varies for the duration of the breathing, receiving air at the ambient temperature (25 °C), and releasing it at the body temperature (37 °C). Depending on the maximum flow rate, a laminar or turbulent model may be applicable. For this analysis, a laminar model is adopted. The initial temperature (22 °C) equals that of the ambient. The inhale temperature, when the person breathes in, is the same as the mask inlet temperature (22 °C), while the exhale temperature is the same as that of the body (37 °C) as the person breathes out.

Breathing consists of two stages, inhale and exhale. Each inhale and exhale have a sinusoidal flow rate profile with its own characteristics—amplitude and duration. Together, they make up the breathing cycle, consisting of one inhale and one exhale period. The total time of a single cycle (period) of breathing consists of an inhale period followed by an exhale period. The inhale time is usually shorter than the exhale time by about one second, giving the total breath period of 5.44 s (an average male subject compared to 4.03 s for an average female subject). The pattern for the breath flow depends on the gender and physical activity level. In addition, factors such as body mass and height affect the body metabolism and therefore the breathing pattern. For a typical human breathing candidate, body height, surface area, mass, mass index, inhale and exhale respiratory frequencies, mass flow rate, inhale and exhale durations, as well as amplitudes should be included in the breathing calculations.

The examples provided herein are for average female and male humans. For each case, appropriate typical parameters are listed and equations are provided to calculate the breathing patterns (mass or volume flow rate). Female parameters are 1.5 m height, 1.7 m^2 body surface area, 45 kg weight, and 20 kg/m^2 body mass index (Table 3). Male parameters are 1.9 m height, 2.1 m^2 body surface area, 78.3 kg weight, and 21.7 kg/m^2 body mass index (Table 4).

Table 3. Female breathing pattern parameters.

Parameter	Equation and Values		Definition	Dimension
	Female	Value		
Height	1.5 (m)	1.5	Body Height	m
BSA	1.7 (m^2)	1.7	Body Surface Area	m^2
BMI	20 (kg/m^2)	20.0	Body Mass Index	kg/m^2
Mass	BMI × $Height^2$	45.0	Body Mass	Kg
MV	4.634 × BSA × (1E-03) [m^3/min]	1.28E-04	Minute Volume	m^3/s
RF_in	46.43 [1/min] – 18.85 [1/(m.min)] × Height	0.303	Inhale Respirator Factor	1/s
RF_out	54.47 [1/min] – 25.48 [1/(m.min)] × Height	0.271	Exhale Respirator Factor	1/s
TV	MV × [RF_in + RF_out]/ [2 × RF_in × RF_out]	4.48E-04	Tidal Volume	m^3
beta_in	Pi × RF_in/30	0.032	Inhale Phase	1/s
beta_out	Pi × RF_out/30	0.028	Exhale Phase	1/s
alpha_in	beta_in × TV/2	4.26E-04	Inhale Amplitude	m^3/s
alpha_out	beta_out × TV/2	3.81E-04	Exhale Amplitude	m^3/s

Table 4. Male breathing pattern parameters.

Parameter	Equation and Values		Definition	Dimension
	Male	Value		
Height	1.9 (m)	1.9	Body Height	m
BSA	2.1 (m^2)	2.1	Body Surface Area	m^2
BMI	21.7 (kg/m^2)	21.7	Body Mass Index	kg/m^2
Mass	BMI × $Height^2$	78.3	Body Mass	Kg
MV	5.225 × BSA × (1E-03) (m/min)	1.83E-04	Minute Volume	m^3/s
RF_in	55.55 [1/min] – 32.86 [1/(m.min)] × Height + 0.2602 [1/(kg.min)] × Mass	0.225	Inhale Respirator Factor	1/s
RF_out	77.03 [1/min] – 45.42 [1/(m.min)] × Height + 0.2373 [1 / (kg.min)] × Mass	0.155	Exhale Respirator Factor	1/s
TV	MV × [RF_in + RF_out] / [2 × RF_in × RF_out]	1.66E-05	Tidal Volume	m^3
beta_in	2 × Pi × RF_in	1.414	Inhale Phase	1/s
beta_out	2 × RF_out	0.976	Exhale Phase	1/s
alpha_in	beta_in × TV/2	7.03E-04	Inhale Amplitude	m^3/s
alpha_out	beta_out × TV/2	4.86E-04	Exhale Amplitude	m^3/s

There are a number of practical features highlighted in this work. The first is modeling a periodic input for the flow rate that varies as a function of an independent variable (e.g., time). This means the problem cannot be modeled by a steady-state approach. Similar to the previous scenarios where a flow model is concerned, it is valuable to include Reynolds study analysis; therefore, the effect of the inlet or outlet diameters are included in the model. In this case, the inlet and outlet have their own channels, meaning that the flow enters and leaves via two different openings during the inhalation and exhalation processes. There are two openings that act as the exhale ports, one on the left and another on the right side of the mask. During the exhale phase, a valve prevents the outward airflow via the inlet, which is located on the front of the mask. The total breathing period consists of the inhale and exhale periods.

The inhale period starts from the beginning of the breathing period (zero seconds), while the exhale period starts at the end of the inhale period, meaning that instead of starting from zero seconds, it is offset by the inhale period. The offset function is then a rectangular function (Figure 208 for female and Figure 209 for male case studies), which has a magnitude of one during the exhale and zero during the inhale. This function is multiplied by the inhale pattern to form *Analytic Function* (Figure 210 for female and Figure 212 for male case studies). Another *Analytic Function* is defined (using a similar approach to that of the inhale) for the exhale pattern (Figure 211 and Figure 213). A new *Analytic Function* then can be defined, combining the inhale and exhale patterns for the single breathing period, which can be repeated for any required number of breathing periods (cycles) (Figure 214 and Figure 215). These functions are defined under *Global Definitions* (Figure 216).

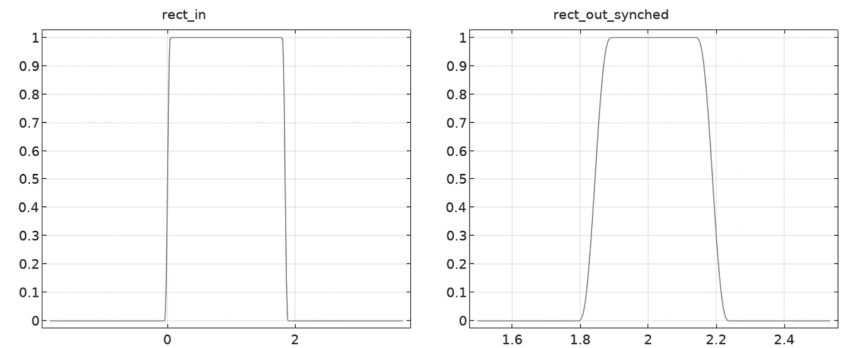

(*a*) (*b*)

Figure 208. Transient female breathing patterns modeled using rectangular function: (a) Inhale, (b) Exhale.

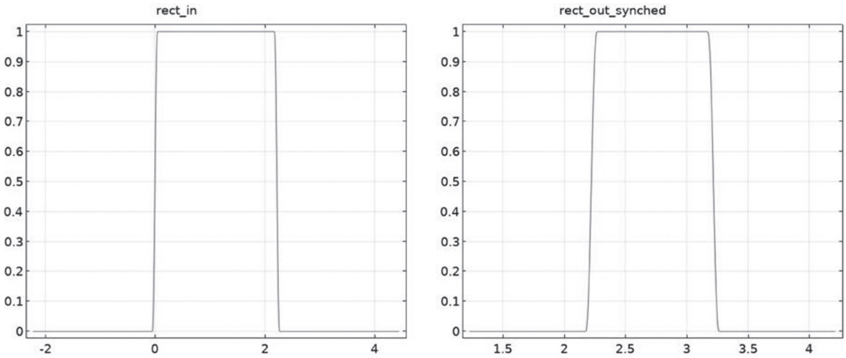

(*a*) (*b*)

Figure 209. Transient male breathing patterns modeled using rectangular function: (a) Inhale, (b) Exhale.

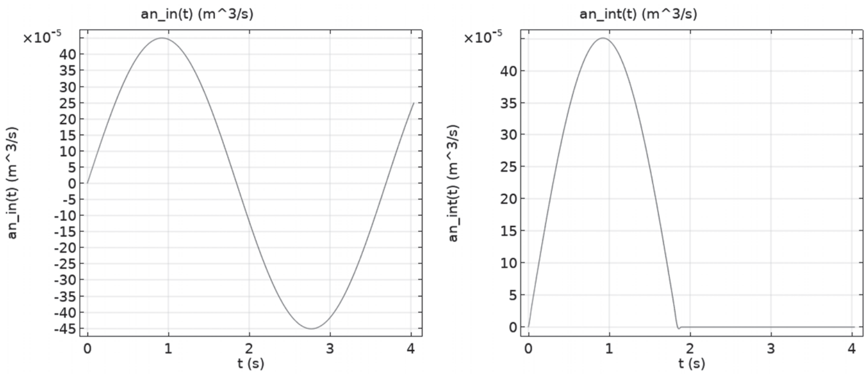

(*a*) (*b*)

Figure 210. Transient female breathing patterns modeled using *Analytic Functions*: (a) Inhale, (b) Inhale combined with breathing in period.

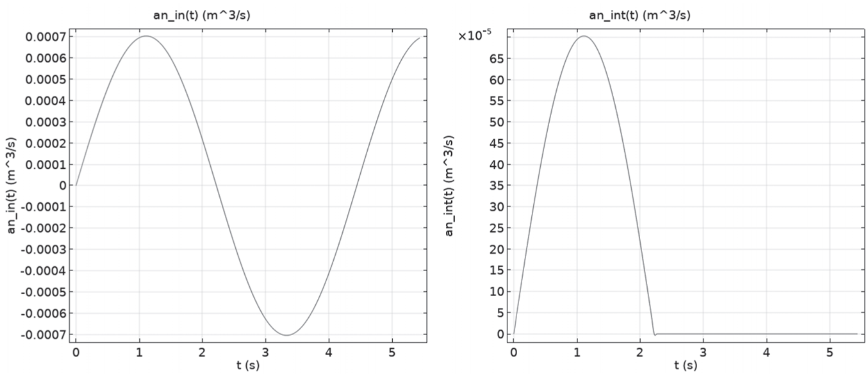

(*a*) (*b*)

Figure 211. Transient male breathing patterns modeled using *Analytic Functions*: (a) Inhale, (b) Inhale combined with breathing in period.

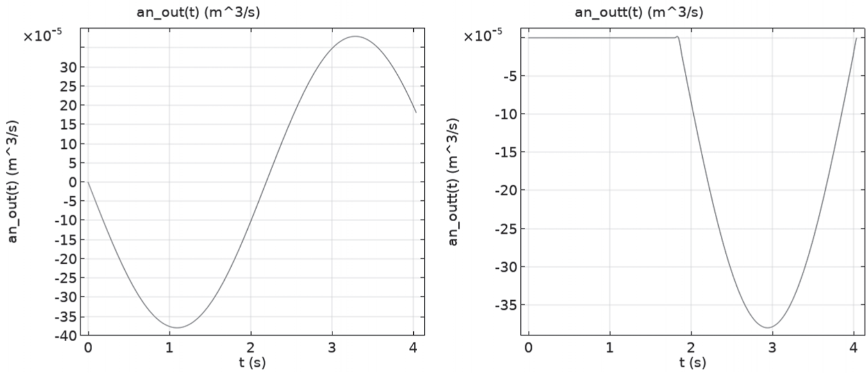

(a) (b)

Figure 212. Transient female breathing patterns modeled using *Analytic Functions*: (a) Exhale, (b) Exhale combined with breathing out period.

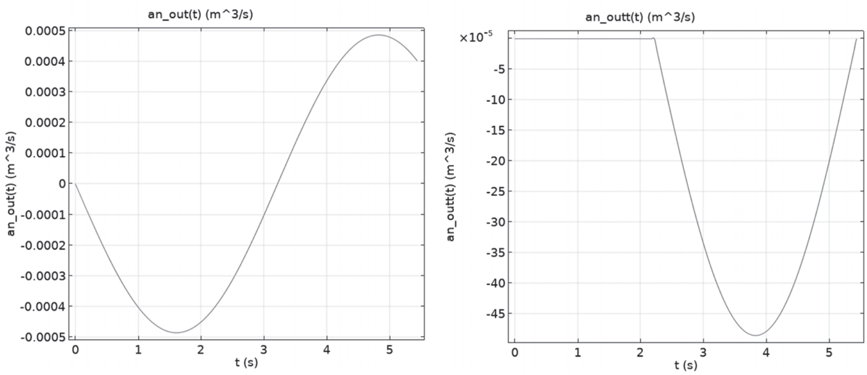

(a) (b)

Figure 213. Transient male breathing patterns modeled using *Analytic Functions*: (a) Exhale, (b) Exhale combined with breathing out period.

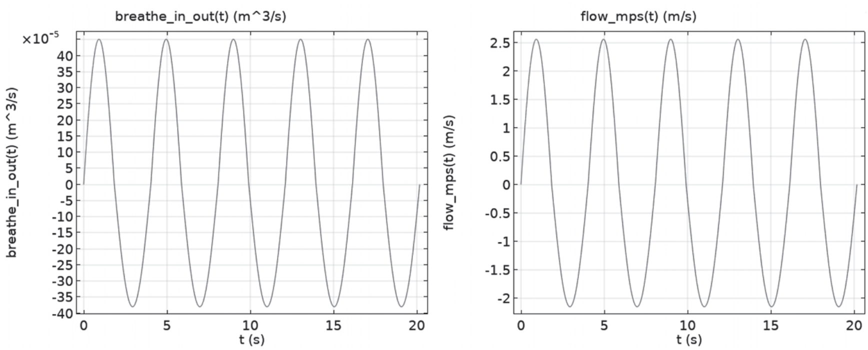

(a) (b)

Figure 214. Transient female breathing patterns modeled using *Analytic Functions*, inhale-exhale patterns combined with breathing in and out periods: (a) Flow rate, (b) Flow velocity based on the inlet dimensions.

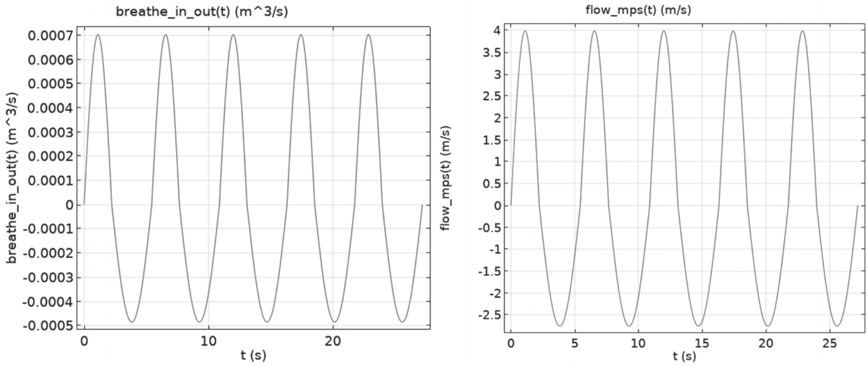

(*a*) (*b*)

Figure 215. Transient male breathing patterns modeled using *Analytic Functions*, inhale-exhale patterns combined with breathing in and out periods: (a) Flow rate, (b) Flow velocity based on the inlet dimensions.

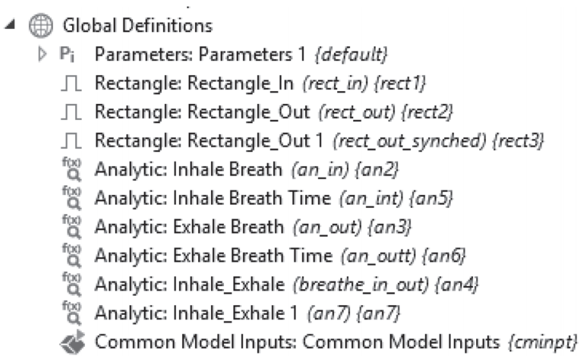

Figure 216. Oxygen face mask functions tree.

The volumetric flow rate during the inhale, entering the mask inlet, is substituted with the volumetric flow rate during the exhale, exiting the mask outlet. The flow is normal to the inlet and outlet in this study, although, in general, it is also possible for the flow velocity field to be defined (with given x, y, and z components). It is possible to define the inlet as the outlet and the outlet as the inlet when setting up the physics, keeping in mind that the flow directions and patterns should be selected correctly.

Post-processing visualization tools such as the use of arrow lines in order to study the transient flow direction in the vicinity of the outlet or inlet are useful tools that can assist with understanding the *transient* flow direction. Parameters used in COMSOL Multiphysics model are presented in Figure 217 and Figure 218 for female and male case studies, respectively.

Settings

Parameters

Label: Parameters 1

Parameters

Name	Expression	Value	Description
Height	height_female	1.6 m	01- body height
BSA	bsa_female	1.7 m^2	02- body surface area
BMI	bmi_female	20 kg/m^2	03- body mass index
Mass	mass_female	51.2 kg	04- mass
MV	mv_female	1.313E-4 m^3/s	05- minute volume
RF_in	RF_in_female	0.27117 1/s	06- inhale respirator factor
RF_out	RF_out_female	0.22837 1/s	07- exhale respirator factor
TV	tv_female	5.2956E-4 m^3	08- tidal volume
beta_in	beta_in_female	1.7038 1/s	09- inhale phase
beta_out	beta_out_female	1.4349 1/s	10- inhale angle
alpha_in	alpha_in_female	4.5113E-4 m^3/s	11- inhale amplitude
alpha_out	alpha_out_female	3.7993E-4 m^3/s	12- exhale amplitude
breath_period	breath_period_female	4.0333 s	13-breath period
Tamb	Tinit	308.15 K	ambient temperature
Patm	1[atm]	1.0133E5 Pa	atmospheric pressure
Tbody	25[degC]	298.15 K	body temperature
hc	5[W/(m^2*K)]	5 W/(m^2·K)	convective coefficient
exhale_period	1/(2*RF_out)	2.1895 s	exhale period
height_female	1.6[m]	1.6 m	female body height
mass_female	bmi_female*height_female^2	51.2 kg	female body Mass
bmi_female	20[kg/m^2]	20 kg/m^2	female body mass index
bsa_female	1.7[m^2]	1.7 m^2	female body surface area
breath_period_female	1/(2*RF_in_female)+1/(2*RF_out_female)	4.0333 s	female breath period
alpha_out_female	beta_out_female*tv_female/2	3.7993E-4 m^3/s	female exhale amplitude
beta_out_female	2*pi*RF_out_female	1.4349 1/s	female exhale angle
RF_out_female	54.47[1/min]-25.48[1/(m*min)]*height_female	0.22837 1/s	female exhale respirator factor
alpha_in_female	beta_in_female*tv_female/2	4.5113E-4 m^3/s	female inhale amplitude
beta_in_female	2*pi*RF_in_female	1.7038 1/s	female inhale angle
RF_in_female	46.43[1/min]-18.85[1/(m*min)]*height_female	0.27117 1/s	female inhale respirator factor
mv_female	(4.634*bsa_female/60000)[m/s]	1.313E-4 m^3/s	female minute volume
tv_female	mv_female*(RF_in_female+RF_out_female)/(2*RF_in_female*RF_out_female)	5.2956E-4 m^3	female tidal volume
inhale_period	1/(2*RF_in)	1.8439 s	inhale period
Tinit	35[degC]	308.15 K	initial temperature
inlet_area	(2*8.8154E-5)[m^2]	1.7631E-4 m^2	inlet area
inlet_diameter	(4*inlet_area/pi)^0.5	0.014983 m	inlet inside diameter
Tinlet	25[degC]	298.15 K	inlet temperature
height_male	1.9[m]	1.9 m	male body height
mass_male	bmi_male*height_male^2	78.337 kg	male body mass
bmi_male	21.7[kg/m^2]	21.7 kg/m^2	male body mass index
bsa_male	2.1[m^2]	2.1 m^2	male body surface area
breath_period_male	1/(2*RF_in_male)+1/(2*RF_out_male)	5.4408 s	male breath period
alpha_out_male	beta_out_male*tv_male/2	4.8561E-4 m^3/s	male exhale amplitude
beta_out_male	2*pi*RF_out_male	0.97613 1/s	male exhale angle
RF_out_male	77.03[1/min]-45.42[1/(m*min)]*height_male+0.2373[1/(kg*min)]*mass_male	0.15536 1/s	male exhale respirator factor
alpha_in_male	beta_in_male*tv_male/2	7.0327E-4 m^3/s	male inhale amplitude
beta_in_male	2*pi*RF_in_male	1.4136 1/s	male inhale angle
RF_in_male	55.55[1/min]-32.86[1/(m*min)]*height_male+0.2602[1/(kg*min)]*mass_male	0.22499 1/s	male inhale respirator factor
mv_male	(5.225*bsa_male/60000)[m/s]	1.8287E-4 m^3/s	male minute volume
tv_male	mv_male*(RF_in_male+RF_out_male)/(2*RF_in_male*RF_out_male)	9.9498E-4 m^3	male tidal volume
outlet_area	3.7654E-5[m^2]	3.7654E-5 m^2	outlet area
outlet_diameter	(4*outlet_area/pi)^0.5	0.0069241 m	outlet inside diameter
Tref	293.15[K]	293.15 K	reference temperature
time_step	breath_period/50	0.080667 s	time step

Figure 217. Parameters used for oxygen face mask study, female case study (global level).

Settings

Parameters

Label: Parameters 1

Parameters

Name	Expression	Value	Description
Height	height_male	1.9 m	01- body height
BSA	bsa_male	2.1 m^2	02- body surface area
BMI	bmi_male	21.7 kg/m^2	03- body mass index
Mass	mass_male	78.337 kg	04- mass
MV	mv_male	1.8287E-4 m^3/s	05- minute volume
RF_in	RF_in_male	0.22499 1/s	06- inhale respirator factor
RF_out	RF_out_male	0.15536 1/s	07- exhale respirator factor
TV	tv_male	9.9498E-4 m^3	08- tidal volume
beta_in	beta_in_male	1.4136 1/s	09- inhale phase
beta_out	beta_out_male	0.97613 1/s	10- inhale angle
alpha_in	alpha_in_male	7.0327E-4 m^3/s	11- inhale amplitude
alpha_out	alpha_out_male	4.8561E-4 m^3/s	12- exhale amplitude
breath_period	breath_period_male	5.4408 s	13-breath period
Tamb	Tinit	308.15 K	ambient temperature
Patm	1[atm]	1.0133E5 Pa	atmospheric pressure
Tbody	25[degC]	298.15 K	body temperature
hc	5[W/(m^2*K)]	5 W/(m^2·K)	convective coefficient
exhale_period	1/(2*RF_out)	3.2184 s	exhale period
height_female	1.6[m]	1.6 m	female body height
mass_female	bmi_female*height_female^2	51.2 kg	female body Mass
bmi_female	20[kg/m^2]	20 kg/m^2	female body mass index
bsa_female	1.7[m^2]	1.7 m^2	female body surface area
breath_period_female	1/(2*RF_in_female)+1/(2*RF_out_female)	4.0333 s	female breath period
alpha_out_female	beta_out_female*tv_female/2	3.7993E-4 m^3/s	female exhale amplitude
beta_out_female	2*pi*RF_out_female	1.4349 1/s	female exhale angle
RF_out_female	54.47[1/min]-25.48[1/(m*min)]*height_female	0.22837 1/s	female exhale respirator factor
alpha_in_female	beta_in_female*tv_female/2	4.5113E-4 m^3/s	female inhale amplitude
beta_in_female	2*pi*RF_in_female	1.7038 1/s	female inhale angle
RF_in_female	46.43[1/min]-18.85[1/(m*min)]*height_female	0.27117 1/s	female inhale respirator factor
mv_female	(4.634*bsa_female/60000)[m/s]	1.313E-4 m^3/s	female minute volume
tv_female	mv_female*(RF_in_female+RF_out_female)/(2*RF_in_female*RF_out_female)	5.2956E-4 m^3	female tidal volume
inhale_period	1/(2*RF_in)	2.2223 s	inhale period
Tinit	35[degC]	308.15 K	initial temperature
inlet_area	(2*8.8154E-5)[m^2]	1.7631E-4 m^2	inlet area
inlet_diameter	(4*inlet_area/pi)^0.5	0.014983 m	inlet inside diameter
Tinlet	25[degC]	298.15 K	inlet temperature
height_male	1.9[m]	1.9 m	male body height
mass_male	bmi_male*height_male^2	78.337 kg	male body mass
bmi_male	21.7[kg/m^2]	21.7 kg/m^2	male body mass index
bsa_male	2.1[m^2]	2.1 m^2	male body surface area
breath_period_male	1/(2*RF_in_male)+1/(2*RF_out_male)	5.4408 s	male breath period
alpha_out_male	beta_out_male*tv_male/2	4.8561E-4 m^3/s	male exhale amplitude
beta_out_male	2*pi*RF_out_male	0.97613 1/s	male exhale angle
RF_out_male	77.03[1/min]-45.42[1/(m*min)]*height_male+0.2373[1/(kg*min)]*mass_male	0.15536 1/s	male exhale respirator factor
alpha_in_male	beta_in_male*tv_male/2	7.0327E-4 m^3/s	male inhale amplitude
beta_in_male	2*pi*RF_in_male	1.4136 1/s	male inhale angle
RF_in_male	55.55[1/min]-32.86[1/(m*min)]*height_male+0.2602[1/(kg*min)]*mass_male	0.22499 1/s	male inhale respirator factor
mv_male	(5.225*bsa_male/60000)[m/s]	1.8287E-4 m^3/s	male minute volume
tv_male	mv_male*(RF_in_male+RF_out_male)/(2*RF_in_male*RF_out_male)	9.9498E-4 m^3	male tidal volume
outlet_area	3.7654E-5[m^2]	3.7654E-5 m^2	outlet area
outlet_diameter	(4*outlet_area/pi)^0.5	0.0069241 m	outlet inside diameter
Tref	293.15[K]	293.15 K	reference temperature
time_step	breath_period/50	0.10882 s	time step

Figure 218. Parameters used for oxygen face mask study, male case study (global level).

Another point to consider is the flow type selection (i.e., *Incompressible* versus *Weakly compressible flow*). A variation of density with temperature for *Compressible flow* with Mach under 0.3 is also possible to be captured; however, *Weakly compressible flow* option facilitates non-isothermal flow modeling in regions with small temperature variations, occasionally with better solution converging conditions.

10.2 Face Mask Geometry

The oxygen face mask geometry was created using Solid Edge CAD software. After creating the geometry as a solid filled volume, a *Thin-Wall* command was used to define a shell with uniform walls with 1.5 mm thickness and an opening where the wearer's face would fit plus holes for the two inlets and one outlet. This geometry was then imported into COMSOL Multiphysics and further processing steps were applied (Figure 219).

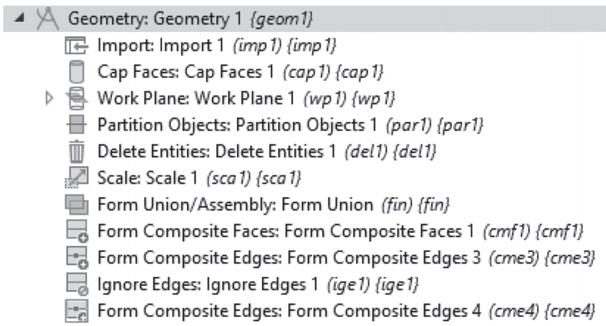

Figure 219. Oxygen face mask model geometry tree.

To model the flow, the model needs to include the fluid domain, which is to be added to the imported solid part. The approach used to create such a domain is by capping the open volume of a solid model. To achieve this, the perimeter edges of an opening to be filled with fluid are selected and *Cap Faces* command is applied (Figure 220). The model is symmetrical with respect to the *z-x* plane and thus can be reduced by half. To remove one half of the model, a work-plane is used to partition the geometry volume into two equal halves (Figure 221a). Then, the unneeded half, highlighted with purple in Figure 221b, is deleted.

The imported file consists of many geometrical features such as volumes, surfaces, edges, or layers. Some of those features (e.g., surfaces)

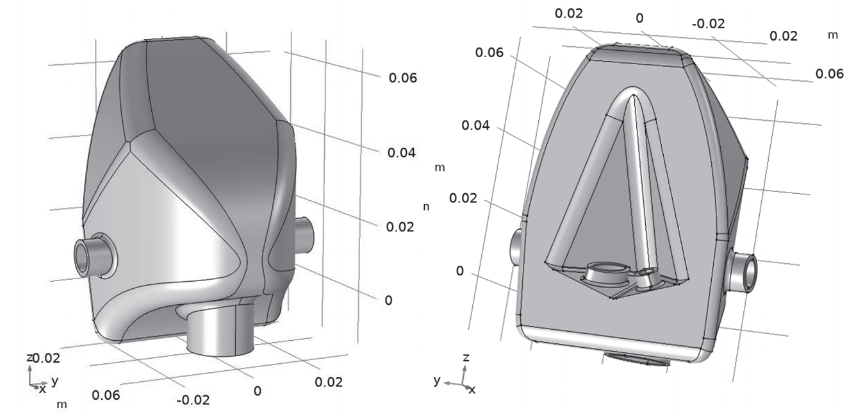

(*a*) (*b*)

Figure 220. Oxygen face mask model: (a) Imported geometry, (b) Capped faces.

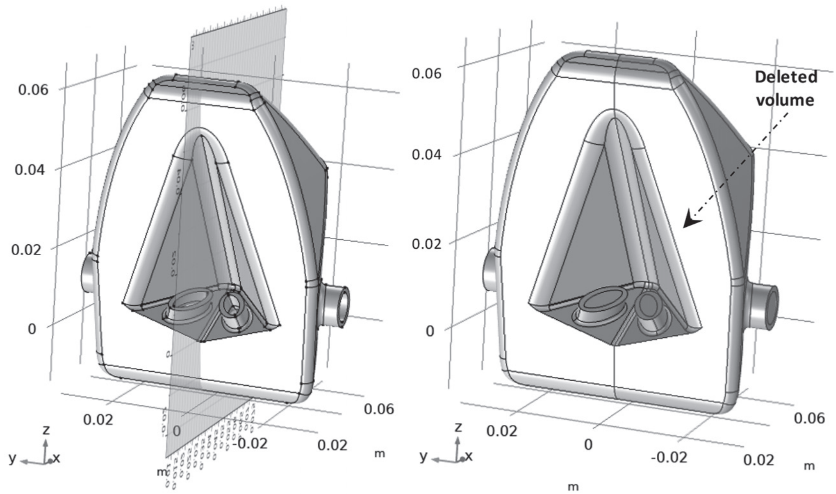

(*a*) (*b*)

Figure 221. Oxygen face mask model:
(a) *Work Plane* partitioning the model, (b) Partitioned model by symmetry.

have been combined to create composite surfaces (Figure 222). This way, when meshing the part, one does not need to account for the surfaces or edges that are too small to fit within the mesh size definitions. Although the latter does not necessarily jeopardize the solution or increase the convergence time, it is a good practice to help the program mesh the part with the least number of warning messages.

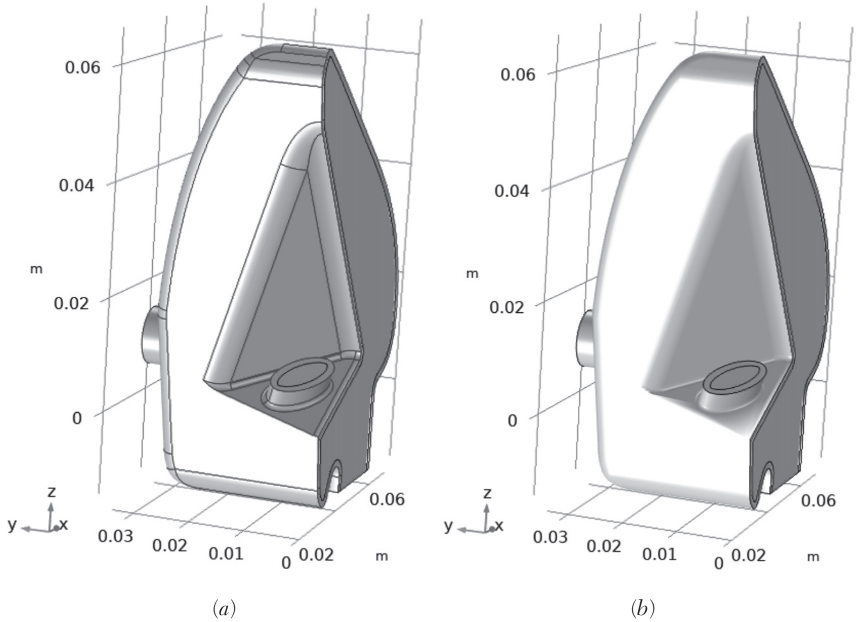

Figure 222. Oxygen face mask model: (a) Partitioned half model, (b) Composite surfaces.

10.3 Face Mask Materials, Physics, and Meshing

A face mask model tree is shown in Figure 223. Oxygen thermo-physical properties are presented in Figure 215; the flow patterns used have been shown in Figure 224. Parameters used for this part of the investigation are adopted from the male case study data presented in Figure 218. When solving a challenging problem such as those involving conjugate heat transfer, one way to improve the likelihood of a converging solution is to first obtain a solution for a hypothetical fluid with high viscosity and then use the results as the initial state for the model with the actual viscosity value.

The flow regime is also of great importance. Given that a laminar flow regime is used in this case study, care should be taken to ensure the flow *Reynolds number* is within the laminar flow regime. This dimensionless number, which is the ratio of the dynamic to viscous forces, is calculated for the openings, and the results are shown in Figure 225 as a function of the time and temperature for the atmospheric pressure (101.325 kPa). Transient breathing patterns for the inhale and exhale intervals for the mask inlet and outlet as well as the nostril are shown in Figure 226 and Figure 227. These are the model inputs. The flow rates (m^3/s) are divided by the inlet or outlet areas when calculating these patterns.

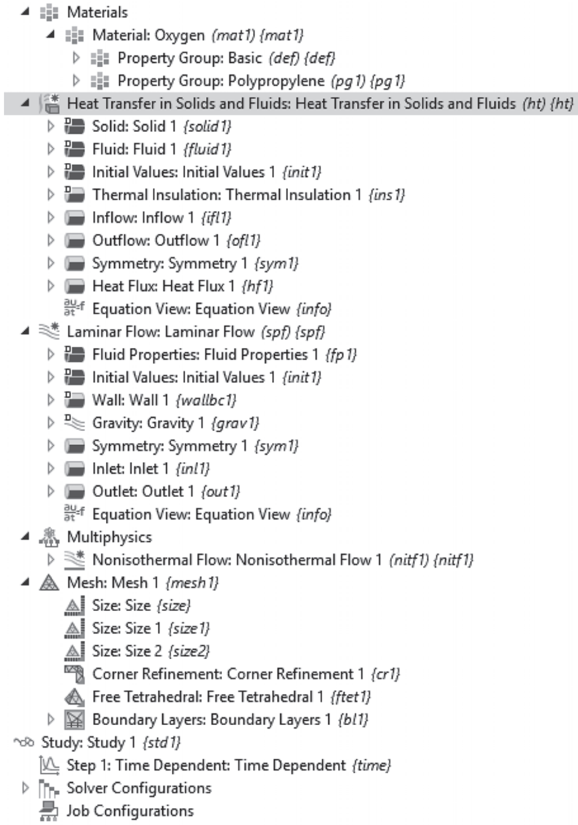

Figure 223. *Heat Transfer and Flow* physics tree for oxygen face mask study.

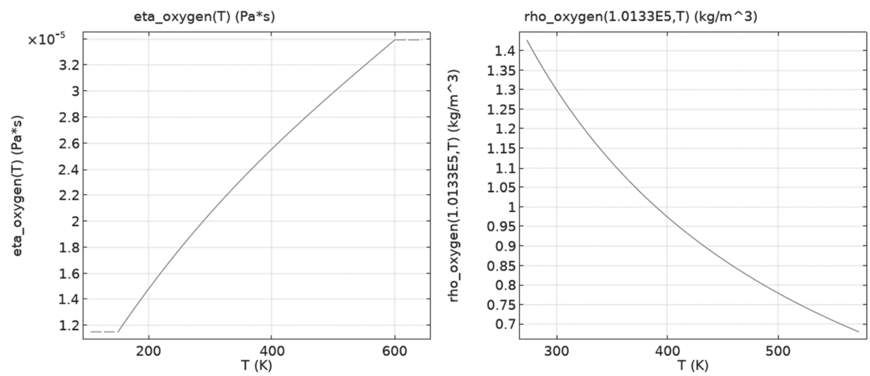

(*a*) (*b*)

Figure 224. Oxygen thermo-physical properties versus the temperature: (a) Dynamic viscosity, (b) Density.

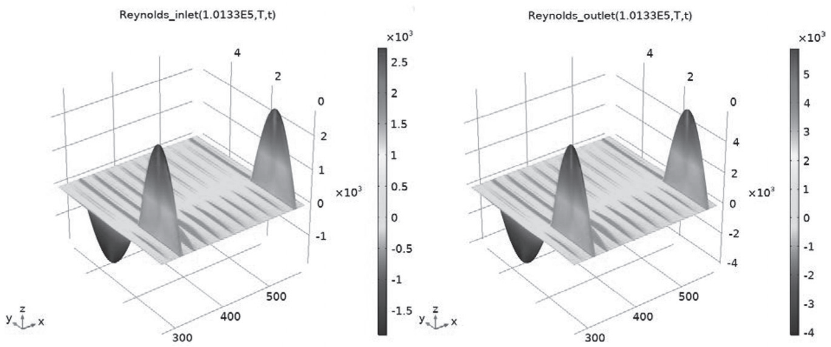

(*a*) (*b*)

Figure 225. Transient *Reynolds number* versus the temperature based on: (a) Inlet, (b) Outlet.

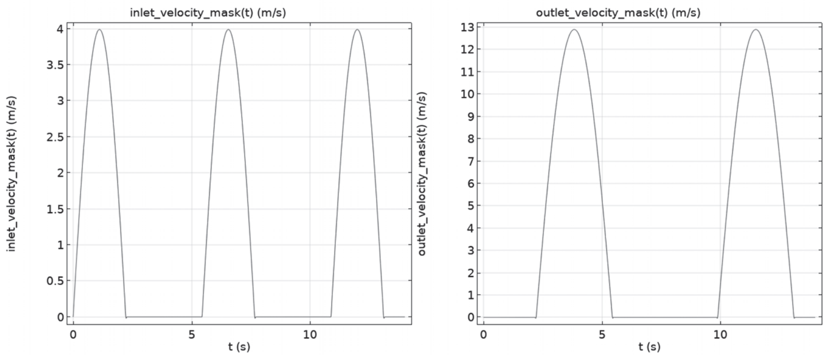

(*a*) (*b*)

Figure 226. Transient male breathing patterns modeled using *Analytic Functions*, inhale-exhale patterns combined with breathing in and out periods: (a) Inlet velocity, (b) Outlet velocity.

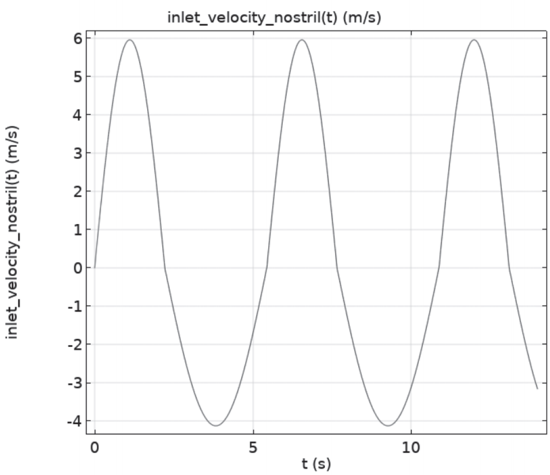

Figure 227. Transient male breathing patterns (inhale and exhale) from the nostril modeled using *Analytic Functions*.

The model is meshed by tetrahedral elements at *Fine* setting with a maximum element size of 0.0055 m for the fluid and 0.0069 m for the solid domains (Figure 228). The fluid enclosed within the propylene enclosure is meshed using fluid dynamics elements. If a user-defined meshing is selected, boundary elements can be selected for the fluid with the desired number of *Maximum element depth to process*.

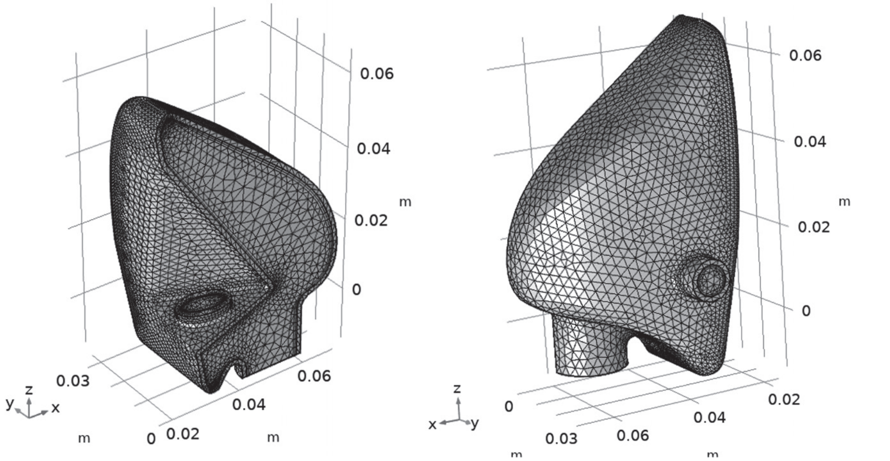

(*a*) (*b*)

Figure 228. Meshed oxygen face mask: (a) Back view, (b) Front view.

Another point of consideration when setting up the flow models with convergency difficulties is to ensure the pressure constraints are correctly applied. This measure is particularly helpful in symmetrical problems, and where there are openings (outlets) which direct the flow in or out of the domain. This pressure constraint point can be attached to any interior point, in contact with the fluid, on the symmetry plane, and at the opening or close to it. Note that where openings exist, assuming that the opening do not move and the flow is nonslip, flow wakes can occur at the openings or in their vicinity. This situation may happen even though the normal flow velocity is selected for the inflow or outflow conditions—the flow does not necessarily leave or enter the opening surface in a normal direction.

10.4 Face Mask Solution Results

The solution was carried out over a total of one breath period (5.44 s) to see the effect of repeated breathing cycles. The solution was run on a Windows 10 PC, with Intel Core i7-5820K CPU and 64 GB of RAM. It took about five days to compute the solution for this study, with the convergence tolerance of 0.01. The problem was solved in multiple steps: (1) heat transfer in solids and fluids model was first solved, by employing *User controlled*, *Initial expression*, *Zero solution* settings for *Initial values of variables solved for*; (2) the same procedure was conducted for the laminar flow model; and (3) the third analysis (*transient*) was performed in which the two physics were combined and solved under *Multiphysics* nodes with the initial conditions being selected as *User controlled*, *Initial expression*, *Study i* under *Initial values of variables solved for* node. *Study i* represents *Study* ID (number) to which the specific analysis is set (e.g., *Study 2—std2*). The three previously described steps were applied to the inhale and exhale models.

Note that in the inhale case, the ambient air enters the mask from the mask inlet as the person breathes in the air, and when exhale occurs, the air enters the mask from the nostril at the body temperature. During the exhale period, the mask inlet closes and the air exits the mask at the outlet, while during the inhale period, the mask outlet is closed. The nostril functions as both inlet and outlet, directing the air into and out of the mask. The inhale and exhale models are solved separately.

The fact that the boundary conditions change between the inhale and exhale periods poses a particular challenge in this solution and requires the use of a new solution setup approach. By selecting *Modify model configuration for study step*, it is possible to change the model physics between study steps. After making this selection, a setting window will be activated in which model physics can be turned on or off. For this solution, this allows activation and deactivation of certain boundary conditions during each step. Thus, the outlet can be defined to be closed during the inhale and open during the exhale. Boundary conditions on all the openings can be varied as needed using this approach.

The total breathing period for which the solution was obtained is 5.44 s. It comprises 2.22 s inhale and 3.22 s exhale intervals. The solution results are presented in Figure 229 through Figure 233. The plots for this case study show surface data (temperature, T), maximum and minimum temperature (T), streamline (velocity field—u,v,w), and arrow lines (velocity field—u,v,w). Arrows visible on the inlets and outlet show the flow direction and speed. Temperature contours for times of 0.5, 1, 1.5, and 2 s (during the inhale) for male settings are shown in Figure 229 and Figure 230. The flow patterns are shown with the blue arrow lines. Cooler air (blue) is seen coming into the inlet during the inhale. Circular flow patterns form shortly after initiation of the inhale. The exhale contour plots at 2.5 s to 5 s (0.5 s time interval) are seen in Figure 231 through Figure 233. Here the arrows at the outlet show the air coming out of the mask. One can also observe

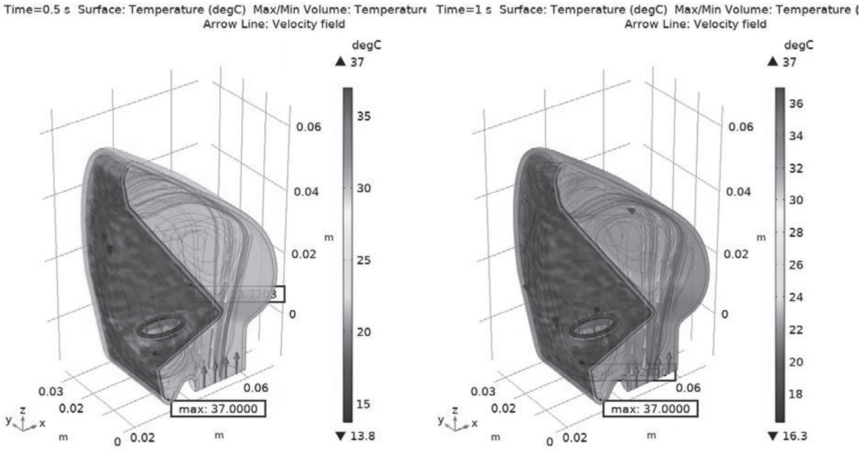

(*a*) (*b*)

Figure 229. Temperature contours, male case study, inhale: (a) t = 0.5 s, (b) t = 1.0 s.

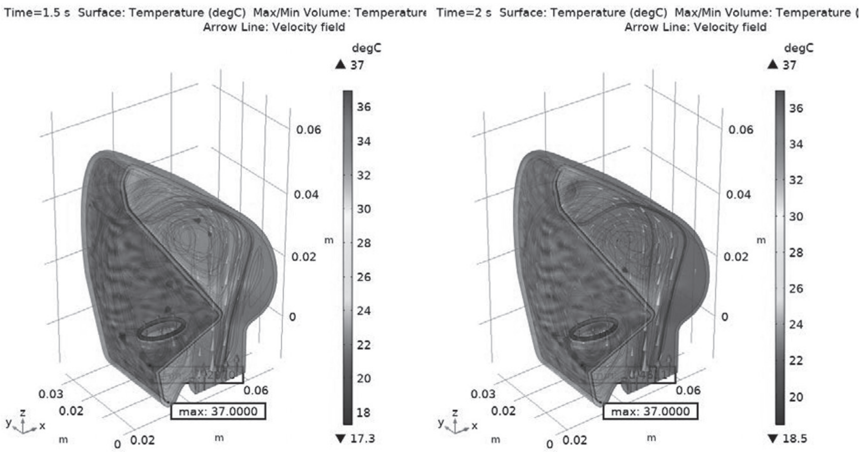

(*a*) (*b*)

Figure 230. Temperature contours, male case study, inhale: (a) t = 1.5 s, (b) t = 2.0 s.

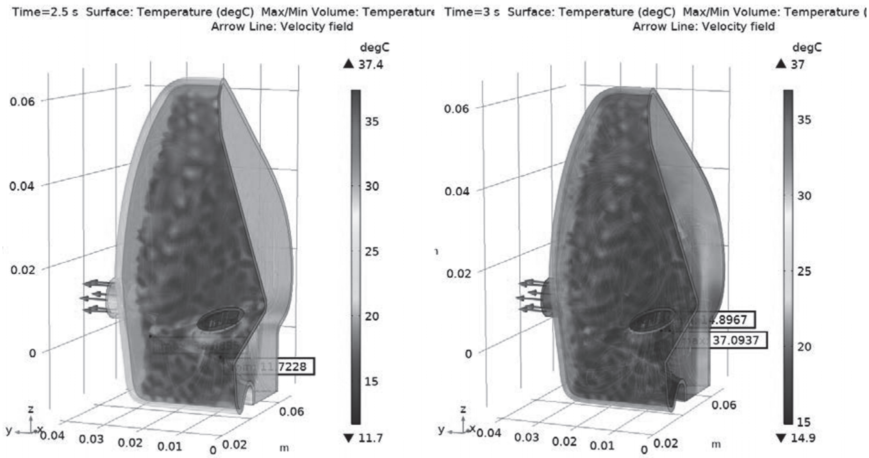

(*a*) (*b*)

Figure 231. Temperature contours, male case study, exhale: (a) t = 2.5 s, (b) t = 3 s.

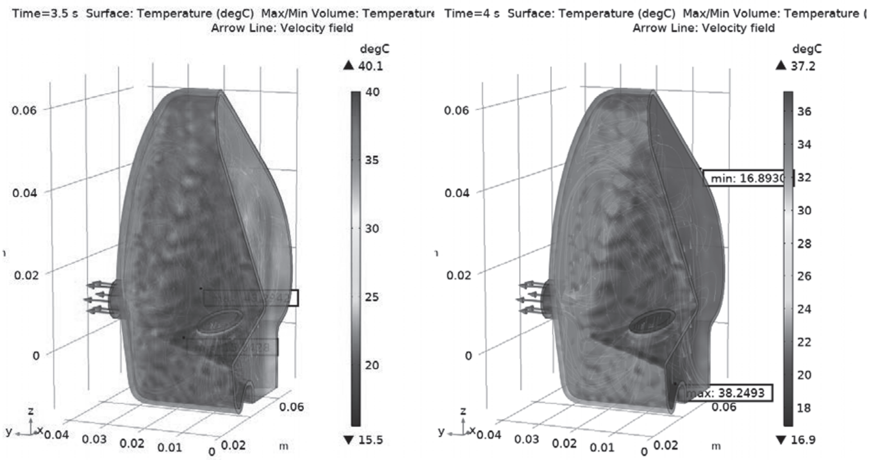

(*a*) (*b*)

Figure 232. Temperature contours, male case study, exhale: (a) t = 3.5 s, (b) t = 4 s.

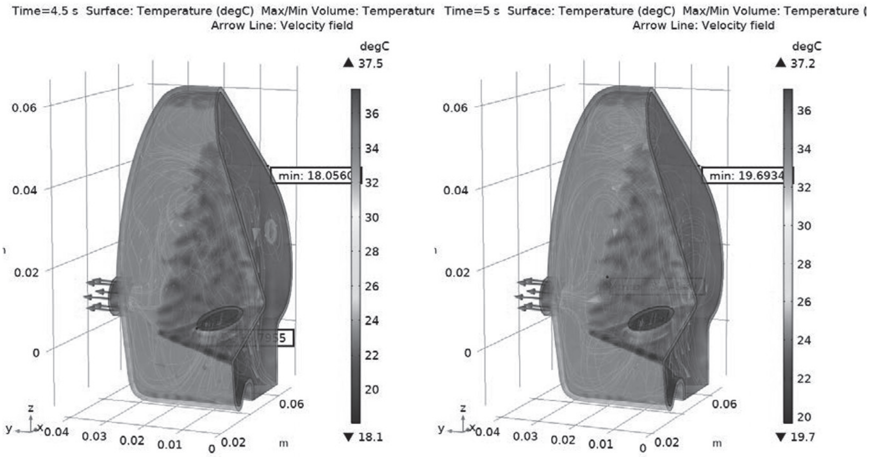

(*a*) (*b*)

Figure 233. Temperature contours, male case study, exhale: (a) t = 4.5 s, (b) t = 5.0 s.

how the mask is filling up with warm air as the exhale progresses—the mask interior color changes from blue to red as the time progresses.

Spatial temperature profiles are presented in Figure 235, Figure 237, and Figure 239 for the temperature distributions along the x- (Figure 234), y- (Figure 236), and z-coordinates (Figure 238). They are obtained by defining *Cut Lines 3D* as shown. Figure 241 shows the transient temperature for the location presented in Figure 240, defined by *Cut Point 3D*. The temperature distributions are presented for both inhale and exhale periods.

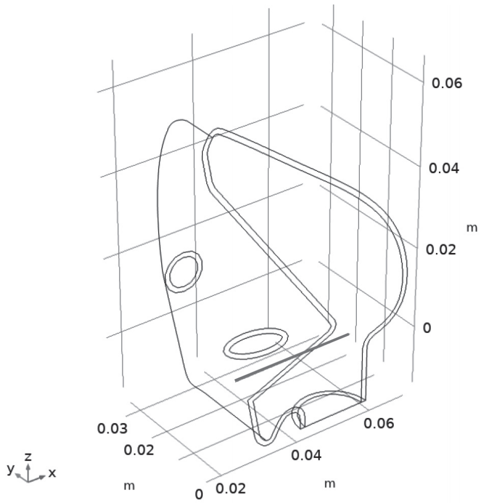

Figure 234. Face mask *Cut Line 3D* along the length (x-coordinate).

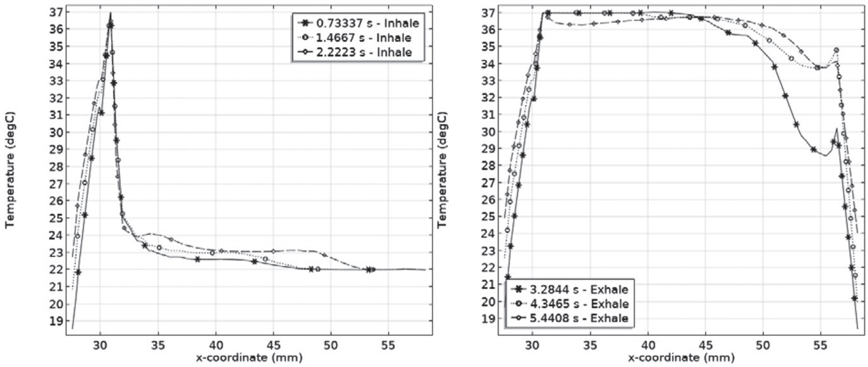

(a) (b)

Figure 235. Spatial temperature profiles at selected line versus the length for different time steps (*x*-coordinate), male case study: (a) Inhale, (b) Exhale.

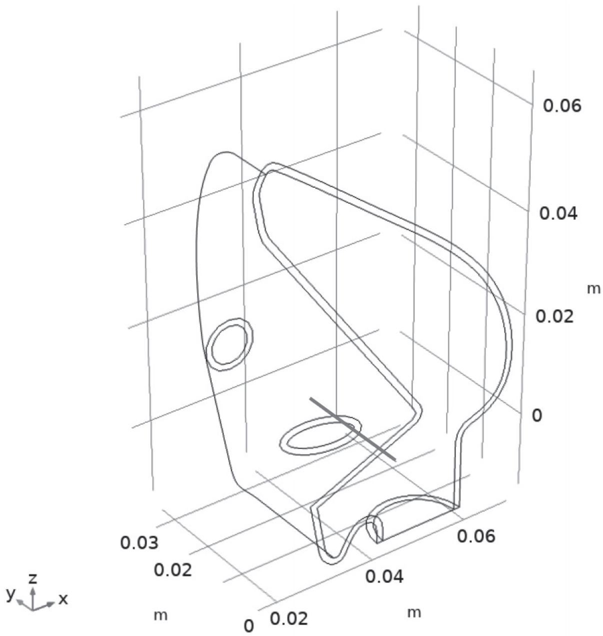

Figure 236. Face mask *Cut Line 3D* along the depth (*y*-coordinate).

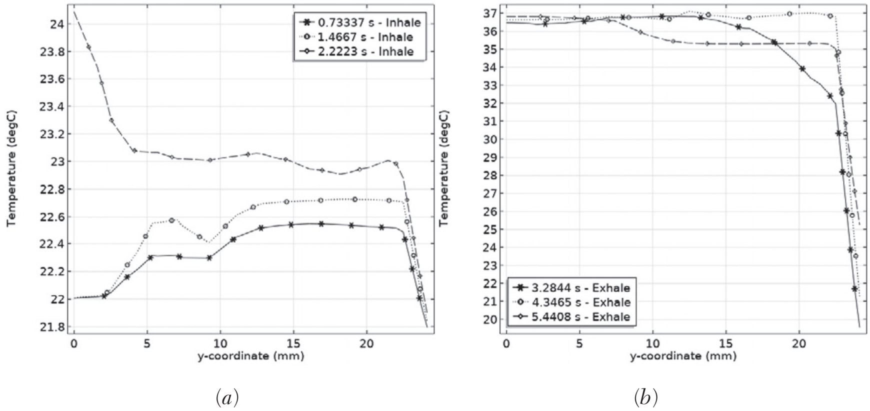

Figure 237. Spatial temperature profiles at selected line versus the depth for different time steps (*y*-coordinate), male case study: (a) Inhale, (b) Exhale.

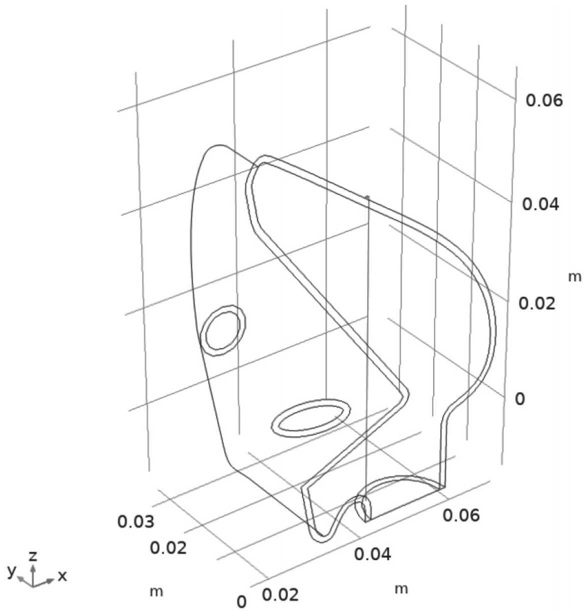

Figure 238. Face mask *Cut Line 3D* along the height (*z*-coordinate).

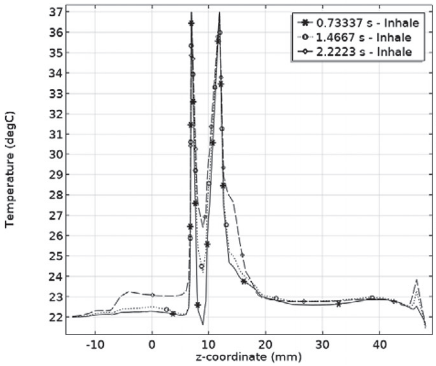

(a)

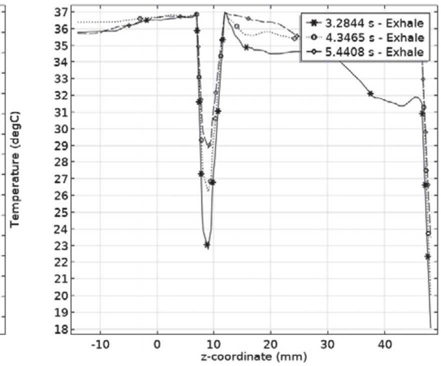

(b)

Figure 239. Spatial temperature profiles at selected line versus the height for different time steps (*z*-coordinate), male case study: (a) Inhale, (b) Exhale.

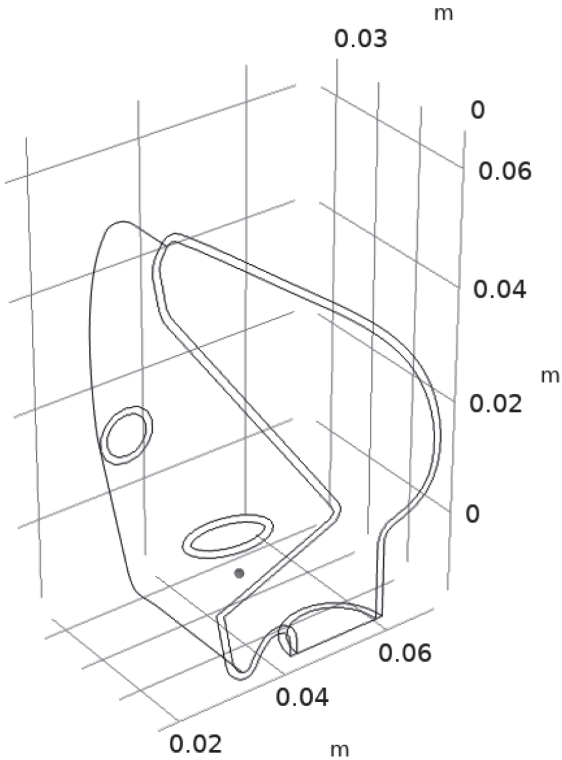

Figure 240. Face mask *Cut Point 3D*.

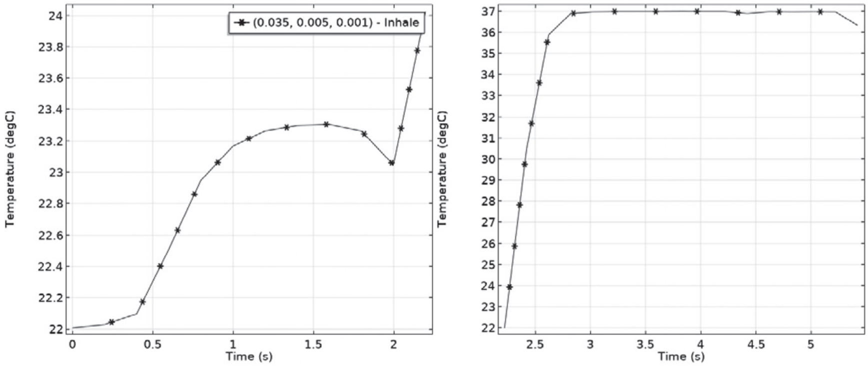

(*a*) (*b*)

Figure 241. Transient temperature profiles at selected point, male case study: (a) Inhale, (b) Exhale.

CHAPTER 11

Case Study 6—Solidified Molten Rock

Molten rock, also known as the *magma*, is generated by means of geothermal energy, finding its way to the surface of the Earth either by eruption or through crust rupture. The non-erupting flow cools down as lava moves and sweeps the ground. Along its path, materials with similar or lower flash points are molten and join the flow, while the ones with higher flash points survive. Flowing lava's internal temperature is on average 950 °C, and some molten flows can occupy areas over 500 km^2. As the lava flows, it cools, the exterior surface in contact with the air cooling faster than the flow's center. It can travel a long distance due to its reduction of viscosity and decrease of the flow shear strain over time as a result. This behavior is similar to what you may have experienced when dispensing ketchup. Recall that to get the ketchup to leave the bottle more easily, you should shake the bottle first. The lava flow eventually solidifies and forms magnetic rocks, also known as the *igneous rocks*. The degree of magnetism depends on the temperature at which the molten rock erupted and the temperature gradient while it cools. For example, for ultramafic lava, where maximum temperatures above 1,600 °C are observed, after solidification, rocks with maximum magnetic properties are observed; one reason could be due to the lack of polymerization at this extremely high temperature and high fluidity of the lava flow.

The glowing yellow and orange colors seen inside the flowing lava are due to the thermal radiation emitted from its center, temperature being the highest at the center. Formation of land on volcanic islands is one of the consequences of the lava flow as it falls into the surrounding sea, expanding the land—as is the case for the Big Island of Hawaii. Lava's chemical composition and temperature depend on the extraction layer from which lava exits the Earth. Lava's properties, in turn, affect how it interacts with its surroundings. Thus, there are different types of lavas, known as the *carbonatite*, *iron oxide*, *sulfur*, *and olivine nephelinite lavas*, named after their dominant element.

Thermo-physical as well as mechanical properties of lava, such as viscosity, are affected by the chemical composition, and viscosity determines the manner in which the lava flow spreads. This, in combination with the land slope, are the determining factors in lava formations and depositions. If they have low viscosity, the flow speed and the fluidity are higher, leading to formation of flat sheets of rocks after cooling; higher viscosity leads to slower flow and formation of dimpled lands with creases and rough or localized elevated rocks. As most of the Earth's surface is covered with water or ice, most volcanic eruptions occur either under the water or ice, expediting the magma's cooling process and therefore the formation of rocks, also known as the *pillow lavas*[133].

If the initial temperature of the magma embedded in the lava is uniform, one can model the stationary matter using the lumped capacity technique to obtain the transient temperature over time. For example, one can thus estimate the time it takes for the magma to cool to its solidification temperature. When it flows, the lava is exposed to another form of heat

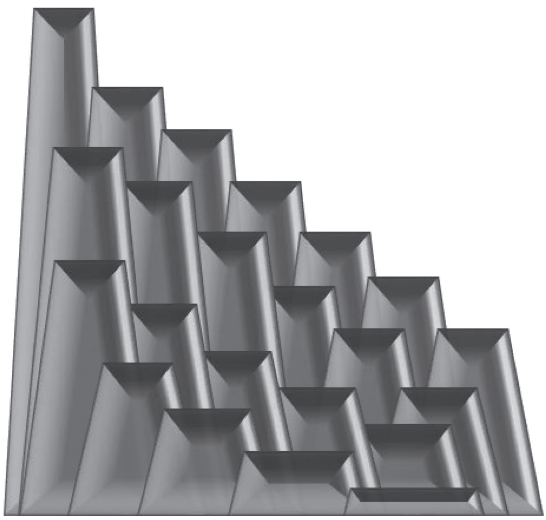

Figure 242. A model of solidified molten rock.

transfer, advection, due to the fluid bulk flow, and therefore the heat transfer regime is more efficient. The interior lava flow, being thermally insulated by the thick layer of the rock surrounding it, has a higher temperature and lower viscosity, and therefore moves faster than the upper layers; it effectively forms a tube over time, allowing the molten material to travel over long distances.

An example of a volcanic rock formation can be seen in the two famous paintings by Leonardo da Vinci known as the *Virgin (or Madonna) of the Rocks*. The first version (located in the Louvre Museum, Paris) depicts the position of Jesus versus Ariel, the angel, in an oblique fashion, with the angel pointing his finger at the child. The second version (located in the National Gallery, London) depicts Ariel looking in the distance with a dreamy eye, perhaps waiting for a miracle to happen. The plants, herbs and primrose, under Jesus' feet, with light falling from above, are beautifully depicted.

The formation of rocks shown indicates their volcanic origin, with the characteristic form produced as the moving lava cools down in stages. The part that is directly exposed to the air cools down and solidifies faster, while it takes some time for the central part to cool down. During this transient heat transfer, the volcanic rocks form layers—which is due to the temperature variations and cooling process from the exterior surfaces of the lava to the interior parts, with the interior parts cooling last. Therefore, longer structures are formed, as the interior parts are built upon the freshly provided molten flow of lava that continue to move along their path, decreasing their rate of cooling as they move forward. This rock variation, in its scientific fundamentals, its shape, perspective, and proportions, is meticulously depicted in these da Vinci works.

Solidification of the molten rock creates *igneous rocks*. It can either happen below the Earth, allowing for the gradual formation of large crystals during the slow cooling process, or during the eruption above the surface, where cooling happens quickly and smaller crystals are formed. The former method creates what are known as the *intrusive igneous rocks* while the latter one creates *extrusive igneous rocks*. Basalt, a fine-grained rock, which is the subject of this study, belongs to the latter group. Basalt forms most of the Earth's bedrock, and that includes areas in the oceans. The floods of basalt are under many land surfaces. Basalt can also be found on the Moon and Mars. Most of the volume under the Moon's surface, also known as the *lunar maria*, is occupied by a lava flow of basalt. It is believed that the impact of significant lunar events has caused the surface of the Moon to change. Scientists employ the density of the impact craters in order to identify the age of the *lunar maria*. Olympus Mons, the highest mountain on Mars and the largest volcano in the solar system, was formed from basaltic lavas.

Underwater convection currents can transport hot lava from under the ground (mantle). The diverging rock bed causes the rock flow, which is molten under the convection heat and change of pressure, to erupt and flow under the oceanic surfaces and crystallize into pillow-shaped rocks. This is a fissure eruption and most of such events are not visible to humans, being deep under the ocean. In Iceland, a mid-ocean ridge is above the sea, where its activities are visible. Oceanic hotspots are other locations in which basalt rocks are formed. Hawaii is formed by such activities, where a cluster of lava flows over the Earth's mantle. This is visible by the occasional hotspots seen on the Big Island of Hawaii. The eruption takes place from underground. If it continues, the created cone spreads to the surface of the Earth, generating land. The islands of Hawaii, which are about 300,000 to 600,000 years old, have been formed by such activities. It is hypothesized that only 100,000 years ago, the lava-formed land emerged above the oceanic surface. Continental events can also transport molten lava in large volumes to the Earth's surface by means of fissures or other openings. Colorado River Flood Basalts and Giant's Causeway in Ireland are examples of these [134].

Lava cooling starts from the surface until it gradually freezes and shrinks to form a solid structure. The interior is less exposed to the environment; therefore, it cools at a lower rate. Because of this temperature difference—which can be as low as 120 °C—solidified rock may shrink and eventually crack under the stress, forming hexagons within a period of ten to twenty years. This closely describes the process of formation of the land, where the Earth that is covered with the molten rock is cooled and frozen, forming solid rocks. How wide the formed columns of rock are depends on the cooling rate, which is affected by their proximity to the ambient.

Basalt can be used as a construction material; for that it is crushed into smaller pieces, where the particles then can be used to form tiles, asphalt pavement, and railroad track foundations. Basalt is a dark rock, which can change to a yellowish-brown color due to weathering; it is made of plagioclase and pyroxene minerals. The word itself is derived from Latin and means *very hard stone*. Depending on the elements existing in basalt, its color may vary, demonstrating the lighter ones due to feldspar and quartz or darker ones such as pyroxene and olivine. The lava reaching the Earth's surface at about 1,250 °C cools down quickly within hours or days. *'a'a* and *pahoehoe* are two Hawaiian terms used for the volcanic basalts. The former has rough surfaces formed by fast flowing lava (making barefoot people scream Ah! Ah! as they walk on its surface). The latter are smooth and glassy, looking like waves (or multiple ropes).

Energy density, which is specific heat multiplied by density, is a measure that is used to characterize how much heat can be retained within the volume of a material. Basalt is among the most heat-absorbing rocks, being placed after gypsum and soapstone. It releases this heat slowly, meaning that it has low thermal conductivity. This property is widely used for rock applications that are sensitive to heat, such as around the fireplace, cooktop, or in heated pavement systems. At temperatures below 300 °C, rock thermal conductivity decreases sharply as temperature increases. At temperatures above 300 °C, although some sources report a decrease of this property with an increase in temperature, others show the opposite trend. It is suspected that the latter case may be due to the radiative effects occurring at high temperatures. For this reason, measurements of the optical properties of a variety of minerals have been conducted, resulting in equivalent radiative thermal conductivity that depends on the extinction coefficient (e), refractive index (n), absolute temperature (T), and Stefan-Boltzmann constant (σ)—$K_{\text{rad}} = 16n^2\sigma T^3/3e$ [135].

For basalt rocks, the heat transfer coefficient (i.e., convection coefficient) is about 46.88 W/m^{2}K at 1,088 °C. Basalt melting temperature is between 984 and 1,260 °C, forming a temperature band of about 276 °C [136]. Magma formed from basalt is usually very dense, with density varying from 2,250 kg/m^3 to about 2,800 to 3,000 kg/m^3 [137]. Based on the literature data, temperature-dependent thermo-physical properties of basalt were adopted for this study. The temperature of magma is about 1,350 °C, crystallization temperature is about 1,200 °C, and the latent heat is on the order of 400 kJ/kg [138,139]. Solid magma shows a lower specific heat at constant pressure than the liquid one (1,000 J/kgK versus 1,400 J/kgK). Looking at the specific heat capacity curve, one notices the sharp increase and decrease of this property at the melting temperature [140,141].

11.1 Problem Definition

This study adds phase change to the model, allowing to demonstrate the use of this COMSOL Multiphysics feature. *Phase Change* is an option available under the material (liquid and solid) when setting up a fluid or *Solid-Fluid Heat Transfer* physics. It should also be noted that temperature-dependent heat capacity affects the thermal response of the system, and therefore its temperature-dependent expression should be included. When considering phase change, this option can be added to the fluid or solid physics by selecting *Phase Change Material* option. Under *Settings*, properties such as the number of *Phase Transitions* and *Phase Change* characteristics such as latent heat, melting temperature, and transition temperature interval between the two phases are identified. Note that the phase transition physics get activated as the solution approaches the melting point. At this stage, due to the rapid change of physical properties, the solution may face challenges that are to be addressed by adopting a gradual approach toward the melting point. Therefore, a transition interval is specified, which sets a temperature difference of about x (e.g., 100 °C) for the heating process. This dT (= x) then reduces to zero degrees in multiple steps, and the results of each solution are fed into the next solution as the initial conditions.

It is challenging to obtain solution convergence when solving a phase change problem; one approach to achieve such convergence is by defining a temperature difference (dT) and using *Auxiliary Sweep* feature (under *Study Extensions*) to introduce a value that is relatively large (e.g., 200 °C) and reduce it in multiple steps (e.g., increments of 0.5 dT) so that one reaches the melting point in multiple finite steps. The results of each temperature iteration step are then used as the input (initial conditions) to the next step. When displaying the results, it is also possible to assess the sensitivity of the solution (calculated temperature) to the identified temperature interval. This is achieved by selecting the temperature interval from the list of the solution variables.

There is another option available to improve accuracy of the solution. It is called *Adaptive Mesh Refinement*. When setting up this feature, the user may activate *Adaptation and Error Estimates* settings, selecting the last solution in order to use it as the input to the next one. The type of mesh adaptations available are *General modification*, *Rebuild mesh*, *Regular refinement*, and *Longest edge refinement*. These features define the method of mesh regeneration. This case study takes advantage of these techniques.

Parameters used in the analysis are presented in Figure 243. Thermo-physical properties of basalt rock from the Hawaiian islands are adopted in this study. Figure 244 shows the rock thermal conductivity versus the temperature. Rock's temperature-dependent heat capacity is presented in Figure 245 for temperatures up to 1,200 °C. Figure 246 presents the heat capacity for temperatures above 1,200 °C, where the rock is likely in the molten state. Melting temperature as a function of the depth from the ground surface is presented in Figure 247. This data is used when the molten phase portion is predicted. It is seen that with increasing depth, the melting temperature increases, starting from 1,100 °C at the surface to about 1,600 °C at a depth of 140 km. The convective heat transfer coefficient between the molten rock and its environment (the atmosphere) is *h_air* = 106.3 W/m^{2}K and between the molten and solid rocks is *h_melt* = 25 W/m^{2}K.

Settings

Parameters

Label: Parameters 1

Parameters

Name	Expression	Value	Description
A_mush	6e3[kg/(m^3*s)]	6000 kg/(m^3·s)	Volume force damping constant
Cp_l	1583[J/(kg*K)]	1583 J/(kg·K)	Heat capacity at constant pressure, solid phase, 1400
Cp_s	1065[J/(kg*K)]	1065 J/(kg·K)	Heat capacity at constant pressure, liquid phase, 1000
dH	400[kJ/kg]	4E5 J/kg	Latent heat of solidification
dT	30[K]	30 K	Temperature transition zone half width
eps_s	0.95	0.95	Surface emissivity, air exposure
epsilon	1e-3	0.001	Volume force damping constant
flow_rate	10[m^3/s]	10 m^3/s	flow rate
h_air	106.3244[W/(m^2*K)]	106.32 W/(m^2·K)	air convection coefficient
h_melt	25[W/(m^2*K)]	25 W/(m^2·K)	Heat transfer coefficient, brake ring
inlet_area	(pi*inlet_opening^2)/4	0.094705 m^2	inlet area
inlet_opening	0.34725[m]	0.34725 m	inlet opening
inlet_velocity	flow_rate/inlet_area	105.59 m/s	inlet velocity
P_exit	5[atm]	5.0663E5 Pa	exit pressure
T_inlet	1250[degC]	1523.2 K	Melt inlet temperature 1350
T_melt	1100[degC]	1373.2 K	Melting temperature 984-1260 degC
Tamb	45[degC]	318.15 K	ambient tempeature
Tinit	T_inlet-100[degC]	1150 K	initial tempeature
v_flow	(1.6)[mm/s]	0.0016 m/s	Casting speed

Figure 243. Parameters used for rock model study (global level).

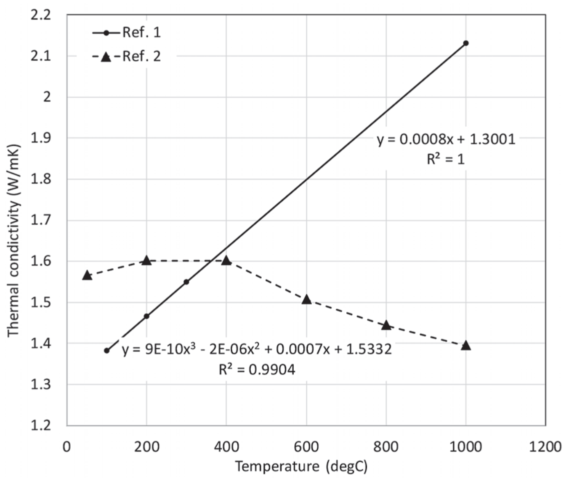

Figure 244. Basalt thermal conductivity versus the temperature, raw data from references 1 [142] and 2 [143].

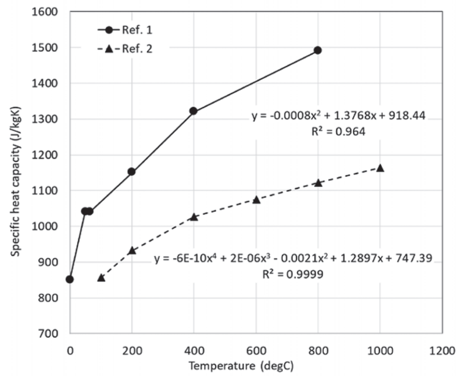

Figure 245. Basalt specific heat capacity versus the temperature, raw data taken from references 1 [142] and 2 [143].

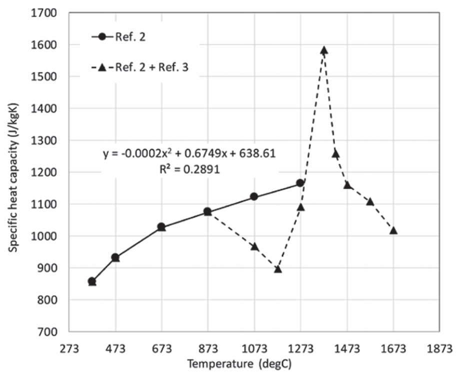

Figure 246. Basalt specific heat capacity versus the temperature, raw data taken from references 2 [143] and 3 [144].

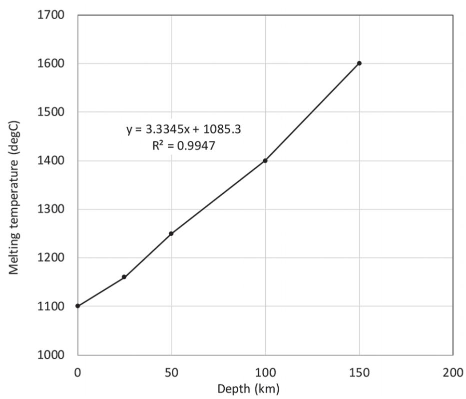

Figure 247. Basalt melting temperature versus the depth within the Earth, raw data taken from [145].

11.2 Molten Rock Model Setup

In this model, the rock and the embedded molten material are represented by a 2D axisymmetric model. This makes it possible to represent a 3D geometry using a 2D model, which requires less time and computational resources. The rock is modeled, given the selected geometry, as if the molten flow leaves the Earth at a certain depth, flows through its layers, and reaches the top surface. This molten rock then flows over the surface down to the bottom of the rock bed, cooling down along the way. In this model, *Solid-Fluid Heat Transfer* physics are adopted, with the boundary and flow conditions that are presented herein.

The model consists of the solid domain that is originally at a constant initial temperature. This temperature is below the melting point, therefore letting the rock remain at a solid state. The molten rock moving inside the solid channel causes the temperature of the surrounding environment to increase and, at the same time, the flow's temperature decreases as it moves inside the channel and eventually solidifies. The purpose of this case study is to show the phase change variables to depict the phase-related contour plots for the solid and molten rock and identify the molten zone and its extent in a stationary study.

Simplified solid-flow domains are presented in Figure 248a, with molten rock highlighted in purple. The axisymmetric border is shown in Figure 248b. Depending on the location, *Wall conditions* setting is either *Slip* (vertical inner wall) or *No slip* (horizontal and step surfaces) (Figure 249). The choice of the *Slip* (Figure 249a) versus the *No slip* (Figure 249b) condition depends on the nature of the moving fluid. The

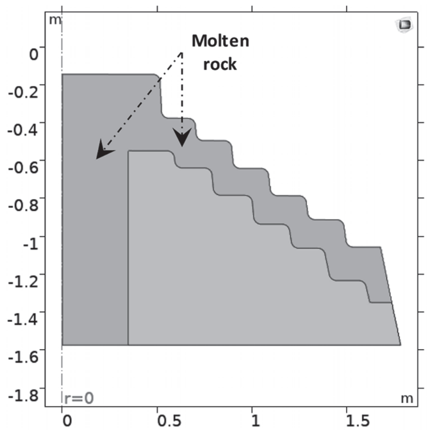

(*a*)

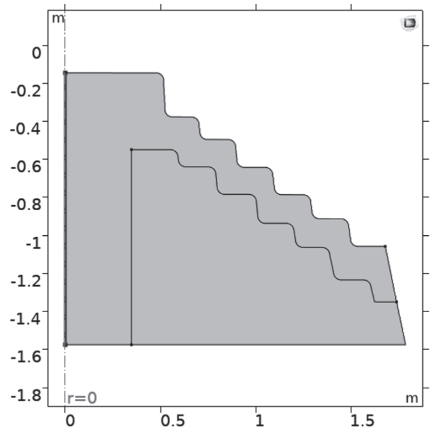

(*b*)

Figure 248. Solid and flow model domains: (a) Molten rock domain, (b) Axial symmetry boundary.

molten rock layers show this slip behavior. An additional benefit of setting a slip flow condition is that it facilitates convergence, which is beneficial given the geometry complexity.

Figure 250 shows the inlet (Figure 250a) and outlet (Figure 250b) boundaries by which the flow is transferred to or removed from the domain. Figure 251 shows the interfaces by which the molten rock is exchanging heat with the solid cooler rock channel walls by convection (Figure 251a) and its environment by radiation (Figure 251b).

Generally speaking, when using *Adaptive Mesh Refinement*, the problem can be divided into multiple regions or domains whose mesh distributions

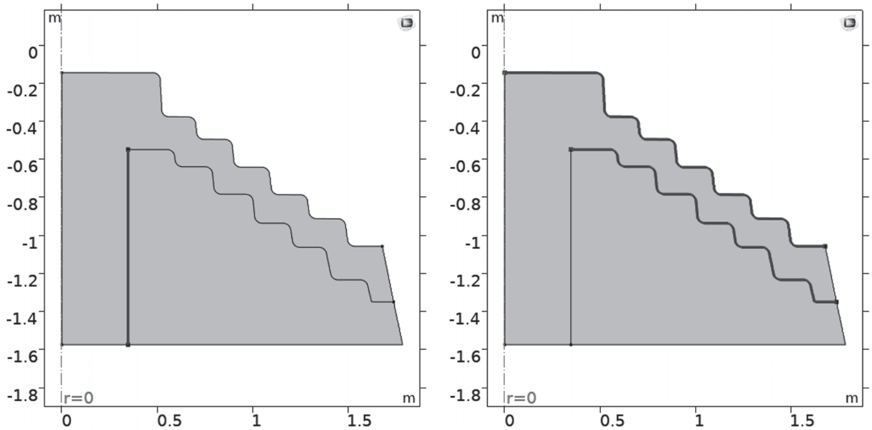

(*a*) (*b*)

Figure 249. Rock wall conditions: (a) *Slip*, (b) *No slip*.

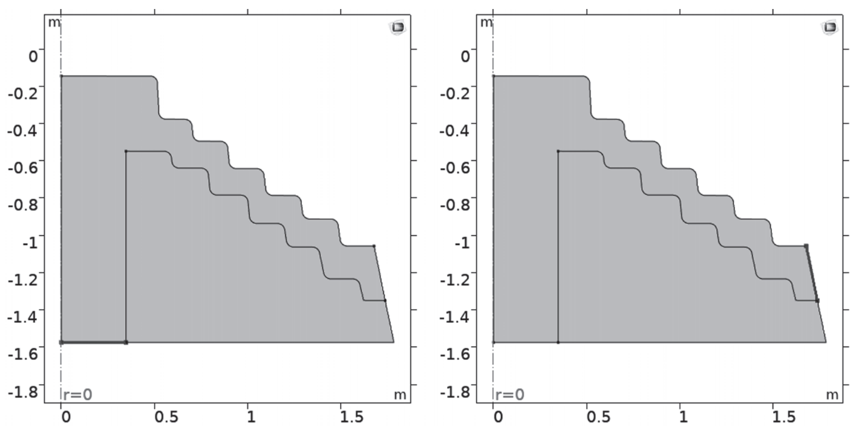

(*a*) (*b*)

Figure 250. Molten rock model: (a) Inlet (inflow), (b) Outlet (outflow).

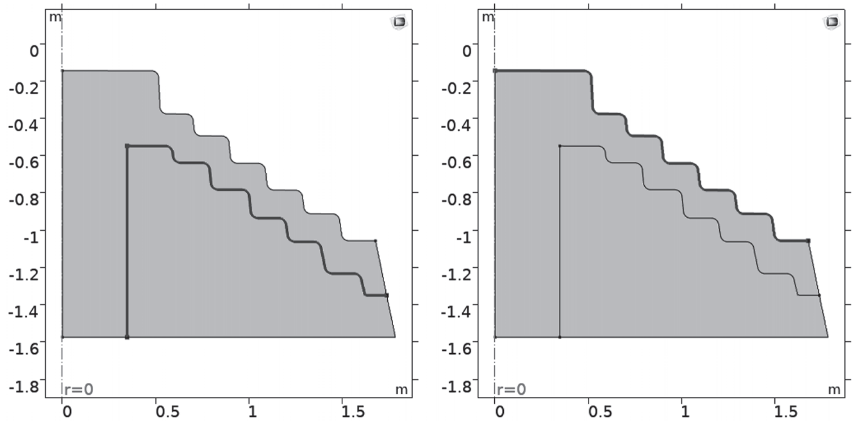

(a) (b)

Figure 251. Heat flux: (a) Molten rock-solid rock interface, (b) Molten rock-environment interface (surface-to-ambient radiation).

can be created as appropriate, given the physics and boundary conditions. In this scenario, the fluid region (where molten rock flows) is assumed as a single domain, where fluid dynamics physics and boundary conditions are applicable. Within this domain, boundary layer meshing is applied at the wall vicinity. Corner refinement options were included in the fluid domains. To mesh this geometry, free triangles were chosen and edges were refined.

11.3 Scenario 1—Molten Rock Solution Results

Results for two modeled scenarios are presented. For each scenario, properties are controlled using parameter *nn*, which is the convection heat transfer coefficient multiplier with the base conditions for the heat exchange between the molten rock and solid rock (*h_melt* = 25 W/m^{2}K) and molten rock and ambient (*h_air* = 106.3 W/m^{2}K). *Stationary Solver* settings are presented in Figure 252. To set up *Adaptive Mesh Refinement* feature, *Maximum number of adaptations* was set to 2 within *Adaptation and Error Estimates* option found under *Stationary Solver* settings. The surface-to-ambient radiation boundary condition is applied to the exterior surfaces exposed to the ambient with the emissivity coefficient of 0.95.

Pressure iso-contours are presented on Figure 253 along the *y-z* plane for *nn* = 1 (heat transfer coefficient multiplier). Temperature iso-contours are presented in Figure 254. The difference between the two scenarios is almost negligible—there are an equal number of isotherm contours (140) for both scenarios. Figure 255 presents the flow velocity contours for the convection coefficient presented in the caption. Figure 256 presents the

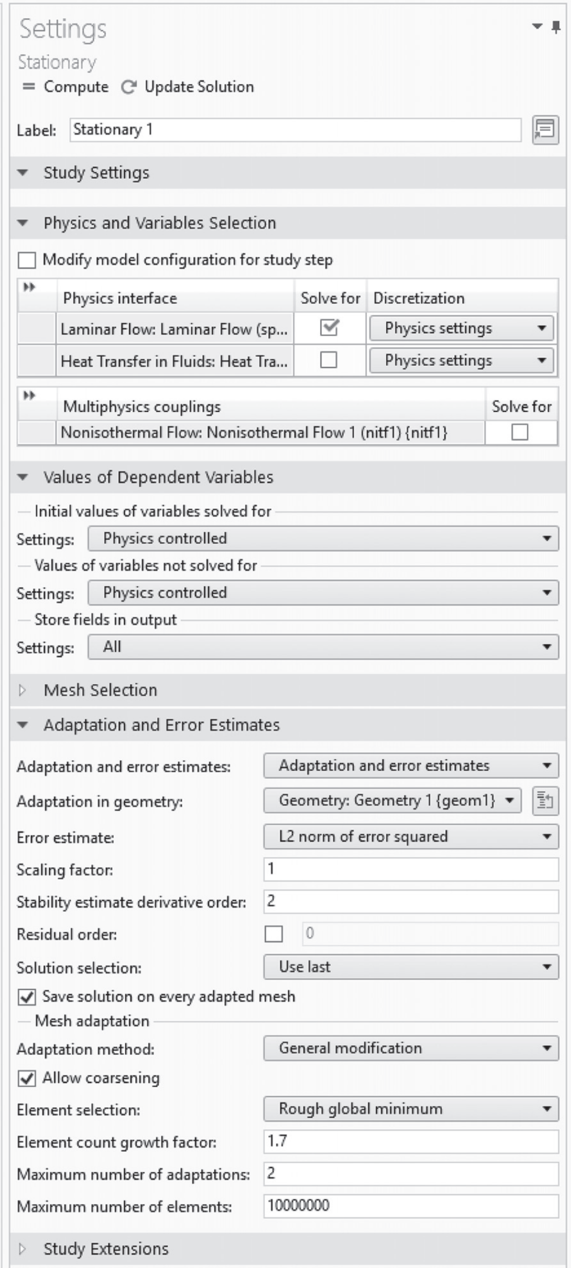

Figure 252. *Stationary Solver* settings for molten rock model.

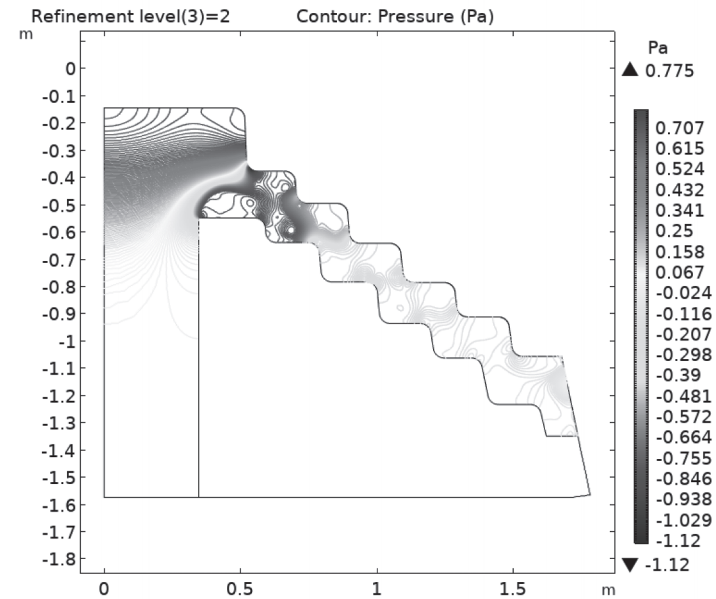

Figure 253. Pressure iso-contours (*y-z* plane), *nn* = 1 (*h_air* = 106.3 W/m^{2}K*, h_melt* = 25 W/m^{2}K).

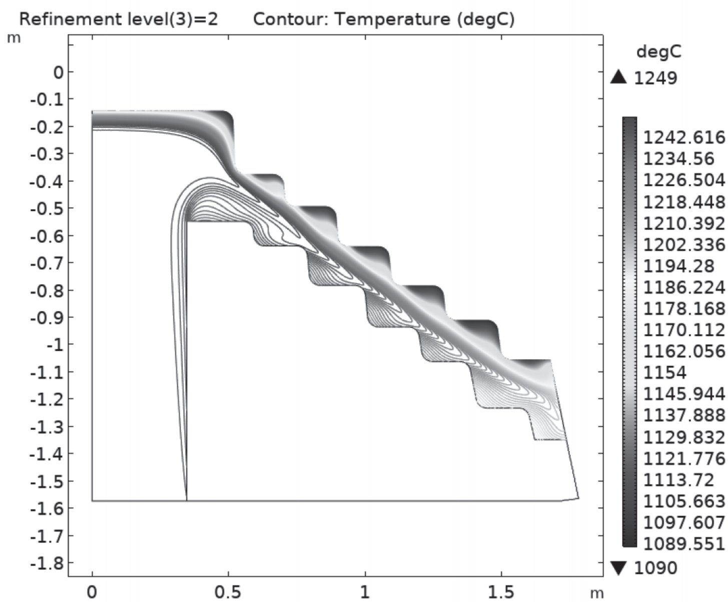

Figure 254. Temperature iso-contours (*y-z* plane), *nn* = 1 (*h_air* = 106.3 W/m^{2}K*, h_melt* = W/m^{2}K).

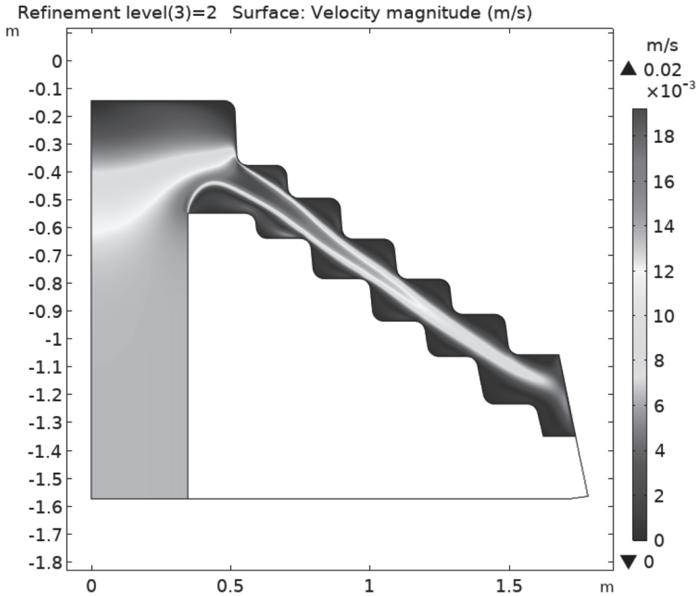

Figure 255. Surface flow velocity contours (*y-z* plane), *nn* = 1 (*h_air* = 106.3 W/m^{2}K, *h_melt* = 25 W/m^{2}K).

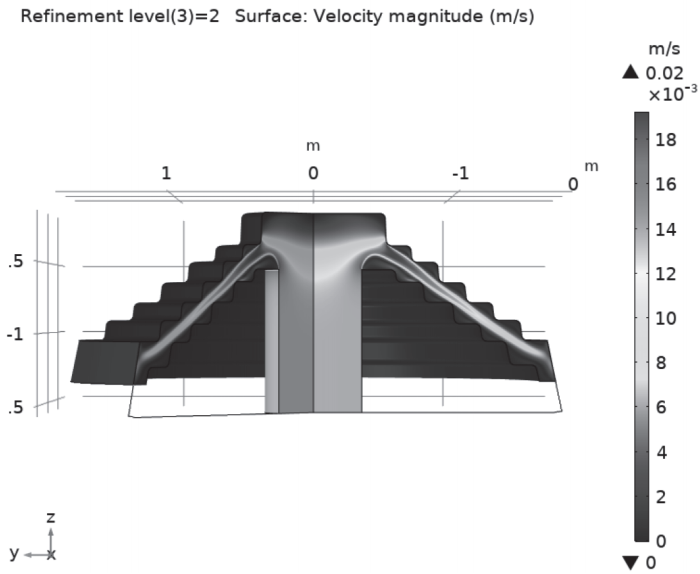

Figure 256. Surface flow velocity contours (*y-z* plane), *nn* = 1 (*h_air* = 106.3 W/m^{2}K, *h_melt* = 25 W/m^{2}K).

flow velocity for the 3D scenario at the isometric view but also for the *x-z* plane. It is seen that the temperature at the surfaces is lower than in the interior. Figure 257 presents the 2D temperature contours along the *y-z* plane and the 3D temperature contours for the high and low convection coefficients. Figure 258 presents the temperature contours for the *x-z* plane.

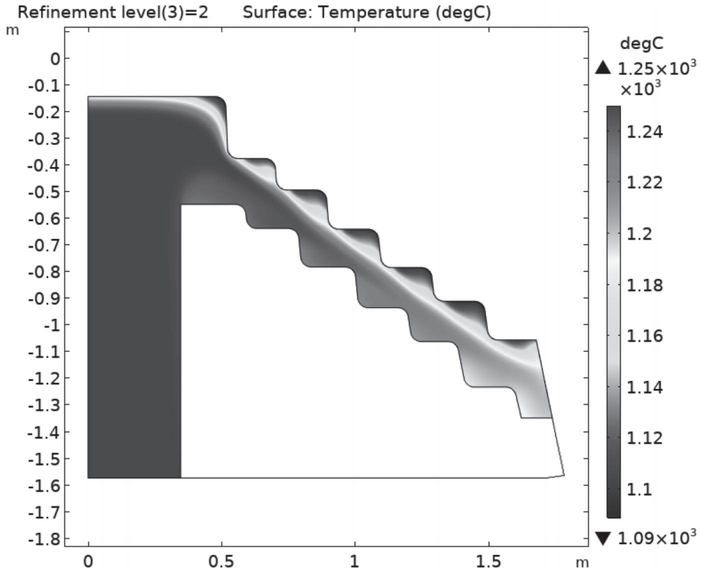

Figure 257. Surface temperature contours (*y-z* plane), *nn* = 1 (*h_air* = 106.3 W/m²K, *h_melt* = 25 W/m²K).

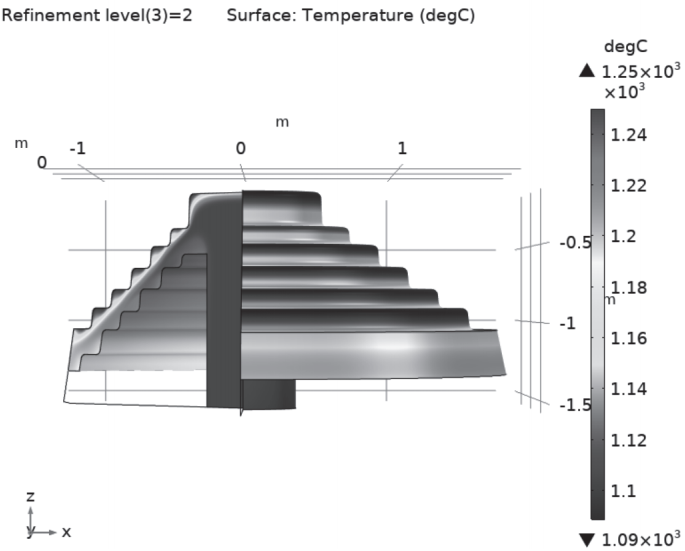

Figure 258. Surface temperature contours (*x-z* plane), *nn* = 1 (*h_air* = 106.3 W/m²K, *h_melt* = 25 W/m²K).

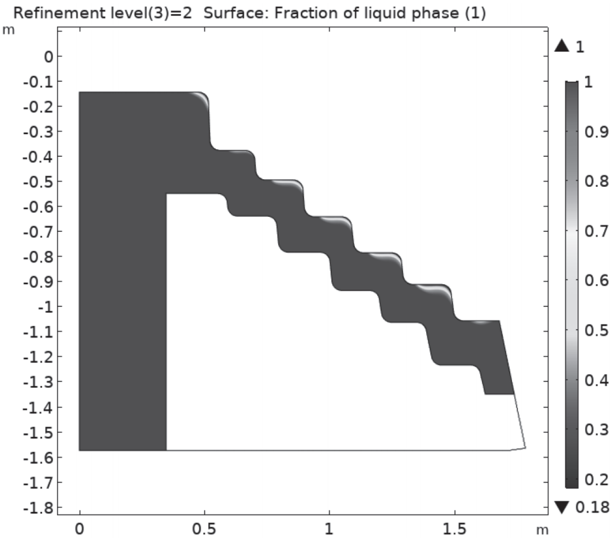

Figure 259. Surface fraction of liquid phase (*y-z* plane), *nn* = 1 (*h_air* = 106.3 W/m²K, *h_melt* = 25 W/m²K).

Figure 259 shows the molten phase fraction of the domain that remains after cooling has taken place in the stationary scenario. A red color corresponds to 100 percent liquid, while blue is a 100 percent solid phase. Most of the domain is still in a liquid state, with some transitioning to solid near the exterior boundaries. The fastest cooling is seen to happen on the protruding corners, where the molten material has the greatest exposure to the cooler environment.

Figure 260a and Figure 261a present the lines across which normal conductive heat fluxes are calculated for the selected domain. These fluxes describe the rate at which the heat is transferred across the interface between the molten and solid rocks. The one in Figure 260b shows the heat removed from the molten rock as it travels vertically toward the top. The plot in Figure 261b shows the heat removed toward the interior, as the molten rock flows down the "stairs." In both cases, these fluxes are plotted versus the z-coordinate. In Figure 260b, the flux is seen to decrease with increasing z values, as lava flows upward and cools, leading to a decreasing heat transfer rate to the surrounding rock. In Figure 261b, the lava flow is downward, and so the plot should be viewed from right to left. The lava is hottest on the right, closest to the top, and so the highest heat flux is seen there. The flux is seen to decrease more quickly from right to left, as there is greater heat loss here, with heat being lost both to the interior rock and to the exterior air.

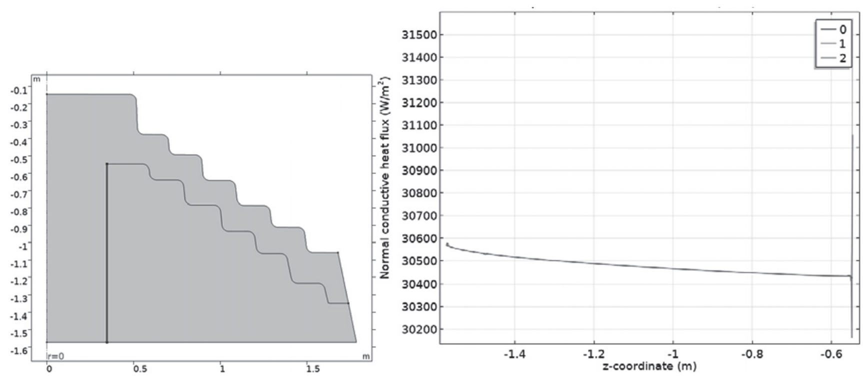

(*a*) (*b*)

Figure 260. Normal spatial conductive heat flux (*z*-coordinate), *nn* = 1 (*h_air* = 106.3 W/m^{2}K*, h_melt* = 25 W/m^{2}K: (a) Location, (b) Magnitude.

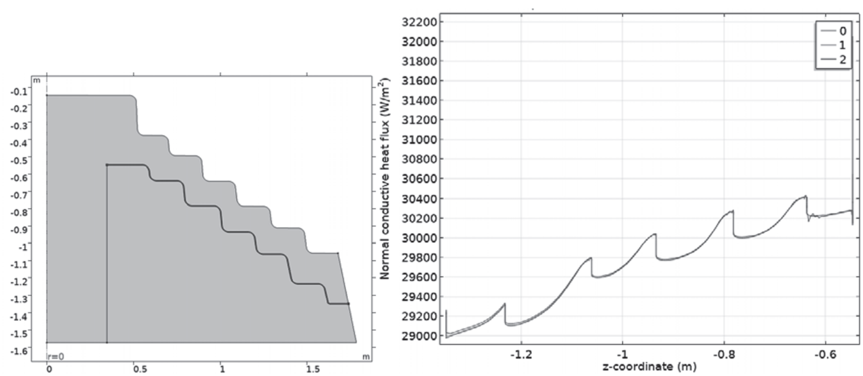

(*a*) (*b*)

Figure 261. Normal spatial conductive heat flux (*z*-coordinate), *nn* = 1 (*h_air* = 106.3 W/m^{2}K*, h_melt* = 25 W/m^{2}K: (a) Location, (b) Magnitude.

The numbers 0, 1, 2 displayed in the legend in the top-right corner of the plots indicate that the associated plots are from the corresponding mesh refinement steps. To obtain the normal conductive heat flux plots such as these, one needs to select for plotting the variable (*ht.ndflux*) from the variables offered by COMSOL Multiphysics *y-Axis Data* (*Expression*) and also can be found among *Variables* under *Equation View*, along with its other settings (identifiers) such as *Expression* (*0.5*(ht.ndflux_d-ht.ndflux_u)*), *Unit* (W/m^2), *Description* (*Normal conductive heat flux*), and *Selection* (Boundary 1-3, 6-7).

11.4 Scenario 2—Varying Molten Temperature

Results for additional runs are presented for two different melting temperatures (984 and 1,150 °C), given the same inlet, ambient, and initial temperatures. The main difference seen in the temperature contours (Figure 262) is the temperature variation that is more significant for the second scenario, where the melting temperature is closer to the inlet temperature. This means that not all the liquid remains in the molten state and that it mainly solidifies at the interface between the liquid and the adjoining environment. Figure 263 is the temperature contour for the *x-z* plane. Figure 264 is the molten fraction content for the two scenarios. It is seen that the molten fraction is at a maximum (1.0) for the lower assumed

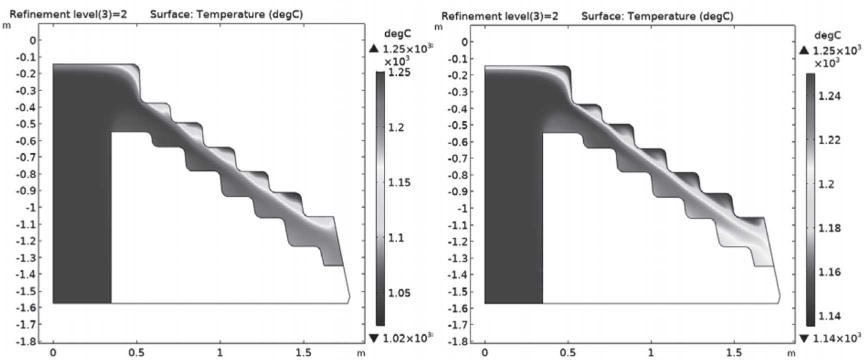

(*a*) (*b*)

Figure 262. Surface temperature contours (y-*z* plane), *nn* = 1 (*h_air* = 106.3 W/m²K, *h_melt* = 25 W/m²K): (a) T_m = 984 °C, (b) T_m = 1,150 °C.

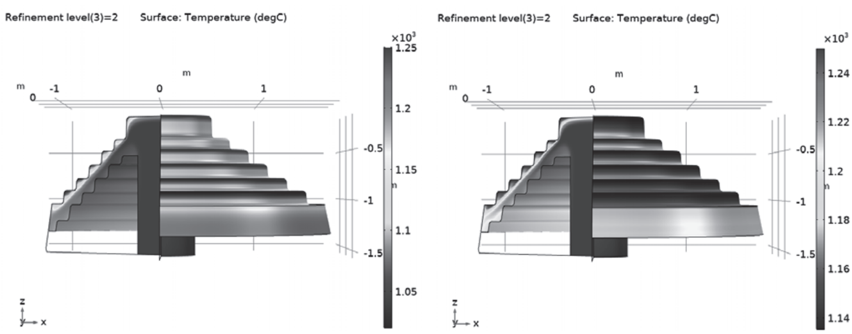

(*a*) (*b*)

Figure 263. Surface temperature contours (*x-z* plane), *nn* = 1 (*h_air* = 106.3 W/m²K, *h_melt* = 25 W/m²K): (a) T_m = 984 °C, (b) T_m = 1,150 °C.

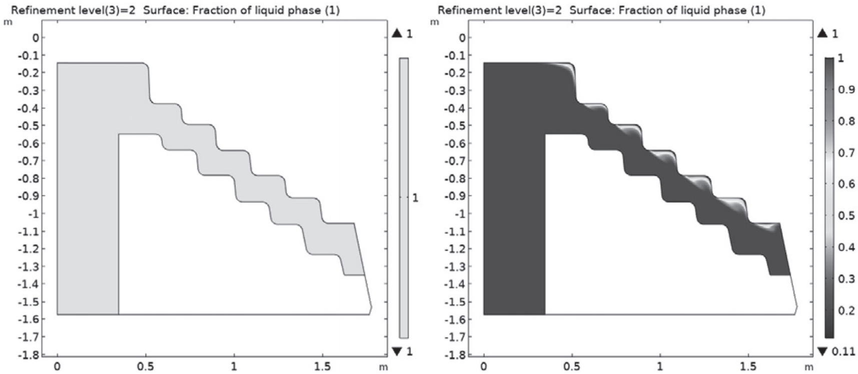

(*a*) (*b*)

Figure 264. Surface fraction of liquid phase (*y-z* plane), *nn* = 1 (*h_air* = 106.3 W/m^{2}K, *h_melt* = 25 W/m^{2}K): (a) T_m = 984 °C, (b) T_m = 1,150 °C.

melting temperature; a setting of a higher melting temperature results in the reduced molten zone seen in the image on the right.

Stationary Solver settings may slightly vary from those of Figure 252, which is to select the method of input variable selection; for example, the scholar may decide to take a multistep approach to problem solving, using the results from the previous step as the initial value to the next step.

CHAPTER 12

CASE STUDY 7—ROTINI FIN, A FIN WITH A TWIST

Rotini pastas are short and are corkscrew shaped. *Rotini* is an Italian term meaning *small wheels*. It is not only a shape that is geometrically interesting with its twists and turns, but it also works well as a pasta, with its large surface area taking up all that sauce. If an observant reader ever made a rotini pasta, they would soon learn that these pasta shapes cool faster than other types such as spaghetti (the long stranded thin ones) [146]. The author believes that this fast cooling must be due to the very good heat dissipation properties, which can be explained by the rotini's large surface area. This hypothesis is investigated in this case study. A comparison is then made with a straight slab to examine the effect of their shape difference.

12.1 Problem Definition

The rotini pasta piece can be considered as a type of fin structure. Fins are extended surfaces expected to transfer heat from their base, and therefore base temperature can be thermally managed (i.e., kept within an acceptable range), depending on the fin thermal efficiency. The 3D rotini fin model employed in this study is shown in Figure 265a. In addition to the rotini fin itself, it includes a vertical block on one end representing a wall to which the fin attaches. To create this complex 3D geometry, a dedicated third-party CAD tool (Solid Edge) was employed. The fin is 100 mm long and its cross section can be inscribed in a 10 mm-diameter circle (Figure 265b). The 3D geometry of the model was obtained by combining components imported from the CAD tool (the rotini) with those created internally in COMSOL

Multiphysics (the block). All fins in this study are made of aluminum with the properties shown in Figure 266. The geometrical and heat transfer model parameters are shown in Figure 267.

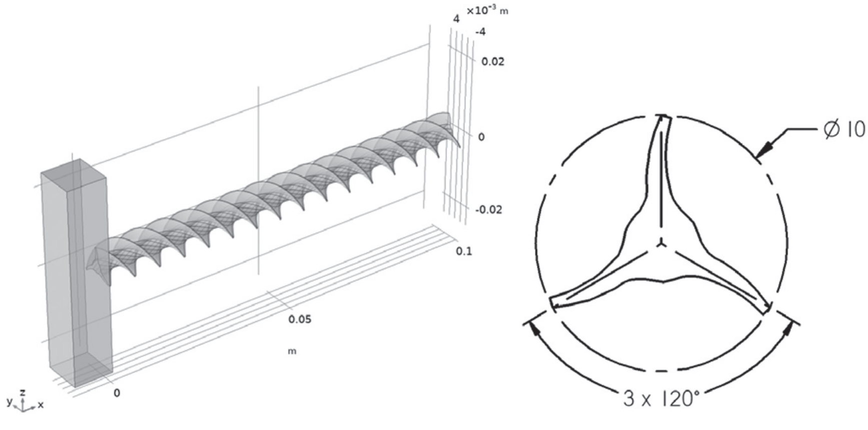

(*a*) (*b*)

Figure 265. Rotini fin geometry (a) COMSOL Multiphysics model, (b) Cross section (dimensions in mm, created in Solid Edge).

Material: Material: Aluminum Solid (mat5) {mat5}

Material Contents

	Property	Variable	Value	Unit	Property group
☑	Heat capacity at constant pressure	Cp	Cp_s	J/(kg·K)	Basic
☑	Thermal conductivity	k_iso ; kii = k_iso, kij = 0	238[W/(m*K)]	W/(m·K)	Basic
☑	Density	rho	2700[kg/m^3]	kg/m³	Basic
	Relative permeability	mur_iso ; murii = mur_iso, murij = 0	1	1	Basic
	Electrical conductivity	sigma_iso ; sigmaii = sigma_iso, sigmaij = 0	3.774e7[S/m]	S/m	Basic
	Relative permittivity	epsilonr_iso ; epsilonrii = epsilonr_iso, epsilonrij = 0	1	1	Basic
	Coefficient of thermal expansion	alpha_iso ; alphaii = alpha_iso, alphaij = 0	23e-6[1/K]	1/K	Basic
	Young's modulus	E	70e9[Pa]	Pa	Young's modulus and Poisson's ratio
	Poisson's ratio	nu	0.33	1	Young's modulus and Poisson's ratio
	Murnaghan third-order elastic moduli	l	-2.5e11[Pa]	N/m²	Murnaghan
	Murnaghan third-order elastic moduli	m	-3.3e11[Pa]	N/m²	Murnaghan

Figure 266. Aluminum material properties.

As was pointed out in Section 4.2 on geometry creation in FEM, one should strive to take advantage of any symmetry to reduce the modeled geometry size and consequently reduce the required computational resources. Later on in this study, the rotini fin is compared to a simpler fin shape, one with a circular cross section. While the cylindrical fin geometry presented herein is symmetric about the two planes, the rotini fin is not truly symmetric about any plane. However, one may hypothesize that, for the purposes of heat transfer analysis, the key factors that affect it are the volume of the part and its surface area. Thus, an astute analyst may test the idea of dividing the rotini fin into two halves with an *x-z* plane and checking whether results comparable to the full model solution can be obtained.

Settings
Parameters

Label: Parameters 1

▾ Parameters

Name	Expression	Value	Description
L	0.1[m]	0.1 m	fin wall length
th1	0.01[m]	0.01 m	wall width
th2	th1	0.01 m	wall depth
height	L/2	0.05 m	wall height
mesh_size	0.04[m]	0.04 m	mesh size
h_air	(n*5)[W/(m^2*K)]	5 W/(m²·K)	convection air coefficient
T_base	(n*100)[degC]	373.15 K	base temperature
Tinit	20[degC]	293.15 K	initial temperature
Tamb	25[degC]	298.15 K	ambient temperature
n	1	1	multiplier
time	60*10[s]	600 s	exposure time
P_atm	1[atm]	1.0133E5 Pa	initial pressure
emissivity	0.3	0.3	aluminum (rough) emissivity
T_m	660.3[degC]	933.45 K	melting temperature
dT	10[K]	10 K	temperature difference
dH	398[kJ/kg]	3.98E5 J/kg	latent heat
Cp_l	1.18[kJ/(kg*degC)]	1180 J/(kg·K)	heat capacity of aluminum liquid
Cp_s	0.91[kJ/(kg*degC)]	910 J/(kg·K)	heat capacity of aluminum solid
HG	(nn*10)[W]	10 W	internal heat source
rotini_volume	1.49E-6[m^3]	1.49E-6 m³	rotini fin volume
rotini_area	0.0037549[m^2]	0.0037549 m²	rotini fin area
cylinder_volume	rotini_volume	1.49E-6 m³	cylinder volume
cylinder_area	rotini_area	0.0037549 m²	cylinder area
cylinder_radius	(cylinder_volume/(pi*L))^0.5	0.0021778 m	cylinder radius
RH	0.54	0.54	
wind	3[m/s]	3 m/s	wind velocity
nn	1	1	multiplier

Figure 267. Parameters used for rotini fin study (global level).

If this proves to be the case, and if one needs to do multiple solutions with varying parameters, one can then shorten the solution time by working with only half of the geometry. For the heat transfer analysis presented here, a full-size fin has been used. The author encourages the reader to compare the results of the half-fin with those of the full model to investigate the previously described hypothesis.

Figure 268 presents the mesh for the finalized geometry. Tetrahedral mesh elements were employed to mesh the fin and wall; each was selected as separate domain so that the element size can be individually controlled (4,534 for the fin versus the 1,196 for the wall). Figure 269 and Figure 270

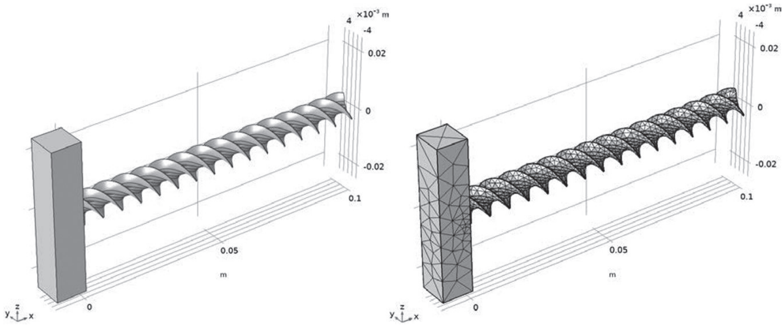

(*a*) (*b*)

Figure 268. Rotini fin: (a) Geometry, (b) Meshed geometry.

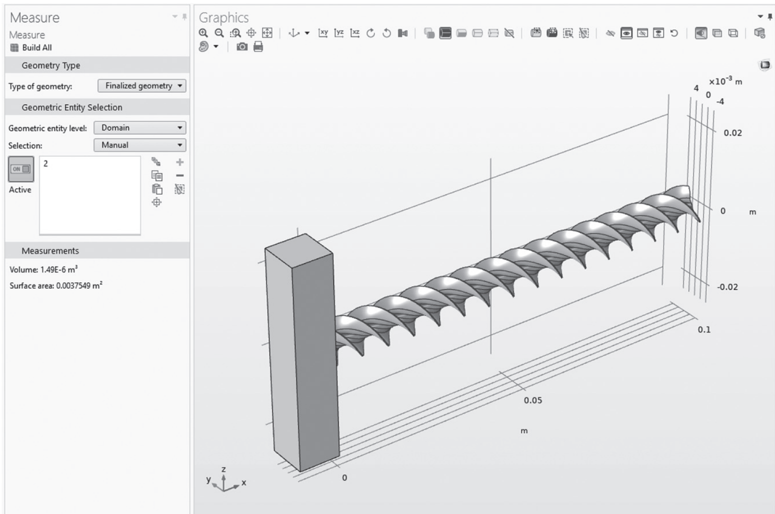

Figure 269. Measuring volume for rotini fin.

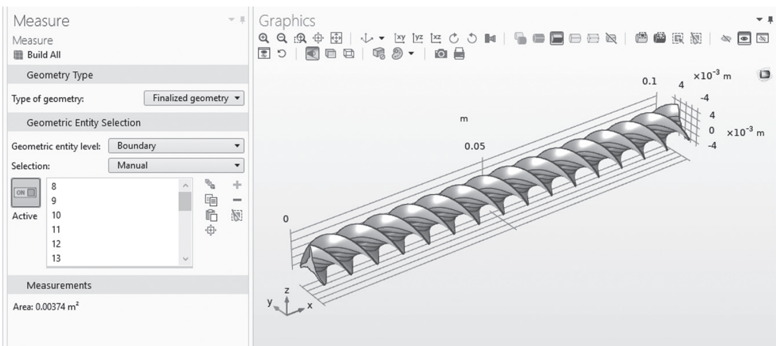

Figure 270. Measuring convective area for rotini fin.

show volume and surface area measurements for the full-size rotini fin. Figure 271 shows *Ambient Thermal Properties*, identifying the temperature and the atmospheric conditions, relative humidity, wind velocity, and normal beam irradiance; however, only the ambient temperature is used for this solution. Figure 272, Figure 273, and Figure 274 present the locations (planes, lines, and point) at which the spatial and temporal temperature profiles are presented. Figure 274 shows the points at which temporal temperature profiles are presented.

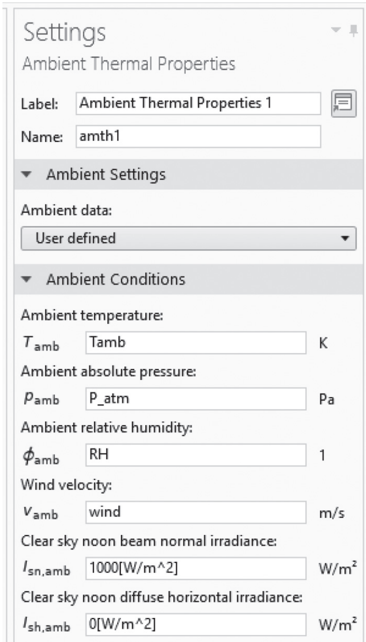

Figure 271. Ambient thermal properties.

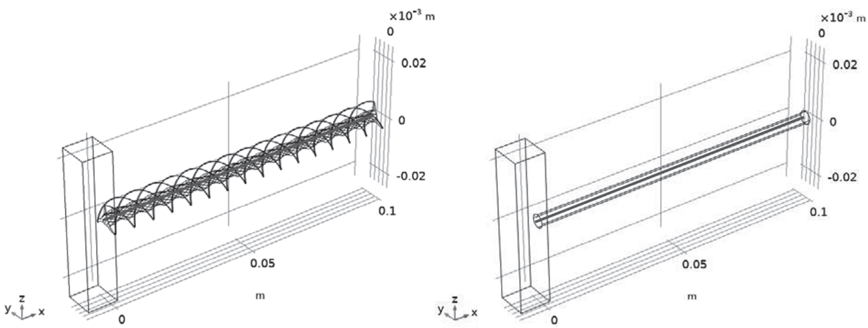

(*a*) (*b*)

Figure 272. *Cut Lines 3D* along the length (*x*-coordinate): (a) Rotini fin, (b) Cylindrical fin.

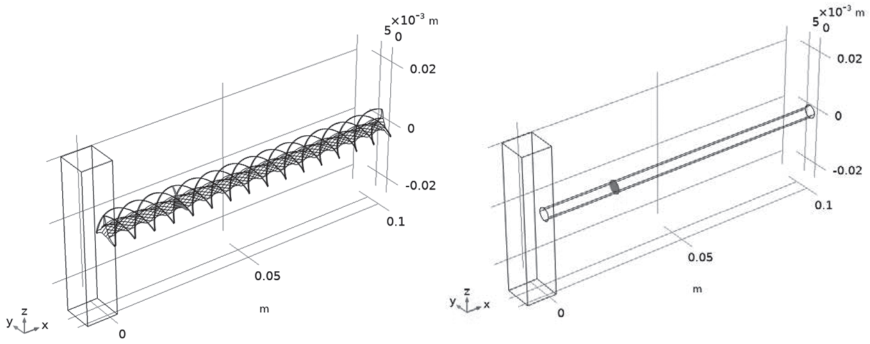

(*a*) (*b*)

Figure 273. *Cut Planes 3D*: (a) Rotini fin, (b) Cylindrical fin.

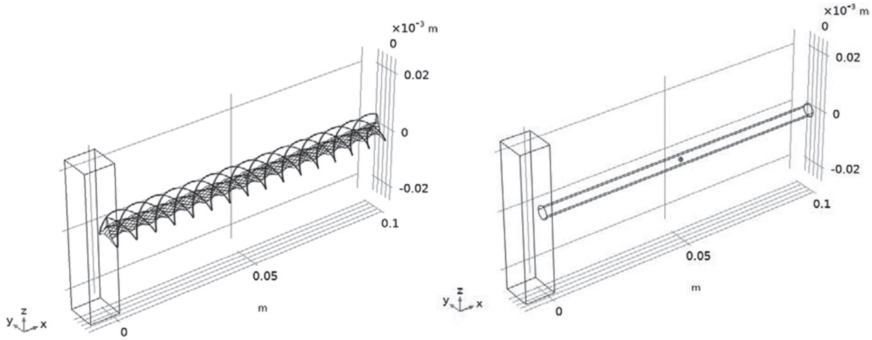

(*a*) (*b*)

Figure 274. *Cut Points 3D*: (a) Rotini fin, (b) Cylindrical fin.

12.2 Rotini Fin Solution Results

The rotini fin has been analyzed, assuming convection heat transfer for the external surfaces in contact with the ambient (h_{air} = 5 W/m^{2}K). Two heat source types have been investigated: (1) the wall is set at a fixed temperature of either 100 or 200 °C; and (2) the wall generates heat at a constant rate of 10 W. For the former heat source, parameter n is used to vary the temperature by multiplying the base temperature setting of 100 °C by n = 1 or 2. Figure 275 shows the result of the analysis for n = 1 (T_{base} = 100 °C). The left plot shows the temperature variation over the fin's surface, and the right plot shows the temperature on a section through the fin.

As the fin's function is to dissipate the heat from the structure to which the fin is attached, it is of interest to calculate the conductive heat flux close to the boundary between the fin and the wall. To accomplish this, *Surface*

Integration under *Derived Values* was used, where a specific variable was selected (*ht.dfluxx*) to be integrated over the appropriate surface (*cpl4*). This surface was defined as *Cut Plane 3D* (*y-z* plane), located in close proximity to the wall-fin interface ($x = 1$ *mm*). Figure 276a shows the selected *y-z* plane, while the surface integration setup is shown in Figure 276b. The plot of the total conductive heat flux versus the time is presented in Figure 277. The plot shows that the heat flux stabilizes to a steady value after about 150 s. The value is 2 W for 100 °C (n = 1) and 4 W for 200 °C (n = 2) cases. The data can be also presented in *Table Graph* (under *1D Plot Group*).

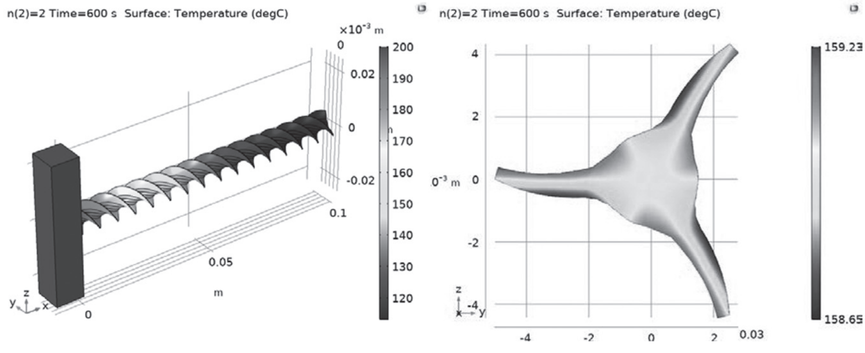

(*a*) (*b*)

Figure 275. Rotini fin, n = 1 (T_{base} = 100 °C), temperature contours: (a) Isometric view, (b) Cross section at x = 25 mm.

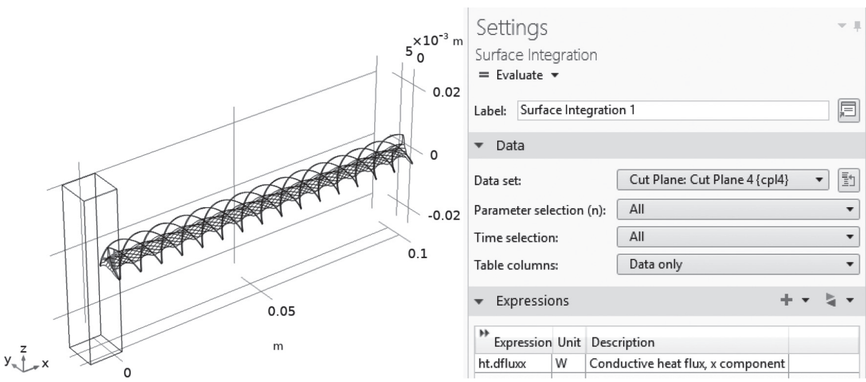

(*a*) (*b*)

Figure 276. Conductive heat flux x-component integration over the surface area: (a) Rotini fin plane of integration at x = 1 mm, (b) Integration settings.

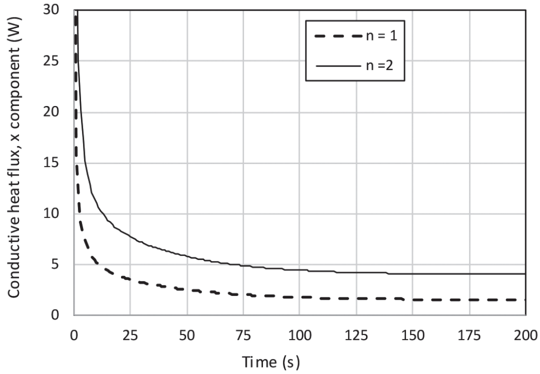

Figure 277. Rotini fin transient integrated conductive heat flux x-component over the surface area at x = 1 mm, n = 1 (T = 100 °C) and n = 2 (T = 200 °C).

The results of this analysis are then compared to those for the cylindrical fin. This fin has the same length as the rotini (100 mm) and its diameter is 4.36 mm. This diameter value was calculated to make the volume of the two fins equal and thus enable a meaningful comparison of their heat dissipation capabilities.

Table 5 shows the comparison between the fin convective areas and volumes as well as the surface-to-volume ratios. Figure 278 graphically compares the surface-to-volume ratios. It demonstrates how much higher this value is (more than 2.5 times) for the rotini fin compared to the cylindrical one.

Table 5. Area and volume for the two fins.

Fin type	Volume (m^3)	Area (m^2)	Convective Surfaces (m^2)	Convective Area/ Volume (1/m)
Cylindrical	1.4804E-06	1.40E-03	1.38E-03	9.33E+02
Rotini	1.49E-06	3.75E-03	3.74E-03	2.51E+03

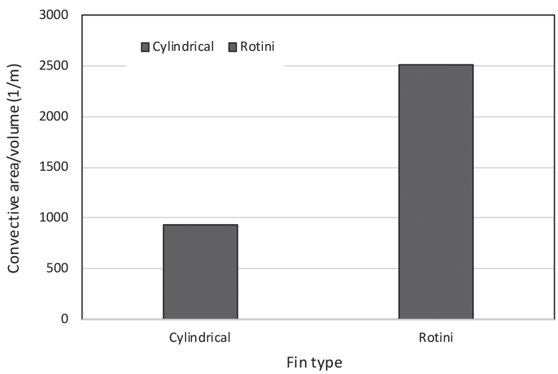

Figure 278. Comparison of surface-to-volume ratios of the two fins.

Figure 279 shows the temperature distribution on the cylindrical fin's surface and variation over the cross-sectional plane located at $x = 25\,mm$, for the case of wall temperature fixed at 100 °C ($n = 1$). Figure 280 compares the temperature variation along the length of the rotini and cylindrical fins, for both high ($n = 2$) and low ($n = 1$) fixed-wall-temperature cases, after 600 s (10 min). The wall temperature corresponds to the left side of the plot. The rotini fin shows the faster temperature decay along the length, corresponding to the greater heat flux along the x-coordinate direction, as seen in Figure 277.

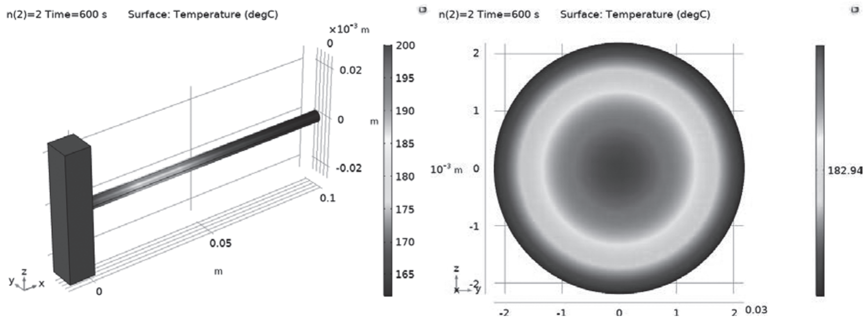

(a) (b)

Figure 279. Surface temperature contours for cylindrical fin, $n = 1$ ($T_{base} = 100$ °C): (a) Temperature surface plot, 3D view, (b) Temperature surface plot for section located at $x = 25$ mm.

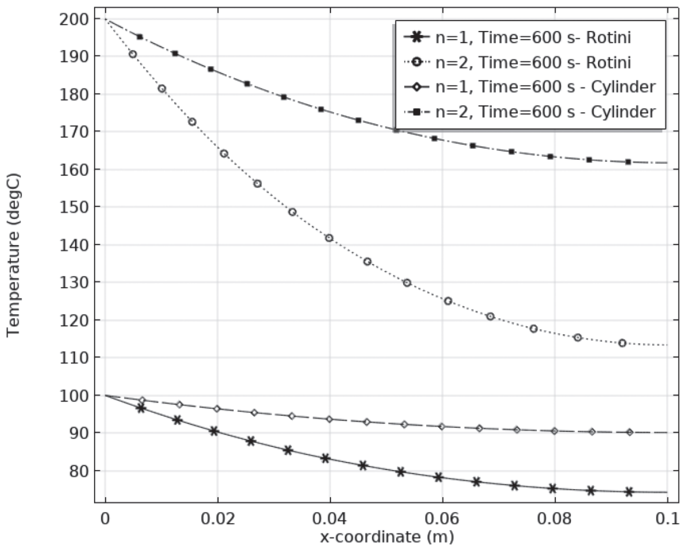

Figure 280. Comparison between spatial temperature profiles along the fin length (x-coordinate), $n = 1$ ($T_{base} = 100$ °C) and $n = 2$ ($T_{base} = 200$ °C).

Transient temperatures at the centers of the two fins are presented in Figure 281. The curves show that the temperature has nearly stabilized at around 200 s. For the lower wall temperature setting of 100 °C (n = 1), the rotini is at 80 °C and the cylinder is at 92 °C; for the higher wall temperature setting of 200 °C (n = 2), the rotini is at 132 °C and the cylinder is at 171 °C. Again, these show the higher heat dissipation of the rotini geometry.

Figure 282 and Figure 283 show the temperature contours for the vertical planes passing through the fin's central axis, as indicated on the far-left side of these figures.

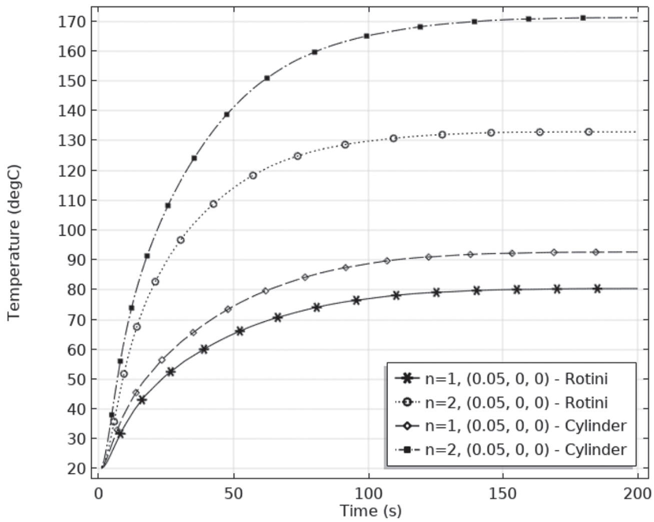

Figure 281. Comparison between transient temperature profiles at fin center, n = 1 (T_{base} = 100 °C) and n = 2 (T_{base} = 200 °C).

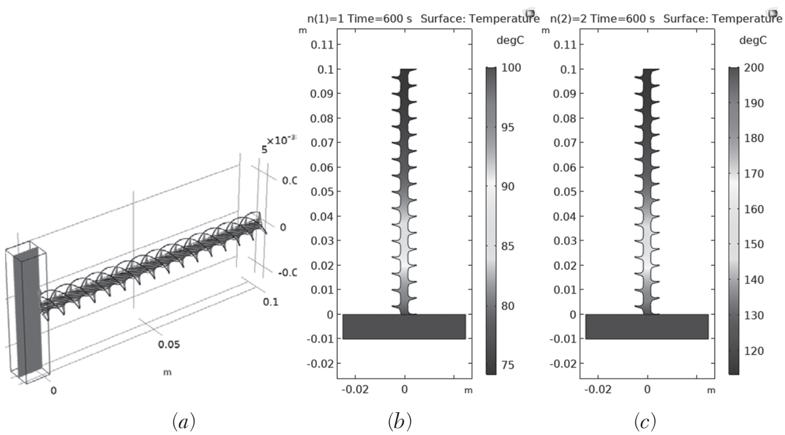

Figure 282. Surface temperature contours for rotini fin at y = 0 (z-x plane), n = 1 (T_{base} = 100 °C): (a) *Cut Plane 3D*, (b) n = 1 (T_{base} = 100 °C), (c) n = 2 (T_{base} = 200 °C).

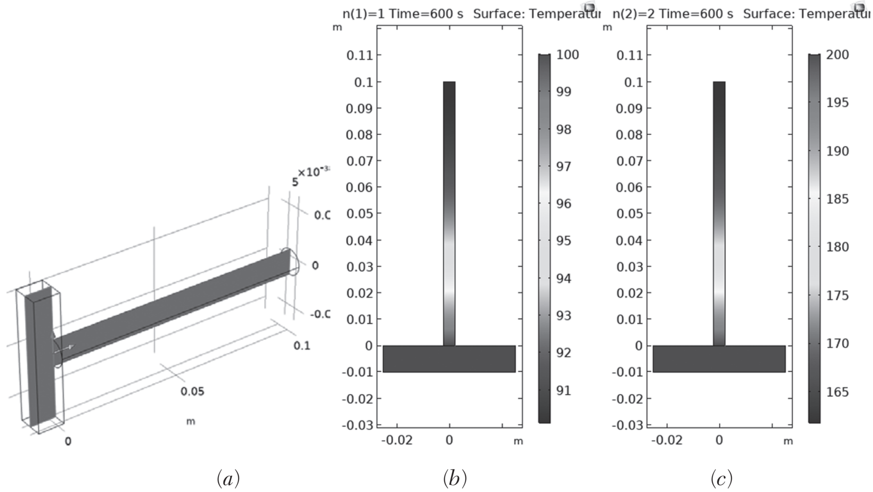

Figure 283. Surface temperature contours for cylindrical fin at $y = 0$ (z-x plane), $n = 1$ ($T = 100$ °C): (a) *Cut Plane 3D*, (b) $n = 1$ ($T_{base} = 100$ °C), (c) $n = 2$ ($T_{base} = 200$ °C).

Next, results are presented for the second case considered, where the wall generates heat at a constant rate (as opposed to using a fixed wall temperature). Also, a stationary (steady-state) study is carried out for this case instead of the transient one. A base heat generation rate of 10 W is considered, with a parameter *nn* value that multiplies this rate, determining the heat generation. Runs with two levels of heat generation (*HG*) are presented, a low-power case of $HG = 2.5\ W$ ($nn = 0.25$) and a high-power case of $HG = 5$ W ($nn = 0.5$).

Figure 284 and Figure 285 present the temperature distributions for the rotini and cylindrical fins for the previous conditions. Figure 286 compares temperature variation along the length for the two fins. The results show the effectiveness of the rotini fin, with its high surface-to-volume ratio, in reducing the temperature of the wall block. The temperature at the wall-fin interface at the high-power setting is about 370 °C for the cylinder versus about 230 °C for the rotini fin, a reduction of 140 °C. For the low-power case, it is 240 °C for the cylinder versus 140 °C for the rotini fin, a reduction of 100 °C. Looked at in another way, at twice the power, the rotini fin can maintain about the same temperature of the wall as the cylindrical fin.

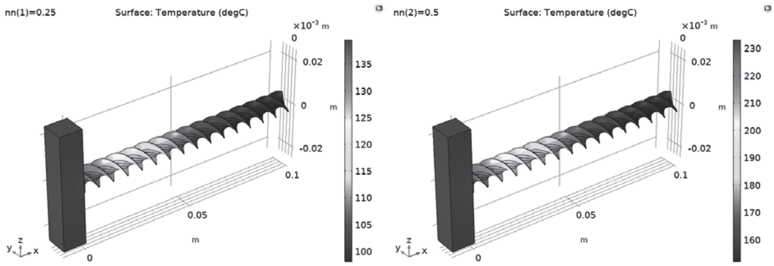

(a) (b)

Figure 284. Surface temperature contours for Rotini fin:
(a) *nn* = 0.25 (*HG* = 2.5 W), (b) *nn* = 0.5 (*HG* = 5 W).

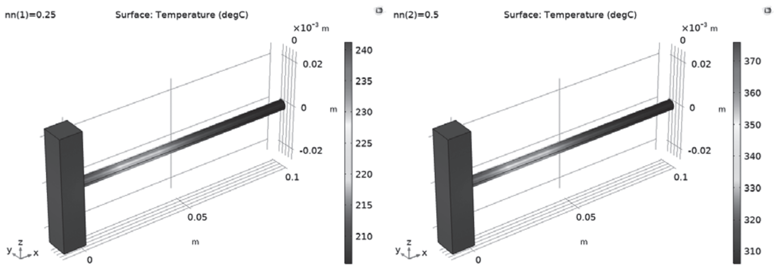

(a) (b)

Figure 285. Surface temperature contours for cylindrical fin:
(a) *nn* = 0.25 (*HG* = 2.5 W), (b) *nn* = 0.5 (*HG* = 5 W).

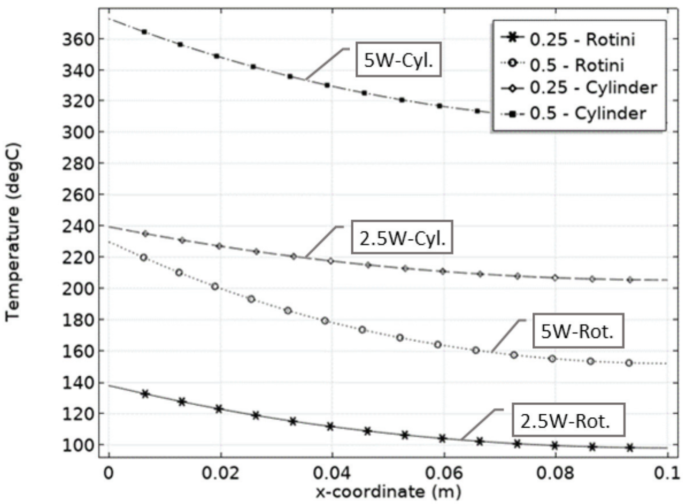

Figure 286. Comparison between spatial stationary temperature profiles along the fin length for rotini and cylindrical fins (*x*-coordinate), *nn* = 0.25 and 0.5 (*HG* = 2.5 and 5 W).

CHAPTER 13

Case Study 8—Flow Inside a Pipe

Pipelines have been used to transport a wide variety of substances (liquids, gases, and solids), over short or long distances. Most commonly the substances are carried from their place of origin to wherever they need to be processed further or as end-products to be used for their intended purpose. For water or any fluid to flow inside a conduit, pressure difference is the driving force. This can be created by a pump, gravity, or due to the temperature difference. If the walls of the pipe are exposed to heat at different rates, this temperature variation results in the fluid flow, with its direction being from areas with higher to those with lower temperature.

Gravity-driven pressure difference is a very common way to move liquid through pipes. That is how we get water in many of our homes—it comes from those elevated water tower tanks. Until the nineteenth century, fountains, such as the famous ones in Versailles, France, used to work only with gravity. A source of water higher than the fountain was required to convert the potential energy of the height into the kinetic energy of the water exiting the fountain's nozzle. Many such fountains are still part of the English countryside, perhaps placed there by the famous eighteenth-century British landscape architect Capability Brown.

The non-isothermal flow inside the ducts can by characterized by different flow regimes. In a laminar regime, the fluid moves smoothly along its flow lines; in a turbulent regime, current eddies are formed, and the fluid undergoes a lot of mixing, with a variation of flow direction and speed. A flow within a conduit will transition from laminar to turbulent above a certain flow velocity; this limit depends on the fluid properties and the conduit cross-section size. Any sudden disruption in the fluid flow due to barriers or sharp corners will cause the formation of local turbulent flows, with the potential to produce excessive noise in some applications.

13.1 Pipeline Applications

Natural gas is transported by pipelines after it is extracted from wells: (1) gas at low pressure is transferred by pipelines with small diameters from the wells to the manufacturing facilities, where they are processed into other products; (2) gas at high pressure is transported from the manufacturing facilities to interstate, intrastate, and international destinations—this high pressure is maintained by the pumping stations through which the gas passes; and (3) gas delivered to the main processing or distribution facility is carried by small-diameter pipelines. The main difference between the pipes and tubing is their sizing. Pipelines are also used to transport irrigation and portable water, waste (e.g., sewer waste), slurry (e.g., coal), and chemicals (e.g., ammonia).

Depending on the fluid types, there are different challenges faced when designing pipelines. For example, some of these materials (e.g., ammonia) are highly toxic. Therefore, not only the piping routes need to meet the right-of-way constraints but also the pipe's physical, thermal, and mechanical characteristics need to comply with regulations. In addition, all the fittings such as valves, intersections, and seaming materials—with which the pipes are joined together—should be carefully selected according to the performance requirements. In Canada, interprovincial pipelines are under the supervision of the National Energy Board; the equivalent U.S. agency is the Federal Energy Regulatory Commission (FERC).

Pipelines have been used to transport a surprising variety of substances. For example, a pipeline in Brazil is used to transport coal, liquified into a slurry, from a Minas-Rio mine to a port in Açu. In Germany, famous for its beer-drinking enthusiasts, the pubs located throughout Veltines-Arena stadium are connected by 5-km of pipelines to several large underground distribution tanks, where the beer is kept cool. Possibly the oldest industrial pipeline can be found in the village of Hallstatt in Austria, which has a rich history of salt mining. The 40-km pipeline, originally built in 1595, transports brine from Hallstatt to Ebensee. The pipes were made of 13,000 hollowed out tree trunks. Until 1994, 30,000 liters of milk from Ameland Island were transported daily to the Netherlands mainland by means of an 8-km pipeline laid at the bottom of Wadden Sea.

One may not think of wood as a suitably durable pipe material, but actually wooden pipelines have shown characteristics such as resistance to corrosion, electrolysis, and decay (rot); they are also easy to transport, especially in hard-to-reach areas, such as mountainous regions, making them a relatively easy-maintenance option for piping systems. The thick walls of wooden pipes provide good insulation for the transported substance, much diminishing the possibility of pipes freezing. Wood does not expand or contract easily with temperature changes, and that minimizes the need for the installation of expansion joints. Wooden pipes are made with staves and hoops, similar to barrels. It is believed that redwood found in the western United States can resist acids, insects, fungus, and weathering. In the seventeenth-century London, the pipes were tapered at the end and sealed by means of hot animal fat. It is reported that about 100,000 ft of wooden pipes were installed during World War II in army camps and airfields [147,148].

Teleheating, also known as the *district heating*, is a method of heat distribution by means of hot water or steam. Although the pipes are insulated, the heat wastage is significant (e.g., 10 percent in Norway district heating networks). Such piping systems are typically laid underground; stations along the pipeline routes may be added that can store heat and release it when the demand is high. This generated heat is then transferred to the users' central heating system by means of heat exchangers, isolating the heating fluid in the local system.

Temperature extremes and mechanical loads must be carefully considered in pipe design to avoid failure due to accumulation of residual thermal stresses, fatigue due to thermal cycling, or exceeding the material strength. The types of load vary depending on the environment in which the pipes are operated. Conditions that may need to be addressed in pipe design are installations in earthquake-prone regions, high winds, vibrations, and fluid hammer due to the bends in the pipes. The existence of sharp corners can cause high-stress regions within the pipe, and so pipe bend radii must be chosen appropriately. Cryogenic pipes, which transport extremely cold fluids, must be carefully designed to avoid the steel structures becoming brittle when exposed to such low temperatures.

In industrial installations, it is often needed to monitor the operating conditions of the pipelines. Instruments, such as temperature and pressure gauges, may be employed for this purpose. They can communicate by wire or wirelessly, using satellites or cellular networks, with central controllers using Supervisory Control and Data Acquisition (SCADA) systems.

This information can be processed, for example, to detect leaks. Comparing the flow rate data between two different locations along the pipe can provide this information by calculating the difference between the two values.

A heated or cooled fluid moving through a pipe is an important means of transporting heat to or from the system of interest; such an arrangement is used in various thermal management systems (e.g., heat exchangers). Internal or external fins are often connected to pipes to increase the heat transfer rate. An example of an effective thermal management system that can operate without using any powered fluid pumping mechanism is a heat pipe. Its reliability and effectiveness has led to its use in aerospace cooling applications. A heat pipe has an array of narrow channels within it that perform a wick function. The vaporized liquid molecules travel via these channels upstream to the cool end (condenser) where they are drawn in by the capillary forces, lose the absorbed excess heat, and form liquid, which then flows back to the warm end (evaporator) of the pipe to repeat the cooling cycle.

For some private homes and industrial spaces, heating can be done using a non-isothermal heated water flow inside the network of pipes built into the floor. These systems deliver heat by warming up the large surface area of the floor slab, delivering heat by radiation and gentle convection. Humans are actually quite sensitive to radiant heat—it adds to a sense of comfort, just like standing in front of a lit fireplace. On the other hand, poorly insulated cold walls will make one feel chilled. How much more pleasant it is to walk over a gently heated floor than over a cold one on a winter night as one wakes up from a dream, tiptoeing through the kitchen to the refrigerator, getting ready to practice fasting.

An HVAC duct is another example where the fluid (air in this case) flows through a channel that can be straight, bent, or split into many smaller branches. If the HVAC system is used for heating or cooling, not just ventilation, in addition to the flow rate, one also needs to be concerned that the air at an appropriate temperature reaches the diffusers where it enters the intended service space. It must provide comfort to people or meet cooling or heating requirements of the equipment. Thus, heat transfer modeling is an important element of HVAC system design.

Pipes do not just serve utilitarian purposes. They have been used in some modern art creations, showing the infinite creativity of the human mind. Pipes are used in fountains, which can be said to embody the human spirit and its love for purity (water) and life (movement). Water, the source of life, is the most responsive being to forces and energies, seen during its crystallization process forming ice, melting to bring life to the Earth, and flowing to clear the mundane [149]. The soothing sound of the water flowing inside the underground pipes and finding its way to the exterior environment is affected by the pipes' characteristics—from the material to the length and shape.

If you have witnessed water dancing to music during a water show, you see that water exits the pipe outlets at different heights with patterns that are affected by the size of the outlet nozzles. In these shows, water is moved by means of pumps that power the super and mini shooters delivering water in mist or liquid forms. Modern fountain installations can use tremendous quantities of water and electrical power. The iconic Bellagio Hotel fountains in Las Vegas, NV, reportedly contain about 20 million gallons of water which are delivered via 12,000 nozzles. Thus, resource management, such as water quantity, pressure, and temperature, is an important element of running such shows [150,151].

There is another vital piping system that all humans make use of and without which we could not survive—the human circulatory system. The human body incorporates perhaps the most complex flow system of them all, operating reliably for decades in a nearly unfailing fashion. Hemodynamics, the dynamics of the blood flow within the veins and arteries, is responsible for this operation, ensuring the transportation of the nutrients and hormones, gases such as oxygen and carbon dioxide, as well as metabolic wastes. Of course, heat transfer plays a critical role here as well. Blood flow regulates body temperature, directing heat to the parts of the body where it is needed most, which may sometimes leave your fingers freezing as your body decides that maintaining your core temperature is more critical to your survival. Blood is a non-Newtonian fluid, meaning that its viscosity can change depending on the environmental conditions. The vessels are also flexible to accommodate flow variation and facilitate fluid movement.

Pipes running on the exterior of structures may be exposed to harsh environmental conditions due to extreme temperatures, wind, and the Sun's radiation, such as those found in arid climates. In these applications, the choice of the material is as vital as the design's geometry. In some aerospace applications, aluminum sheets are used for the heat pipe envelope [152]. They are used to maintain space nuclear systems within the recommended temperature range of 130 to 280 °C. Although aluminum is easily machinable, manufacturing the interior longitudinal grooves in order to increase the surface area of the heat pipe envelope does not produce a strong structure for the given weight requirements. Therefore, titanium, which has a high strength-to-weight ratio, is suggested as an aluminum substitute. These characteristics, in addition to its anticorrosive properties, make titanium a desirable material in aerospace applications. The main challenge in using this material is its machinability.

The pipes that are used to convey the fluids are made of materials such as wood, fiberglass, glass, plastics, metal (e.g., steel, copper, and aluminum), and occasionally concrete. Surface roughness is one of the factors that affects the flow regime inside the pipes. There are also other materials used for constructing pipes such as steel alloys, Inconel, titanium, and chrome-moly. Copper pipelines were used extensively through the twentieth century in residential plumbing and are still found in many older homes; however, due to copper's higher material and installation costs, it has been generally replaced by plastics such as PEX (cross-linked polyethylene). In addition to a higher installation cost, copper, being an excellent heat conductor, also can waste some notable fraction of heat when used to deliver domestic hot water, especially if a hot-water recirculation system is being used. Such energy waste may be reduced by adding insulation around the pipes, for example, in the form of closed-cell polyethylene foam semi-slit tube sleeves.

There has been one interesting application of pipes where their function as a conduit of liquid was combined with a structural function. This was for the construction of Beesat Bridge on the southern section of the river Arvand in Iran. This river starts at the confluence of Tigris and Euphrates Rivers and empties into the Persian Gulf about 160 km downstream. The southern section of this river forms the border between Iraq and Iran. In 1986, a bridge crossing needed to be quickly constructed across Arvand River. The river at this point was flowing at 11-km/h; it was 1-km wide, 12-m deep, with a 3 to 5-m tidal depth variation. To address this challenge, the engineers assigned to the task had an innovative idea. Nearby, there was a sunken ship that carried a large load of pipes intended for an oil pipeline. They were 1.42-m in diameter, 12-m in length, with a 16 mm wall thickness (Figure 287).

To make Beesat Bridge, these pipes were placed into the river while oriented along the direction of the water flow. This allowed the water to pass by unimpeded while creating the bridge structure. Pipes were stacked, starting at the bottom, until sufficient height was reached above the water level. The rows of pipes were then linked by means of earing hooks and welded. After placing smaller diameter pipes between the large ones to make a flatter upper surface, asphalt was laid on top to cover the crevices, creating a 12 m drivable road surface. In all, 3,400 pipes making a total length of 80 km were used in this bridge construction [153].

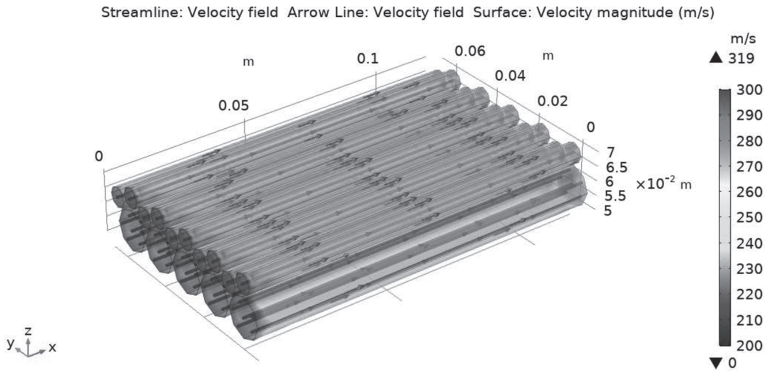

Figure 287. A flow analysis for Beesat Bridge constructed on the southern section of the river Arvand (Iran) in 1998.

The rest of this chapter describes three exercises related to pipe flow which are presented as an opportunity for the reader to practice setting up the models and solving them. The first exercise applies a fixed-temperature boundary condition to the pipe's exterior while a fluid flows through the interior at either constant or temperature-dependent velocities. Two modeling approaches are suggested: using a single physics or using a conjugate heat transfer model. The second exercise involves a non-isothermal flow inside an underground gas pipe. Finally, the third exercise suggests modeling of a non-isothermal flow through a converging-diverging nozzle.

13.2 Exercise 1—Constant Wall Temperature

This exercise applies a constant-temperature boundary condition to the exterior wall of the pipe. Different temperature settings are used for two fluids—water and air. Two modeling approaches are suggested: (1) a single physics solid-fluid heat transfer model; and (2) a conjugate solid-fluid heat transfer model. For the second scenario, temperature-dependent flow velocity is introduced, replacing the constant flow velocity employed in the first scenario.

As an additional variation, the reader may replace the constant-temperature boundary condition with a constant heat flux and repeat the previous solutions. A parametric study is recommended with progressively increasing values of power, starting from 45 W and increasing by a factor of 1.5 up to 228 W. A parameter named *Power*, which can be used to define this heat flux, is listed among *Study* settings (Figure 296).

13.2.1 Problem Definition

In this example, flow passes through a constant-diameter pipe. The pipe is 25-cm long, with an exterior diameter of 5-cm and an interior diameter of 3.33-cm (Figure 288). Since a round pipe is axisymmetric, if all the boundary conditions were also axisymmetric, a 2D axisymmetric model could have been used in this case. However, a 3D model is selected here, giving the possibility of applying non-axisymmetric boundary conditions, if desired. For example, if one wanted to model the pipe exposed to solar radiation, it would be heated unequally over its external surface. In such a case, a 2D axisymmetric model would not be suitable.

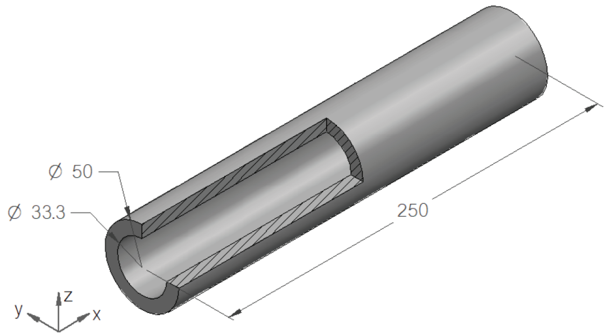

Figure 288. Pipe geometry with cutout showing internal structure (dimensions in mm).

The pipe geometry was generated internally with COMSOL Multiphysics built-in tools. Since the pipe is symmetrical about the *x-z* and *x-y* planes, both in terms of the geometry and the boundary conditions applied, the pipe geometry was cut in half with a vertical plane (Figure 289). The pipe material is copper (Figure 290).

For this exercise, it is desired that fluid (e.g., water or air) flows inside the pipe at a sufficiently low velocity to form a laminar flow. For the flow to remain in the laminar regime, *Reynolds number* should be below 2,300; if it exceeded this value, the flow regime would transition to turbulent. Since the pipe interior diameter does not change, *Reynolds number* mainly depends on the flow velocity, in addition to the fluid density and dynamic viscosity. Assuming that the latter two parameters vary with temperature, one may conclude that the maximum velocity below which the flow remains within the laminar flow range also varies with temperature. Therefore, one method to choose flow velocity, fulfilling the laminar condition, is to make sure *Reynolds number* remains under 2,300 (Figure 291). The flow enters the pipe at the inlet temperature (30 °C) and velocity 0.0068 m/s (which is 1/22th of the maximum velocity below which the flow should remain

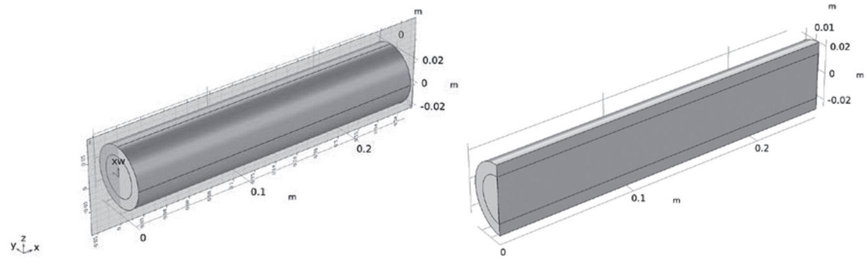

(*a*) (*b*)

Figure 289. Pipe with a central embedded channel: (a) *Work Plane* partitioning the model, (b) Partitioned model by symmetry.

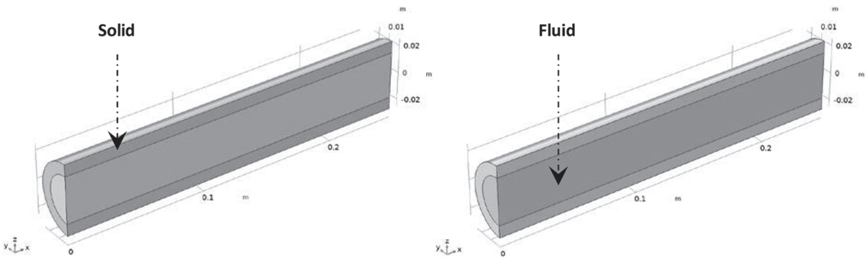

(*a*) (*b*)

Figure 290. Pipe flow model domains: (a) Solid, (b) Fluid.

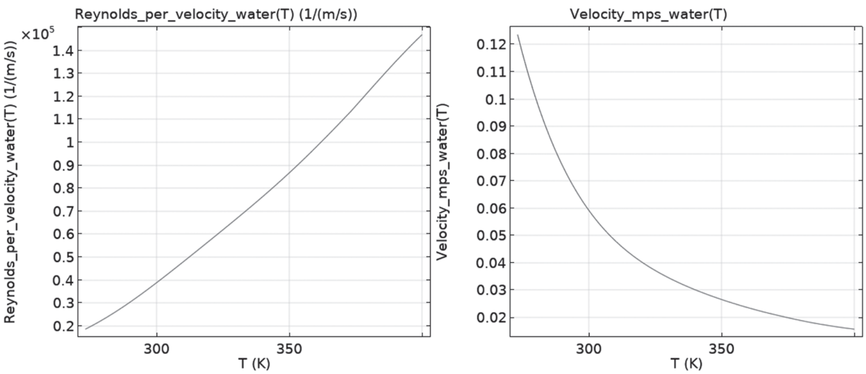

(*a*) (*b*)

Figure 291. Water temperature-dependent properties: (a) *Reynolds number* per flow velocity, (b) Laminar flow velocity inside the pipe (*Re* = 2,300).

laminar, given the pipe dimensions and mass flow rate—equivalent to a 2,300 *Reynolds number*). For water, this velocity magnitude results in a *Reynolds number* of about 1,886, while for air, it is about 206 (Figure 292 and Figure 293).

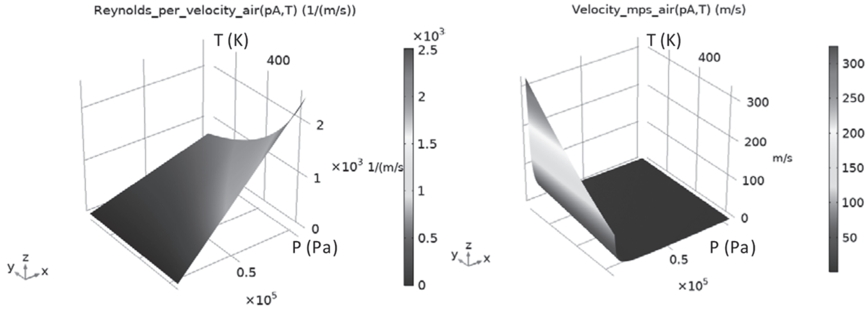

(a) (b)

Figure 292. Air temperature and pressure-dependent: (a) *Reynolds number* per flow velocity, (b) Laminar flow velocity inside the pipe (*Re* = 2,300).

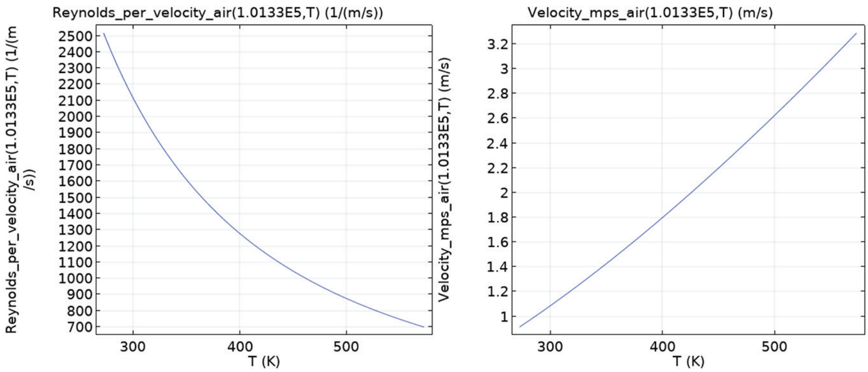

(a) (b)

Figure 293. Air temperature-dependent properties at 101 kPa: (a) *Reynolds number* per flow velocity, (b) Laminar flow velocity inside the pipe (*Re = 2,300*).

Figure 294 shows how the boundary conditions were defined in the model. A symmetry condition was applied to the central vertical plane (Figure 294a). The exterior surfaces transfer heat to the ambient by convection. This includes the exterior cylindrical surface (Figure 294b) and the exposed surfaces at the front and back (Figure 294e). The flow enters the pipe via the inlet (Figure 294c). The flow leaves the pipe via the outlet at the atmospheric pressure (Figure 294d). The interface between the interior wall surface and exterior fluid surface is a wall in the flow analysis (Figure 294f). Figure 295 shows the meshing of the 3D model. Parameters used to create the pipe flow models are presented in Figure 296.

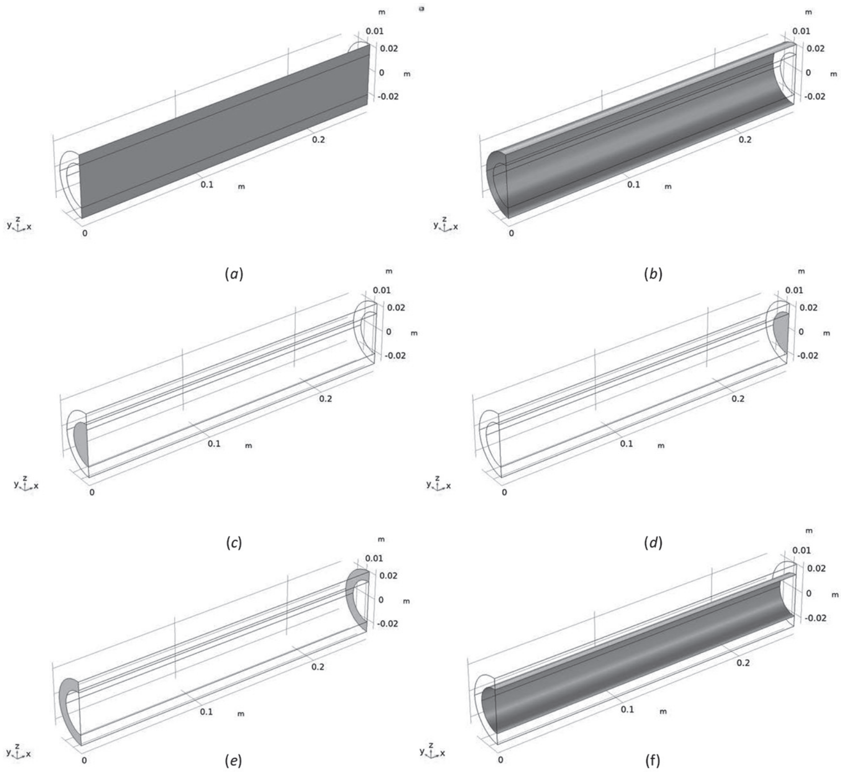

Figure 294. Model boundary conditions: (a) Symmetry plane, (b) Exterior convective surface, (c) Inlet, (d) Outlet, (e) Convective end surfaces, (f) Interior wall surface.

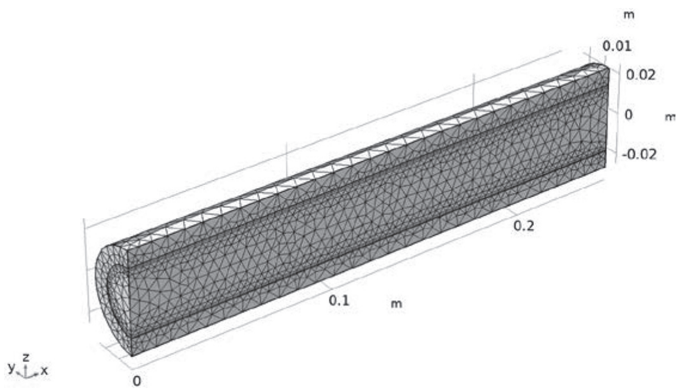

Figure 295. Meshed pipe.

Settings
Parameters

Label: Parameters 1

Parameters

Name	Expression	Value	Description
Amp	5[A]	5 A	amperage
area	(0.5*pi*(diameter/2)^2)-(0.25*diameter)^2	8.255E-4 m²	fin tip area
contact_p	100[kPa]	1E5 Pa	contact pressure
diameter	0.05[m]	0.05 m	fin external diameter
diameter_in	2*diameter/3	0.033333 m	
final_temp_source	nt1*Tinlet	303.15 K	final temperature of the coil
flow_pressure	860[kPa]	8.6E5 Pa	flow pressure
h_horizontal	5[W/(m^2*K)]	5 W/(m²·K)	convective coefficient, horizontal surfaces
h_vertical	10[W/(m^2*K)]	10 W/(m²·K)	convective coefficient, vertical surfaces
L	0.25[m]	0.25 m	fin length
mesh_size	0.0025[m]	0.0025 m	mesh size
mu	0.0018[Pa*s]	0.0018 Pa·s	dynamic viscosity
n	1	1	multiplier
NGL_below	30[in]	0.762 m	natural gas line below the surface depth
NGL_depth_ground	6[ft]	1.8288 m	natural gas line depth inside ground
NGL_diameter	42[in]	1.0668 m	natural gas line diameter
NGL_length	NGL_diameter*5	5.334 m	natural gas line length
NGL_thickness	80[mm]	0.08 m	natural gas line thickness
nnn	1	1	multiplier for velocity
nnq	1	1	multiplier
nnt	1	1	multiplier
nt1	1	1	multiplier
Patm	1[atm]	1.0133E5 Pa	atmospheric pressure
peropane_temperature	60[degF]	288.71 K	
Power	n*45[W]	45 W	seat electric power
premiter	0.5*(2*pi*diameter/2)+(diameter-0.25*diameter)+3*0.25*diameter	0.15354 m	fin tip perimeter
propane_flow_rate	Upropane*pi*(NGL_diameter/2)^2	9.9305 m³/s	propane flow rate
Q_time	nnq*400[W/m^2]	400 W/m²	power density
radius_exterior	1000*diameter/2	25 m	
radius_interior	1000*diameter/3	16.667 m	
Reynolds	(2/3)*rho*Uinlet*diameter/mu	1257	reynolds number
rho	998.2071[kg/m^3]	998.21 kg/m³	density
rotation	90	90	rotatio of the seat back
sun_radiation	1000[W/m^2]	1000 W/m²	sun's radiation
Tamb	84.4[degF]	302.26 K	ambient temperature
tfinal	1800[s]	1800 s	final time
Tground	70.6[degF]	294.59 K	ground tempeature
time	3600[s]	3600 s	time
time_heat	nnt*2[min]	120 s	heating time
time2	90[s]	90 s	conjugate time
Tinit	20[degC]	293.15 K	initial temperature
tinitial	960[s]	960 s	initial time
Tinlet	30[degC]	303.15 K	inlet temperature
Toutlet	50	50	outlet temperature
Tref	20[degC]	293.15 K	reference temperaure
Twall	(n*25)[degC]	298.15 K	wall temperature
Uinlet	nnn*0.068[m/s]	0.068 m/s	inlet velocity
Upropane	11.11[m/s]	11.11 m/s	propane velocity
Volt	12[V]	12 V	voltage
wall_length	0.05[m]	0.05 m	wall length

Figure 296. Parameters used for pipe flow study (global level).

13.2.2 Single Physics

Attempt the following case study.

Here, the flow inside a pipe with constant wall temperature is modeled using a conduction model. An example of such a model application is in the design of heat exchangers and thermal management systems. The solution obtained here with a single physics solid-fluid heat transfer can be compared with that in the next exercise, where different physics is used.

The wall temperature here remains constant through the length of the pipe and over time. Two temperature settings are to be investigated—50 and 100 °C for the two fluids (water and air). The fluid enters the inlet at

30 °C and leaves the outlet at the atmospheric pressure. The minimum inlet flow velocity (to generate laminar flow) is about 0.068 m/s, resulting in *Reynolds number* of about 1,886. This number is below the 2,300 transitional criterion value of *Reynolds number*, ensuring the flow is laminar. The initial fluid velocity condition is set at 0.068 m/s.

Predict the isosurface temperature contours (isotherms) for the same heating times as previously (one hour) for the wall temperatures of 50 °C (n = 2) and 100 °C (n = 4) for both water and air fluids. Apply the automatic range option for the plot color legend.

Note that if one chooses to explore the results with a different temperature range (minimum and maximum values), they may achieve this by selecting *Coloring and Style* under the requested *3D Plot Group* (e.g., *Isosurface* node), and choose variable (e.g., *T* for temperature) under *Expression*, its *Range* (maximum and minimum values for the color bar), and *Color table* under *Coloring and Style* (e.g., *Rainbow* and *Thermal*). This will change *Color legend* to the desired one.

Since the selected transient scenarios consist of two wall temperature values (50 and 100 °C) and two materials (water and air), with *All combinations* setting activated in *Parametric Sweep* setup, there are four scenarios in total. The solution convergence may be more of an issue when air is the fluid; therefore, it is a good idea to first solve the problem with a more viscous flow (e.g., water) and then use the results of this model as the initial state (or initial guess) to the problem with air as the main fluid. To solve this model, the material selection is suggested to be incorporated as *Switch* node, with water being *Material 1* and air *Material 2* in the list.

In specification of the boundary conditions, the pipe entrance settings include a fully developed inlet flow, meaning that the inlet flow velocity conditions are set as part of the flow initial conditions. An *entrance length* (distance from the entrance) is defined, after which the flow velocity or temperature profile does not vary within the pipe length. In such a case, the flow profile becomes uniform (fully developed) within a very short distance from the entrance (entrance length). The temperature profiles along the radial direction within the pipe are expected to be parabolic. To confirm this, present radial temperate distributions using *Cut Lines 3D* feature and the sliced temperature contours using *Cut Plane 3D* feature.

13.2.3 Conjugate Heat Transfer

In this exercise, it is suggested to model the pipe flow using conjugate heat transfer consisting of the solid-fluid model in addition to the flow model, with water and air as the two fluids, as before. When setting up the solution in *Study* node, you can employ *Parametric Sweep* feature to study the effect of the wall temperature and *Material Sweep* to investigate the influence of the material selection (i.e., water versus air) on the analysis results (Figure 297 and Figure 298). Use *Material Switch* feature to define options for the fluid domain (Figure 297), with water being *Material 1* and air being *Material 2*. Then, select *Material Sweep* and choose the appropriate *Switch*.

In this example, instead of using a fixed inlet velocity value, it is defined as a function of the wall temperature (Figure 299). As the wall temperature increases, so does the possibility for the flow to transition from a laminar to a turbulent regime. This is due to the kinematic viscosity of the fluid being affected by the temperature. Thus, fluid velocity value is calculated using a function (*Velocity_mps_steam* = 2,300/*Reynolds_per_velocity_steam(pA,T)*), which takes into account this dependence.

Figure 291, Figure 292, and Figure 293 present *Reynolds number* per velocity (1/m/s) and velocity (m/s) as functions of absolute temperature (K) for water and air. These diagrams are obtained based on the assumption that the laminar flow criterion to transition to turbulent flow is 2,300.

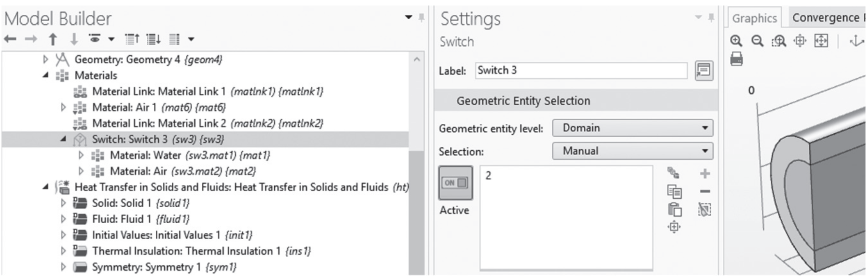

Figure 297. *Material* and *Switch* definitions.

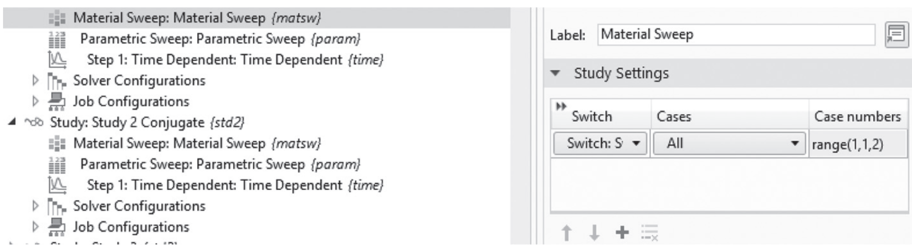

Figure 298. *Material* and *Parametric Sweep* definitions.

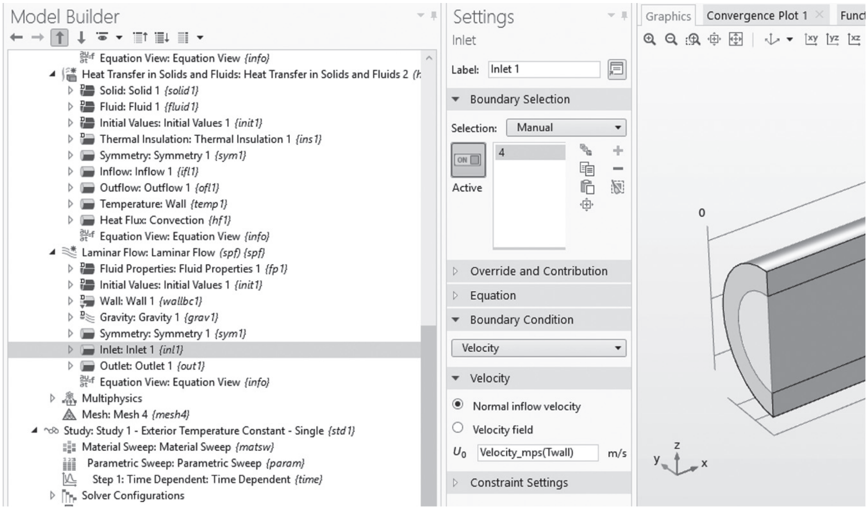

Figure 299. *Conjugate Heat Transfer* physics and temperature-dependent inlet velocity.

13.3 Exercise 2—Oil and Gas Pipelines and Analytic Functions

13.3.1 Background on Oil and Gas Pipelines

Pipes are used as means of transporting oil and natural gas between the processing and distribution centers. Examples include the pipelines crossing Africa, Asia, Europe, North America (e.g., Canada, Mexico, Puerto Rico, and the United States), South America, and Oceania. To deliver propane gas to customers in large volumes, it is more efficient for it to be converted to fluid using very high pressures.

Natural gas transmission pipelines also require high pressure for transmission. The pressure is maintained by the compressor stations located (about every 65 to 160 km) along the way. These compressors are very powerful, outputting about 36,000 hp, a rate comparable to a large jet engine. Natural gas moves inside the pipeline at about 40 km/hr (11.1 m/s).

Natural gas, which comprises gases such as butane, propane, and ethane, is discretized at the processing facility, with the excess contents and contaminants such as hydrogen sulfide removed. Usually, ethanethiol is added to the natural gas to make it smell like rotten eggs, in case it leaks, since natural gas is odorless. The storage is usually done inside waterproof underground storage facilities.

Pipelines have diameters that vary from 0.5 to 48 inches. The larger ones transfer the fluids from the processing center to the major distribution stations, while the smaller ones connect the distribution and processing centers. Transmission pipelines are usually made of steel coated with corrosion-protection materials (e.g., coal tar enamel or light blue fusion bond epoxy) [154,155,156].

Underground pipelines would normally be placed about 1.8 m (6 ft) deep below the surface. Interestingly, gas pipelines are intentionally not laid out in an exactly straight fashion; instead gentle *S-curves* are added. The reason is to avoid pipe damage due to thermal expansion. While the seasonal temperature variation below the ground surface declines with depth, there is still significant variation at the typical pipe-laying depth. For example, soil temperature observations were made for oil pipeline projects in 2004–2005 in Mackenzie River valley, in Fort Simpson area of the Northwest Territories. These measurements recorded seasonal variations from a minimum of 2.0 °C to a maximum of 6.3 °C. While a temperature change of 4.3 °C does not appear to be large, when the thermal expansion is calculated for the tens of kilometers of the pipeline, the effect becomes significant. Using this temperature difference with the steel thermal expansion coefficient of 11.7×10^{-6} m/mK for 10 km of pipeline results in a length change of 0.5 m. If the pipes were laid in a straight line, this expansion would cause significant sideways movement, likely leading to pipe damage [157,158,159,160,161].

13.3.2 Setup for Oil and Gas Pipeline Study

Attempt the following case study.

An underground pipeline is to be modeled here. The thermal load is due to the solar heating of the soil's surface. The propane gas can be assumed to be initially at high pressure, ensuring that it is transported in a liquid state. The 3D model is shown in Figure 300. There are a number of considerations when setting up such a model. The physics are set as a combination of heat transfer in solids and fluids, flow, and radiation heat transfer. The first two and the second two form *Multiphysics* nodes that are then simultaneously solved with the solid-fluid heat transfer data as the floating data interacting between the two *Multiphysics* nodes.

As for any flow model, the analyst needs to check which flow regime is being investigated. In order to do this for the flow inside a pipe, *Reynolds number* is adopted as the flow transition regime criteria. This means that with *Reynolds numbers* below 2,300, one expects a laminar flow. Since propane gas is adopted for this study, assuming that this number is to be satisfied to ensure laminar flow inside the pipes, Figure 301 to Figure 304

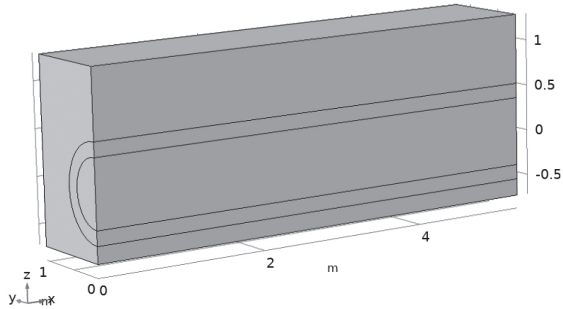

Figure 300. Model for an underground natural gas pipeline.

are presented for the propane *Reynolds number* per velocity and velocity for the defined temperature and pressure ranges. Surfaces are used to plot this value, since the quantity depends on two independent variables (predictors), which are temperature and pressure.

Note that dynamic viscosity is mainly a function of the temperature in COMSOL Multiphysics material definitions, taking on a constant value outside the defined temperature range. Liquid densities, which are also temperature-dependent, are specified similarly. Density of gases, however, is a somewhat different case, for it is temperature- and pressure-dependent.

Data ranges should be set properly if the intention is to extract the data for visualization purposes or in order to compare them with the corresponding ones in the literature for certain conditions (e.g., the atmospheric ones), similar to what is shown in Figure 301 through Figure 304, which present the ratio of *Reynolds number* over the flow velocity and velocity—assuming *Reynolds number* is 2,300—for a range of pressure from zero up to the atmospheric one (Figure 301) and at the atmospheric pressure (Figure 303).

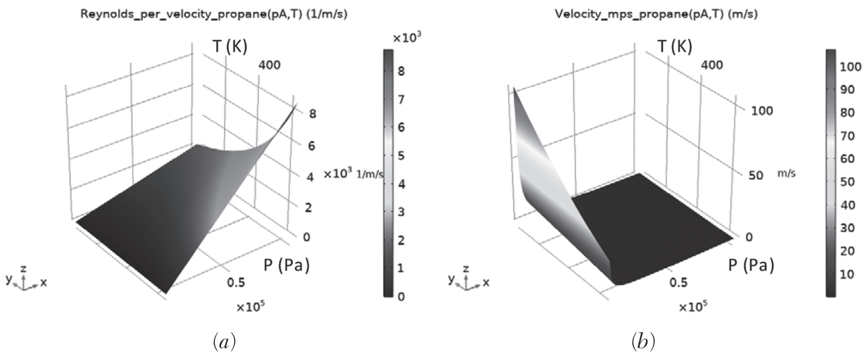

Figure 301. Propane, $0 < P < 101$ kPa, $0 < T < 300$ °C: (a) *Reynolds number* per flow velocity, (b) Velocity for a laminar flow ($Re = 2{,}300$).

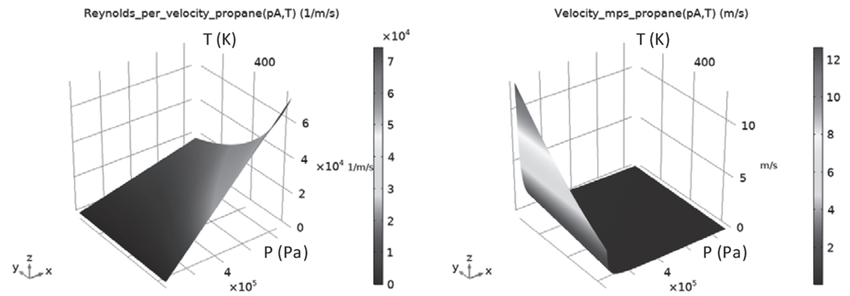

(*a*) (*b*)

Figure 302. Propane 0 < *P* < 860 kPa, 0 < *T* < 300 °C: (a) *Reynolds number* per flow velocity, (b) Velocity for a laminar flow (*Re* = 2,300).

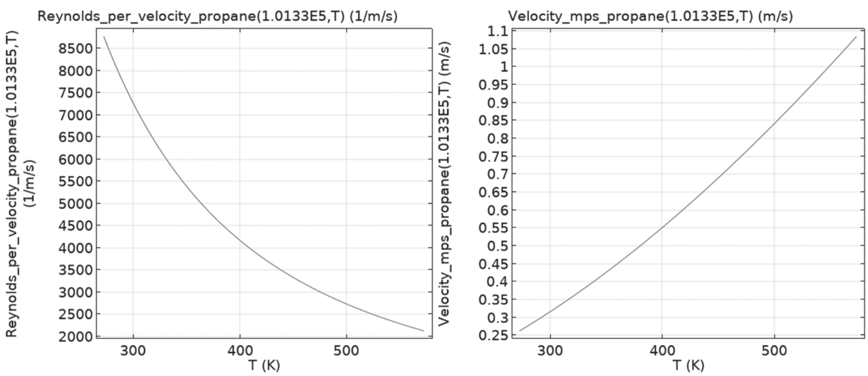

(*a*) (*b*)

Figure 303. Propane temperature-dependent properties at 101 kPa: (a) *Reynolds number* per flow velocity, (b) Laminar flow velocity inside the pipe (*Re* = 2,300).

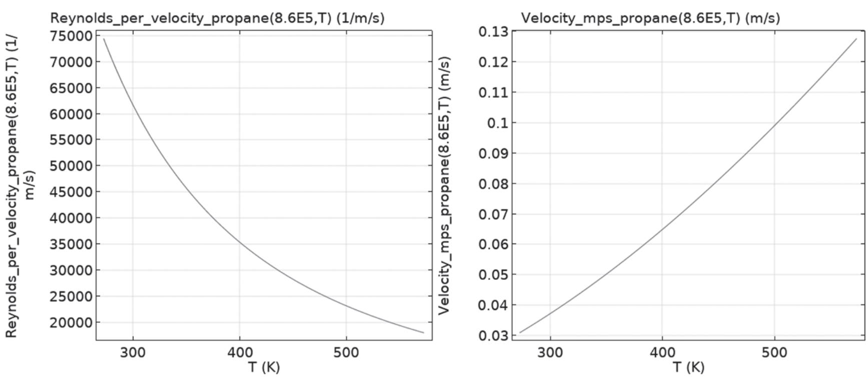

(*a*) (*b*)

Figure 304. Propane temperature-dependent properties at 860 kPa: (a) *Reynolds number* per flow velocity, (b) Laminar flow velocity inside the pipe (*Re* = 2,300).

Figure 304 provides similar plots for high-pressure scenarios. The atmospheric and high-pressure magnitudes are assumed to be 101 and 860 kPa, respectively. Figure 305 and Figure 306 present the *Analytic Functions* to describe *Reynolds number* per velocity ($\rho d/\mu$) and velocity ($2{,}300 \times \mu/\rho d$) functions versus the temperature and pressure to help with visualizing these relationships but also to identify the regions in which *Reynolds number* is within the laminar range (2,300).

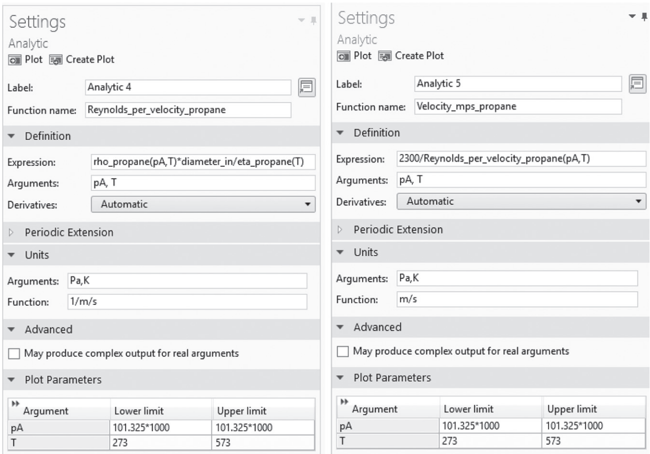

(*a*) (*b*)

Figure 305. Propane velocity function settings for constant pressure and temperature range P = 101 kPa, $0 < T < 300$ °C: (a) *Reynolds number* per flow velocity, (b) Laminar flow velocity inside the pipe (Re = 2,300).

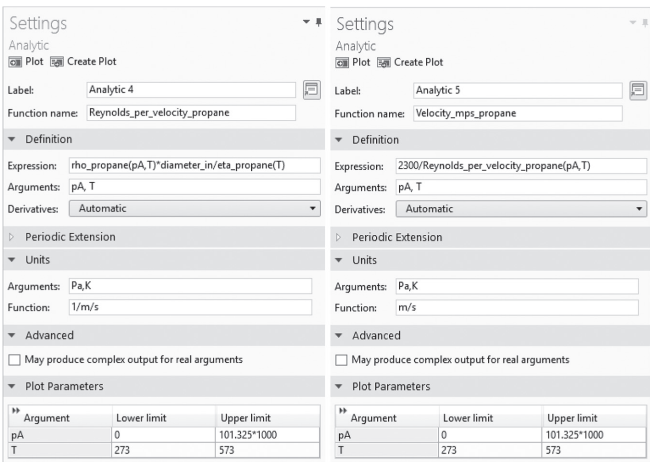

(*a*) (*b*)

Figure 306. Propane velocity function settings for pressure and temperature ranges $0 < P < 101$ kPa, $0 < T < 300$ °C: (a) *Reynolds number* per flow velocity, (b) Laminar flow velocity inside the pipe (Re = 2,300).

As input to this model, one needs to define temperature-dependent thermo-physical properties, such as temperature and pressure. To do this, *Analytic Function* feature is used, which is adopted from the material library defined in COMSOL Multiphysics. Note that to define *Analytic Function* feature (temperature-dependent thermo-physical properties in this case), *Function name* with no spaces should be used. This name is later used to reference this function when used as input for other functions or variable placeholders within the physics settings. The next input variable is *Expression* under *Definition* category that is associated with the mathematical expression. Note that in these scenarios, the input variables are the previously defined functions (e.g., air density). *Arguments* are the next set of input entities that present the variable (e.g., *pA* and *T*). The function derivatives that are used in order for the resulting function slopes to be properly defined may be selected as *Automatic* (recommended by the program) or *Manual*, in which the argument along with its partial derivative are provided as inputs. Under *Units* section of *Analytic Settings*, the units are provided for both arguments and function. Under *Plot Parameters*, the data ranges for the defined arguments are supplied.

13.4 Exercise 3—Converging-Diverging Nozzle

Attempt the following case study.

This scenario is a special case of the previous case study. Here, instead of a constant pipe cross section, there is a segment of the pipe where its cross-section diameter linearly narrows and then expands again to the original value. The constriction in the middle of the pipe, where the flow converges and then diverges again, is known as the *nozzle*.

Figure 307 shows the geometry of the converging-diverging nozzle, with the original geometry shown in Figure 307b and the one remaining after being cut into two halves due to symmetry shown in Figure 307b. This example has a wide variety of applications. Many similar examples can be found in the literature. Completion of this exercise may require extensive use of COMSOL Multiphysics *CFD* module. Therefore, this section mainly introduces the idea of developing such a model due to its importance in propulsion applications.

Karl Gustaf Patrik de Laval, a nineteenth-century Swedish engineer and inventor, built a nozzle in which an upstream high-pressure steam jet was transformed to a fluid with supersonic speed at the exit of the nozzle to the atmosphere. This design was part of an impulse steam turbine. This

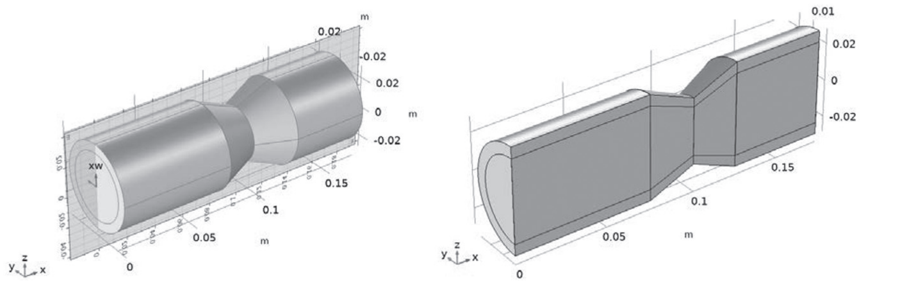

(*a*) (*b*)

Figure 307. Converging-diverging nozzle: (a) *Work Plane*, (b) Partitioned geometry.

method trades off the steam pressure for the kinetic energy. Modern rocket engines use this constricted structure as well, and it is referred to as the *de Laval nozzle*.

His work was originally used in turbines with bearings that were coated with oil. Thus, as the steam passed through the nozzle, oil contamination was present in it, affecting the efficiency of the engine. To address this issue, he invented a centrifugal machine that was able to separate the oil and steam. As an interesting side point, later on the inventor transferred the idea of the centrifugal separator to separating cream from milk.

The fluid behavior in a nozzle is governed by Bernoulli equation—a simplified form of Navier Stokes flow equation based on the conservation of energy principle. The law states that the sum of the kinetic, potential, and internal energies (summation of dynamic pressure and hydraulic head) remain constant. Since the process is a reversible adiabatic one, no heat is generated during the passage of the flow inside the constricted channel, and therefore it can be ignored. Since the flow continuity is to be satisfied within the structure, the smaller the flow cross-sectional area, the faster the constricted flow becomes. Following Bernoulli's principle, this higher speed results in lower pressure.

One of the features of this nozzle is that, given that fluid flows from high-pressure to low-pressure regions, the lower the back pressure (pressure of the flow destination) is, the higher the flow rate becomes. However, decreasing the back pressure to a smaller value than a critical one does not change the flow rate any further; this condition is called the *flow choking*.

As part of the problem definition, one needs to define conditions at the inlet and outlet. For this problem, these need to be defined by inlet and outlet pressures. This is different from previous exercises where a flow velocity was defined instead. Ideally, the maximum flow rate should be directed through the pipe for the maximum power to be generated. This flow rate is related to the ratio of the flow pressure at the upstream to that of the downstream (Table 6). It is noted that maximum velocity is achieved when Mach number, which is the ratio of the speed of the flow to that of the sound, equals one. For Mach numbers greater than one, the flow experiences choking, limiting the flow velocity, which is not desirable.

This flow characteristic is useful in propulsion applications operating with homogeneous fluids, where managing the flow upstream pressure and temperature is sufficient to achieve the desired flow rate, despite the downstream pressure. In order to increase the flow rate, the constricted area can also be widened. However, the same result is still obtained when decreasing the backpressure flow to lower than its critical value, where Mach at the constricted zone becomes one. In other words, after such a condition is reached, with decreasing the backpressure further, the flow rate does not change to what is achieved with Mach one; having said that, the downstream flow pattern may change. Up to this stage, when Mach is under one, flow is subsonic.

Temperature distribution inside the nozzle is essentially uniform—the same as the pressure distribution is. The fluid inside the converging-diverging nozzle is assumed to be an ideal gas. Table 6 lists values for several gases of the upstream-to-downstream absolute pressure ratios and heat capacity ratios, which are needed to calculate the critical conditions. For steam, the pressure ratio is 1.851, which is related to the ratio of the heat capacities. Note that the absolute pressure is the summation of the gauge and the atmospheric pressures. The pressure used in COMSOL Multiphysics can be defined as either a relative or absolute pressure. Inlet

Table 6. Properties of selected ideal gases [162].

Gas	Hydrogen	Steam (Water)	Helium	Dry Air Oxygen	Propane	Nitrogen-Carbon Monoxide
Heat capacity ratio $\gamma = C_p/C_v$	1.140	1.330	1.660	1.400	1.131	1.404
Minimum upstream-to-downstream absolute pressure ratio (P_u/P_d) $P_u/P_d = (2/(\gamma+1))^{-\gamma(\gamma-1)}$	1.899	1.851	2.049	1.893	1.729	1.895

and outlet temperatures can be obtained using the ideal gas law ($P = \rho RT$); assuming that the steam leaves the chamber at about 100 °C (373.15 K) at the atmospheric pressure, and that the steam gas constant is about 461.52 J/kgK, density (ρ) can be obtained as 0.588 kg/m^3. This density then can be employed, given the upstream pressure, in order to calculate the upstream temperature (670.55 K = 417.40 °C).

Calculations can be made in which the pressure ratio along with the area ratio (ratio of the open to the restricted spaces) may be employed along with the mass flow rate continuity and Bernoulli's principle to calculate the inlet (570 m/s) and outlet (175 m/s) velocities. This is also to expedite the solution convergence. Some of these calculations as well as parameters used are presented in Figure 308. For *Reynolds numbers* below 2,300, one expects a laminar flow. Figure 309 is presented for steam *Reynolds number* per velocity and velocity for the defined temperature and pressure ranges.

Settings
Parameters

Label: Parameters 1

Parameters

Name	Expression	Value	Description
area_inside	pi*(4*diameter_in/2)^2	0.0015518 m²	pipe interior surface area
area_outside	pi*(4*diameter_out/2)^2	0.0025023 m²	pipe exterior surface area
area_ratio	area_inside/converged_area	2.9308	ratio of the area to the constricted area, m
constricted_velocity	flow_rate/converged_area	83.882 m/s	
converged_area	pi*(4*(diameter_in-diameter_dif)/2.5)^2	5.2948E-4 m²	constricted area
diameter_dif	diameter_out-diameter_in	0.0029986 m	pipe thickness
diameter_in	(7/16)[in]	0.011112 m	pipe internal diameter
diameter_out	(5/9)[in]	0.014111 m	pipe external diameter
flow_downstream_pressure	(nn*101.325)[kPa]	1.0133E5 Pa	downstream pressure
flow_rate	open_velocity*area_inside	0.044414 m³/s	flow rate
flow_upstream_pressure	pressure_ratio*(flow_downstream_pressure)	1.0315E5 Pa	upstream pressure
flow_velocity	flow_rate/(area_inside)	28.621 m/s	flow velocity
h_horizontal	5[W/(m^2*K)]	5 W/(m²·K)	convective coefficient, horizontal surfaces
h_vertical	10[W/(m^2*K)]	10 W/(m²·K)	convective coefficient, vertical surfaces
L	0.1[m]	0.1 m	pipe length
mesh_size	0.0025[m]	0.0025 m	mesh size
minrec_pressure_ratio	minrec_pressure_ratio2*0.55	1.0181	
minrec_pressure_ratio2	1.851	1.851	ratio of the upstream to downstream absolute pressures, n
mu	0.0014[Pa*s]	0.0014 Pa·s	dynamic viscosity
n	1	1	multiplier for wall tempeature
nn	1	1	
nnn	1	1	multiplier for velocity
open_velocity	((2*flow_downstream_pressure/rho_steam)*((pressure_ratio-1)/(area_ratio^2-1)))^0.5	28.621 m/s	steam flow velocity
Patm	1[atm]	1.0133E5 Pa	atmospheric pressure
premiter	0.5*(pi*diameter_in)	0.017455 m	pipe tip perimeter
pressure_ratio	minrec_pressure_ratio*1	1.0181	
Reynolds_constricted	(2/3)*rho_steam*constricted_velocity*(4*diameter_in)/mu	1044.6	
Reynolds_open	(2/3)*rho_steam*open_velocity*diameter_in/mu	89.108	reynolds number
rho	998.2071[kg/m^3]	998.21 kg/m³	density
rho_steam	flow_downstream_pressure/(steam_gas_constant*steam_temp)	0.58836 kg/m³	
steam_gas_constant	461.52[J/(kg*K)]	461.52 J/(kg·K)	
steam_temp	100[degC]	373.15 K	
sun_radiation	1000[W/m^2]	1000 W/m²	sun's radiation
Tamb	22[degC]	295.15 K	ambient temperature
time	5400[s]	5400 s	time
Tinit	22[degC]	295.15 K	initial temperature
Tinlet	(flow_upstream_pressure)/(rho_steam*steam_gas_constant)	379.89 K	steam inlet temperature
Tref	20[degC]	293.15 K	reference temperaure
Twall	(n*25)[degC]	298.15 K	wall temperature
wall_height	L/2	0.05 m	wall height

Figure 308. Parameters used for converging-diverging nozzle study (global level).

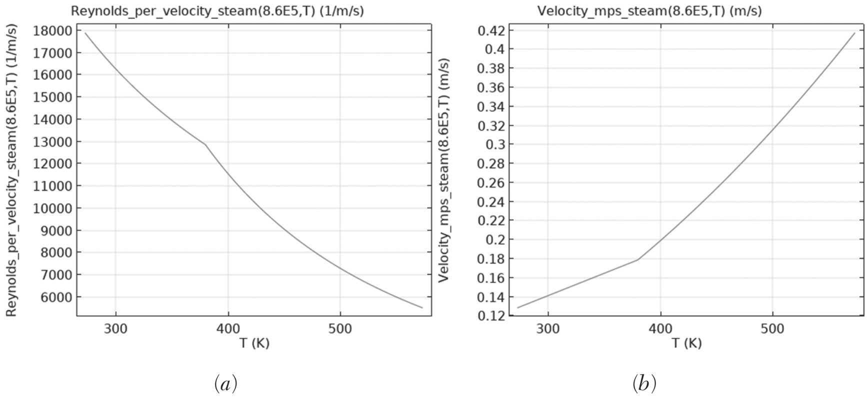

Figure 309. Steam temperature-dependent properties at 860 kPa: (a) *Reynolds number* per flow velocity, (b) Laminar flow velocity inside the pipe (*Re* = 2,300).

CHAPTER 14

GOOD PRACTICES

The term *best practices* is a well-known expression in a variety of engineering disciplines in which the product CDIO (Conceive, Design, Implement, and Operate) lifecycle concept is used. When working on a model, analysis, or process of any kind, a variety of techniques may be employed, revised, and expanded upon. Hence, the author does not necessarily agree with the expression *best practices*; instead there are *good practices*—those more likely to lead to a useful outcome. Nevertheless, the challenge endures to improve processes and designs. This is to ensure refining performance and eliminating waste (i.e., *Muda*; a Japanese term for Futility, Uselessness, and Wastefulness), focusing on critical-to-quality characteristics [163].

There is no preferred approach to design geometries; the process usually fits in three categories: (1) approach, (2) order, and (3) interface. The approach tells the story of the origin of the assembly or part, where and how it is created, and the environment in which it is grown to its full maturation. The order informs the successive steps that have been taken for the geometry to be generated—if it is *ordered* (each step is the milestone for the next steps) or *unordered* (steps are independent of one another). The interface tells the interconnectivity between the assembled parts and their relation to the new environment. The host environment in these scenarios are usually the FEM specialized tools, while the originator can be either the CAD or FEM tool, or even a combination of both.

As science progresses, the approach, order, and interface improve through the introduction of new commercial software packages in analysis and geometry-generation fields. With this knowledge progression, the concept of standardization becomes even more important, since the cost associated with converting the geometries generated in prior revisions of the specialized tools (FEM or CAD) becomes prohibitive. Projects are delayed when the geometries created with an older-version CAD tool cannot be easily translated to the one compatible with the new CAD tool—the only acceptable version to a newly developed FEM tool. Note that FEM is used often in this book; however, it may be extended to other types of models where physics of any kind are investigated (e.g., Computational Fluid Dynamics, CFD). Although the community of the fields' specialists may propose workarounds—and the vendors attempt to introduce compatible products—costly challenges remain both in terms of human effort and project delivery timelines.

There are multiple steps to be taken on the way to an accurate heat transfer model. Geometry creation is among the first steps, and so it will affect all the subsequent ones. Thus, one must devote appropriate care to this stage of model development. The geometry must be carefully reviewed before and after import into the analysis tool. One should be particularly careful if there is any change in the units used, such as a change from meters to millimeters. Confusion with units has caused trouble countless times, as long as humans have been using technology. In one well-known airplane accident in 1983, an Air Canada jet ended up running out of fuel at 41,000 ft but managed to make a safe landing by gliding into an airport in Gimli, Manitoba, thanks to the incredible skill of the pilot. This became known as the *Gimli Glider case* [164]. The cause was later found to be due to an error with fuel quantity calculations, which confused pounds and kilograms at one point. While this example is not one of thermal analysis, nevertheless it shows how one such small error can have enormous consequences.

Use of variables or parameters when setting up the models is always a good practice. This approach facilitates the interface between multiple platforms, allowing for synchronization between the tools. Following this practice facilitates carrying out sensitive analysis studies. When selecting parameter names, take care to choose meaningful ones that will allow you to correctly recognize each variable. Do the work methodically; doing it right the first time saves future work.

Another good practice to follow is to watch out for devoting excessive resources in the pursuit of minor issues. One needs to keep in mind the overall sense of the level of uncertainty of the model and avoid working on areas which are likely to have minute effects on the model predictions.

Thus, if one can only estimate the heat transfer coefficient to within 10 percent of the actual value, there is little benefit to measuring density to eight decimal places. On the other hand, resources devoted to pursuit of the issues with little impact on the outcome could be better spent in other areas, with greater return on your resource investment.

The last note is that the designers should always try to think ahead while they are in the middle of the creation process. They need to remember to occasionally step away from the day-to-day details they are focusing on and take a broader outlook on the big picture. They should be asking themselves: what is happening next and one more step after that; what kind of accessibility features do I need to include in my design? Will I need to define additional boundary conditions or reinforce the structure? Do I need to incorporate redundancy systems for safety purposes such as the ones seen in the Boeing 747 design? Do I need to check the historical data for lessons learned and compatibility of my chosen design with the environment such as Challenger space shuttle O-ring experience? What are the steps to be taken to ensure a socially responsible, environmentally friendly, and personally fulfilling project? What is happening after that? How the creation is being used? What would be the possible outcomes if the product were not employed as intended?

Thinking ahead is critical for anyone working on a project that will be used by others. So, while in the middle of some busy day, as you are working on an apparently minor task, you make a little shortcut, just to get things done, a month, a year, or a decade later, it may come back to you with some unpleasant consequences. So, be on the lookout for these small decisions that can have serious consequences [3,165].

CHAPTER 15

LEAN SIX SIGMA IMPLEMENTATION

A project's or a product's journey starts with the idea conception and ends when it is fully operational. All involved would like to extract as much benefit from the project as possible, be it the company's bottom line or society's interests. To make any improvement, one needs to take into account the historical data, the current situation, and any future trends. But it is impossible to improve anything if one cannot quantify accurately the base conditions. One must be able to both determine those base conditions and the current situation in order to predict for the future and to make sound plans. This is what makes it so important to have an effective methodology by which to make this assessment.

The Lean Six Sigma concepts provide tools to measure process progress, quantify the deviations, and predict their effects on the process trend. It is the trio of quality, time, and cost that plays the decisive role in defining how satisfied you are with the project's progress and how successful it will be. Just about all cases contain room for improvement. Empirical statistical techniques are used to analyze the collected *qualitative* and *quantitative* data. This data analysis identifies the critical-to-quality characteristics and variables that then serve as input for the process model. This approach also helps to isolate those variables that are trivial and should be disregarded in the decision-making process.

The concept of a quantitative study based on the critical variables can be explored by looking at a project that many people undertake these days—losing weight. Imagine that your current weight prevents you from fulfilling your dream of a tandem skydiving jump, where there is a strict weight limit of 200 lb, and there is a once-in-a-lifetime opportunity for such a jump that is coming in eight weeks. Your current weight is the baseline and 190 lb is the desired weight that you would like to achieve in six weeks, leaving yourself two weeks as a precaution. Let us assume that you do not consider using extreme measures like surgery to achieve the desired weight. You are then to follow a diet (exercise and food) to ensure that your weight trend follows the interpolated weight points you have projected from the initial start date to the end of the timeline. The weekends might be the times to check for process milestones—when you check your actual weight against your planned values. If for whatever reason this trend has deviated from the set path, and the variation is significant, you will know that something is not going right with your current approach and you should make a correction as soon as possible to be able to experience the exhilaration of the freefall that you have been dreaming of.

The same approach can be brought to the engineering applications. The engineers or scientists decide upon a target value and strive to achieve it by (1) recognizing that the improvement is necessary and feasible; (2) defining the areas in which improvements can and should be made; (3) measuring the maximum rate of return in each identified area; (4) analyzing how the changes influence the overall bottom line; (5) improving the methodology to introduce revisions by making educated decisions; (6) controlling the output by monitoring the processes—adhering to the recognized best practices; (7) standardizing the processes and establishing new best practices; and (8) integrating the methodology throughout theprocesses or operations by allocating appropriate resources—expertise, time, and funding.

The product of this effort is an improved relationship between cost, quality, and time achieved by removing the unnecessary steps (wastage or redundancy)—the visible or hidden steps that add no value to the experience [166]. The main potential sources of waste are Transportation, Inventory, Material, Waiting, Overproduction, Overprocessing, Defects, and Skills (TIMWOODS). Being responsible citizens, the engineers and scientists strive to reduce waste to the extent possible in order to respect (1) nature, (2) people or the surrounding world including the resources they indirectly interact with, and (3) immediate environment. The value entitlement defines this interaction, which is merely a business transaction in the form of services, products, or experiences, and the responsibilities of individuals to respect others.

Lean Six Sigma defines quality as the state of the realization of the full value of entitlement in all aspects of business relationships. Entitlement is the right value of expectation, which takes the form of utility (form, fit, and function), access (volume, time, and location), and worth (economical, emotional, and intellectual). Entitlement is what you are entitled given the available resources. It is the rightful level of expectation of every aspect of a business relationship.

One way to implement Lean Six Sigma is to design smart experiments. Saying *smart* here not only means a synonym of "clever" but it is also a memory aid, standing for Specific, Measurable, Attainable, Relevant, and Timely (SMART). Before undertaking any project or an experiment, it pays to review these points to check that the project satisfies all of them to a large extent.

1. Specific: you know exactly what you will be doing—the scope is defined clearly;
2. Measurable: you would be able to collect good quality data;
3. Attainable: everything you plan to do is within your capabilities and you are aware that there are things out of your control that can interfere;
4. Relevant: the project addresses some of the needed deficiencies (i.e., its usefulness is confirmed); and
5. Timely: it can be completed within an acceptable timeframe.

For example, one can try to apply these considerations to the thermal imaging experiment reported in this book; in this experiment, a cup of hot water was observed using a thermal camera.

1. **S**: the experiment goals are clearly defined: measuring temperature at specific locations on the glass using a thermal camera;
2. **M**: the camera is able to collect temperature measurements of acceptable accuracy for the required purpose;
3. **A**: an affordable thermal camera is available, working properly, calibrated, and does not need to be borrowed from someone else;
4. **R**: the experimental results are useful in validating the numerical model predictions; and
5. **T**: all the experimental equipment is easily available on site and the work can be completed within one day, or within a reasonable time investment.

To perform the root cause analysis to identify error sources, the first step is to find these sources by different means such as brainstorming. The ideas generated by brainstorming, when you are questioning the process and methodology, can be organized by means of 5S methodology (Sort, Set in order, Shine, Standardize, and Sustain).

Imagine you organized your graduation party. You brought all the supplies: the teacups, plates, cutlery, napkins, bowl, cake, soft drinks, and party hats. After the party, you were left with cleaning up the mess left afterward. It looked like an unnerving task, but you remembered 5S methodology you learned during your Lean Six Sigma black-belt training.

1. Sort: you sorted items into appropriate categories and identified which you needed to deal with immediately and which you could take care of later;
2. Set in order: you took those items that required immediate attention and separated them into categories, such as *to recycle*, *to throw away*, *to put away*;
3. Shine: you cleared the place to create an area where you could move and work;
4. Standardize: you made a note of your procedure so you can repeat it in the future under similar circumstances;
5. Sustain: you ensured that the improvements can be sustained. For this reason, design standards were developed that include systems of measurements and acceptable tolerances.

Implementing good practices is a systematic approach that should be implemented when planning, executing, and reporting the design-related tasks to comply with the certification requirements. After recognizing the parameters that may affect the process or product outcome, a number of tests may be conducted in which the critical ones among them may be selected for further review. Sensitivity analysis characterizes the rate at which the dependent variable changes as a function of the significant critical variables identified previously. Select the most important contributing items, the ones that make the most impact—the few critical to quality variables, and eliminate the rest—the trivial many.

When designing experiments, create a table encompassing the critical variables and decide on the tests and the number of repeats. The rows of the table are associated with the experiments and the columns with critical process parameters. You may decide to run experiments for complete sets of variables along with their combinations. For example, for two and three sets of process parameters you can set up three and seven sets of experiments. The effect of each critical variable on the dependent variable can then be analyzed using a regression analysis—a mathematical relationship that identifies *goodness of fit* to data by statistical tools. Report *key performance indices* as the last step.

CHAPTER 16

CONCLUSION

When creating thermal designs, creativity is as important as adhering to the known and tested techniques. If designers, engineers, doctors, and decorators were to just follow the old-fashioned knowledge and construction techniques, humans would have still lived in the Flintstones versions of cave homes. Though actually, contemporary cave homes do offer modern amenities within a primeval setting [167,168,169]. Thinking outside the construction square is the reason for exceptional creations at any time and in any place.

Independent thinking in an unrestricted environment is an indispensable part of this process. The fuel of resources and experiences available to a creative mind ignited by its imagination propels the development of new ideas into reality. Interconnections among diverse fields of study, such as art, engineering, and fashion, have brought us the innovative products that enrich our lives—think about the lifestyle changes brought about by the introduction of smart phones and tablet computers such as iPad.

Creative and independent thinking requires courage, as there are often pressures to conform to the accepted practices. Historically, brave scientists and innovators have made sacrifices to bring new ideas and better life to humanity. In the seventeenth century, Galileo Galilei realized that the old concepts of planetary motion simply did not make sense in light of the new ideas proposed by Copernicus and considering what Galileo saw himself with the new telescope that he built. However, he lived in a time when the church wanted to protect the *status quo*, and so he was punished for his ideas; but the ideas could not be suppressed and flourished despite all the reactionary efforts.

Innovative and responsible designs are not only rewarding for the designers who create them, but they also benefit immensely all of humanity and the environment. Looking around us, there are numerous examples in which this brilliance of the human mind can be seen. These projects show how our natural resources can be used responsibly by designing, constructing, or retrofitting intelligent, efficient, and eco-friendly projects that educate and give solace to the people. Mentioned here are some examples of ethical leadership in the use of thermal management techniques.

1. Vertical gardens as a platform for planting, working, and shading environments—an example is Supertrees Grove at Gardens in central Singapore, which improves quality of life by introducing greenery into this densely populated city. These trees not only provide homes to exotic plants and birds but also exist in harmony with their surroundings, mimicking a living tree by harvesting solar energy with the photovoltaic cells and collecting rainwater for irrigation and fountain displays [170].
2. Passive house designs being incorporated into new building architecture or as a retrofit into the existing ones—they heat and cool the structure so as to minimize its ecological footprint. Examples are the Vauban residences in Freiburg, Germany, and Cornell's green 26-story high-rise campus on Roosevelt Island in New York City [171,172,173].
3. Energy harvesting from the waves using PowerBuoy, which can be either connected to an electrical grid using power transmission cables or can operate autonomously in a deep-water environment—PowerBuoys installed in Cromarty Firth, Scotland, can generate 3 MW of power—they convert into electricity the energy of the rising and falling of waves. They are aesthetically pleasing due to their low surface profiles and small horizontal footprints, and can operate in severe conditions [174,175].
4. Efficient residential apartments that people wish to live in even though they seemingly lack basic amenities, such as a parking garage or air conditioning and, in addition, are located next to a train track—an apartment building in Melbourne, Australia, was designed to keep the heat in winter and cool in summer with the ultra-thick exterior walls shielding them from the train noise; they have a rooftop garden to provide additional insulation and a green environment [176].

5. Sustainable cities that are both aesthetically pleasing and functional—an example is Dubai Smart Sustainable City project. It looks like a flower in the middle of a desert, with shiny roofs covered by solar panels generating 200 MW of electricity [177].

6. Sunshine harvest in the most remote and underprivileged villages, in places that are exposed to sunshine most of the year—Sichanloo is a remote location in arid rural Iran, with simple clay houses which have been recently decorated with new high-tech rooftops made from photovoltaic cells provided by a government-subsidized project. These are part of a growing effort to provide steady power for a fossil-fuel country that counts on oil and natural gas sources for 40 and 37 percent of its energy intake with an increasing energy demand predicted to be 30 percent between 2010 and 2020. Sichanloo and similar communities are recovering from noise and pollution that gas-fueled power generators imposed on their lives for decades [178].

7. LEED (Leadership in Energy and Environmental Design) *certified* designs that improve efficiency and health to achieve a sustainable environment—these initiatives can transform a tornado-hit American city such as Greensburg, Kansas, into a model of a green village [179,180]. They can transform a fading clay pit in Cornwall, England, into a thriving green community by building an eco-friendly park, museum, and indoor rainforest that educate us on the responsible use of natural resources such as composting waste, water treatment, geothermal, and wind energy [181].

16.1 A Universe in a Cup of Tea

The complexity of the world around us is unimaginable. Even the vacuum, the so-called the *empty space*, may not be as empty as we think. Physicists are saying it is full of *energy*. They are discovering patterns that can connect the microscopic world of the quanta with the large-scale phenomena that we can experience with our senses. The most radical ideas are often brought to light by misfits, those who are blessed with the power of curiosity and who can think critically about their surroundings as opposed to being preoccupied with fitting in to avoid being intimidated. One of them is Nassim Haramein, a contemporary Swiss-Egyptian amateur physicist, who claims to have developed a unified field theory that he, along with his collaborator in the academic-but-fringe physics community, Elizabeth Rauscher, have named *Haramein-Rauscher Metric*. This new approach integrates Coriolis and torque effects in Einstein's field equations. Very small quantities of energy are made of larger quantities of energy on a quantum level—also known as the *vacuum fluctuations*.

In his 2016 TEDx talk, Haramein explains how atomic structures parallel the cosmic ones, and how the singularity of a black hole is similar to that of an atomic nucleus. The matter itself is mostly empty space. If the atom were the size of St. Peter's Cathedral dome, the nucleus would be the size of a pin head. So, perhaps it is the empty space that defines the material world, and not the other way around? A dynamical Casimir effect has been demonstrated, which provides proof for the vacuum energy fluctuations and space filled with virtual particles, which flit in and out of existence [182].

Haramein measures the world using a constant called *Planck length*. It is an extremely small number (1.616×10^{-35} m) equal the distance light travels in one unit of *Planck time*. If one were to scale up *Planck length* to the size of a grain of sand, then the proton size would be equal to the distance between the Sun and Alpha Centauri. He calculates that *Planck density* of a vacuum is 10^{93} g/cm^3. The number is so large that fitting the entire known universe inside a 1 cm^3 results in density of 10^{55} gm/cm^3, which is still many orders of magnitude smaller.

He was able to connect the quantum world of *Planck density* with a large-scale world by studying a Cygnus X-1 black hole. This work enabled him to provide an accurate estimation of the proton's diameter, with recent experimental work adjusting the previously known proton size to more closely match his prediction [183].

These latest breakthroughs may lead to humanity mastering the gravitational field the way we have mastered the electromagnetic field over the past two centuries. Just like the technology based on the understanding of the electromagnetism has transformed our lives, so the gravitational field knowledge may lead in the future to technologies that we cannot even begin imagining today. The sky will not be the limit anymore!

An eighteenth-century Persian (Iranian) poet, Seyyed Ahmad Hatef Esfahani, wrote poems of complex lyrical structures with recurrent themes of a mystical nature, known as the *tarji'-bands*. One of these, known as *There is Only One and No One but Him*, says that if you open the heart of each particle, you will see the *Sun* inside it. Perhaps this is not just a poetic turn of phrase? If so, maybe there is *a universe in a cup of tea*?

APPENDIX A

Glossary

APDL	ANSYS Parametric Design Language
CAD	Computer Aided Design
CADAM	Computer-Augmented Design and Manufacturing
CAE	Computer Aided Engineering
CAM	Computer Aided Manufacturing
CATIA	Computer-Aided Three-dimensional Interactive Application
CDIO	Conceive, Design, Implement, and Operate
CFD	Computational Fluid Dynamics
CMB	Cosmic Microwave Background
CUORE	Cryogenic Underground Observatory for Rare Events
DAEAC	Direct Analogy Electric Analog Computer
DEM	Discrete Element
DSC	Differential Scanning Calorimetry
DTA	Differential Temperature Analysis
ECAD	Electronic and Electrical Computer-Aided Design
EES	Engineering Equation Solver
FDM	Finite Difference Method

FEM	Finite Element Method
FERC	Federal Energy Regulatory Commission
FLT	Fish, Lettuce, and Tomatoes
Fo	Fourier Number ($\alpha t/L^2$)
FVM	Finite Volume Method
Gr	Grashof Number ($g\beta \Delta TL^3/\nu^2$)
HG	Heat Generation
HPC	High-Performance Computing
HVAC	Heating, Ventilation, and Air Conditioning
IDE	Integrated Development Environment
ISS	International Space Station
Laser	Light Amplification by Stimulated Emission of Radiation
LED	Light Emitting Diode
LEED	Leadership in Energy and Environmental Design
LFA	Laser Flashing Analysis
LIM	Linear Induction Motor
LTW	Laser Transmission Welding
MOS	Model Output Statistics
MRI	Magnetic Resonance Imaging
Muda	Futility, Uselessness, and Wastefulness
Nu	Nusselt Number (hL/k)
OAI	Object Action Interface
PDE	Partial Differential Equation
PLM	Product Lifecycle Management
PRT	Part
QGS	Quadruple Gas Spectrometer
RAM	Random-Access Memory
SCADA	Control and Data Acquisition
SCUBA	Self-Contained Underwater Breathing Apparatus

SLD	Solid
SMART	Specific, Measurable, Attainable, Relevant, and Timely
TAF	Terminal Aerodrome Forecast
TIMWOODS	Transportation, Inventory, Material, Waiting, Overproduction, Overprocessing, Defects, and Skills
TGM	Thermogravimetric Method
TMA	Thermomechanical Analysis
TMS	Thermal Module Suite
TOA	Thermo-Optical Analysis
TPS	Thermal Protection System
WHO	Wold Health Organization
1D	One Dimensional
2D	Two Dimensional
3D	Three Dimensional
5M	Material, Machine, Method, Measurement, Man, and Money
5S	Sort, Simplify, Shine, Standardize, and Sustain

APPENDIX B

List of Symbols

B.1 Variables

a	constant value
a	fit parameter
$atan$	arc tangent operator
A	surface area (m^2, ft^2)
A'	constant value
b	constant value
b	fit parameter
B'	constant value
c	constant value
c	fit parameter
c_p	specific heat capacity at constant pressure (J/kgK)
c_v	specific heat capacity at constant volume (J/kgK)
C	heat capacity (J/kgK)
C_p	heat capacity at constant pressure (J/K)
C_v	heat capacity at constant volume (J/K)
C'	constant value

Cos	cosine operator
$Cotan$	cotangent operator
Csc	cosecant operator
d	constant value
d	fit parameter
dx	finite difference along the x-coordinate (m)
dy	finite difference along the y-coordinate (m)
dz	finite difference along the z-coordinate (m)
e	error
e	constant value
e_{in}	specific internal energy at input (J/kg)
e_{gen}	specific internal energy generated (J/kg)
e_{out}	specific internal energy at output (J/kg)
e_{st}	specific internal energy storage (J/kg)
$\dot{e}_{in}$	rate of specific internal energy at input (W/kg)
$\dot{e}_{gen}$	rate of specific internal energy generated (W/kg)
$\dot{e}_{out}$	rate of specific internal energy at output (W/kg)
$\dot{e}_{st}$	rate of specific internal energy storage (W/kg)
E_{in}	internal energy at input (J)
E_{gen}	internal energy generated (J)
E_{out}	internal energy at output (J)
E_{st}	internal energy storage (J)
$\dot{E}_{in}$	rate of internal energy at input (W)
$\dot{E}_{gen}$	rate of internal energy generated (W)
$_{out}$	rate of internal energy at output (W)
$\dot{E}_{st}$	rate of internal energy storage (W)
f	function
f	constant value
F'	angle (°, rad)

g	gravity acceleration (m/s^2)
h	constant value
h	fit parameter
i	unit vector
j	unit vector
k	unit vector
k	thermal conductivity (W/mK)
k	Boltzmann constant (J/K)
k_x	thermal conductivity along the x-coordinate (W/mK)
k_y	thermal conductivity along the y-coordinate (W/mK)
k_z	thermal conductivity along the z-coordinate (W/mK)
l	characteristic length (m)
ln	natural logarithm operator
log	logarithm operator
L	fin length (m, ft, in)
m	mass (kg)
n	multiplier
nn	multiplier
$nnnn$	multiplier
nnq	multiplier
nnt	multiplier
nt_i	multiplier
P	power (W)
P	pressure (Pa)
$Power$	power (W)
q_{fin}	heat transfer from the fin (W/m^2)
q_x	heat flux along the x-coordinate (W/m^2)
q_y	heat flux along the y-coordinate (W/m^2)
q_z	heat flux along the z-coordinate (W/m^2)

q_0	initial heat generation (W/m^3)
$\dot{q}_{gen}$	heat generation (W/m^3)
r	radius (m), radius ratio
r_i	internal radius (m, ft, in)
r_o	external radius (m, ft, in)
S	view factor
t	time (s)
th	fin height (m), thickness (m, ft, in)
$Scale$	scale
Sec	secant operator
Sin	sine operator
T	temperature (ºC, K)
T_{amb}	ambient temperature (ºC, K)
T_b	bulk temperature (ºC, K)
T_i	initial temperature (ºC, K)
T_{init}	initial temperature (ºC, K)
T_m	melting temperature (ºC, K)
T_s	surface temperature (ºC, K)
T_∞	surroundings temperature (ºC, K)
u	dependent variable
u	response function
u	axis along the x-coordinate
u_i	dependent variable component along the x-coordinate
u_x	change of dependent variable along the x-coordinate
u_{xx}	derivative of change of dependent variable along the x-coordinate
u_ψ	angular change of dependent variable about the x-coordinate
v	dependent variable
v	response function
v	axis along the y-coordinate

v_i	dependent variable component along the y-coordinate
v_x	change of dependent variable along the y-coordinate
v_{xx}	derivative of change of dependent variable along the y-coordinate
v_φ	angular change of dependent variable about the y-coordinate
V	volume (m^3, ft^3, in^3)
w	dependent variable
w	axis along the z-coordinate
w_i	weight fraction for content "i" (kg of content/kg of the total, grains per grains)
w_i	dependent variable component along the z-coordinate
w_x	change of dependent variable along the z-coordinate
w_{xx}	derivative of change of dependent variable along the z-coordinate
w_θ	angular change of dependent variable about the z-coordinate
x	coordinate along the x-axis
x	distance along the x-coordinate (m, ft, in)
x_i	dependent variable component along the x-coordinate
x_i	length along the x-coordinate (m, ft, in)
x_0	reference length (m, ft, in)
y	fit parameter
y	coordinate along the y-axis
y	distance along the y-coordinate (m, ft, in)
y_i	dependent variable component along the y-coordinate
y_i	depth along the y-coordinate (m, ft, in)
y_0	reference depth (m, ft, in)
z	coordinate along the z-axis
z	distance along the z-coordinate (m, ft, in)
z_i	dependent variable component along the z-coordinate
z_i	height along the z-coordinate (m, ft, in)
z_0	reference height (m, ft, in)

B.2 Greek Symbols

α	thermal diffusivity (m^2/s)
α	absorptivity
β	coefficient of thermal expansion for gas (1/K)
ε	emissivity
Δ	difference operator
Δt	time step (s)
Δt	time difference (s, min, hr)
ΔT	temperature rise (°C, K)
Δx	step size along the x -coordinate (m, ft, in)
Δy	step size along the y-coordinate (m, ft, in)
Δz	step size along the z-coordinate (m, ft, in)
θ	rotation angle about the vertical axis, z-coordinate (°, rad)
θ	dimensionless temperature
θ_{amb}	dimensionless ambient temperature
θ_b	dimensionless bulk temperature
θ_i	dimensionless initial temperature
θ_m	dimensionless melting temperature
θ_s	dimensionless surface temperature
θ_∞	dimensionless surroundings temperature
$\dot{\theta}$	angular velocity about the vertical axis, z-coordinate (rad/s)
$\ddot{\theta}$	angular acceleration about the vertical axis, z-coordinate (rad/s^2)
λ	wavelength (nm)
μ	dynamic viscosity (kg/ms)
ϑ	kinematic viscosity (m^2/s)
ρ	density (kg/m^3)
ρ	reflectivity
σ	Stefan Boltzmann constant (W/m^2K^4)
σ	standard deviation

τ	transmissivity
φ	rotation angle about the lateral axis, y-coordinate (°, rad)
$\dot{\varphi}$	angular velocity about the lateral axis, y-coordinate (rad/s)
$\ddot{\varphi}$	angular acceleration about the lateral axis, y-coordinate (rad/s^2)
ψ	rotation angle about the longitudinal axis, y-coordinate (°, rad)
$\dot{\psi}$	angular velocity about the longitudinal axis, y-coordinate (rad/s)
$\ddot{\psi}$	angular acceleration about the longitudinal axis, y-coordinate (rad/s^2)

B.3 Subscripts

amb	ambient
gen	generated
i	initial state
in	input
init	initial state
o	initial, reference
out	output
m	melting point
x	along the x-coordinate
y	along the y-coordinate
z	along the z-coordinate
st	stored
t	time
∞	surroundings

APPENDIX C

List of Figures

APPENDIX D

LIST OF TABLES

BIBLIOGRAPHY

1 Shaykh Abbas Qummi (Author), Ali Quli Qarai (Translator), Mafatih al-Jinan: A Treasury of Islamic Piety (Translation & Transliteration): Volume Two: The Book of Ziyarah, CreateSpace Independent Publishing Platform, First Edition, p. 676, 2018.

2 Layla S. Mayboudi, Heat Transfer Modelling Using COMSOL: Slab to Radial Fin (Multiphysics Modeling Series), p. 272, Mercury Learning and Information, 2018.

3 Layla S. Mayboudi, Geometry Creation and Import with COMSOL Multiphysics®, p. 260, Mercury Learning and Information, 2019.

4 https://www.britannica.com/biography/Katherine-Johnson-mathematician

5 https://www.britannica.com/biography/Alan-Turing

6 https://en.oxforddictionaries.com/definition/heat

7 https://www.britannica.com/biography/Robert-Boyle

8 https://www.thoughtco.com/the-discovery-of-fire-169517

9 http://gby.huji.ac.il/

10 Katharine MacDonald, “The Use of Fire and Human Distribution,” Temperature (Austin), vol. 4, no. 2, pp. 153–165, 2017; https://www.ncbi.nlm.nih.gov/pmc/articles/PMC5489006/

11 https://en.wikipedia.org/wiki/Classical_element

12 https://www.britannica.com/biography/Francis-Bacon-Viscount-Saint-Alban

13 James Riddick Partington, An Advanced Treatise on Physical Chemistry, Prentice Hall Press, p. 728, 1953.

14 https://www.britannica.com/biography/Johann-Joachim-Becher

15 https://www.britannica.com/biography/Georg-Ernst-Stahl

16 https://www.britannica.com/biography/Antoine-Lavoisier

17 https://www.britannica.com/biography/Thomas-Newcomen

18 https://www.britannica.com/biography/Joseph-Black
19 https://www.britannica.com/biography/James-Watt
20 Nicolas Léonard Sadi Carnot was born in Paris into a family that was distinguished in both science and politics. He was the first son of Lazare Carnot, an eminent mathematician, military engineer, and leader of the French Revolutionary Army. Lazare chose his son's third given name (by which he would always be known) after the Persian (Iranian) poet Sadi of Shiraz. Sadi was the elder brother of statesman Hippolyte Carnot and the uncle of Marie François Sadi Carnot, who would serve as President of France from 1887 to 1894; https://www.britannica.com/biography/Sadi-Carnot-French-scientist
21 John J. O'Connor, Edmund F. Robertson, Nicolas Léonard Sadi Carnot, MacTutor History of Mathematics archive, University of St Andrews, Scotland.
22 Homa Katouzian, Sa'di, the Poet of Life, Love, and Compassion (A Comprehensive Study of Sa'di and His Works), p. 160, Oneworld Publications, 2006.
23 https://www.britannica.com/biography/Robert-Brown-Scottish-botanist
24 https://www.britannica.com/biography/Jan-Ingenhousz
25 https://en.wikipedia.org/wiki/List_of_things_named_after_Leonhard_Euler
26 https://www.britannica.com/biography/Joseph-Baron-Fourier
27 https://www.britannica.com/biography/Jean-Baptiste-Biot
28 https://www.britannica.com/biography/Claude-Louis-Marie-Navier
29 https://www.britannica.com/biography/Sir-George-Gabriel-Stokes-1st-Baronet
30 https://www.britannica.com/biography/Georg-Ohm
31 https://www.britannica.com/biography/Adolf-E-Fick
32 https://www.britannica.com/biography/Pierre-Simon-marquis-de-Laplace
33 Hourly History, Galileo Galilei: A Life from Beginning to End, p. 50, Amazon Digital Services LLC Kindle Edition, 2017.
34 https://www.britannica.com/biography/Jean-Leurechon
35 https://www.britannica.com/biography/Elijah-Delmedigo
36 https://www.britannica.com/biography/Ferdinand-II-grand-duke-of-Tuscany
37 https://fr.wikipedia.org/wiki/Carlo_Renaldini
38 James Gleick, Isaac Newton, p. 288, Vintage, 2004.
39 https://www.britannica.com/biography/Daniel-Gabriel-Fahrenheit
40 https://www.britannica.com/biography/Anders-Celsius
41 https://www.britannica.com/biography/William-Thomson-Baron-Kelvin
42 https://www.britannica.com/biography/Thomas-Clifford-Allbutt
43 https://patents.justia.com/inventor/francesco-pompei
44 https://www.nist.gov/si-redefinition/kelvin-thermodynamic-temperature
45 https://www.sciencealert.com/after-a-century-of-debate-cooling-to-absolute-zero-has-been-declared-mathematically-impossible
46 https://timesofindia.indiatimes.com/home/science/Lowest-temperature-ever-in-universe-recorded-at-Italian-lab/articleshow/44907265.cms
47 http://hyperphysics.phy-astr.gsu.edu/hbase/Solids/maglev.html

48 https://www.nibib.nih.gov/science-education/science-topics/magnetic-resonance-imaging-mri
49 https://en.wikipedia.org/wiki/University_of_Basel
50 https://learn-xpro.mit.edu/quantum-computing?utm_medium=sem&utm_source=mitxpro&utm_campaign=quantum-3t-2019&utm_content=aw-a&gclid=EAIaIQobChMIiI_YkYXE5AIVjI7ICh0Z2QTJEAAYASAAEgLVr_D_BwE
51 http://www.ccg-gcc.gc.ca/icebreaking/home
52 https://www.carolina.com/teacher-resources/Interactive/the-science-of-popcorn/tr23952.tr
53 http://www.dgfett.de/material/physikalische_eigenschaften.pdf
54 https://solarsystem.nasa.gov/planets/venus/overview/
55 https://www.goldennumber.net/body-temperatures/
56 https://www.khanacademy.org/science/biology/principles-of-physiology/metabolism-and-thermoregulation/a/animal-temperature-regulation-strategies
57 R. Yagil, Camels and Camel Milk, Animal Production and Health Paper, M21, p. 69, Food and Agriculture Organization of the United Nations (FAO) Rome, 1982; http://www.fao.org/3/X6528E/X6528E00.htm#TOC
58 https://wilderness-safaris.com/blog/posts/10-amazing-facts-you-probably-didn-t-know-about-giraffe
59 Edited by Bernd Heinrich, Encyclopedia of Insects, p. 1168, Second Edition, 2009.
60 Bernd Heinrich, "Insect Thermoregulation," Science Direct, Endeavour, vol. 19, no. 1, pp. 28–33, 1995; https://www.sciencedirect.com/science/article/pii/016093279598891I
61 https://www.britannica.com/animal/reptile/Growth-and-longevity
62 https://www.britannica.com/animal/Komodo-dragon
63 https://www.disabled-world.com/calculators-charts/degrees.php
64 https://www.livescience.com/34128-limits-human-survival.html
65 https://emedicine.medscape.com/article/1125851-overview
66 https://www.cancer.org/treatment/treatments-and-side-effects/treatment-types/hyperthermia.html
67 Scott F. Nadler, Kurt Weingand, Roger J. Kruse, "The Physiologic Basis and Clinical Applications of Cryotherapy and Thermotherapy for the Pain Practitioner," Pain Physician, pp. 395–399, vol. 7, 2004; https://www.painphysicianjournal.com/current/pdf?article=MTU3&journal=20
68 https://www.britannica.com/biography/Bartolomeu-Lourenco-de-Gusmao
69 https://www.grc.nasa.gov/www/k-12/TRC/Aeronautics/Hot_Air_Balloon.html
70 https://www.britannica.com/biography/Montgolfier-brothers
71 https://en.wikipedia.org/wiki/Vijaypat_Singhania
72 https://www.britannica.com/technology/glassblowing
73 https://www.britannica.com/topic/blacksmith

74 Robert D. Quinn, Leslie Gong, "Real-Time Aerodynamic Heating and Surface Temperature Calculations for Hypersonic Flight Simulation," pp. 44, NASA Technical Memorandum 4222, 1990; https://www.nasa.gov/centers/dryden/pdf/88193main_H-1602.pdf
75 https://www.grc.nasa.gov/WWW/BGH/stagtmp.html
76 https://www.faa.gov/about/office_org/headquarters_offices/avs/offices/aam/cami/library/online_libraries/aerospace_medicine/tutorial/media/iii.4.1.7_returning_from_space.pdf
77 https://www.sciencedirect.com/topics/materials-science/negative-thermal-expansion
78 https://earthsky.org/space/the-coldest-place-in-the-universe
79 https://www.pbs.org/wgbh/nova/article/absolute-hot/
80 https://www.space.com/25945-cosmic-microwave-background-discovery-50th-anniversary.html
81 https://www.britannica.com/topic/Bell-Laboratories
82 https://www.britannica.com/topic/Antikythera-mechanism
83 https://www.britannica.com/biography/Apollonius-of-Perga
84 Michio Yano, "Bīrūnī: Abū al Rayḥān Muḥammad ibn Aḥmad al Bīrūnī," The Biographical Encyclopedia of Astronomers, Thomas Hockey et al. (eds.), pp. 131–133, Springer, 2007; https://islamsci.mcgill.ca/RASI/BEA/Biruni_BEA.htm
85 Petra G. Schmidl, "Fārisī: Muḥammad ibn Abī Bakr al Fārisī," The Biographical Encyclopedia of Astronomers, Thomas Hockey et al. (eds.), pp. 357–359, Springer, 2007; https://islamsci.mcgill.ca/RASI/BEA/Farisi_BEA.htm
86 https://en.wikipedia.org/wiki/Analog_computer#Timeline_of_analog_computers
87 https://www.britannica.com/technology/automaton
88 https://youtu.be/zYQnV7xRhko
89 https://www.britannica.com/science/slide-rule
90 https://www.analogictips.com/analog-computation-part-1-what-and-why/
91 Icon Group International, Analog Computer: Webster's Timeline History, 1904–2006, pp. 28, ICON Group International, Inc., 2010.
92 Charles Care, Technology for Modelling: Electrical Analogies, Engineering Practice, and the Development of Analogue Computing, p. 203, Springer, 2010.
93 https://www.britannica.com/technology/computer/History-of-computing
94 https://www.britannica.com/biography/Alan-Turing
95 https://www.britannica.com/event/Manhattan-Project
96 https://www.tdworld.com/distribution/damage-prediction-model-improves-storm-response
87 https://web.stanford.edu/~cantwell/AA283_Course_Material/AA283_Course_Notes/AA283_Aircraft_and_Rocket_Propulsion_Ch_09_BJ_Cantwell.pdf
98 Layla S. Mayboudi, Heat Transfer and Thermal Modelling of Laser Transmission Welding of Thermoplastics, PhD dissertation, Queen's University, 2009.
99 https://www.researchgate.net/publication/222784800_Physical_and_Thermal_Properties_of_Ground_Beef_During_Cooking

100 https://www.ijera.com/papers/Vol3_issue1/IV3116551661.pdf
101 https://www.researchgate.net/publication/256295618_Evaluation_of_Some_Physical_Properties_of_Cucumber_Cucumis_sativus_L
102 https://www.researchgate.net/publication/222232320_Physical_properties_of_three_onion_varieties_as_affected_by_the_moisture_content
103 https://www.ijera.com/papers/Vol3_issue1/IV3116551661.pdf
104 https://www-tandfonline-com.proxy.queensu.ca/doi/full/10.1081/JFP-120015594?scroll=top&needAccess=true
105 https://www.engineeringtoolbox.com/specific-heat-capacity-food-d_295.html
106 https://en.wikipedia.org/wiki/List_of_physical_properties_of_glass
107 https://www.engineeringtoolbox.com/heat-loss-open-water-tanks-d_286.html
108 https://www.flir.com/products/flir-one-pro/
109 https://www.mcmaster.com/3m-electrical-tape
110 https://www.britannica.com/topic/samovar
111 https://youtu.be/pXE6CDOhRB8
112 https://youtu.be/RuJWpl7W6mc
113 https://www.goldenmoontea.com/blogs/tea/is-your-teapot-releasing-toxins
114 https://www.thoughtco.com/flame-temperatures-table-607307
115 https://www.thenakedscientists.com/articles/questions/how-many-watts-burning-candle
116 https://www.quora.com/How-much-energy-heat-does-one-standard-tea-light-candle-produce
117 https://www.explainthatstuff.com/candles.html
118 S. Paulke, E. Kreppold, "The Application of Thermal Simulation Techniques for Seat Comfort Optimizations," pp. 27, 2008; https://www.theseus-fe.com/ths_content/publications/articles/2008_paper_simvec_the-application-of-thermal-simulation-techniques-for-seat-comfort-optimizations_en.pdf
119 E.C. Chan, G. Karimi, D. Rose, and J.R. Culham, "Mechanical-Thermal Simulation of Passenger-Loaded Vehicle Seat in Severe Winter Conditions," pp. 10, Society of Automotive Engineers, 2004-01-1507; https://pdfs.semanticscholar.org/912a/2f52d216f688b8cecfe747dd9ffc5646c740.pdf
120 M. Kolich, P. Hoke, D. Dooge, M. Doroudian, E. Litovsky, and J. Kleiman, "Influence of Temperature and Mechanical Compression on Thermo-Physical Properties of Car Interior Foam Plastics Insulation," Journal of Elastomers & Plastics, vol. 46, no. 2, pp. 132–143, 2014.
121 Jason A. Lustbader, "Evaluation of Advanced Automotive Seats to Improve Thermal Comfort and Fuel Economy," Society of Automotive Engineers, NREL/CP-540-37693, pp. 7, 2005-01-2056.
122 Sally Shahzad, Ben Hughes, John Kaiser Calautit, Diana S.N.M. Nasir, "Computational and Field Test Analysis of Thermal Comfort Performance of User-Controlled Thermal Chair in an Open Plan Office," Energy Procedia, vol. 105, pp. 2635–2640, 2017.
123 https://www.britannica.com/biography/Christian-James-Lambertsen

124 Michael Menduno, Richard D. Vann, Petar J. Denoble, Neal W. Pollock, "Building a Consumer Rebreather Market: Lessons from the Technical Diving Revolution," Rebreather Forum 3 Proceedings, Durham, NC: AAUS/DAN/PADI, pp. 2–23, 2012; http://media.dan.org/RF3_web.pdf

125 https://opentextbc.ca/clinicalskills/chapter/5-5-oxygen-therapy-systems/

126 During the first Persian Gulf war in 1988, the Iraqi regime used chemical weapons against the Sardasht people of Iran and Halabja Kurdish people of Iraq, killing 5,000 people and injuring 10,000. The survivors needed to wear oxygen masks on a regular basis to carry on their daily activities. The author wishes to acknowledge her classmate, the warrior whom she witnessed walking up and down the stairs in a high-rise engineering school, with his wife following him, carrying an oxygen mask, putting himself through graduate studies in an engineering field. He and his peers, who stood up to protect their land, people, and values are remembered and revered. Only love for humanity and personal conviction to do things right can explain such sacrifice. They are surely among the individuals who elevate the human spirit and set an example for the rest.

127 https://en.wikipedia.org/wiki/Chemical_weapon#India

128 Unlike a G-Suit, a Space-Suit is to protect you against extreme temperature and zero-pressure conditions as well as protection against UV radiation, and collision with high velocity small objects while flying in space.

129 Chris Hadfield, An Astronaut's Guide to Life on the Earth, p. 320, First Edition, Random House Canada, 2013.

130 https://se.intersurgical.com/products/oxygen-och-aerosolprodukter/paediatric-medium-concentration-oxygen-masks#downloads

131 https://www.shinetsusilicone-global.com/catalog/pdf/rubber_e.pdf

132 https://www.wacker.com/cms/media/publications/downloads/6709_EN.pdf

133 Tephra is another by-product of volcanic activities; these are fragmental materials that can also be airborne. They cause the largest lava fragments to fall on the ground, or remain in the atmosphere, absorbing the Sun's radiation, causing the Earth's temperature to decrease considerably and occasionally generating volcanic winter or acidic precipitation in the form of rain and snow. They can be as small as ash, with particles under 2 mm (0.08 in), or as large as 64 mm (2.5 in).

134 https://www.naturalstoneinstitute.org/stoneprofessionals/technical-bulletins/rvalue/

135 http://www.minsocam.org/msa/collectors_corner/arc/tempmagmas.htm

136 http://www.tulane.edu/~sanelson/Natural_Disasters/volcan%26magma.htm

137 https://sciencestruck.com/basalt-rock-properties-uses

138 http://www.science.smith.edu/geosciences/petrology/Assignments/Enthalpy.pdf

139 http://www.dartmouth.edu/~ears5/handouts/heat.html

140 http://www.dartmouth.edu/~ears5/handouts/heat.html

141 http://volcano.oregonstate.edu/flow-rates

142 Eugene C. Robertson, The United States Department of the Interior Geological Survey, "Thermal Properties of Rocks," pp. 110, 1988; https://pubs.usgs.gov/of/1988/0441/report.pdf

143 P. Hartlieba, M. Toiflb, F. Kucharc, R. Meiselsc, T. Antretterb, "Thermo-Physical Properties of Selected Hard Rocks and Their Relation to Microwave-Assisted Comminution," Journal of Minerals Engineering, vol. 91, pp. 34–41, 2016; https://www.sciencedirect.com/science/article/pii/S0892687515301278
144 Rebecca A. Lange, Katharine V. Cashman, Alexandra Navrotsky, "Direct Measurements of Latent Heat during Crystallization, Contributions to Mineralogy and Petrology," vol. 118, no. 2, pp 169–181, 1994.
145 https://www.fusd1.org/cms/lib/AZ01001113/Centricity/Domain/883/eslbw10.pdf
146 https://pastafits.org/pasta-shapes/
147 https://www.britannica.com/technology/coal-slurry
148 https://www150.statcan.gc.ca/t1/tbl1/en/tv.action?pid=2510005601
149 Masaru Emoto, Hidden Messages in Water, Atria Books, 2005
150 https://www.reviewjournal.com/local/the-strip/heres-a-behind-the-scenes-look-at-how-the-bellagio-fountains-are-maintained/
151 https://youtu.be/kvOJ37pPKaM
152 K.N. Shukla, "Heat Pipe for Aerospace Applications—An Overview," Journal of Electronics Cooling and Thermal Control, vol. 5, pp. 1–14, 2015.
153 https://www.aparat.com/v/Xp9YB/
I am negotiating with the green flag of content, seeking the untold secrets of Beesat Bridge, having become acquainted with the memories of lovers; I am the interpreter of the eighth sunrise passage—Valfajr 8; the land of sadness is the meeting place of divine people; it is the turning point of all stories. When is it possible for the the Traveller to return and find the lost ones of Fave? I am mesmerised by the sunset at the shores of the river Arvand and the sparrows of the South reeds.
154 https://www.aboutpipelines.com/en/pipeline-101/whats-in-the-pipelines/natural-gas-lines/
155 https://www.shell.com/about-us/major-projects/perdido.html
156 https://en.wikipedia.org/wiki/List_of_natural_gas_pipelines
157 https://chemicalengineeringresearchandr.weebly.com/pipeline-transport.html
158 http://naturalgas.org/naturalgas/transport/
159 https://www.engineeringtoolbox.com/pipes-temperature-expansion-coefficients-d_48.html
160 http://pstrust.org/wp-content/uploads/2015/09/2015-PST-Briefing-Paper-02-NatGasBasics.pdf
161 https://www.builditsolar.com/Projects/Cooling/EarthTemperatures.htm
162 https://neutrium.net/fluid_flow/choked-flow/
163 The Lean Six Sigma approach focuses on enhancing the bottom line by improving performance and eliminating waste (i.e., Muda; a Japanese word for Futility, Uselessness, and Wastefulness), focusing on critical to quality characteristics. The training for Lean Six Sigma is provided through a belt-based training system. The belt personnel are designated as white, yellow, green, black, and master black belts, similar to judo.
164 https://en.wikipedia.org/wiki/Gimli_Glider

165 Layla S. Mayboudi, Flight Science: Mathematics Techniques Sensibility, p. 500, Mercury Learning and Information, 2019.
166 Hans Skalle, Bill Hahn, Applying Lean, Six Sigma, BPM, and SOA to Drive Business Results, Redguides for Business Leaders, p. 76, Redbooks, 2013; http://www.redbooks.ibm.com/redpapers/pdfs/redp4447.pdf
167 https://www.bing.com/images/search?q=cave+homes&qpvt=cave+homes&FORM=IGRE
168 https://www.britannica.com/topic/The-Flintstones
169 https://inhabitat.com/amazing-transformation-of-a-decrepit-cave-into-a-beautiful-modern-home/
170 https://www.gardensbythebay.com.sg/
171 https://www.theatlantic.com/magazine/archive/2016/01/the-height-of-efficiency/419124/
172 https://tech.cornell.edu/campus
173 https://www.greenbuildermedia.com/buildingscience/passive-house-is-it-worth-the-upfront-cost
174 https://www.oceanpowertechnologies.com/
175 https://www.waveenergyscotland.co.uk/
176 https://www.nbcwashington.com/news/national-international/Five-Innovative-Green-Projects-from-Around-the-World-375893561.html
177 http://www.middleeastgreenbuildings.com/11864/top-10-green-building-projects/
178 https://www.thenational.ae/world/iran-looks-to-solar-alternative-for-energy-1.456219
179 https://new.usgbc.org/leed
180 https://www.usgbc.org/articles/rebuilding-and-resiliency-leed-greensburg-kansas
181 https://en.wikipedia.org/wiki/Eden_Project#Environmental_aspects
182 https://youtu.be/xJsl_klqVh0
183 Nassim Haramein, "Addendum to Quantum Gravity and the Holographic Mass in View of the 2013 Muonic Proton Charge Radius Measurement," pp. 2, Hawaii Institute for Unified Physics, 2013; https://resonance.is/wp-content/uploads/2014/05/Addendum-to-Quantum-Gravity-and-the-Holographic-Mass.pdf
184 Mark Ahlers, Aircraft Thermal Management: Integrated Energy Systems Analysis, p. 109, SAE International, 2016.
185 Mark Ahlers, Aircraft Thermal Management: Systems Architectures, p. 99, SAE International, 2016.
186 Vedat S. Arpaci, Conduction Heat Transfer, p. 550, Addison-Wesley, 1966.
187 Andrew Aziz, T. Y. Na, Perturbation Methods in Heat Transfer, p. 199, Springer, 1984.
188 Thomas Bertels, Rath and Strong's Six Sigma Leadership Handbook, p. 566, John Wiley and Sons, 2003.
189 Marshall Brain, The Engineering Book: From the Catapult to the Curiosity Rover, 250 Milestones in the History of Engineering, p. 528, Sterling, 2015.

190 Yunus A. Cengel, M. A. Boles, p. 1024, Thermodynamics: An Engineering Approach, Eighth Edition, McGraw-Hill Education, 2014.
191 Yunus Cengel, Afshin Ghajar, Heat and Mass Transfer: Fundamentals and Applications, p. 992, Fifth Edition, McGraw-Hill Education, 2014.
192 Clifford A. Pickover, The Physics Book: From the Big Bang to Quantum Resurrection, 250 Milestones in the History of Physics, p. 528, Sterling, 2011.
193 Iain G. Currie, Fundamental Mechanics of Fluids, p. 548, Fourth Edition, CRC Press, 2012.
194 Mark Denny, Alan McFadzean, Engineering Animals: How Life Works, p. 385, Belknap Press of Harvard University Press, 2011.
195 Abraham S. Dorfman, Applications of Mathematical Heat Transfer and Fluid Flow Models in Engineering and Medicine, p. 410, First Edition, Wiley-ASME Press Series.
196 Russell C. Eberhart, Avraham Shitzer, Heat Transfer in Medicine and Biology: Analysis and Applications: 002, p. 462, Springer, 2008.
197 Federal Aviation Administration (FAA)/Aviation Supplies & Academics (ASA), Pilot's Handbook of Aeronautical Knowledge: FAA-H-8083-25B, p. 528, Aviation Supplies and Academics, Trotter Publishing, 2016.
198 Richard Haberman, Elementary Applied Partial Differential Equations with Fourier Series and Boundary Value Problems, p. 736, Third Edition, Prentice Hall, 1997.
199 William L. Haberman, James E. A. John, Introduction to Fluid Mechanics, p. 448, Third Edition, Prentice Hall, 1998.
200 Mikel Harry, Richard Schroeder, Six Sigma: The Breakthrough Management Strategy Revolutionizing the World's Top Corporations, p. 320, Crown Business, 2006.
201 Russell C. Hibbeler, Kai Beng Yap, Mechanics for Engineers, Dynamics, p. 736, Thirteenth Edition, Pearson, 2013.
202 Jack P. Holman, Heat Transfer, p. 752, Tenth Edition, McGraw Hill, 2009.
203 Robert Siegel, Thermal Radiation Heat Transfer, p. 1096, McGraw-Hill Series in Transportation, Third Edition, Taylor & Francis, 1992.
204 Frank P. Incropera, David P. DeWitt, Introduction to Heat Transfer, p. 912, Fifth Edition, John Wiley and Sons, 2006.
205 Frank P. Incropera, Fundamentals of Heat and Mass Transfer, p. 1024, Sixth Edition, John Wiley and Sons, 2006.
206 Walter Isaacson, Leonardo da Vinci, p. 625, Simon & Schuster, 2017.
207 Walter Isaacson, Einstein: His Life and Universe, p. 675, First Edition, Simon & Schuster, 2007.
208 Erwin Kreyszig, Advanced Engineering Mathematics, p. 1001, Tenth Edition, John Wiley and Sons, 2015.
209 P. E. Liley, 2000 Solved Problems in Mechanical Engineering Thermodynamics, p. 406, First Edition, McGraw Hill, 1989.

210 Seymour Lipschutz, Murray R. Spiegel, J. Liu, Schaum's Outline of Mathematical Handbook of Formulas and Tables, p. 271, Fifth Edition, McGraw- Hill Education, 2017.
211 Norman G. McCrum, Craig P. Buckley, Principles of Polymer Engineering, p. 464, Second Edition, Oxford University Press, 1997.
212 Bruce R. Munson, Alric P. Rothmayer, Theodore H. Okiishi, Wade W. Huebsch, Fundamentals of Fluid Mechanics, Seventh Edition, p. 792, John Wiley and Sons, 2012.
213 John Murphy, Numerical Analysis, Algorithms, and Computation, p. 158, Ellis Horwood Ltd, Publisher, 1988.
214 Glen E. Myers, Analytical Methods in Conduction Heat Transfer, p. 429, Second Edition, Amch, 1998.
215 National Aeronautics and Space Administration (NASA), Inside the International Space Station (ISS): NASA Thermal Control System (TCS) and Simplified Aid for EVA Rescue (SAFER) Astronaut Training Manuals, World Spaceflight News, Progressive Management, 2011.
216 Necati Ozisik, Heat Transfer: A Basic Approach, p. 576, ISE Edition, McGraw-Hill Education, 1984.
217 Suhas Patankar, Numerical Heat Transfer and Fluid Flow, p. 214, First Edition, Taylor and Francis, 2018.
218 Junuthula N. Reddy, An Introduction to the Finite Element Method, p. 816, Fourth Edition, 2018.
219 Shames, Mechanics of Fluids, p. 864, Fourth Edition, McGraw-Hill, 2002.
220 Frederick S. Sherman, Viscous Flow, p. 746, ISE Edition, McGraw-Hill Education, 1990.
221 Tien-Mo Shih, Numerical Heat Transfer, p. 467, First Edition, CRC Press, Hemisphere Publishing Corporation, 1984.
222 https://www.skygod.com/quotes/
223 Richard E. Sonntag, Gordon J. Van Wylen, Fundamentals of Statistical Thermodynamics, Series in Thermal and Transport Sciences, p. 370, John Wiley and Sons, 1966.
224 Claus Borgnakke, Richard E. Sonntag, Fundamentals of Thermodynamics, p. 912, Eighth Edition, John Wiley and Sons, 2012.
225 George B. Thomas Jr. (Author), Ross L. Finney Late (Author), Jan D. Weir (Author), Giordano (Author), Thomas' Calculus, p. 1280, Fourth Edition, Pearson, 2002.
226 Kenneth Wark, Advanced Thermodynamics for Engineers, p. 576, McGraw-Hill College, 1994.
227 Joel R. Hass (Author), Christopher E. Heil (Author), Maurice D. Weir (Author), Thomas' Calculus, p. 1224, Fourteenth Edition, Pearson, 2017.
228 Frank M. White, Heat and Mass Transfer, p. 736, First Edition, 1988.
229 Mark W. Zemansky, Basic Engineering Thermodynamics, p. 492, Second Edition, McGraw-Hill, 1975.

INDEX

D

E

F

G